ΠΑΝΕΠΙΣΤΗΜΙΟ ΘΕΣΣΑΛΙΑΣ

ΤΜΗΜΑ ΠΟΛΙΤΙΚΩΝ ΜΗΧΑΝΙΚΩΝ

ΤΟΜΕΑΣ ΓΕΩΤΕΧΝΙΚΗΣ

UNIVERSITY OF THESSALY

DEPARTMENT OF CIVIL ENGINEERING

GEOTECHNICAL DEPARTMENT

Διδακτορική Διατριβή

Παθητική σταθεροποίηση εδαφών έναντι ρευστοποίησης: πειραματική διερεύνηση εισπιεσιμότητας σταθεροποιητή – αριθμητική διερεύνηση σεισμικής απόκρισης σταθεροποιημένων εδαφών και θεμελιώσεων

PhD Thesis

Passive soil stabilization against liquefaction: experimental investigation of stabilizer permeation potential – numerical investigation of seismic response of stabilized soils and foundations

Γεωργία Ι. Αγαπουλάκη

Πολιτικός Μηχανικός

Georgia I. Agapoulaki

Civil Engineer

Συν-επιβλέποντες Καθηγητές

Παναγιώτης Ντακούλας, Καθηγητής, Π.Θ.

Αχιλλέας Παπαδημητρίου, Επικ. Καθηγητής, Ε.Μ.Π.

Co-Supervisors

Panagiotis Dakoulas, Professor, U.Th.

Achilleas Papadimitriou, Assistant Professor, N.T.U.A.

Βόλος, 2017

Volos, 2017

ΠΑΝΕΠΙΣΤΗΜΙΟ ΘΕΣΣΑΛΙΑΣ

ΤΜΗΜΑ ΠΟΛΙΤΙΚΩΝ ΜΗΧΑΝΙΚΩΝ

ΤΟΜΕΑΣ ΓΕΩΤΕΧΝΙΚΗΣ

Παθητική σταθεροποίηση εδαφών έναντι ρευστοποίησης: πειραματική διερεύνηση εισπιεσιμότητας σταθεροποιητή – αριθμητική διερεύνηση σεισμικής απόκρισης σταθεροποιημένων εδαφών και θεμελιώσεων

Διδακτορική διατριβή

Γεωργίας Ι. Αγαπουλάκη

Η διατριβή υποβλήθηκε στο Τμήμα Πολιτικών Μηχανικών της Πολυτεχνικής Σχολής του Πανεπιστημίου Θεσσαλίας προς εκπλήρωση των προϋποθέσεων του τίτλου του Διδάκτορος Μηχανικού.

ΤΡΙΜΕΛΗΣ ΣΥΜΒΟΥΛΕΥΤΙΚΗ ΕΠΙΤΡΟΠΗ:

Π. Ντακούλας, Καθηγητής, Π.Θ.
(Συν-επιβλέπων)

Αχ. Παπαδημητρίου, Επ. Καθηγητής, Ε.Μ.Π.
(Συν-επιβλέπων)

Γ. Μπουκοβάλας, Καθηγητής, ΕΜΠ

ΕΠΤΑΜΕΛΗΣ ΕΞΕΤΑΣΤΙΚΗ ΕΠΙΤΡΟΠΗ:

Π. Ντακούλας , Καθηγητής, Παν. Θεσσαλίας

Αχ. Παπαδημητρίου, Επ. Καθηγητής, Ε.Μ.Π.

Γ. Μπουκοβάλας , Καθηγητής, ΕΜΠ

Α. Κωμοδρόμος, Καθηγητής, Παν. Θεσσαλίας

Θ. Τίκα – Βασιλικού, Καθηγήτρια, Α.Π.Θ.

Μ. Πανταζίδου, Αν. Καθηγήτρια, Ε.Μ.Π.

Π. Καλλιόγλου, Λέκτορας, Παν. Θεσσαλίας

Η παρούσα έρευνα έχει συγχρηματοδοτηθεί από την Ευρωπαϊκή Ένωση (Ευρωπαϊκό Κοινωνικό Ταμείο - ΕΚΤ) και από εθνικούς πόρους μέσω του Επιχειρησιακού Προγράμματος «Εκπαίδευση και Δια Βίου Μάθηση» του Εθνικού Στρατηγικού Πλαισίου Αναφοράς (ΕΣΠΑ) – Ερευνητικό Χρηματοδοτούμενο Έργο: ΘΑΛΗΣ. Επένδυση στην κοινωνία της γνώσης μέσω του Ευρωπαϊκού Κοινωνικού Ταμείου.

UNIVERSITY OF THESSALY

DEPARTMENT OF CIVIL ENGINEERING

GEOTECHNICAL DEPARTMENT

Passive soil stabilization against liquefaction: experimental investigation of stabilizer permeation potential – numerical investigation of seismic response of stabilized soils and foundations

PhD Thesis by

Georgia I. Agapoulaki

The thesis is submitted to the Department of Civil Engineering at the University of Thessaly in fulfilment of the requirements for the Degree of Doctor of Philosophy.

ADVISORY COMMITTEE:

P. Dakoulas, Professor, Univ. of Thessaly (Co-Supervisor)

A. Papadimitriou, Assistant Professor, N.T.U.A. (Co-supervisor)

G. Bouckovalas, Professor, N.T.U.A.

EXAMINATION COMMITTEE:

P. Dakoulas, Professor, Univ. of Thessaly

A. Papadimitriou, Assistant Professor, N.T.U.A.

G. Bouckovalas, Professor, N.T.U.A.

E. Comodromos, Professor, Univ. of Thessaly

Th. Tika - Vasilikou, Professor, A.U.Th.

M. Pantazidou, Associate Professor, N.T.U.A.

P. Kallioglou, Lecturer, Univ. of Thessaly

This research has been co-financed by the European Union (European Social Fund ESF) and Greek national funds through the Operational Program "Education and Lifelong Learning" of the National Strategic Reference Framework (NSRF) Research Funding Program: Thales. Investing in knowledge society through the European Social Fund.

ABSTRACT

Seismic liquefaction hazard is efficiently mitigated by a large number of existing ground improvement techniques. However, at developed sites, most liquefaction mitigation techniques are either difficult (e.g. soil mixing), or even impossible (e.g. vibro-replacement) to implement. In such cases, confinement methods (underpinning, diaphragm walls), high pressure (and viscosity) grouting, or perforated drains are often prescribed. However, these techniques cannot mitigate liquefaction under the whole structure at risk, since they are usually performed at its perimeter, while they may also create structural problems (e.g. footing heave due the pressures involved in high viscosity grouting). In addition, normal operation is obstructed during improvement works and the treatment of large areas is costly. If liquefaction mitigation is required around lifelines, similar problems may arise, since the majority of existing ground improvements techniques may impose damage to the pipelines, while the related cost is prohibitive given their large total lengths.

An alternative technique without these drawbacks is passive (site) stabilization, which includes the low-pressure injection in the soil pores of colloidal silica (CS), an aqueous dispersion of fine silica particles. This material retains low viscosity values (slightly higher than that of water) up until a well-controlled time after mixing (named gel time) when its viscosity increases rapidly. The CS injection in situ may be performed by injection and pumping wells on either side of a structure at risk of liquefaction in its foundation soil. The gelation of CS alters the mechanical response of the soil skeleton–pore fluid system, making it less vulnerable to plastic strain accumulation related to liquefaction or cyclic mobility.

This ground improvement technique is currently still at an experimental stage worldwide. Some of the fundamental issues that need to be resolved before this technique becomes applicable in practice are: (a) the control of CS gelation, since the under- and over-prediction of the gel time leads in situ to over- and under-delivery of CS, respectively, (b) the depiction and simulation of the transport mechanisms that affect the efficient delivery of CS into the soil pores over large distances, (c) the numerical simulation of the mechanical response of stabilized soils, to be used in analyses of pertinent boundary value problems, (d) the knowledge of seismic response of stabilized soil layers, since this affects the vibration of thereby founded structures and finally (e) the effectiveness of passive stabilization for usual structures (with shallow foundations) in terms of settlement reduction from a performance-

based design point of view. In this respect, the scope of this Thesis is to aid in resolving the foregoing fundamental issues, as explained

Particularly, this Thesis initially presents results from viscosity measurements on CS solutions. These measurements complement the existing literature, which shows that the gel time of CS solutions depends on the pH value, decreases with normality of cations and the concentration of CS in the solution, CS(%), but also depends on the dimensions of the CS particles (or the CS type, in general). The viscosity measurements were performed on a total of 60 different samples of different concentrations of Ludox-SM® fine colloidal silica, diluted with deionized water and enriched with pure NaCl in different normalities, while the pH was controlled by adding small quantities of HCl. The tests corroborated the effects of the aforementioned parameters on the gelation of CS, but also depicted a significant decreasing effect of temperature on the gel time. Then, a statistical analysis of the available laboratory data (measurements, complemented by the literature wherever possible) was performed and a set of design charts was devised for predicting the gel time of CS solutions. In addition, a multi-variable equation was proposed for predicting the viscosity versus time curve of CS solutions, which may be used for predicting the rheology of any CS solution. The proposed design charts and equations yield results that compare very satisfactorily with the laboratory data.

Then, a series of 1D injection tests investigated the injectability of different CS solutions in granular columns. The tests measured the flow rate and travel distance of CS with time during injections with low hydraulic gradients (0.05 to 0.25) in sand and silty sand columns of 20 to 100cm height. These tests corroborate the literature-depicted increasing effects of hydraulic gradient and hydraulic conductivity on the flow rate, as well as the fundamental finding that that injection essentially stops when the CS viscosity reaches 4–7cP, at least for the tested low hydraulic gradients. In addition, these tests underline the important role of the higher density of CS in comparison to the water that it displaces from the soil pores. Hence, the CS injectability is affected by both the time-increasing viscosity of CS and the density-driven flow component outlined above. These tests also show that the NaCl existing in sea water does not essentially affect the injectability of CS in marine sands, at least for injections lasting up to a day. Finally, a recently proposed simple analytical tool is employed for predicting the CS flow rate in 1D injection tests, which is based on the Darcy's law after appropriate adjustments for the differences in viscosity and density of CS as compared to that of the water it displaces.

In the sequel, since a dedicated constitutive model for stabilized sands has not been established yet, this Thesis explored the potential of using existing models for untreated

sands, after appropriate modifications. For this purpose, the bounding surface plasticity model NTUA-SAND was selected, since it is well-established for liquefaction analyses in the literature. Two (2) simulation approaches were explored: (a) recalibration of model constants (leading to a stiffer and less contractive response of the soil skeleton), (b) decrease of pore fluid bulk modulus K in comparison to the value K_w for water (simulating the seemingly increased compressibility of CS in comparison to water). Comparison of model simulations to laboratory element tests shows that both these approaches are potentially capable of simulating the behavior of stabilized sands. However, further comparison with two (2) dynamic centrifuge tests for the seismic response of a horizontal layer and a gently sloping layer of stabilized sand show that only approach (b) can provide quantitative accuracy in fully coupled dynamic analyses of boundary value problems involving stabilized sands. In practice, a simple relation for the moduli ratio of K_w/K is proposed as a function of the percentage per weight CS(%) as a uniform framework for the simulation of stabilized sand response, along with an appropriate model for sands (like the NTUA-SAND model employed here).

Subsequently, numerical parametric analyses were conducted for investigating the 1D seismic response of stabilized soil layers using the above simulation methodology. It was found that the seismic response of fully stabilized layers is reminiscent of the corresponding response of the untreated soil under fully drained conditions, and identical to it for low intensity excitations. It has to be underlined here that fully drained conditions imply zero excess pore pressures, a condition that never appears for sands or silty sands in situ during shaking. For surficially only stabilized layers, the seismic response at the ground surface is mostly determined by the response of the underlying untreated soil layer, e.g. if this latter layer is quite thick and liquefies, then de-amplification may be observed. In addition, a statistical processing of the input data and the results of the ground response analyses for fully stabilized layers led to the proposal of a set of multi-variable relations, which estimate the surface-to-base amplification of the elastic response spectrum (5% damping) at stabilized layers.

Finally, numerical parametric analyses were conducted for investigating the seismic response of a surface strip foundation lying on stabilized soil using again the proposed simulation methodology. It was found that if the foundation lies on a fully stabilized layer, the accelerations may be important, but seismic settlements are significantly smaller than those of an untreated layer. On the other hand, if the foundation lies on a surficially only stabilized layer, its accelerations may be de-amplified due to the underlying liquefied layer. Important problem parameters are the factor of safety against bearing capacity failure and the

characteristics of the excitation (intensity, duration, predominant period). From a performance-based design point of view, it was found that if the thickness of the surficially only stabilized layer is twice the width of the foundation, the seismic settlements are reduced significantly, i.e. almost as much as if the layer was fully stabilized. However, if the surficially only stabilized layer thickness is equal to the width of the footing, the benefit in seismic settlements is very small.

Ευχαριστίες

Με την ολοκλήρωση αυτής της διατριβής φτάνουμε στο τέλος μιας μεγάλης και δύσκολης διαδρομής. Μέσα σ' αυτά τα πέντε χρόνια εκπόνησής της υπήρχαν στιγμές πίεσης και άγχους, υπήρχαν όμως και στιγμές χαράς, ικανοποίησης και ευχαρίστησης. Κοιτώντας λοιπόν πίσω, και κάνοντας έναν απολογισμό, μπορώ με βεβαιότητα να πω πως οι ευχάριστες στιγμές σκιάζουν τις δυσάρεστες, πως οι στιγμές πίεσης και άγχους ξεχνιούνται και τη θέση τους παίρνουν όμορφες αναμνήσεις. Όμως, η υλοποίηση αυτής της διατριβής δε θα ήταν δυνατή χωρις την παρουσία, την υποστήριξη και την ανεκτικότητα κάποιων ανθρώπων. Για το λόγο αυτό, νιώθω την ανάγκη να «κλέψω» λίγο χώρο από αυτές εδώ τις σελίδες για να εκφράσω την ευγνωμοσύνη μου και να πω ένα μεγάλο ευχαριστώ σε όλους αυτούς που με τις πράξεις ή τα λόγια τους, με τις γνώσεις ή την αγάπη τους συνέβαλαν στην ολοκλήρωση αυτής εδώ της εργασίας.

Πρώτα απ'όλα, θα ήθελα να ευχαριστήσω τον κ. Αχιλλέα Παπαδημητρίου, Επίκουρο Καθηγητή Ε.Μ.Π., ο οποίος μου έβαλε το «μικρόβιο» των γεωτεχνικών ήδη από τα προπτυχιακά μου χρόνια και συνεπέβλεψε αυτήν εδώ τη διατριβή. Με τις συμβουλές, τις γνώσεις του και την υπομονή του με βοήθησε σε όλα τα στάδια εκπόνησης της διατριβής, όντας πάντα έτοιμος να δώσει λύσεις σε κάθε πρόβλημα ή απορία καθώς και να με «ταρακουνήσει» τις στιγμές που ένιωθα αγχωμένη. Είναι ένας εξαιρετικός καθηγητής και επιστήμονας, μα πάνω απ'όλα ένας υπέροχος Άνθρωπος, που ακόμα και στις δύσκολες και δυσάρεστες προσωπικές μου στιγμές έδειξε κατανόηση και υπομονή.

Θα ήθελα να εκφράσω τις θερμές μου ευχαριστίες και στον κ. Ντακούλα Παναγιώτη, Καθηγητή Π.Θ., συνεπιβλέποντα της διαδακτορικής διατριβής για την πνευματική και επιστημονική υποστήριξη που μου παρείχε κατά τη διάρκεια εκπόνησης της διατριβής αλλά και τα χρόνια των προπτυχιακών μου σπουδών. Ιδιαίτερη μνεία αξίζει ο κ. Μπουκοβάλας Γεώργιος, Καθηγητής Ε.Μ.Π., μέλους της τριμελούς Συμβουλευτικής Επιτροπής, του οποίου οι συμβουλές υπήρξαν πολύτιμες για την επίτευξη του βέλτιστου αποτελέσματος. Επίσης, θα ήθελα να ευχαριστήσω και τα υπόλοιπα μέλη της Επταμελούς Επιτροπής κ. Κωμοδρόμο Αιμίλιο, Καθηγητή Π.Θ., κ. Θεοδώρα Τίκα-Βασιλικού, Καθηγήτρια Α.Π.Θ., κ. Μαρίνα Πανταζίδου, Αναπληρώτρια Καθηγήτρια Ε.Μ.Π. και κ. Πολυξένη Καλλιόγλου, Λέκτορα Π.Θ. για τη συμβολή τους στην τελική διαμόρφωση της διατριβής.

Θα ήταν παράλειψη να μην αναφέρω την πολύτιμη συνεισφορά του Δρ. Κων/νου Ανδριανόπουλου στην ολοκλήρωση αυτής της εργασίας, του Κυριάκου Κανδρή για τις

συμβουλές του, όποτε τις χρειάστηκα, και του Δρ. Ιωάννη Χαλούλου στην εκμάθηση του λογισμικού. Επίσης, ένα ευχαριστώ οφείλω στον Ιωάννη Τσιάπα για τις αισθητικές του παρεμβάσεις και για όλες τις φορές που «γιάτρεψε» τον υπολογιστή μου.

Φυσικά, δε θα μπορούσα να μην πω ένα μεγάλο ευχάριστώ στα «παιδιά» μου, όπως τα αποκαλώ, τους προπτυχιακούς φοιτητές των οποίων συνεπέβλεψα τις διπλωματικές εργασίες μαζί με τον κ. Αχιλλέα Παπαδημητρίου. Ευχαριστώ λοιπόν τον Άντώνη Ντουντουλάκη για την πολύτιμη βοήθεια στα πολύωρα πειράματα στο εργαστήριο, καθώς και την Ηλιάνα Πανάγου και την Ντένη Σιάμπου, οι οποίες υπήρξαν πολύτιμες συνεργάτες, και η συμβολή τους ήταν πολύ σημαντική.

Θα ήθελα μέσα από την καρδιά μου να ευχαριστήσω και όλους τους ανθρώπους οι οποίοι όλα αυτά τα χρόνια είναι δίπλα μου και μου συμπαραστέκονται. Ίσως κάποιοι από αυτούς να μην έχουν τις επιστημονικές γνώσεις να μου δώσουν συμβουλές επί του ερευνητικού μου έργου, όμως με την αγάπη τους ήταν πάντα εκεί να μου φτιάξουν τη διάθεση και να μου προσφέρουν ένα χαμόγελο κάθε φορά που ήμουν αγχωμένη. Αναφέρομαι φυσικά στην οικογένειά μου και στους φίλους μου, όσους ήξερα από πριν αλλά και όσους γνώρισα αυτά τα πέντε χρόνια, που υπήρξαν σιωπηλοί συνοδοιπόροι μου σε όλη αυτή τη διαδρομή. Περισσότερο από όλους θα ήθελα να ευχαριστήσω το Νίκο, ο οποίος ήταν πάντα εκεί να με επαναφέρει στην πραγματικότητα όταν το χρειάστηκα και μου στάθηκε στις πιο δύσκολες αλλά και στις πιο όμορφες στιγμές.

Το πιο μεγάλο όμως ευχαριστώ από όλα το οφείλω στους γονείς μου Γιάννη και Μαρία και στον αδερφό μου Βασίλη, που με την αγάπη τους όλα αυτά τα χρόνια με κάνουν πιο δυνατή και χαρούμενη, που ακόμα και όταν τα πράγματα ήταν πολύ δύσκολα, τα έκαναν να φαντάζουν εύκολα με μια κουβέντα τους και με ένα χαμόγελο. Χωρίς αυτούς τίποτα από όλα αυτά που έχω καταφέρει δε θα είχε γίνει και σίγουρα θα ήμουν ένας διαφορετικός άνθρωπος. Σας ευχαριστώ πολύ.

Γεωργία Ι. Αγαπουλάκη

Διδακτορική Διατριβή

Παθητική σταθεροποίηση εδαφών έναντι ρευστοποίησης: πειραματική διερεύνηση εισπιεσιμότητας σταθεροποιητή – αριθμητική διερεύνηση σεισμικής απόκρισης σταθεροποιημένων εδαφών και θεμελιώσεων

Γεωργία Ι. Αγαπουλάκη

ΕΚΤΕΝΗΣ ΠΕΡΙΛΗΨΗ

1. Αντικείμενο και σκοπός της εργασίας

Η σεισμική ρευστοποίηση είναι μία από τις πλέον επιβλαβείς φυσικές καταστροφές για τα δομικά έργα και τα έργα υποδομής. Προκύπτει σε χαλαρά μη συνεκτικά εδάφη, κάτω από τη στάθμη του υδροφόρου ορίζοντα, αν υποβληθούν σε ισχυρή σεισμική διέγερση, και οι επιπτώσεις αυτής στις κατασκευές μπορεί να είναι τεράστιες (π.χ. αστοχίες θεμελίων ή πασσάλων, μεγάλες καθιζήσεις, ολισθήσεις και στροφές τοίχων, ανατροπές κτιρίων, επιπλεύσεις υπόγειων κατασκευών). Το εν δυνάμει πρόβλημα ειδικά για υφιστάμενες κατασκευές γίνεται εμφανές αν αναλογιστεί κανείς ότι μόλις τη δεκαετία του ’80 προέκυψε μια ολοκληρωμένη μεθοδολογία ανάλυσης του προβλήματος στη διεθνή βιβλιογραφία, ενώ όλα τα παραλιακά μέτωπα αστικών κέντρων είχαν ήδη κατασκευαστεί, τόσο στην Ελλάδα όσο και στο εξωτερικό.

Σε θέσεις υφισταμένων κατασκευών θεμελιωμένων επί ρευστοποιήσιμου (χαλαρού μη συνεκτικού) εδάφους, η χρήση των περισσοτέρων από τις υπάρχουσες μεθοδολογίες βελτίωσης του εδάφους είναι δυσχερής (π.χ. λόγω λειτουργίας της κατασκευής ή λόγω δυσχερούς πρόσβασης), ακόμη και αδύνατη (π.χ. λόγω των δομικών ζημιών που μπορούν να προκληθούν). Έτσι, για τη βελτίωση του εδάφους σε τέτοιες θέσεις συνήθως χρησιμοποιούνται τεχνικές όπως: μικροπάσσαλοι/ διαφραγματικοί τοίχοι, εισπίεση ενεμάτων υψηλού ιξώδους (με υψηλές πιέσεις) καθώς και η έμπηξη πλαστικών στραγγιστηρίων. Παρόλα αυτά, οι συγκεκριμένες μεθοδολογίες δεν μπορούν ευχερώς να βελτιώσουν το έδαφος σε ολόκληρη την κάτοψη του κτηρίου, ενώ μπορούν να δημιουργήσουν και κατασκευαστικά προβλήματα (π.χ. η εισπίεση ενεμάτων με υψηλές πιέσεις μπορεί να προκαλέσει ανασήκωμα θεμελίων). Επιπλέον, κατά τη διάρκεια των

εργασιών της βελτίωσης προκαλούνται δυσχέρειες στην κανονική λειτουργία της κατασκευής και η βελτίωση μεγάλων περιοχών αποδεικνύεται σχετικά υψηλού κόστους

Μία εναλλακτική μέθοδος βελτίωσης μη συνεκτικών εδαφών που δεν έχει τα παραπάνω μειονεκτήματα και μπορεί να χρησιμοποιηθεί ευχερώς στο έδαφος θεμελίωσης υφισταμένων κατασκευών (αλλά και γύρω από υπόγειους αγωγούς) είναι η παθητική σταθεροποίηση (passive site stabilization: Gallagher, 2000). Σύμφωνα με αυτή, γίνεται εμπλουτισμός του υγρού των πόρων του ρευστοποιήσιμου εδάφους με έναν σταθεροποιητή, ο οποίος αποτελείται από περιβαλλοντικώς ασφαλή νανο-σωματίδια (π.χ. κολλοειδής πυριτία, αργιλικά ορυκτά, μικρο-οργανισμοί). Αυτός ο εμπλουτισμός αλλάζει τη μηχανική συμπεριφορά του συστήματος εδαφικού σκελετού – υγρού πόρων, καθιστώντας το λιγότερο ευάλωτο σε συσσώρευση πλαστικών παραμορφώσεων που σχετίζονται με ρευστοποίηση ή την ανακυκλική κινητικότητα (cyclic mobility), κατά τη διάρκεια και αμέσως μετά τη σεισμική διέγερση, και των καταστροφικών συνεπειών που έχουν αυτές για τη συνορεύουσα κατασκευή. Η διήθηση του σταθεροποιητή μπορεί να γίνει μετά από διάνοιξη φρέατος και μέσω της φυσικής ροής του υγρού των πόρων (εξασφαλίζοντας ότι δε θα γίνει ανεξέλεγκτη διήθηση προς τα κατάντη), ή συνηθέστερα επιβάλλοντας συνθήκες ροής με τη χρήση φρεάτων υψηλού και χαμηλού υδραυλικού ύψους εκατέρωθεν της κατασκευής (βλ. Εικόνα 1).

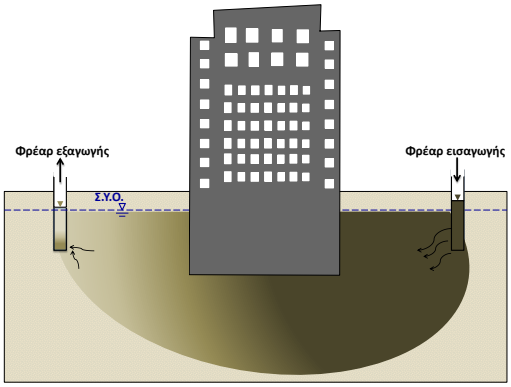

Εικόνα 1 *Διαδικασία εκτέλεσης παθητικής σταθεροποίησης στο έδαφος θεμελίωσης κατασκευής*

Η επιτυχής εφαρμογή της παθητικής σταθεροποίησης έγκειται στην εισπίεση του βέλτιστου σταθεροποιητή στην επιθυμητή θέση μέσα σε έναν προκαθορισμένο χρόνο. Στην παρούσα διατριβή, η έμφαση δίνεται στο βέλτιστο σταθεροποιητή με βάση την βιβλιογραφία, δηλαδή την κολλοειδή πυριτία. Σκοπός της παρούσας διατριβής είναι αρχικώς να εμπλουτίσει τα εργαστηριακά αποτελέσματα της βιβλιογραφίας που αφορούν τόσο στα ρεολογικά

χαρακτηριστικά της κολλοειδούς πυριτίας όσο και στην εισπιεσιμότητά της σε μη συνεκτικά εδάφη.

Καθώς αυτή η νέα τεχνική βελτίωσης του εδάφους εξακολουθεί να βρίσκεται σε πειραματικό στάδιο διεθνώς και ελλείψει ενός εξειδικευμένου καταστατικού προσομοιώματος, η παρούσα διατριβή διερευνά επίσης τη δυνατότητα χρήσης υφιστάμενων καταστατικών προσομοιωμάτων για άμμους προκειμένου να προσομοιωθεί η ανακυκλική απόκριση των παθητικά σταθεροποιημένων εδαφών. Για το σκοπό αυτό, χρησιμοποιείται ένα σοφιστευμένο προσομοίωμα για άμμους για την προσομοίωση τόσο ανακυκλικών δοκιμών εδαφικού στοιχείου, όσο και δύο δυναμικών δοκιμών φυγοκέντρισης στις οποίες προσομοιώνεται η σεισμική απόκριση μιας οριζόντιας σταθεροποιημένης στρώσης άμμου και μιας αντίστοιχης υπό μικρή κλίση. Για να επιτευχθεί αυτό, πραγματοποιήθηκαν συζευγμένες δυναμικές αναλύσεις πεπερασμένων διαφορών θεωρώντας αλλαγές στον εδαφικό σκελετό ή στο υγρό των πόρων.

Για την εφαρμογή της παθητικής σταθεροποίησης στην πράξη απαιτείται η ολοκληρωμένη γνώση της σεισμικής απόκρισης του σταθεροποιημένου εδάφους και των κατασκευών που θεμελιώντονται επ' αυτού. Στη βιβλιογραφία υπάρχουν μόνο αποσπασματικά δεδομένα τα οποία υποδεικνύουν ότι τα σταθεροποιημένα εδάφη όχι μόνο δεν οδηγούν σε απομείωση της ταλάντωσης (όπως στη ρευστοποίηση) αλλά αντίθετα την ενισχύουν (Gallagher et al., 2007a). Αυτή η πτυχή της απόκρισης των σταθεροποιημένων εδαφών έχει μεγάλη πρακτική σημασία, καθώς επηρεάζει την ένταση της σεισμικής φόρτισης που φτάνει στις κατασκευές, οι οποίες είναι θεμελιωμένες επί σταθεροποιημένων εδαφών. Ελλείψει άλλων δεδομένων, η διατριβή αυτή διερευνά αριθμητικά την μονοδιάστατη σεισμική απόκριση των σταθεροποιημένων εδαφών με τη βοήθεια μιας κατάλληλα βαθμονομημένης αριθμητικής μεθοδολογίας. Στη συνέχεια, η ίδια αριθμητική μεθοδολογία χρησιμοποιείται για τη μελέτη της απόκρισης μιας επιφανειακής θεμελιολωρίδας που εδράζεται σε μια σταθεροποιημένη στρώση. Για το λόγο αυτό, διερευνώνται οι επιδράσεις των χαρακτηριστικών της διέγερσης και του εδάφους στη σεισμική απόκριση τέτοιων θεμελίων μέσω παραμετρικών αναλύσεων.

Με βάση τα ανωτέρω, η παρούσα διατριβή αποτελεί μία συνδυασμένη εργαστηριακή και υπολογιστική συμβολή στην προσπάθεια να καταστεί η παθητική σταθεροποίηση πρακτικώς εφαρμόσιμη. Η παρούσα εκτενής περίληψη έχει επιμέρους κεφάλαια, η αρίθμηση και το αντικείμενο των οποίων αντιστοιχούν στα κεφάλαια της διατριβής.

2. Κολλοειδής πυριτία στη βιβλιογραφία

Η κολλοειδής πυριτία (Colloidal Silica, CS) είναι ένα διάλυμα νανο-σωματιδίων του πυριτίου σε νερό, η οποία προκύπτει από τον πολυμερισμό του μονομερούς $Si(OH)_4$. Όταν αραιωθεί σε συγκέντρωση 4-10% κατά βάρος έχει αρχικό ιξώδες και πυκνότητα ελαφρώς μεγαλύτερα από το νερό και σχηματίζει ταχέως μια σταθερή γέλη μετά από ένα ρυθμιζόμενο χρονικό διάστημα, το οποίο μπορεί να κυμαίνεται από μερικά λεπτά έως αρκετούς μήνες. Αυτή η διαδικασία σχηματισμού γέλης προκαλείται από το σχηματισμό δεσμών σιλοξάνης μεταξύ των νανο-σωματιδίων της πυριτίας. Κατά τη διάρκεια αυτού του χρόνου οι τιμές του ιξώδους παραμένουν χαμηλές, επιτρέποντας στο διάλυμα να διηθηθεί μέσω των πόρων του εδάφους στην επιθυμητή θέση. Ο χρόνος που απαιτείται για τη δημιουργία γέλης μπορεί να ρυθμιστεί με μεταβολή της συγκέντρωσης CS(%) στο διάλυμα, της τιμής του pH, της συγκέντρωσης αλάτων (NaCl ή άλλου) και της θερμοκρασίας του διαλύματος (Agapoulaki and Papadimitriou 2015; Gallagher 2000a). Επισημαίνεται ότι κολλοειδής πυριτία είναι μη τοξική, βιολογικά και χημικά αδρανής, άοσμη, μη εύφλεκτη, ανθεκτική και δεν απαιτεί ειδικό εξοπλισμό για την προετοιμασία και την εφαρμογή της μεθόδου. Η ανθεκτικότητα της CS εκτιμάται από τον Whang (1995) ως υψηλότερη από 25 χρόνια. Στην παρούσα διδακτορική διατριβή, έμφαση θα δοθεί στην Ludox-SM®, η οποία είναι ο πιο συχνά χρησιμοποιούμενος τύπος κολλοειδούς πυριτίας καθώς διαθέτει τη μεγαλύτερη ειδική επιφάνεια ($345 m^2/g$) και το μικρότερο μέγεθος σωματιδίων (7nm), καθιστώντας έτσι πιο μικρούς του χρόνους γέλης, σε σχέση με τους άλλους τύπους πυριτίας. Αντίστοιχα, χρειάζεται και μικρότερες ποσότητες κατά βάρος για να δημιουργηθεί γέλη, όντας έτσι η πιο οικονομική επιλογή (Gallagher, 2000).

3. Μηχανική συμπεριφορά σταθεροποιημένων εδαφών

Μονοτονική συμπεριφορά

Τα πειραματικά δεδομένα που αφορούν στην μονοτονική συμπεριφορά των σταθεροποιημένων εδαφών στη βιβλιογραφία είναι περιορισμένα και αποσπασματικά, αδυνατώντας να περιγράψουν ολοκληρωμένα την απόκρισή τους. Σε γενικές γραμμές, τα υπάρχοντα δεδομένα υποδεικνύουν μία αρκετά βελτιωμένη συμπεριφορά του σταθεροποιημένου εδάφους σε σχέση με το (φυσικό) μη σταθεροποιημένο.

Για παράδειγμα, οι Kodaka et al. (2005) πραγματοποίησαν δοκιμές στρεπτικής διάτμησης σε σταθεροποιημένα με κολλοειδή πυριτία (ο τύπος της οποίας δεν καθορίζεται στη δημοσίευση: Ludox-SM® ή άλλος) και φυσικά δοκίμια άμμου Toyoura (με D_r=22%, e_{max}=0.821, e_{min}=0.464, D_{50}=0.44mm) για διαφορετικές τιμές κατακόρυφης τάσης. Τα

αποτελέσματα καταδεικνύουν μια εν γένει πιο διαστολική και πιο δύστμητη συμπεριφορά των σταθεροποιημένων εδαφών. Στην Εικόνα 2 παρουσιάζονται τα εν λόγω αποτελέσματα, όπου με συνεχείς γραμμές φαίνεται η απόκριση του φυσικού εδάφους και με διακεκομμένες η αντίστοιχη συμπεριφορά των σταθεροποιημένων εδαφών με συγκέντρωση πυριτίας CS=4%. Τα δεδομένα για διαφορετικές κατακόρυφες τάσεις απεικονίζονται με διαφορετικά χρώματα.

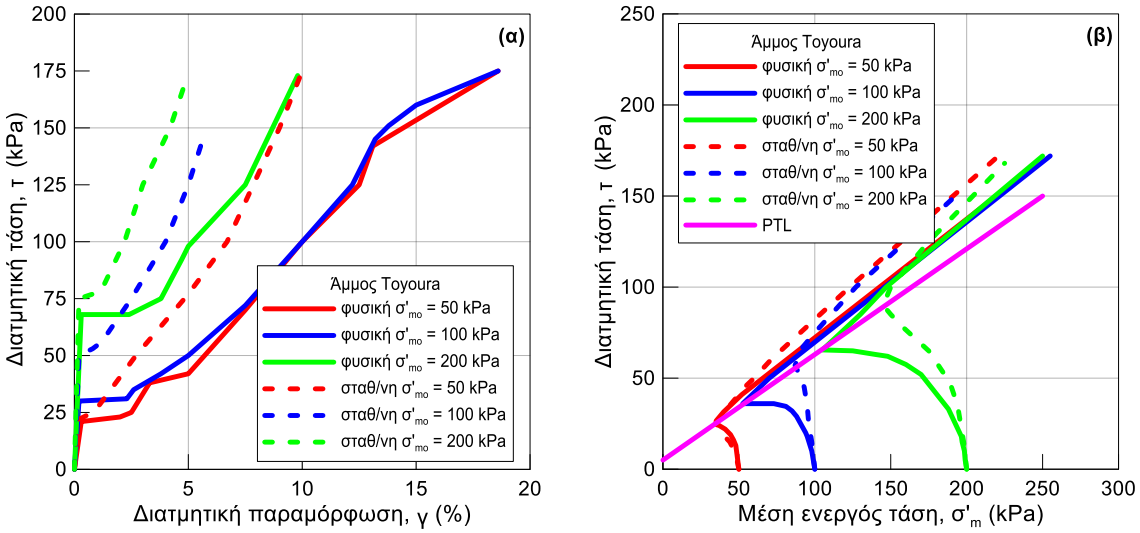

Εικόνα 2 *Αποτελέσματα δοκιμών στρεπτικής διάτμησης σε άμμο Toyoura φυσική και σταθεροποιημένη με CS=4% κατά βάρος σε όρους: (α) διατμητικής τάσης – διατμητικής παραμόρφωσης, (β) διατμητικής τάσης – μέσης ενεργού τάσης (δεδομένα από: Kodaka et al. 2005).*

Πέρα από τη συγκεκριμένη προσπάθεια, οι υπόλοιπες δοκιμές που υπάρχουν στη βιβλιογραφία αφορούν δοκιμές ανεμπόδιστης θλίψης σε διαφορετικές άμμους ή ιλυώδεις άμμους σταθεροποιημένες με διαφορετικά ποσοστά κολλοειδούς πυριτίας και στοχεύουν κυρίως στον έλεγχο της ποιότητας βελτίωσης του εδάφους. Τα αποτελέσματα των δοκιμών παρουσιάζονται συγκεντρωτικά στην Εικόνα 3 και όπως προκύπτει, η σταθεροποίηση με CS προσφέρει μια σημαντική αύξηση της αντοχής σε ανεμπόδιστη θλίψη (q_u), η οποία αυξάνεται με αύξηση της συγκέντρωσης CS(%) κατά βάρος που χρησιμοποιείται. Τα αποτελέσματα για διαφορετικά είδη άμμων παρουσιάζονται με διαφορετικά χρώματα.

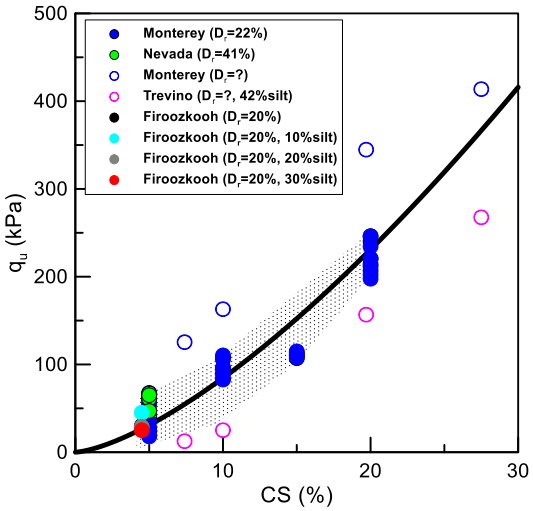

Εικόνα 3 *Αντοχή q_u σε ανεμπόδιστη θλίψη από δοκιμές σε σταθεροποιημένες άμμους και ιλυώδεις άμμους σε συνάρτηση με τη συγκέντρωση CS(%) κατά βάρος που χρησιμοποιήθηκε (δεδομένα από : Gallagher and Mitchell 2002; Gallagher 2000; Gallagher et al. 2007a; Moradi and Seyedi 2015; Persoff et al. 1999)*

Ανακυκλική συμπεριφορά

Εστιάζοντας στην ανακυκλική απόκριση σε μικρές ανακυκλικές παραμορφώσεις, τα βιβλιογραφικά αποτελέσματα δείχνουν ότι η σταθεροποίηση με CS οδηγεί σε μια μικρή αύξηση του ελαστικού μέτρου διάτμησης G_{max}, κατά μέσο όρο 10-25% (Papadimitriou and Agapoulaki 2013; Spencer et al. 2008). Αντίθετα, σε μεσαίες ανακυκλικές παραμορφώσεις, τα αποτελέσματα (Spencer et al. 2008) δε δείχνουν σημαντική επίδραση στις καμπύλες απομείωσης του κανονικοποιημένου μέτρου διάτμησης G / G_{max} και στις καμπύλες αύξησης της υστερητικής απόσβεσης D. Ωστόσο, σε μεγάλες ανακυκλικές παραμορφώσεις, οι δοκιμές καταδεικνύουν μια πολύ πιο σταθερή συμπεριφορά των σταθεροποιημένων εδαφών σε σύγκριση με τα αντίστοιχα (φυσικά) μη σταθεροποιημένα εδάφη. Συγκεκριμένα, ανακυκλικές (τριαξονικές και απλής διάτμησης) δοκιμές στη βιβλιογραφία υποδεικνύουν ρευστοποίηση (η οποία ορίζεται όταν το διπλό εύρος παραμόρφωσης, DA, υπερβεί μία προκαθορισμένη τιμή π.χ. 2-5%) μετά από ένα πολύ αυξημένο αριθμό κύκλων, σε σύγκριση με τα αποτελέσματα για τη μη σταθεροποιημένη άμμο κάτω από τις ίδιες συνθήκες (π.χ. Díaz-Rodríguez et al. 2008; Gallagher and Mitchell 2002). Για παράδειγμα, στην Εικόνα 4 φαίνονται τα αποτελέσματα τριαξονικών ανακυκλικών δοκιμών σε σταθεροποιημένο έδαφος με συγκέντρωση CS= 5% και 10%, από όπου είναι σαφής η σημαντική αύξηση της αντίστασης σε ρευστοποίηση σε όρους λόγου ανακυκλικών τάσεων CSR για ένα δεδομένο αριθμό κύκλων που απαιτούνται για ρευστοποίηση, η οποία μάλιστα αυξάνεται με αύξηση της

συγκέντρωσης CS(%) κατά βάρος που χρησιμοποιείται (δεδομένα από: Gallagher and Mitchell 2002).

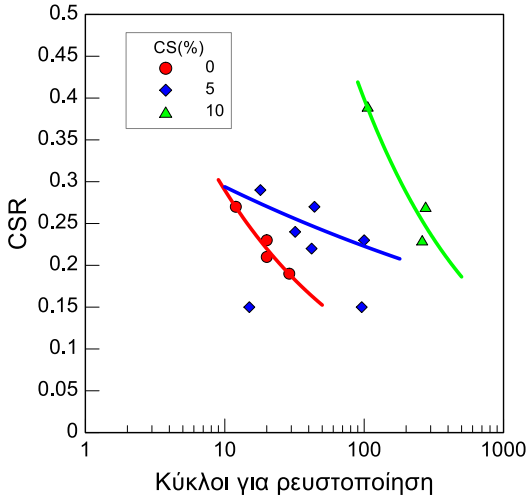

Εικόνα 4 *Επίδραση της κολλοειδούς πυριτίας (που ποσοτικοποιείται σε όρους CS(%) κατά βάρος) στο λόγο ανακυκλικών τάσεων CSR που απαιτείται για ρευστοποίηση για δεδομένο αριθμό κύκλων N_L από ανακυκλικές τριαξονικές δοκιμές (Gallagher and Mitchell 2002)*

Σεισμική απόκριση σε προβλήματα συνοριακών τιμών

Η επίδραση της σταθεροποίησης με κολλοειδή πυριτία σε προβλήματα συνοριακών τιμών έχει εξεταστεί περιορισμένα στη βιβλιογραφία, δηλαδή με λιγοστές δυναμικές δοκιμές φυγοκέντρισης (Conlee et al. 2012; Gallagher et al. 2007a; Pamuk et al. 2007) και με μια δοκιμή πεδίου (Gallagher et al. 2007b). Από την έρευνα των Pamuk et al. (2007), βασικός στόχος της οποίας ήταν η σταθεροποίηση ενός ρευστοποιήσιμου εδάφους με CS προκειμένου να μειωθεί ο κίνδυνος βλαβών εξαιτίας της ρευστοποίησης σε βαθιές θεμελιώσεις προέκυψε ότι υπάρχει μείωση των ροπών και των μετακινήσεων της πασσαλομάδας μετά τη σταθεροποίηση, καθώς το σταθεροποιημένο έδαφος δεν ρευστοποιήθηκε, παρά το γεγονός ότι παρατηρήθηκε μια ενίσχυση της σεισμικής ταλ'αντωσης σε μικρά βάθη. Από τις δοκιμές φυγοκέντρισης τόσο για διέγερση υπό μονοδιάστατες (Gallagher et al. 2007a) όσο και σε δισδιάστατες (Conlee et al. 2012) συνθήκες (όχι οριζόντιο έδαφος) προέκυψε ότι στο σταθεροποιημένο έδαφος προκύπτει ενίσχυση των επιταχύνσεων καθ' ύψος της εδαφικής στήλης, ενώ οι καθιζήσεις που προέκυψαν ήταν σημαντικά μειωμένες σε σχέση με αυτές του φυσικού εδάφους.Αντίστοιχη μείωση των καθιζήσεων παρατηρήθηκε και στη δοκιμή πεδίου (Gallagher et al., 2007b), όπου δοκιμάστηκε η αποτελεσματικότητα της παθητικής σταθεροποίησης στη μείωση καθιζήσεων επίπεδου φυσικού εδάφους λόγω ρευστοποίησης μέσω μικρο-εκρήξεων. Επιπλέον, οι

δοκιμές των Conlee et al (2012) έδειξαν και σημαντική μείωση των οριζόντιων μετατοπίσεων του κεκλιμένου εδάφους.

4. Μετρήσεις ιξώδους σε διαλύματα κολλοειδούς πυριτίας

Στη βιβλιογραφία έχουν εκτελεστεί μετρήσεις ιξώδους σε διάφορους τύπους κολλοειδούς πυριτίας. Δεδομένου του εύρους των μετρήσεων της βιβλιογραφίας, είναι σημαντικό οι μετρήσεις ιξώδους να επικεντρωθούν στην ποσοτικοποίηση των διαφόρων παραμέτρων που επηρεάζουν την εξέλιξη του ιξώδους με το χρόνο στον βέλτιστο τύπο CS για το σκοπό της παθητικής σταθεροποίησης. Για το λόγο αυτό, έγιναν μετρήσεις στο Εργαστήριο Γεωτεχνικής Μηχανικής στο Πανεπιστήμιο Θεσσαλίας (ΠΘ), με χρήση πυριτίας Ludox-SM®, ένα από τα είδη CS με το μικρότερο μέγεθος σωματιδίων (μέση διάμετρος ίση με 7 ηm), το οποίο έχει βρει και τη μεγαλύτερη χρήση στη σχετική βιβλιογραφία.

Προκειμένου να διερευνηθούν οι σημαντικότερες παράμετροι που επηρεάζουν το χρόνο γέλης και της καμπύλες ιξώδους – χρόνου (μ vs t), πραγματοποιήθηκαν μετρήσεις σε ένα μεγάλο σύνολο διαλυμάτων CS. Οι μετρήσεις αυτές έγιναν με τη βοήθεια ενός περιστροφικού ιξωδομέτρου τύπου Brookfield LVDV-II+PX (εξοπλισμένο με έναν UL μετατροπέα, UL adapter, για την μέτρηση των πολύ χαμηλών τιμών ιξώδους) και ενός υδατόλουτρου τύπου Brookfield TC- 150 για την διατήρηση σταθερής θερμοκρασίας. Η παρασκευή των διαλυμάτων CS έγινε αναμειγνύοντας απιονισμένο νερό με κολλοειδή πυριτία (Ludox-SM®) και καθαρό χλωριούχο νάτριο (NaCl), ενώ η τιμή του pH προσαρμόστηκε προσθέτοντας μικρές ποσότητες υδροχλωρικού οξέος (HCl) στο διάλυμα με βάση μετρήσεις που γίνονταν με πεχάμετρο τύπου Metrohm 826.

Στην Εικόνα 5(α) παρουσιάζονται οι μετρημένες καμπύλες ιξώδους - χρόνου για διαλύματα CS με συγκέντρωση πυριτίας CS=5% κατά βάρος, κανονικότητας 0.1N (NaCl), θερμοκρασίας T=25^{o}C και με διαφορετικές τιμές pH, οι οποίες κυμαίνονται από 4.23 – 6.53. Για όλες τις τιμές pH που εξετάστηκαν, οι τιμές του ιξώδους αρχικά παραμένουν πολύ χαμηλές (λίγο μεγαλύτερες από του νερού, 1cP) και έπειτα αυξάνονται απότομα σε μερικές χιλιάδες cP. Αυτή η ξαφνική αύξηση του ιξώδους οδηγεί στη μετατροπή του διαλύματος σε γέλη που θα σταθεροποιούσε ένα ρευστοποιήσιμο έδαφος αν το διάλυμα αυτό είχε εισπιεστεί στους πόρους του. Παρά το γεγονός ότι όλα τα διαλύματα CS παρουσιάζουν ποιοτικά την προαναφερθείσα ρεολογική συμπεριφορά, διαφέρουν σημαντικά στο χρόνο που απαιτείται για να μετατραπούν σε γέλη. Επειδή στη βιβλιογραφία δεν υπάρχει σαφής ορισμός του χρόνου γέλης (t_g), στην παρούσα έρευνα ο χρόνος αυτός ορίζεται ως ο χρόνος που απαιτείται

για να φτάσει το ιξώδες σε τιμές μεγαλύτερες ή ίσες των 100cP, καθώς από τη στιγμή αυτή και μετά, ο χρόνος για τη δημιουργία μιας σταθερής γέλης είναι πρακτικώς αμελητέος.

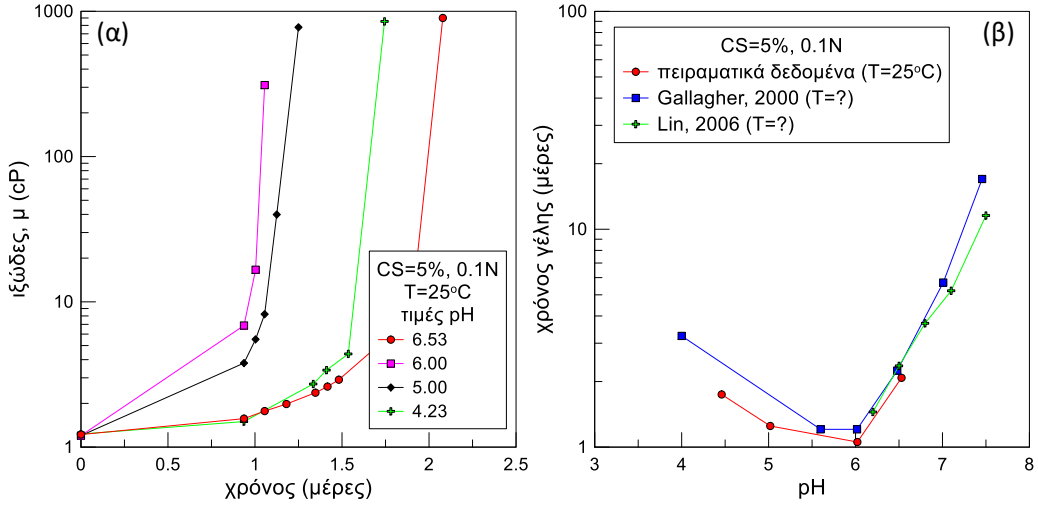

Εικόνα 5 *(α)Τυπική επίδραση της τιμής του pH στην καμπύλη ιξώδους – χρόνου για διάλυμα κολλοειδούς πυριτίας με CS(%)= 5 , 0.1N, T=25°C (β) καμπύλες χρόνου γέλης για διαλύματα με CS(%)= 5, 0.1N, T=25°C και διαφορετικές τιμές pH από μετρήσεις στο Π.Θ. σε σύγκριση με τα αποτελέσματα της βιβλιογραφίας (Gallagher 2000, Lin 2006)*

Υιοθετώντας τον παραπάνω ορισμό του χρόνου γέλης t_g (ο οποίος είναι σύμφωνος με τη βιβλιογραφία, βλ. Gallagher 2000) στην Εικόνα 5(α) φαίνεται ότι το αρχικό στάδιο, που το ιξώδες παραμένει χαμηλό, συνήθως διαρκεί $0.8t_g$ – $0.9t_g$. ενώ στον υπολειπόμενο χρόνο ($0.1t_g$ - $0.2t_g$) το ιξώδες αυξάνεται ραγδαία. Αυτή η συμπεριφορά παρατηρήθηκε σε όλους τους συνδυασμούς (CS(%),N,pH,T) που εξετάστηκαν. Ενδιαφέρον παρουσιάζει επίσης το γεγονός ότι η επίδραση του pH φαίνεται ότι είναι πολύ σημαντική, όχι όμως μονοτονική. Συγκεκριμένα, για μια τιμή pH = 6, παρατηρείται ο ελάχιστος χρόνος γέλης (t_{gmin}), ενώ μεγαλύτερες ή μικρότερες τιμές pH (από αυτή τη «βέλτιστη» τιμή pH_{opt}=6)οδηγούν σε μεγαλύτερο χρόνο γέλης. Υπογραμμίζεται ότι η μορφή των καμπυλών (μ – t) της Εικόνας 5(α) είναι ποιοτικά παρόμοια ανεξαρτήτως CS, κανονικότητας N, θερμοκρασίας T και pH του διαλύματος. Παρακάτω, θα παρουσιαστούν οι βασικές παράμετροι που επηρεάζουν τη ρεολογική συμπεριφορά των διαλυμάτων CS, όπως προέκυψαν από τις δοκιμές που εκτελέστηκαν.

Επίδραση τιμής pH

Όπως αναφέρθηκε προηγουμένως η επίδραση της τιμής του pH δεν είναι μονοτονική. Η συμπεριφορά αυτή αντικατοπτρίζεται σαφέστερα στα διάγραμματα χρόνου γέλης (t_g) ως συνάρτηση του pH («καμπύλη χρόνου γέλης»), όπως αυτό της Εικόνας 5(β) που παρουσιάζει

τους χρόνους γέλης των διαλυμάτων της Εικόνας 5(α) και αντίστοιχα αποτελέσματα από τη βιβλιογραφία (Gallagher 2000). Από την Εικόνα 5(β) προκύπτει ότι οι μετρήσεις συμφωνούν και συμπληρώνουν τη βιβλιογραφία, ενώ καταδεικνύουν ότι η «καμπύλη χρόνου γέλης» (t_g – pH) έχει τη μορφή ανεστραμμένης συμμετρικής «καμπάνας» με ακρότατο τον ελάχιστο χρόνο γέλης t_{gmin} που προκύπτει στην «βέλτιστη» τιμή pH_{opt}.

Επίδραση συγκέντρωσης CS κατά βάρος και κανονικότητας ιόντων

Μια άλλη σημαντική παράμετρος που επηρεάζει το χρόνο γέλης είναι η συγκέντρωση CS(%) στο διάλυμα, η οποία σχετίζεται άμεσα με το κόστος της παθητικής σταθεροποίησης. Δοκιμές από τη βιβλιογραφία δείχνουν ότι οι συγκεντρώσεις CS μεταξύ 5% και 10% αρκούν για την αποτροπή της ρευστοποίησης σε υφιστάμενες κατασκευές επί ρευστοποιήσιμου εδάφους (Gallagher και Mitchell 2002). Η Εικόνα 6(α) παρουσιάζει τις καμπύλες ιξώδους σε σχέση με το χρόνο σε διαλύματα με διαφορετικές συγκεντρώσεις CS(%) με pH = 6.00 και κανονικότητα (NaCl) 0.10N. Είναι σαφές ότι η τυπική απόκριση όλων των διαλυμάτων που συμπεριλαμβάνονται σε αυτήν την Εικόνα είναι ίδια σε όλες τις δοκιμές, και ότι υπάρχει σημαντική μονοτονική φθίνουσα επίδραση της συγκέντρωσης CS(%) σε συνάρτηση με το χρόνο γέλης.

Η προσθήκη αλάτων στο διάλυμα (στην παρούσα έρευνα NaCl) επηρεάζει επίσης το χρόνο γέλης. Για την μελέτη αυτής της επίδρασης, στην Εικόνα 6(β) παρουσιάζονται οι μετρήσεις ιξώδους με το χρόνο για τρία (3) διαλύματα CS με συγκέντρωση πυριτίας CS=10% με ίδια όλα τα χαρακτηριστικά πέραν της κανονικότητας NaCl. Είναι σαφές ότι μία αύξηση της συγκέντρωση NaCl από 0N σε 0.1N προκαλεί υποτετραπλασιασμό του χρόνου γέλης.

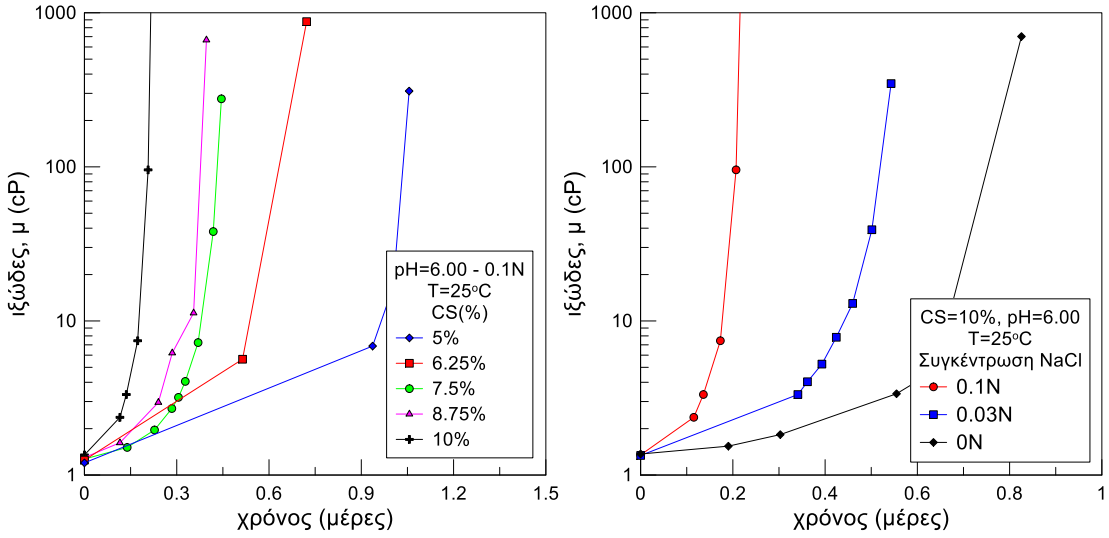

Εικόνα 6 *(α) Τυπική επίδραση της συγκέντρωσης πυριτίας CS(%) στην καμπύλη ιξώδους – χρόνου για διάλυμα κολλοειδούς πυριτίας με pH=6.00 , 0.1N, T=25°C, (β) Τυπική επίδραση της συγκέντρωσης αλάτων στην καμπύλη ιξώδους – χρόνου για διάλυμα κολλοειδούς πυριτίας με CS(%)=10, pH=6.00 , T=25°C από μετρήσεις στο Π.Θ.*

Επίδραση θερμοκρασίας

Η θερμοκρασία T του διαλύματος CS επίσης διαδραματίζει σημαντικό ρόλο στη διαδικασία σχηματισμού γέλης. Για το σκοπό αυτό, μια σειρά από μετρήσεις ιξώδους επαναλήφθηκε για διαφορετικές θερμοκρασίες, ώστε η επίδραση της θερμοκρασίας να ποσοτικοποιηθεί (για τη Ludox-SM®). Στην Εικόνα 7 φαίνονται οι «καμπύλες χρόνου γέλης» για CS = 10%, 0.1 N σε τέσσερεις (4) διαφορετικές θερμοκρασίες T = 5, 15, 20, 25 ° C για διαφορετικές τιμές του pH.

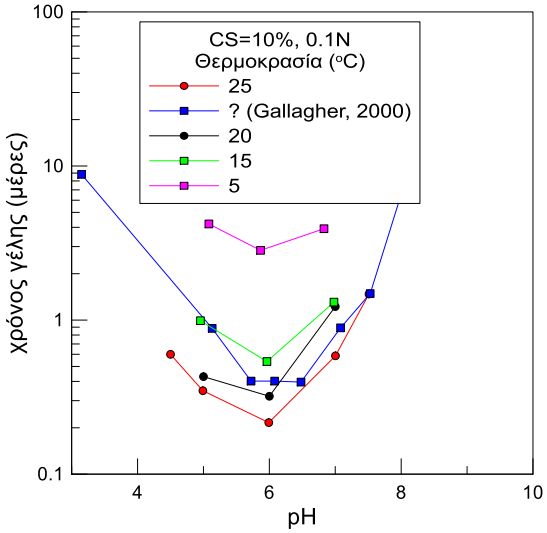

Εικόνα 7 *Επίδραση της θερμοκρασίας T στην καμπύλη χρόνου γέλης για διάλυμα με CS=10%, 0.1N, T= 5 -25°C και διαφορετικές τιμές του pH από μετρήσεις στο Π.Θ. και σύγκριση με τη βιβλιογραφία (Gallagher, 2000)*

Τα δεδομένα των δοκιμών επιβεβαιώνουν την μειωτική επίδραση της θερμοκρασίας στο χρόνο γέλης, αφού η αύξηση της θερμοκρασίας οδηγεί σε σημαντική μείωση του χρόνου γέλης Για όλους τους συνδυασμούς (CS(%), N) που εξετάστηκαν η μορφή της «ανεστραμμένης καμπάνας» των καμπυλών χρόνου γέλης παραμένει η ίδια, ενώ η τιμή του pH_{opt} παραμένει ουσιαστικά αμετάβλητη, ως συνάρτηση μόνο της συγκέντρωσης CS(%) και της κανονικότητας NaCl του διαλύματος.

Διαγράμματα σχεδιασμού για το χρόνο γέλης t_g και την καμπύλη μ - t

Μία σημαντική παράμετρος προκειμένου να εφαρμοστεί η μέθοδος της παθητικής σταθεροποίησης στην πράξη είναι η σωστή επιλογή του συνδυασμού (CS(%), N, pH, T) προκειμένου να επιτευχθεί ο επιθυμητός χρόνος γέλης t_g καθώς και ο χρόνος που οι τιμές του ιξώδους παραμένουν χαμηλές έτσι ώστε να είναι δυνατή η εισπίεση του διαλύματος στο έδαφος. Προς αυτήν την κατεύθυνση, η Εικόνα 8 συνοψίζει τις τιμές των ελάχιστων χρόνων γέλης t_{gmin} για όλους τους συνδυασμούς (CS(%), N, T=25°C), καθώς και τις αντίστοιχες τιμές pH_{opt}. Επιπλέον, στην Εικόνα 9 παρουσιάζεται η συσχέτιση μεταξύ του κανονικοποιημένου χρόνου γέλης t_g / t_{gmin} με το κανονικοποιημένο pH/pH_{opt} για όλες τις δοκιμές. Είναι σαφές ότι η μορφή «ανεστραμμένης καμπάνας» είναι κοινή για όλες τις καμπύλες χρόνου γέλης, και ότι για όλους τους συνδυασμούς που ερευνήθηκαν μπορεί να οριστεί μία μέση καμπύλη σχεδιασμού (κόκκινη συνεχής γραμμή). Προκειμένου να συμπεριληφθεί η επίδραση της θερμοκρασίας T στο σχεδιασμό, στο Σχήμα 10 ορίζεται ένας σχετικός διορθωτικός συντελεστής για το χρόνο γέλης.

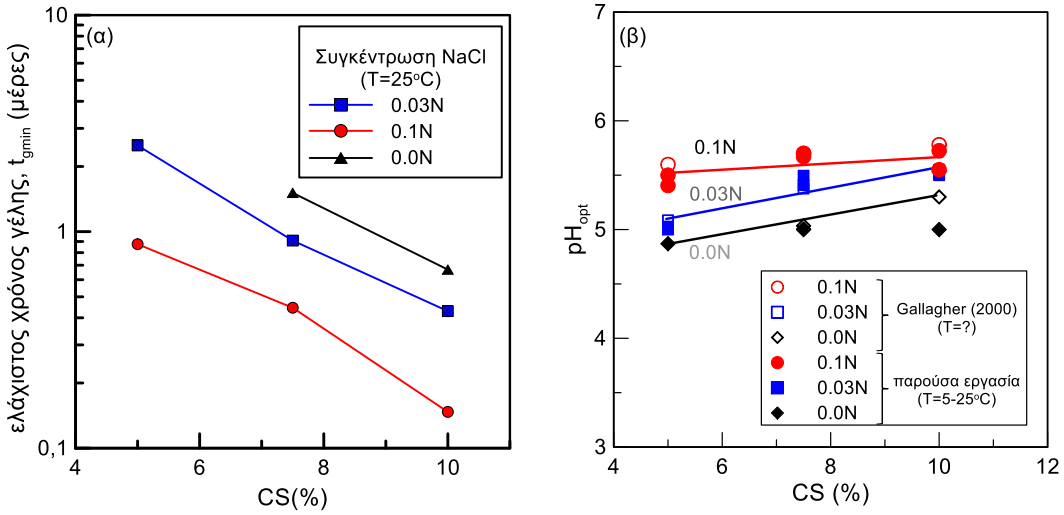

Εικόνα 8 *Διαγράμματα σχεδιασμού (από μετρήσεις στο Π.Θ. και τη βιβλιογραφία) για τον υπολογισμό: (α) του ελάχιστου χρόνου γέλης (t_{gmin}) με βάση την συγκέντρωση CS(%) κατά βάρος και κανονικότητας NaCl για T=25°C, (β) της βέλτιστης τιμής του pH (pH_{opt}) με βάση την συγκέντρωση CS(%) κατά βάρος και κανονικότητας NaCl για οποιαδήποτε θερμοκρασία T.*

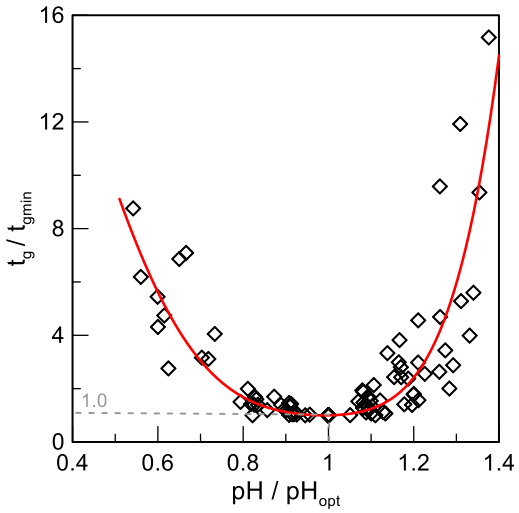

Εικόνα 9 *Συσχέτιση του κανονικοποιημένου χρόνου γέλης t_g/t_{gmin} με το κανονικοποιημένο pH/pH_{opt} για όλες τις δοκιμές που εκτελέστηκαν, και η μέση καμπύλη σχεδιασμού, με βάση μετρήσεις στο Π.Θ.*

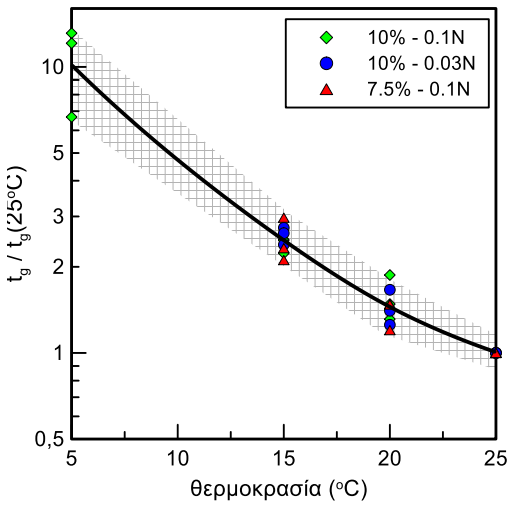

Εικόνα 10 *Κανονικοποιημένη φθίνουσα επίδραση της θερμοκρασίας Τ στον χρόνο γέλης t_g για διαλύματα πυριτίας (CS = 7.5 – 10%,κανονικότητας NaCl 0.03 – 0.1N), και η μέση καμπύλη σχεδιασμού, με βάση μετρήσεις στο Π.Θ..*

Επισημαίνεται ότι το βασικό συμπέρασμα που επιτρέπει τη χρήση μόνο ενός συντελεστή διόρθωσης για τη θερμοκρασία Τ είναι ότι η τιμή του pH_{opt} παραμένει η ίδια (βλ. Εικόνα 7) και επομένως η επίδραση της θερμοκρασίας εφαρμόζεται μόνο επί του ελάχιστου χρόνου γέλης t_{gmin} στην κανονικοποιημένη «καμπύλη χρόνου γέλης» της Εικόνας 9.

Αντίστοιχα με τις καμπύλες χρόνου γέλης, παρατηρήθηκε πως και οι καμπύλες ιξώδους – χρόνου αν κανονικοποιηθούν ως προς την αρχική τιμή του ιξώδους (μ_0) και ως προς τον χρόνο γέλης της εκάστοτε δοκιμής (t_g, όπως υπολογίστηκε παραπάνω) συμπίπτουν σε μία κοινή καμπύλη (Εικόνα 11) η οποία εκφράζεται από την Εξίσωση (1). Επισημαίνεται ότι σύμφωνα

με τις μετρήσεις σε διαλύματα με διαφορετικούς συνδυασμούς (CS(%), N, T) οι αρχικές τιμές του ιξώδους εξαρτώνται πρακτικώς μόνο από τη συγκέντρωση CS(%) και είναι ίσες κατά μέση τιμή με μ_0= 1.24, 1.29, 1.39cP για CS=5, 7.5 και 10% αντίστοιχα.

$$\frac{\mu}{\mu_0} = 1 + 0.54 \frac{\frac{t}{t_g}}{\left|\frac{t}{t_g} - 1\right|^{1.2}} \qquad (1)$$

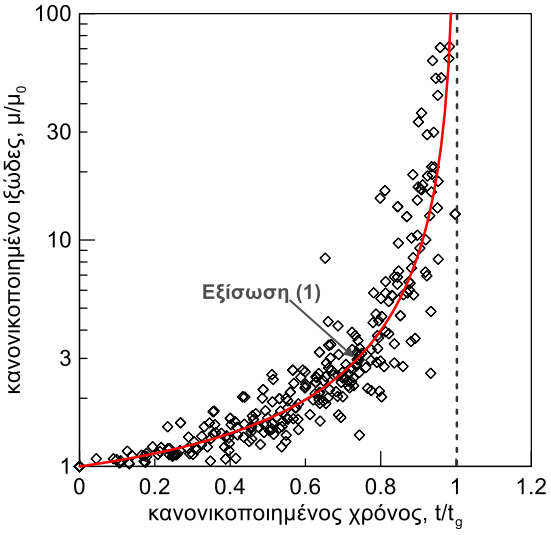

Εικόνα 11 *Μέση καμπύλη σχεδιασμού για το κανονικοποιημένο ιξώδες, μ/μ_0, ως συνάρτηση του κανονικοποιημένου χρόνου, t/t_g, για τα 61 διαλύματα κολλοειδούς πυριτίας που μερήθηκαν στο Π.Θ. (εύρη CS=5-10%, 0.0N-0,1N, pH=4.23-7.5, T=5-25°C)*

5. Δοκιμές εισπίεσης κολλοειδούς πυριτίας σε κοκκώδη εδάφη

Προκειμένου να εφαρμοστεί αποτελεσματικά η παθητική σταθεροποίηση στην πράξη, είναι πολύ σημαντική η διερεύνηση της εισπιεσιμότητας των διαλυμάτων κολλοειδούς πυριτίας (CS) σε κοκκώδη εδάφη. Ο όρος «εισπιεσιμότητα» αναφέρεται στην δυνατότητα των διαλυμάτων CS να εισπιέζονται ομοιόμορφα στο έδαφος για σχετικά μεγάλες αποστάσεις με μικρές υδραυλικές κλίσεις. Ως εκ τούτου, στο παρόν κεφάλαιο περιγράφεται η πειραματική διερεύνηση της εισπιεσιμότητας των διαλυμάτων CS σε ρευστοποιήσιμες άμμους και ιλυώδεις άμμους και η κατανόηση των μηχανισμών που την επηρεάζουν. Αυτό διερευνάται εδώ πειραματικά, μέσω μονοδιάστατων (1Δ) δοκιμών εισπίεσης σε στήλες κοκκώδους εδάφους, όπου γίνεται μέτρηση της παροχής της CS (όγκος διαλύματος που εισπιέζεται στη στήλη ανά μονάδα χρόνου), της απόστασης διήθησης της CS εντός της στήλης, της συγκένρωσης CS(%) κατά βάρος σε δείγματα του υγρού πόρων και του χρονικά αυξανόμενου ιξώδους του διαλύματος. Οι δοκιμές αυτές εκτελέστηκαν σε στήλες ύψους 20 έως 100 cm

χρησιμοποιώντας διαφορετικά διαλύματα CS, διαφορετικούς τύπους εδάφους και διαφορετικές αρχικές υδραυλικές κλίσεις.

Υλικά, εξοπλισμός και διαδικασία

Για τις 1Δ δοκιμές κατακόρυφης εισπίεσης κατασκευάστηκε διάταξη «διαπερατόμετρου» (από plexiglass) με ειδικές απαιτήσεις κατασκευής, όπως παρουσιάζεται στην Εικόνα 12 για τη στήλη ύψους 20 cm. Η κατασκευή αποτελείται από ένα κύριο κυλινδρικό τμήμα (1) με διάμετρο 10cm και ύψος 20cm, δειγματοληψίες πάνω στα τμήματα από τις οποίες γίνεται εξαγωγή του υγρού των πόρων (2), ένα κάτω τμήμα με δύο βαλβίδες για την εισπίεση του διαλύματος CS και του νερού (3), ένα πάνω τμήμα για την εξαγωγή του διαλύματος CS με μία βαλβίδα (4) και μία τάπα στο πάνω μέρος του δοκιμίου (5). Οι κάτω και άνω βαλβίδες συνδέονται με τρεις δεξαμενές: μια δεξαμενή εισόδου για την εισαγωγή του νερού, μια δεξαμενή εξόδου για την εξαγωγή νερού ή διαλύματος CS και μια δεξαμενή εισόδου για την εισαγωγή του διαλύματος CS.

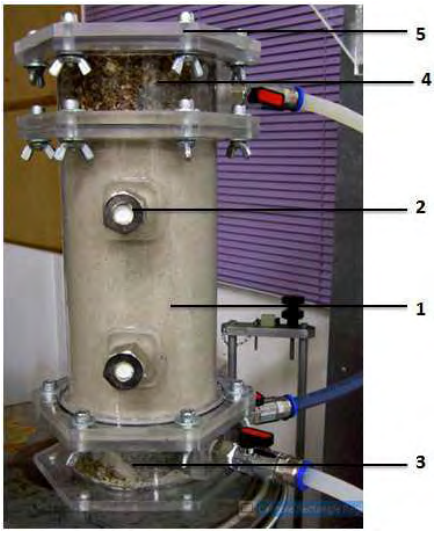

Εικόνα 12 *Συσκευή για την εκτέλεση των 1Δ δοκιμών εισπίεσης με τα επιμέρους τμήματά της*

Τα εδάφη που χρησιμοποιήθηκαν ήταν η άμμος M31 και η ιλύς D6, τα οποία δημιούργησαν επιπλέον και μίγμα 85%M31 και 15%D6 με τελικό ποσοστό λεπτόκοκκων f_c=10%. Οι κοκκομετρικές καμπύλες των εδαφών αυτών παρουσιάζονται στην Εικόνα 13.

Για την ομοιόμορφη εισπίεση της CS μέσω των βαλβίδων, μια στρώση πάχους 5cm από χαλικώδη άμμο τοποθετήθηκε στο κάτω μέρος της εδαφικής στήλης, δηλαδή στο κάτω τμήμα (3) με τις 2 βαλβίδες εισαγωγής. Τα εδαφικά δοκίμια διαμορφώθηκαν με την μέθοδο υποσυμπύκνωσης (Ladd, 1978) στην επιθυμητή πυκνότητα. Μετά την προετοιμασία τους

αφέθηκαν να κορεστούν μέσω ενυδάτωσης (hydration) που πραγματοποιήθηκε επιτρέποντας την κυκλοφορία καθαρού νερού μέσω των δεξαμενών για 1-2 μέρες και υπό χαμηλή πίεση. Το διάλυμα CS παρασκευάστηκε ανάλογα με τον επιθυμητό χρόνο γέλης t_g με βάση τα όσα αναφέρθηκαν στην Ενότητα 4 και χρωματίστηκε με μπλε χρώμα ζαχαροπλαστικής, προκειμένου να είναι ορατό στο εσωτερικό της στήλης όταν εισπιέζεται.

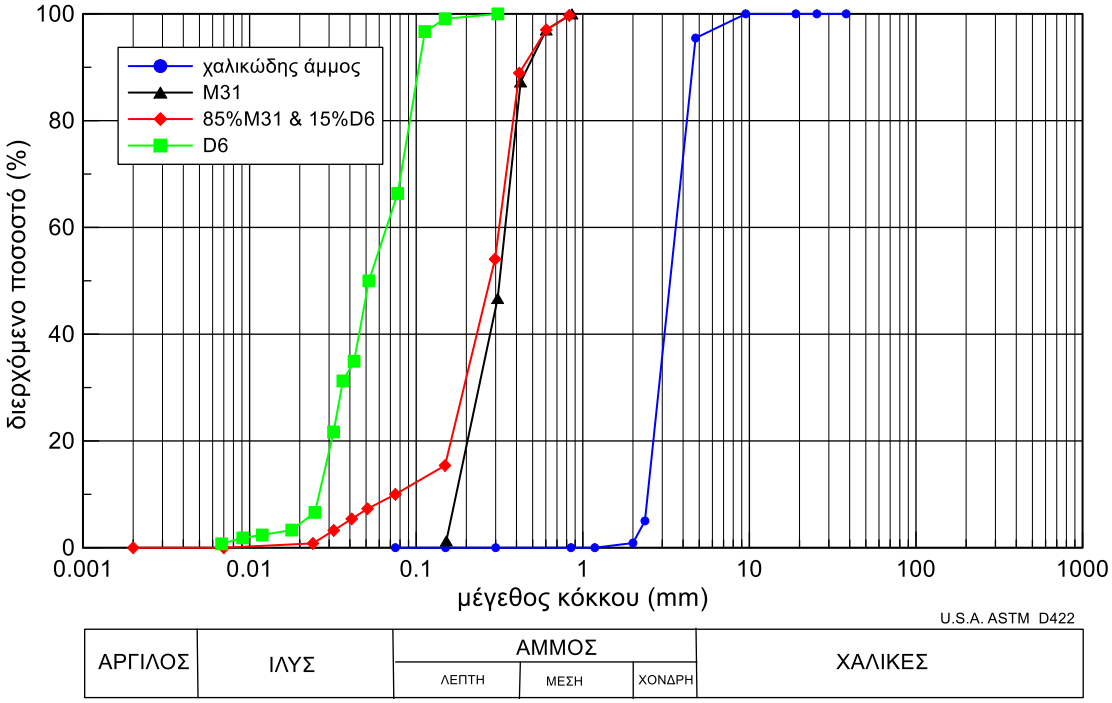

Εικόνα 13 *Κοκκομετρικές καμπύλες των εδαφών που χρησιμοποιήθηκαν στις δοκιμές εισπίεσης*

Ο στόχος των πειραμάτων ήταν να εκτελέστει μία κατακόρυφη 1Δ προς τα άνω εισπίεση των διαλυμάτων CS χρησιμοποιώντας χαμηλές υδραυλικές κλίσεις. Λόγω της ελαφρώς υψηλότερης πυκνότητας του διαλύματος CS (σε σύγκριση με το νερό) εάν οι στάθμες CS και νερού στις δεξαμενές εισόδου και εξόδου βρίσκονται στο ίδιο ύψος τότε υπάρχει ροή εξαιτίας της διαφορετικής πυκνότητας των δύο υλικών (density driven flow, Post et al., 2007). Εάν αυτά τα επίπεδα διατηρηθούν σταθερά, τότε αυτή η ροή λόγω διαφοράς πυκνότητας θα συνεχιστεί με μειούμενο ρυθμό μέχρι τερματισμού της. Έτσι, προκειμένου να επέλθει ισορροπία (συνθήκες μηδενικής ροής) η στάθμη του διαλύματος CS είχε αρχικά οριστεί ελαφρώς χαμηλότερα από εκείνη του νερού (βλέπε Εικόνα 14). Στη συνέχεια, η στάθμη του διαλύματος CS (h_1) αυξήθηκε, προκειμένου να επιτευχθεί η επιθυμητή αρχική υδραυλική κλίση i_0.

Όταν ξεκίνησε η εισπίεση της CS, οι στάθμες της δεξαμενής εισόδου πυριτίας (h_1) και της δεξαμενής εξόδου (h_2) παρέμειναν σταθερές καθόλη την διάρκεια του πειράματος εισπίεσης

Αυτό επιτεύχθηκε με τη διαρκή προσθήκη πυριτίας στην ομώνυμη δεξαμενή εισόδου και την ταυτόχρονη αφαίρεση υγρού από τη δεξαμενή εξόδου, όποτε χρειαζόταν. Με τον τρόπο αυτό, η μέτρηση των όγκων της προστιθέμενης πυριτίας με τον χρόνο αντιστοιχήθηκε στη μετρούμενη παροχή πυριτίας Q_{meas} που εισπίεζεται μέσα στο δοκίμιο. Επιπλέον, κατά τη διάρκεια της δοκιμής εισπίεσης, καταγραφόταν ο απαιτούμενος χρόνος για την μετακίνηση του μετώπου της πυριτίας (μπλέ χρώματος) μέχρι προδιαγεγραμμένα σημεία κατά μήκος του δοκίμιου (ύψους L_g στην Εικόνα 14), καθώς και τα αποτελέσματα από τη μέτρηση της σχέσης ιξώδους – χρόνου του διαλύματος CS ώστε να προκύψει το μετρούμενο ιξώδες της πυριτίας, και το πως αυτό αλλάζει με το χρόνο. Η μέτρηση αυτή γινόταν ανεξάρτητα της εισπίεσης στο διάλυμα CS της δεξαμενής εισόδου.

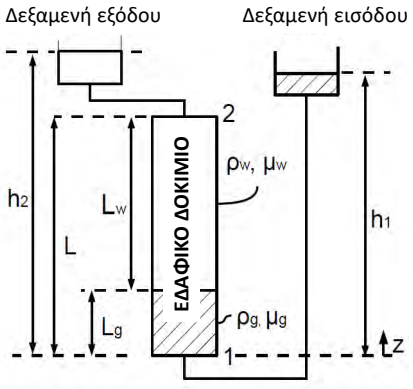

Εικόνα 14 *Σχηματική πειραματική διάταξη 1Δ δοκιμών εισπίεσης και ορισμός σημαντικών παραμέτρων φυσικού προβλήματος*

Παράλληλα με τη μέτρηση παροχής (Q_{meas}), θέσης μετώπου CS (L_g) και ιξώδους CS (μ_{meas}) γινόταν και δειγματοληψία του υγρού πόρων για τη μέτρηση του ποσοστού κατά βάρος της πυριτίας CS(%) σε αυτό. Η δειγματοληψία ικανοποιητικής ποσότητας υγρού των πόρων γινόταν με φαρμακευτική σύριγγα. Τα δείγματα τοποθετήθηκαν σε ανοξείδωτους υποδοχείς και αφέθηκαν στο φούρνο στους 200^{o}C για δύο ημέρες, μια διαδικασία που έχει χρησιμοποιηθεί στο παρελθόν (Lin 2006, Gallagher and Lin 2009), ώστε να προκύψει το ποσοστό CS(%). Οι δειγματοληψίες γίνονταν μέσω συγκεκριμένων υποδοχών (2 στην Εικόνα 12) στο «διαπερατόμετρο», και ως σημαντική παράμετρος θεωρήθηκε το ποσοστό CS(%) που μετράται σε κάθε θέση μέσα στο δοκίμιο, συγκριτικά με τη θέση που βρίσκεται το μέτωπο της CS εκείνη τη στιγμή. Με άλλα λόγια, δεν είχε σημασία από ποια υποδοχή καθ' ύψος στο δοκίμιο γινόταν η δειγματοληψία, αλλά η σχετική θέση της υποδοχής συγκριτικά με τη θέση του μετώπου CS κατά τη στιγμή που γινόταν η δειγματοληψία από αυτήν.

Αποτελέσματα δοκιμών εισπίεσης

Αποτελέσματα δειγματοληψίας υγρού πόρων

Τα ποσοστά πυριτίας κατά βάρος CS(%) στα δείγματα που εξήχθησαν από όλες τις δοκιμές ως συνάρτηση της θέσης (απόστασης) της δειγματοληψίας από το οπτικά εκτιμώμενο μέτωπο της πυριτίας παρουσιάζονται στην Εικόνα 15. Οι δειγματοληψίες που αναφέρονται σε αρνητικές τιμές απόστασης στον άξονα x αφορούν δείγματα που ελήφθησαν από υποδοχείς που βρίσκονταν κατάντη του μετώπου CS, δηλαδή σε θέσεις πιο ψηλά από τη θέση του μετώπου στην κατακόρυφη προς τα άνω εισπίεση της CS. Αντίστοιχα, οι δειγματοληψίες που αναφέρονται σε θετικές τιμές απόστασης στον άξονα x αφορούν δείγματα που ελήφθησαν από υποδοχείς που βρίσκονταν ανάντη του μετώπου, δηλαδή σε θέσεις πιο χαμηλά από τη θέση του μετώπου CS στην κατακόρυφη προς τα άνω εισπίεση της πυριτίας.

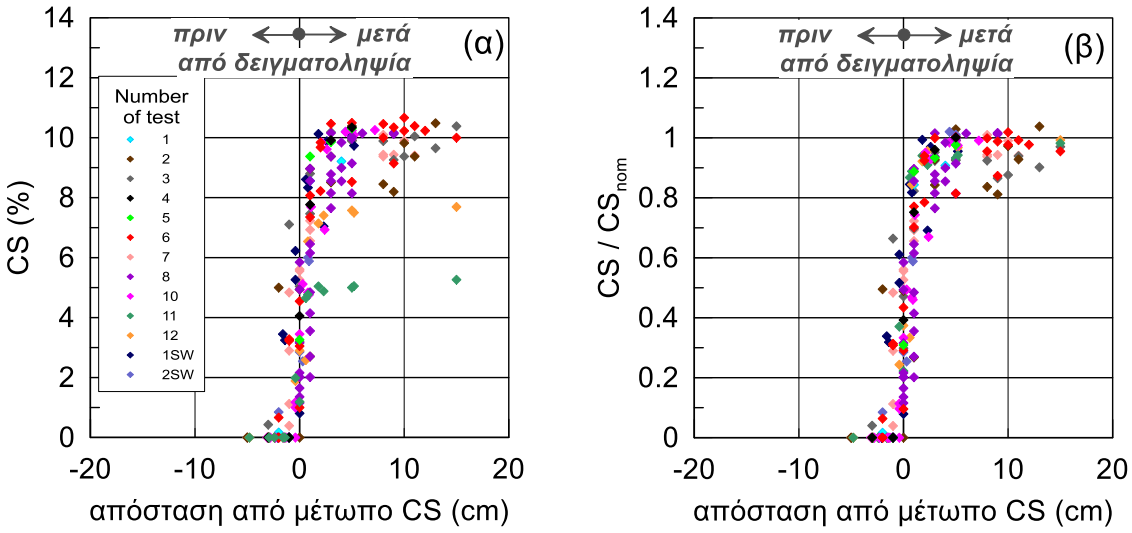

Εικόνα 15 *(α) Συγκέντρωση CS(%) κατά βάρος που εξήχθη από τις θέσεις δειγματοληψίας για όλες τις δοκιμές, (β) Συγκέντρωση CS(%) που εξήχθη από τις θέσεις δειγματοληψίας κανονικοποιημένη με την αρχική συγκέντρωση* CS_{nom}*(%) σε σχέση με την απόσταση του μετώπου CS από την εκάστοτε θέση δειγματοληψίας*

Με βάση τα συνολικά αποτελέσματα των μετρήσεων συγκέντρωσης κατά βάρος πυριτίας CS(%) από τις δειγματοληψίες προκύπτει:

- Η ύπαρξη μιας καμπύλης τύπου S στη σχέση θέσης δειγματοληψίας (συγκριτικά με το μέτωπο CS) και συγκέντρωσης κατά βάρος CS(%) στο υγρό των πόρων. Η ύπαρξη τιμών CS λίγο μεγαλύτερων της ονομαστικής CS_{nom} αποδίδονται στη (πολύ μικρή) μάζα αλατιού και χρώματος στα δείγματα, αλλά οι διαφοροποιήσεις είναι αμελητέες για πρακτικές εφαρμογές.

- Σε δείγματα από θέσεις όπου το μέτωπο CS δεν έχει φτάσει στο σημείο δειγματοληψίας (< –2cm) δεν προκύπτει ουσιώδης συγκένρτωση κατά βάρος CS(%), ενώ το ποσοστό CS = 0% σε απόσταση 4cm πριν το μέτωπο CS.
- Σε δείγματα από θέσεις όπου το μέτωπο CS έχει προσπεράσει το σημείο δειγματοληψίας (≥ 2cm) δεν προκύπτει ουσιώδης διαφορά στη συγκένρτωση κατά βάρος CS(%) σε σχέση με την ονομαστική τιμή της (διαφορά < 20% από την ονομαστική συγκέντρωση), αν και χρειάζεται απόσταση ίση με 10cm από το μέτωπο CS, ώστε η τιμή της CS(%) να έχει διαφορά μικρότερη από 10% της ονομαστικής τιμής
- Σε μια περιοχή πάχους 4cm (2cm πριν και μετά το μέτωπο CS), προκύπτει μια μεταβατική ζώνη στις τιμές συγκένρτωσης CS(%), με ενδιάμεσες τιμές συγκέντρωσης (από μηδέν έως 80% της ονομαστικής), με τις μικρότερες τιμές στα κατάντη του μετώπου CS.
- Με βάση τα ανωτέρω, προκύπτει ότι η προς τα άνω 1Δ εισπίεση της CS με χαμηλή υδραυλική κλίση πρακτικώς εκτοπίζει το νερό από τους πόρους της άμμου, με μια μικρού πάχους μεταβατική ζώνη, ειδικά στα κατάντη του μετώπου CS σε συμφωνία με τη βιβλιογραφία (π.χ. Gallagher and Lin, 2009)

Συγκριτική αξιολόγηση των αποτελεσμάτων των δοκιμών εισπίεσης

Πέραν των αρχικών πιλοτικών δοκιμών, έγιναν δεκατρείς (13) δοκιμές εισπίεσης σε αμμώδη δοκίμια διερευνώντας τις επιδράσεις διαφόρων παραγόντων. Εδώ παρουσιάζονται ενδεικτικά κάποια αποτελέσματα των δοκιμών εισπίεσης σε όρους μετρούμενων παροχών, ιξώδους και θέσης μετώπου CS ανά ζεύγη, προκειμένου να αναδειχθούν οι μελετούμενες επιδράσεις.

Στην Εικόνα 16 παρουσιάζεται η επίδραση της αρχικής υδραυλικής κλίσης i_0 στην μετρούμενη παροχή Q_{meas} και στη θέση του μετώπου CS στην εδαφική στήλη. Η δοκιμή No4 πραγματοποιήθηκε χρησιμοποιώντας χαμηλή αρχική υδραυλική κλίση $i_0 = 0.05$, ενώ η Δοκιμή No8 με αρκετά υψηλότερη $i_0 = 0.23$. Τα διαλύματα CS και στις δυο δοκιμές είχαν παρόμοιο χρόνο γέλης. Κατά το αρχικό στάδιο της εισπίεσης, η υψηλότερη υδραυλική κλίση οδηγεί σε αυξημένη παροχή, η οποία σταματά όταν το ιξώδες του διαλύματος CS φθάσει σε τιμή ίση με 5-7cP, ανεξάρτητα από την αρχική υδραυλική κλίση i_0. Συνολικά, η απόσταση που διανύει το διάλυμα CS μέσα στις εδαφικές στήλες είναι πολύ μεγαλύτερη για τη δοκιμή με την υψηλότερη υδραυλική κλίση, στον ίδιο συνολικό χρόνο εισπίεσης.

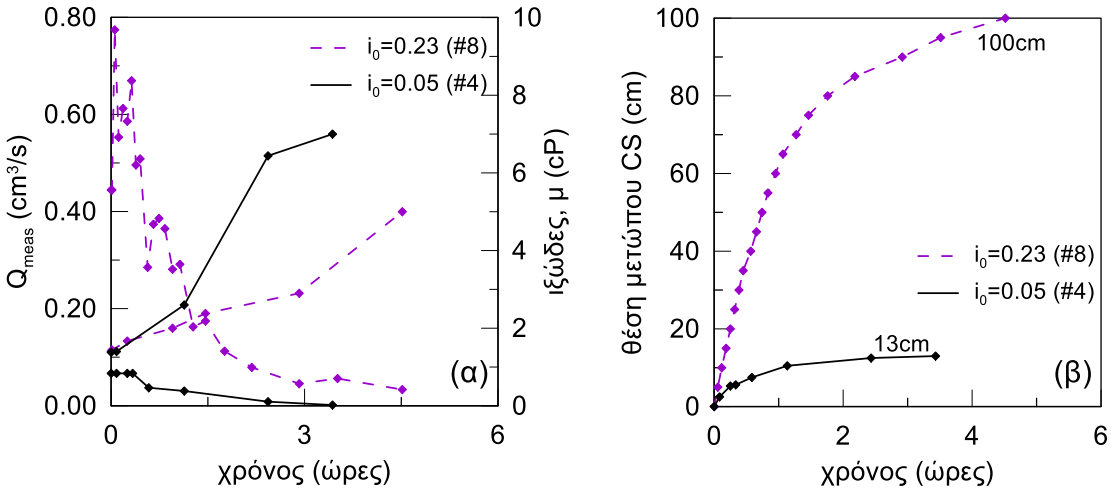

Εικόνα 16 *Επίδραση αρχικής υδραυλικής κλίσης i_0 (α) στην μετρούμενη παροχή σε σχέση με το χρόνο (β) στην απόσταση που διανύει το διάλυμα της πυριτίας μέσα στην εδαφική στήλη, με βάση εισπιέσεις με διαλύματα με παρόμοιους χρόνους γέλης (δοκιμές 4 και 8)*

Για σχεδόν όλες τις δοκιμές εισπίεσης, η παροχή Q_{meas} μειώνεται εξαιτίας δύο διαφορετικών μηχανισμών δηλαδή την αύξηση του ιξώδους και τη διαφορετική πυκνότητα των δύο υγρών (CS και νερού). Προκειμένου να εξαλειφθεί η επίδραση του ιξώδους στη ροή, στη Δοκιμή No9 το ιξώδες παρέμεινε σταθερό και ίσο 1.47cP (με κατάλληλη επιλογή της κανονικότητας NaCl και του pH του διαλύματος CS). Η Εικόνα 17 δείχνει την επίδραση του χρονικά αυξανόμενου ιξώδους στην παροχή Q_{meas} και στην μετατόπιση του μετώπου της CS, καθώς για τη Δοκιμή No9 η παροχή μειώνεται μόνο λόγω της διαφοράς πυκνότητας του διαλύματος CS και του νερού, ενώ για τη Δοκιμή No4 η παροχή Q_{meas} επηρεάζεται και από την αύξηση του ιξώδους της CS. Και οι δύο δοκιμές έχουν την ίδια αρχική υδραυλική κλίση (i_0 = 0,05) και την ίδια υδραυλική αγωγιμότητα και ως εκ τούτου, οι αρχικές τους τιμές του Q_{meas} πρακτικά συμπίπτουν. Ωστόσο, η παροχή στη Δοκιμή No4 μειώνεται γρηγορότερα και τελικά σταματά μετά 3.4 ώρες όταν το ιξώδες έχει φθάσει μία τιμή 7cP, ενώ στη Δοκιμή No9 η εισπίεση συνεχίζεται περαιτέρω, αλλά με πολύ μειωμένη παροχή, κάτι που οδηγεί σε μια ελαφρώς μόνο μεγαλύτερη απόσταση του μετώπου της CS μέσα στο δοκίμιο.

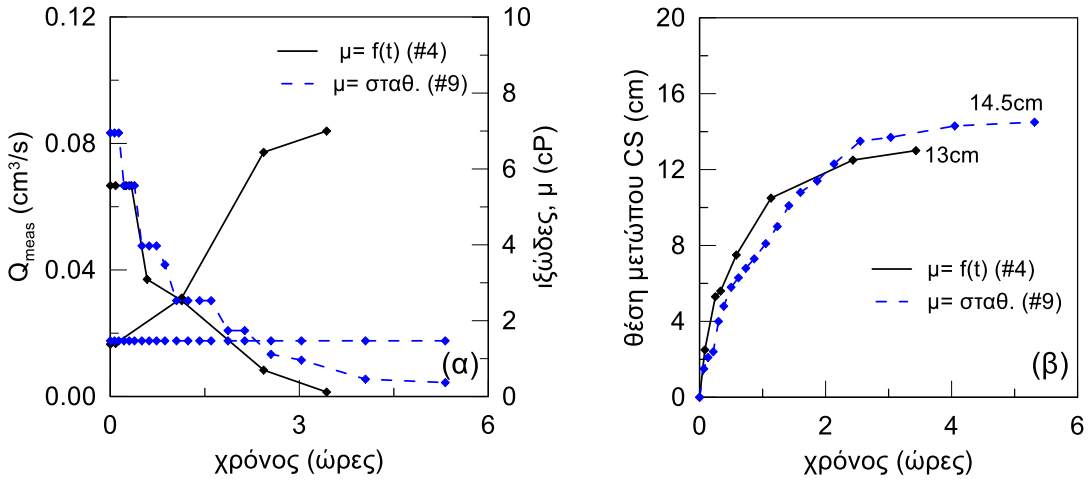

Εικόνα 17 *Επίδραση αύξησης ιξώδους του διαλύματος CS: α) στην μετρούμενη παροχή σε σχέση με το χρόνο (β) στην απόσταση που διανύει το διάλυμα της πυριτίας μέσα στην εδαφική στήλη, με βάση εισπιέσεις με διαλύματα με διαφορετική συγκέντρωση NaCl και pH (δοκιμές 4 και 9)*

Τα αποτελέσματα των δοκιμών εισπίεσης σε άμμο (100%M31) και ιλυώδη άμμο (85% M31 & 15%D6) με χρήση του ίδιου διαλύματος CS και της ίδιας αρχικής υδραυλικής κλίσης i_0, φαίνονται στην Εικόνα 18. Η Q_{meas} μειώνεται ασυμπτωτικά με το χρόνο και στις 2 δοκιμές και τελικά η ροή σταματά την ίδια χρονική στιγμή, δηλαδή όταν το ιξώδες έχει φθάσει μία τιμή ίση με 4-7cP. Θα πρέπει να αναφερθεί εδώ ότι το μέτωπο της CS στη Δοκιμή No1S δεν μπορούσε να παρατηρηθεί εύκολα, όμως η διαφορά στην υδραυλική αγωγιμότητα αντικατοπτρίζεται ξεκάθαρα στις διαφορετικές αποστάσεις που διάνυσε το διάλυμα CS. Αυτό υποδεικνύει ότι η εισπίεση είναι δύνατη και στις ιλυώδεις άμμους, αλλά απαιτεί υψηλότερες υδραυλικές κλίσεις ή / και διαλύματα CS με μεγαλύτερους χρόνους γέλης.

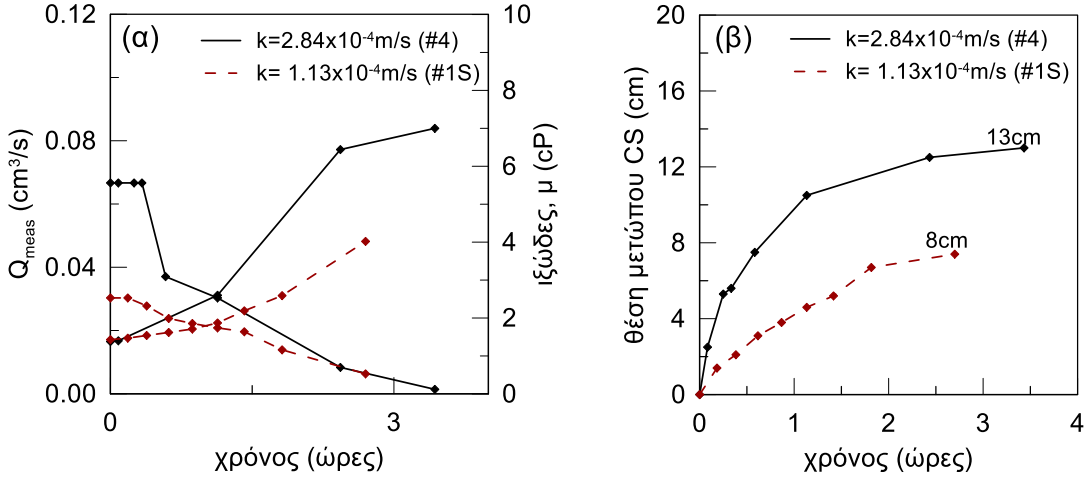

Εικόνα 18 *Επίδραση της υδραυλικής αγωγιμότητας του εδάφους: (α) στην μετρούμενη παροχή σε σχέση με το χρόνο, (β) στην απόσταση που διανύει το διάλυμα της πυριτίας μέσα στην εδαφική στήλη, με βάση εισπιέσεις του ίδιου διαλύματος CS σε διαφορετικούς εδαφικούς σχηματισμούς (δοκιμές 4 και 1S)*

Αναλυτική προσομοίωση των μονοδιάστατων δοκιμών εισπίεσης

Η ενότητα αυτή επιχειρεί μια αναλυτική προσομοίωση της εισπίεσης των διαλυμάτων CS που μελετήθηκε μέσω των 1Δ δοκιμών. Η σχηματική απεικόνιση των παραμέτρων των δοκιμών σε τυχαίο χρόνο κατά την εισπίεση του διαλύματος CS παρουσιάζεται στην Εικόνα 14. Συγκεκριμένα, καθώς το διάλυμα CS εισάγεται από τη δεξαμενή εισόδου, κινείται προς τα πάνω εκτοπίζοντας το νερό των πόρων. Έτσι, με την πάροδο του χρόνου το διάλυμα CS καταλαμβάνει μία περιοχή της εδαφικής στήλης με ύψος ίσο με L_g (<L, του συνολικού ύψους του δοκιμίου). Αυτή η περιοχή ορίζεται από την κάτω ίνα του εδάφους και το οριζόντιο μέτωπο του διαλύματος CS. Στην περιοχή αυτή, οι πόροι γεμίζουν με το διάλυμα CS, το οποίο είναι βαρύτερο (πυκνότητα CS, ρ_g> 1000 kg / m^3) και με μεγαλύτερο ιξώδες από το νερό (ιξώδες CS, μ_g> 1.0cP από την αρχή της εισπίεσης). Για συνήθη ποσοστά CS αυτές κυμαίνονται ως: ρ_g = 1021- 1048kg / m^3, αρχικές $\mu_g \geq$ 1.24cP - 1.39cP για CS = 5-10% αντίστοιχα (σε T=25^{o}C). Με άλλα λόγια, η εισπίεση ενός διαλύματος CS σε κορεσμένο πορώδες μέσο αποτελεί ένα πρόβλημα ροής υπό συνθήκες μεταβαλλόμενου ιξώδους και πυκνότητας.

Γενικεύοντας το νόμο Darcy, οι Post et al (2007) έλαβαν υπόψη την ροή λόγω διαφορετικής πυκνότητας υγρών, με χρήση μιας μέσης πυκνότητας για το υγρό πόρων που αλλάζει όσο προχωρά η εισπίεση. Κάνοντας το ίδιο οι Agapoulaki et al. (2015) και για ένα μέσο ιξώδες για το υγρό πόρων που επίσης αλλάζει όσο προχωρά η εισπίεση, προτείνουν τη σχέση:

$$Q_{calc} = \frac{k\rho_w g}{\left(\mu_g L_g + \mu_w L_w\right)}\left\{\left[\left(\frac{\rho_g}{\rho_w}\right)h_1 - h_2\right] - \left(\frac{\rho_g}{\rho_w} - 1\right)L_g\right\}A \qquad (2)$$

όπου h_1 και h_2 είναι τα μετρημένα υδραυλικά ύψη που αντιστοιχούν στις βάνες εισόδου και εξόδου των δοκιμίων, K η περατότητα του εδάφους (m^2), g η επιτάχυνση της βαρύτητας (m/s^2), μ_g το (χρονικά αυξανόμενο) ιξώδες του διαλύματος CS (kg m/s), μ_w το ιξώδες του υγρού των πόρων πριν την εισπίεση (kg m/s), L_g το ύψος μέχρι το μέτωπο του διαλύματος CS (m) (όπου $L=L_w+L_g$), L_w το ύψος της στήλης στο οποίο δεν έχει φτάσει το διάλυμα CS (m), ρ_w η πυκνότητα του υγρού των πόρων πριν την εισπίεση (kg/m^3), ρ_g η πυκνότητα του διαλύματος CS (kg/m^3) και A το εμβαδό της επιφάνειας κάθετα στη διεύθυνση της ροής (m^2).

Η ανωτέρω αναλυτική λύση που αναπτύχθηκε από τους Post et al. (2007) και τροποποιήθηκε από τους Agapoulaki et al (2015), παρουσιάζεται στις Εικόνες 19 και 20 ως Q_{calc} δείχνοντας ότι αναπαράγει ικανοποιητικά τις μετρούμενες παροχές Q_{meas} για τις 4 ενδεικτικές εισπιέσεις που παρουσιάστηκαν αναλυτικά ανωτέρω. Στα σχήματα αυτά με συνεχή γραμμή και σύμβολα παρουσιάζεται η παροχή Q_{calc} όπως υπολογίστηκε χρησιμοποιώντας ως τιμές

ιξώδους τις μετρούμενες (μ_{meas}), ενώ με διακεκομμένη μαύρη γραμμή παρουσιάζονται οι αναλυτικές προβλέψεις της Q_{calc} με τιμές ιξώδους CS όπως αυτή εκτιμήθηκε από τη σχέση (1) και τα διαγράμματα σχεδιασμού της Ενότητας 4.

Συνεπώς, η αναλυτική σχέση (2) προσδίδει επαρκή ακρίβεια στην πρόβλεψη της παροχής Q_{meas}, ακόμη κι αν δεν υπάρχουν διαθέσιμες μετρήσεις του ιξώδους της CS, και σε αυτήν την περίπτωση μπορεί να χρησιμοποιηθεί η μεθοδολογία της ενότητας 4 (και η εξίσωση 1).

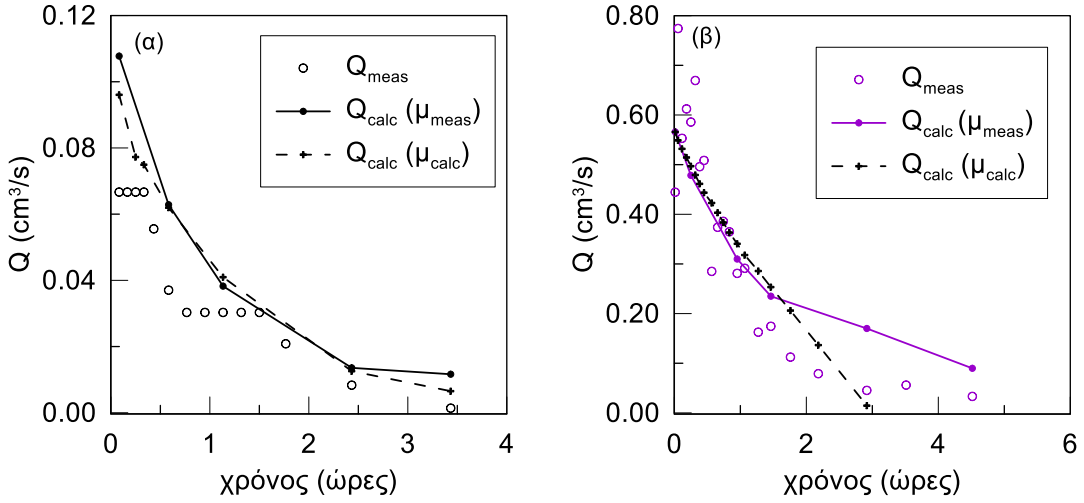

Εικόνα 19 *Μετρούμενη Q_{meas} και εκτιμώμενη παροχή Q_{calc} (με χρήση του μετρούμενου ιξώδους (μ_{meas}), καθώς και του εκτιμώμενου από την Εξίσωση (1) (μ_{calc})) σε σχέση με τον χρόνο, για τις δοκιμές (α) No4 [i_0=0.05, k=2.54x10^{-4}m/s, μ=f(t)] και (β) No 8 [i_0=0.23, k=3.1x10^{-4}m/s, μ=f(t)].*

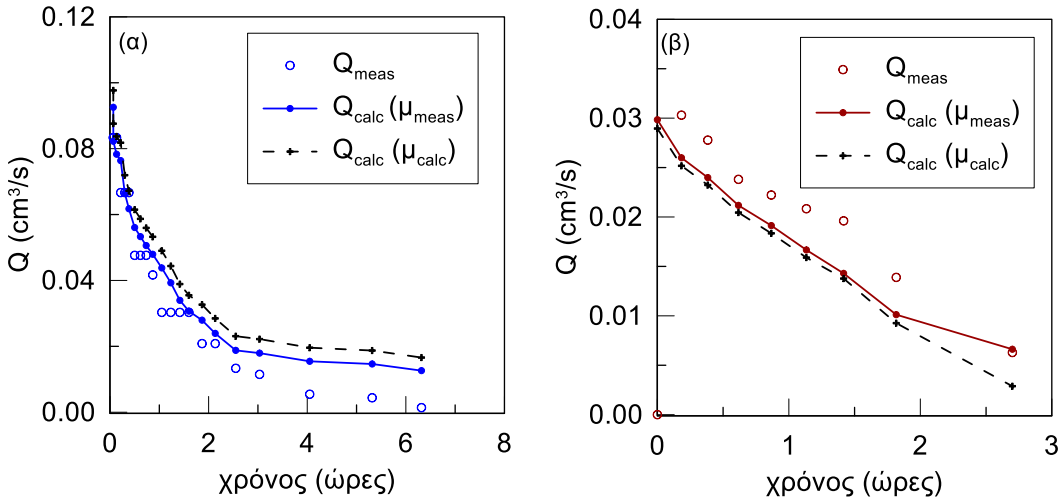

Εικόνα 20 *Μετρούμενη Q_{meas} και εκτιμώμενη παροχή Q_{calc} (με χρήση του μετρούμενου ιξώδους (μ_{meas}), καθώς και του εκτιμώμενου από την Εξίσωση (1) (μ_{calc})) σε σχέση με τον χρόνο, για τις δοκιμές (α) No9 [i_0=0.05, k=2.83x10^{-4}m/s, μ=σταθ.] και (β) No 1S [i_0=0.05, k=1.13x10^{-4}m/s, μ=f(t)].*

6. Αριθμητική προσομοίωση της μηχανικής απόκρισης σταθεροποιημένων εδαφών σε επίπεδο εδαφικού στοιχείου

Η μηχανική συμπεριφορά των σταθεροποιημένων εδαφών έχει αποτελέσει αντικείμενο διεθνούς έρευνας μόλις τα τελευταία 15 χρόνια. Η έρευνα αυτή έως τώρα είναι σχεδόν αποκλειστικά πειραματικής φύσης. Ωστόσο, η εφαρμογή της νέας μεθόδου βελτίωσης εδαφών στην πράξη χρειάζεται επιπλέον και μια μεθοδολογία αριθμητικής προσομοίωσης της σεισμικής συμπεριφοράς του σταθεροποιημένου εδάφους, με απώτερο σκοπό τη χρήση της για το σχεδιασμό έργων Πολιτικού Μηχανικού. Στόχος της παρούσας ενότητας είναι η διατύπωση και η διακρίβωση της αξιοπιστίας μιας τέτοιας αριθμητικής μεθοδολογίας, βασιζόμενη αρχικά σε συγκρίσεις με πειραματικές μετρήσεις σε επίπεδο εδαφικού στοιχείου. Ελλείψει εξειδικευμένου καταστατικού προσομοιώματος για σταθεροποιημένες άμμους, επιχειρείται εναλλακτικά η «ευφυής» χρήση ενός υπάρχοντος σοφιστευμένου προσομοιώματος κρίσιμης κατάστασης, NTUA-SAND (Andrianopoulos et al. 2010a, b), που έχει αποδείξει την ικανότητά του να περιγράφει επακριβώς τη μονοτονική και ανακυκλική συμπεριφορά αμμωδών εδαφών.

Η «ευφυής» χρήση του προσομοιώματος συνίσταται στην εκτέλεση συζευγμένων δυναμικών αναλύσεων χρησιμοποιώντας τη μέθοδο των πεπερασμένων διαφορών τροποποιώντας ορισμένες από τις παραμέτρους της προσομοίωσης. Όπως έχει ήδη αναφερθεί στην Ενότητα 3, η σταθεροποίηση με CS έχει ως αποτέλεσμα μια πιο δύστμητη και λιγότερο συστολική συμπεριφορά συγκριτικά με το ίδιο έδαφος χωρίς σταθεροποίηση.

Επιπλέον, σύμφωνα με πειράματα που έκανε ο Towhata (2007, 2008) σε δείγματα καθαρής κολλοειδούς πυριτίας υπάρχουν ενδείξεις ότι το υλικό αυτό έχει συμπιεστότητα, σε αντίθεση με το νερό το οποίο είναι πρακτικώς ασυμπίεστο. Τα αποτελέσματα των πειραμάτων καταδεικνύουν ότι η αντοχή του ίδιου του υλικού είναι ουσιαστικά αμελητέα, ενώ ο λόγος της αξονικής προς την πλευρική παραμόρφωση, δηλαδή ο λόγος του Poisson, προκύπτει ίσος με 0.3. Είναι δηλαδή πιθανό, ότι η αντοχή σε ρευστοποίηση βελτιώνεται εξαιτίας της συμπιεστότητας της πυριτίας στους πόρους. Το γεγονός αυτό μπορεί να εισαχθεί στην συζευγμένη αριθμητική ανάλυση μέσω της αύξησης της συμπιεστότητας του υγρού των πόρων. Συγκεκριμένα, σύμφωνα με τη θεωρία του Biot, που αποτελεί τη βάση της συζευγμένης ανάλυσης, αλλάζοντας την τιμή του μέτρου συμπιεστότητας του υγρού πόρων, υπάρχει άμεση επίδραση στις αναπτυσσόμενες πιέσεις πόρων και ως εκ τούτου στην συνολική απόκριση του σταθεροποιημένου εδάφους, με βάση την αρχή των ενεργών τάσεων.

Με βάση, λοιπόν, τα παραπάνω, για την αριθμητική προσομοίωση της σεισμικής απόκρισης της σταθεροποιημένης άμμου με το καταστατικό προσομοίωμα NTUA-SAND, έχουν χρησιμοποιηθεί τρεις (3) διαφορετικές προσεγγίσεις θεωρώντας μεταβολές είτε στον εδαφικό σκελετό (Α ή Β) ή στο υγρό των πόρων (Γ):

(Α) η αύξηση της αδιάστατης θετικής σταθεράς h_0 του πλαστικού μέτρου του προσομοιώματος για τον εδαφικό σκελετό της άμμου, με τη λογική ότι τα σταθεροποιημένα εδάφη εμφανίζουν πιο δύστμητη συμπεριφορά.

(Β) Η μείωση της αδιάστατης θετικής σταθεράς A_0 που υπεισέρχεται στο συντελεστή διαστολικότητας D του προσομοιώματος, με τη λογική ότι το σταθεροποιημένο έδαφος εμφανίζει λιγότερη συστολική συμπεριφορά.

(Γ) Η μείωση του μέτρου συμπιεστότητας K υγρού πόρων σε σχέση με αυτό του νερού, K_w, αποδίδοντας ότι η κολλοειδής πυριτία φαίνεται να έχει μεγαλύτερη συμπιεστότητα από το νερό.

Στην Εικόνα 21 παρουσιάζεται η σχετική αύξηση της αντίστασης σε ρευστοποίηση σε όρους διαφοράς CSR για συγκεκριμένους κύκλους φόρτισης (N_L) ανάμεσα στα (φυσικά) μη σταθεροποιημένα και στα αντίστοιχα σταθεροποιημένα εδάφη. Όπως φαίνεται στην εικόνα, η μέγιστη τιμή της διαφοράς μεταξύ σταθεροποιημένου και μη σταθεροποιημένου εδάφους κυμαίνεται περί το 0.20, με τα δεδομένα των Diaz-Rodriguez et al (2008) να αποτελούν μια καλή μέση εκτίμηση της επίδρασης της σταθεροποίησης σε όρους διαφοράς CSR. Επίσης με βάση τα αποτελέσματα αυτά, η επίδραση των αρχικών συνθηκών (σχτικής πυκνότητας D_r και αρχικής κατακόρυφης ενεργού τάσης σ'_{v0}) δε διαφαίνεται καθοριστική. Τα αποτελέσματα των τριών (3) προσεγγίσεων προσομοίωσης για τις βέλτιστες τιμές των παραμέτρων όπως αυτές προέκυψαν από διαδικασία δοκιμής – λάθους παρουσιάζονται στην Εικόνα 22, από όπου γίνεται σαφές ότι και οι τρεις (3) αυτές οδοί είναι εν δυνάμει κατάλληλες για την προσομοίωση της συμπεριφοράς του σταθεροποιημένου εδάφους. Επισημαίνεται ότι η στόχευση της βαθμονόμησης ήταν τα δεδομένα των Diaz-Rodriguez et al (2008) σε αυτή την προσπάθεια.

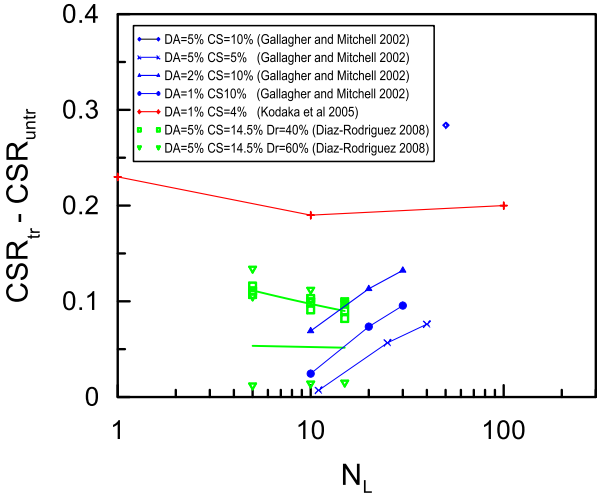

Εικόνα 21 *Επίδραση της CS στο λόγο ανακυκλικών τάσεων CSR που απαιτείται για ρευστοποίηση για δεδομένο κάθε φορά αριθμό κύκλων N_L (δεδομένα: Diaz-Rodriguez et al 2008, Kodaka et al 2005 and Gallagher and Mitchell 2002).*

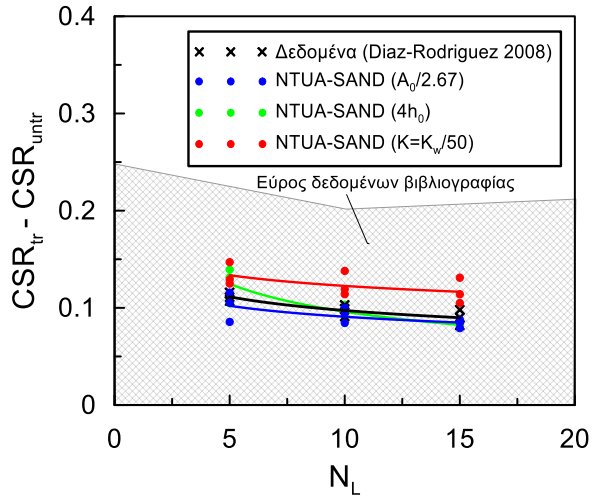

Εικόνα 22 *Επίδραση της CS στο λόγο ανακυκλικών τάσεων CSR απαιτούμενο για ρευστοποίηση για δεδομένο κάθε φορά αριθμό κύκλων N_L και σύγκριση με αριθμητικές αναλύσεις με το NTUA-SAND για τιμές παραμέτρων $A_0/2.67$, $4h_0$ και $K_w/50$ (δεδομένα από: Diaz-Rodriguez et al (2008))*

7. Αριθμητική προσομοίωση της μονοδιάστατης σεισμικής απόκρισης οριζόντιας σταθεροποιημένης εδαφικής στρώσης

Στην παρούσα ενότητα διερευνάται η ακρίβεια της αριθμητικής προσομοίωσης της μηχανικής συμπεριφοράς των σταθεροποιημένων με κολλοειδή πυριτία (CS) εδαφών σε προβλήματα συνοριακών τιμών, με «ευφυή» χρήση του καταστατικού προσομοιώματος NTUA-SAND, όπως παρουσιάστηκε στην Ενότητα 6. Για το σκοπό αυτό, έμφαση δίνεται στην προσομοίωση μίας δυναμικής δοκιμής φυγοκέντρισης επίπεδης σταθεροποιημένης

εδαφικής στρώσης υπό διέγερση βάσης, που αντιστοιχεί σε συνθήκες σεισμικής απόκρισης ελευθέρου πεδίου.

Συγκεκριμένα, η δοκιμή που θα εξεταστεί, διεξήχθη από τους Gallagher et al (2007a) και πρόκειται για δοκιμή φυγοκεντριστή με άμμο Nevada No.120, η οποία σταθεροποιήθηκε με διάλυμα CS=6% (Ludox-SM®). Για τη δοκιμή, χρησιμοποιήθηκε ένα μεταλλικό δοχείο με εύκαμπτα τοιχώματα (Laminar box), και διαστάσεις σε κάτοψη 460mm επί 370mm και ύψος ίσο με 260mm. Στην Εικόνα 23 απεικονίζεται η τομή του εύκαμπτου δοχείου, καθώς επίσης και οι θέσεις των οργάνων μέτρησης επιταχύνσεων και μετατοπίσεων. Για τη μέτρηση των οριζόντιων επιταχύνσεων τοποθετήθηκαν πέντε ζεύγη επιταχυνσιογράφων (AH) σε διάφορα ύψη, ενώ για τις οριζόντιες και κατακόρυφες μετακινήσεις χρησιμοποιήθηκαν πέντε LVDTs, τέσσερα για μέτρηση της πλευρικής εξάπλωσης (LH) και μόνο ένα στην επιφάνεια του εδάφους για τη μέτρηση των καθιζήσεων (LV), θεωρώντας τις ομοιόμορφες.

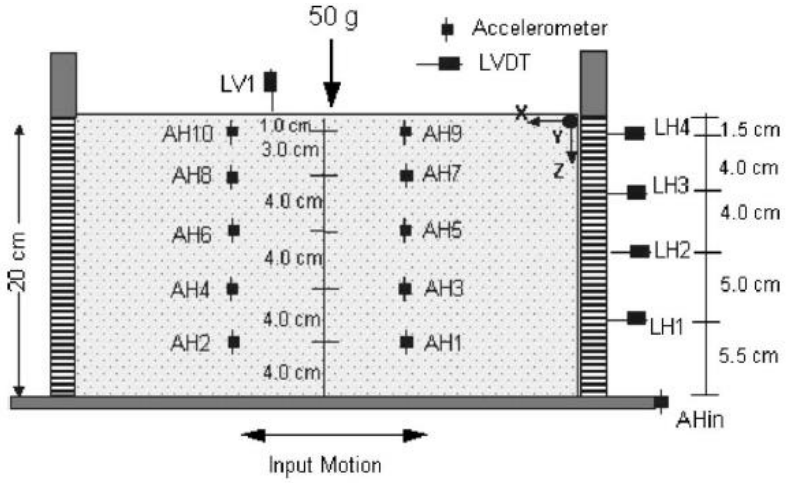

Εικόνα 23 *Διάταξη και όργανα μέτρησης στο δοχείο του φυγοκεντριστή (Gallagher 2007a), σε μονάδες προσομοιώματος*

Αριθμητική προσομοίωση δυναμικής δοκιμής φυγοκέντρισης

Η αριθμητική προσομοίωση του πειράματος φυγοκεντριστή που παρουσιάστηκε ανωτέρω, έγινε με το λογισμικό FLAC (Itasca Inc. 2011), με χρήση του καταστατικού προσομοιώματος NTUA-SAND, το οποίο βαθμονομήθηκε κατάλληλα για άμμο Nevada (Andrianopoulos 2006). Ο κάνναβος που χρησιμοποιήθηκε είναι διαστάσεων 23x10m με ζώνες εμβαδού 1x1m. Οι κάτω κόμβοι του καννάβου που αντιστοιχούν σε βάθος 10m δεσμεύτηκαν σε μετακίνηση κατά τον x και τον y άξονα λόγω του ανένδοτου πυθμένα του υποδοχέα και επειδή μέσω αυτών επιβλήθηκε η διέγερση βάσης της δοκιμής. Στα πλευρικά σύνορα δεσμεύτηκαν καθ' ύψος οι ακραίοι κόμβοι του καννάβου (μέθοδος tied nodes) στο ίδιο ύψος, ώστε να δίνουν

την ίδια οριζόντια και κατακόρυφη μετατόπιση. Με αυτό τον τρόπο μπορούν να προσομοιωθούν σωστά οι συνοριακές συνθήκες που επιβάλλει το εύκαμπτο δοχείο (Laminar box) του φυγοκεντριστή.

Στη βάση του καννάβου επιβλήθηκε ημιτονοειδής οριζόντια διέγερση με μέγιστη τιμή επιτάχυνσης ίση με 0.20g και συχνότητας 2Hz και θεωρήθηκε αρχική απόσβεση (local damping), δηλαδή ανεξάρτητη της συχνότητας, 2% για την άμμο Nevada. Επισημαίνεται ότι η χρήση του NTUA-SAND για την προσομοίωση συνεπάγεται ότι προκύπτει επιπλέον υστερητκή απόσβεση ανάλογα με την ένταση της διέγερσης.

Για την αριθμητική προσομοίωση του σταθεροποιημένου εδάφους χρησιμοποιήθηκαν οι τρεις (3) προσεγγίσεις που προαναφέρθηκαν στην ενότητα 6 και πιο συγκεκριμένα: (α) την αύξηση της σταθεράς h_0 του πλαστικού μέτρου του προσομοιώματος για τον αμμώδη σκελετό, (β) τη μείωση της σταθεράς A_0 της διαστολικότητας του προσομοιώματος για τον αμμώδη σκελετό, και (γ) τη μείωση του μέτρου συμπιεστότητας $K=K_W/n$ του υγρού των πόρων. Αρχικά εξετάστηκαν οι τιμές των παραμέτρων που απέδωσαν βέλτιστα την συμπεριφορά του σταθεροποιημένου εδάφους για ανακυκλικές δοκιμές εδαφικού στοιχείου ($A_0/2.67$, $4h_0$ και $K_W/50$), όμως παρατηρήθηκε ότι η αναβαθμονόμηση των σταθερών του προσομοιώματος (h_0 και A_0) και του μέτρου συμπίεσης K του υγρού πόρων με βάση μόνο δοκιμές εδαφικού στοιχείου είναι ποιοτικά ορθές, αλλά ποσοτικά υποεκτιμούν την αποδοτικότητα της βελτίωσης στο πρόβλημα συνοριακών τιμών. Παρόλα αυτά, προέκυψε ότι μόνο η μείωση του μέτρου συμπίεσης K του υγρού των πόρων ως συνάρτηση της συγκέντρωσης πυριτίας CS (%) κατά βάρος (για συνήθεις τιμές 5-10%), μπορεί να αποτελέσει ένα ενιαίο πλαίσιο προσομοίωσης για προβλήματα συνοριακών τιμών, καθώς μόνο εκείνη προσεγγίζει τόσο τις επιταχύνσεις, όσο και τις μόνιμες μετατοπίσεις (π.χ. καθιζήσεις) του σταθεροποιημένου μέσου.

Πιο συγκεκριμένα, ακολουθώντας τη λογική της μείωσης της τιμής του διαιρέτη του μέτρου συμπιεστότητας του υγρού των πόρων K_w, διερευνήθηκε πιθανή συσχέτιση αυτής της τιμής με την τιμή της συγκέντρωσης CS(%) κατά βάρος στο διάλυμα που χρησιμοποιήθηκε στο πείραμα. Κατόπιν παραμετρικών αναλύσεων που έγιναν τόσο για το πείραμα της Gallagher (2007a) όσο και για το πείραμα των Conlee et al (2012) που παρουσιάζεται στην Ενότητα 8, μέσω δοκιμαστικών προβλέψεων προέκυψε η ακόλουθη σχέση για την εκτίμηση του μέτρου K:

$$K = K_w / \left[\left(CS(\%) + 2.25 \right) \cdot 100 \right] \quad (3)$$

όπου: K_w το μέτρο συμπιεστότητας του νερού των πόρων ίσο με $2.1x10^6$kPa και CS(%) η τιμή της συγκέντρωσης κατά βάρος κολλοειδούς πυριτίας (πχ. για 6% κατά βάρος CS=6%)

Για την τιμή της συγκέντρωσης κολλοειδούς πυριτίας CS=6% που χρησιμοποιήθηκε στο πείραμα των Gallagher eta al. (2007), προκύπτει η τιμή 825 για τον διαιρέτη n του μέτρου συμπιεστότητας του υγρού των πόρων K_w στη σχέση (3). Επιπλέον παρουσιάζεται και η τιμή του διαιρέτη 50, η οποία προέκυψε από τη βαθμονόμηση με βάση ανακυκλικές δοκιμές στην Ενότητα 6. Στα σχήματα που ακολουθούν παρουσιάζονται τα αποτελέσματα των αναλύσεων για τις δύο αυτές τιμές (K_w/825 και K_w/50) σε όρους χρονοϊστοριών επιταχύνσεων και λόγου υπερπιέσεων πόρων (Εικόνα 24), καθώς και σε όρους χρονοϊστοριών καθιζήσεων (Εικόνα 25).

Από τις συγκρίσεις στις Εικόνες 24 και 25 προκύπτε τόσο η επαρκώς επιτυχής προσομοίωση για διαιρέτη n=875, όσο και η προαναφερθείσα υποεκτίμηση της αποδοτικότητας της σταθεροποίησης για n=50.

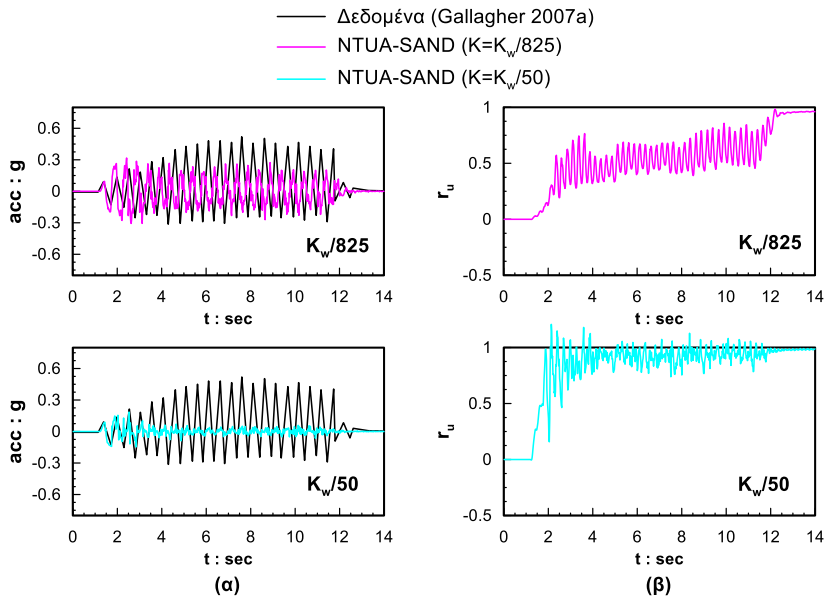

Εικόνα 24 *Σύγκριση των χρονοϊστοριών επιταχύνσεων, όπως μετρήθηκαν σε βάθος 2m στο πείραμα (Gallagher 2007a) με τα αντίστοιχα αποτελέσματα των αριθμητικών αναλύσεων για K_w/825 και K_w/50 και οι αντίστοιχες χρονοϊστορίες του λόγου πιέσεων πόρων r_u από την αριθμητική ανάλυση σε βάθος 1.5m (δεν υπάρχουν καταγραφές στο πείραμα).*

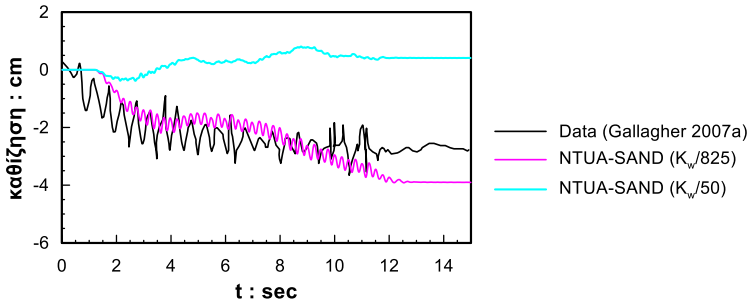

Εικόνα 25 *Σύγκριση των χρονοϊστοριών καθιζήσεων όπως μετρήθηκαν στην επιφάνεια του εδάφους στο πείραμα (Gallagher 2007a) με τα αντίστοιχα αποτελέσματα των αριθμητικών αναλύσεων για K_w/825 και K_w/50.*

8. Αριθμητική προσομοίωση σεισμικής απόκρισης σταθεροποιημένης στρώσης υπό μικρή κλίση

Πέραν της αριθμητικής προσομοίωσης της 1Δ σεισμικής απόκρισης σταθεροποιημένων εδαφών, η οποία παρουσιάστηκε στη Ενότητα 7, στην παρούσα ενότητα διερευνάται περαιτέρω η «ευφυής» χρήση του NTUA-SAND για την προσομοίωση της σεισμικής απόκρισης σταθεροποιημένης εδαφικής στρώσης υπό μικρή κλίση με βάση καταγραφές από μια σειρά από δοκιμές φυγοκέντρισης σταθεροποιημένης εδαφικής στρώσης υπό μικρή κλίση (Conlee et al, 2012, Conlee, 2010).

Το προσομοίωμα αποτελείται από δύο συμμετρικά πρανή με κλίση 3° προς ένα κεντρικό κανάλι πλάτους 3m , όπως φαίνεται στην Εικόνα 26. Τα πρανή αποτελούνται από 3 στρώσεις: (α) μία κάτω στρώση πάχους 0.75m πυκνής άμμου Monterey No.0/30, (β) μία ενδιάμεση στρώση πάχους 4.8m από ρευστοποιήσιμη άμμο Nevada No120 και (γ) μία επιφανειακή στρώση πάχους 1m συμπαγούς, ιλυώδους αργίλου Yolo loam. Συνολικά πραγματοποιήθηκαν δύο δοκιμές με ονομασίες CTC01 και CTC02. Στην πρώτη δοκιμή (CTC01) οι άμμοι Nevada και Monterey στο αριστερό πρανές σταθεροποιήθηκαν με Ludox-SM® CS=9%, ενώ στο δεξιό πρανές παρέμειναν τα αντίστοιχα (φυσικά) μη σταθεροποιημένα εδάφη. Στη δεύτερη δοκιμή (CTC02) οι ίδιες στρώσεις του αριστερού πρανούς σταθεροποιήθηκαν με Ludox-SM® CS=4%, ενώ στο δεξιό πρανές οι εν λόγω στρώσεις σταθεροποιήθηκαν με Ludox-SM® CS=5% (Conlee 2010). Για την καταγραφή των χρονοϊστοριών επιταχύνσεων, πιέσεων πόρων και μετατοπίσεων, στη ρευστοποιήσιμη στρώση τοποθετήθηκαν 10 επιταχυνσιογράφοι, 9 μετρητές πιέσεων πόρων σε κατακόρυφη διάταξη σε κάθε πρανές, καθώς και μετρητές οριζόντιων (Horizontal LP/LVDT) και κατακόρυφων (Vertical LP/LVDT) μετατοπίσεων στην επιφάνεια του προσομοιώματος για την εκτίμηση της οριζόντιας εξάπλωσης και των

καθιζήσεων, αντίστοιχα. Η γεωμετρία των δύο δοκιμών παρουσιάζεται στην Εικόνα 26 μαζί με τις θέσεις των μετρητών που τοποθετήθηκαν στο προσομοίωμα.

Το προσομοίωμα υποβλήθηκε σε εννιά σεισμικές διεγέρσεις σε φυγοκεντρική επιτάχυνση 15g. Κάθε μία διέγερση αποτελούνταν από είκοσι (20) ημιτονοειδείς κύκλους συχνότητας 2Hz (περίοδος T=0.5sec). Η ακολουθία των σεισμικών γεγονότων αποτελούνταν από 9 ξεχωριστές διεγέρσεις με διαφορετικές μέγιστες τιμές της επιτάχυνσης βάσης (PBA) που εφαρμόστηκαν διαδοχικά στο προσομοίωμα. Η παρούσα διατριβή θα επικεντρωθεί στις μεσαίας έντασης διεγέρσεις 3 και 4 με μέγιστη επιτάχυνση βάσης 0.1g και 0.19g αντίστοιχα, για την δοκιμή CTC01, οι οποίες έπονται των μικρής έντασης δονήσεων 1 και 2 με μέγιστη επιτάχυνση βάσης 0.007g και 0.03g αντίστοιχα που δεν έχουν πρακτικό ενδιαφέρον. Δεν πραγματοποιήθηκαν προσομοιώσεις για τις υπόλοιπες διεγέρσεις της CTC01, καθώς η αρχική γεωμετρία αυτών δεν ήταν πια η γεωμετρία σχεδιασμού και κάποιες από τις διεγέρσεις ήταν εξαιρετικά ισχυρές και μικρού πρακτικού ενδιαφέροντος (π.χ. 1.28g).

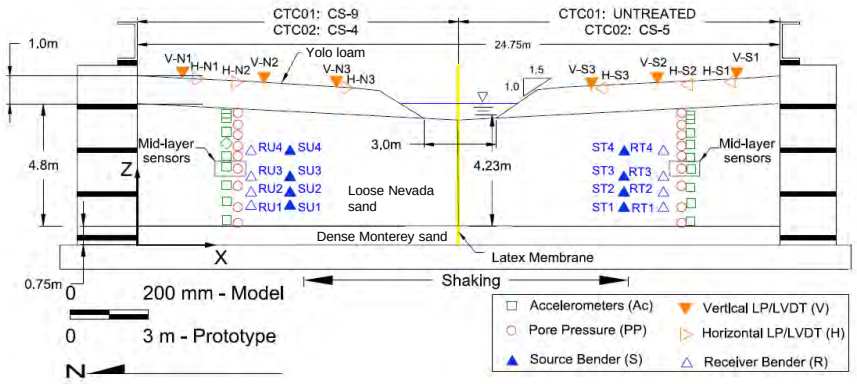

Εικόνα 26 *Γεωμετρία και θέσεις μερητών προσομοιώματος δοκιμών φυγοκεντριστή CTC01 και CTC02 (Conlee, 2010)*

Για την αριθμητική προσομοίωση του πειράματος CTC01 χρησιμοποιήθηκε το λογισμικό FLAC (Itasca Inc. 2011). Ο κάνναβος που επιλέχθηκε έχει συνολικό μήκος 24.75m (στο πρωτότυπο), το μέγιστο ύψος του καννάβου είναι 6.73m και αποτελείται από 676 στοιχεία μεταβλητού εμβαδού. Για την αριθμητική προσομοίωση των δύο αμμώδων στρώσεων του αριστερού πρανούς που σταθεροποιήθηκαν με κολλοειδή πυριτία, τροποποιήθηκαν οι παράμετροι A_0, h_0, και $K=K_w/n$ ακολουθώντας τη λογική που αναφέρθηκε στην Ενότητα 6, αλλά χάριν συντομίας θα παρουσιαστούν μόνο οι τελικές αναλύσεις που υποθέτουν την μείωση του μέτρου συμπιεστότητας του υγρού των πόρων ως συνάρτηση της συγκέντρωσης CS(%) κατά βάρος που χρησιμοποιείται, σύμφωνα με την Εξίσωση (3), προσέγγιση η οποία, όπως αποδείχτηκε, μπορεί να αποτελέσει ένα ενιαίο πλαίσιο προσομοίωσης της απόκρισης των

σταθεροποιημένων εδαφών. Η τιμή του διαιρέτη που θα παρουσιαστεί είναι η τιμή n=1125 που προέκυψε για συγκέντρωση πυριτίας CS=9% από την εξίσωση (3). Σύμφωνα με τους Persoff et al (1999) η υδραυλική αγωγιμότητα του σταθεροποιημένου εδάφους για συγκέντρωση πυριτίας CS=9% προκύπτει ίση με $3x10^{-10}$m/s, δηλαδή η σταθεροποιημένη άμμος αποκτά υδραυλική αγωγιμότητα αργίλων. Για τα φυσικά αμμώδη εδάφη (Nevada, Monterey) θεωρήθηκε ίση με $2.94x10^{-6}$m/s, ενώ για το Yolo loam η τιμή ήταν $1.97\ 10^{-9}$m/s Τέλος, στη βάση του καννάβου επιβλήθηκε ημιτονοειδής διέγερση με μέγιστη τιμή επιτάχυνσης ίση με 0.10g και συχνότητας 2Hz, που αντιστοιχεί στις επιλεγμένες διεγέρσεις της ακολουθίας και εισήχθη αρχική απόσβεση (local damping), δηλαδή ανεξάρτητη της συχνότητας, 2% για τα μη συνεκτικά εδάφη και 10% για την επιφανειακή στρώση (Yolo loam) και στα δύο πρανή.

Από τις παρακάτω Εικόνες 27 και 28 διαφαίνεται ότι η τιμή του $K=K_w/1125$ του μέτρου συμπιεστότητας του υγρού των πόρων προσεγγίζει ικανοποιητικά την απόκριση του σταθεροποιημένου αριστερού πρανούς με CS=9%. Συγκεκριμένα, η Εικόνα 27 παρουσιάζει συγκρίσεις σε όρους χρονοϊστοριών επιτάχυνσης στην επιφάνεια του εδάφους (z=0.6m,x=10.0m), ενώ η Εικόνα 28 σε όρους καθιζήσεων (x=10.4m) και οριζόντιων μετακινήσεων κοντά στο τοίχωμα (x=10.4m). Ενδιαφέρον παρουσιάζει και η ταυτόχρονα ικανοποιητική προσομοίωση της απόκρισης του μη σταθεροποιημένου δεξιού πρανούς, δεδομένου ότι υπάρχει αλληλεπίδραση μεταξύ των δύο πρανών.

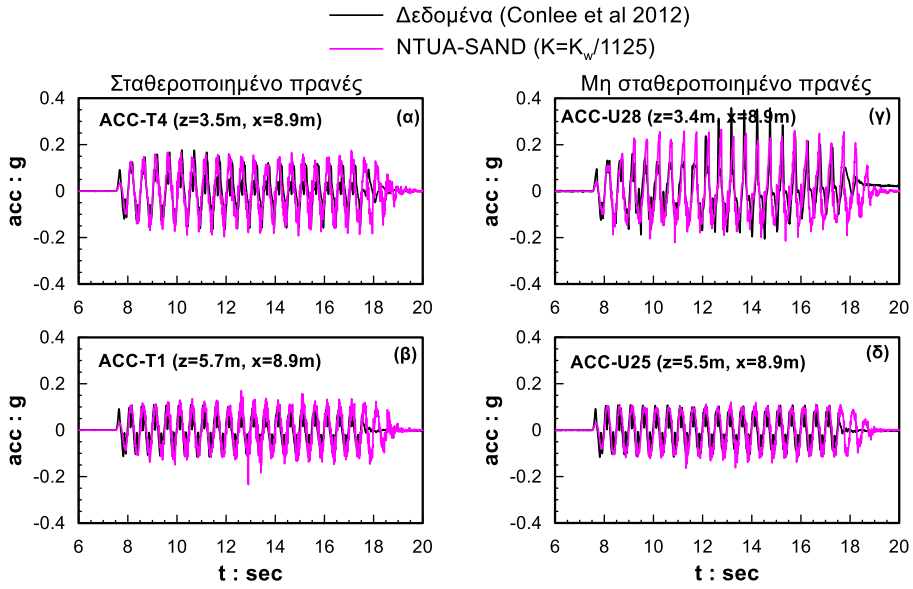

Εικόνα 27 *Σύγκριση των χρονοϊστοριών επιταχύνσεων όπως μετρήθηκαν για διαφορετικά βάθη z σε διαφορετικές αποστάσεις x από την κεντρική μεμβράνη στο πείραμα CTC01 (Shake 4 των Conlee et al 2012) με τα αντίστοιχα αποτελέσματα των αριθμητικών αναλύσεων για $K=K_w/1125$ στο σταθεροποιημένο αριστερό πρανές.*

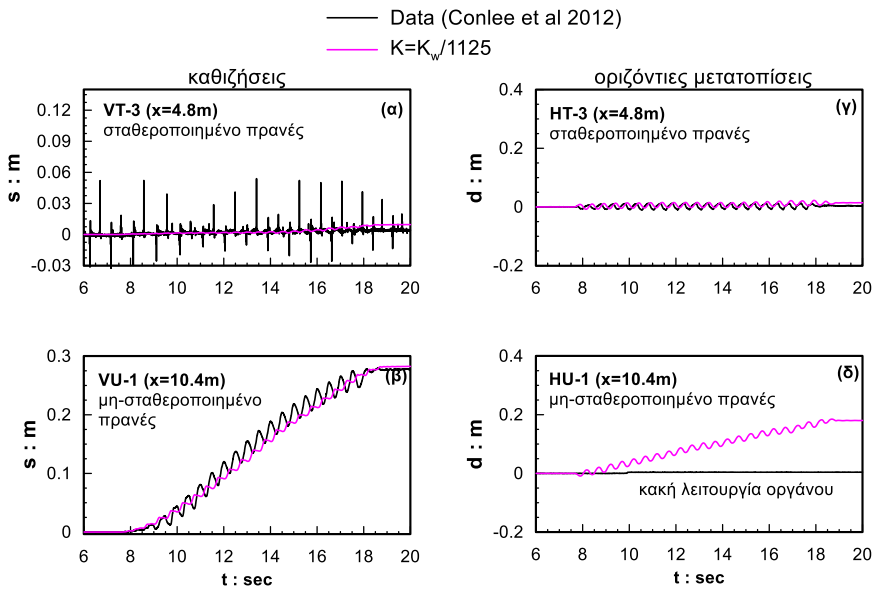

Εικόνα 28 *Σύγκριση των χρονοϊστοριών καθιζήσεων και των οριζόντιων μετατοπίσεων όπως μετρήθηκαν στο πείραμα CTC01 (Shake 4 των Conlee et al 2012) στην επιφάνεια του εδάφους σε διαφορετικές αποστάσεις x από την κεντρική μεμβράνη, με τα αντίστοιχα αποτελέσματα των αριθμητικών αναλύσεων για K=K_w/1125 στο σταθεροποιημένο αριστερό πρανές.*

Επιπλέον, διερευνήθηκε η αξιοπιστία της μεθόδου προσομοίωσης των σταθεροποιημένων εδαφών και για περιπτώσεις με άλλες τιμές CS. Για το σκοπό αυτό θα χρησιμοποιηθεί το πείραμα CTC02 των Conlee et al (2012). Στο πείραμα αυτό διατηρείται η ίδια γεωμετρία, αλλά σε αντίθεση με το CTC01, σταθεροποιούνται και τα δύο πρανή, το αριστερό με συγκέντρωση πυριτίας CS=4% και το δεξί με CS=5%. Η ημιτονοειδής διέγερση που επιβλήθηκε στη βάση είχε μέγιστη τιμή επιτάχυνσης 0.15g και συχνότητα 2Hz, δηλαδή λίγο πιο ισχυρή από τη διέγερση 3 του CTC01 που παρουσιάστηκε πριν. Η αριθμητική προσομοίωση του πειράματος CTC02 έγινε στο FLAC (Itasca Inc. 2011) ομοιοτρόπως με εκείνη για το CTC01, ενώ η σταθεροποίηση εισήχθηκε με την μείωση της συμπιεστότητας του υγρού των πόρων K (συγκριτικά με εκείνη του νερού K_w) λαμβάνοντας υπόψιν τη συγκέντρωση πυριτίας που υπήρχε σε κάθε πρανές με βάση την Εξίσωση (3). Έτσι προέκυψαν οι τιμές K_w/625 για το αριστερό και K_w/725 για το δεξί πρανές. Επιπλέον, οι διαπερατότητες των αμμώδων στρώσεων που σταθεροποιήθηκαν με συγκέντρωση πυριτίας CS=4% και CS=5% υπολογίστηκαν 10^{-8} και $5.1x10^{-9}$ m/s αντίστοιχα σύμφωνα με τους Persoff et al (1999).

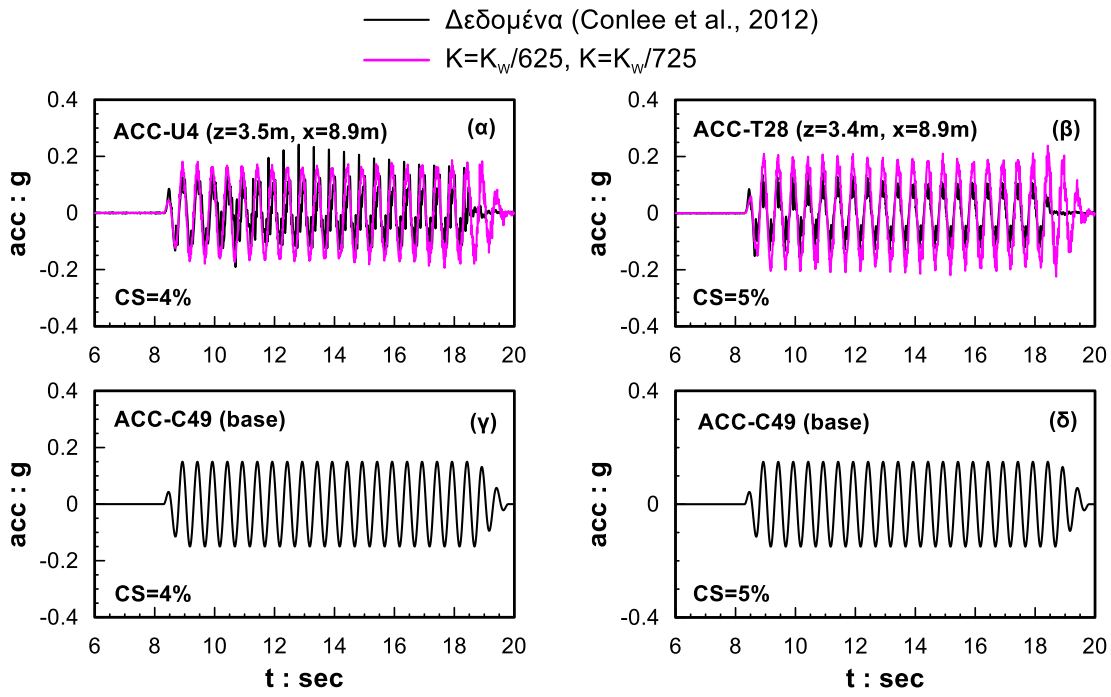

Εικόνα 29 *Σύγκριση των χρονοϊστοριών επιταχύνσεων όπως μετρήθηκαν από τους επιταχυνσιογράφους U4 και T28 στο πείραμα CTC02 (Shake 3) (Conlee et al 2012) με τις αντίστοιχες από τις αριθμητικές αναλύσεις: για K=Kw/625 για το αριστερό πρανές με CS=4% και K=Kw/725 για το δεξιό πρανές με CS=5%.*

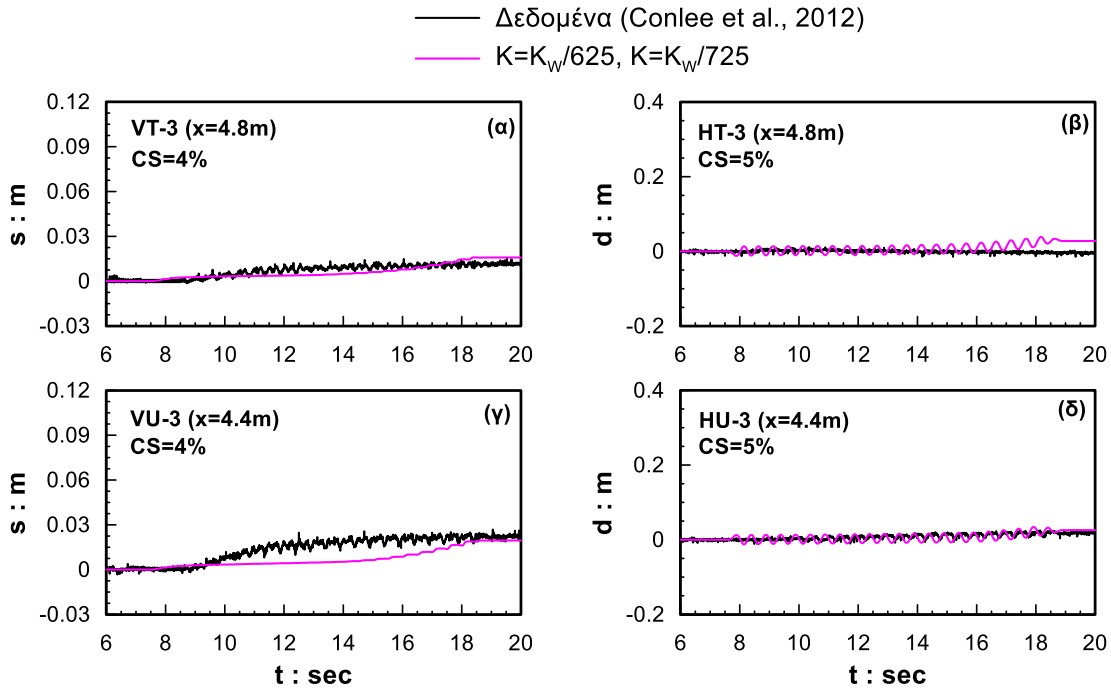

Εικόνα 30 *Σύγκριση των χρονοϊστοριών καθιζήσεων και των οριζόντιων μετατοπίσεων όπως μετρήθηκαν στο πείραμα CTC02 (Shake 3) (Conlee et al 2012) με τα αντίστοιχα αποτελέσματα των αριθμητικών αναλύσεων για διαφορετικές τιμές του μέτρου συμπιεστότητας: K_w/625, K_w/725 για το αριστερό πρανές με CS=4% και το δεξιό πρανές με CS=5% αντίστοιχα*

Οι συγκρίσεις καταγραφών και προσομοιώσεων σε όρους επιταχύνσεων παρουσιάζονται στην Εικόνα 29, ενώ σε όρους καθιζήσεων και οριζόντιων μετατοπίσεων στην Εικόνα 30. Από τις συγκρίσεις διαφαίνεται ότι η εν λόγω φαινομενολογική μεθοδολογία προσομοίωσης μπορεί να αποδώσει τη σεισμική απόκριση των σταθεροποιημένων εδαφών και σε προβλήματα συνοριακών τιμών.

9. Φασματική ενίσχυση επιταχύνσεων σταθεροποιημένων εδαφών

Στόχος του παρόντος κεφαλαίου είναι ο καθορισμός των ελαστικών φασμάτων απόκρισης στην επιφάνεια σταθεροποιημένων εδαφών, που θα μπορούσαν να χρησιμοποιηθούν για το σχεδιασμό κατασκευών Πολιτικού Μηχανικού. Ελλείψει σχετικών καταγραφών, γίνεται μία προσπάθεια εκτίμησης των ελαστικών φασμάτων σχεδιασμού για σταθεροποιημένα εδάφη με βάση δυναμικές συζευγμένες ελαστοπλαστικές αναλύσεις. Για το σκοπό αυτό, γίνεται χρήση της βαθμονομημένης αριθμητικής μεθοδολογίας των προηγούμενων ενοτήτων, δηλαδή γίνεται παραμετρική διερεύνηση με χρήση του καταστατικού προσομοιώματος NTUA-SAND (Andrianopoulos et al. 2010a, b) για άμμο Nevada με D_r=40% και κατάλληλη απομείωση του μέτρου συμπίεσης του υγρού πόρων K (βλ. Εξίσωση 3), για μία εδαφική στήλη ύψους 9m υπό 11 πραγματικές διεγέρσεις.

Συνολικά εξετάστηκαν 4 εδαφικά προφίλ: (α) 9m φυσικού εδάφους, (β) 9m σταθεροποιημένου εδάφους, (γ) 6m σταθεροποιημένης στρώσης πάνω από 3m (φυσικού) μη σταθεροποιμένου εδάφους και (δ) 3m σταθεροποιημένης στρώσης πάνω από 6m (φυσικού) μη σταθεροποιμένου εδάφους, τα οποία υποβλήθηκαν στις 11 διεγέρσεις βαθμονομημένες σε 3 επίπεδα ενεργών επιταχύνσεων a_{eff} ίσα με 0.25g, 0.125g και 0.025g. Για την αριθμητική προσομοίωση της σεισμικής απόκρισης της στήλης 9m με χρήση του FLAC (Itasca Inc. 2011) με κάνναβο διαστάσεων 3m επί 9m με ζώνες μήκους 1m και ύψους 0.5m, με εξαίρεση τα σημεία που βρίσκονται οι διεπιφάνειες σταθεροποιημένου και μη εδάφους (δηλαδή σε βάθος 3m και 6m) όπου ο κάνναβος είναι πυκνωμένος με ζώνες διαστάσεων 1x0.25m. Η προσομοίωση της σταθεροποίησης έγινε με μειωμένη τιμή στο μέτρο συμπίεσης του υγρού πόρων K συγκριτικά με την τιμή K_w του νερού, χρησιμοποιώντας την τιμή 975 ως διαιρέτη της, μια τιμή που αντιστοιχεί σε CS=7.5% (μέση τιμή του συνήθους εύρους CS=5-10%) με βάση την εξίσωση (3). Επίσης, η διαπερατότητα του σταθεροποιημένου εδάφους για τη μέση συγκέντρωση πυριτίας (CS=7.5%) εκτιμήθηκε ως $8x10^{-10}$m/s, με βάση τους Persoff et al (1999).

Το σύνολο των αναλύσεων της διατριβής εξετάζει την επίδραση της παθητικής σταθεροποίησης, της έντασης της διέγερσης, των συνθηκών στράγγισης, του πάχους της σταθεροποιημένης εδαφικής στρώσης καθώς και την επίδραση της μερικής (επιφανειακής μόνο) σταθεροποίησης. Στην παρούσα εκτενή περίληψη, χάριν συντομίας, θα παρουσιαστούν συνοπτικά μόνο τα αποτελέσματα των αναλύσεων που αφορούν στην επίδραση της παθητικής σταθεροποίησης, της έντασης της διέγερσης και των συνθηκών στράγγισης.

Συνεπώς, για να εξεταστεί πόσο ευνοϊκά επιδρά η σταθεροποίηση στη σεισμική απόκριση μίας ρευστοποιήσιμης αμμώδους στρώσης, εξετάστηκαν τρεις (3) περιπτώσεις στήλης ύψους 9m κορεσμένης άμμου Nevada με D_r=40%: (α) (φυσικής) μη-σταθεροποιημένης, (β) πλήρως σταθεροποιημένης με συγκέντρωση πυριτίας CS=7.5% κατά βάρος και (γ) (φυσικής) μη σταθεροποιημένης άμμου με την παραδοχή πλήρως στραγγιζόμενων συνθηκών. Και στις τρεις αυτές περιπτώσεις επιβλήθηκαν στη βάση της οι 11 διεγέρσεις που προαναφέρθηκαν, αλλά εδώ παρουσιάζονται αναλυτικά αποτελέσματα μόνο για μία εξ' αυτών, τη σχετικά χαμηλόσυχνη διέγερση Northridge με a_{eff}=0.25g.

Τα αποτελέσματα παρουσιάζονται στην Εικόνα 31 σε όρους λόγου φασματικής ενίσχυσης κορυφής προς βάση A_{Sa}, απ' όπου φαίνεται ότι οι τιμές των φασματικών αυτών λόγων για T=0 (συνοπτικά A_α) για το φυσικό κορεσμένο έδαφος υπό πλήρως στραγγιζόμενες συνθήκες, το σταθεροποιημένο και εν συνεχεία το φυσικό κορεσμένο έδαφος προκύπτουν ίσοι με 1.2, 1.0 και 0.4 αντίστοιχα, δηλαδή η μέγιστη επιτάχυνση στο φυσικό έδαφος απομειώνεται έντονα, στο σταθεροποιημένο παραμένει πρακτικώς αμετάβλητη και στο έδαφος με τις πλήρως στραγγιζόμενες συνθήκες ενισχύεται ελαφρώς.

Επιπλέον, σε όρους ιδιοπεριόδων στήλης, προκύπτει ότι η στήλη 9m του σταθεροποιημένου εδάφους με T_s=0.47sec είναι σχεδόν ίδια αλλά ελαφρώς αυξημένη από την ιδιοπερίοδό της για φυσικό κορεσμένο έδαφος με πλήρως στραγγιζόμενες συνθήκες (T_s=0.45sec). Αυτά τα αποτελέσματα υπονοούν ότι το σταθεροποιημένο έδαφος αναπτύσσει πρακτικώς μηδενικές υπερπιέσεις πόρων και σχετικά μικρή απόσβεση, όπως σχεδόν στις πλήρως στραγγιζόμενες συνθήκες, σε πλήρη αντίθεση με το φυσικό μη-σταθεροποιημένο έδαφος, όπου αναπτύσσονται σημαντικές υπερπιέσεις πόρων, και ρευστοποίηση που οδηγεί σε έντονη απομείωση της ταλάντωσης.

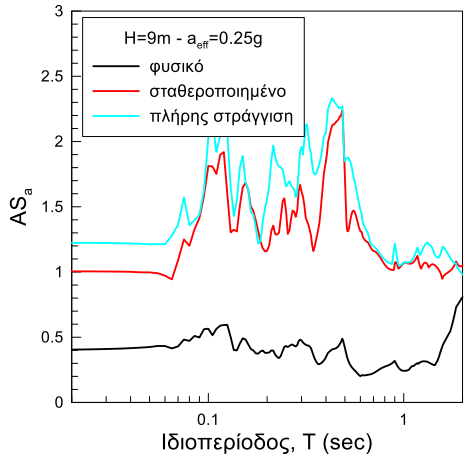

Εικόνα 31 *Φασματικοί λόγοι επιφάνειας προς βάση A_{Sa} για τη στήλη των 9m υπό διέγερση Northridge με a_{eff}=0.25g για: (α) φυσικό έδαφος, (β) σταθεροποιημένο έδαφος και (γ) φυσικό έδαφος με πλήρως στραγγιζόμενες συνθήκες.*

Ακόμη, διερευνήθηκε η συσχέτιση της σεισμικής συμπεριφοράς του σταθεροποιημένου εδάφους με εκείνη του φυσικού εδάφους με και χωρίς πλήρη στράγγιση, αλλά για επίπεδο έντασης διέγερσης πολύ μικρότερο, που αντιστοιχεί σε a_{eff}=0.025g. Έτσι, παρατηρώντας την Εικόνα 32, η οποία αναφέρεται ξανά στη διέγερση Northridge με a_{eff}=0.025g, προκύπτει πλήρης ταύτιση της απόκρισης του φυσικού εδάφους με πλήρως στραγγιζόμενες συνθήκες με την απόκριση του σταθεροποιημένου εδάφους, στο οποίο πλέον αναπτύσσονται μηδενικές υπερπιέσεις πόρων.

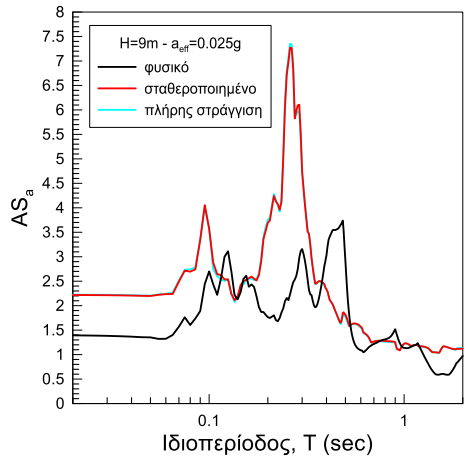

Εικόνα 32 *Φασματικοί λόγοι επιφάνειας προς βάση A_{Sa} για τη στήλη των 9m υπό διέγερση Northridge με a_{eff}=0.025g για: (α) φυσικό έδαφος, (β) σταθεροποιημένο έδαφος και (γ) φυσικό έδαφος με πλήρως στραγγιζόμενες συνθήκες.*

Συγκεκριμένα, η τιμή του φασματικού λόγου για T=0sec, ήτοι $AS_a(T=0)=A_\alpha$ λαμβάνει την τιμή 2.2 για το σταθεροποιημένο έδαφος και το φυσικό έδαφος υπό πλήρως στραγγιζόμενες συνθήκες, ενώ για το φυσικό έδαφος την τιμή 1.4. Αν και το φυσικό έδαφος δεν

ρευστοποιείται για τη χαμηλής έντασης διέγερση, είναι εμφανής η μειωμένη δυστμησία του με την αύξηση της ιδιοπεριόδου της στήλης των 9m από την ιδιοπερίοδό της για τις δύο άλλες περιπτώσεις (T_s=0.26sec) σε T_s=0.48sec.

Στη συνέχεια έγινε κατάστρωση απλών πολυ-παραμετρικών σχέσεων εκτίμησης της ενίσχυσης του ελαστικού φάσματος απόκρισης της επιτάχυνσης σε σταθεροποιημένες στρώσεις, μέσω στατιστικής επεξεργασίας των δεδομένων και αποτελεσμάτων των αριθμητικών αναλύσεων. Δίνοντας έμφαση στις προβλέψεις για πλήρως σταθεροποιημένες στρώσεις, μπορούν να εκτιμηθούν πολύ-παραμετρικές σχέσεις εκτίμησης του A_{Sa} γενικής εφαρμογής. Στη γενική μορφή του ο φασματικός λόγος A_{Sa} μπορεί να αποτυπωθεί με βάση 3 μεγέθη: την ιδιοπερίοδο T_s, την ενίσχυση της μέγιστης επιτάχυνσης A_α=A_{Sa}(T=0) και τη μέγιστη φασματική ενίσχυση A_{Sap}=A_{Sa}(T=T_s). Για την προσομοίωση των αριθμητικών αποτελεσμάτων χρησιμοποιείται η αναλυτική σχέση που έχει προταθεί από τους Bouckovalas & Papadimitriou (2003), η οποία όμως χρησιμοποιεί τα κανονικοποιημένα ως προς A_α μεγέθη A^*_{Sa}, A^*_{Sap}. Η σχέση αυτή, η οποία εκφράζεται από την (4) χρησιμοποιείται εδώ και για τα σταθεροποιημένα εδάφη με τη βαθμονόμηση των A_{Sa} και A_{Sap} που ακολουθεί:

$$A^*_{Sa}=\frac{1+\frac{1}{A_\alpha}\left(\frac{T}{T_s}\right)}{\sqrt{\left(1-\left(\frac{T}{T_s}\right)^2\right)^2+\left(\frac{1+\frac{1}{A_\alpha}}{A^*_{Sap}}\left(\frac{T}{T_s}\right)\right)^2}} \quad (4)$$

Έτσι, συλλέχτηκαν τα αποτελέσματα για πλήρως σταθεροποιημένες με CS εδαφικές στρώσεις των 3m, 6m και 9m υπό τις 11 προαναφερθείσες διεγέρσεις με ένταση διέγερσης (μικρή) 0.1λ και (μέση) 0.5λ με έμφαση στις τιμές των τριών (3) σημαντικών μεγεθών: T_s, A_α, $A^*_{Sαp}$= $A_{Sαp}/A_\alpha$. Επισημαίνεται εδώ ότι τα δεδομένα από τις αναλύσεις για μεγάλη ένταση διέγερσης (a_{eff}=0.25g) δεν ελήφθησαν υπόψη για την εξαγωγή των σχέσεων, καθώς οι αναλύσεις υποδεικνύουν έντονα μη-γραμμική συμπεριφορά του σταθεροποιημένου εδάφους και η αριθμητική μεθοδολογία δεν έχει επαρκώς διακριβωθεί για τέτοιας έντασης διεγέρσεις.

Προέκυψε ότι η σχέση που προβλέπει την ιδιοπερίοδο T_s της σταθεροποιημένης εδαφικής στήλης, και δίνεται από:

$$T_s(s)=\alpha\left[H_{tr}(m)\right]^{0.89}, \text{ όπου } \alpha=0.04\left(1+\frac{a_{eff}}{g}\right) \quad (5)$$

Στην παρούσα ενότητα, έμφαση δίνεται στην ενίσχυση της μέγιστης επιτάχυνσης $A_\alpha=A_{Sa}(T=0)$. Υιοθετείται η σχέση των Bouckovalas & Papadimitriou (2003), ως γενική σχέση εκτίμησης του μεγέθους A_α των φυσικών εδαφών, που εδώ θα βαθμονομηθεί ξανά για τα σταθεροποιημένα. Η σχέση αυτή για τον λόγο A_α έχει τη γενική μορφή (Bouckovalas & Papadimitriou 2003):

$$A_\alpha = \frac{\left[1+C_1\left(\frac{T_s}{T_e}\right)^2\right]}{\sqrt{\left[\left(1-\left(\frac{T_s}{T_e}\right)^2\right)^2+\left(C_2\left(\frac{T_s}{T_e}\right)^2\right)\right]}} \quad (6)$$

όπου για το σταθεροποιημένο έδαφος παίρνει τιμές: $C_1=0.26\left(0.1+\frac{a_{eff}}{g}\right)^{-0.8}$ και $C_2=3.10\left(\frac{a_{eff}}{g}\right)^{0.4}$

Στην Εικόνα 33 παρουσιάζονται οι τιμές του A_α όπως προέκυψαν από τις αναλύσεις (σύμβολα) και από τη σχέση (6) (γραμμές) για ενεργές επιταχύνσεις a_{eff}=0.025g και a_{eff}=0.125g, αντίστοιχα. Όπως είναι εμφανές, η μορφή της εξίσωσης (6) έχει φυσική σημασία, με την έννοια ότι η αρχική της τιμή για T_s/T_e=0 είναι πάντα μονάδα (πλήρως άκαμπτη εδαφική στήλη), ενώ για την τιμή συντονισμού (T_s/T_e=1) η εξίσωση προβλέπει τη μέγιστη δυνατή ενίσχυση. Παράλληλα, η σχέση μπορεί να αποδώσει ακόμη και την μείωση της ενίσχυσης με περαιτέρω αύξηση της ενεργού επιτάχυνσης a_{eff} (π.χ. βλέπε διαφορά μεταξύ a_{eff}=0.025g και a_{eff}=0.125g στην Εικόνα 33).

Τέλος, για την ολοκλήρωση της μεθόδου σχεδιασμού απαιτείται και ο προσδιορισμός της μέγιστης φασματικής ενίσχυσης A_{Sap}, ή, όπως αναφέρεται πιο πριν, της κανονικοποιημένης τιμής αυτής $A^*_{Sap}=A_{Sap}/A_\alpha$. Στατιστική επεξεργασία των τιμών A^*_{Sap} οδήγησε στην διατύπωση της ακόλουθης σχέσης εκτίμησής τους:

$$A^*_{S\alpha p}=1+C_0\left(\frac{T_s}{T_e}\right)^{C_t} H(m)^{C_h}\left(\frac{a_{eff}}{g}\right)^{C_\alpha} \quad (7)$$

όπου C_0=3.97, C_h=-1, C_t=0.4 και C_α=-0.2

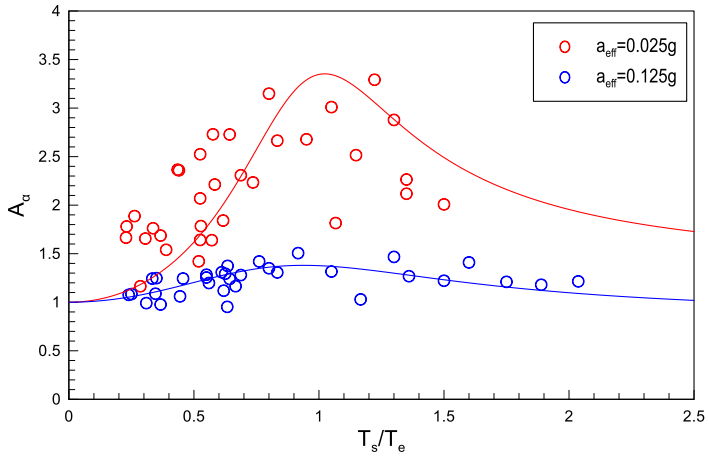

Εικόνα 33 *Ενίσχυση της μέγιστης επιτάχυνσης από τη βάση στην κορυφή της σταθεροποιημένηςεδαφικής στήλης $A_α$, όπως προέκυψε από τις αναλύσεις (σύμβολα) και από την εξίσωση (6) (γραμμές) για a_{eff}=0.025g και a_{eff}=0.125g αντίστοιχα.*

Προκειμένου να γίνει πιο κατανοητός ο τρόπος χρήσης και η αξιοπιστία της προτεινόμενης μεθόδου εκτίμησης της φασματικής ενίσχυσης σταθεροποιημένων στρώσεων, ακολουθούν ένα (1) ενδεικτικό παράδειγμα εφαρμογής της και η σύγκριση του με τα αποτελέσματα των αναλύσεων για την διέγερση Coyote Lake. Η σύγκριση παρουσιάζεται σε όρους φασματικού λόγου επιφάνειας προς βάση της σταθεροποιημένης στήλης.

Η διαδικασία που ακολουθήθηκε ήταν η εξής: Αρχικώς υπολογίστηκαν με βάση τις πολύ-παραμετρικές σχέσεις και με δεδομένη τη δεσπόζουσα περίοδο της διέγερσης Coyote Lake (T_e=0.42sec), την ενεργό επιτάχυνση a_{eff} και το ύψος της σταθεροποιημένης στήλης H_{tr}=6m (ενδεικτικά), η ιδιοπερίοδος της στήλης T_s, και οι λόγοι $A_α$ και $A^*_{sαp}$, αντίστοιχα. Έτσι βαθμονομήθηκε η πλήρως κανονικοποιημένη φασματική ενίσχυση $A^*_{sα}$ ως προς την κανονικοποιημένη ιδιοπερίοδο της κατασκευής T/T_s, και στη συνέχεια προέκυψε η τελική φασματική ενίσχυση $A_{sα}(T)$ με βάση τις προβλεφθείσες τιμές των $A_α$ και T_s. Η καμπύλη $A_{sα}(T)$ που προέκυψε συγκρίθηκε με την καμπύλη του αντίστοιχου φασματικού λόγου των σχετικών αναλύσεων, απ'όπου προκύπτει ικανοποιητική συμφωνία με τις λεπτομερείς αριθμητικές αναλύσεις.

Επισημαίνεται ότι οι προτινόμενες σχέσεις αποτελούν ουσιαστικά ανα-βαθμονόμηση των σχέσεων των Bouckovalas and Papadimitriou (2003). Η αναβαθμονόμηση κρίθηκε αναγκαία κυρίως λόγω της αυξημένης διασποράς που προκύπτει από τη χρήση των σχέσεων Bouckovalas and Papadimitriou (2003) για σταθεροποιημένα εδάφη.

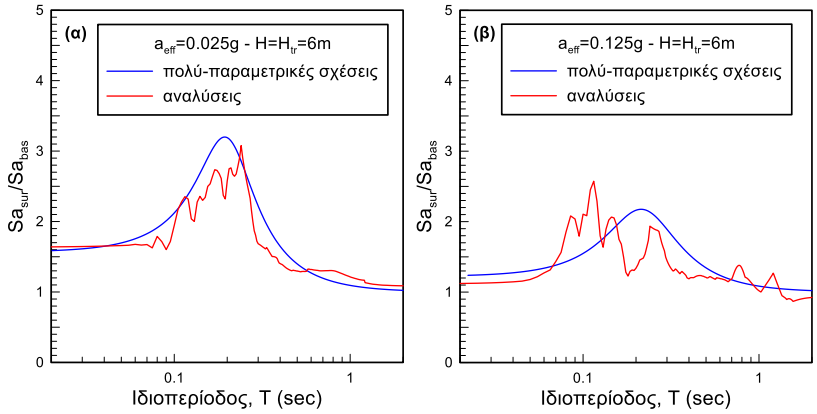

Εικόνα 34 *Σύγκριση εκτιμηθέντος λόγου φασματικής ενίσχυσης A_{Sa} (μπλε καμπύλη) με το λόγο A_{Sa} όπως προέκυψε από τις αναλύσεις (κόκκινη καμπύλη) για τη διέγερση Coyote Lake σε σταθεροποιημένη στήλη πάχους 6m με (α) a_{eff}=0.025g και (β) a_{eff}=0.125g.*

10. Σεισμική απόκριση επιφανειακής θεμελιολωρίδας επί σταθεροποιημένης εδαφικής στρώσης

Σύμφωνα με τους ισχύοντες αντισεισμικούς κανονισμούς, σε εδάφη με κίνδυνο ρευστοποίησης, η κατασκευή τεχνικών έργων με επιφανειακή θεμελίωση, είναι απαγορευτική χωρίς την εκ των προτέρων βελτίωση του εδάφους. Στόχος του παρόντος κεφαλαίου είναι να διερευνηθεί η σεισμική απόκριση επιφανειακής θεμελιολωρίδας η οποία εδράζεται πάνω σε σταθεροποιημένη στρώση, καθώς τέτοιες θεμελιώσεις είναι οι πλέον συνήθεις για κτηριακά έργα, ειδικά σε παλαιότερες δεκαετίες. Επειδή για το συγκεκριμένο ζήτημα δεν υπάρχουν πειραματικά δεδομένα διαθέσιμα στη βιβλιογραφία, η μεθοδολογία που θα ακολουθηθεί είναι αμιγώς αριθμητική, ακολουθώντας την διαδικασία προσομοίωσης που καταρτίστηκε και βαθμονομήθηκε σε προηγούμενες ενότητες. Με άλλα λόγια, η σταθεροποίηση προσομοιώνεται με μείωση του μέτρου συμπιεστότητας του υγρού των πόρων K με βάση την εξίσωση (3), ως προς τη συγκέντρωση CS(%) κατά βάρος. Η προσομοίωση έγινε με χρήση του λογισμικού FLAC (Itasca Inc. 2011), ενώ χρησιμοποιήθηκε το καταστατικό προσομοίωμα NTUA-SAND (Andrianopoulos et al 2010a, b), το οποίο έχει βαθμονομηθεί κατάλληλα για άμμο Nevada (η οποία θεωρείται ότι αποτελεί το ρευστοποιήσιμο έδαφος). Το επιφανειακό θεμέλιο (πέδιλο) θεωρείται απειρομήκης λωρίδα πλάτους 3m, άρα χρησιμοποιείται ανάλυση επίπεδης παραμόρφωσης με κάνναβο διαστάσεων 106m επί 9m.

Η διαδικασία που ακολουθήθηκε στις επιμέρους αναλύσεις περιγράγεται παρακάτω. Αρχικώς, υπολογίστηκε η φέρουσα ικανότητα του πέδιλου σε (φυσική) μη σταθεροποιημένη στρώση άμμου Nevada με ανάλυση υπό πλήρως στραγγιζόμενες συνθήκες (θεμελίωση επί

άμμου). Η φέρουσα ικανότητα του αμμώδους εδάφους θεμελίωσης (με D_r=40%) του πέδιλου πλάτους B_f=3m, προέκυψε ίση με q_{ult}=601KPa.

Στη συνέχεια, πραγματοποιήθηκε δυναμική ανάλυση με διέγερση βάσης για τάση έδρασης λειτουργίας q=200KPa, το οποίο αντιστοιχεί σε (σχετικά μικρό για άμμους) στατικό συντελεστή ασφαλείας $FS=q_{ult}/q=3$. Για το πέδιλο επιλέχτηκε μία πολύ μικρή τιμή διαπερατότητας ίση με 10^{-10}m/s προκειμένου να θεωρηθεί αδιαπέρατο (π.χ. σκυρόδεμα). Εδώ θα παρουσιαστούν δύο αναλύσεις αναφοράς, μία για (φυσική) μη σταθεροποιημένη κορεσμένη στρώση άμμου και μία για πλήρως σταθεροποιημένη, οι οποίες αποτελούν και τις αναλύσεις αναφοράς για q=200kPa και FS=3 (αγνοώντας την όποια θετική επίδραση της σταθεροποίησης στη στατική φέρουσα ικανότητα). Για το φυσικό έδαφος εισήχθη τιμή διαπερατότητας $k=3.31x10^{-3}$m/s (η οποία αντιστοιχεί σε μία χονδρόκοκκη άμμο), ενώ για το σταθεροποιημένο έδαφος με κολλοειδή πυριτία συγκέντρωσης CS=7.5% (μέση τιμή του αποδεκτού εύρους συγκεντρώσεων CS=5-10%) εκτιμήθηκε τιμή διαπερατότητας $k_{tr}=10^{-9}$ m/s (Persoff et al 1999). Για την προσομοίωση της σεισμικής απόκρισης της αμμώδους στρώσης χρησιμοποιήθηκε το NTUA-SAND με τις δυναμικές τιμές των παραμέτρων του για άμμο Nevada (Andrianopoulos et al, 2010a,b), ενώ για τη σεισμική απόκριση του σταθεροποιημένου εδάφους μεταβλήθηκε το μέτρο συμπίεσης του υγρού των πόρων σύμφωνα με τη σχέση: $K=K_w/n$ (εξίσωση 3), όπου $n= (CS(\%)+2.25)x100$ = 975. Στα πλευρικά σύνορα δεσμεύτηκαν καθ' ύψος οι ακραίοι κόμβοι (μέθοδος tied nodes) ώστε να δίνουν την ίδια οριζόντια και κατακόρυφη μετατόπιση στο ίδιο ύψος. Κατόπιν, για τις δύο αναλύσεις αναφοράς επιβλήθηκε στη βάση του καννάβου ημιτονοειδής διέγερση 10 κύκλων (n=10), με μέγιστη τιμή επιτάχυνσης ίση με 0.15g και περιόδου T_e=0.15sec και θεωρήθηκε αρχική απόσβεση (local damping), δηλαδή ανεξάρτητη της συχνότητας, 2% για την άμμο Nevada. Προκειμένου να διερευνηθεί περαιτέρω η επίδραση των χαρακτηριστικών της διέγερσης και του εδάφους στην απόκριση του πέδιλου επί σταθεροποιημένης στρώσης, πραγματοποιήθηκαν παραμετρικές αναλύσεις, τα αποτελέσματα των οποίων παρουσιάζονται αναλυτικά στο Κεφάλαιο 10 της παρούσας διατριβής.

Ενδεικτικά εδώ, στην Εικόνα 36 συγκρίνονται οι χρονοϊστορίες επιταχύνσεων στην επιφάνεια και σε βάθη 3m και 6m κάτω από το πέδιλο (πλάτους B_f=3m), καθώς και σε μεγάλη απόσταση από αυτό (περίπου 42m=14B_f από το μέσον του) έτσι ώστε να αποτυπώνουν συνθήκες σεισμικής απόκρισης ελεύθερου πεδίου. Παρατηρείται ότι κάτω από το πέδιλο διατηρούνται τα χαρακτηριστικά της διέγερσης τόσο για το μη σταθεροποιημένο όσο και για το σταθεροποιημένο έδαφος, με μια μικρή απομείωση της μέγιστης επιτάχυνσης στην

επιφάνεια στην πρώτη περίπτωση. Αντίθετα, στο ελεύθερο πεδίο το σταθεροποιημένο έδαφος εμφανίζει ενίσχυση της επιτάχυνσης πλησίον της επιφάνειας (βλέπε Ενότητα 9), ενώ το (φυσικό) μη σταθεροποιημένο εμφανίζει έντονη απομείωση της ταλάντωσης. Η συμπεριφορά επεξηγείται από τις χρονοϊστορίες του λόγου υπερπιέσεων πόρων r_u (Εικόνα 37) από όπου φαίνεται ότι προκύπτει ρευστοποίηση του φυσικού εδάφους σε βάθη z≤3m και ειδικά πλησίον της επιφάνειας, σε αντίθεση με το σταθεροποιημένο όπου οι υπερπιέσεις είναι πρακτικώς μηδενικές παντού. Τονίζεται εδώ ότι η μειωμένη τιμή του λόγου υπερπιέσεων πόρων r_u κάτω από το πέδιλο συγκριτικά με την αντίστοιχη τιμή του στο ελεύθερο πεδίο οφείλεται στην αύξηση της ενεργού κατακόρυφης τάσης $σ'_v$ λόγω του φορτίου ανωδομής του πεδίλου τόσο στο φυσικό όσο και στο σταθεροποιημένο έδαφος.

Στην Εικόνα 38 παρουσιάζονται οι χρονοϊστορίες των καθιζήσεων στην επιφάνεια κάτω από το πέδιλο και στο ελεύθερο πεδίο. Παρατηρείται ότι οι καθιζήσεις κάτω από το πέδιλο προκύπτουν κατά τη διάρκεια της δόνησης λόγω διατμητικής φόρτισης και όχι λόγω αποτόνωσης υπερπιέσεων μετά το τέλος της. Είναι σαφώς μεγαλύτερες για τη φυσική σε σχέση με τη σταθεροποιημένη άμμο, η οποία δείχνει σημαντικά βελτιωμένη συμπεριφορά. Μάλιστα η απόλυτη τιμή της τελικής καθίζησης στην περίπτωση της φυσικής στρώσης κρίνεται απαγορευτικά μεγάλη (περίπου 13cm) για την ομαλή λειτουργία της κατασκευής σε αυτήν την αναφορά ανάλυσης, σε αντίθεση με αυτήν στην περίπτωση του σταθεροποιημένου εδάφους που είναι εντός, εν δυνάμει αποδεκτών, ορίων (περίπου 4cm) ειδικά για τη σχετικά μικρή τιμή συντελεστή ασφαλείας FS=3 που επελέγη εδώ. Επίσης, προκύπτουν σχεδόν μηδενικές καθιζήσεις στο ελεύθερο πεδίο όπου δεν υπάρχει επιφόρτιση και στατικές διατμητικές τάσεις (στο οριζόντιο και κάθετο επίπεδο), και αυτό τόσο για το φυσικό όσο και για το σταθεροποιημένο έδαφος. Το γεγονός ότι είναι ασήμαντες οι καθιζήσεις ελευθέρου πεδίου συγκριτικά με εκείνες κάτω από το πέδιλο είναι αναμενόμενο, και με τη λογική και με βάση πειραματικά αποτελέσματα για ρευστοποιημένα εδάφη (π.χ. σύγκριση Velacs No. 1 έναντι Velacs No. 12, βλ. Andrianopoulos et al 2010b).

Επιπλέον, εκτελέστηκαν δυναμικές συζευγμένες ελαστοπλαστικές αναλύσεις οι οποίες κατέδειξαν πως οι βασικές παράμετροι που επηρεάζουν την απόκριση του συστήματος θεμελιολωρίδας- πλήρους σταθεροποιημένου εδάφους είναι η δεσπόζουσα περίοδος της διέγερσης T_e, η μέγιστη επιτάχυνση βάσης (PGA), ο στατικός συντελεστής ασφαλείας (FS) και η ύπαρξη ή υποκείμενης μη σταθεροποιημένης στρώσης. Άλλες παράμετροι όπως ο αριθμός κύκλων φόρτισης και η σχετική πυκνότητα του εδάφους πριν τη σταθεροποίηση δεν προέκυψαν ως μεγάλης σημασίας.

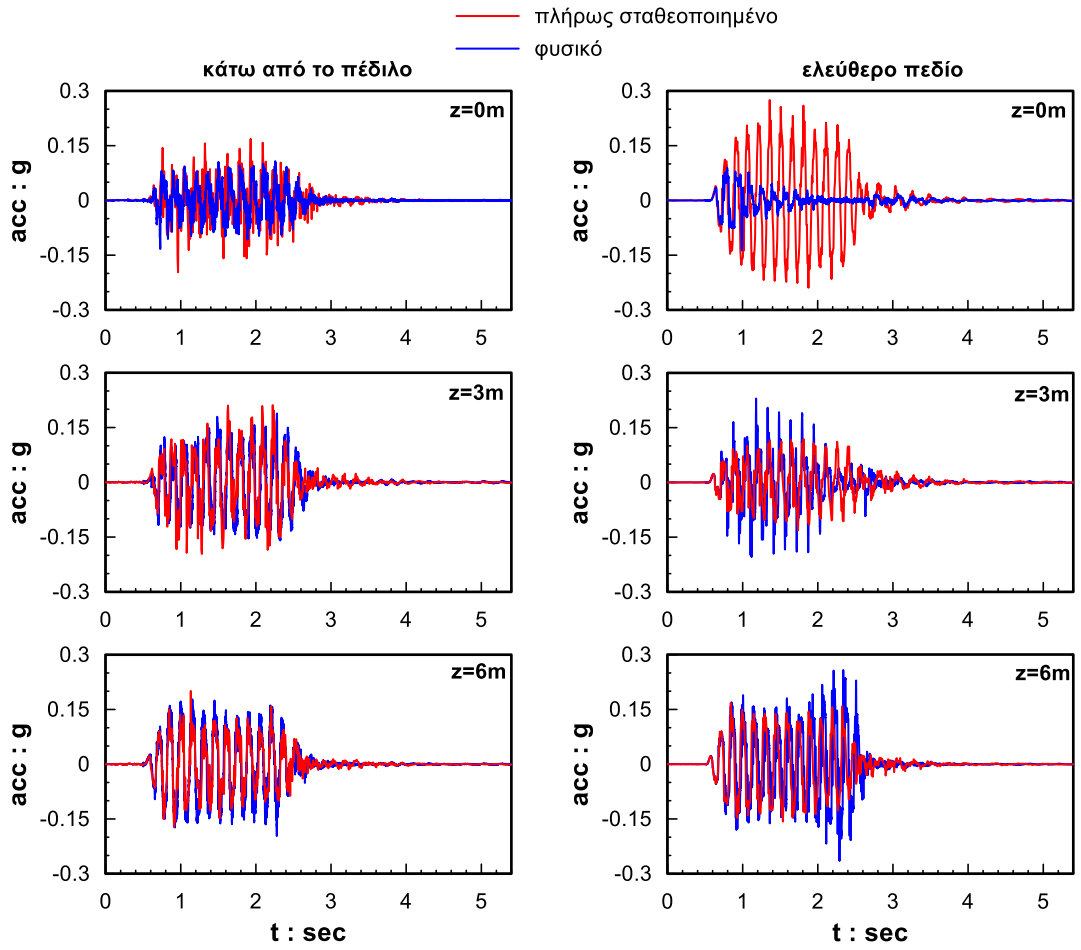

Εικόνα 35 *Σύγκριση χρονοϊστορίων επιταχύνσεων σε διάφορα βάθη κάτω από το πέδιλο (αριστερή στήλη) και στο ελεύθερο πεδίο (δεξιά στήλη) για σταθεροποιημένη (κόκκινο) και μη σταθεροποιημένη (μπλε) εδαφική στρώση ύψους 9m υπό την ίδια σεισμική διέγερση βάσης.*

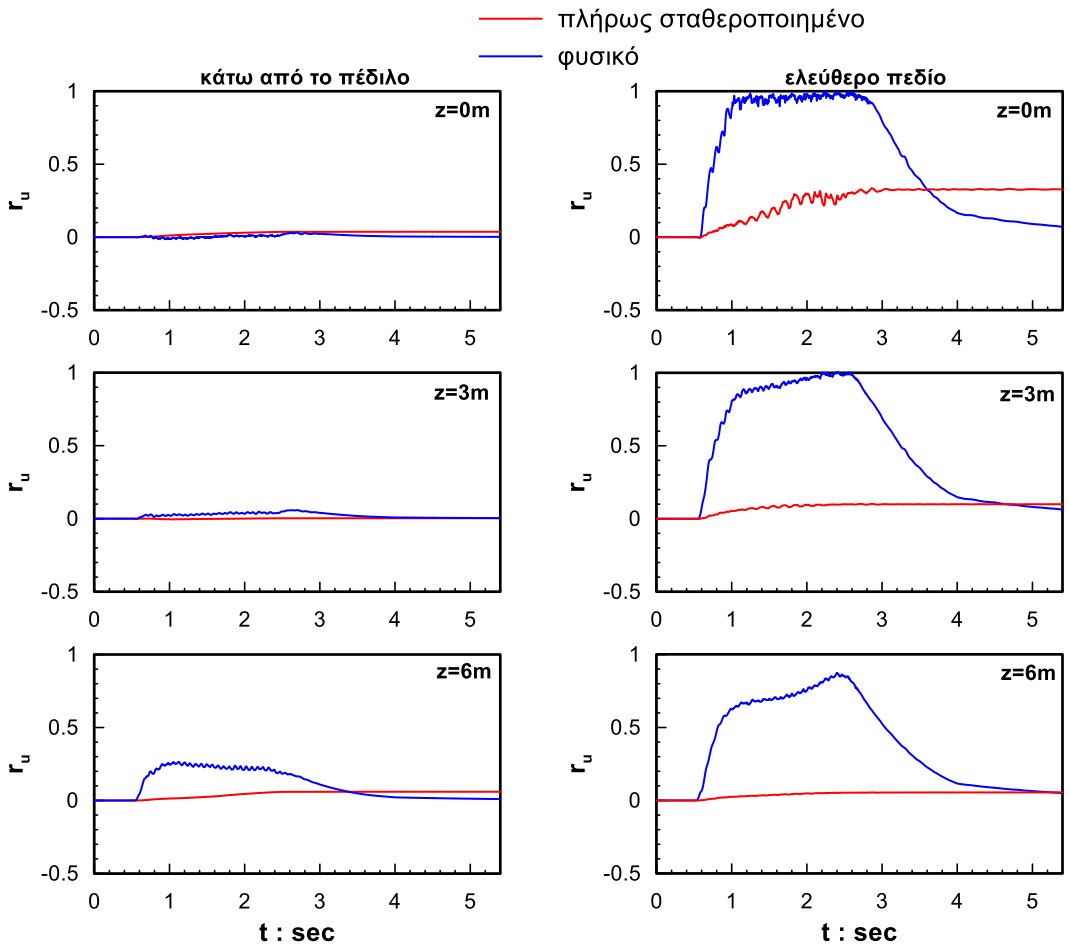

Εικόνα 36 *Σύγκριση χρονοϊστορίων του λόγου υπερπιέσεων πόρων r_u σε διάφορα βάθη κάτω από το πέδιλο (αριστερή στήλη) και στο ελεύθερο πεδίο (δεξιά στήλη) για σταθεροποιημένη (κόκκινο) και μη σταθεροποιημένη (μπλε) εδαφική στρώση ύψους 9m υπό την ίδια σεισμική διέγερση βάσης.*

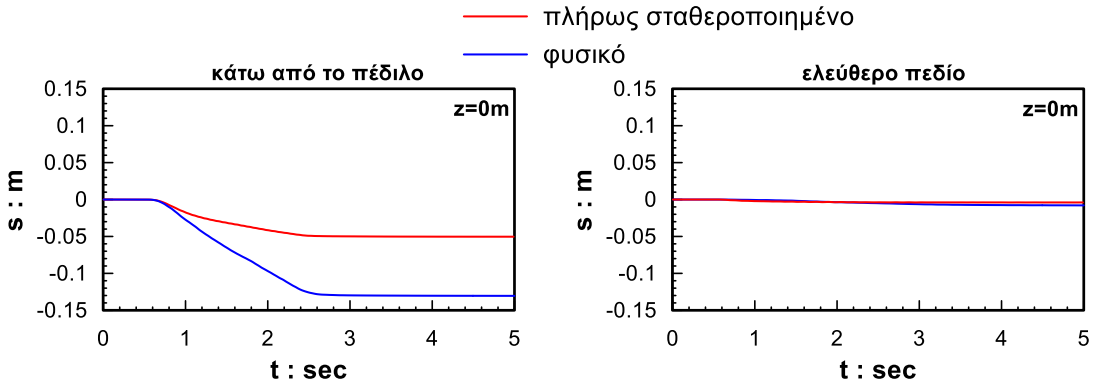

Εικόνα 37 *Σύγκριση χρονοϊστορίων καθιζήσεων κάτω από το πέδιλο (αριστερή στήλη) και στο ελεύθερο πεδίο (δεξιά στήλη) στην επιφάνεια της σταθεροποιημένης (κόκκινο) και μη σταθεροποιημένη (μπλε) εδαφική στρώση ύψους 9m υπό την ίδια σεισμική διέγερση βάσης.*

11. Συμπεράσματα

Τα βασικά συμπεράσματα της βιβλιογραφικής ανασκόπησης που αφορούν στα ρεολογικά χαρακτηριστικά της κολλοειδούς πυριτίας CS (*Κεφάλαιο 2*), καθώς και στη μηχανική συμπεριφορά των σταθεροποιημένων με CS εδαφών (*Κεφάλαιο 3*) συνοψίζονται παρακάτω:

- Η κολλοειδής πυριτία (CS) είναι ένας οιωνοί ιδανικός σταθεροποιητής, καθώς έχει σχετικά χαμηλό κόστος (συγκριτικά με άλλα χημικά ενέματα), ενώ διαθέτει αποδεκτή χημική σύσταση (περιβαλλοντικώς ασφαλής) και κατάλληλα ρεολογικά χαρακτηριστικά (χαμηλό αρχικό ιξώδες που επιτρέπει την εισπίεση και μετατροπή σε γέλη σε έναν προκαθορισμένο χρόνο)
- Το ιξώδες του διαλύματος CS και ως επακόλουθο ο χρόνος γέλης επηρεάζονται σημαντικά από την τιμή του pH, την συγκέντρωση CS(%) κατά βάρος και την συγκέντρωση αλάτων στο διάλυμα. Καθώς η τιμή του ιξώδους αυξάνεται, η απόσταση εισπίεσης της CS μειώνεται δραματικά, ενώ με χαμηλή υδραυλική κλίση η εισπίεση τερματίζεται όταν η τιμή του ιξώδους φτάσει σε τιμές μερικών λίγων cP. Εκτός από το ιξώδες, μια άλλη σημαντική παράμετρος που διαδραματίζει σημαντικό ρόλο στην εισπίεση της CS είναι η υδραυλική κλίση, ενώ η εισπίεση σε μεγάλες αποστάσεις μπορεί να πραγματοποιηθεί αν το ιξώδες παραμείνει σε χαμηλές τιμές για τον αναγκάιο χρόνο.
- Με βάση εργαστηριακές δοκιμές σε επίπεδο εδαφικού στοιχείου, οι σταθεροποιημένες με CS άμμοι έχουν μη μηδενική αντοχή σε ανεμπόδιστη θλίψη, η οποία βαίνει αυξανόμενη όσο αυξάνεται η συγκέντρωση CS(%) κατά βάρος που χρησιμοποιείται. Τα αποτελέσματα υποδεικνύουν μια εν γένει πιο δύστμητη και πιο διαστολική συμπεριφορά σε σχέση με τα φυσικά εδάφη που υποβλήθηκαν στην ίδια φόρτιση υπό ίδιες αρχικές συνθήκες φόρτισης.
- Η σταθεροποίηση μιας άμμου με CS οδηγεί σε μικρή αύξηση (10% κατά μέσο όρο) του ελαστικού μέτρου διάτμησης (σε μικρές ανακυκλικές διατμητικές παραμορφώσεις), αλλά δεν φαίνεται να έχει σημαντική επίδραση στις καμπύλες μείωσης του κανονικοποιημένου μέτρου διάτμησης και αύξησης της υστερητικής απόσβεσης με την ανακυκλική διατμητική παραμόρφωση.
- Από ανακυκλικές δοκιμές (τριαξονικές, απλής διάτμησης κλπ) σε σταθεροποιημένες άμμους προκύπτει ότι η ρευστοποίηση παρατηρείται μετά από ένα μεγάλο αριθμό κύκλων φόρτισης σε αντίθεση με τις μη σταθεροποιημένες άμμους που υποβλήθηκαν στην ίδια φόρτιση υπό τις ίδιες αρχικές συνθήκες και στις οποίες η ρευστοποίηση παρουσιάστηκε μετά από τους λίγους μόνο κύκλους φόρτισης.

Τα αποτελέσματα από τις δοκιμές μέτρησης ιξώδους που εκτελέστηκαν στο Π.Θ. για ένα μεγάλο εύρος διαλυμάτων CS και παρουσιάζονται στο *Κεφάλαιο 4* συνοψίζονται ως εξής¨

- Ο χρόνος γέλης (t_g) των διαλυμάτων CS επηρεάζεται από τέσσερεις (4) βασικούς παράγοντες, την συγκέντρωση CS(%) κατά βάρος, την προσθήκη NaCl (σε όρους κανονικότητας), το pH και την θερμοκρασία T του διαλύματος. Η συγκέντρωση CS(%), η κανονικότητα NaCl και η θερμοκρασία έχουν μονοτονική μειωτική επίδραση στον t_g, ενώ η τιμή του pH έχει μη μονοτονική επίδραση. Ο καθορισμός του t_g (από μερικές ώρες έως αρκετές ημέρες) μπορεί να πραγματοποιηθεί με κατάλληλη προσαρμογή αυτών των τεσσάρων (4) παραμέτρων.
- Για όλους τους συνδυασμούς [CS(%), κανονικότητα NaCl, T], υπάρχει μία τιμή του pH (pH_{opt}) που οδηγεί στον ελάχιστο χρόνο γέλης (t_{gmin}). Η τιμή του pH_{opt} επηρεάζεται από την συγκέντρωση CS(%) και την κανονικότητα NaCl αλλά όχι από τη θερμοκρασία T.
- Η αρχική τιμή του ιξώδους (μ_0) είναι γενικώς μικρότερη από 1.5cP (για CS≤10%) και εκφράζεται από μια αυξητική συνάρτηση της συγκέντρωσης CS(%) κατά βάρος.
- Με βάση τις δοκιμές μέτρησης ιξώδους που εκτελέστηκαν που είναι συμβατές με μετρήσεις της βιβλιογραφίας, προτείνονται μια σειρά διαγραμμάτων σχεδιασμού και μια πολύ-παραμετρική σχέση για τον υπολογισμό τόσο του t_g όσο και της πλήρους καμπύλης ιξώδους – χρόνου, για δεδομένες τιμές των προαναφερθέντων τεσσάρων παραμέτρων [CS(%), κανονικότητα NaCl, T, pH]

Από τις μονοδιάστατες δοκιμές εισπίεσης διαλυμάτων CS σε άμμους και ιλυώδεις άμμους σε εδαφικές στήλες διαφορετικών υψών που πραγματοποιήθηκαν στο Π.Θ. και μελετήθηκαν στο *Κεφάλαιο 5* παρατηρήθηκε ότι:

- Η δυνατότητα εισπίεσης ενός διαλύματος CS σε αμμώδεις εδαφικές στήλες εξαρτάται από την υδραυλική αγωγιμότητα του εδάφους, τα χαρακτηριστικά του διαλύματος CS που χρησιμοποιείται και την υδραυλική κλίση. Προκειμένου να επιτευχθεί η εισπίεση του διαλύματος CS στην επιθυμητή απόσταση, θα πρέπει να προσαρμοστούν καταλλήλως τα χαρακτηριστικά του διαλύματος (pH, κανονικότητα NaCl, CS(%), T), καθώς για τιμές ιξώδους πάνω από 4-7cP η εισπίεση τερματίζεται (τουλάχιστον για το εύρος αρχικών υδραυλικών κλίσεων που εξετάστηκαν: 0.03 ως 0.23).
- Προκειμένου να σχεδιαστεί η εισπίεση επιτόπου, θα πρέπει να ληφθούν υπόψη δύο χαρακτηριστικά ενός διαλύματος CS: η αύξηση του ιξώδους (η οποία είναι συνάρτηση των τεσσάρων (4) παραμέτρων [CS(%), κανονικότητα NaCl, T, pH]) και το μεγαλύτερο ειδικό

βάρος του [που είναι συνάρτηση της συγκέντρωσης CS(%)] συγκριτικά με το νερό που εκτοπίζει.

- Η εισπιεζόμενη παροχή του διαλύματος CS κατά τη διάρκεια της εισπίεσης μπορεί να προσομοιωθεί ικανοποιητικά μέσω της αναλυτικής σχέσης των Post et al (2007) όπως τροποποιήθηκε από τους Agapoulaki et al. (2015), η οποία βασίζεται στο νόμο Darcy τροποποιώντας τον κατάλληλα ώστε να λαμβάνονται υπόψη το χρονικά αυξανόμενο ιξώδες και το μεγαλύτερο ειδικό βάρος του διαλύματος CS συγκριτικά με το νερό.

Ελλείψει εξειδικευμένου καταστατικού προσομοιώματος για σταθεροποιημένες άμμους, στο *Κεφάλαιο 6* επιχειρείται εναλλακτικά η «ευφυής» χρήση ενός υπάρχοντος σοφιστευμένου προσομοιώματος για άμμους μετά από κατάλληλες τροποποιήσεις. Για αυτό το λόγο, χρησιμοποιήθηκε το προσομοίωμα κρίσιμης κατάστασης NTUA-SAND (Andrianopoulos et al., 2010a, b) διερευνώντας δύο (2) βασικές οδούς προσομοίωσης: (α) την αναβαθμονόμηση των σταθερών του προσομοιώματος για τον εδαφικό σκελετό (αποδίδοντας την πιο δύστμητη και λιγότερο συστολική συμπεριφορά) και (β) τη μείωση του μέτρου συμπίεσης K του υγρού των πόρων, συγκριτικά με την τιμή K_w του νερού (αποτυπώνοντας τη διαφαινόμενη αυξημένη συμπιεστότητα της πυριτίας συγκριτικά με το νερό στους πόρους). Συγκρίσεις με εργαστηριακές ανακυκλικές δοκιμές εδαφικού στοιχείου υποδεικνύουν ότι και οι δύο (2) αυτές οδοί προσομοίωσης είναι εν δυνάμει κατάλληλες για την προσομοίωση της ανακυκλικής συμπεριφοράς του σταθεροποιημένου εδάφους. Αντίστοιχα, προσομοιώνουν σωστά τη σχετική μείωση της διαστολικότητας και της ενδοσιμότητας του σταθεροποιημένου εδάφους υπό μονοτονική φόρτιση.

Έπειτα, στο *Κεφάλαιο 7* και στο *Κεφάλαιο 8* διερευνάται η ακρίβεια των δύο αυτών οδών προσομοίωσης σε προβλήματα συνοριακών τιμών συγκρίνοντας τα αποτελέσματα από σχετικές συζευγμένες μη γραμμικές αναλύσεις σε κώδικα πεπερασμένων διαφορών με τις αντίστοιχες μετρήσεις από δυναμικές δοκιμές φυγοκέντρισης που αφορούν σε σταθεροποιημένες άμμους. Στο *Κεφάλαιο 7* δίνεται έμφαση στην 1Δ σεισμική απόκριση μίας σταθεροποιημένης αμμώδους στρώσης (Gallagher et al., 2007) στην οποία εμφανίζεται η συνήθως παρατηρούμενη ενίσχυση της σεισμικής κίνησης λόγω μη- ρευστοποίησης του εδάφους. Στο *Κεφάλαιο 8* παρουσιάζεται η απόκριση μίας στρώσης σταθεροποιημένου εδάφους υπό μικρή κλίση (Conlee et al., 2012), στην οποία παρατηρούνται ελάχιστες μετατοπίσεις και καθιζήσεις σε αντίθεση με το πλευρικώς εξαπλούμενο και καθιζάνον ρευστοποιημένο έδαφος ίδιας γεωμετρίας υπό την ίδια διέγερση βάσης. Η σύγκριση των προσομοιώσεων με τα πειραματικά αποτελέσματα υποδεικνύουν ότι:

- Η αναβαθμονόμηση των σταθερών του προσομοιώματος και του μέτρου συμπίεσης K του υγρού πόρων που βασίζεται μόνο σε ανακυκλικές δοκιμές εδαφικού στοιχείου αποδεικνύεται μεν ποιοτικά ακριβής, αλλά υποεκτιμά ποσοτικά την αποδοτικότητα της σταθεροποίησης σε προβλήματα συνοριακών τιμών,
- Παρόλα αυτά, μόνο η μείωση του μέτρου συμπίεσης K (= K_w/n) του υγρού των πόρων ως συνάρτηση της συγκέντρωσης πυριτίας CS (%) κατά βάρος (για συνήθεις τιμές 5-10%), είναι ικανή να προσφέρει ποσοτικά ακριβείς προβλέψεις της μηχανικής συμπεριφοράς σταθεροποιημένων εδαφών και για τα δύο εξεταζόμενα προβλήματα συνοριακών τιμών.
- Η προτεινόμενη φαινομενολογική μεθοδολογία αριθμητικής προσομοίωσης της δυναμικής απόκρισης σταθεροποιημένων εδαφών μπορεί να εφαρμοστεί για το εύρος των συνθηκών των εξετασθέντων δοκιμών φυγοκέντρισης στις οποίες βασίστηκε, δηλαδή για τα συνήθη ποσοστά συγκέντρωσης κατά βάρος CS (=4-10%) και για μικρής και μεσαίας έντασης διεγέρσεις (με μέγιστη επιτάχυνση 0.20g)

Στη συνέχεια, στο *Κεφάλαιο 9* έγινε παραμετρική αριθμητική διερεύνηση της 1Δ σεισμικής απόκρισης σταθεροποιημένων εδαφικών στρώσεων με χρήση του ως άνω πλαισίου προσομοίωσης, απ' όπου προέκυψε ότι:

- Η σεισμική απόκριση πλήρως σταθεροποιημένης στρώσης προσεγγίζει την αντίστοιχη απόκριση του φυσικού εδάφους υπό πλήρως στραγγιζόμενες συνθήκες, και μάλιστα για μικρής έντασης διεγέρσεις οι δύο αυτές αποκρίσεις ταυτίζονται (μηδενική ανάπτυξη υπερπιέσεων πόρων και στις δύο περιπτώσεις)
- Η φασματική ενίσχυση της επιτάχυνσης (επιφάνεια προς βάση) σε πλήρως σταθεροποιημένα εδάφη είναι ποιοτικά παρόμοια με εκείνη των σταθερών μη σταθεροποιημένων εδαφών, όπως οι άργιλοι. Για παράδειγμα, μια αύξηση της έντασης της διέγερσης προκαλεί αύξηση της ιδιοπεριόδου της εδαφικής στήλης T_s και μείωση της φασματικής ενίσχυσης εξαιτίας της αυξημένης μη γραμμικότητας, ενώ παρατηρούνται και φαινόμενα συντονισμού όταν η ιδιοπερίοδος του εδάφους T_s προσεγγίζει τη δεσπόζουσα περίοδο της διέγερσης T_e.
- Σε μερικώς (μόνο επιφανειακά) σταθεροποιημένη στρώση, η σεισμική απόκριση καθορίζεται κυρίως από τη συμπεριφορά της υποκείμενης μη σταθεροποιημένης στρώσης, η οποία, αν έχει επαρκές πάχος και ρευστοποιηθεί, οδηγεί σε έντονη απομείωση της ταλάντωσης στην επιφάνεια του εδάφους.
- Με βάση τις 66 παραμετρικές αριθμητικές αναλύσεις που πραγματοποιήθηκαν, προτείνονται πολύ-παραμετρικές σχέσεις για τον υπολογισμό της φασματικής ενίσχυσης

της επιτάχυνσης (επιφάνεια προς βάση), οι οποίες χρησιμοποιούν ως δεδομένα τα χαρακτηριστικά της διέγερσης (ενεργός επιτάχυνση, δεσπόζουσα περίοδος T_e) και το πάχος της σταθεροποιημένης στρώσης H_{tr}. Η αναγκαιότητα κατάστρωσης νέων σχέσεων προκύπτει από το γεγονός ότι οι ήδη υπάρχουσες σχέσεις για τα σταθερά, φυσικά εδάφη οδηγούν σε αυξημένη διασπορά όταν χρησιμοποιούνται για σταθεροποιημένα εδάφη.

Τέλος, στο *Κεφάλαιο 10* έγινε παραμετρική αριθμητική διερεύνηση της σεισμικής απόκρισης επιφανειακής θεμελιολωρίδας επί σταθεροποιημένης στρώσης, με χρήση του ίδιου πλαισίου φαινομενολογικής προσομοίωσης, με τα ακόλουθα συμπεράσματα:

- Η πλήρης σταθεροποίηση του εδάφους θεμελίωσης μειώνει σημαντικά τις καθιζήσεις, συγκριτικά με αυτές που αναμένονται σε ένα μη σταθεροποιημένο έδαφος. Ωστόσο, ποιοτικά, και στην περίπτωση του σταθεροποιημένου εδάφους (όπως και σε εκείνη του μη σταθεροποιημένου), οι καθιζήσεις του θεμελίου είναι αποτέλεσμα διάτμησης και εμφανίζονται κατά τη διάρκεια της διέγερσης, δηλαδή δεν σχετίζονται με την αποτόνωση των υπερπιέσεων των πόρων μετά το τέλος της διέγερσης.
- Η σεισμική επιτάχυνση στην διεπιφάνεια εδάφους – θεμελίου είναι σημαντική στα πλήρως σταθεροποιημένα εδάφη και συγκρίσιμη με εκείνη στα μη σταθεροποιημένα. Στο ελεύθερο πεδίο του θεμελίου η σεισμική απόκριση είναι αρκετά διαφορετική (π.χ. το μη σταθεροποιημένο έδαφος παρουσιάζει σημαντική απομείωση της επιτάχυνσης εξαιτίας της ρευστοποίησης, αντίθετα με το σταθεροποιημένο έδαφος), σε συμφωνία με τα ευρήματα του *Κεφαλαίου 9*.
- Οι καθιζήσεις κατά τη διάρκεια της διέγερσης αυξάνονται με αύξηση της επιτάχυνσης βάσης, της δεσπόζουσας περιόδου και του αριθμού των κύκλων φόρτισης, με σημανικότερη την επίδραση των δύο πρώτων. Αντίθετα, αύξηση του στατικού συντελεστή ασφαλείας ή/ και της σχετικής πυκνότητας της άμμου (πριν τη σταθεροποίηση) μειώνει τις καθιζήσεις μετά τη σταθεροποίηση.
- Αν το θεμέλιο εδράζεται σε μερικώς (μόνο επιφανειακά) σταθεροποιημένη στρώση, οι επιταχύνσεις στη στάθμη έδρασης μπορεί να απομειωθούν, λόγω της υποκείμενης πιθανώς ρευστοποιήσιμης στρώσης. Ωστόσο, μια επιφανειακή σταθεροποίηση άπειρου πλάτους και πάχους ίσου με το εύρος του θεμελίου δε δείχνει επαρκής να απομειώσει τις σεισμικές καθιζήσεις, ενώ, αντίθετα, για πάχος σταθεροποίησης διπλάσιο του εύρους θεμελίου προκύπτει σχεδόν το πλήρες σχετικό όφελος σε όρους καθιζήσεων.

Table of Contents

Chapter 1

INTRODUCTION

1.1 Soil improvement against liquefaction

Liquefaction is a phenomenon in which the strength and the stiffness of a granular saturated soil are dramatically reduced due to large excess pore pressure development. This phenomenon may appear in non-cohesive soils (gravels, sands, non-plastic silts) and is considered these days one of the most important reasons for structural failures during earthquakes. For this reason, according to existing seismic codes (e.g. EC8), the construction of civil engineering structures is prohibited on soils which are at risk of liquefaction, unless the soil is first improved.

Depending on the particle size and the fines content of the problematic soil, the appropriate liquefaction mitigation method should be employed. Figure 1.1 presents a list of currently available soil improvement techniques for liquefaction mitigation based on the soil type and range of grain-size distribution, as reported by Idriss and Boulanger (2008).

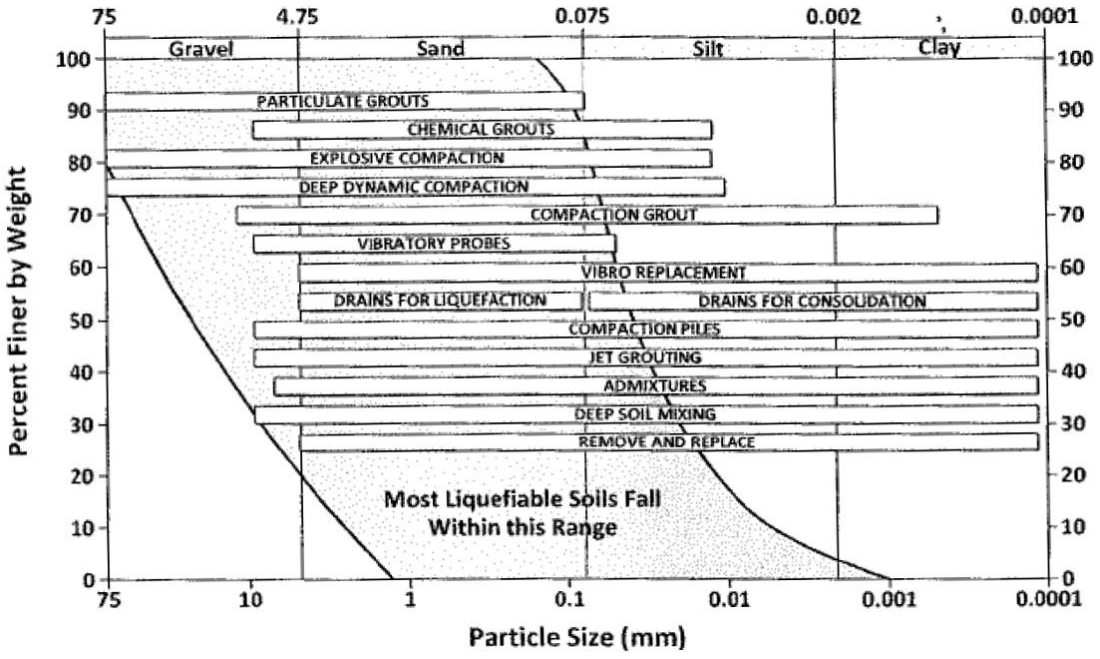

Figure 1.1 *Available soil improvement techniques for liquefaction mitigation (Idriss and Boulanger, 2008)*

In practice, the list of currently available liquefaction mitigation techniques for undeveloped sites is longer that what is shown in Figure 1.1. The reason is that when the site does not contain a structure or a lifeline, there is no technical problem hindering the application of a multitude techniques. The choice is really a matter of cost- effectiveness, rather than a matter of applicability. In general, the available ground improvement techniques against liquefaction can be categorized depending on their mitigation concept into the following groups: (a) densification methods, (b) stabilization/ grouting methods, (c) methods increasing drainage, (d) confinement/ strain reducing methods.

In the first category (densification methods) the soil density is increased by the application of mechanical force or vibration. Pertinent methods include dynamic compaction, vibro-compaction and preloading, although the latter is not so effective for non- cohesive soils. Obviously, these methods are only applicable at non developed sites.

The category of stabilization/ grouting includes (among many) deep soil mixing, injection of chemical grouts and premixing. This type of improvement technique serves three purposes: firstly to increase the strength and cohesion of the granular soil by increasing its load-bearing capacity, to decrease the permeability of the soil and to lower its compressibility. These methods can be applied at developed sites but the equipment size may not fit the available space, while their application can cause structural problems (footing upheave) due to high pressure grouting.

Drainage increasing methods aim to increase dissipation rates for the excess pore water pressures that are generated during shaking, or simply to modify the dissipation patterns and thus alleviate potential damage from pore pressure redistribution. (Idriss and Boulanger 2008). The main goal of the drain installation is to dissipate pore pressures which develop during any cyclic loading and thus reduce the liquefaction risk of the soil formation, and secondly to reinforce the foundation soil since the mean shear strength of the mixed formation is increased (if gravel drains are installed). Unfortunately, such methods cannot mitigate liquefaction under the whole structure or developed area.

In the confinement methods, the soils under a structure are enclosed with the help of surrounding sheet piles or walls, and hence cannot easily spread outwards in case of shear strength loss. It can be applied for small structures, but the confinement is not sufficient if the structure is quite spacious. Similarly, strain- reducing methods employ stiff inclusions, which

reduce the straining of the surrounding untreated soil, but do not necessarily disallow liquefaction (unless the inclusions are very closely located).

Based on the above, at developed sites (e.g. under a structure, around pipelines) the very large majority of these techniques proves inapplicable or problematic. In such cases, underpinning (micropiles), grouting (high pressure injection of viscous grouts) or prefabricated drains (installed without vibration) are usually prescribed (Gallagher and Mitchell 2002), but even these may prove problematic, as described below.

Particularly, underpinning has been used effectively in many ground improvement applications in order to increase the bearing capacity and reduce settlement, i.e. for strengthening existing foundations. A micropile is a small-diameter (typically less than 300 mm), drilled and grouted non-displacement pile that is typically reinforced. It is constructed by drilling a borehole, placing steel reinforcement, and grouting the hole. Micropiles are traditionally used in foundation retrofit and rehabilitation projects due to their high flexibility, ductility, capacity to withstand extension forces, as well as their good performance during earthquakes (Wang et al., 2008). Micropiles are used mainly as foundation support elements to resist static and seismic loads. This method essentially falls within the confinement category of liquefaction mitigation techniques, if the micropiles are used at the perimeter only, and in the related strain- reducing methods if they are used throughout the plan view.

(Jet) grouting is a method of constructing soil piles, by the following procedure: (a) break-up of existing soil structure by a grout (viscous fluid) injected into the soil at high pressure, (b) in-situ mixing and partial replacement of the soil particles with a hydraulic binder (slurry). The grout (or viscous fluid) used for the break-up of the geomaterial can usually also constitute the necessary binder for the formation of the soil pile. This method improves the mechanical properties of the soil using the fluid jetting with very high kinetic energy and creates a homogeneous mass of a high strength reinforced soil – stabilizer material. This type of stabilization does not face problems of equipment size fitting in the available space (e.g. like for deep soil mixing), but may create structural problems from footing heave due to the used high pressures.

Prefabricated vertical drains consist of synthetic (usually) band-shaped material that is installed vertically into soft soils. The drains are approximately 10cm wide by 5mm thick and composed of a plastic strip with drainage channels, wrapped in a filter fabric. The installation of the drains is performed using vibratory hammers and/or static methods, and the wick drain

layout typically consists of a triangular or square pattern. This type of drainage technique cannot always be installed underneath the whole of an existing structure and hence its benefit may only be partially effective especially for large structures. tIn addition, clogging may affect their long-term effectiveness if the soil has condisiderable amount of fines.

To conclude, all existing mitigation techniques focusing on developed sites cannot readily mitigate liquefaction effects underneath the whole structure and in some cases structural problems may arise. Moreover, operation is obstructed during improvement works (a problem for critical infrastructure like hospitals) and the mitigation of large areas, like the waterfronts of large cities in seismically active areas like Greece, Italy, Turkey built before the 70's (when seismic liquefaction was first identified as a measurable potential risk) is generally of prohibitive cost. The next section presents one possible alternative technique, without many of the foregoing drawbacks, named passive (site) stabilization whose concept was first proposed by Gallagher (2000).

1.2 Passive (site) stabilization

Passive (site) stabilization concerns the low pressure injection of a stabilizer-enriched pore fluid with time-increasing viscosity at the up-gradient side of a developed site followed by delivery under the structure via groundwater flow. The enrichment of the pore fluid with the stabilizer (environmentally safe nano-particles) with different possible chemical compositions (like colloidal silica and clay particle mixtures) alters the mechanical response of the soil skeleton–pore fluid system, making it less vulnerable to plastic strain accumulation related to seismic liquefaction.

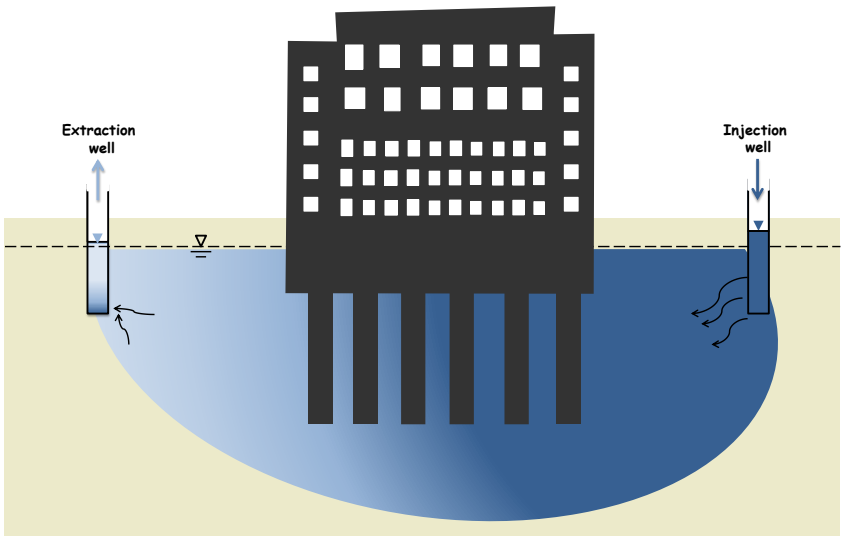

Figure 1.2 *Concept of passive stabilization, via augmented (induced) groundwater flow.*

The delivery of the stabilizer in place as a pore fluid may be performed either by natural ground flow, or more realistically by altering it using boreholes with high and low hydraulic head on either side of the developed site (see Figure 1.2). Based on this concept, it becomes possible to stabilize the whole area underneath a structure, and this without obstructing its normal operation. Given the low gradient flow, no high pressure injection is necessary and hence no structural problems are expected. This also means that there is no need for specialized equipment or personnel. For the same reasons, this technique may be used for improving the ground at shallow depths and around urban lifelines (e.g. pipelines under pavements). In addition, its cost is expected to be sufficiently low and practically comparable to that of chemical grouting.

Basic prerequisites for potential nano-size solutions for use in passive (site) stabilization are: a) time-increasing but controllable viscosity, b) non-toxicity, c) high durability and d) low cost. Applying these basic criteria reduces the list of candidate nano-size solutions to the following: colloidal silica, clay particles, bio-grouts, chemical grouts, zero-valent iron. Based on Gallagher (2000), a series of chemical grouts may be excluded for various reasons (e.g. acrylamide because of its toxicity and cost), while zero-valent iron because it is highly sensitive to oxidation and thus raising issues of durability. In addition, the use of bio-grouts is attracting attention in the literature (e.g. Paassen et al., 2009), since micro-organisms in the pore fluid may catalyze chemical reactions leading to the precipitation of calcium carbonate crystals turning sand into stone. Such procedures may be used for liquefaction mitigation, but issues of durability arise since these chemical reactions may be reversed. The same may occur with other microbial processes that produce pore-blocking bio-films (Gallagher, 2000). Hence, based on the literature, the use of two (2) stabilizers has so far taken the lead: a) mixtures of nano-size clay particles, and, most commonly, b) colloidal silica.

The characteristics of the former have been outlined by Papadimitriou & Agapoulaki (2014), while details may be found in: Haldavnekaret al. (2004); El Mohtar. (2008); El Mohtar et al. (2008a); El Mohtar et al. (2008b). In summary it is mentioned here that, the use of bentonite (high plasticity clayey particles) in small percentages per weight (3-5%) in water solutions creates a thixotropic mixture. This mixture may be permeated as a pore fluid only if its viscosity is small enough, e.g. after its alteration with sodium pyrophosphate (El Mohtar 2008). This chemical alteration is not permanent (given hydrolysis of sodium pyrophosphate) and hence the enriched pore fluid regains its thixotropic nature with time. Cyclic testing depicts that for the same relative density and cyclic stress ratio, sand with bentonite exhibits

increased liquefaction resistance, which increases as a function of the percentage per weight of the bentonite, as well as with time due to the thixotropic nature of the mixture (El Mohtar et al. 2008b). Rheometer testing shows that the thixotropic pore fluid exhibits elastic response with non-zero shear modulus (Haldavnekar et al., 2004). Hence, its existence in the pores seems to obstruct grain sliding (as compared to clean water), leading macroscopically to excess pore pressure generation only under very large cyclic shear strains. This improvement mechanism is backed by limited microscopic measurements, but it is still unclear whether it is the same with that of sands with high plasticity fines, that also show similar increase of liquefaction resistance. Element testing focuses on permeation and cyclic response exclusively on sand samples stabilized with small percentages of bentonite. No physical modeling has been performed for the study of this type of stabilizer, while there is no measurement of permeability changes when the thixotropic pore fluid is in place. Nevertheless, there are tests showing that if the improved soil liquefies due to intense shaking, its cyclic strength is regained with time (self-healing material). In order to avoid problems related to quality control of chemical alteration, smaller clay nano-particles may be used, like laponite, i.e. synthetic, high plasticity clay, with particles one order of magnitude smaller than that of bentonite

This Thesis deals with the use of colloidal silica as a stabilizer and its basic characteristics are the subject of the following paragraph.

1.3 Colloidal silica

Colloidal silica (CS) is a dispersion of silica particles (size 7-22nm usually) in water. At a concentration of 5-10% per weight, a colloidal silica aqueous dispersion has initially density and viscosity values slightly higher than that of water. While its density remains constant its viscosity increases with time and thus colloidal silica becomes a permanent gel abruptly after a controlled amount of time ranging from a few hours to a few months. Before gelation, the viscosity remains small (allowing its low pressure injection in place; see Figure 1.2), while the duration of this pre-gelation period is affected by the percent per weight of silica, the size of the silica particles, the pH and the normality of ions (e.g. Na^{+}, Ca^{++}) in the dispersion (Gallagher 2000a). Colloidal silica is non-toxic, biologically and chemically inert and is considered quite durable, in general.

Figure 1.3 presents a schematic illustration of a silica particle (H_4SiO_4). Due to its small particle size and its negatively-charged surface, electro-static forces between the particles control the response of the dispersion. Gelation occurs by the formation of siloxane (Si-O-Si) bonds between silica particles, releasing H_2O into the solution. The procedure of gelation is

perpetual, and the time required for its formation depends on the intensity of the electro-static interaction between the particles. Hence, it may be controlled by introducing ions and/or by altering the pH of the dispersion, since these two parameters affect the repulsive forces between the silica particles in the dispersion. For example, the introduction of NaCl in the silica dispersion reduces the double layer of water attached to the silica particles that is created by the electro-static attraction of bipolar H_2O molecules. As a result, the repulsive forces between silica particles are reduced, thus accelerating the formation of siloxane bonds, i.e. the prerequisite for gelation.

There are 3 common types of colloidal silica in the literature of passive (site) stabilization: Ludox®-SM, Ludox®-HS-40 and Ludox®-TM. The basic properties of these CS types are presented in Table 1-1. In comparative terms, Ludox®-SM is characterized by the largest specific surface ($345m^2/g$) and the smallest particle size (7nm), thus minimizing its gel time. Based on Gallagher (2000), these characteristics lead to smaller required concentrations per weight to create a firm gel, thus making this type the least costly among the 3 foregoing Ludox colloidal silica types. For this reason, Ludox-SM® was selected as the optimal Ludox CS type for use in this Thesis. An overview of the literature for the chemical and rheological properties of Ludox-SM® can be found in Chapter 2. The same Chapter also includes the pertinent literature on the injectability of CS in granural soils.

Table 1-1 *Properties of Ludox colloidal silica solutions (Gallagher, 2000)*

	Ludox-SM	Ludox HS-40	Ludox TM
SiO_2/Na_2O (by weight)	50	95	225
Stabilizing counter ion	Sodium	Sodium	Sodium
Particle charge	Negative	Negative	Negative
Silica (as SiO_2), weight %	30	40	50
PH	10.0	9.7	9.0
Viscosity (cP)	5.5	16	40
Average Particle Size (nm)	7	12	22
Specific Surface Area (m^2/g)	345	220	140

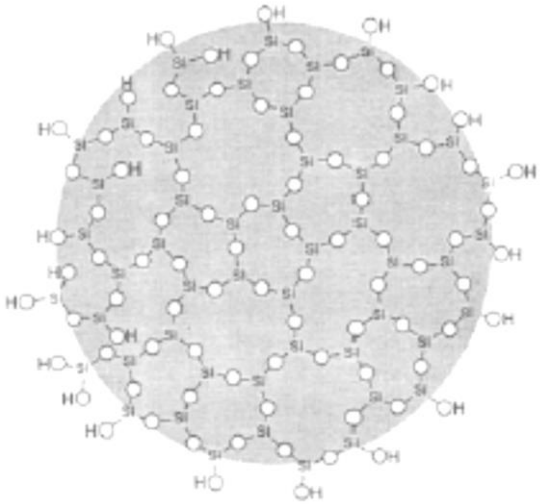

Figure 1.3 *Schematic illustration of a (colloidal) silica particle with negatively charged surface (Silco Inc, 2005)*

Macroscopically, once the CS gels in the pores of the sand, the thus stabilized sand is characterized by reduced straining (e.g. at large cyclic shear strains, see results of triaxial tests in Figure 1.4. Also, the gel drastically reduces the permeability of the virgin soil (Persoff et al. 1999).

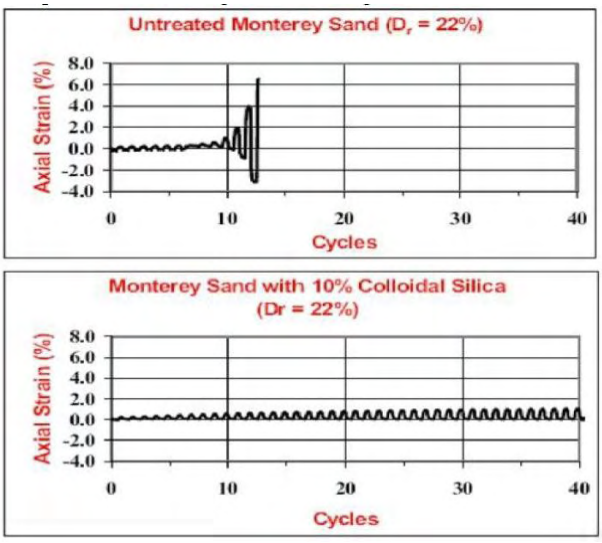

Figure 1.4 *Axial strain during cyclic triaxial loading (with a Cyclic Stress Ratio: CSR=0.27): a) pure (Monterey) sand, b) (Monterey) sand stabilized with colloidal silica (10% per weight), from Gallagher (2000).*

Mechanical element testing in the literature focuses on cyclic tests, mostly on sand samples stabilized with different (small) percentages of colloidal silica (e.g. Gallagher and Mitchell 2002; Kodaka et al. 2005), but lately testing has been extended to silty sands (Díaz-Rodríguez

et al. 2008). Pertinent physical modeling has been performed in the centrifuge (Conlee et al. 2012; Pamuk et al. 2007) and in field conditions (Gallagher et al. 2007a). These tests provided promising but partially inconclusive results. For example, despite the stabilization, excess pore pressures did nullify effective stresses of the stabilized-soil in the field test (Gallagher et al. 2007a), while settlements were reduced but not eliminated. An overview of the literature for the mechanical response of stabilized sands and its simulation can be found in Chapter 3.

1.4 Scope of Thesis

The long term goal of this Thesis is to aid in establishing passive (site) stabilization as a practical tool for engineers worldwide, when dealing with seismic liquefaction. To do so, this Thesis attempts to fill a number of literature gaps on the use of colloidal silica for this novel ground improvement technique. Particularly, the successful application of passive (site) stabilization lies on the delivery of the CS solution at the right place during a predefined time (see concept in Figure 1.2). Hence, a first goal of this research is to enrich the laboratory experiments that already exist in the literature that are related to the rheological properties of CS and its injectability in granular soils. Both these experimental efforts ended with simple analytical tools for predicting these critical elements for designing passive stabilization.

As this novel ground improvement technique is currently still at an experimental stage worldwide and in lack of a reliable dedicated constitutive model, this Thesis also explores the potential of using a state-of-the-art constitutive model for simulating the cyclic response of sands passively stabilized with colloidal silica. Its successful use is verified via comparisons with element tests, but mostly with the results of two independently executed series of centrifuge tests.

Having this novel numerical tool at hand, it is then used parametrically for analyzing two (2) very fundamental issues for using this ground improvement technique in practice. The first is the amplification of seismic motion at the ground surface of stabilized soil layers, since limited data from the literature indicate that amplifications may appear which would affect the intensity of seismic loading reaching the structures founded on such soils. The second issue deals with the seismic response of footings laying on passively stabilized sand, an issue of obvious importance for practice which has not been investigated in the literature, and its study was made possible with the new numerical tool.

1.5 Contents of Thesis

This first *Chapter 1* outlined the concept of passive (site) stabilization for liquefaction mitigation, the basic characteristics of the optimal stabilizer material (colloidal silica) and the scope of this Thesis, i.e. to aid in making this novel ground improvement technique applicable in practice.

In order to better understand the stabilizer material (colloidal silica), *Chapter 2* presents the chemical, rheological and mechanical properties of pure colloidal silica (CS) found in the literature, as well as its injectability in granular soils on the basis of the literature.

Chapter 3 outlines the existing literature data that refer to the monotonic and cyclic response of stabilized soils, as well as the behavior of stabilized soils under dynamic excitation (e.g. centrifuge tests).

In *Chapter 4* the rheological properties of CS are presented through viscosity measurements conducted for a wide range of CS solutions at the University of Thessaly. These tests enrich the literature measurements by also considering temperature as a controlling factor on top of the percentage per weight of CS in the solution, the pH and the normality of cations. In addition, a simple analytical methodology for predicting the viscosity versus time curve of CS solutions is proposed.

Chapter 5 investigates the injectability of CS solutions by executing one-dimensional column injection tests in the laboratory at the University of Thessaly. These tests were performed in sand and silty sand columns of different heights, injected with different solutions of CS. These tests study the effects of hydraulic gradient, CS (%), pH value, hydraulic conductivity, as well as the salinity of the sand (prior to injection) on the flow rate and the travel distance of CS solutions. Hence, they complement the literature, while they aid in validating an analytical tool for predicting the flow rate in practice.

Then, *Chapter 6* explores the potential of using a state-of-the-art constitutive model for sands (NTUA-SAND) for predicting the behavior of stabilized sands, by appropriately adjusting different aspects of the simulation components. This work is performed on the basis of literature results from element tests.

In the sequel, the established numerical methodology is used for simulating dynamic centrifuge tests on stabilized sands. Firstly, in *Chapter 7*, this methodology is used for simulating a test on the 1D seismic response of a uniform stabilized sand layer, and then, in

Chapter 8 the same methodology is used for simulating multiple tests on the laterally11 spreading response of passively stabilized layers towards a free face. In all cases the simulations show reliability of the numerical methodology.

Chapter 9 studies the 1D seismic ground response of stabilized sands. In lack of pertinent data other than the centrifuge experiment in *Chapter 7*, this study is performed numerically by parametrically employing the verified numerical methodology. The study includes the effects of layer thickness, intensity and duration of shaking, as well as of other parameters and ends with a set of multi-variable relations for predicting the pertinent spectral amplification.

In addition, *Chapter 10* employs again the verified methodology for studying a very common problem in the practice of civil engineering, that of the seismic response of shallow footings but when these lay on stabilized sand. Unfortunately there are no measurements related to this problem. Hence, the study is performed purely numerically and focuses on the effects of layer thickness, seismic intensity, footing factor of safety as well as other parameters and shows the effectiveness of passive (site) stabilization for reducing seismic settlements.

Finally, *Chapter 11* includes the main conclusions of this research effort and proposes issues for further investigation in the future.

Chapter 2

LITERATURE REVIEW OF COLLOIDAL SILICA PROPERTIES AND ITS INJECTABILITY IN GRANURAL SOILS

2.1 Chemical properties of Colloidal Silica

Colloidal silica (CS) is a suspension of silica nanoparticles (size: 7-22nm, depending on the type) in water. When CS is diluted in water at a concentration of 5-10%per weight (p.w.), immediately after dilution it has viscosity and density slightly higher than that of water, while it forms rapidly a firm gel after a specific amount of time (named gel time), which can vary from a few minutes to several months or even more. This gelling procedure is caused by the formation of siloxane bonds between silica nanoparticles. During this time, before the formation of a firm gel, viscosity values remain low, allowing CS to "travel" through the soil pores to the desirable location without the need for high pressure injection. The time required for gelation (gel time) of a specific type of CS can be adjusted by altering the CS(%) concentration in the solution, the pH value, salt (NaCl or other) concentration (Gallagher 2000b), as well as the temperature of the solution (Agapoulaki and Papadimitriou. 2015). Colloidal silica is also nontoxic, biologically and chemically inert, odorless, non-flammable, durable and does not require special equipment for preparation and application of the solution within the context of passive site stabilization. For better maintenance, CS should be stored in a dry environment of 20-25^{o}C until its mixture. The durability of CS is estimated from Whang (1995) as higher than 25 years, but it is still an issue requiring further investigation.

As mentioned in *Chapter 1*, at least three types of CS were tested in the literature in regards to viscosity evolution and the time required for gelation (gel time) in order to choose the appropriate type of CS for the application of passive stabilization. Further investigation was conducted by Gallagher (2000), who compared the following CS types: Ludox-SM®, Ludox-HS-40®, Ludox-TM®. Some of the details of this comparison effort are presented in *Chapter 1*, whereas this Chapter (and this Thesis) emphasizes on Ludox-SM®, which is the most commonly type of CS used in the literature of passive stabilization.

Many attempts have been made to explain the rheological behavior of CS solutions. According to Iler (1979), the formation of silica gel follows three steps. Firstly, the monomers $Si(OH)_4$

polymerize (or else condense) and form colloidal particles. The structure of a CS monomer is presented in Figure 2.1.

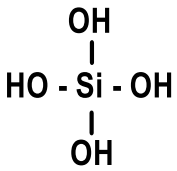

Figure 2.1 *Monomer of colloidal silica.*

Colloidal silica particles, then, grow in size through polymerization which can lead either to particles of massive silica or the particles link together into chains, then networks thus eventually transforming the liquid into a gel. More specifically, according to Iler (1979) the formation of silica gel takes place in two stages. In the first, initially formed Si(OH), condenses to form colloidal particles. In dilute solution, a further slow increase in particle size is the only change, but at low concentrations (i.e. CS=1%), these initially formed particles are able to condense together in order to give a very open but continuous structure, extending throughout the medium, thus offering a certain degree of rigidity upon it. In both stages of polymerization, the mechanism is the same: condensation to form Si-0-Si links, but in the first stage, condensation leads to particles of massive silica, while in the second, since it is not possible to fit two particles accurately together over a common face, the number of Si-0-Si linkages between particles is fewer in number than those within the particles themselves. They are merely sufficient to bind adjacent particles together, in a fixed position relative to one another, and thereby lead to a rigid, highly porous, tangled network of branching chains.

At low pH values (4<pH<7) the surfaces of the monomer are not intensively charged, they do not repel each other and siloxane bonds, chains and gel networks are formed. More specifically, at pH values of 5-6 the monomer is converted rapidly to particles, which aggregate and finally gel. The polymerization reaction is presented in Figure 2.2. Hydroxyl ions (OH^-) at pH values smaller or equal to 7 result from self-ionization of water, an ionization reaction in water or an aqueous solution, in which a water molecule, H_2O, deprotonates (loses the nucleus of one of its hydrogen atoms) in order to become a hydroxyl ion, OH^-. The hydrogen nucleus, H^+, immediately protonates another water molecule to form hydronium, H_3O^+ at small concentrations. This hydroxyl ion takes the H^+ from ≡Si-OH and transforms it to the negatively charged ≡Si-O^-, which reacts with CS monomer (Figure 2.1) and a siloxane bond is formed, as shown in Figure 2.3. As it is concluded from behavior the reaction of Figure 2.3,

siloxane bond formation produces hydroxyl ions (OH^-) which acts as a catalyst and will be used again at another reaction (Figure 2.2).

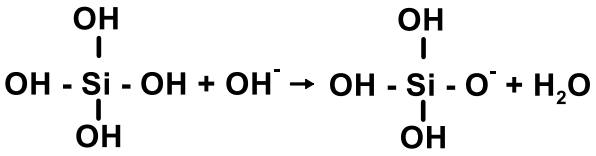

Figure 2.2 *Monomer reaction with hydroxyl ions producing water (polymerization).*

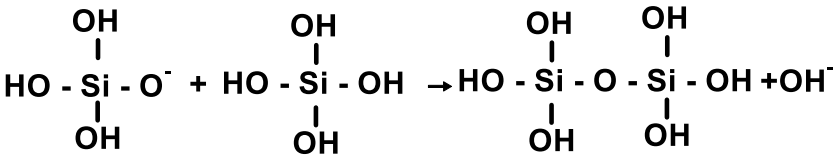

Figure 2.3 *Siloxane bond formation between a monomer and the polymerization product of Figure 2.2.*

When hydroxyl ion concentration is high, i.e. at high pH values (>7) and in an alkaline environment (e.g. in the presence of NaOH), most of the ≡Si-OH groups have become ≡Si-O and there are no monomers like those in Figure 2.1 to allow for siloxane bond formation (the reaction of Figure 2.3). According to Iler (1979) at pH > 6-7 the ionization of polymer species is much higher so that monomer polymerizes and decreases in concentration very rapidly, even in a matter of minutes at 25°C. At the same time, the particles grow rapidly to a size that depends mainly on temperature. However, if no salt is added no aggregation or chaining together of particles occurs because they are similarly charged and mutually repel each other: If salt is present, for example NaCl, ≡Si-O- react with Na+ forming Si-ONa which is hydrolyzed to Si-OH and can be used in the polymerization reaction of Figure 2.2.

The typical effects of pH and salt concentration effect on gel time of CS are presented in Figure 2.4. Curve ABC shows the behavior of CS when no salt is added and a rapid gelling at pH value of 5-6 is observed. At pH > 7, a gel cannot be formed since particles repel each other. When salt is added, as presented by the DEF curve, the gel times become smaller. In addition, at low pH values the salt addition has a relatively small effect and in a region of pH=5-6 the minimum solution stability is higher, with the term “stability” referring to the ability to resist change in its properties over time.

The growth of the primary particles occurs by an Oswald ripening mechanism, where particles grow in size and decrease in number. This particle growth depends on solubility, which, in

turn, depends on both pH value and temperature. Generally, for a chemical reaction to occur, there must be collisions between atoms or molecules to form a product, in this case a gel. In order for the collisions to occur the atoms or molecules must have enough kinetic energy. The average kinetic energy of molecules can be measured in terms of temperature. Molecules with a high temperature have a greater kinetic energy than molecules with a low temperature. According to Karol (2003) chemical reactions slow down as temperature decreases and this can lead to a twofold decrease in gel time as temperature increases for almost 8°C.

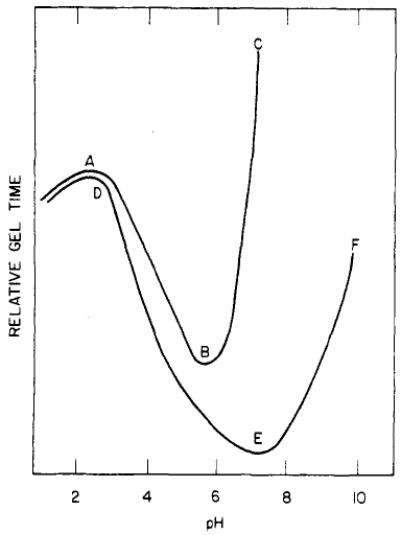

Figure 2.4 *Gel time curves of colloidal silica solutions with (DEF) and without (ABC) salt addition (Iler, 1979).*

2.2 Rheological properties of Colloidal Silica

The time required for gelation of a CS solution is of vital importance, as it defines available time for injection and delivery of the solution. In the literature, this time and more specifically the time from the end of mixture until CS viscosity increases rapidly and transforms the solution into a firm gel is called gel time. Gel time is considered to be the most important parameter for CS injection, because the CS solution should be delivered at the target location at the right time and then be transformed into a firm gel, thus ending the injection process. If the gelling procedure is delayed, then the CS solution will overtake the target location leading to increased cost due to extra material being used. On the contrary, if it gels prematurely, then the stabilizer will not be able to reach the target location and the stabilization will not be materialized, even though some material has been injected.

For the quality control of a low pressure injection of CS, the total gel time is not the only parameter that should be taken into account. The viscosity value at the initial stage of

injection should also be considered, because this value is directly linked to the injection velocity of CS in the soil. Particularly, as viscosity increases, the velocity of CS decreases even if the hydraulic gradient remains constant. As a result, rheological properties of CS solutions (from the mixing of silica particles in water all the way to gelation) is the main factor controlling the successful application of passive stabilization in practice.

The time required for gelation depends on the interaction rate between the particles and according to Gallagher (2000) it is a function of several parameters. The most important are:

- Particle size of CS, with an increasing effect
- CS(%) concentration in the solution, with a decreasing effect
- Ion concentration in the solution in terms of normality N with a decreasing effect
- pH of the solution with a non-monotonic effect
- temperature of the solution with a decreasing effect (Agapoulaki and Papadimitriou, 2015)

The effect of particle size of CS is presented in detail in *Chapter 1*. Gel times of CS solutions recorded in the literature have a minimum value of 30 minutes (Noll et al. 1992) but the upper limit is practically undetermined, as gel time is remarkably increased for very low (<3) and high (>8) pH values. As stated before, solutions with a high pH value with no addition of salt cannot essentially form a gel, and hence such alkaline environments can be used for storage of CS prior to mixing.

Figure 2.5 presents typical viscosity versus time curves of CS solutions from the literature. Observe that the viscosity – time curve has an initial almost linear part which begins from the initial viscosity value (slightly higher than water) until a value of 3-6cP and then it increases rapidly to a few thousands cPs, where a firm gel is formed. This type of rheological response is general and holds true for any combination of CS(%), salt concentration, pH, temperature which can lead to gelation, and is observed in all pertinent literature studies (Gallagher and Lin 2005, 2006, 2009; Gallagher et al. 2002; Jurinak and Summers 1991; Koch 2002; Persoff 1999). Despite the fact that all CS solutions have the same qualitative rheological response, the time required for gelation differs significantly. For example, in the results of Figure 2.5, the gel time ranges between 10 and 19 hours approximately. In practice, this gel time (t_g) can be defined as the time until viscosity reaches a value of 100cP (compatible with the definition of Gallagher, 2000), because the time required for the formation of a firm gel after this moment is essentially negligible.

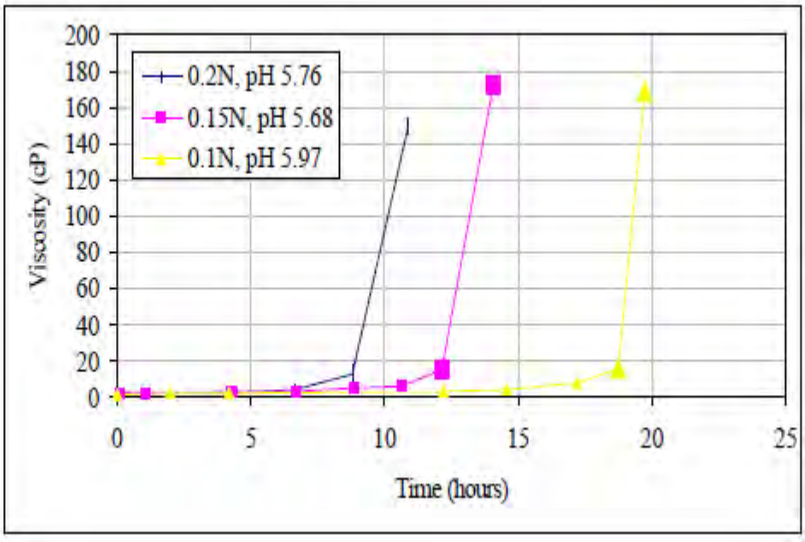

Figure 2.5 *Typical viscosity versus time curves for solutions with CS(%)=5 and different normalities and pH values* (Koch 2002).

The pH value is an important parameter which affects gel time, as shown in Figure 2.6, where the gel time ranges from a couple of days up to several tens of days. Based on the chemical properties of CS (see Section 2.1) and the research conducted by Iler (1979) it is widely believed that the minimum gel time can be achieved by adjusting the pH value between 5 and 7 (with or without salt addition). However, it is important to underline that the effect of pH is not monotonic. As shown in Figure 2.6 and Figure 2.7 shows that the minimum gel time is not observed at the minimum pH value but at a value between the range of 5.5 and 6.5 (Gallagher 2000).

Ion normality, namely the quantity and ionic strength of salt in the solution is also an important parameter affecting gel time. Normality is defined as the concentration of an aqueous solution or how many gram equivalents of the ion are diluted into one liter of the solution. This effect is monotonic, because as normality increases gel time decreases for the same combination of CS(%)-pH. This effect is shown in Figure 2.7 where the effect of NaCl on gel time is illustrated for four different normalities of 0.1N, 0.03N, 0.01N and 0N. It is observed that for the same pH value higher normalities lead to smaller gel times.

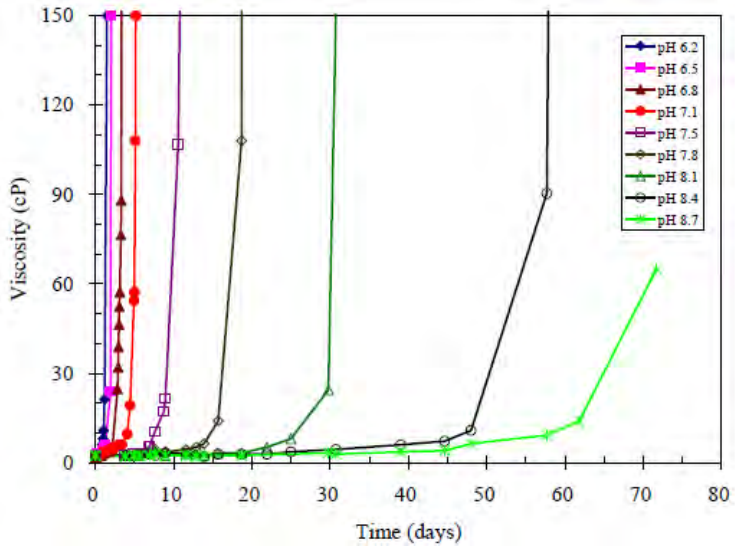

Figure 2.6 *Effect of pH on viscosity versus time curve for a solution with CS(%)=5 and normality 0.1N* (Lin 2006).

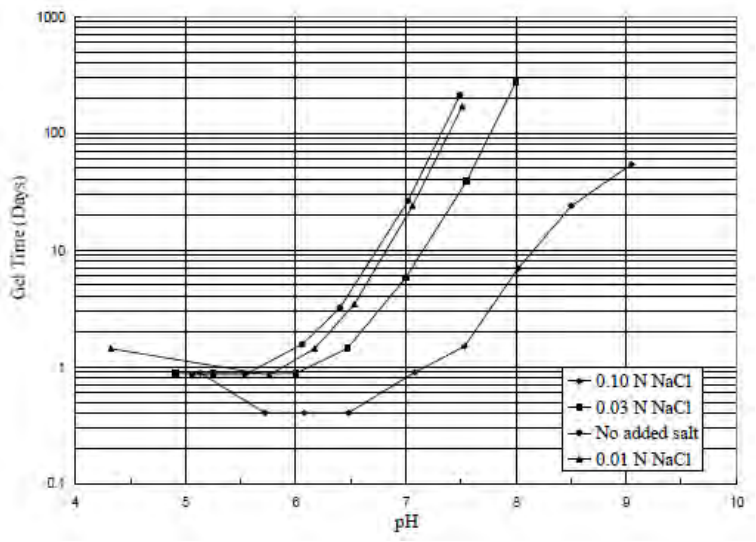

Figure 2.7 *Gel time curves for different NaCl normalities for solutions with CS(%)=10 and different pH values (Gallagher 2000).*

The concentration of CS (%) per weight in the solution also affects gel time and is a parameter directly connected with the cost of passive stabilization. Similarly with salt addition, its effect is monotonic because as CS (%) concentration increases, the gel time decreases, for the same combination of N- pH.

Temperature is also an important parameter affecting gel time, but it has not been investigated in detail in the literature. Apart from Iler (1979) who defines temperature as a major parameter controlling the solubility of silica, Otterstedt and Greenwood (2005) have

also depicted this effect for a specific (N,CS,pH) combination. However all studies related to passive stabilization with the use of CS consider this variable as negligible. This effect has been recently investigated by Agapoulaki and Papadimitriou (2015) and is presented in detail in *Chapter 4*.

2.3 Mechanical behavior of gelled colloidal silica

Towhata (2007) performed a series of unconfined compression strength tests in order to understand better the mechanical behavior of gelled CS without the presence of soil. The samples used were 7cm in height, 4.7cm in diameter and 129g in weight. Typical results of the tests are presented in Figure 2.8 andFigure 2.9 2.9 in terms of deviatoric stress versus axial strain and lateral versus axial strain, respectively. It is observed that unconfined compression strength of gelled CS is negligible, somewhat higher than 5kPa and thus cannot explain the improved mechanical behavior of stabilized soils. In addition the shear modulus of gelled CS is quite low, in the order of a few hundreds of kPa, on the basis of these tests.

In order to measure lateral and axial strains two sets of laser displacement transducers were placed at 1/3 and 2/3 of the samples height and sheets of white paper were placed at the surface so that the reflection of laser beams was facilitated. Figure 2.9 shows that the ratio of axial to lateral strain, or else Poisson's ratio is approximately equal to 0.3, which means that the material itself has volume compressibility (Poisson's ratio equal to 0.5 corresponds to uncompressible materials). If this compressibility is verified via more appropriate procedures, then it may be considered a possible explanation for the increased liquefaction resistance of stabilized soils.

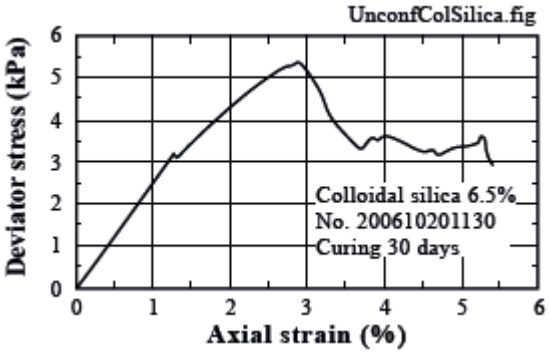

Figure 2.8 *Stress- strain relation of gelled CS as measured in an unconfined compression test* (Towhata 2007a).

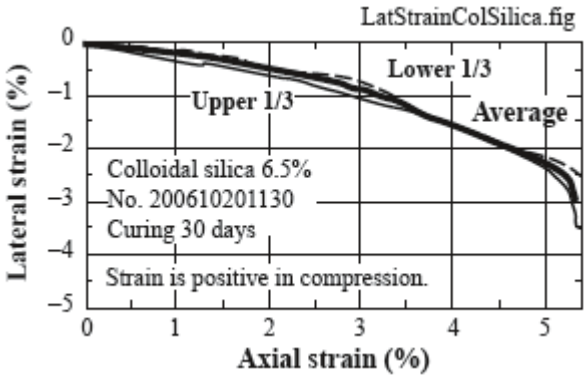

Figure 2.9 *Lateral- axial strain relation of gelled CS as measured in the unconfined compression test of Figure 2.12* (Towhata 2007a).

In order to use colloidal silica as a stabilizer it should transform into a gel at a predefined time. This means that the appropriate solution properties should be chosen, namely pH, temperature, salt and colloidal silica concentration. In order to investigate the properties of a silica solution for grouting in crystalline rock at relatively shallow depths Axelsson (2006) performed measurements on colloidal silica solutions (with CS(%)=35, $CaCl_2$(%)=2.9 and pH=10, not specified if it is Ludox-SM® or other) at low temperature, 8°C, and three different relative humidities (RH=75%,95% and 100%). The goal of the experiment was to measure some of the most important mechanical parameters of CS solutions: drying shrinkage, compressive strength, modulus of elasticity, shear strength and flexural strength. The measurements of compressive strength are shown in Figure 2.10 and indicate a significant increase from 0.6kPa after one day up to 5kPa after one week. This increase continues as curing time increases and differs depending on the RH of the sample.

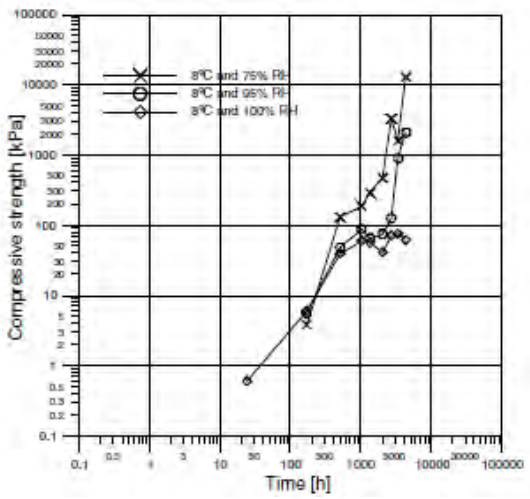

Figure 2.10 *Compressive strength of CS solutions at 8°C as a function of curing time for three different relative humidity RH values* (Axelsson 2006)

Figure 2.11 shows the force versus deformation relation, which indicates a practically linear elastic behavior and so the Young modulus was calculated from Hook's law (Figure 2.12). For the higher RH =100% the modulus seems to have a constant value of almost 3MPa but seems to increase with curing time for higher RH values.

As implied from the combination of Young's modulus values and compressive strength, the failure mode becomes more brittle as strength increases. The measurements of the shear strength are shown in Figure 2.13 and at the sample with the lower RH shear strength increases after a time of 40 days. The evolution of shrinkage and flexural strength show that shrinkage increases over curing time and this increase is faster as humidity lowers. An increase of flexural strength is observed for samples kept at lower humidities.

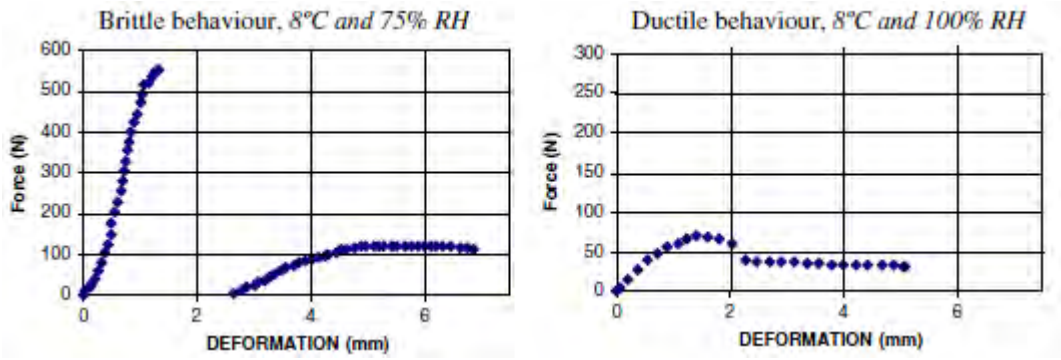

Figure 2.11 *Two examples of the failure mode for pure CS solutions* (Axelsson 2006).

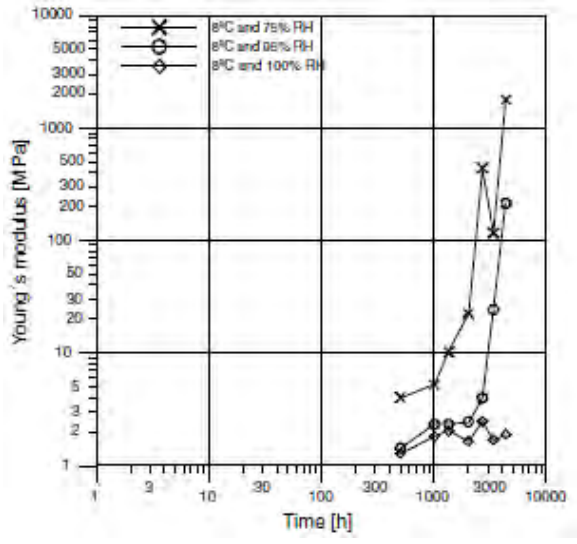

Figure 2.12 *Measured Young's modulus of CS solutions at 8°C as a function of curing time for three different relative humidity RH values* (Axelsson 2006).

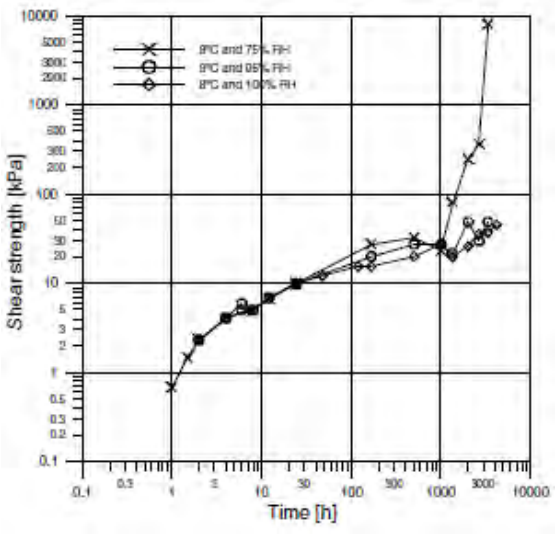

Figure 2.13 *Shear strength of CS solutions at 8°C as a function of curing time for three different relative humidity RH values* (Axelsson 2006).

In addition, Scherer et al. (1988) measured the elastic modulus and viscosity of silica gels as a function of the curing age using a beam-bending method. The gels used in this study were prepared using a recipe developed by Klein et al (1984). Results showed an increase of shear modulus with time due to the increase in bonds produced by condensation reactors which continue long after gelation. Figure 2.14 shows this evolution of shear modulus. The gel time was estimated to be 14 hours and is measured from the time the solution was mixed.

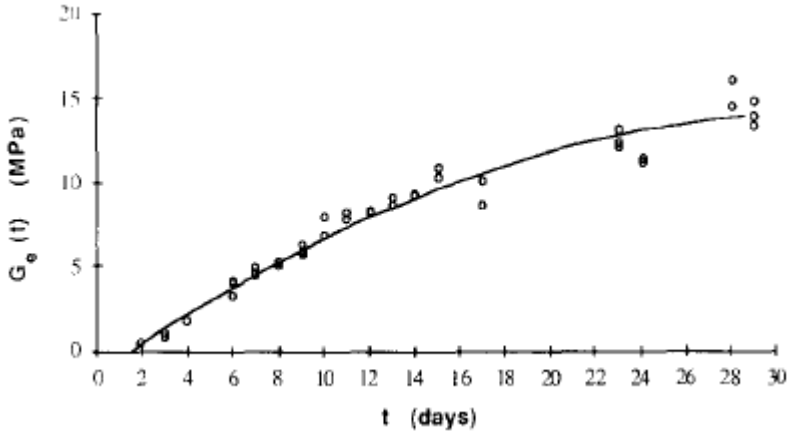

Figure 2.14 *Shear modulus evolution as a function of curing/ aging time* (Scherer et al. 1988)

Drabarek et al. (2002) used constant shear rate and dynamic rheological measurements to investigate how shear can affect the structural evolution of CS solutions during gelation. When no shear is applied, both the storage/elastic (G') and the loss/viscous (G'') moduli increase slowly prior to gelation due to the slow growth of particle size and network and then increase

with a higher rate because the particle growth becomes faster than network formation. Also, Drabarek et al. (2002) related gel time with the storage/elastic and loss/viscous moduli. Figure 2.15 compares the evolution of these two moduli with time for Ludox-SM® at pH values of 6 and 8. It is clear that for pH=6 gel time (180s) is less that this of pH=8 (4250s). However the strength of the network for pH=8 seems to be higher (50Pa) than that obtained by pH=6 (23Pa).

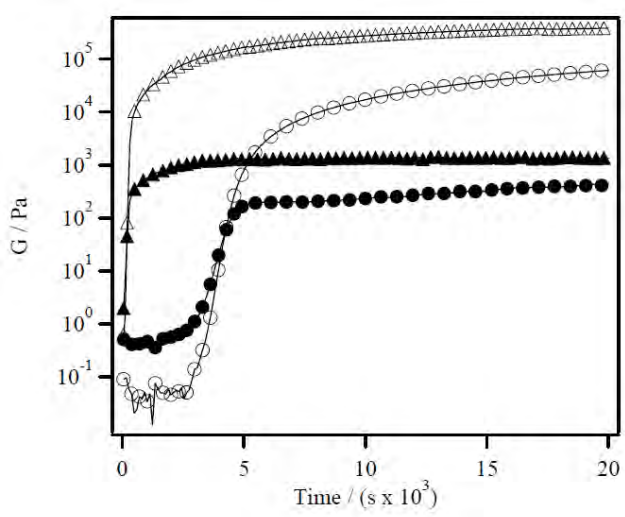

Figure 2.15 *Evolution of G' and G'' versus time as a function of the initial pH (open symbols, G', solid symbols G'', triangle pH=6, circle pH=8) (Drabarek et al. (2002)).*

Finally, Huang et al. (2007) used stable aqueous emulsions prepared by emulsification technique using colloidal silica particles combined with very small amount of emulsifiers. They used three kinds of nano-silica sols (10, 20, and 100 nm, pH 9–10) were the products of Eka Chemicals (Sweden). They investigated the effects of colloidal silica particle size and concentration on the rheological behavior of the emulsion by measuring the dynamic modulus. They found that the emulsions where CS was added, exhibited shear-thinning behavior and for smaller silica particles and/or higher CS concentration this behavior became more obvious. In terms of dynamic modulus, results showed that the smaller the particle size and/or CS concentration the higher the storage modulus and lower the loss modulus, which indicates that interparticulate interaction is stronger and elasticity is higher.

2.4 Injectability of Colloidal Silica in granular soils

A crucial parameter for the effective application of passive site stabilization is the injectability of the CS, i.e. how fast, how uniformly and how far can CS be injected into granular soils. Saiers

et al. (1994) concluded that CS delivery through a heterogenous media can be understood and even predicted in a laboratory system. However, the in situ parameters that should be taken into account are more complicated. According to many researchers, the main factor affecting stabilizer injectability is the increasing viscosity of colloidal silica solutions which governs their ability to "travel" through the soil formation (Jurinak and Summers 1991; Gallagher and Finsterle 2004; Gallagher and Lin 2005, 2009; Koch 2002; Lin and Gallagher 2006; Persoff et al. 1994). The remainder of this section presents the main findings of various CS injection attempts in the literature that were not always related to the use of CS for passive stabilization. Then, in sections 2.4.1 and 2.4.2 emphasis is set on the most prominent studies using 1D and 2D injection tests respectively, for the use of CS for passive stabilization, while section 2.4.3 provides information on the hydraulic conductivity of stabilized sands after gelation of CS in the pores.

Noll et al. (1992) performed pilot injection tests in order to investigate the formation of a water flow barrier using colloidal silica solutions (Ludox-SM®) at a concentration of 5%. A box 3.6mx1.8mx1.2m was filled with sand with a mean diameter of 0.3mm, porosity n=0.3, permeability $k=3x10^{-2}$cm/s and an estimated gel time of t_g=16h. Four injection and 6 extraction wells were used and colloidal silica was successfully delivered after 14 hours and the final soil permeability was reduced top $4x10^{-6}$cm/s.

Noll et al. (1993) performed a field scale pilot study to investigate the ability of colloidal silica to stabilize contamination hot spots and construct horizontal containment barriers. The injection and extraction wells system was determined to be a hexagonal array of extraction wells with a single injection well located at the center. One central injection well was used and six extraction wells were placed at a distance of 10 feet from the injection well. The injection and extraction rate was 3 gallons per minute with a travel time of 20 hours. The sand layer used was 9.15 m thick and had a permeability of $1.3x10^{-2}$cm/s with a porosity of 0.17 and colloidal silica was Ludox-SM® diluted at a concentration of 5% per weight. Finally, the CS traveled through the formation and managed to treat an area of 4.88 m diameter and 3.05 m thick.

Persoff et al. (1994) performed 0.9m column injection tests with Hanford sand stabilized with Nyacol 1440 colloidal silica solutions with a concentration of 50%, 20% and 13% and found that gelation of the solution caused a rapid end of the injection procedure and only when CS was diluted at a concentration of 13% was delivered through a distance of 0.9m. Taking into

account the results of these laboratory tests, it is of vital importance that analysis of site chemistry and heterogeneity should be conducted prior to CS injection.

Moridis et al (1996) conducted field testing in order to investigate the injection potential of CS solutions into heterogenous unsaturated alluvial deposits of clay, silt sand and gravel. Colloidal silica Nyacol DP5110 was used diluted at a concentration of 30% per weight with a pH value of 6.5 and the results showed that CS solutions could successfully travel through these soil formations.

Chaney et al. (1998) performed column injection tests with colloidal silica solutions with per weight concentrations of 32.2%, 31.8% and 27.8% and a particle diameter 14, 7 and 8nm respectively. Gel time in the soil was assessed by the injection tests in-soil columns and the monitoring of gelling in the columns. They concluded that if gel time equals to 2 hours then a CS solution with 2 pore volumes could be permeated with low pressures. On the contrary, if smaller gel times are used (e.g. 1 hour), then the pressure required increases dramatically reaching a value of 700kPa before the same volume can be injected. This is due to the increased viscosity values related to the reduced gel times.

Manchester et al (2001) performed small and large scale laboratory testing with nine CS variants with different particle size in order to investigate gel time, grout column injection and saturated hydraulic conductivity of stabilized soils. Column injection results showed that in all cases the CS solutions were able to travel through the columns and CS with larger particle size did not cure as fast as these with a smaller particle size. This is because the larger colloid particle size variants produce a more stable silica sol and therefore take longer to cure.

Koch (2002) performed two - dimensional box model tests with a central chamber filled with Nevada No120 sand and two reservoirs for groundwater control. The CS used was Ludox-SM® diluted at a concentration of 5% per weight. Results showed that CS delivery depends on viscosity evolution, which is a function of gel time. More details of these experiments can be found in paragraph 2.4.2.

Gallagher and Finsterle (2004) used the same set up to perform physical modeling experiments. For their research 1.5 pore volume of 5% diluted Ludox-SM® was used and delivered through the box during a period of 10 hours. Viscosity of CS was chosen so that it would increase 10 times compared to its initial value after these 10 hours. These results indicated that CS solutions could be delivered through loose sands using low head injection and extraction wells.

Gallagher et al. (2007b) performed a field test in order to investigate the ability of a 5% Ludox-SM® CS solution to cover a travel distance larger than 4.5m. One central extraction and eight injection wells which were equally spaced around the perimeter of the 9-m-diameter test area were used in order to maintain an injection rate of 13L/min. The injection of CS was done with a two stage bottom-up procedure and a 2m thick sand layer was saturated with CS. It was found that the injection rate of the grout was highly dependent on the viscosity value of CS, due to the permeability reduction caused by the increasing viscosity. Once viscosity values were significantly increased, flow could not continue even if the injection pressure increased.

Gallagher and Lin (2009) via 1D injection tests showed that for low gradient (pressure) injection of CS, the flow practically stops when viscosity has reached a value of approximately 4cP. This publication is based on Dr Lin's PhD thesis (Lin, 2006), which is presented in more detail in paragraph 2.4.1.

Moradi and Seyedi (2015) performed a similar box model test with silty sand mixtures of sand with variations in silt from 0 up to 30%. Colloidal silica Ludox-SM® was again used diluted at a concentration of 5% per weight. The box model had dimensions of 125x30x30cm and used five low head injection and two extraction wells. The model was tested for four different soil samples, the hydraulic gradient used was 0.03 and the viscosity of the CS solution was kept constant at 1.5cP during its delivery. The tests showed that a change in hydraulic conductivity, under identical conditions, can lead to a corresponding change in delivery time of CS solutions and this change is highly dependent on the silt content of the soil formation. This can be attributed to the change in the permeability of the soil due to the change in its silt content.

2.4.1 One dimensional injection tests *(Lin 2006)*

In his PhD thesis, Dr. Lin conducted 15 injection tests in cylindrical columns of 0.9m, 3m and 9m length. The goal of this research was to investigate the ability of CS to "travel" uniformly in liquefiable soil in adequate concentration in order to passively stabilize the soil. Loose Nevada 120 and Ottawa 20/30 sands were used and also 5% or 10% per weight graded silty sand. The CS used was Ludox-SM® at a concentration of 5% per weight, which according to Gallagher and Mitchell (2002) is the minimum required concentration to effectively improve soil strength. The tests investigated the effect of many parameters such as viscosity, pH, ionic strength and hydraulic gradient and different soil types. The grain size distribution of the soils used are shown in Figure 2.16 and the experimental set up is shown in Figure 2.17. The CS solution was injected into the sample with low gradient using the inlet and outlet chambers. The gradient was held constant during the entire test and it was chosen as a representative

of in situ gradients. The CS was then injected after it was colored with red food dye for visual observation. Chloride concentration, pH value, viscosity and flow rate were recorded during testing. For estimating CS(%) concentration in the pores, samples of 5ml were extracted (from sampling ports) and then burned at 200^{o}C for 2-3 days. The remaining material after burning was considered representative of the CS(%) concentration at the time of the sampling.

The injection tests led to the following conclusions:

- Viscosity and as a result gel time are strongly affected by pH value and ionic strength of the CS solution. As viscosity increases, the travel time of CS decreases dramatically and as the increasing rate is higher the time required until the end of the test becomes lower. A viscosity value of 3.6cP seems to cause an 80% reduction of CS delivery time when a low gradient is used. Hence, when injecting CS solutions, the injection should have finished when viscosity reaches this crucial value.
- Chloride concentration is a good indicator for the concentration of CS within the pores of the column.
- Hydraulic gradient is of vital importance for the stabilizer transportation through the porous medium. The flow rate of CS increases as the hydraulic gradient increases.
- In silty sand columns, the CS solution could not be easily delivered through the column. Flow rate of CS depends on the permeability of the column and two times larger permeability leads to a two-fold flow rate of CS.
- The long column tests proved that CS can be delivered through any chosen distance, when using the appropriate CS solution properties to control the gel time.

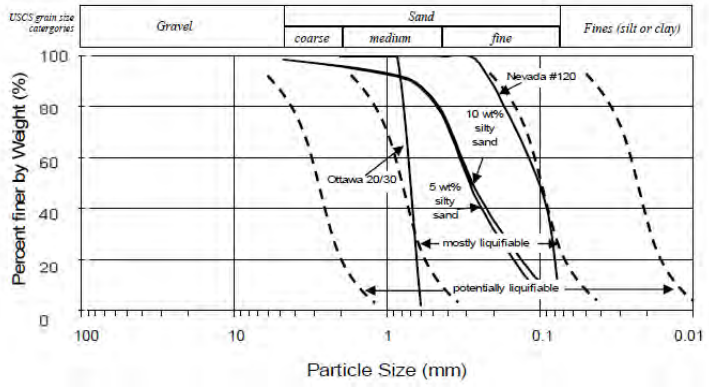

Figure 2.16 *Grain size distribution of soils used for 1D injection tests of CS in sand columns* (Lin 2006).

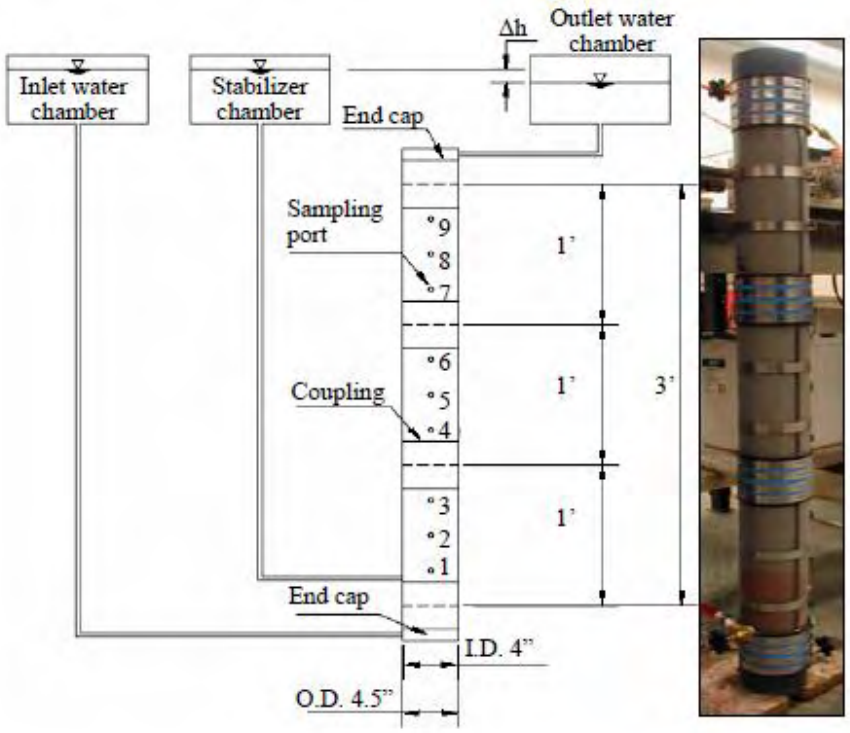

Figure 2.17 *Experimental set up for 1D injection tests of CS in sand columns* (Lin 2006).

2.4.2 Two dimensional injection tests *(Koch 2002)*

Koch (2002) investigated the ability of colloidal silica to be uniformly delivered into loose sands using low gradient injection wells via 15 two dimensional tests. Nevada sand No120 with a relative density of 40% was used in this study and as a stabilizer a CS solution (Ludox-SM®) with CS=5% per weight. The model used has dimensions 30.5x76x26.5cm and is presented at Figure 2.18. It consists of three parts, a central chamber where sand was placed and two chambers on either side of the central one for the groundwater flow control. The flow length through the sand was 46 cm and each water chamber has a length of 15 cm. As shown at Figure 2.18 on the front size of the model small holes are used as sampling ports in order to extract pore fluid during the test and estimate the CS(%) concentration.

After sand saturation, a hydraulic gradient of 0.04 was established and the CS was injected through the inlet reservoir, which had holes on its vertical interface with the sand chamber enabling horizontal injection. Here, one test will be presented with CS=5%, pH=6.3, 0.1N for a total quantity of two times the pore volume of the sand. The gel time for this CS solution is 2 days, which corresponds to a travel time equal to half day. Gallagher (2000) defined the travel time as the period of time during which the viscosity of the solution increases to ten times the initial viscosity. The CS solution was colored with blue food dye for visual observation. Twenty

minutes after the test began, the CS appeared at the lateral sides of the sand and after three hours it appeared on the sand surface. Because of the slightly higher density of CS in comparison to water, the stabilization tended to occur at the bottom half of the sand layer. Figure 2.19 shows the CS travelling into the soil during the first ten hours

The tests showed that a minimum of one and a half pore volumes are required in order to achieve full coverage of the box model at least for this injection setup and gradient. Also, the required travel time depends on both the amount of the stabilizer needed for full coverage and the injection rate and the adequate coverage depends on the injection and extraction wells used. Finally, the right choice of CS solution properties is the most important parameter for its delivery through the soil.

Figure 2.18 *Experimental set up for 2-D injection tests* (Koch 2002).

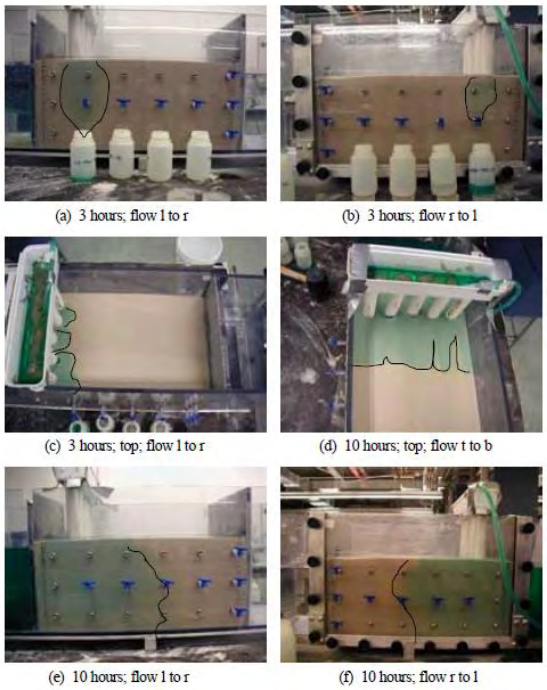

Figure 2.19 *(Dyed) Colloidal silica progression during a 2-D injection test* (Koch 2002).

2.4.3 Hydraulic conductivity of stabilized soils

Persoff et al. (1999) conducted hydraulic conductivity measurements on stabilized sands with different CS(%) concentrations and found that it becomes significantly lower than that of the untreated sand before injection of CS. In particular, values of $4*10^{-9}$ m/s – $3*10^{-10}$ m/s were measured for CS(%)=5-10% as presented in Figure 2.20.

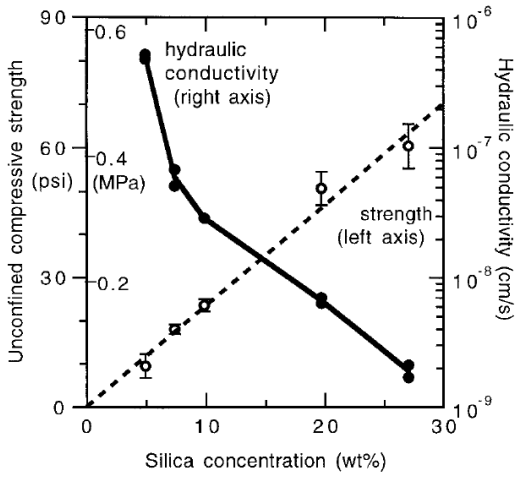

Figure 2.20 *Permeability of stabilized sands in relation with CS(%) concentration (Persoff et al, 1999).*

Chapter 3

LITERATURE PREVIEW OF THE MECHANICAL BEHAVIOR OF STABILIZED SANDS AND ITS NUMERICAL SIMULATION

3.1 Monotonic behavior of stabilized sands

The existing literature data that refer to monotonic behavior of soils stabilized with colloidal silica are not sufficient to fully describe their response. However, these data clearly show that colloidal silica solutions offer a significantly improved mechanical behavior.

Particularly, Kodaka et al. (2005) performed undrained cylinder torsional shear tests on Toyoura sand (D_r=40%, e_{max}=1.17, e_{min}=0.77, D_{50}=0.17mm) hollow cylindrical samples stabilized with a CS solution with concentration of 4% the type of which (Ludox-SM® or other) is not defined in the publication. Results showed that mechanical behavior of stabilized sands seems to be comparatively more dilative and stiffer and has a higher shear strength compared to the untreated sand sample under the same initial stress and density conditions. Figure 3.1 and 3.2 show this trend for the untreated and the stabilized sand, respectively.

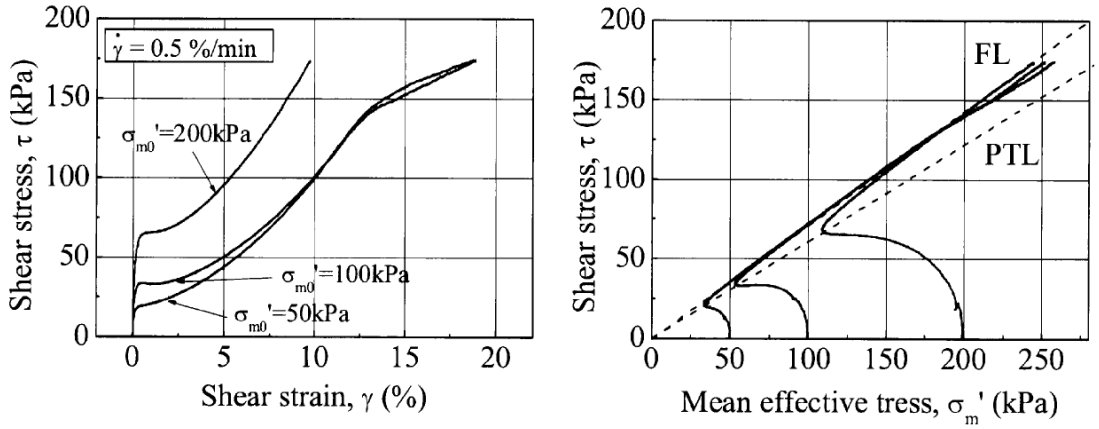

Figure 3.1 *Results of undrained torsional shear tests for untreated Toyoura sand for different vertical effective stresses (a) Stress (τ) – strain (γ) relation (b) Mean stress σ_m' – shear stress τ relation* (Kodaka et al. 2005).

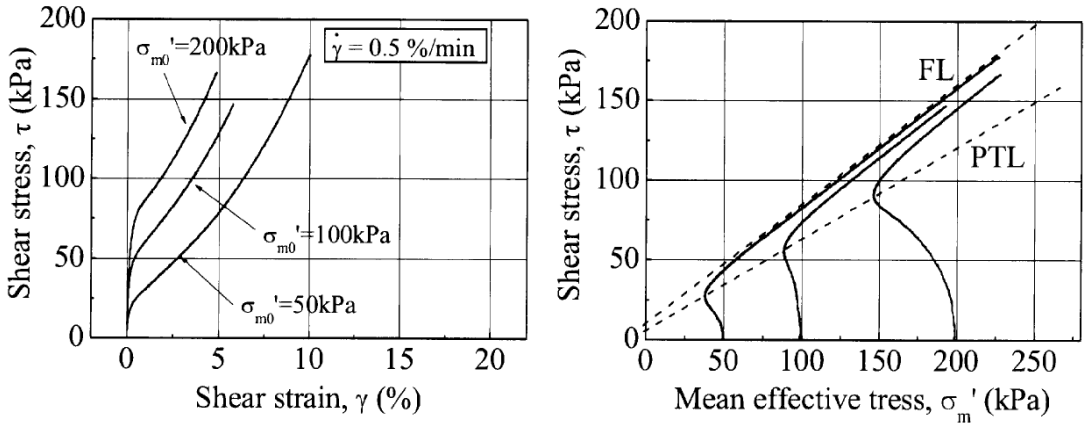

Figure 3.2 *Results of undrained torsional shear tests for stabilized Toyoura sand for different vertical effective stresses (a) Stress (τ) – strain (γ) relation (b) Mean stress σ_m' – shear stress τ relation* (Kodaka et al. 2005).

Towhata (2007) performed laboratory shear tests in order to better understand the mechanical behavior of stabilized sands using CS solutions. The specimens were prepared by loose saturated sand and consolidated in K_0 conditions in a container under a stress of 100kPa. The samples were cured for 5 weeks and under sustained stress. The results of undrained triaxial monotonic shear (for compression and extension) are shown in Figure 3.3, where the dashed lines depict the untreated sand while the solid lines the stabilized with 4.5% CS (uncertain whether it is Ludox-SM®).

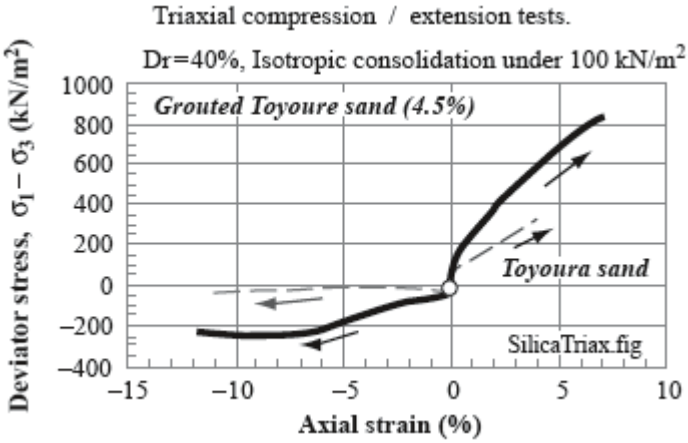

Figure 3.3 *Results of monotonic undrained triaxial tests on stabilized and untreated Toyoura sand (Towhata 2007)*

Apart from these laboratory experiments, all other literature testing related to the monotonic behavior of stabilized sands are unconfined compression (UC) tests. Persoff et al. (1999) performed UC strength tests at stabilized sands, which were stabilized with CS and cured for

7 days. The soils used were Monterey sand (D_r=22%, e_{max}=0.821, e_{min}=0.464, D_{50}=0.44mm) and Trevino sandy loam (D_{50}=0.095mm). The results showed that unconfined compression strength increased as the CS(%) concentration increased, i.e. sands acquire UC strength.

Gallagher (2000) performed UC strength tests and unconsolidated undrained (UU) tests on Monterey sand stabilized with four different concentrations of Ludox-SM® colloidal silica solutions. The UC strength was again non-zero and ranged from 45kPa for a solution with CS(%)=5 up to 223kPa for a solution with CS(%)=20. Similar results were presented by Gallagher and Mitchell (2002), who performed UU tests on samples grouted with CS(%)=10 and measured strengths with an average value of 51kPa.

UC tests on Nevada sand (D_r=41%, e_{max}=0.89, e_{min}=0.51, D_{50}=0.15mm) were also conducted by Gallagher and Lin (2005, 2009) on samples taken from most sections along the columns during 1D injection tests for CS solutions with CS(%)=5%. They found that stabilized sand had an average strength of 47-67kPa with a standard deviation of 6-18kPa and 40-60kPa with a standard deviation of 4.4-13.4kPa respectively.

Mollamahmutoglu and Yilmaz (2009) conducted UC tests on grouted samples with 70mm diameter and 140mm height. The sand used in this study had a specific gravity of 2.62, e_{max}=0.985, e_{min}=0.61 and was classified as poorly graded. Colloidal silica Meyco MP 320 and table salt (for adjusting ionic strength) were used to stabilize the sand at different CS and salt concentrations. It is interesting that no testing was performed at specimens with CS(%)=5 because of the soft gel that was reportedly formed. Typical results of these tests are presented in Figure 3.4 where it is obvious that stabilized sands acquired UC strength for all combinations of (CS, salt). This strength increased as the curing time increased but more or less stabilized after 28 days.

Moradi and Seyedi (2015) performed UC strength tests on silty sand samples stabilized with 4.5% Ludox-SM® colloidal silica solution. The undisturbed samples were extracted from a box model test and left curing for 6 weeks. Results showed an UC strength of 35, 60, 42 and 40kPa for sand with 0, 10, 20 and 30% silt respectively. The UC strength was higher when the silt content was 10% and as the percentage of silt increased, the UC strength decreased. The authors claim that, at silt content of 10% the voids between the sand particles are filled with silt and lead to an increasing strength, but as silt particles become abundant, they form a loose bridge between sand grains. Typical results from these tests are shown in Figure 3.5.

An overall review of these results is presented in Figure 2.1 in terms of UC strength (q_u) versus CS(%) concentration. It is observed that for all types of soil, stabilization offers a non-zero strength which increases almost linear as the concentration of CS used increases. Of practical interest are the data for CS≤10%, which correspond to q_u up to 90kPa approximately.

A more recent research was performed by Vranna and Tika (2015) who conducted undrained isotropically consolidated tests on untreated and unconfined compression, as well as undrained consolidated tests on stabilized silty sand specimens. The colloidal silica used was Ludox-SM® at concentrations CS=6% and 10%. The soil used in that study was a silty sand with non-plastic fines content of fc = 10%, Gs =2.653, emax = 0.682 and emin = 0.414, D50 = 0.30mm and Cu = 4.13 and D_r=31-37%. The results of the tests in terms of Mohr circles at peak stress are presented in Figure 3.7 and Figure 3.8 where it is clear that stabilization increases the strength of the stabilized specimens and this increase is due to the increase in both friction angle, but mainly in the apparent cohesion. The same conclusions were drawn by Vranna and Tika (2015b) for clean sand samples stabilized with CS=10% (Ludox-SM®).

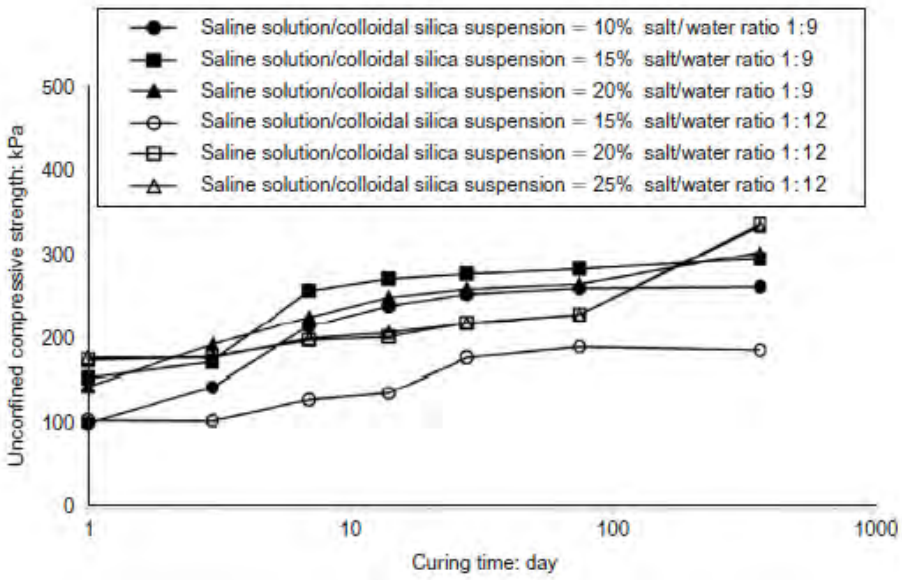

Figure 3.4 *Unconfined compression strengths of stabilized sand (with different CS and salt concentrations) for different curing time* (Mollamahmutoglu and Yilmaz 2009)

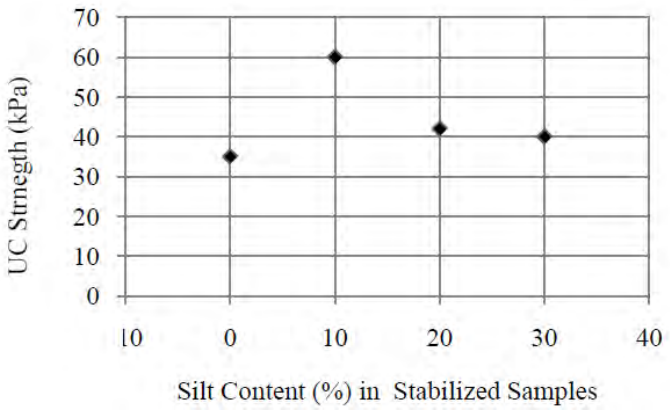

Figure 3.5 *Unconfined compression strengths of stabilized sand with CS=4.5% for different silt contents* (Moradi et al. 2015)

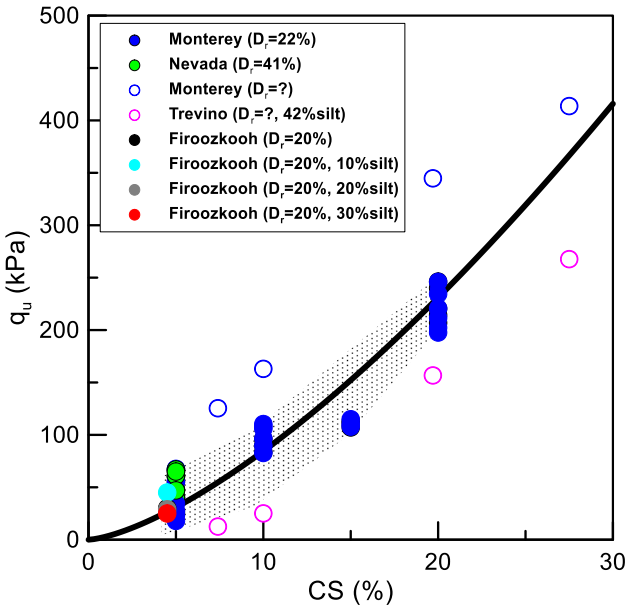

Figure 3.6 *Unconfined compression strength as a function of CS(%) concentration for different sands (data:* Gallagher and Mitchell 2002; Gallagher 2000b; Gallagher et al. 2007a; Persoff 1999; *Moradi and Seyedi, 2015a*)

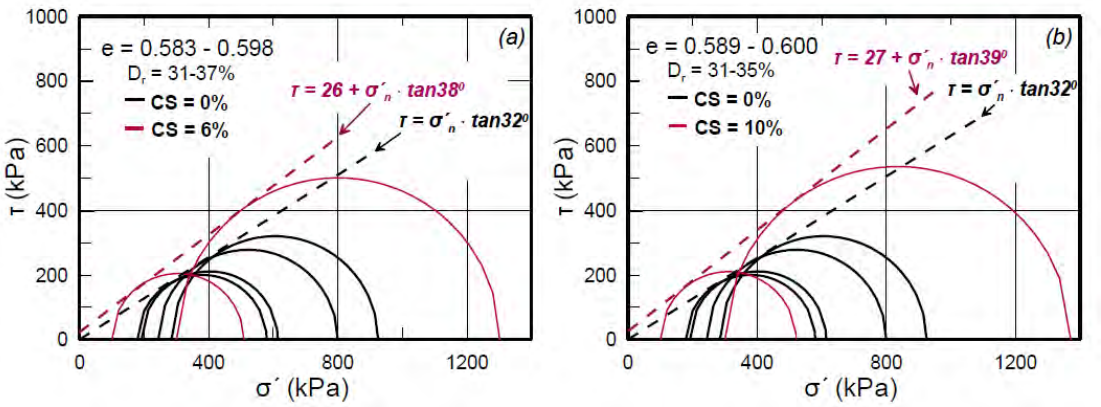

Figure 3.7 *Peak shear strength envelopes for untreated and stabilized specimens with (a) CS = 6% and (b) CS = 10%* (Vranna and Tika 2015a)

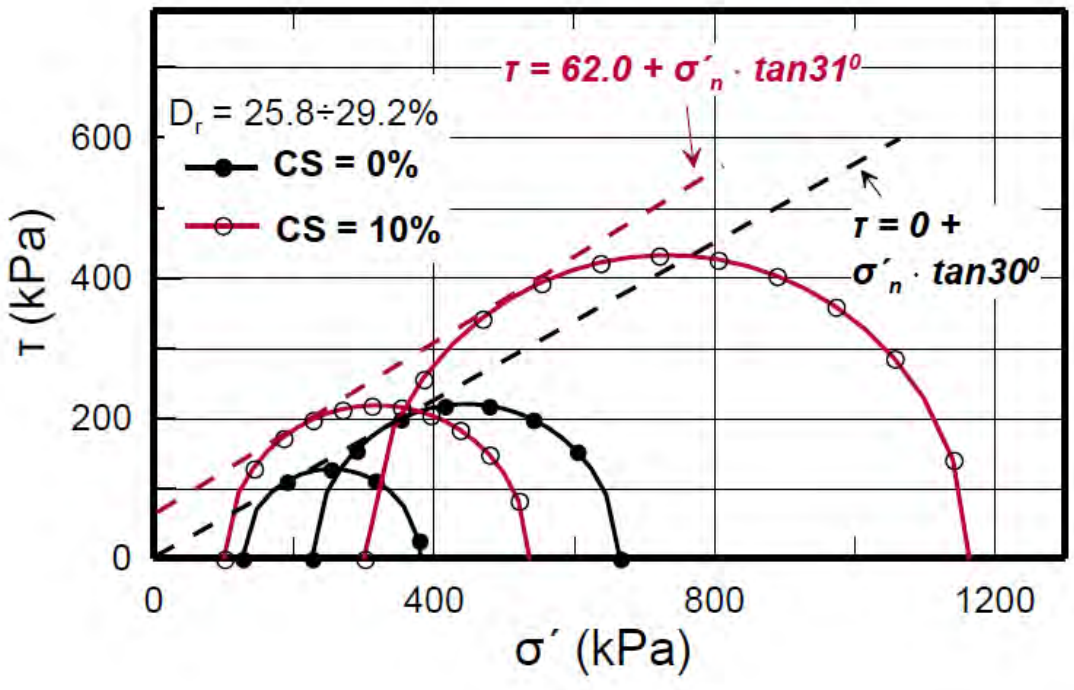

Figure 3.8 *Peak shear strength envelopes for untreated and stabilized specimens with (a) CS = 6% and (b) CS = 10%* (Vranna and Tika 2015b)

From a practical point of view, it is also important to evaluate the durability of passive stabilization, namely the behavior of the stabilized sand after being subjected to cyclic loading, as an indication of its potential degradation. Gallagher and Mitchell (2002) and Gallagher (2000) performed UC tests on Monterey (No30) sand samples (D_r=22%, e=0.75) stabilized with CS(%)=10% Ludox-SM®, which were previously subjected to cyclic triaxial loading. The measured q_u was correlated with the maximum double amplitude (DA) cyclic strain developed during the preceding cyclic loading phase. It should be noted that DA is defined as the

maximum strain difference during a whole compression – extension cycle. Figure 3.9(a) presents this relation of q_u with DA and in Figure 3.9(b) the q_u values of Figure 3.9(a) are normalized with the average q_u of these samples before cyclic loading, noted as q_{max} (DA=0). Observe that stabilized sand seems to retain its q_u value if the maximum DA cyclic strain caused by the cyclic loading is smaller than 1.5%. After this critical value (which corresponds to a high intensity excitation in practice) as the maximum DA strain increases, the post-cyclic q_u value decreases and may reach as low as 40% of the initial (pre-cyclic) strength when the maximum DA strain from the cyclic loading is as high as 5.5%.

Towhata (2007) performed a similar effort by executing undrained monotonic shear tests on samples stabilized with CS solutions of CS=4.5% and 6.5%, which were previously subjected to cyclic loading until a predefined level. As shown in Figure 3.10 these tests show that stabilized sand is stiffer than untreated sand even after cyclic loading has been concluded.

Similarly, Mollamahmutoglu and Yilmaz (2009) performed UC strength tests after their samples were subjected to cyclic loading. The results are presented in Figure 3.11 in terms of q_u versus cyclic stress ratio, CSR, and no significant loss of strength is observed as CSR increases.

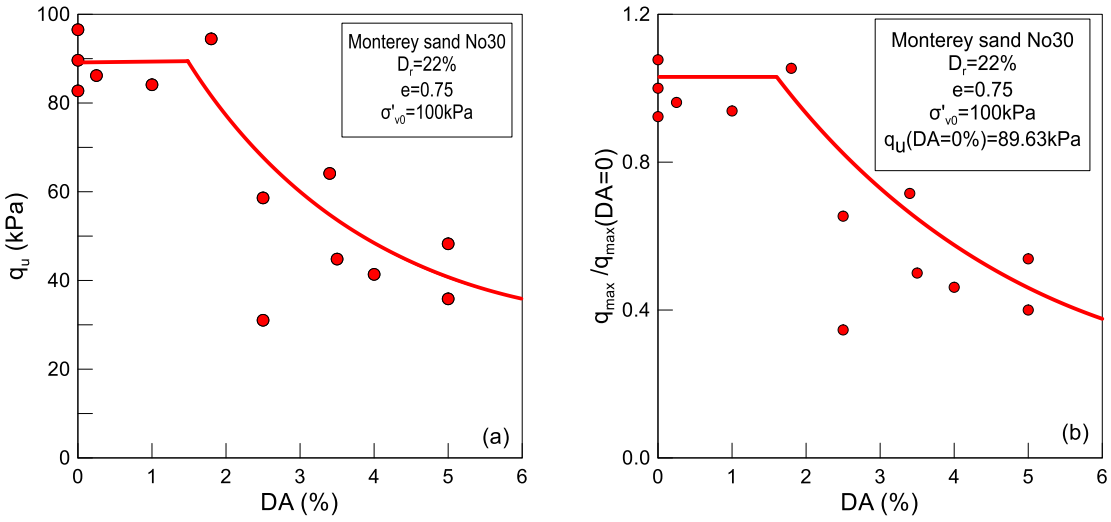

Figure 3.9 (a) *UC strength q_u test results after cyclic loading versus double amplitude cyclic shear strain DA(%) at stabilized samples with CS(%)=10* ***(b)*** *normalized q_u over the average q_u of samples before cyclic loading versus DA(%) of cyclic loading of stabilized samples with CS(%)=10 (data: Gallagher 2000, Gallagher and Mitchell 2002)*

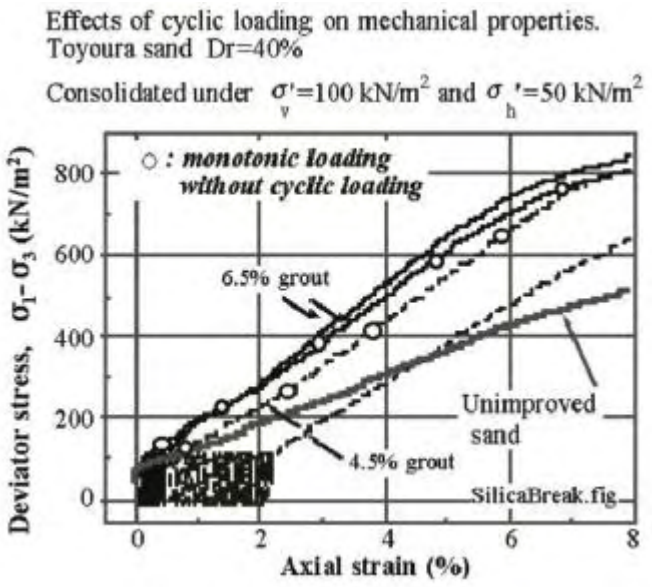

Figure 3.10 *Results from undrained monotonic shear tests for stabilized Toyoura sand samples with CS=4.4 and 6.5% after subjected to cyclic loading* (Towhata 2007b)

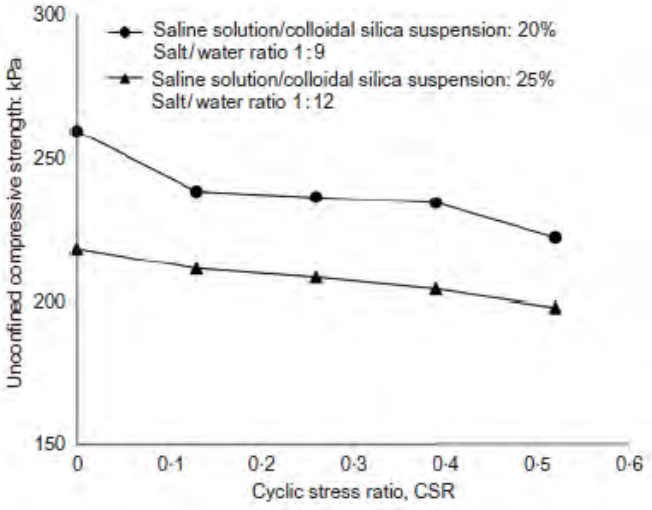

Figure 3.11 *UC strength results after cycling loading on stabilized sand samples in relation with the CSR of preceding cyclic loading* (Mollamahmutoglu and Yilmaz 2009)

3.2 Cyclic behavior of stabilized sands

The improvement mechanism of pore fluid enrichment with CS solutions has not been fully understood microscopically, but results from laboratory experiments systematically indicate the important contribution of CS on the increase of liquefaction resistance of stabilized soils. For example, Gallagher and Mitchell (2002) first presented the results of cyclic undrained

triaxial tests on Monterey 0/30 sand samples with and without the addition of CS solution. Stabilization with Ludox-SM® led to a significant increase of liquefaction resistance in comparison with untreated sand samples. Figure 3.12 (a) and (b) present the axial strain evolution during cyclic loading for stabilized and untreated sand samples respectively. Stabilized sand samples developed double amplitude axial strain DA=5% after 12 loading cycles and at the 13th cycle they essentially collapsed. On the contrary, stabilized sand samples with CS(%)=10 developed smaller axial strains which accumulated progressively during the cyclic loading.

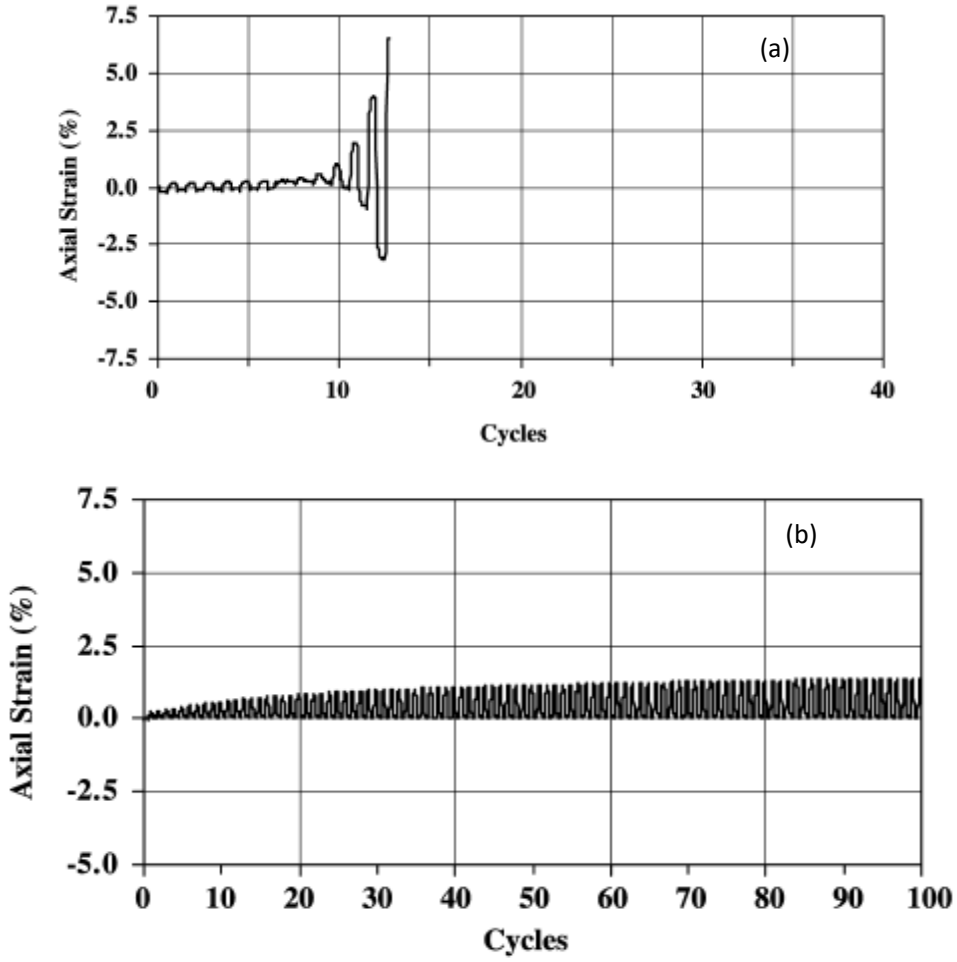

Figure 3.12 *Comparison of axial strain accumulation with loading cycles from cyclic (undrained) triaxial tests with CSR=0.27 on Monterey sand (Dr-22%) (a) untreated, (b) stabilized with CS(%)=10* (Gallagher and Mitchell 2002)

Liao et al. (2003) performed cyclic undrained triaxial tests on sand samples which were taken from a hydraulic fill site in Taiwan. The stabilized sand samples with CS concentration of CS(%)=50 per volume developed liquefaction resistance 4 to 7 times greater than the untreated samples. The effect of treatment with CS on liquefaction resistance further

increased with an increase of curing time. As resulted from undrained triaxial tests performed by Towhata and Kabashima (2001) on Toyoura sand (D_r=40%, e_{max}=1.17, e_{min}=0.77, D_{50}=0.17mm), stabilized samples with CS(%)=4.5 had similar response in terms of strains and liquefaction resistance with this of much denser untreated sands (with relative density of almost 80%).

Kodaka et al. (2005) performed cyclic undrained torsional shear tests on sand samples stabilized with CS(%)=4, the type of which is not defined in the publication (Figure 3.13). They found that stabilized sand develops large strains even at the initial stages of loading, which do not significantly increase as loading continues and do not lead to collapse or cyclic mobility of the stabilized sample, unlike what happens to the untreated sample.

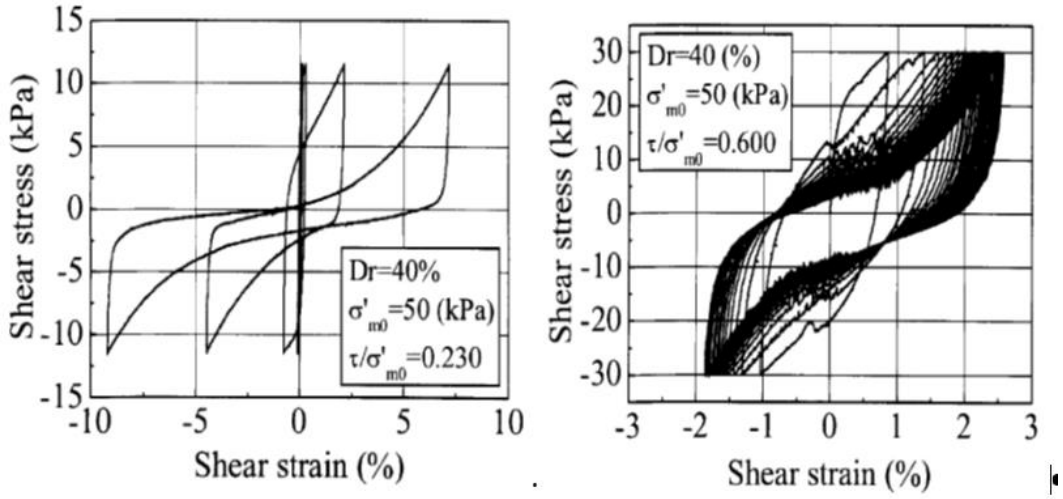

Figure 3.13 *Shear stress – shear strain relation for cyclic undrained torsional shear tests for Toyoura sand (a) untreated (b) stabilized with CS(%)=4* (Kodaka et al. 2005)

Mollamahmutoglu and Yilmaz (2009) performed cyclic triaxial tests on stabilized sand with Meyco MP320 colloidal silica with a concentration of CS=20% and 25% with different salt concentrations. The stabilized sand samples were cured for 28 days and were then subjected to sinusoidal loading with a period of 1s at cyclic stress ratios (CSR) of 0.13, 0.26, 0.39 and 0.52. None of the samples collapsed, even though the loading continued for 1000 cycles. The pertinent results in terms of CSR versus the post-cyclic unconfined compression were presented in Figure 3.11 and are not repeated here.

Corral and Whittle (2007) performed cyclic direct simple shear tests on Nevada sand with D_r=40% after its stabilization with 5% of colloidal silica. They show increased liquefaction resistance of stabilized sand which increases further as curing time increases. Similar results

were presented by Towhata (2007) who showed liquefaction resistance curves for stabilized sand with CS(%)=4.5 (not Ludox-SM®) at DA=2% and 5% and a relative density of 40%. These results (shown in Figure 3.14were compared to the liquefaction resistance curve for untreated Toyoura sand with D_r=50% as reported by Toki et al (1986). It is obvious that for any maximum DA strain value the liquefaction resistance of stabilized sand is significantly increased.

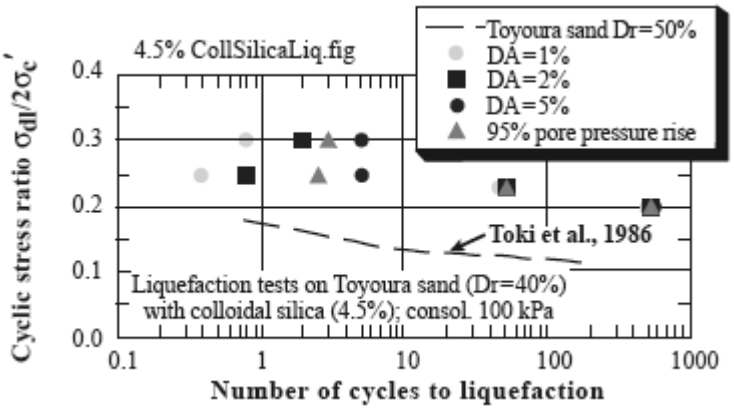

Figure 3.14 *Increase of liquefaction resistance of sand stabilized with colloidal silica* (Towhata 2007b)

Díaz-Rodríguez et al. (2008) conducted a series of 21 cyclic simple shear tests under constant volume on samples of untreated and stabilized Lazaro Cardenas sand, with CS(%)=14.4 (the type of colloidal silica used is not defined). This is a poorly graded sand which contains fines content of 11.5%, and has e_{max}=1.17, e_{min}=0.77, D_{50}=0.17mm. The tests were conducted on samples under different initial conditions, namely different initial vertical stress σ'_{v0} and different initial relative density D_r(%). The results indicate a significant increase of the shear strength of the stabilized samples and a corresponding decrease of excess pore pressure development, leading thus to an important increase of liquefaction resistance. It is worth noticing that CS has a more beneficial effect on sands with small relative densities and large vertical stresses (Figure 3.15), namely it acts more effectively on sands which are most likely to liquefy. On the contrary, the benefit seems to diminish for low vertical stresses and higher densities (Figure 3.16).

A more recent research by Moradi and Seyedi (2015a) showed that untreated samples of Firoozkooh No161 sand with 0, 10, 20 and 30% of non-plastic Firoozkooh silt liquefied under cyclic triaxial loading, developed large deformations when liquefaction was triggered and finally collapsed. The clean sand sample withstood a total of 7 cycles before it collapsed, whereas the samples with silt content collapsed immediately after the 1st cycle. However, at

stabilized sand samples with 5% of Ludox-SM® colloidal silica, axial strain was smaller and none of them collapsed. The results of a clean sand sample are shown in Figure 3.17 in terms of deviatoric stress versus loading cycles for the stabilized sand sample with D_r=20% at CSR=0.2. The corresponding results for the stabilized clean sand sample are shown in Figure 3.18.

Vranna and Tika (2015a,b) performed cyclic triaxial tests on a quartz sand (M31) stabilized with CS (Ludox-SM®). Figure 3.19 presents, the CSR required to reach three levels of ε_{DA} = 1, 2.5 and 5%, for various N values for the stabilized samples at a loose state with CS = 6% (Figure 3.19a) and 10% (Figure 3.19b), under p'_0 = 100kPa. The numbers of cycles required to reach ε_{DA} = 1, 2.5 and 5% are considerably different from each other for both CS = 6% and 10%. Moreover, as observed in Figure 3.20 there is a remarkable increase of the number of cycles for liquefaction for the stabilized samples as compared to the corresponding number for the untreated. In the same figure, it is obvious that the Nl values for samples with CS = 6% and 10% are very similar with each other at high CSR values.

Typical results are shown in Figure 3.21 and indicate that the untreated sand samples experience much larger strain in fewer loading cycles, N, than the corresponding stabilized samples with the same void ratio e = 0.696-0.700 and CSR ≈ 0.43 value under σ′0 = 100kPa.

The same researchers also conducted cyclic tests on quartz silty sand with non-plastic fines content of fc = 10%.sands Figure 3.22 presents the variation of CSR with number Nl for εDA = 5%, for stabilized and untreated samples under p'_0 = 100kPa. There is an increase of Nl for loose stabilized samples with CS = 6%, as compared to the corresponding of the untreated ones. Furthermore, the Nl for samples stabilized with CS=10% is higher and approximately double the corresponding of the untreated specimens.

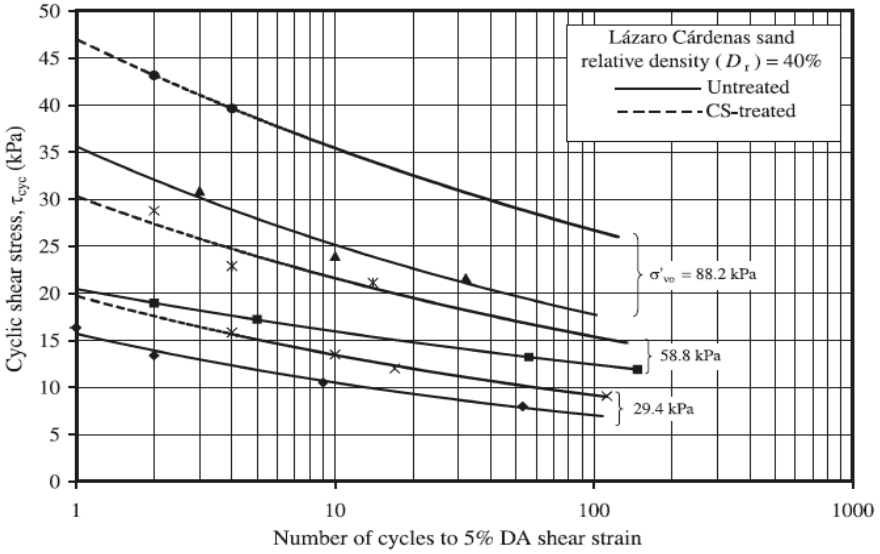

Figure 3.15 *Liquefaction resistance curves of untreated and stabilized with CS(%)=14.5 Lazaro Cardenas sand subjected to cyclic constant volume simple shear tests with Dr=40% and different initial vertical effective stresses (Díaz-Rodríguez et al. 2008)*

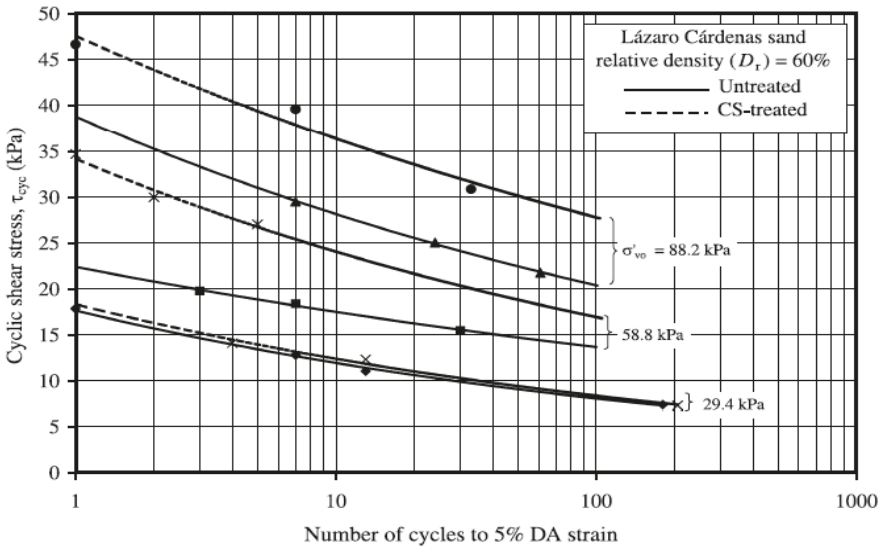

Figure 3.16 *Liquefaction resistance curves of untreated and stabilized with CS(%)=14.5 Lazaro Cardenas sand subjected to cyclic constant volume simple shear tests with D_r=60% and different initial vertical effective stresses (Díaz-Rodríguez et al. 2008)*

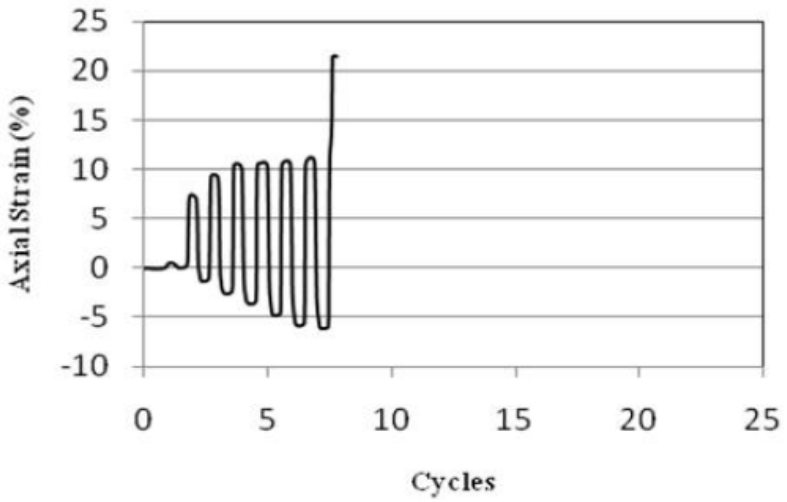

Figure 3.17 *Axial strain during cyclic loading for untreated Firoozkooh No161 clean sand at CSR=0.20 (Moradi and Seyedi 2015).*

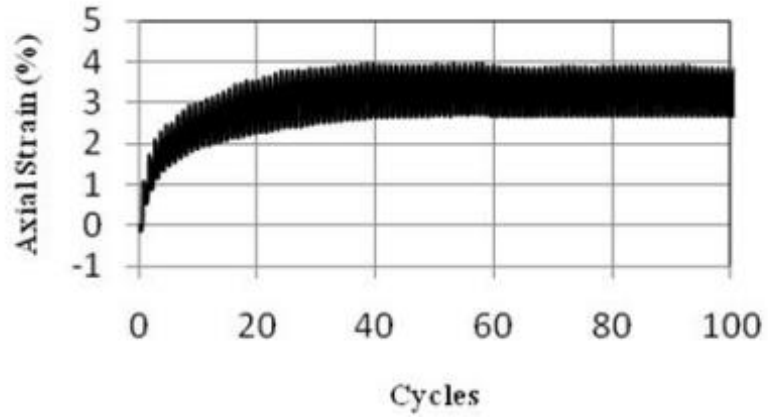

Figure 3.18 *Axial strain during cyclic loading for stabilized clean Firoozkooh No161 sand at CSR=0.20 (Moradi and Seyedi 2015).*

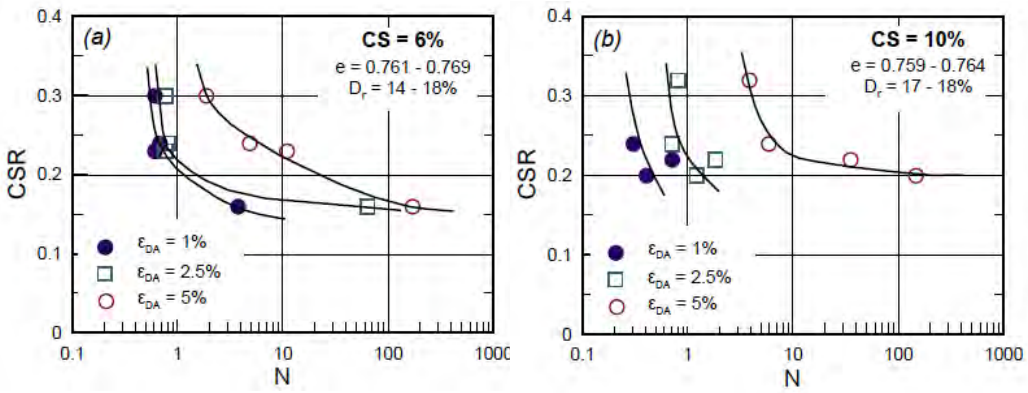

Figure 3.19 *Variation of CSR, with number of cycles N, for stabilized samples with (a) CS = 6% and (b) 10%, at various values of ε_{DA}, at p'_0 = 100kPa* (Vranna and Tika 2015a).

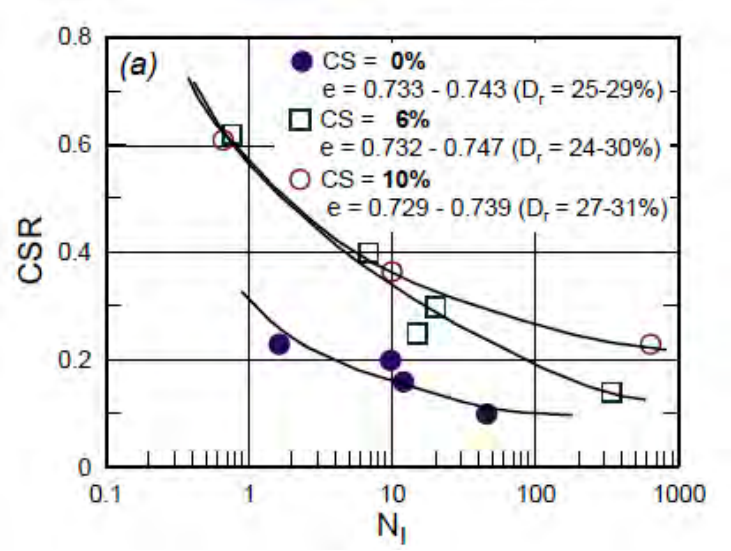

Figure 3.20 *Variation of CSR, with number of cycles, N_l, required for ε_{DA} = 5% for untreated and stabilized with CS=6,10% M31 sand* (Vranna and Tika 2015a).

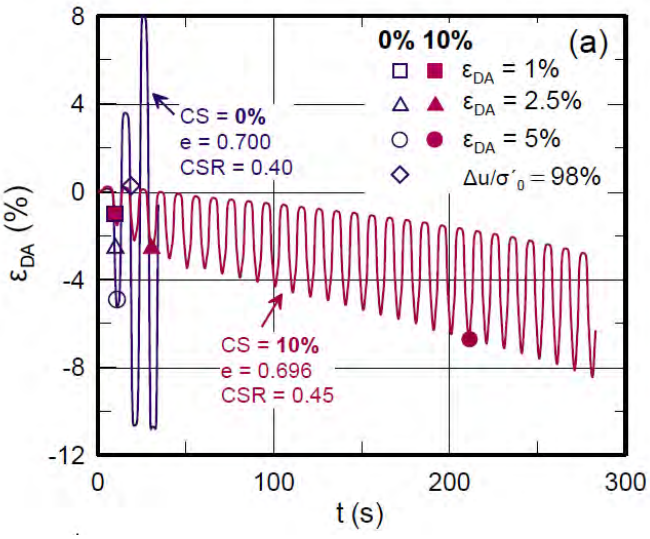

Figure 3.21 *Variation of double amplitude axial strain, ε_{DA} with time, t, for stabilized and untreated sands, for e = 0.696-0.700 and CSR ≈ 0.43 under σ΄0 = 100kPa (Vranna and Tika, 2015b).*

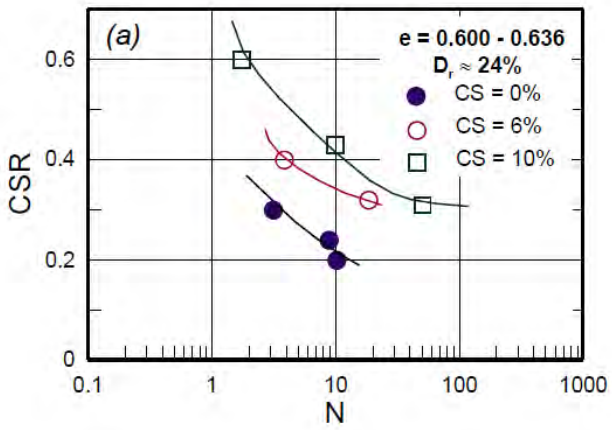

Figure 3.22 *Variation of CSR, with number of cycles, N_l, required for ε_{DA} = 5% for untreated and stabilized with CS=6,10% quartz silty sand.refrenxipkl*

3.3 Dynamic behavior of stabilized soils

In this paragraph the dynamic behavior of stabilized soils will be presented, firstly in terms of the (small - strain) shear modulus G_{max}, as measured from resonant column tests and shear wave velocity measurements of the new geomaterial, and then in terms of the minimum hysteretic damping D_{min} (again at small strains). Then, emphasis will be given on the normalized shear modulus (G/G_{max}) degradation versus cyclic shear strain and also on the corresponding increase of hysteretic damping D.

Spencer et al. (2008) conducted resonant column tests at samples stabilized with CS (%)=5 and 9 using Ludox-SM. A small difference in the shear modulus G with increasing concentration of colloidal silica in the gel-sand mixtures was observed and the shear modulus of all colloidal silica gel-sand mixtures seems to be slightly higher than the shear modulus of untreated sand in the small cyclic strain region, as shown in Figure 3.23. The corresponding damping ratio of stabilized and untreated sand are compared in Figure 3.24. It can be concluded that the effect of introducing colloidal silica into the soil matrix on the damping ratio is negligible.

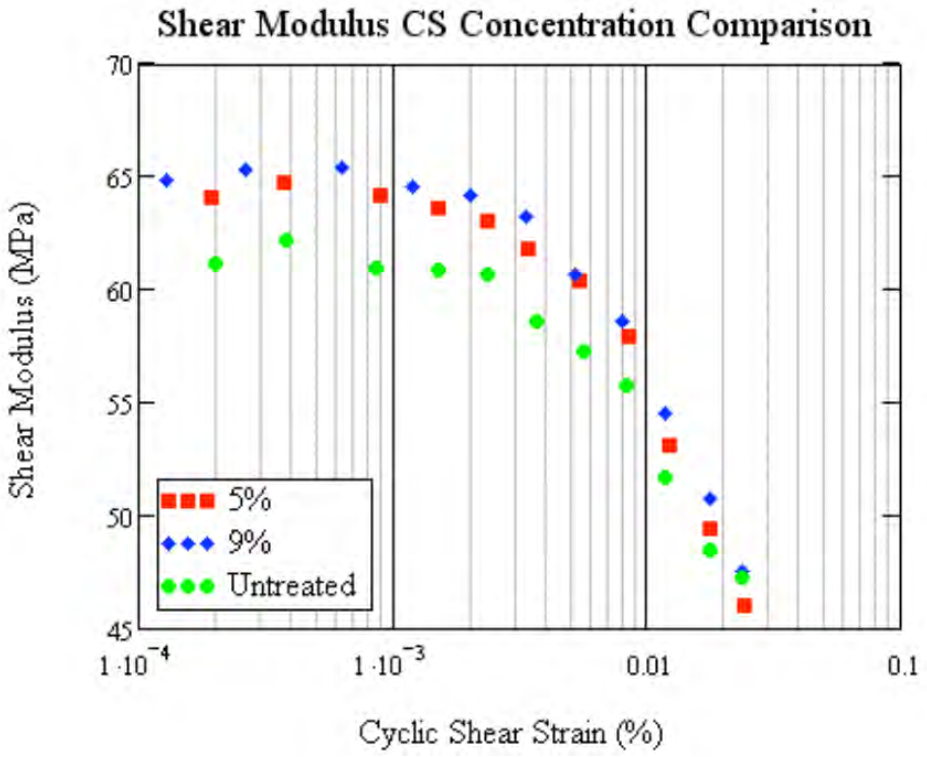

Figure 3.23 *(Secant) shear modulus for stabilized and untreated sand samples of Nevada sand at mean stress 50kPa and relative density 50%* (Spencer et al. 2008a).

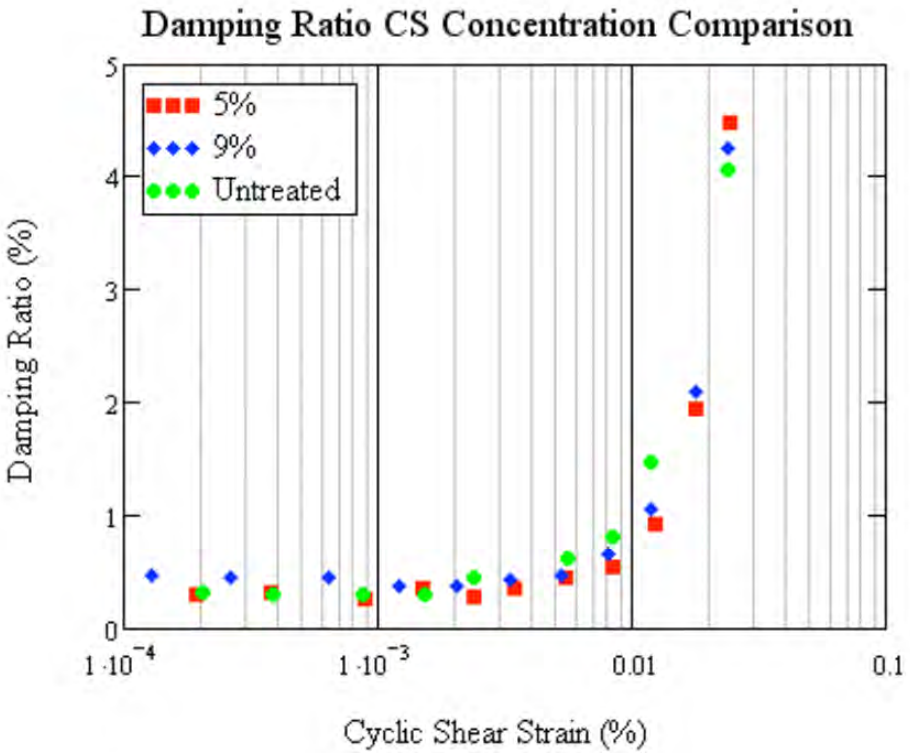

Figure 3.24 *Hysteretic damping ratio for stabilized and untreated sand samples of Nevada sand at mean stress 50kPa and relative density 50%* (Spencer et al. 2008a).

Particularly, focusing on the dynamic response at small cyclic strains, the same data show that stabilization with colloidal silica leads to a generally small increase in the elastic shear modulus Gmax, of 10% on average (Spencer et al. 2008). On the contrary, at medium cyclic strains, the same data show no substantial effect on the normalized shear modulus G/Gmax degradation (Figure 3.25) with cyclic shear strain based on the interpretation of Andrianopoulos et al. (2015), i.e. the stabilization effect may be considered important for G_{max} only.

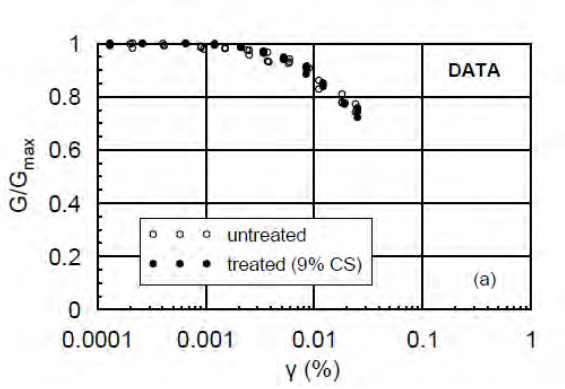

Figure 3.25 *Effect of colloidal silica on the normalized shear modulus G/G_{max} degradation curves with cyclic shear strain level (Andrianopoulos et al. 2015, data from Spencer et al. 2008).*

Conlee (2010) conducted shear wave velocity measurements using pulse wave and bender element testing on Nevada No120 sand with relative density Dr=41% stabilized with different concentrations per weight of colloidal silica (Ludox-SM®). The pulse wave testing was performed within the centrifuge container inflight sand. For example, Figure 3.26 presents the locations of accelerometers in one model configuration (named CTC01), where the left side was stabilized with CS(%)=9 and the right side was left untreated. The measurements resulted from five different pulse waves with different peak base acceleration (PBA) values. The bender element testing was used to estimate the shear wave velocities of the stabilized (and untreated) soils at various depths. Similar measurements were performed in a second model configuration (named CTC02) the left side was stabilized with CS(%)=4 and the right side with CS(%)=5.

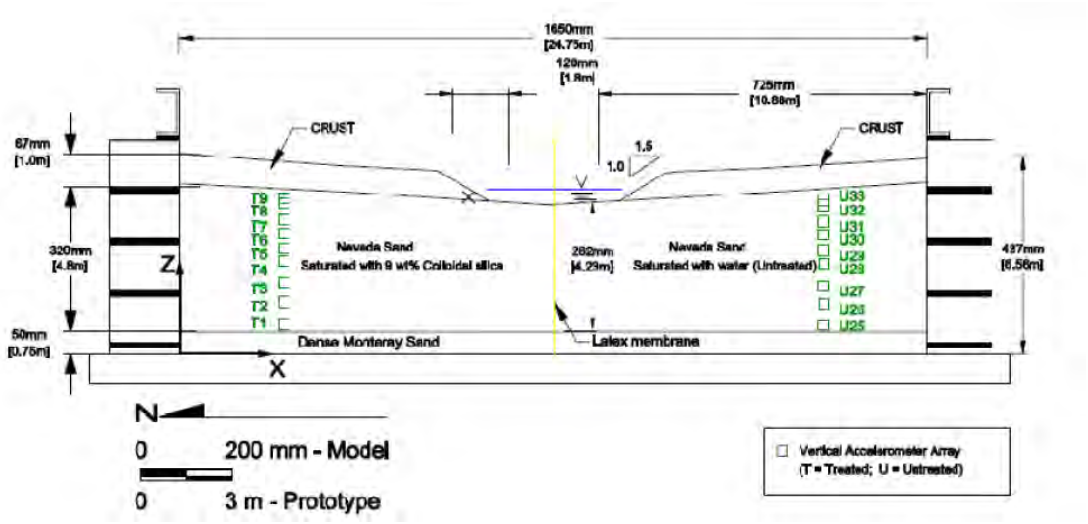

Figure 3.26 *Instrumentation Layout for Pulse-wave testing in CTC01* (Conlee 2010).

In order to make the comparison of the shear wave velocity V_s results of the stabilized and untreated sand more direct, Figure 3.27 shows the comparison of the V_s measurements of the untreated sand versus the corresponding measurements of the stabilized sand at the same depth, assuming different symbols for the different CS(%) concentrations, based on the CTC01 and CTC02 test results of Conlee (2010). Since accelerometers were not all located necessarily at the same depths, the reference V_s values (and depths) were those of the untreated sand, and the corresponding values of stabilized V_s were obtained by assuming linear interpolation (in terms of depth) between measurements slightly above and below. The diagonal line in this diagram corresponds to a fully independent of passive stabilization V_s value. The results indicate a systematic increase of V_s due to stabilization which is approximately equal to 12% (with significant scatter). However, the exact value of CS(%) concentration does not seem to affect the values of V_s, as for CS(%) values of 5 and above the effect of stabilization seems practically the same on the value of V_s at least for CS values up to 9%. Note that this 12% higher V_s corresponds to a 25% higher G_{max} value, thus making the stabilization effect on G_{max} ranging from 10% - 25%.

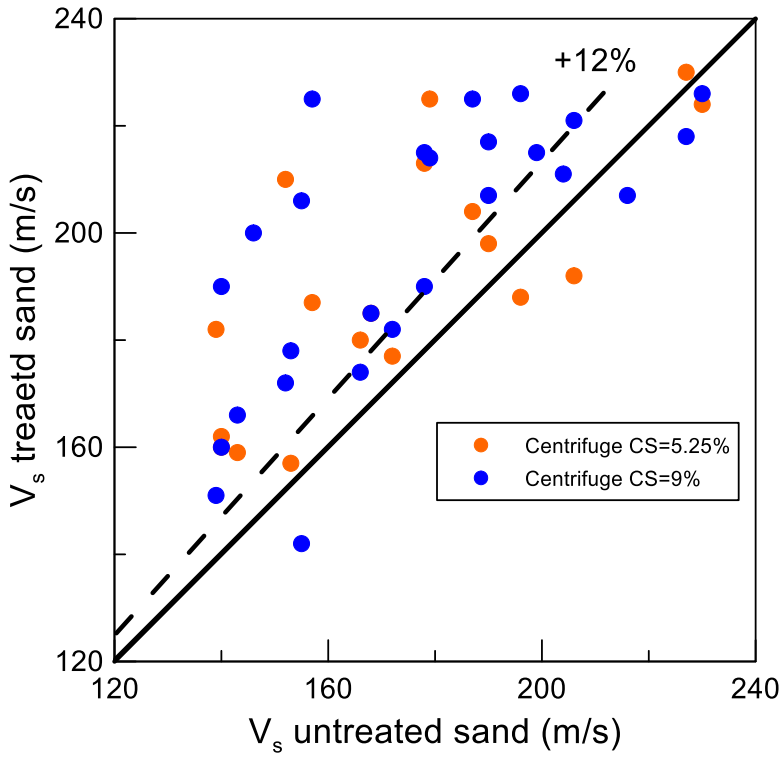

Figure 3.27 *Comparison of V_s values of a stabilized sand (with CS(%)=5.25 and 9) with those of untreated similar sand at the same depths based on the results of Conlee (2010).*

3.4 Centrifuge and field testing of stabilized soils

There are only a few centrifuge and field tests on stabilized sands in the literature, testing their liquefaction resistance. Firstly, emphasis is set on Gallagher et al. (2007a) who performed centrifuge tests using Ludox-SM® colloidal silica with a concentration of CS(%)=6 in order to stabilize a loose horizontal liquefiable Nevada No120 sand layer under two base excitations. The sand layer had a height of 10m in prototype units and was subjected to two (2) seismic excitations with 20 sinusoidal cycles at a frequency of 2Hz with uniform peak ground accelerations of 0.20 and 0.25g (in prototype scale) parallel to the base of the laminar box. It was found that the soil layer stabilized with CS did not liquefy at neither of the two (2) seismic events and the ground motion was amplified at the surface of the layer. For the stabilized sand, measured shear strains reached approximately 1%, while the untreated layer with similar depth and density exhibited shear strain values which ranged from 3% to 5% according to Taboada's results (1986) for base accelerations of 0.23g and 0.25g respectively. For both shaking events the stabilized sand did not liquefy during shaking and did not depict de-amplification of the ground motion; rather it even showed significant amplification after the 3-4 cycles. Settlements of stabilized sand were much smaller than those of the untreated sand

but are not nullified. It should be mentioned that there are uncertainties arising from this experiment, since the settlements developed during the second shaking event (0.25g) were smaller than those developed during the first event of lower intensity (0.20g). The time-histories of these settlements are presented in Figure 3.28.

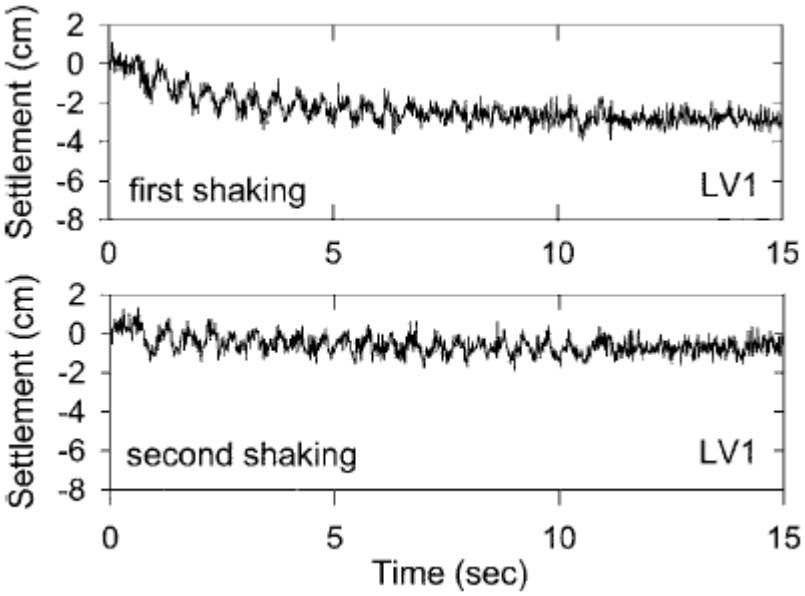

Figure 3.28 *Accumulation of settlements for the first (0.20g) and the second (0.25g) 1D shaking event (Gallagher et al. 2007a) for a 10m-thick stabilized sand layer.*

Conlee et al. (2012) performed two centrifuge set of tests in order to evaluate the effectiveness of CS solutions to mitigate liquefaction at soil layers with a small inclination, at which lateral spreading is highly possible to occur towards a free face. The model consisted of two slopes with a 3^{o} inclination towards a 3m wide central channel. The slopes consisted of three (3) layers with the following properties: (a) a 0.75m bottom layer of dense Monterey No0/30 sand, (b) a 4.8m middle layer of liquefiable Nevada No120 sand and (c) a superficial layer of Yolo loam silty clay which is of low permeability. In the first set of tests, (CTC01) the left slope was stabilized with CS(%)=9% Ludox-SM® and the right slope remained untreated, whereas in the second set of tests (CTC02) both slopes were stabilized with CS(%)=4 and CS(%)=5, respectively. The geometry is indicatively shown in Figure 3.26. Eight (8) sequential base excitations were applied which consisted of 20 sinusoidal cycles with peak accelerations that ranged from 0.007g to 1.3g and had a frequency of 2Hz. The results of the tests indicate that passive stabilization reduces significantly both soil settlement and lateral spreading displacements at soil layers with small inclination as shown in the respective time-histories in Figure 3.29.

In terms of accelerations, it was observed that for usual values of peak base accelerations (0.1g<PBA<0.56g), stabilized soils retained their stiffness and strength, in comparison with untreated soil where amplification of the ground motion was observed at the same depth of the layer at the first cycles before liquefaction occurred followed by de-amplification in the subsequent cycles. Based on the acceleration and pore pressure responses the untreated loose sand layer continued to liquefy for successive shaking events. For larger values of peak base acceleration (PBA>0.56g) stabilized soil with CS(%)=4 and 5 also showed amplification of the ground motion, since no liquefaction occurred.

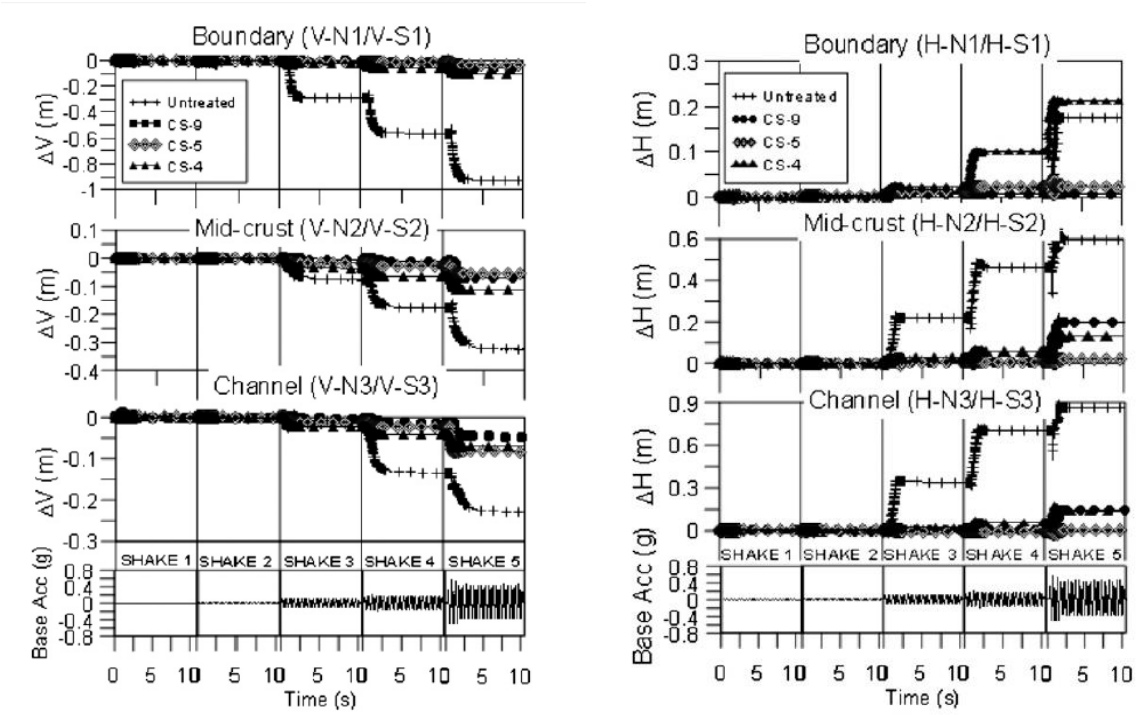

Figure 3.29 *Accumulation of settlements (left) and lateral displacements (right) of the two adjacent banks during the first five shaking events of test series CTC01 and CTC02* (Conlee et al. 2012)

Pamuk et al. (2007) performed two (2) centrifuge tests with centrifugal acceleration of 50g, in an effort to simulate the soil – pile interaction of a 2x2 end bearing pile group embedded on a multilayer soil. In prototype scale, the soil profile included (a) a 2m bottom layer of slightly cemented Nevada sand on which the pile group was founded, (b) a 6m layer of liquefiable Nevada sand with D_r=40% and (c) a 2m superficial layer of slightly cemented sand. The top layer simulated a non-liquefiable layer, where full drainage is allowed and the bottom layer a non-liquefiable medium to dense sand layer. The soil had an inclination of 2^o to the horizontal, which corresponds to 5^o in prototype scale. The piles had a diameter of d=0.6m, stiffness equal to EI=8000kNm^2, were spaced at a distance of 3d and founded on the bottom layer. The pile

cap had dimensions of 3mx3mx0.7m and was placed on the upper layer. The geometry and instrumentation of the test is presented in Figure 3.30. In the first test (model 1), the liquefiable Nevada sand layer remained untreated and in the second test it was stabilized with CS(%)=5, Ludox-SM® (model 2). A significant reduction of lateral displacements was observed in both free field and at the foundation of the pile group, as shown in Figure 3.31. The bending moments and axial forces of the piles were also reduced, since the stabilized sand did not liquefy contrary to what occurred in the untreated sand layer.

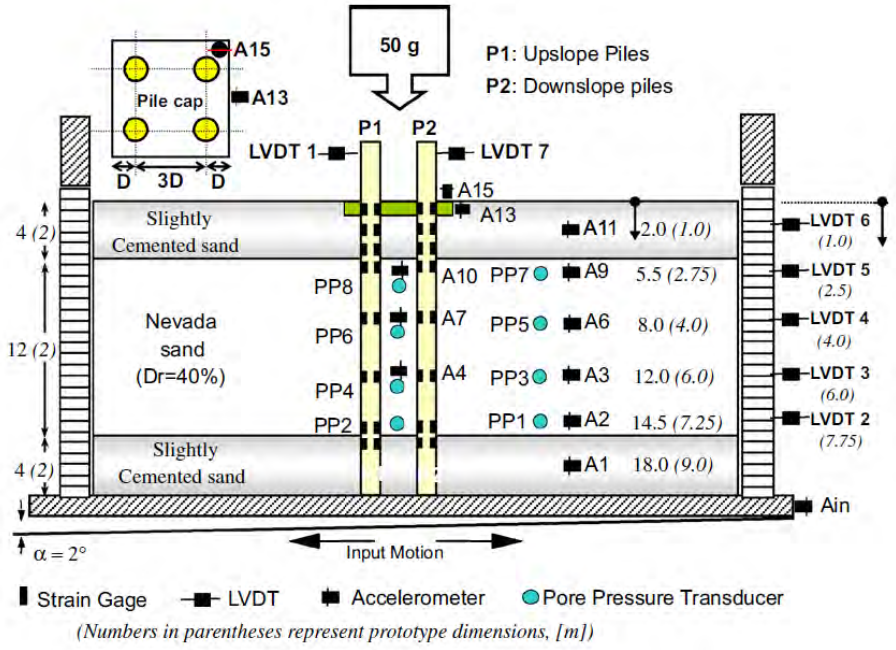

Figure 3.30 *Geometry and instrumentation of the centrifuge model* (Pamuk et al. 2007)

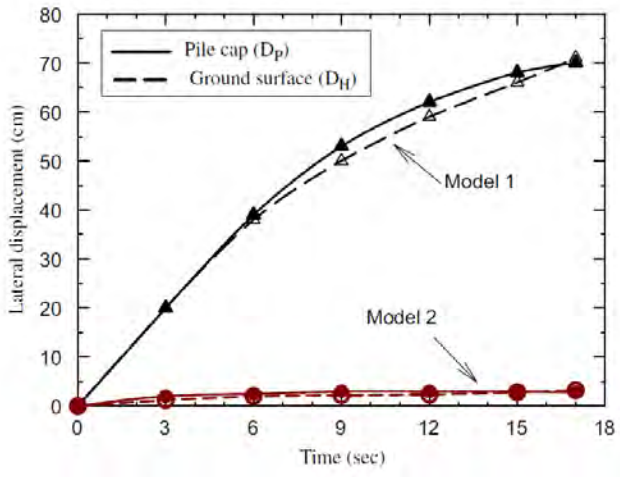

Figure 3.31 *Comparison of lateral displacements on free ground surface and on the pile cap for untreated (Model 1) and stabilized with CS(%)=5 Nevada sand (Model 2)* (Pamuk et al. 2007)

Finally, Gallagher et al. (2007b) performed a full-scale field test in order to investigate the ability of a CS solution to be properly injected in situ and thus reduce the liquefaction induced settlements of a soil layer subjected to a dynamic excitation. They injected a CS(%)=7 solution using a central extraction well and eight (8) equally spaced injection wells at a 9m diameter. The treatment area layout is shown in Figure 3.32. For the permeation of the grout a 2-stage bottom up process was used and the injection rate was approximately 13L/min. The upper one third of a 10m soil layer was stabilized with CS and was subjected to blast induced liquefaction. The results showed a reduction of settlements at the surface of the layer. However, results from CPT and shear wave velocity profiles showed that the cone tip resistance, friction ratio and shear wave velocity were not improved due to stabilization, thus posing a problem for depicting the quality of application of passive stabilization in situ with these methods.

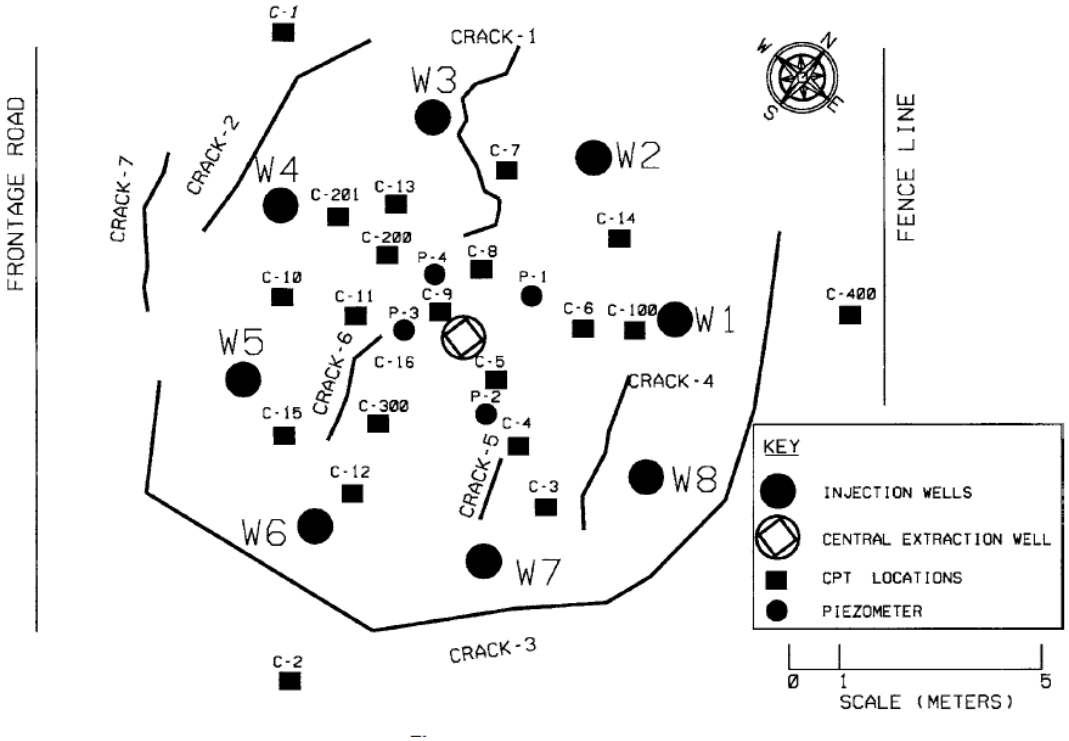

Figure 3.32 *Treatment area layout for the in situ CS injection test* (Gallagher et al. 2007b).

3.5 Numerical simulation of stabilized sand response

This paragraph outlines the single attempt in the literature to numerically simulate the response of stabilized sands. As previously mentioned, the improvement mechanism of pore fluid enrichment with colloidal silica has not been microscopically understood. The mechanical response of stabilized sands has been studied only macroscopically via the tests summarized

in paragraphs 3.1 to 3.4 above. The only effort to simulate the response of stabilized soils was done by Kodaka et al. (2005), who extended an existing elastoplastic constitutive model for sands proposed by Oka (1993) using the work of Adachi and Oka (1993) for soft rocks in order to simulate the seemingly increased "cohesion" resulting from stabilization. The results of the element tests were satisfactorily simulated at least qualitatively, whereas, quantitatively, smaller deformations were simulated for the stabilized soil compared to the laboratory data. More specifically, their numerical simulation was able to simulate both the shear strength increase of the stabilized soil and the shear strain accumulation which occurs when the stress path reaches the Phase Transformation Line (PTL).

In the same publication, a 33.48m sand column was simulated with a typical soil profile of Tokyo Bay. The upper 3.28m of this layer consist of alluvial liquefiable sand and the simulation was performed using the model constants which were calibrated from the element tests. The results of the numerical simulation showed that within the stabilized sand layer, excess pore pressure development is less intense and finally significantly smaller than that of untreated sand as shown in the time-histories of excess pore pressure ratio of Figure 3.33. Moreover, the same analysis shows that the acceleration time histories at various depths of the soil column, a small amplification is to be expected at the surface of the stabilized sand column, contrary to the liquefaction – induced de-amplification of the untreated layer as depicted in Figure 3.34.

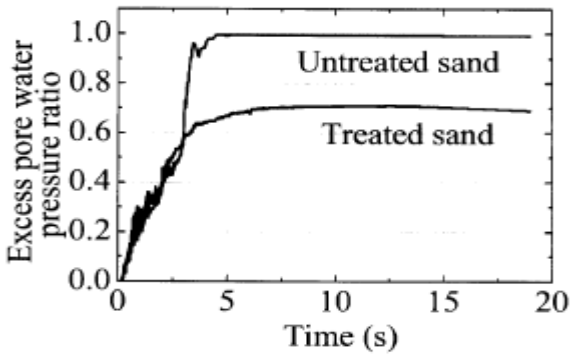

Figure 3.33 *Excess pore pressure development from numerical simulation for stabilized and untreated sand at 4.98 m depth from the surface* (Kodaka et al. 2005)

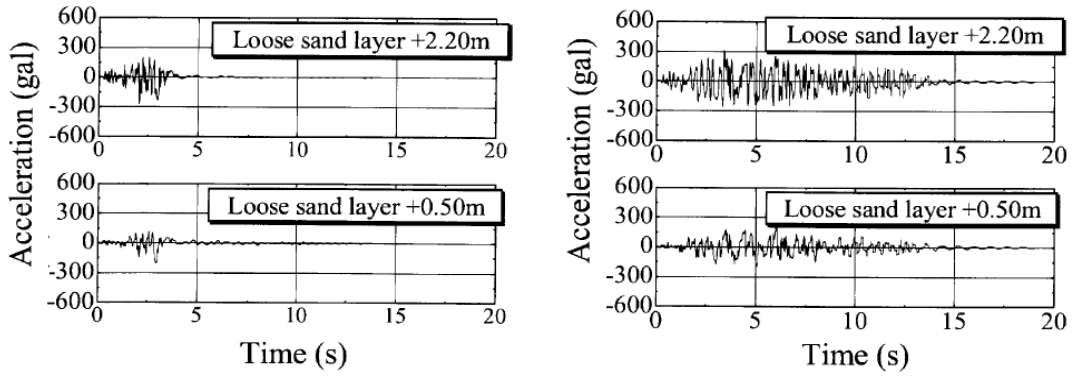

Figure 3.34 *Acceleration time-histories as resulted from numerical simulation of the liquefiable soil for untreated (left) and stabilized (right) cases* (Kodaka et al. 2005)

Chapter 4

VISCOSITY MEASUREMENTS OF COLLOIDAL SILICA SOLUTIONS

4.1 General

The rheological properties of colloidal silica (CS) dispersions, as discussed in previous chapters, make them very attractive stabilizers for the application of passive site stabilization. Their low initial viscosity values, which make them easily injectable and the convenience of achieving the desirable gel times are two of the main advantages of using CS as a stabilizer. The importance of understanding the rheological behavior of CS has led many researchers to conduct viscosity measurements of different CS dispersions and study the effects of different parameters on gel time, as mentioned in Chapter 2. In an effort to further extend the existing data and account for new parameters which significantly affect the evolution of CS viscosity, a wide range of viscosity measurements has been conducted at the University of Thessaly (UTh), Greece, as a part of this Thesis, all for the selected type of CS named Ludox-SM® (see rationale in Chapter 1).

As deduced from Chapter 2, different gel times can be achieved by altering the basic properties of the CS solutions: colloidal silica concentration per weight CS (%) in the solution, pH value, and cation normality N (NaCl in this Thesis). As will be shown here, the results presented herein concur with the literature but also highlight another important parameter that affects gel time and so far was considered negligible, the temperature T of the solution. Viscosity measurements at different temperatures T showed its important effect on the gel time of CS solutions, and this may prove a critical factor if one considers applying passive stabilization in situ (where the temperature remains fairly low, approximately 15^{o}C, below room temperature usually).

In addition, a statistical analysis of a large dataset of viscosity measurements at different temperatures enabled the proposal of a set of design charts and equations for predicting gel time and the viscosity versus time relation of CS solutions (Ludox-SM®). Emphasis is given on different parameters and how they influence gel time, as well as to a comparison of the laboratory data with the literature.

4.2 Equipment – materials – methodology

Viscosity measurements were performed at the Laboratory of Geotechnical Engineering at the University of Thessaly (UTh) in Greece, and are focused on Ludox®-SM, possibly one of the finest types of colloidal silica (CS) in the market (mean diameter of 7nm) for the reasons outlined in Chapter 1. The basic properties of this type of CS are outlined in Table 1-1.

Table 4-1 *Properties of colloidal silica solution Ludox-SM ® (Gallagher, 2000)*

	Ludox-SM
SiO_2/Na_2O (by weight)	50
Stabilizing counter ion	Sodium
Particle charge	Negative
Silica (as SiO_2), weight %	30
PH	10.0
Viscosity (cP)	5.5
Average Particle Size (nm)	7
Specific Surface Area (m^2/g)	345

In order to investigate all the basic parameters that affect gel time as well as the viscosity versus time curves of CS, a wide range of viscosity measurements were performed by employing a Brookfield LVDV-II+PX rotational viscometer (Figure 4.1). The viscometer uses a UL adapter for the accurate measurement of ultra-low viscosity values. The principal of a rotational viscometer is that the torque (amount of torque resistance measured by a rotating spindle immersed in a material) required to turn an object, e.g. a spindle, in a fluid indicates the viscosity of the fluid. It actually measures the torque required to rotate the spindle in the fluid at a known temperature. In order to decide which speed (in rounds per minute, rpm values) will be used for viscosity measurements a trial and error method was performed. The fluid chosen for this procedure was de-ionized water, because it has a known viscosity, equal to 1cP at 25^{o}C which is near the initial viscosity value of diluted CS solutions (where silica is mixed with de-ionized water). According to Brookfield viscometer's manual, an appropriate selection of the speed that will be used will result in measurements made between 10 and 100 on the instrument % torque scale. In practice, when applying a specific speed to the spindle, if the reading of the torque on the viscometer is below 10% or above 100%, then the user must choose another speed to obtain a reading in the recommended range. Considering that, viscosity range is inversely proportional to the rotational speed, the results of this process are shown in Figure 4.2, where the torque (%) and the measured viscosity (cP) of de-ionized water are plotted against spindle speed (rpm) in the same diagram. The right y-axis shows the

viscosity values, which correspond to the red line in the diagram, whereas, torque (%) is shown in the left y-axis and is presented by the blue continuous line in the chart. The blue shaded area shows the acceptable measurements of the torque and the red dashed line the viscosity value of water (=1cP). A speed of 40rpm, seems to offer the best results, as it measures a viscosity value equal to 1.03cP and the torque is 11%, a value within the recommended range. Higher spindle speeds offer acceptable values of torque but not acceptable values of viscosity, whereas lower spindle speeds are out of the acceptable torque range. When measuring the viscosity of CS dispersions, the deviation of the measurements at different rpm values becomes smaller, and negligible when the viscosity increases to almost 3cP, as shown in Figure 4.3, where the spindle speed effect on viscosity of a typical CS dispersion is studied. This procedure shows the sensitivity of viscosity measurements at very low values, and how rpm > 100 may lead to unrealistic values of initial viscosity of CS solutions. Also note, that the calibrated use of 40 rpm for low viscosities required to be reduced when the CS viscosity reached high values (e.g. 100cP), in order to retain the torque within the acceptable range according to the user's manual of the equipment.

Figure 4.1 *Brookfield LVDV-II+PX rotational viscometer at the University of Thessaly.*

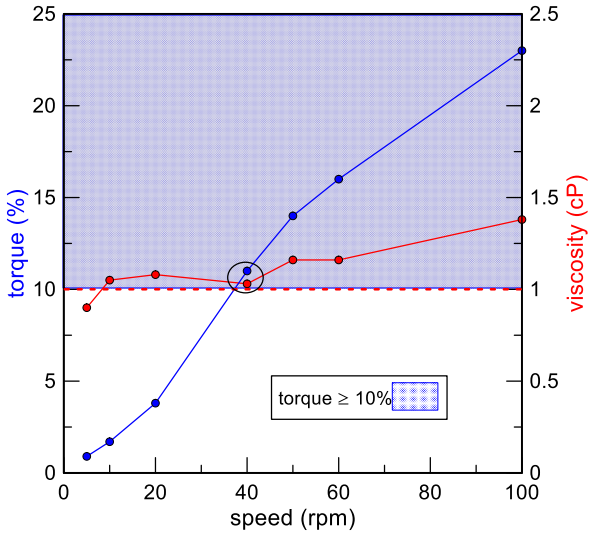

Figure 4.2 *Relation between torque and viscosity measurements at different rpm values using the viscometer of Figure 4.1.*

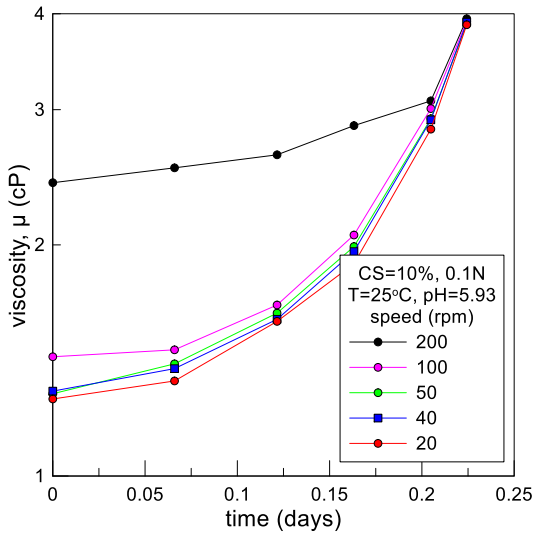

Figure 4.3 *Spindle speed effect as viscosity evolves for CS= 10%, 0.1N, pH=5.93 solution at T=25°C.*

A Brookfield TC-150 water bath was used for retaining constant temperature, which is shown in Figure 4.4. All materials used for the CS dispersions were placed in the water bath before mixing, in order to obtain correct measurements at the initial stages of viscosity evolution. The connection of the water bath with the viscometer was achieved with the assembly presented in Figure 4.5 by circulating water around the black cylinder, within which, the guardleg is placed and the viscosity is measured, by mounting the UL adapter for very low viscosities.

Figure 4.4 *Brookfield TC-150 water bath at the University of Thessaly.*

Figure 4.5 *Connection of water bath to viscometer.*

The Ludox®-SM colloidal silica used herein is a Sigma-Aldrich® product, which is commercially available at a concentration of CS=30%, pH value approximately equal to 10 and a density of 1.22 g/mL at 25°C. CS dilution was achieved by adding deionized water until the desired CS(%) per weight. The pH of the solution was adjusted by adding small quantities of hydrochloric acid (HCl), product of Sigma Aldrich®, with a concentration of 37%, molecular weight MW=36.46g/mole and density 1.20 g/ml at 25°C. The quantity of the added HCl is not considered important, because its weight was negligible in relation with the total weight of the final CS solution. The pH values were measured, using a Metrohm mobile pH-meter, type 826. The salt used for increasing the ionic strength of the final solution was pure sodium

chloride, NaCl (>99.8% purity), product of Sigma-Aldrich® with molecular weight of 58.44mole. The salt concentration was measured in terms of normality, which means that the content of the solution in sodium chloride equal to 1N corresponds to 58.5g in 1lt of solution. Sodium chloride (NaCl) was chosen instead of other salts (for example $CaCl_2$) because it is commonly found in nature and particularly in underground water tables at sites near the sea, where passive stabilization has the potential to be used as a ground improvement method. For the measurement of the quantities of the materials required for the preparation of the solutions a scale of two-decimal accuracy was used (accuracy of ±0.01 gr). When the prepared CS solution reached the desirable values of pH and NaCl concentration, a 60mL sample was removed and the remaining solution was lowered to the next target pH following the same procedure of adding HCl.

A total of 61 colloidal solutions were prepared and their viscosity versus time curves were measured. It should be mentioned that before preparing these 61 solutions, more CS solutions were prepared but temperature was not measured because its effect was not initially considered important based on the literature. Moreover, the spindle speed was set to 200rpms following literature guidelines and the initial viscosity measurements cannot be considered accurate. Only the solutions which take into account the temperature effect and their viscosity was measured with the right spindle speed will be presented hereafter. These solutions cover a wide range of pH values, from 3 to 7.5, three different NaCl concentrations of 0, 0.03 and 0.1N, three different CS (%) concentrations of 5, 7.5 and 10 (and two more samples with CS concentrations of 6.75% and 8.25% at specific pH and N values so that enough CS (%) concentrations have been tested and a safe conclusion of CS effect on gel time can be deduced) and four different temperatures (25 ^{o}C, 20^{o}C, 15 ^{o}C, 5^{o}C) for a limited subset of CS (%), pH and N values The overview of the CS solutions for T= 25^{o}C is presented in Table 4-2, while the overview of CS solutions at T< 25^{o}C is presented in

Table 4-3 . In all tested cases, the gel time ranged from a few hours to almost a month, thus covering practical applications of passive stabilization. This range is an outcome of the selected range of variation of the controlling parameters, for which the following should be noted:

- values of CS lower than 5% do not lead to firm gels, while values larger than 10% are rather costly and unnecessary for passive stabilization (Gallagher and Mitchell 2002)
- pH values lower than 3 and higher than 8 lead to very high gel times, which would not be used in the practice of passive stabilization,

- higher values of NaCl concentration are physically possible, but would not be used in practice since they would lead to very small gel times (in the order of hours, for the CS values of interest)
- temperature below 5°C and above 25°C is not usually attained underground and hence of interest for passive stabilization.

Table 4-2 *Properties of CS solutions tested at T = 25°C (total number of tests 40)*

CS(%)	NaCl concentration (normality, N)	pH range	Number of samples
5	0.03	4.30 – 5.50	3
5	0.1	4.40 – 6.50	5
6.25	0.1	6.00	1
7.5	0	4.40 – 5.70	4
7.5	0.03	4.50 – 6.00	4
7.5	0.1	4.90 – 7.00	5
8.75	0.1	6.00	1
10	0	4.40 – 6.50	5
10	0.03	4.20– 6.50	5
10	0.1	4.50 – 7.50	7

Table 4-3 *Properties of CS solutions tested at T < 25°C (total number of tests 21)*

T	CS (%)	NaCl concentration (normality, N)	pH range	Number of samples
5	10	0.1	5.00 – 7.00	3
15	10	0.1	5.00 – 7.00	3
15	10	0.03	5.00 – 6.00	3
15	7.5	0.1	5.50 – 6.50	3
20	10	0.1	4.40 – 6.00	3
20	10	0.03	4.80 – 6.00	3
20	7.5	0.1	5.50 – 6.40	3

4.3 Controlling parameters of CS rheology

From the previous sections of this Thesis it has become evident that the gel time of a colloidal silica solution is highly affected by five (5) parameters:

- Particle size of colloidal silica used
- Concentration of colloidal silica in the solution, CS (%), per weight
- Cation (salt) concentration in the solution, in terms of normality
- pH value of the solution
- Temperature of the solution

As stated above, the time required for gelation of a CS solution is called gel time and therefore every solution has its own gel time depending on the above parameters. In this study, gel time will be defined as the time from mixing of the solution to when the viscosity reaches a value equal to or greater than 100cP, because from that time and after, the formation of a firm gel is imminent. This definition agrees with the literature (i.e. Gallagher 2000) and results from the inability to perform viscosity measurements on fully formed gels, at least with a rotational viscometer.

The influence of *particle size* of colloidal silica will not be investigated in this research because Ludox®-SM, with a particle size of 7nm, is used in all the CS solutions tested.

Colloidal silica concentration (per weight) of the solution is one of the most important factors affecting gel time based on the literature (see Chapter 2). In order to quantify its effect, measurements were performed on solutions with different CS concentration, but the same pH, NaCl normality and temperature. Figure 4.6 illustrates the viscosity versus time curves of five CS solutions, with pH= 6.00, salt normality equal to 0.1N, measured at constant temperature of T = 25^{o}C and CS (%) increasing gradually from 5% to 10%. These concentrations were chosen because they are cost-effective and can adequately improve the mechanical characteristics of a liquefiable soil. A monotonic effect of CS (%) on gel time is clearly indicated from this figure. The solution with the smaller CS(%)=5 leads to a gel time equal to 1 day and this gel time decreases to 0.22 days as CS(%) is increased by two times. The intermediate CS concentrations give gel times between these two ultimate values.

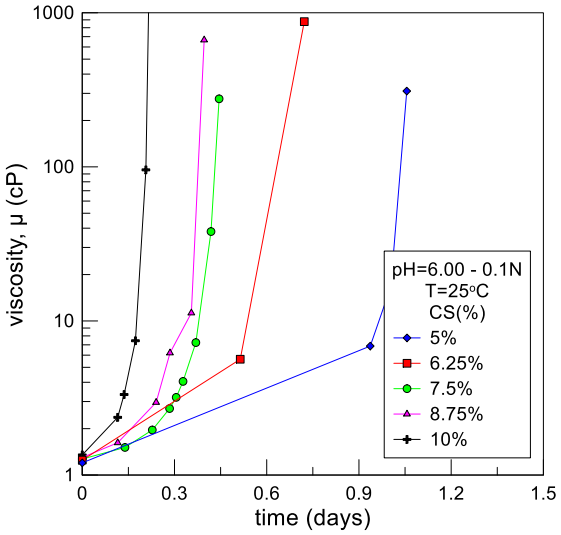

Figure 4.6 *Typical effect of CS (%) on the viscosity versus time curve of CS solutions (pH=6.00, 0.1N, 25°C)*

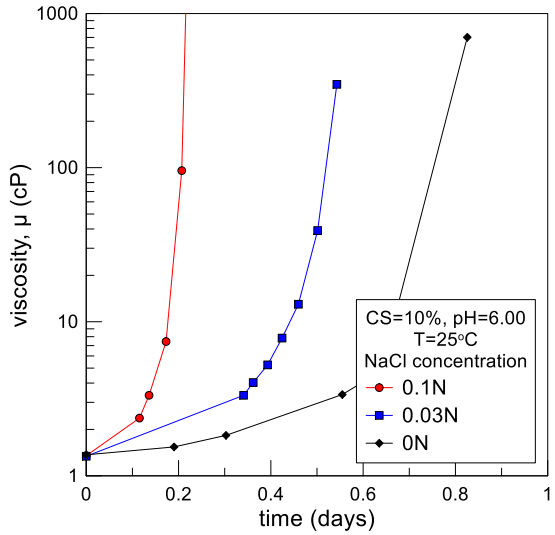

Figure 4.7 *Typical effect of NaCl concentration on the viscosity versus time curve of CS solutions (pH=6.00, CS= 10% , 25°C)*

The influence of *NaCl concentration* on gel time is shown in Figure 4.7 where viscosity versus time curves of three solutions with different normalities, but the same CS (%), pH and temperature are presented. More specifically, the properties of these three CS solutions are: pH=6.00, CS (%) =10, at T = 25°C and their normalities equal to 0, 0.03, 0.1N. A monotonic effect of NaCl concentration is also observed herein, as the solution with the greater salt normality leads to a fairly lower gel time. As the salt concentration increases, gel time decreases, and a change of normality from 0N to 0.1N can cause a 4-fold decrease on gel time. This monotonic effect was found to hold true for all CS solution combinations measured.

The *pH value* of the solution is a crucial parameter for the gel time. As deduced from Figure 4.8, the pH effect is not monotonic, in contrast to the effects of CS (%) and NaCl normality which have a monotonically decreasing effect on gel time. For CS (%) =5, 0.1N and T = 25^{o}C the minimum gel time occurs at pH=6.00 (a value compatible with the literature), while the pH ranges from 4.23 up to 6.53. In order to have a better understanding of the pH effect on gel time, the so-called "gel time curves" were constructed on the basis of data from the viscosity versus time curves for all combinations of (NaCl, CS(%), T) measured by plotting gel times against the corresponding pH values. Figures 4.9-4.11 show these gel time curves for pairs of (NaCl, CS (%)) equal to (0.1N, 5), (0.1N, 10) and (0.03N, 10) in comparison with the literature results (all our data here are for T = 25^{o}C). It is clear from all three figures that the gel time curve has the shape of a symmetric inverted bell, and this was observed for all (CS, N) combinations outlined in Table 4-2. The small differences between the hereby measured gel times and the literature data may be attributed to the fact that temperature of CS solutions in the literature are not reported and probably was neither kept constant nor measured. However, it may be assumed that literature measurements were conducted at room temperature (approximately 20 - 23^{o}C) and so the slightly higher gel times may be rationally justified.

Another conclusion that can be drawn from Figures 4.9 – 4.11, is that for each (CS, N) combination there is an "optimum" pH value (pH_{opt}), which corresponds to a minimum gel time (t_{gmin}) between the values of pH=5-6. This typical response for all (CS, N) combinations has been explained in the literature (Gallagher 2000) and has been presented in detail in Chapter 2. As an effect, similar gel times can be achieved by using many combinations of (CS, N, T, pH) depending on the needs or limitations at hand.

The full set of viscosity measurements performed in this Thesis can be found in Appendix A, and are not presented in this Chapter which emphasizes on the effects of the controlling parameters.

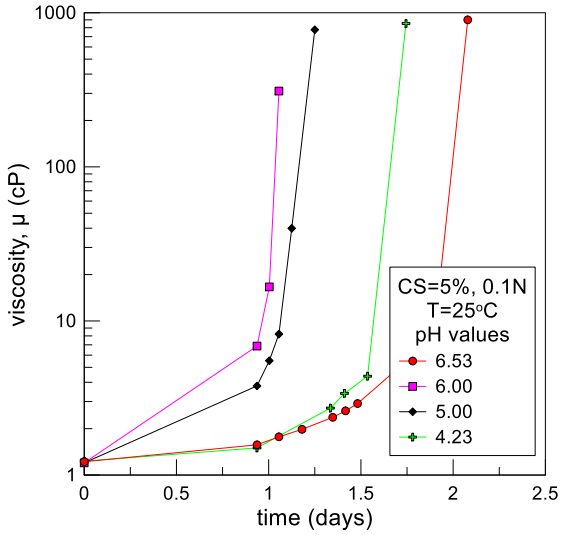

***Figure 4.8**. Typical effect of pH on the viscosity versus time curve of CS solutions (CS= 10% , 0.1N, 25°C)*

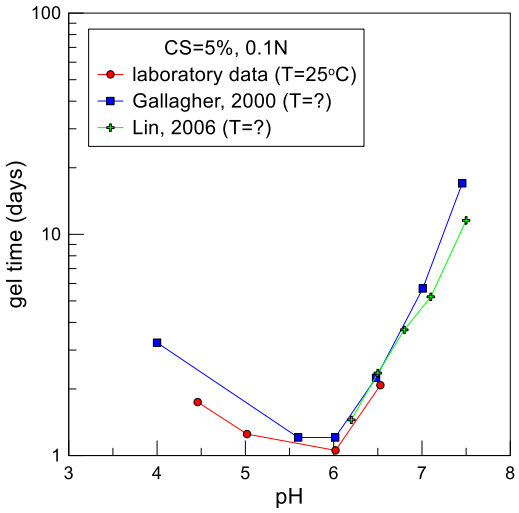

***Figure 4.9** "Gel time curve" for CS=5%, 0.1N, T=25°C and comparison with the literature. (Gallagher, 2000; Lin, 2006)*

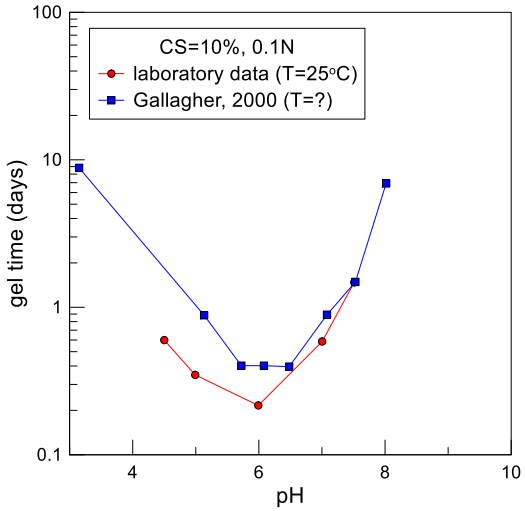

Figure 4.10. *"Gel time curve" for CS=10%, 0.1N, T=25°C and comparison with the literature. (Gallagher, 2000)*

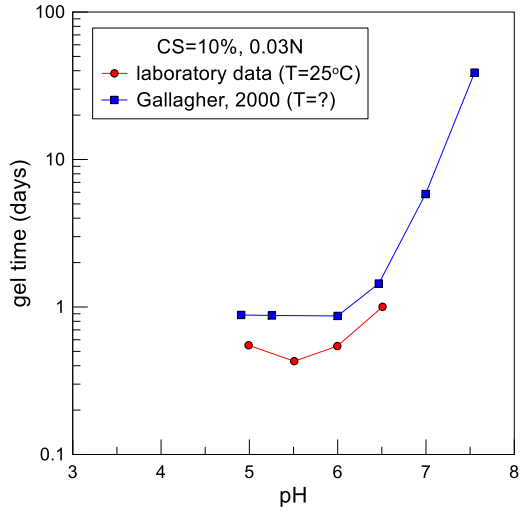

Figure 4.11*. "Gel time curve" for CS=10%, 0.03N, T=25°C and comparison with the literature. (Gallagher, 2000)*

A new parameter systematically introduced herein is the effect of temperature on gel time. Until now, all studies on the rheological behavior of CS solutions that were related to passive stabilization (at least) did not take into account temperature changes and did not mention at which temperature the measurements were conducted. Figure 4.12 shows the importance of temperature T on the rheology of CS solutions. This figure presents the viscosity versus time curves of four CS solutions measured at different temperatures (5°C, 15°C, 20°C and 25°C) and it is clear that when temperature T increases there is a corresponding decrease of gel time. This trend was observed at all pertinent measurements for other combinations of (CS (%), pH and N) and indicates the monotonic influence of temperature on gel time. In Figure 4.13 the

"gel time curves" of three CS solutions with CS (%)=10, 0.03N at temperatures of 15, 20 and 25°C are presented. For CS=10% and 0.03N, a decrease of temperature from 25°C to 15°C is followed by an increase of gel time from 0.43 days to 1.17 days, namely a 2.72 times increase. What is remarkable here is that regardless of temperature, for the same CS solution characteristics, measurements show that the pH value which corresponds to the minimum gel time remains practically the same. Figure 4.14 and Figure 4.15 show the "gel time curves" of CS solutions with CS (%)=10, 0.1N and CS=7.5%, 0.1N, which also lead to the same conclusions. Hence, the value of pH_{opt} for every combination of CS(%), N and T measured ranges from 5-6, in agreement with the literature.

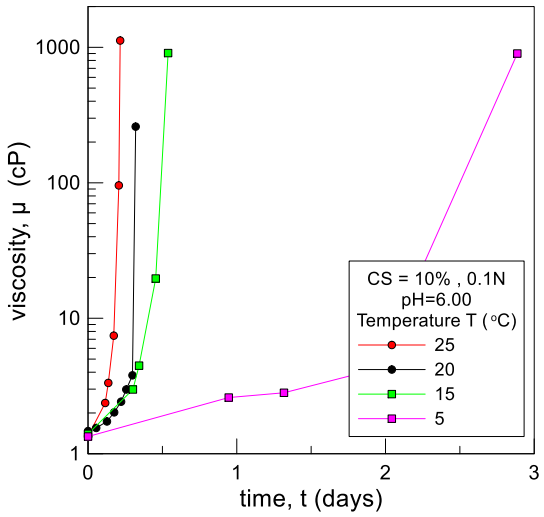

Figure 4.12: *Typical effect of temperature T on the viscosity versus time curves of CS solutions (CS=10%, 0.1N and pH=6.00).*

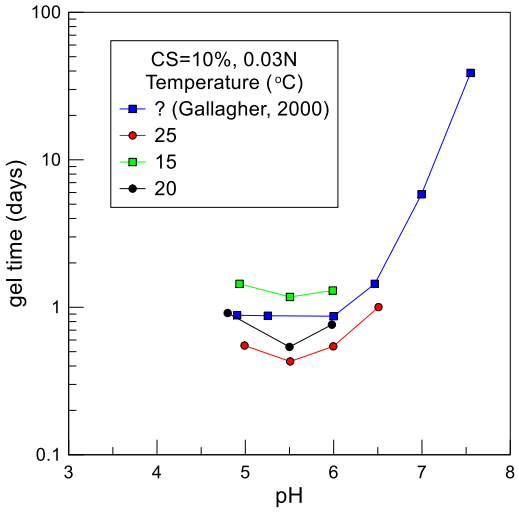

Figure 4.13 *Effect of temperature T on "gel time curves" of CS solutions with CS=10% & 0.03N, and comparison to literature data (performed at unknown room temperature).*

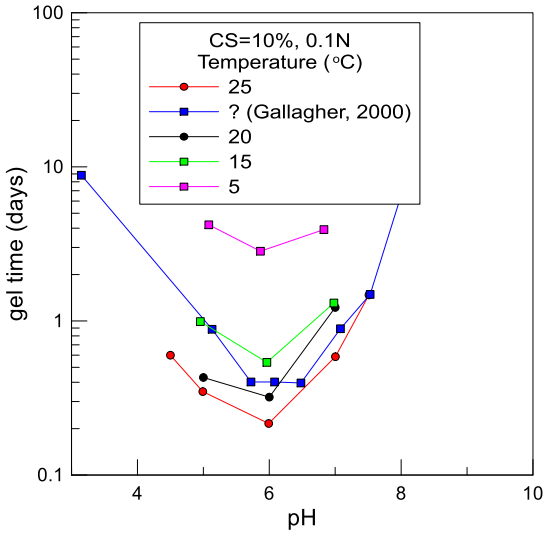

Figure 4.14 *Effect of temperature T on "gel time curves" of CS solutions with CS=10% & 0.1N, and comparison to literature data (performed at unknown room temperature)*

4.4 Gel time of colloidal silica solutions

The effectiveness of passive stabilization relies on the proper delivery of CS solutions at the target location at the appropriate time. If the solution gels prematurely, then the solution will not reach the target location. On the contrary, if the solution gels after the expected time some material will have been injected in vain thus increasing the cost.

Aiming to predict correctly the gel time, all the controlling factors that affect CS rheology, must be taken into account. Hence, this paragraph presents a statistical evaluation of the gel time measurements with the obvious task to propose an approximate methodology for predicting gel time. In order to find a simple way to predict the gel time of different CS solutions, all laboratory data were first gathered in one plot, illustrated on Figure 4.15. It is obvious that the range is huge and requires a methodology of considering the effects of the controlling parameters.

Hence, in this effort, Figure 4.16 presents the minimum gel times (t_{gmin}) measured at different NaCl normalities as a function of CS (%), at the corresponding pH_{opt} for each case, for solutions tested at T = 25°C. The monotonic effects of both CS(%) and NaCl normality become clear in this figure. Particularly, the CS (%) concentration seems to affect more gel time, as a twofold decrease of CS (%) from 10% to 5% is followed by an eightfold increase in gel time. In terms of NaCl normality, the gel time is not so dramatically affected, since an increase from 0.03N to 0.1N leads to an approximately 3.3 times smaller gel time. Minimum gel times of CS

solutions measured at other temperatures are not presented here, because the effect of temperature T is considered in the sequel.

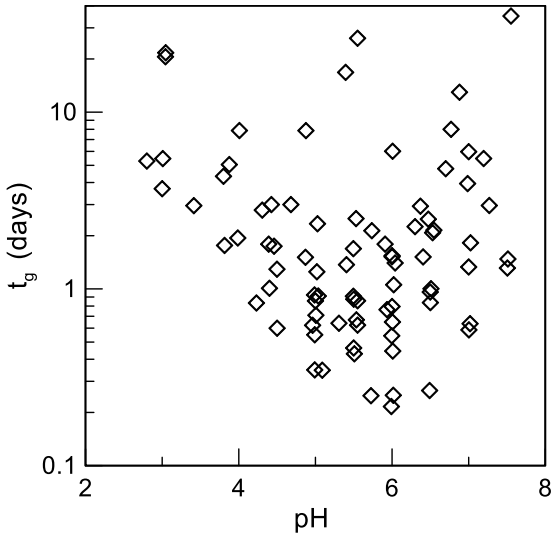

Figure 4.15 *Summary plot of the gel times versus pH for all 61 tested CS solutions.*

In correspondence with Figure 4.16. Figure 4.17 is also constructed, where the pH_{opt} is plotted against CS (%) concentration. This figure also includes three lines which correspond to the average values of pH_{opt} at NaCl normalities of 0, 0.03 and 0.1N. The data included in the graph are from all samples tested both in the laboratory and in the literature regardless of the temperature of the CS solution. The data in this figure show that the pH_{opt} is very slightly (if at all) affected by CS (%), but there is a small increasing effect of normality. More specifically, an increase of NaCl normality causes an increase of pH_{opt}, and this trend seems more intense at low CS concentrations. For example for CS=5% the addition of NaCl from 0N to a normality of 0.1N leads to pH_{opt} from 4.89 to 5.50, whereas for CS=10% the same addition of NaCl changes pH_{opt} from 5.30 to 5.60.

Now, based on Figures 4.9, 4.10, 4.11, 4.13 and 4.14, all "gel time curves" constructed for different combinations (CS (%), N, T) share the same shape of an almost symmetrical inverted bell. Hence, if all such curves are normalized to the corresponding minimum gel time, t_{gmin}, and optimum pH value, pH_{opt}, of each combination, then a unique normalized design curve may be defined as shown in Figure 4.17. In addition, the solid line may be defined as a best fit of the laboratory data. This conclusion is the final step of an approximate and easy to use method for designing passive site stabilization by only choosing the appropriate properties of CS solution to be injected. The reason is that the actual "gel time curve" may be reconstructed, by estimating the t_{gmin} and pH_{opt} via Figures 4.16 and 4.17, respectively.

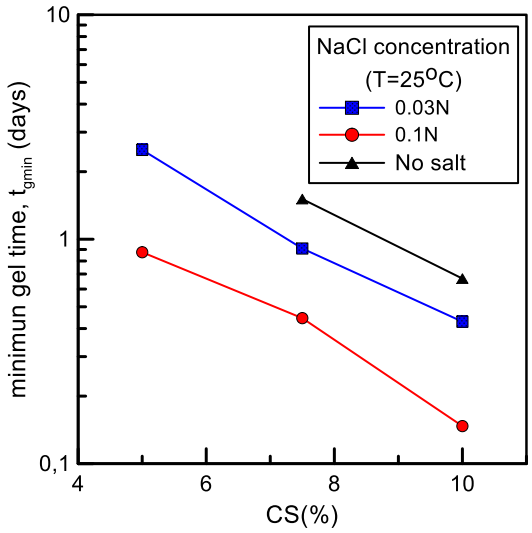

Figure 4.16 *Relation between the minimum gel time, t_{gmin}, of colloidal silica solutions and the CS(%) for three different NaCl normality values and the same temperature (T=25°C)*

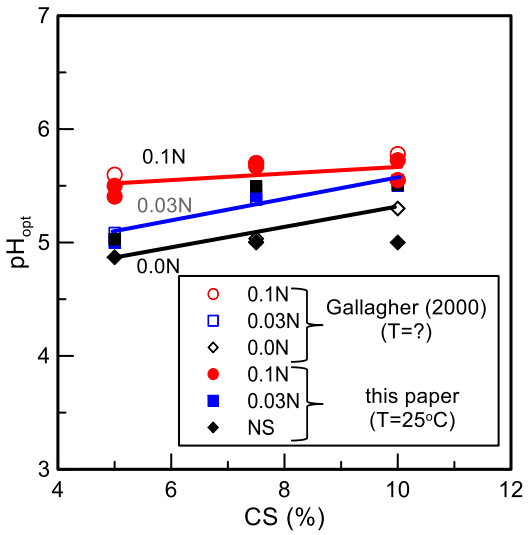

Figure 4.17 *Relation between the optimum pH (related to t_{gmin}), pH_{opt}, of colloidal silica solutions and the CS(%) for three different NaCl normality values and the same temperature (T=25°C), and comparison to literature data (performed at unknown room temperature).*

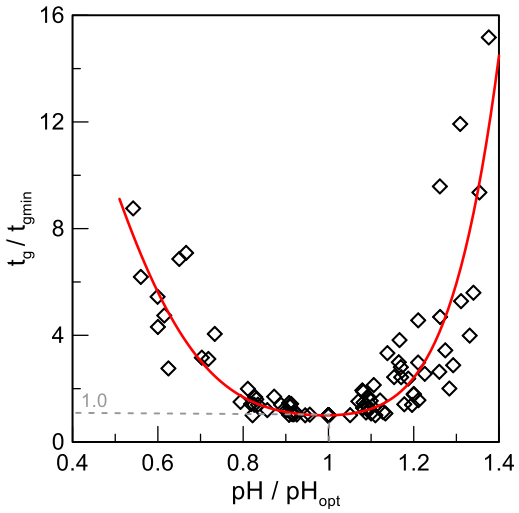

Figure 4.18 *Normalized "gel time curves" of all colloidal silica solutions tested (CS=5–10%, 0.0–0.1N, T=5–25°C) and the average design curve.*

As previously mentioned, temperature T is a parameter that affects the gel time and should be taken into account when designing passive stabilization. In order to include the effect of temperature in the design procedure, a correction factor for temperature T may be defined. The basic conclusion that allows for using just a correction factor for temperature T is that the pH_{opt} remains unaffected and so all the effect may be considered applied on the t_{gmin} of the normalized "gel time curve of Figure 4.18. in order to investigate these effects Figures 4.19 through 4.21 present this effect directly on the gel time of solutions having different combinations of (CS (%), N, pH).

More specifically, Figure 4.19 shows the gel times of solutions with CS=7.5% and NaCl concentration of 0.1N, Figure 4.20 the gel times of solutions with CS=10% and NaCl concentration of 0.1N and Figure 4.21 the gel times of solutions with CS=10% and NaCl concentration of 0.03N. In all these cases, it is obvious that as temperature decreases, the gel time increases significantly. In other words, the minimum gel times appear for the maximum tested temperature of T=25°C.

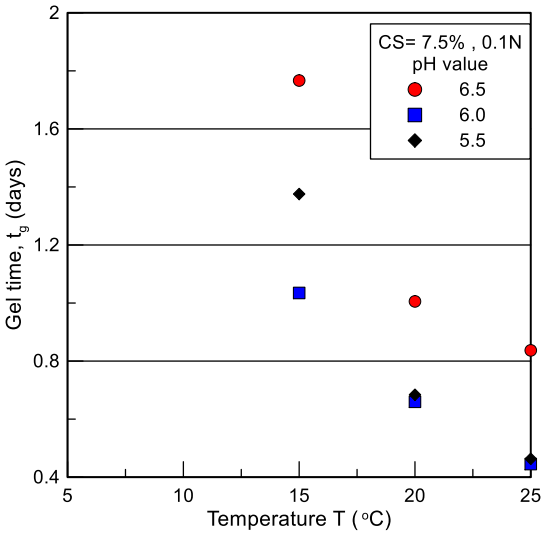

***Figure 4.19**. Effect of temperature on gel time for CS=7.5%, 0.1N at three different pH values (6.5 , 6.0 , 5.5)*

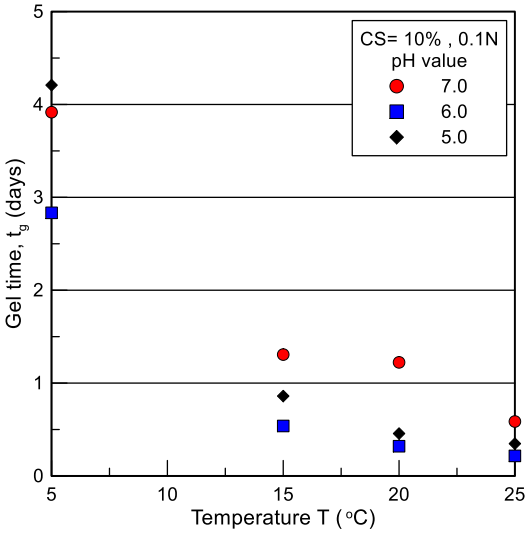

***Figure 4.20** Effect of temperature on gel time for CS=10%, 0.1N at three different pH values (7.0 , 6.0 , 5.0)*

Hence, if all the gel time data are plotted normalized to their minimum value at T=25°C, then Figure 4.22 may be considered, where the normalized gel time ($t_g/t_g(25°C)$) is plotted versus temperature T. Observe that the range is not large and that the average curve gives the correction factor of temperature T, at least in the range of T = 5 - 25°C regardless of the solution characteristics. Note that this effect is not linear, since as temperature increases, there is a corresponding decrease in gel time but the rate of decrease does not remain constant with temperature. More specifically, a 10°C change of temperature from 25 to 15°C

causes an increase of gel time by 2.5 times, whereas a 10°C change from 15 to 10 °C leads to a 4.1 times increase.

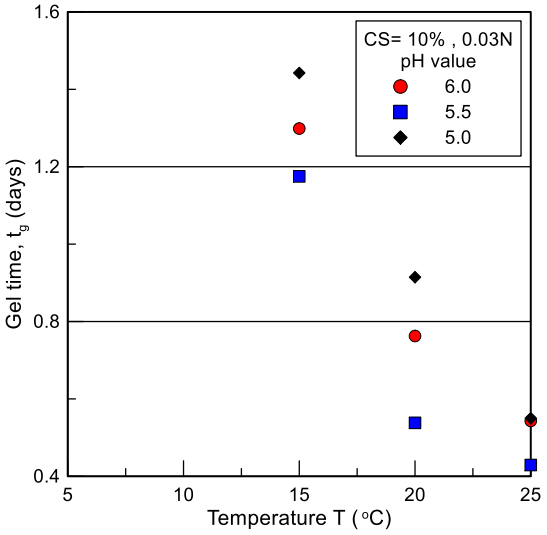

Figure 4.21 *Effect of temperature on gel time for CS=10%, 0.03N at three different pH values (6.0 , 5.5 , 5.0)*

All figures presented before, can be used if someone would like to predict gel time for one specific combination of CS solution properties by following three simple steps. For a given (CS, N) Figure 4.16 and Figure 4.17 give t_{gmin} and pH_{opt}. This t_{gmin} value corresponds to a temperature of T = 25°C, so if the temperature used during the injection is lower, correction of t_{gmin} is necessary. To do so, one may multiply the t_{gmin} at 25°C (from Figure 4.16) with the correction factor taken from Figure 4.22. By estimating all these parameters, "gel time curves" can be reconstructed and the t_g can be calculated through Figure 4.18, as a function of the pH. Note that this procedure may be inversely used as well, by knowing the required t_g and CS (%), one may back estimate the required normality N for a given pH, or the opposite.

The accuracy of this method is evaluated in Figure 4.23, where the horizontal x-axis represents the measured gel times and the vertical axis the predicted gel times of all 61 CS solutions with known properties and temperature. The same figure includes the 100% accuracy line (red continuous line), where the measured gel time equals to the predicted gel time. Overall, the predictions follow closely the measurements, with small uniform scatter and standard deviation of the relative error equal to ±14% (red dashed lines). To better quantify the accuracy of the proposed method of estimating the CS solution gel time (via Figures 4.16, 4.17, 4.18 and 4.22), Figure 4.24 plots the relative error of the predicted gel times versus the controlling parameters: CS (%), T, NaCl normality and pH. The plots in this figure show that

there is no consistent bias of the error as a function of these controlling parameters and that the relative error is uniformly distributed in terms of these parameters.

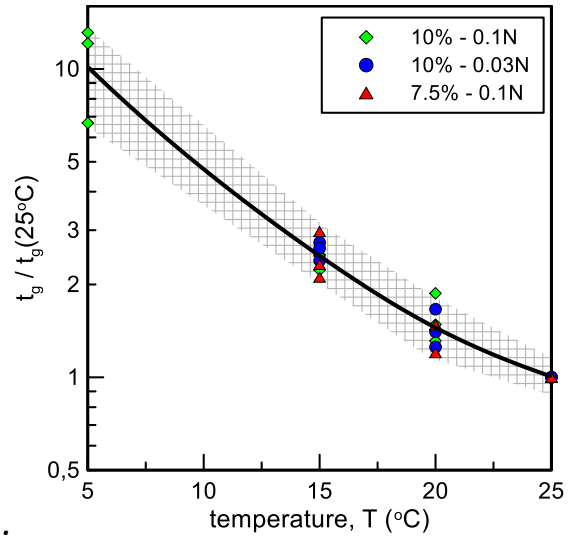

Figure 4.22 *Normalized decreasing effect of temperature T on gel time t_g of CS solutions (CS = 7.5 – 10%, 0.03 – 0.1N), and the average design curve.*

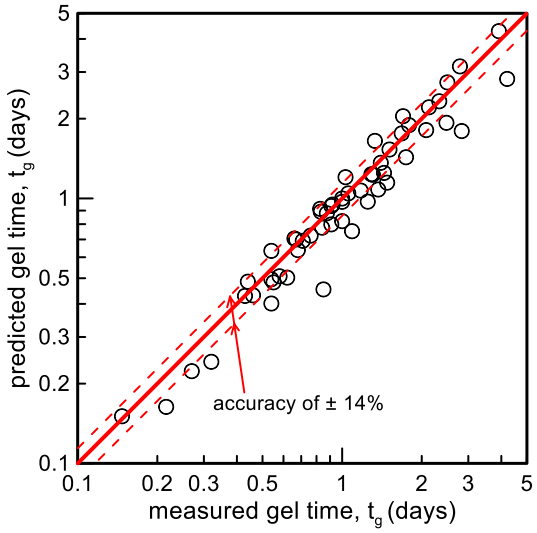

Figure 4.23 *Prediction accuracy of gel time t_g of CS solutions via the proposed design method, on the basis of all 61 tests (CS=5-10%, 0.0N-0,1N, pH=4.23-7.5, T=5-25°C)*

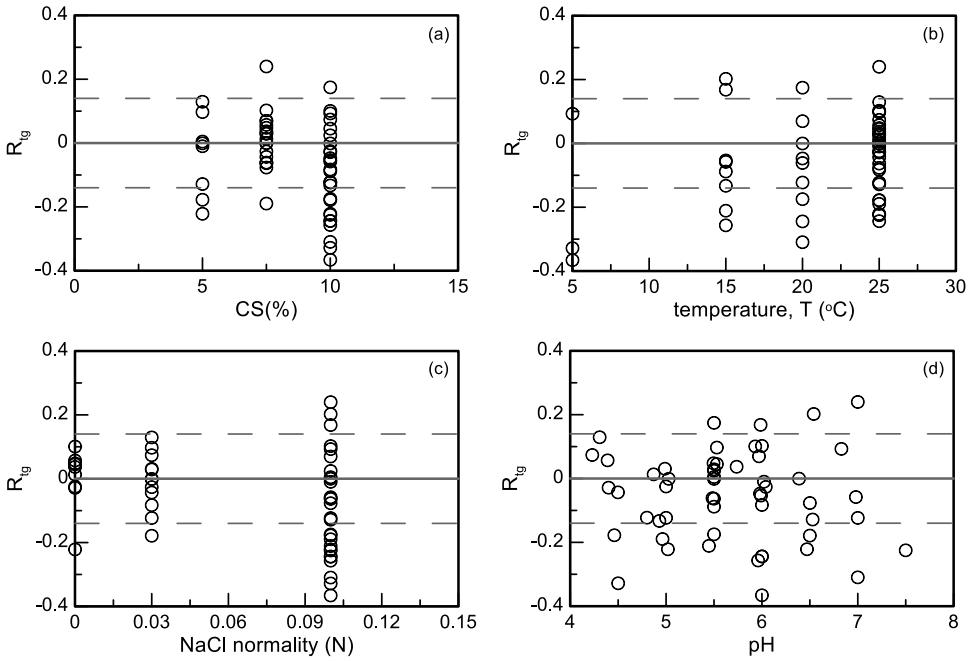

Figure 4.24 *Relative error in predicting gel time t_g of CS solutions, as a function of the four (4) independent controlling parameters: (a) CS(%), (b) T, (c) NaCl normality, (d) pH.*

4.5 Viscosity evolution of CS solutions before gelation

For the quality control of the low pressure injection of CS solutions, the gel time is not the only parameter that should be taken into account. The initial stage of the viscosity versus time curve, i.e. the stage that viscosity increases up to 3-6cP is also a vital parameter for the effective injection of CS. As deduced by the literature findings of Chapter 2, as the viscosity increases, the flow rate decreases (under constant injection pressure). As a result, the prediction of the rheological behavior of the CS solution in this early stage (before gelation) is crucial for its effective delivery at the target location.

In particular, as mentioned in Chapter 2, the delivery of CS essentially stops when its viscosity reaches a value of 3-6cP depending on the gradient (pressure) used for the injection. Hence, a procedure for the accurate prediction of viscosity evolution at these early stages (before gelation) is also significant for the design of passive stabilization. From all the viscosity measurements on the different CS solutions presented above, it is deduced that the viscosity remained low during the initial stage after mixing and it increases rapidly as the gelation of the solution starts. This typical behavior of CS viscosity evolution with time is presented in Figure 4.25(a) for widely different combinations of the controlling parameters CS (%), N, pH

and T. Thus, one may normalize the viscosity μ versus time t curves of all CS solutions, namely the viscosity μ over the initial viscosity μ_0 and over the gel time t_g. This is obvious in Figure 4.25 (b) for the CS solutions presented in Figure 4.25 (a). Observe that after this normalization, the normalized viscosity versus time curves follow the same general trend, which can be approximately described by an exponential equation. The final curve that was chosen to describe the normalized μ vs t curves is shown in Figure 4.26 against the data of all 61 solutions tested herein, and is expressed analytically by:

$$\frac{\mu}{\mu_0} = 1 + \frac{0{,}54\frac{t}{t_g}}{\left|\frac{t}{t_g}-1\right|^{1.2}} \qquad (4.1)$$

Observe in Figure 4.26 that Eq. (4.1) follows the overall trend quite satisfactorily. It is important to underline that this curve can predict the exact viscosity versus time curve for any given CS solution, after providing the values of two variables, the initial viscosity μ_0, and the gel time t_g, which can be obtained from the approximate method presented in paragraph 4.4.

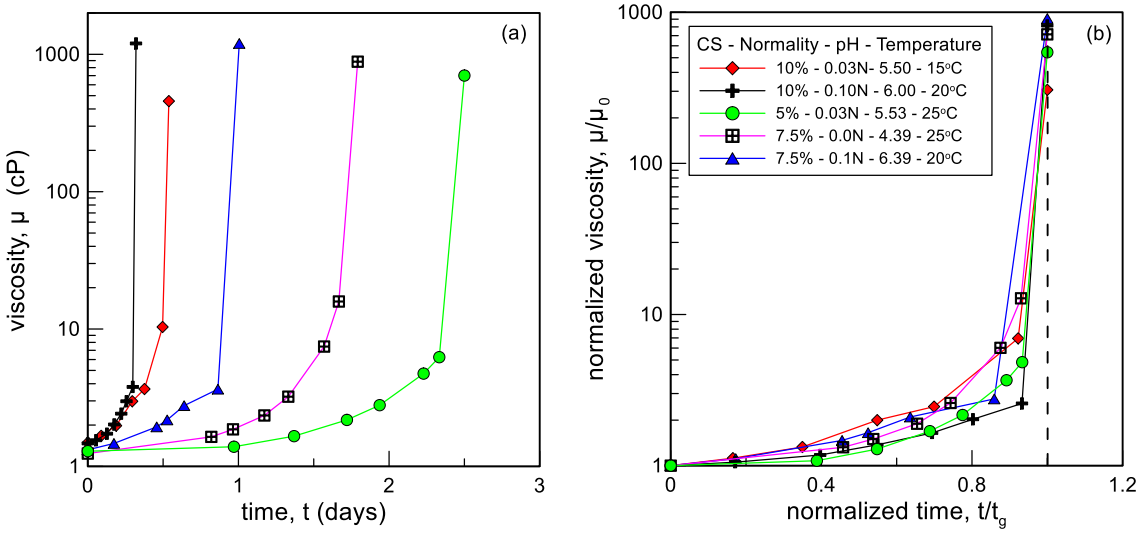

Figure 4.25. *Rheological response of CS solutions with widely different combinations of (CS, N, pH, T) in terms of: (a) viscosity, μ, versus time, t & (b) normalized viscosity, μ/μ_0, versus normalized time, t/t_g.*

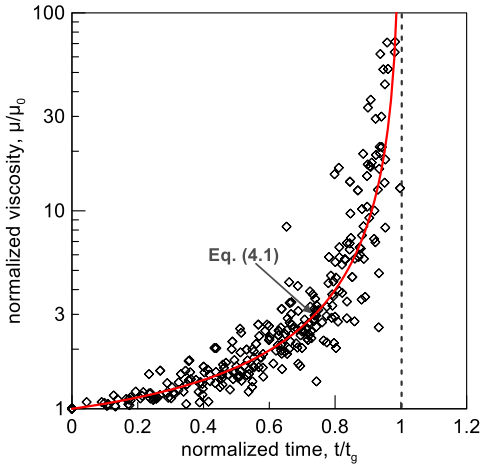

Figure 4.26 *Average design curve for normalized viscosity, μ/μ_0, as a function of the normalized time, t/t_g, of CS solutions, on the basis of all 61 tests performed for various conditions (CS=5-10%, 0.0N-0,1N, pH=4.23-7.5, T=5-25°C)*

The overall accuracy of Eq. (4.1) is illustrated in Figure 4.27, where the measured normalized viscosity is plotted against the predicted normalized viscosity (using Eq. 4.1). The same figure includes the solid diagonal line depicting perfect prediction, as well as the two dashed lines denoting the standard deviation of the relative error which equals ±34%. Observe the good overall predictions especially for the viscosity range of main interest, i.e. μ/μ_0 up to 5 (corresponding to viscosities up to 7cPs approximately). In this range practically all values are within the ±34% range, which is characteristic of the whole dataset.

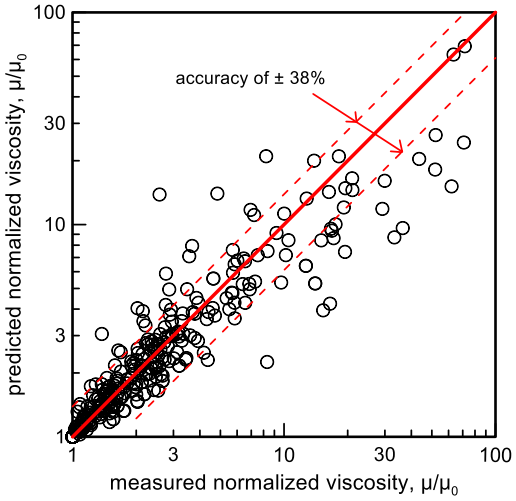

Figure 4.27 *Prediction accuracy of normalized viscosity, μ/μ_0, of colloidal silica solutions (with gel times t_g = 0.14–4.2 days) via the proposed design curve, on the basis of all 61 tests (CS=5-10%, 0.0N-0,1N, pH=4.23-7.5, T=5-25°C).*

Full determination of the viscosity μ versus time t curve still requires a value for μ_0. The value of initial viscosity μ_0 was measured for all CS solutions tested at different temperatures. Figures 4.28- 4.30 show these values of μ_0 for T=25°C, 20°C and 15°C respectively. The three points of each color represent the average value (middle point) at each CS concentration and normality combination as well as the average ± standard deviation values (top and bottom points) for all solutions tested. Based on these Figures it can be deduced that the μ_0 is mostly affected by the CS (%) concentration and secondarily by the other controlling parameters. Particularly, Figure 4.28 shows the effect of CS (%) on μ_0 and it becomes obvious that as the CS (%) becomes higher, the initial viscosity μ_0 increases as well. NaCl concentration does not seem to share the same monotonic effect on μ_0, since its effect is not clear as shown in Figures 4.29 and 4.30 that follow. Figure 4.29 shows the results of similar measurements conducted at 20°C, where higher normality leads to lower initial viscosity μ_0 values. On the contrary, Figure 4.30 shows that this trend is not repeated for the measurements at 15°C where the higher normality leads to higher initial viscosity μ_0 values. With respect to the temperature effect, it has become clear that the effect is not monotonic and an increase of temperature (within the T = 5-25°C range) does not necessarily lead to an increase of initial viscosity as possibly implied by its reducing effect on gel time. To show this, Figure 4.31 shows the increasing effect of CS on initial viscosity μ_0 for the same normality (0.1N) and different temperatures, where no clear effect is observed. Thus, Figure 4.32 shows the initial viscosity value μ_0 as a function of CS (%) on the basis of all 61 CS solutions. In the same figure the shaded area shows the range of all measured initial viscosity values while the thick black line depicts the average trend. It is clear that as CS concentration increases, there is a clear increase of initial viscosity μ_0. For CS=5%, the μ_0 has the lowest average measured value of 1.24cP and for CS=10% this value increases to 1.39cP.

Attempting to show examples of the accuracy in predicting the viscosity μ versus time t curves, the method will be employed by trying to fully reproduce existing viscosity versus time curve from the laboratory measurements (i.e. Eq. 4.1 with μ_0 from Figure 4.32). The value of the gel time, t_g, will result from the procedure presented in paragraph 4.4.

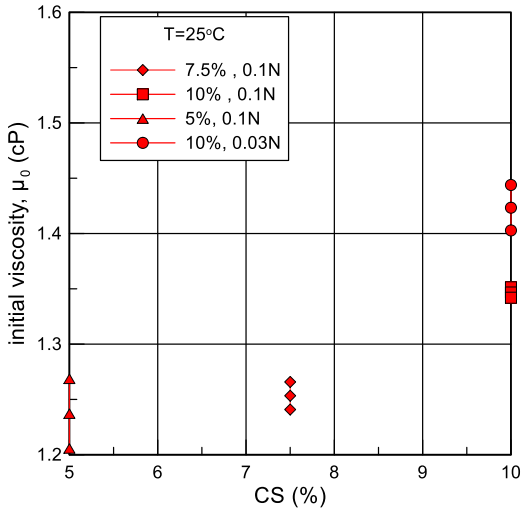

Figure 4.28 *Average values and average ± standard deviation of initial viscosity μ_0 of various for CS solutions measured at T=25°C, as a function of CS (%)*

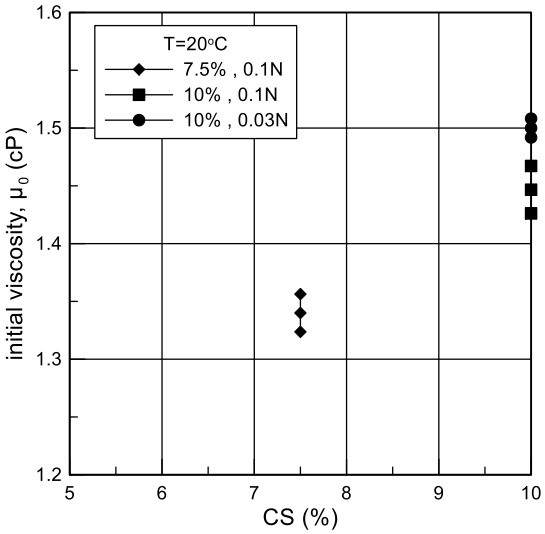

Figure 4.29 *Average values and average ± standard deviation of initial viscosity μ_0 of various for CS solutions measured at T=20°C, as a function of CS (%)*

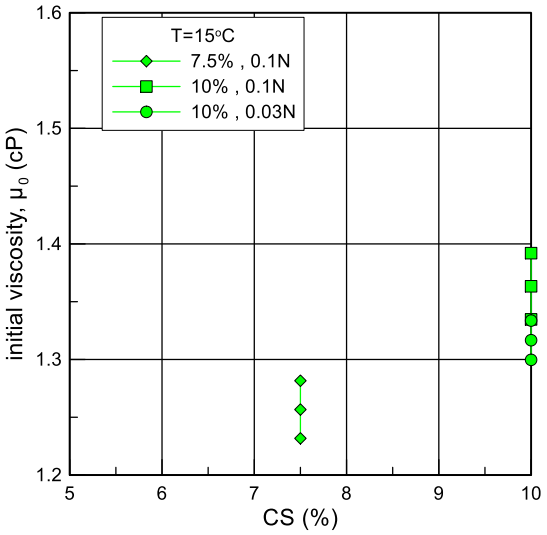

Figure 4.30 *Average values and average ± standard deviation of initial viscosity μ_0 of various for CS solutions measured at T=15°C, as a function of CS (%)*

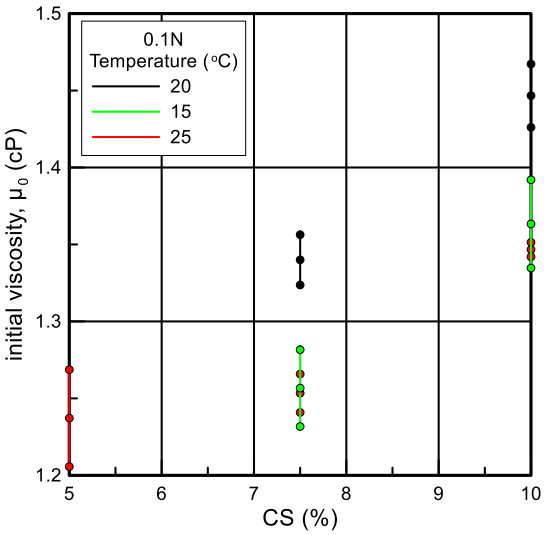

Figure 4.31 *Average values and average ± standard deviation of initial viscosity μ_0 of various for CS solutions measured at T=25, 20 and 15, as a function of CS (%)*

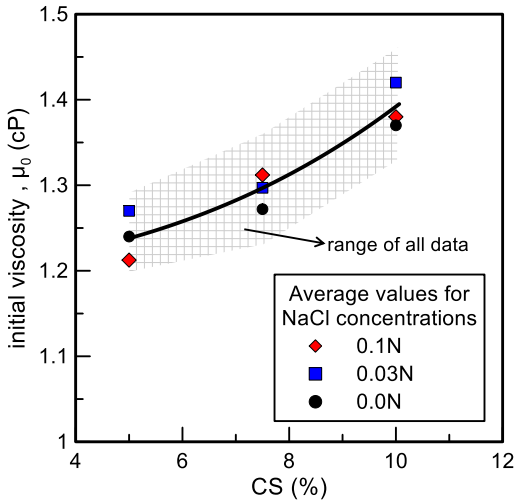

Figure 4.32 *Increasing effect of CS (%) on average initial viscosity, μ_0, of CS solutions irrespective of the combinations of (pH, N, T).*

For example, if the chosen CS and NaCl concentrations are 7.5% and 0.1N, then t_{gmin} = 0.431 days at 25°C (from Figure 4.16) and pH_{opt} = 5.59 (from Figure 4.17). If there is no need for temperature correction (i.e. T=25°C), and t_g = 0.8 days on the basis of the application at hand, then t_g/t_{gmin} = 1.86, and from the average design curve of Figure 4.18 the pH/pH_{opt} = 0.8 or 1.15 (i.e. 2 values may yield the same t_g). Hence, the corresponding pH values for the chosen gel time t_g and combination of (CS(%), N) equal to 4.47 or 6.42. By setting pH=6.42 for example, t_g=0.8 days, μ_0=1.29 cP (for CS=7.5% from Figure 4.32) and by using Equation (4.1), one may fully reconstruct the viscosity μ versus time t curve which is compared to the pertinent data of the closest available CS solution (for CS=7.5% 0.1N, T=25°C and pH=6.5) the comparison of data to simulations is presented in Figure 4.33 and is considered very good.

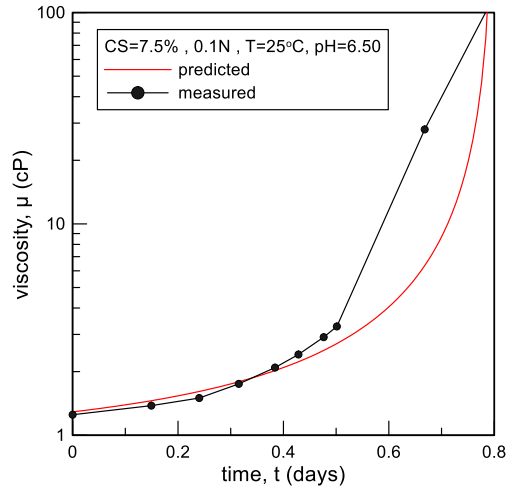

Figure 4.33. *Example of measured versus predicted viscosity μ versus time t curve for CS=7.5%, 0.1N, T=25°C, pH=6.50 (data values).*

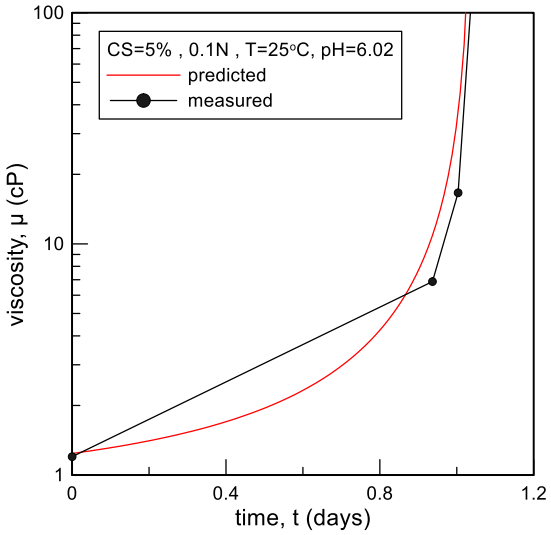

Figure 4.34 *Example of measured versus predicted viscosity μ versus time t curve for CS=5%, 0.1N, T=25oC, pH=6.02 (data values).*

Another example, related to a lower CS concentration is presented in the sequel. Particularly, if the chosen CS and NaCl concentrations are 5% and 0.1N, then t_{gmin} = 0.88 days at T=25°C and pH_{opt} = 5.53 according to Figure 4.16 and Figure 4.17 respectively. Having no need for temperature correction, and pH = 6.02 is enforced, then pH/pH_{opt} = 1.09, and from the average design curve of Figure 4.18, the t_g/t_{gmin} = 1.19. Hence, the corresponding t_g value for the chosen pH and combination of (CS, N) equals to 1.04 days. From the experimental data, for CS = 5% and 0.1N a value of pH=6.02 corresponds to a t_g=1.05 days based on the closest CS solution tested. By using pH=6.02 t_g=1.04 days, μ_0=1.24 cP (for CS=5% from Figure 4.32) and the design curve from Figure 4.26, the comparison of predicted and measured μ versus t curve is shown in Figure 4.34 and is found again quite satisfactory

Chapter 5

INJECTION TESTS OF COLLOIDAL SILICA INTO GRANURAL SOIL

5.1 General

In order to effectively apply passive stabilization in practice, it is of vital importance to investigate the injectability of colloidal silica (CS) solutions into granular soil. The term "injectability" used herein refers to the potential of CS to be pumped into the pores of a soil using low pressures (low gradient flow), as well as to its ability to flow through the pores for relatively large distances in order to be delivered uniformly to the target location. Hence, the goal of this Chapter is to investigate the injectability of CS solutions into liquefiable sand and/ or silty sand layers and to ascertain the uniformity of its delivery within the soil. In other words, the goal is to study the transport mechanisms which control the CS delivery through such soils and depict the parameters that affect them. The results of this study aim to confirm and enrich the literature data outlined in *Chapter 2*. For this purpose, eighteen (18) injection tests were executed in cylindrical saturated sand and silty sand columns. In these tests, the parameters affecting the successful delivery of CS at different distances were investigated, i.e. parameters like the gel time of the CS solution, the hydraulic conductivity of the soil, the hydraulic gradient of the injection and the type of water in the pore fluid of the untreated soil (sea water or not). Finally, a simple analytical tool is validated for estimating the time-dependent one dimensional flow rate of CS through the soil, based on Darcy's law after adjustment for the differences in viscosity and density of CS compared to water.

5.2 Materials, equipment and procedures

The choice of the soil types used in this study took into account the type of soils where liquefaction usually occurs, as well as the type of soils used in other similar research efforts in the literature. More specifically, passive stabilization has been applied to the following sand and silty sands: Trevino soil (Persoff et al., 1999), Monterey No. 30 sand (Gallagher 2000.), Nevada sand (Gallagher and Koch 2003; Lin and Gallagher 2006; Pamuk et al. 2007; Spencer et al. 2008a) Ottawa sand (Lin and Gallagher 2006), Toyoura sand (Kodaka et al. 2005.), Lazaro Cardenas sand (Díaz-Rodríguez et al. 2008a), (unnamed) sand with 5% and 10% of silt (Lin and

Gallagher 2006), M31 sand (Vranna and Tika 2015b), M31/D6 sand – silt mixtures (Vranna and Tika 2015a).

This study investigates the injectability of CS solutions in sands and silty sands (with small percent of fines equal to 10%). In order to compare the response of these two soil types, the silty sand was formed as a mixture of the chosen sand with a fine grained material with the same mineralogical composition. For this purpose, the uniform fine M31 sand was used in combination with the non-plastic sandy silt D6 (67% silt), i.e. exactly the same soils as in the strength tests of Vranna and Tika (2015a; b)

In Figure 5.1 the grain size distribution of all materials used in this research are presented. The shown M31 sand is a natural quartz sand from Belgium. It has a specific gravity G_s = 2.655, maximum and minimum void ratios of e_{max} = 0.805 and e_{min} = 0.558 respectively, a mean diameter D_{50} = 0.31mm and a uniformity coefficient of C_u = 1.5 (Vranna and Tika 2015b). The silty sand mixture used in the study consists of 85% M31 sand and 15% D6 silt. It is a quartz silty sand with non-plastic fines content of fc = 10% with a specific gravity Gs =2.653, maximum and minimum void ratios of emax = 0.682 and emin = 0.414 respectively, a mean diameter D50 = 0.30mm and a uniformity coefficient of Cu = 4.13 (Vranna and Tika 2015a).

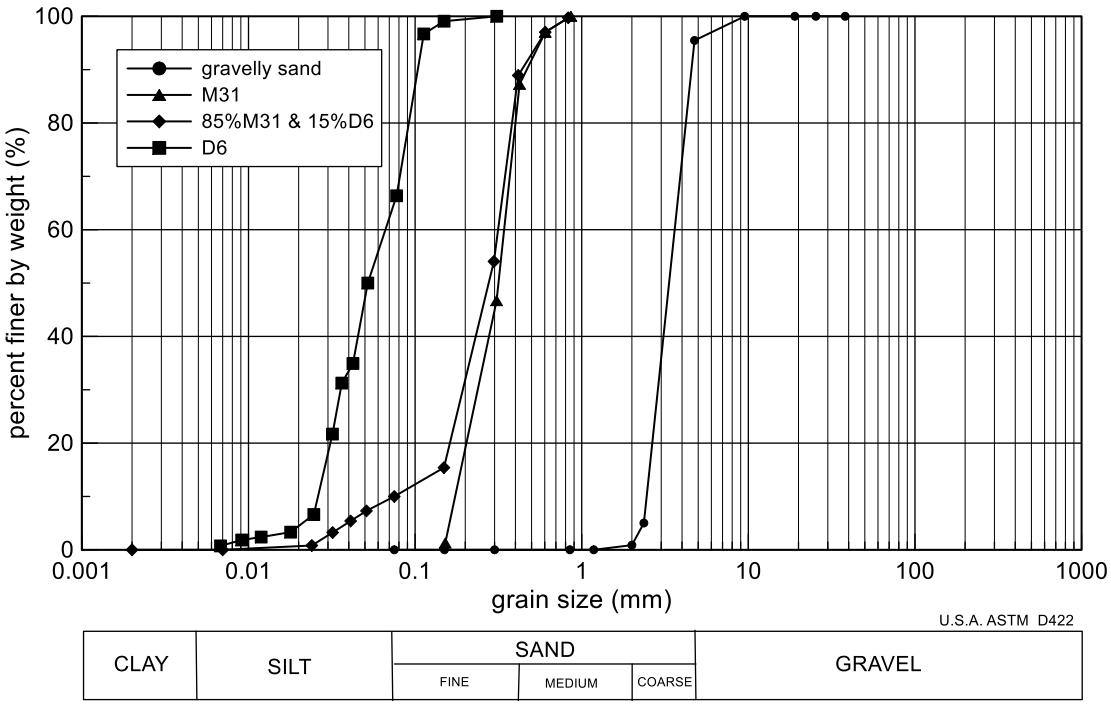

Figure 5.1 *Grain size distribution of all soil materials used in the injection tests*

For the 1D vertical column injection testing a special equipment was constructed, as shown in test setup in Figure 5.2. The equipment was custom-made from Plexiglas and consists of:

- Multiple, inter-connectable cylinder of 20cm height and 10cm diameter used for containing the soil samples as shown in Figure 5.2 and Figure 5.3 (item #1)
- Three separate chambers, one for water injection, one for CS solution injection and one for pore fluid extraction (Figure 5.2)
- Pipes for the connection of chambers and column (Figure 5.2)

Focusing on the cylinder containing the soil sample, Figure 5.3 presents its details:

- Sample ports placed on the cylinders (2 per cylinder) from where samples of the pore fluid were extracted (Figure 5.3 (item #2))
- A bottom cap, i.e. a cylindrical section of 5cm height with one valve for the injection of CS solution and another for water (Figure 5.3 (item #3))
- A top cap, i.e. a cylindrical section of 5cm height with two valves for the extraction of pore fluid (Figure 5.3(item #4))
- An end cap sealing the soil sample (Figure 5.3(item #5))
- O-rings between cylinder and bottom, top and end caps to prevent leakage during the tests.

For the sample preparation of both (M31) sand and silty sand (M31-D6) columns the first 5cm section (bottom cap) of the column was assembled to the (first) 20cm height cylinder using an O-ring between them to prevent leakage. At the bottom section, a metal filter screen was placed in front of the valves and a gravelly sand was then placed in it, so that the CS solution could be uniformly delivered through the bottom of the sand (or silty sand) column. The setup and equipment of these tests was inspired by the pertinent setup and equipment presented by Gallagher andLin (2009).

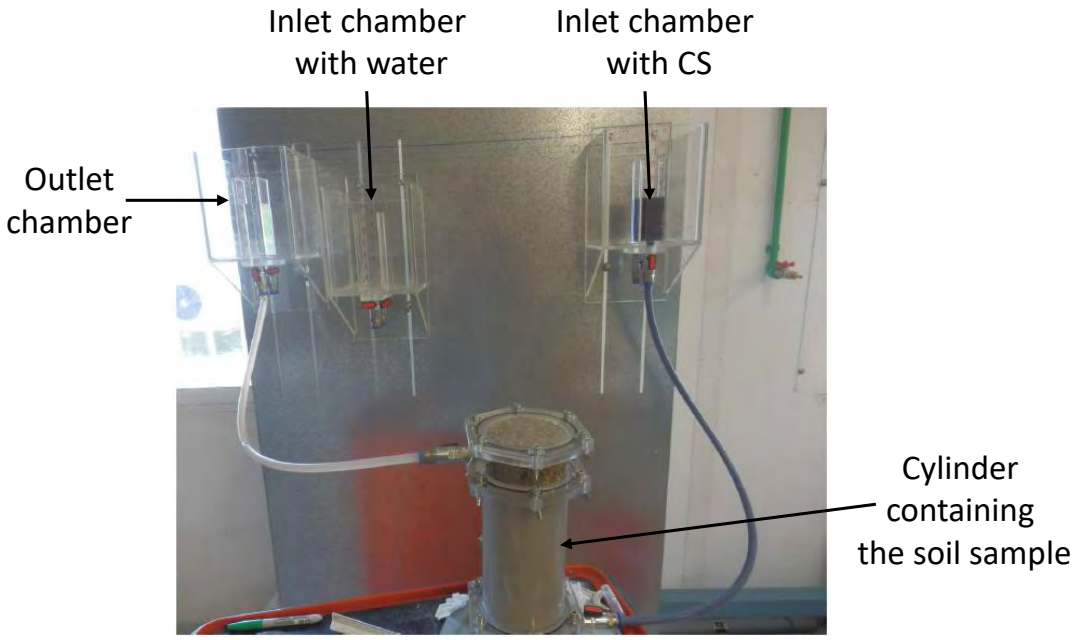

Figure 5.2 *One dimensional column injection test set up.*

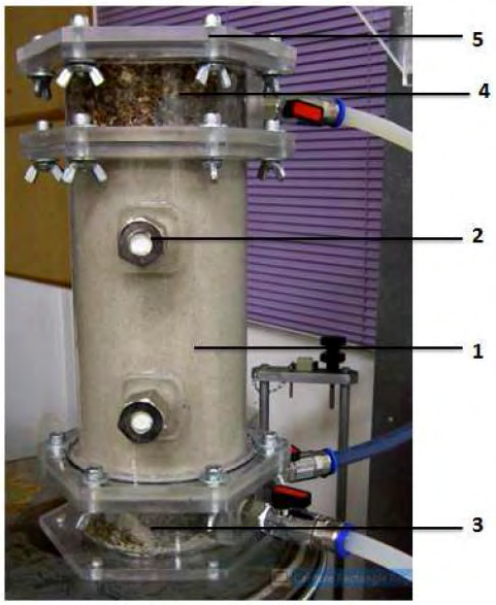

Figure 5.3 *Typical cylinder containing the soil sample for the one dimensional injection tests and its separate sections.*

When the bottom 5cm gravelly sand layer was placed, the sand (or silty sand) samples were formed using the under compaction method (Ladd, 1978) in 9 sub-layers with a tamper (Figure 5.4). Compaction takes places by applying constant force and specific number of hits using the tamper for each one of the nine sub-layers. The tamper diameter was equal to the column diameter and so, every compaction hit imposes the same amount of energy at the same time

to the entire layer diameter. Initial water content used for the sand (or silty sand) column preparation was equal to 6%. Figure 5.5 (a) and (b) show the results of standard Proctor tests for M31 sand and the silty sand mixture (85% M31 and 15% D6), respectively.

Figure 5.4 *Tamper used for the compaction of soil sub-layers within the Plexiglass cylinder used for the one dimensional column injection tests.*

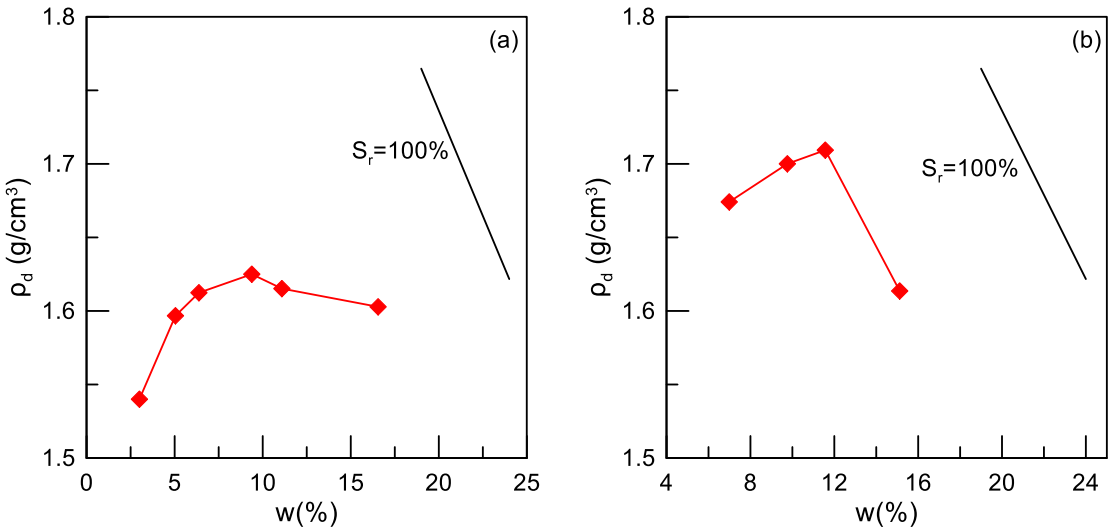

Figure 5.5 *Standard Proctor test results for (a) M31 sand and (b) the silty sand mixture (85%M31 & 15%D6)*

The initial density of M31 sand is estimated to be 1.55g/cm^3, which corresponds to a saturation degree of S_r=30% based on the compaction curve (Figure 5.5a). The remaining 20cm sections were assembled with the same way depending on the final height of the column wanted. At the end cap, another 5cm-thick gravelly sand layer with a metal screen filter were also placed.

After the preparation of the soil columns, they were saturated using hydration which was achieved by allowing water to travel through the column for 1-2 days under a constant low gradient, as also performed by Gallagher and Lin (2009). The degree of saturation achieved using this method is quite high and definitely much higher than the initial one. However, it cannot be accurately measured, only indicatively estimated using measurements at the end of the test (with samples taken after disassembling the column). Such measurements indicated a quite high degree of saturation (e.g. S_r=90-95%).

After hydration, in order to establish hydrostatic conditions the flow was terminated and the column was left in no flow conditions for one more day. Just before CS injection, the hydraulic conductivity k (m/s) of the sample with water as pore fluid was measured (k in m/s) under constant head. The hydraulic conductivity measurements were done by applying downward flow using two (2) different, but constant hydraulic gradients. For all tests, these measurements were conducted by injecting water from the upper valve, which was connected to a water inlet chamber with a pipe and extracting water from the bottom valve which was connected to an outlet chamber with a pipe. The time required for extracting 10, 15, 20, 25, 30, 35 and 50ml of water was recorded and the hydraulic conductivity k was estimated. The detailed presentation of these results is not performed herein, since only the thus measured values of k are of interest. The hydraulic conductivity values of the soil samples with water (deionized or sea water) as the pore fluid prior to the 1D CS injection tests are presented in Table 5-1. Note that these hydraulic conductivity values include not only the main sand or silty sand body, but also the hydraulic conductivity of the gravelly sand of 5cm thickness (2.5cm from the bottom and 2.5cm from the top layers), since the bottom and top valves are placed in the middle of the length of sections 2 and 4 (Figure 5.3). However, taking into account the grain size distribution of the gravelly sand layer (see the comparison with sand and silty sand in Figure 5.1) and the small travel distance of water through it (5cm total versus 20, 40 or 100cm through sand or silty sand) the measured values of k are considered representative of the sand or silty sand samples i.e. they are not affected essentially by the gravelly sand layer. This simplification is practically confirmed by the independent hydraulic conductivity measurement of the gravelly sand, which was measured equal to 8.8×10^{-4} m/s. Note that this value of k for the gravelly sand is 2.3-8.1 times higher than those of the soil columns reported in Table 5-1.

The 1D column injection tests were performed in 20, 40 and 100cm sand and silty sand columns. Different CS solutions were used at each test and their properties are also presented

in Table 5-1. This Table also includes the number of the test (#), the hydraulic conductivity k, the void ratio of the non-stabilized soil, the height of the soil column and the type of water used for saturation. The aqueous suspension of CS was prepared separately and placed in the third chamber (CS inlet chamber in Figure 5.2). The gel times of the CS solutions ranged between 4 and 10 hours, except of the solutions with no added salt and pH=10 (tests 9, 10) where the viscosity retained its initial value during the entire test. Note that the CS solutions were prepared with the method presented in Chapter 4 using deionized water, pure HCl and clean NaCl. Moreover, for visual observation of the CS solution front in the sandy columns, it was colored with blue food dye. The amount of the solution used was at least equal to the pore volume of each column, as the goal of the experiments was to fully fill the pores of the sand, while breakthrough was not targeted in all tests. Note that the term "breakthrough" imlies that the injected CS fills the whole soil column pore volume and exits from the top cap.

The goal of the experiments was to perform 1D vertical upward injection of CS solutions using a low hydraulic gradient. Due to the slightly higher density of the injected CS (when compared with water) if the CS and water levels at the inlet and outlet chambers are set to the same height then a density driven flow of CS through column will occur, a term used by Post et al. (2007). If these levels are kept constant, then this density driven flow will continue at a reducing rate until no-flow conditions appear. Hence, in order to establish equilibrium or no flow conditions at the beginning of the injection, the CS level was initially set slightly lower than that of water outlet level (see Figure 5.6). Then, the CS inlet level was increased (the h_1) in order to apply the initial hydraulic gradient i_0, where $i_0=\Delta h_1/L$ with Δh_1 being the increase of h_1 with respect to its level at initial no-flow conditions. Note that the term "initial" hydraulic gradient is related to the concurrent existence of the aforementioned density- driven flow, which affects the flow rate even when the inlet and outlet chambers remain constant. After that initial setting of h_1 the selected levels of the CS in the inlet chamber and of water in the outlet chamber were held constant during the entire injection test.

Table 5-1 *Characteristics of performed 1D column injection tests of CS in sand and silty sand columns.*

Test (#)	*Column height (cm)*	*Hydraulic conductivity, k (m/s)*	*Void ratio, e*	*CS solution properties*	*Water used for saturation*	*Initial gradient, i_0*
1	20	$1.09*10^{-4}$	0.597	10%CS 0.1N pH=5.55	Deionized	0.05
2	20	$2.25*10^{-4}$	0.597	10%CS 0.1N pH=5.54	Deionized	0.05
3	20	$2.48*10^{-4}$	0.597	10%CS 0.1N pH=5.51	Deionized	0.05
4	20	$2.84*10^{-4}$	0.603	10%CS 0.1N pH=5.53	Deionized	0.05
5	20	$3.17*10^{-4}$	0.613	10%CS 0.1N pH=5.48	Deionized	0.05
6	40	$3.40*10^{-4}$	0.622	10%CS 0.1N pH=6.70	Deionized	0.05
7	40	$2.96*10^{-4}$	0.693	10%CS 0.1N pH=7.00	Deionized	0.05
8	100	$3.1*10^{-4}$	0.645	10%CS 0.1N pH=5.47	Deionized	0.23
9	20	$2.83*10^{-4}$	0.603	10%CS 0.0N pH=10	Deionized	0.05
10	40	$3.21*10^{-4}$	0.630	10%CS 0.0N pH=10.00	Deionized	0.04
11	20	$3.30*10^{-4}$	0.609	5%CS 0.1N pH=5.45	Deionized	0.04
12	20	$3.80*10^{-4}$	0.620	7.5%CS 0.1N pH=5.54	Deionized	0.06
13	40	$3.18*10^{-4}$	0.628	10%CS NS pH=6.75	Deionized	0.04
1S	20	$1.13*10^{-4}$	0.592	10%CS 0.1N pH=5.47	Deionized	0.05
1SW	40	$3.28*10^{-4}$	0.603	10%CS 0.1N pH=7.03	Sea	0.05
2SW	40	$3.28*10^{-4}$	0.629	10% NS pH=6.80	Sea	0.03
3SW	100	$3.30*10^{-4}$	0.675	10%CS NS pH=7.00	Sea	0.03

These constant levels of the fluids in the CS and water chambers were achieved by continuous injection of CS and extraction of water from the inlet and outlet chambers respectively whenever needed. With this procedure, the measured volume of the added CS solution with time was then used in order to estimate the measured flow rate or discharge (Q_{meas}) of CS within the soil sample. Concurrently, measurements of the time evolution of the (dynamic) viscosity of the CS solution and the location of the dyed CS front into the column were performed. The latter was executed by observing and recording the location of the upper level of the dyed CS solution inside the sample. Admittedly, this kind of visual measurement is less accurate than the measurements of the CS flow rate, or the CS viscosity but it proved to be sufficient for the purposes of these tests.

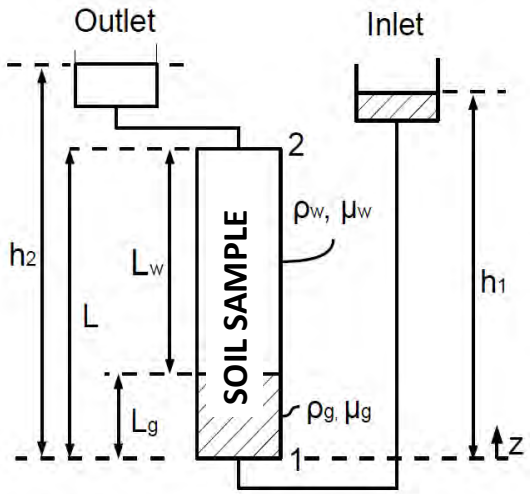

Figure 5.6 *Set up of 1D vertical injection tests.*

Along with the flow rate, the viscosity measurements and the location of the CS front, small samples of the pore fluid were taken in order to estimate the percentage of the CS(%) concentration per weight in them. The main reason for this sampling is that dyed CS helped the visual estimation of injection in sandy soils, but it was not known whether the dye itself injected faster or slower than the CS in the pore fluid. From another point of view, these samples helped to ascertain whether the heavier and more viscous CS solution replaces the water in the pores, or if there is (small or large) diffusion of silica molecules into this water. Therefore, a correlation between the (visually estimated) position of the CS front and the independently measured concentration of the CS(%) would answer both potential inaccuracies of the visual observation method.

Hence, during all tests, CS samples were extracted from the sand with a syringe (Figure 5.7). The column has two sampling ports along each 20cm part, which were used for this purpose. After the extraction of a small (but sufficient) quantity of pore fluid, it was burned at 200^{o}C for two days and the mass measured after burning was considered representative of the CS concentration at the location of the sampling port for the specific time of sampling. This sampled pore fluid mass also includes the salt and dye mass, but these are considered negligible if compared to the CS mass.

The samples were taken through specific ports on the column (see Figure 5.3) and it was found important to correlate the CS(%) concentration measured at each location with the position of the CS front at the time of the sampling. In other words, it does not matter which sampling port is used, but the location of this port in relation with the CS front position during the sampling, i.e. if the CS front is before (upstream) or after (downstream) the sampling port when this is being used for pore fluid sampling.

Figure 5.7 *Syringe used to extract small samples of the dyed pore fluid during 1D column injection tests.*

5.3 Presentation of injection test results

5.3.1 Preliminary set of tests

A detailed description of the 1D injection tests 1, 2, 3, 7 will be given first. During these tests (see Table 5-1 for details) the room temperature was measured approximately constant at an average value of 25^{o}C. The inlet and outlet chambers are presented in Figure 5.8. As it is obvious the diameter of the chambers is large, so the visual observation of the fluid within them is considered relatively inaccurate. Hence, no flow rate measurements were taken during these preliminary tests. However, the movement of the CS front was visually measured and typical images of the testing is presented in Figure 5.9 and Figure 5.10.

Figure 5.8 *Set up of vertical 1D injection tests (large chambers). Observe that breakthrough has been performed (all the sample is dyed blue) and the heavier and more viscous CS can be clearly seen at the bottom of the outlet chamber, as a thin layer below the water-filled chamber.*

Figure 5.9 *Clear image of the CS front at the lower part of a sand column.*

Figure 5.10 *Pore fluid sampling when the CS front is located at a height of 10cm at the time of the sampling and it is before (upstream of) the sampling port.*

No reliable flow rate measurements were taken, but pore fluid sampling was performed. Figure 5.11 shows the results from the sampling procedure for all four 1D injection tests, namely the concentration of CS(%) in the extracted samples as a function of the relative distance of the sampling port from the CS front. Points with negative values on the x-axis refer to samples extracted from ports before the CS front has reached them (i.e. at sampling ports higher than the position of CS front, e.g. as in Figure 5.10). On the contrary, points with positive values of distance (in the x-axis) refer to samples extracted from ports after the CS front has reached them (i.e. at sampling ports lower than the position of the CS front).

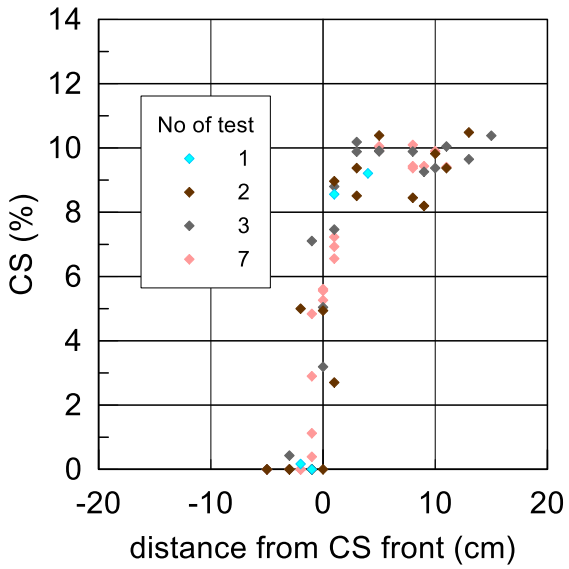

Figure 5.11 *CS(%) concentration per weight in pore fluid extracted from the sampling ports for tests No1, 2,3 and 7.*

As resulted from Figure 5.11, before the CS front reaches the sampling port (for negative values of distance) the percentage of CS(%) is approximately zero. On the contrary, at measurements where the CS front is exactly at the sampling port this percentage increases to a value of 3-7% and is further increased to a value of 9% when the CS front is almost 1cm after the sampling port. For locations of the port lower or equal to 2cm from the front, the CS(%) values are practically equal to the nominal value (in these tests equal to 10%) of the solution used (CS_{nom}), or at least higher than 8%, i.e. 80% of CS_{nom}.

5.3.2 Main set of tests

For the large majority of the executed tests (main set) smaller chambers were built inside the large initial ones, thus enabling more accurate measurement of the level of the liquids within them. This allowed for concurrent measurement of the flow rate, on top of the other measurements of CS front location and CS(%) at different distances from the CS front. These small chambers are shown in Figure 5.12.

The results of the tests will be presented in terms of flow rate, viscosity evolution, CS front position and concentration of CS(%) extracted from the sampling ports. Along with the experimental viscosity measurements, the viscosity versus time curve which resulted from Equation (4.1) as presented in the previous chapter is also illustrated in the viscosity versus time figures with the black dashed line.

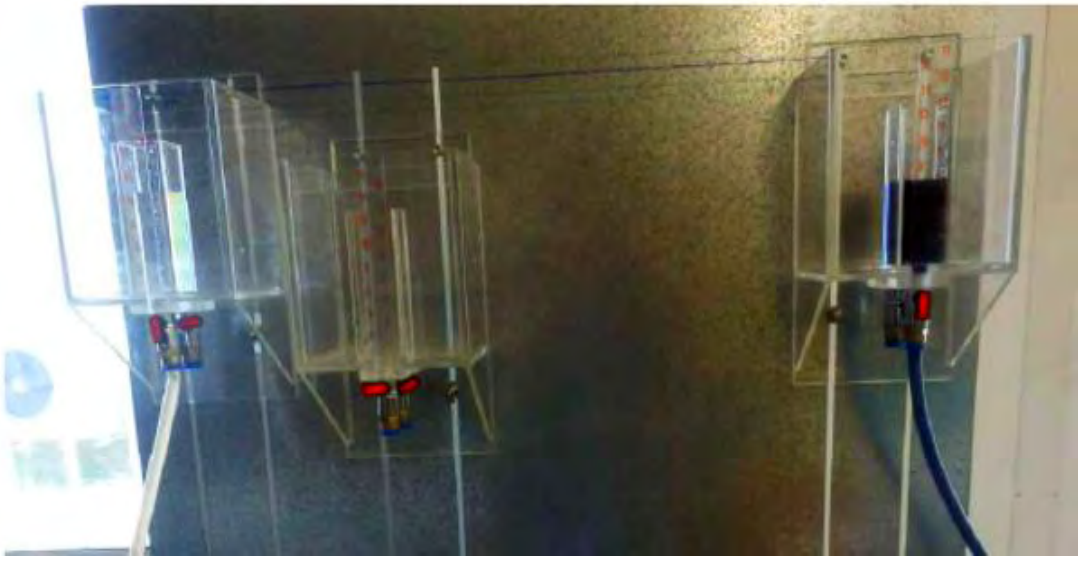

Figure 5.12 *Set up of vertical 1D injection tests for the main set of tests using small inlet and outlet chambers.*

Test No4

In this test the initial hydraulic gradient was set to $i_0=\Delta h_1/20=0.05$. Other details for this test may be found in Table 5-1. As soon as the injection of CS started, the fluid levels in the inlet and outlet chambers were held constant during the whole test. This was achieved by injecting and extracting CS and water from the inlet and outlet chambers, respectively. The volume of CS injected with time represents the measured flow rate (Q_{meas}) which is shown in Figure 5.13 (a). It is observed that as time increases, the measured flow rate decreases. This is explained mainly by the (measured) increasing viscosity of the CS solution, shown in Figure 5.13 (b), which essentially stops the flow when the CS viscosity reaches 7cP. Furthermore, in Figure 5.14 (a) the position of the CS front with time is presented, from where it is deduced that initially the CS front progresses fast (due to initially high flow rates in Figure 5.13(a)), but this rate of CS progression reduces and finally the CS front progression becomes asymptotic with time and stops at a position of 13cm (when the flow rate is essentially zero in Figure 5.13(a)) after 3.2 hours. In addition, pore fluid sampling results from this test are shown in Figure 5.14(b) and seem compatible with those in the preliminary set of tests (Figure 5.11). This test did not lead to a breakthrough of CS and this is clearly shown in Figure 5.15 where a snapshot of the soil column at the end of the test is presented. Finally, note that Figure 5.13b also includes a "blind" prediction of the CS viscosity with time curve using Eq. (4.1) and shows a satisfactory agreement with the test data (up to 7cP).

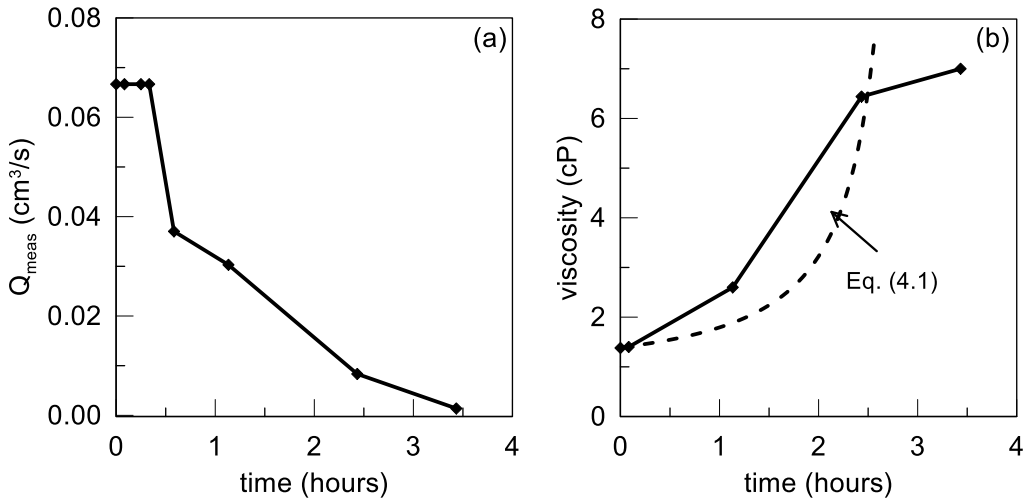

Figure 5.13 *Test No4: (a) Measured flow rate versus time and (b) measured and calculated (from Eq. 4.1) CS viscosity values versus time.*

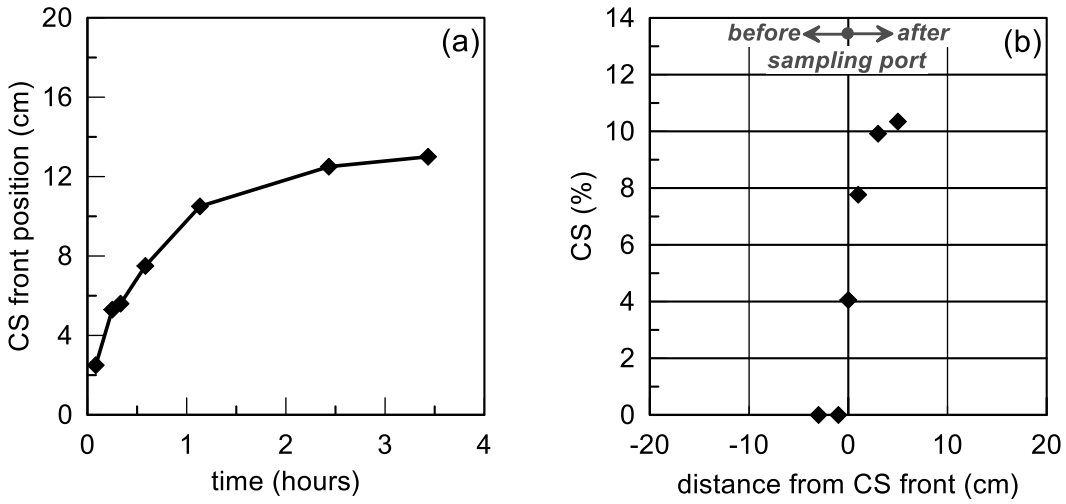

Figure 5.14 *Test No4: (a) Recorded CS front position versus time and (b) CS(%) concentration in the pore fluid, as extracted from the sampling ports.*

Figure 5.15 *Snapshot of CS front at the end of Test No4. Observe that breakthrough was not attained in this test and this clearly depicted by the change of color within the sand sample.*

Test No5

The main characteristics of Test No5 may be found in Table 5-1. This test had the same initial hydraulic gradient i_0 as in test No4 and the CS stopped moving at a position of 11cm into the sand. As shown in Figure 5.16, the main factor responsible for the end of injection is again the increased viscosity of the CS solution (injection ended when 5cP was reached) which is again satisfactorily simulated by Eq. 4.1 (up to 5cP). Figure 5.17 shows results qualitatively similar to those of Figure 5.14 (Test No4).

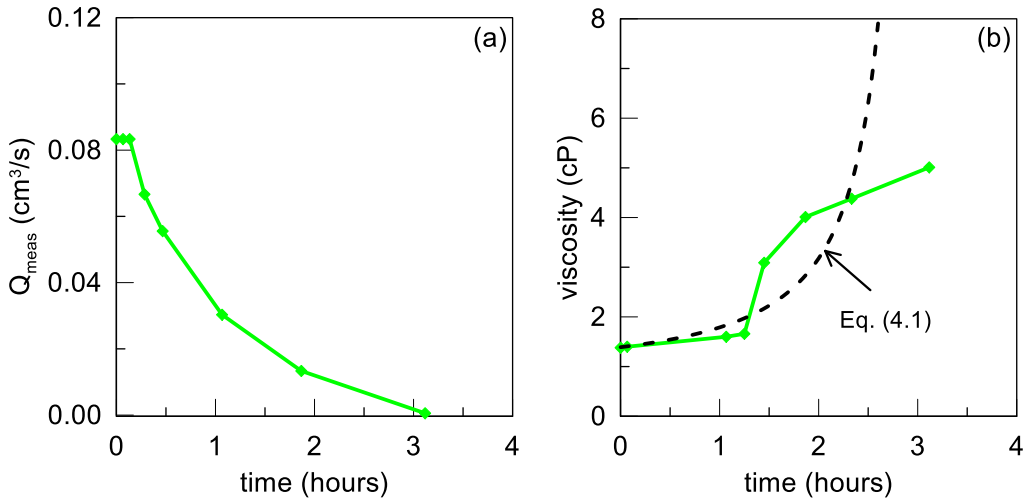

Figure 5.16 *Test No5: (a) Measured flow rate versus time and (b) measured and calculated (from Eq. 4.1) CS viscosity values versus time.*

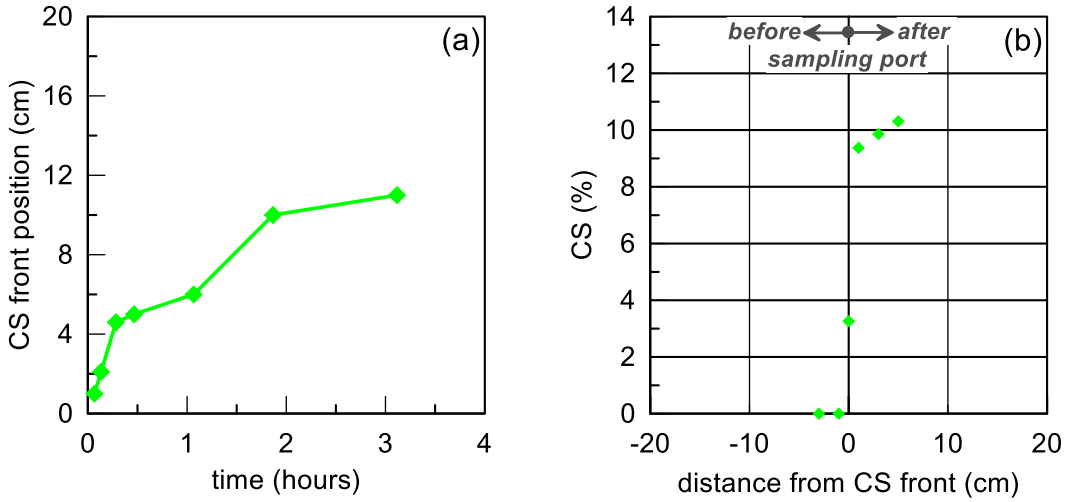

Figure 5.17 *Test No5: (a) Recorded CS front position versus time and (b) CS(%) concentration in the pore fluid, as extracted from the sampling ports.*

Test No6

In comparison to Tests No 4 and 5, in this test (No6) the soil column had double length, i.e. it was assembled with two sections of 20cm. Note that the CS solution has pH=6.7 and this pH increase caused the delay of CS solution gelling, thus allowing for longer CS travel distances using the same initial hydraulic gradient (i_0=0.05). Figure 5.18 shows that the flow rate stopped after 7.9 hrs, i.e. practically twice the travel time of Tests No4 and 5. At that time, the viscosity has reached a value of 4.2cP thus practically nullifying the flow rate. Furthermore, Figure 5.19(a) shows that the asymptotic with time increase of the CS front travel distance, which stops progressing at 28cm, i.e. after performing a breakthrough of the first 20cm.

Finally, Figure 5.19(b) shows measurements for the CS(%) with distance from the CS front that are similar to those of Tests No4 and 5. Observe also that the predicted CS viscosity tends to overpredict the measured values, leading to an underestimation of the gel time.

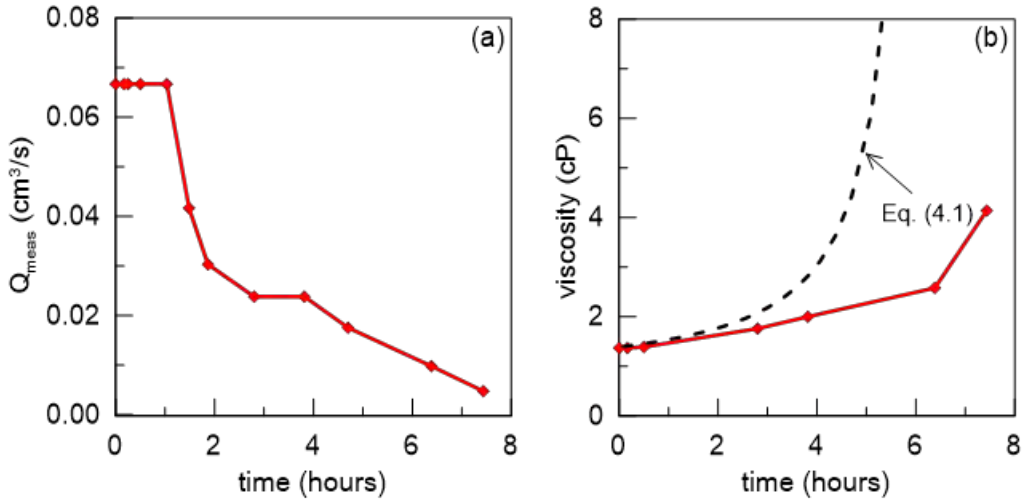

Figure 5.18 *Test No6: (a) Measured flow rate versus time and (b) measured and calculated (from Eq. 4.1) CS viscosity values versus time.*

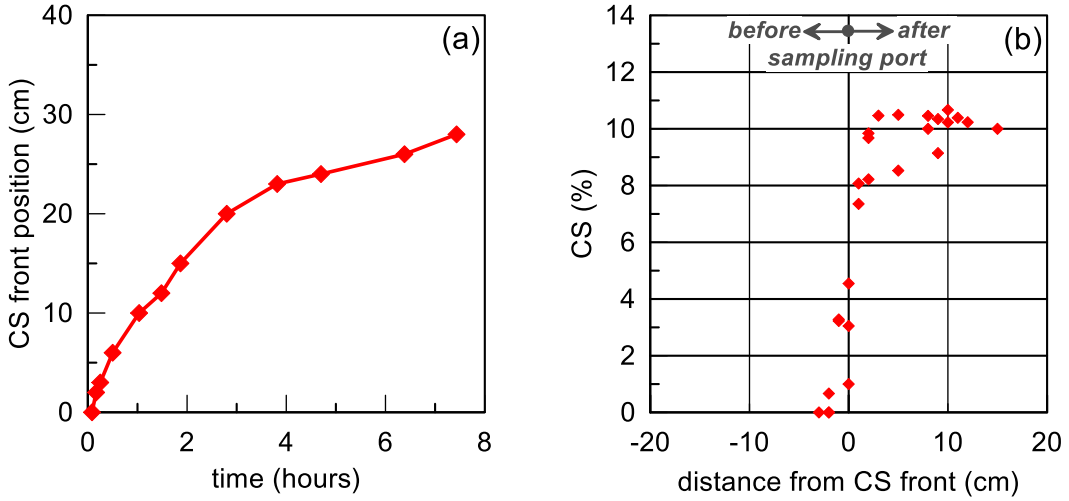

Figure 5.19 *Test No6: (a) Recorded CS front position versus time and (b) CS(%) concentration in the pore fluid, as extracted from the sampling ports.*

Test No8

The column was assembled with five sections of 20cm, i.e. it had a total length of 1m, and initial hydraulic gradient i_0=0.23, i.e. it had a 5 times longer sample and an approximately 5 times higher initial hydraulic gradient than Tests No 4 and 5. The goal of this test was to investigate the ability of CS solutions to travel longer distances within granular soil and also

maintain adequate CS(%) concentration for soil stabilization. The 1m column was assembled section by section with the predescribed procedure. The almost fivefold increase of the initial hydraulic gradient aims to lead to a fivefold larger travel distance (compared with previous tests with the same solution properties and a value of i_0 equal to 0.05) in the same amount of time. Based on Figure 5.20, the overall time required for full coverage of the 1m column (breakthrough) is slightly higher than this of the previous tests (4.5 hours). Interestingly, the CS covered the full column and the flow rate decreased significantly but did not reach a zero value before breakthrough. Again, Figure 5.21 shows qualitatively similar measurements with the previous tests, but of special interest here is that this test shows that CS solutions can be delivered through long distances retaining the nominal CS value with which they are injectedAlso note that, in Test No6, the predicted viscosity versus time curve overpredicts the test data, thus leading to an underprediction of the gel time. Figures 5.22 through 5.25 present photos of this test at different instances, from the setup and beginning all the way to breakthrough of the CS solution.

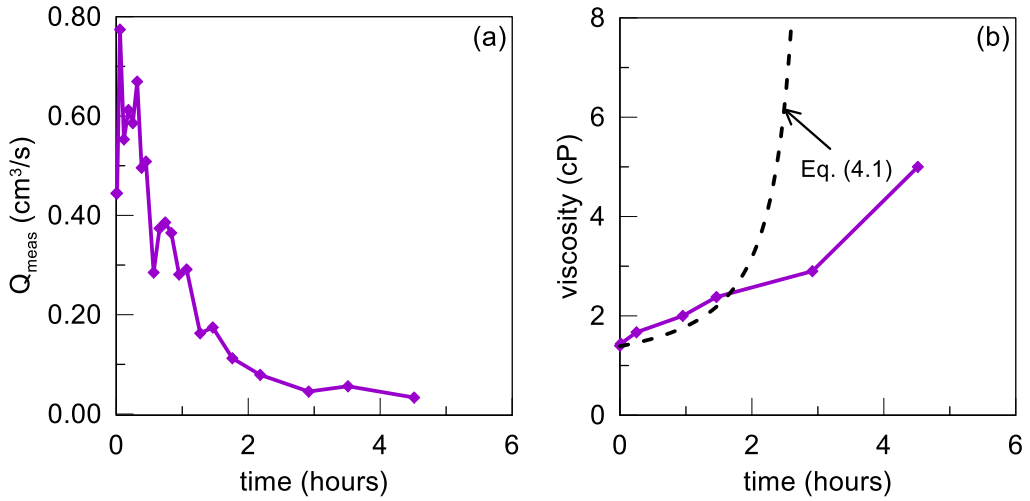

Figure 5.20 *Test No8: (a) Measured flow rate versus time and (b) measured and calculated from Eq. 4.1 CS viscosity values versus time.*

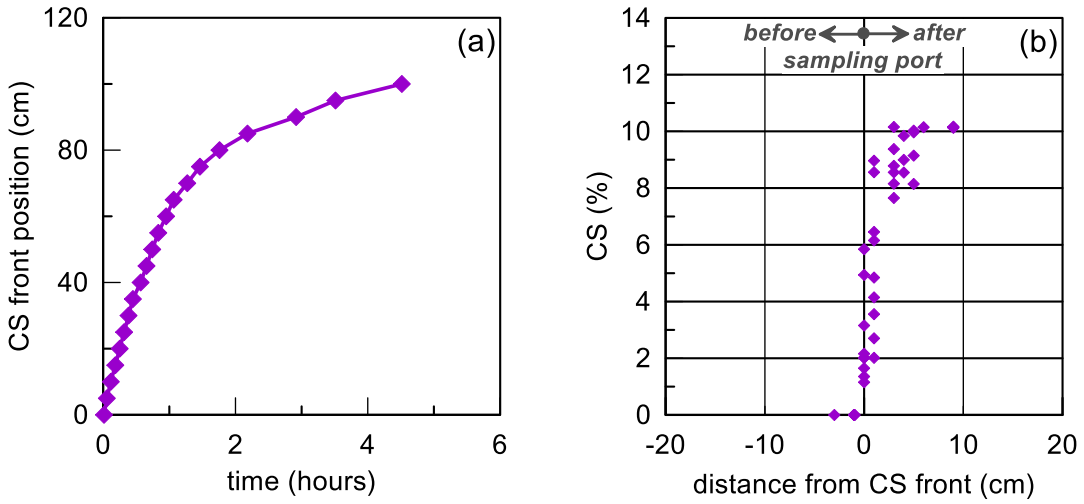

Figure 5.21 *Test No8: (a) Recorded CS front position versus time and (b) CS(%) concentration in the pore fluid, as extracted from the sampling ports..*

Figure 5.22 *Experimental set up for the 1m column injection test (Test No8), where the whole 1m column may be observed.*

Figure 5.23 *Dyed CS appears at the bottom of the sand layer at the beginning of Test No8. Observe the dyed blue pipe injecting the CS solution into the sample.*

Figure 5.24 *CS front at the fourth 20cm section of the 1m column of Test No8. Observe that the pipe leading to the outlet chamber shows no evidence of dye.*

Figure 5.25 *Full coverage (breakthrough) of 1m sand column with injected dyed blue CS solution in Test No8.*

Test No9

In order to better understand the effect of density driven flow on the measured flow rate and on CS delivery through a granular column, Test No9 uses a CS solution with pH=10, zero ionic strength (no added salt) so that its viscosity remains constant and equal to its initial value during the entire injection test (1.47cP). Table 5-1 presents the characteristics of this test, where the column is 20cm tall and the initial hydraulic gradient i_0=0.05. Results in Figure 5.26 show that flow rate decreases due to the density difference between the CS solution and the water it displaces, despite that the viscosity of CS remains constant. No relative figure was deemed necessary here while the methodology of Chapter 4 predicts a gel time of 462 days, thus implying a practically constant viscosity within the time frame of the test (5.3h). As an effect, the stabilizer was not delivered through the entire column, but reached a maximum distance of 15cm within the sand column. This is a clear manifestation of this element of CS delivery, which differentiates this type of flow from what Darcy's law would predict. No pore fluid sampling was performed in this test due to unavailability of required equipment at the time of the experiment.

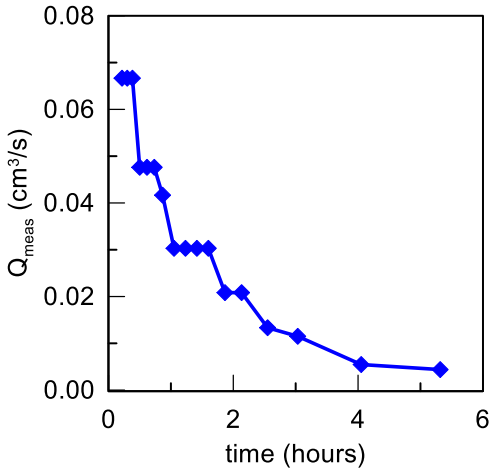

Figure 5.26 *Test No9: Measured flow rate versus time.*

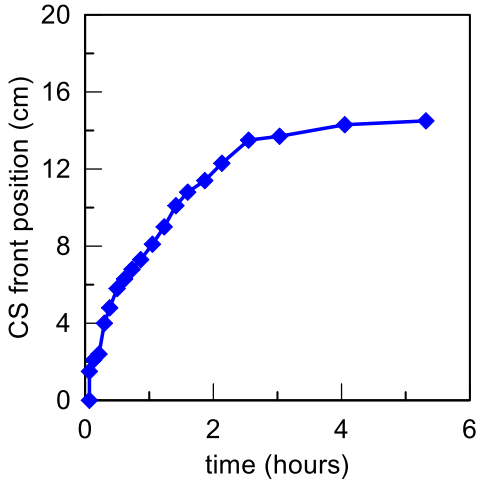

Figure 5.27 *Test No9: Recorded CS front position versus time.*

Test No10

Test No10 is similar to Test No9 (i.e. a CS solution with constant viscosity is injected), but with a height of soil column equal to 40cm. Figure 5.28 presents the decreasing flow rate versus time, while Figure 5.29 shows the visually observed CS front position with time, as well as the measurements of CS(%) from the pore fluid sampling. Observe that the duration of this test is 12.3 hrs, the longest of all previous tests. Nevertheless, the flow rate again diminished before breakthrough, and this even though the viscosity remained practically constant (increased from 1.48cP to 1.50cP in these 12.3hrs). As in Test No9 no viscosity versus time plot is considered necessary. It is merely mentioned here that the CS solution is the same as in Test

No9, and so is the predicted gel time (462 days) implying practically constant viscosity over the 12.3hrs of the injection test.

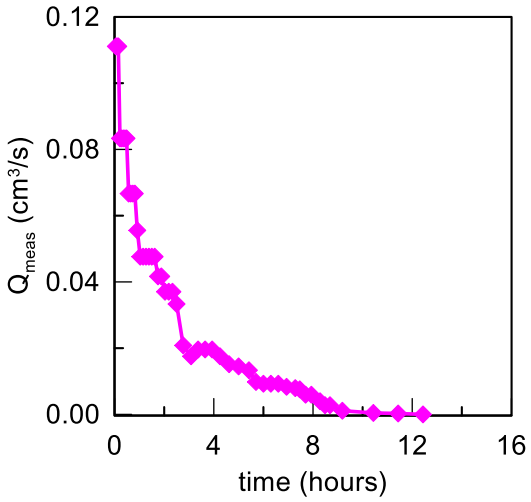

Figure 5.28 *Test No10: Measured flow rate versus time.*

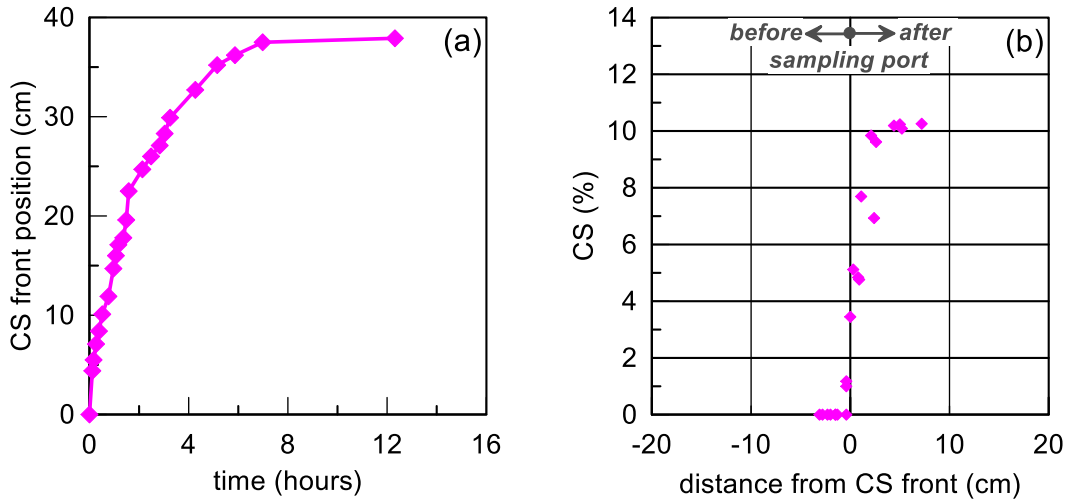

Figure 5.29 *Test No10: (a) Recorded CS front position versus time (b) CS concentration extracted from the sampling ports.*

Test No11

Test No11 used a CS solution similar to that of Test No4, but with CS(%)=5 (and not 10%). Other details of this test are provided in Table 5-1. Note that given the reduction of CS(%), the viscosity remains constant and this predicted by Eq. 4.1 (see Figure 5.30b). However, the flow rate decreases with time (Figure 5.30a), and this is an indication of density- driven flow, which did not prevent breakthrough in this case (see Figure 5.31a). Of interest is also here that the

pore fluid sampling shows qualitatively similar results in terms of CS(%) with distance from the CS front, but for a lower nominal value of CS(%)=5.

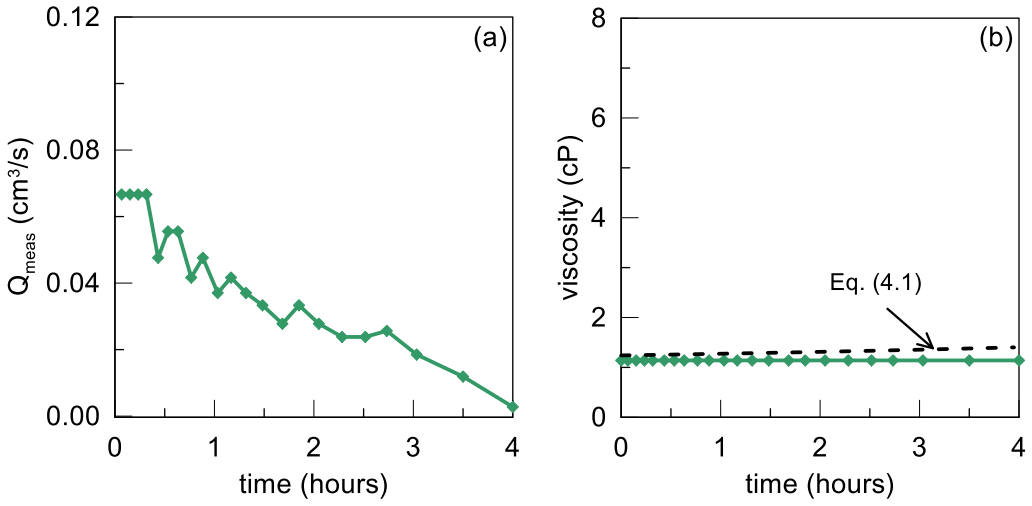

Figure 5.30 *Test No11: (a) Measured flow rate versus time and (b) measured and calculated (from Eq. 4.1) CS viscosity values versus time.*

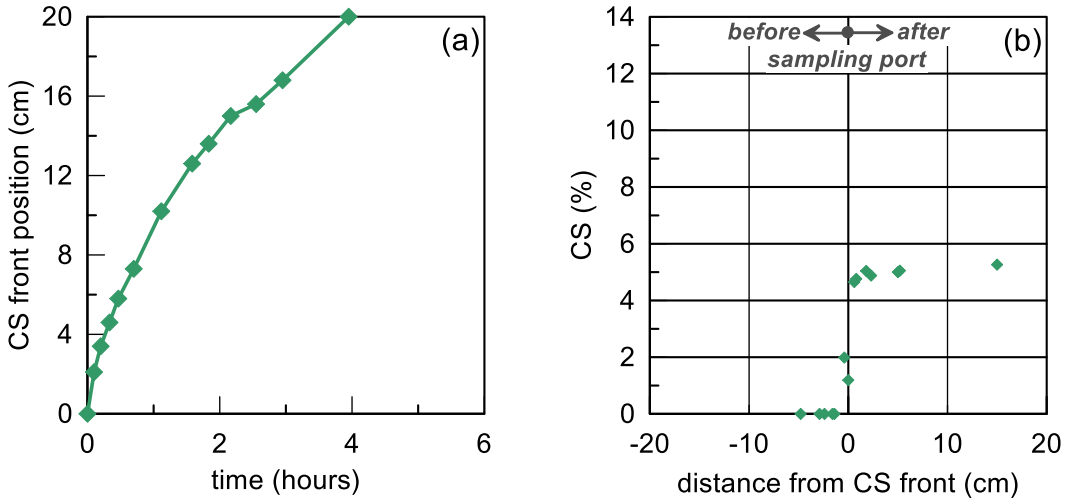

Figure 5.31 *Test No11: (a) Recorded CS front position versus time and (b) CS(%) concentration in the pore fluid, as extracted from the sampling ports.*

Test No12

This test used a CS solution similar to that of Tests No11 and No4, but with an intermediate CS concentration of 7.5%. Observe in Figure 5.32b that the CS viscosity increases slightly (given that the CS is higher than in Test No11) and this is accurately predicted by Eq. 4.1. However, this small increase of CS viscosity did not disallow breakthrough (Figure 5.33a), but overall the flow rate was significantly reduced (Figure 5.32a). Interestingly, the pore fluid sampling gave

qualitatively similar results as all previous tests, but for its pertinent nominal value of CS(%)=7.5 (see Figure 5.33b).

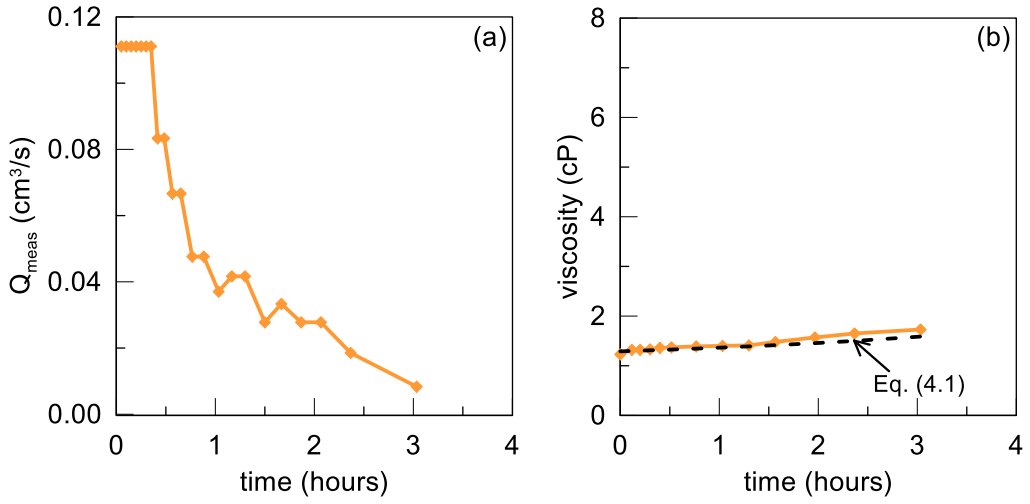

Figure 5.32 *Test No12: (a) Measured flow rate versus time and (b) measured and calculated (from Eq. 4.1) CS viscosity values versus time.*

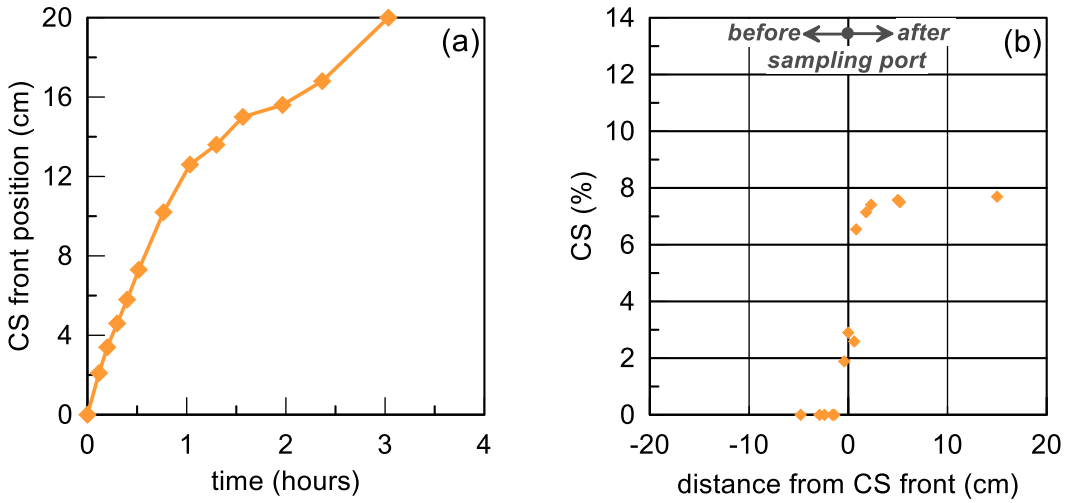

Figure 5.33 *Test No12: (a) Recorded CS front position versus time and (b) CS(%) concentration in the pore fluid, as extracted from the sampling ports.*

Test No13

Test No13 is practically the same with test No10 with the only difference being the pH value of the CS solution (6.75 instead of 10.0), which provides an extremely small increase to the viscosity from 1.45cP to 1.48cP within the time frame of 12.3hrs that is the test duration. This small increase of viscosity affected neither the decreasing flow rate (Figure 5.34, due to density-driven flow), nor the incomplete breakthrough (Figure 5.35). In other words, Test

No10 is practically duplicated here in terms of its CS injection measurements. No pore fluid sampling was performed in this test.

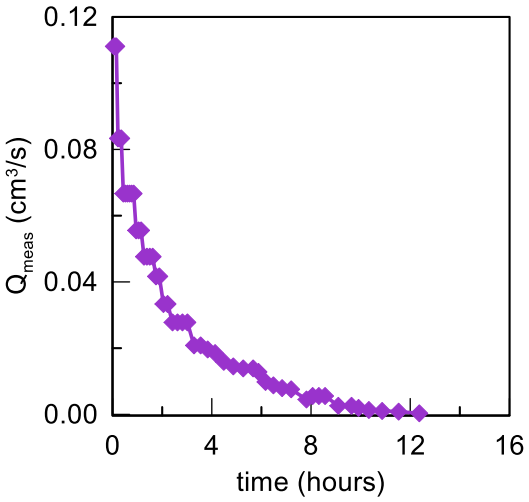

Figure 5.34 *Test No13: Measured flow rate versus time.*

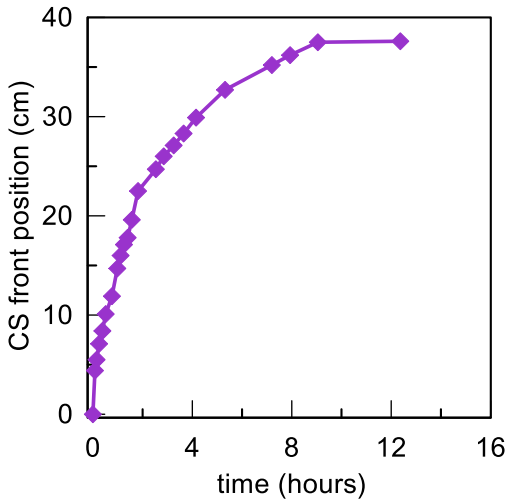

Figure 5.35 *Test No13: Recorded CS front position versus time.*

Test No1S

Test No1S was conducted on a silty sand column, rather than the pure sand columns of the previous tests. Its details are presented in Table 5-1. In comparison to the comparable Test No4 the relatively smaller hydraulic conductivity k of the silty sand column causes firstly a relatively smaller initial flow rate value, as shown at Figure 5.36(a). Other than that, the flow rate decreases, as in sand samples, and nullifies after almost 3 hours. During this time the CS viscosity increased to a value of 4 cP which is accurately simulated by Eq. (4.1), as shown in

Figure 5.36(b). The progression of the CS front versus time is shown in Figure 5.37 and as in tests in sand it has a hyperbolic shape, but stops at a position of just 7.4cm. This is because the flow rates are much lower than in sands due to smaller hydraulic conductivity. Unfortunately, due to the low hydraulic conductivity it was impossible to extract pore fluid from the sampling ports with the use of a syringe.

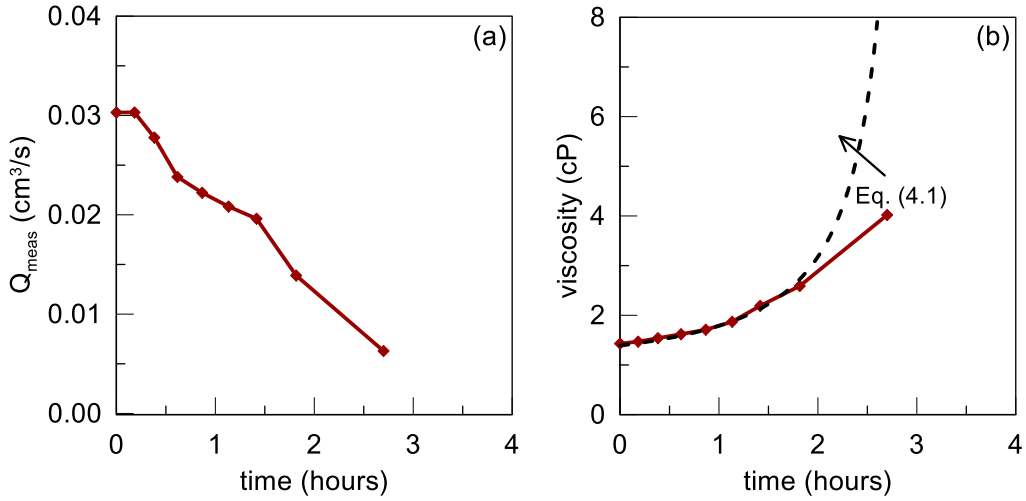

Figure 5.36 *Test No1S: (a) Measured flow rate versus time and (b) measured and calculated (from Eq. 4.1) CS viscosity values versus time*

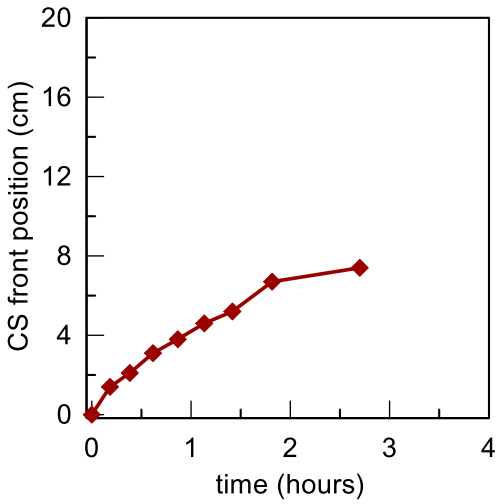

Figure 5.37 *Test No1S : Recorded CS front position versus time.*

On the top of the tests with deionized water as pore fluid, three (3) more tests were conducted using sea water as pore fluid insteado investigate the injectability of CS in a marine environment. The tests were executed in 40m and 100cm sand columns. It should be mentioned that sea water is heavier than deionized water and this is expected to affect the

density- driven flow component of the CS injections. However, the CS solution remains heavier than the sea water it displaces. In addition note the CS solution was prepared again with deionized water, however its potential interaction with the salt in the pore fluid it displaced could affect its rheology.

Test No1SW

The sand column was 40cm tall, and its hydraulic conductivity k was measured using sea water (see Table 5-1 for other details). This test is practically comparable with Test No6 with deionized water. Figure 5.38(a) shows the decreasing flow rate with time which practically becomes zero after 7 hours. The increasing CS viscosity versus time is shown in Figure 5.38(b) from where it is also concluded that this is accurately predicted by Eq. (4.1). Note that the flow rate practically nullifies after the CS viscosity becomes higher than 3cP. The CS front location progresses asymptotically with time and stops evolving after the CS viscosity becomes higher than 3cP (see Figure 5.39a). Finally, the pore fluid sampling gave comparable CS(%) results with previous tests on tests with deionized water (Figure 5.39b). Note that the CS front during the experiment did not move uniformly, maybe because of the not necessarily uniform salt concentration in the sea water in the pores os the sample as shown in Figure 5.40. Otherwise, the overall CS injectability does not seem to be affected considerably, despite the increased salt concentration within the pores of the sand when sea water is used.

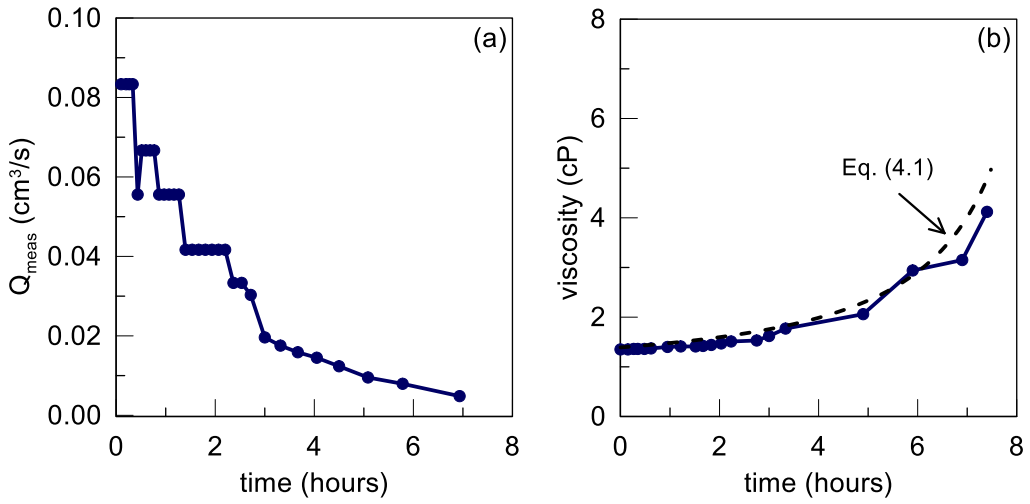

Figure 5.38 *Test No1SW: (a) Measured flow rate versus time and (b) measured and calculated (from Eq. 4.1) CS viscosity values versus time*

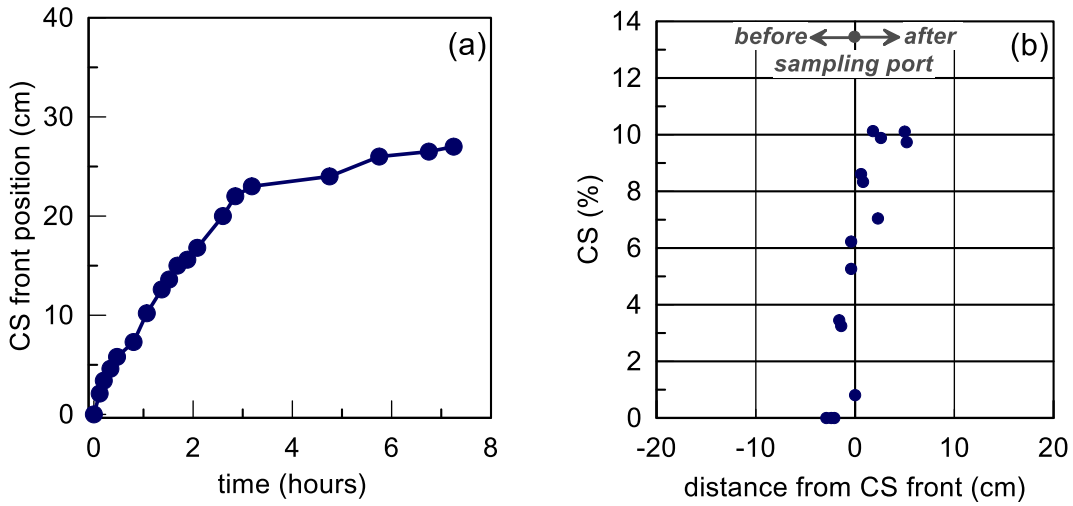

Figure 5.39 *Test No1SW: (a) Recorded CS front position versus time and (b) CS(%) concentration in the pore fluid, as extracted from the sampling ports*

Figure 5.40. *Non-uniform delivery of CS solution through sea water saturated sand column in Test No1SW.*

Test 2SW

Test 2SW uses a CS solution with a pH value of 6.80 and without any added salt, for which the viscosity is expected to remain constant during the test, a change of pH or salt concentration occurs. Its other details are shown in Table 5-1. As shown in Figure 5.41 the flow rate decreases with time, while breakthrough is achieved after 5.7hrs (Figure 5.42a). During this

time the CS viscosity remains constant at a value of 1.45cP on the basis of measurements performed on CS solution samples not injected in the sand.The pore fluid sampling gave the expected results in terms of CS(%). Interestingly, this test shows that injecting a CS solution without any added salt does not affect its expected injectability, at least for the short distances (up to 40cm) and durations (up to 6hrs) tested here.

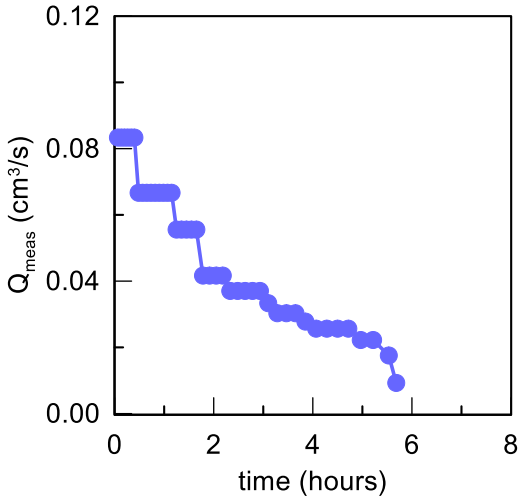

Figure 5.41 *Test No2SW: Measured flow rate versus time.*

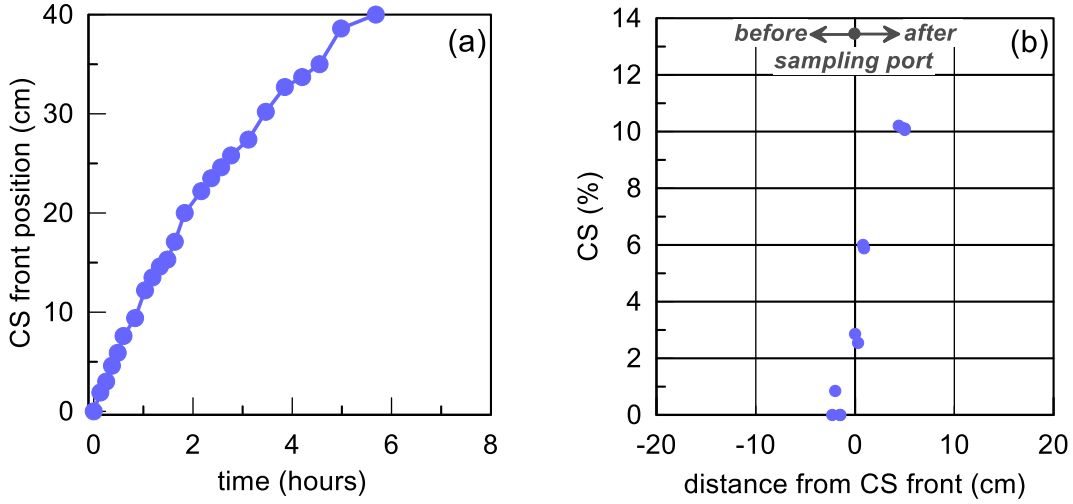

Figure 5.42 *Test No2SW: (a) Recorded CS front position versus time and (b) CS(%) concentration in the pore fluid, as extracted from the sampling ports*

Test 3SW

Test 3SW intended to achieve breakthrough of a 1m sea water saturated sand column using a low initial gradient and a CS solution without added salt having practically constant viscosity (other details may be found in Table 5-1). The results of this test are shown at Figure 5.43 and

Figure 5.44. It is shown that the CS solution managed the breakthrough of the 1m column after 16.4 hours, and this without its flow rate being reduced to zero. This means that the salt water environment again did not seem to considerably affect the rheology of the CS solution even for the larger distances (1m versus 0.4m in Test No2SW) and injection durations (16.4hrs versus 5.7hrs in Test No2SW) tested here.

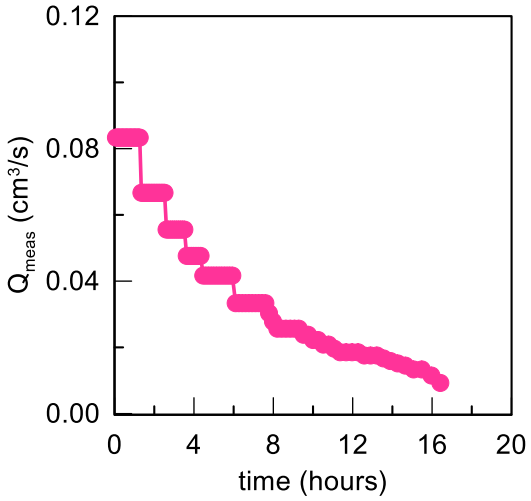

Figure 5.43 *Test No3SW: Measured flow rate versus time.*

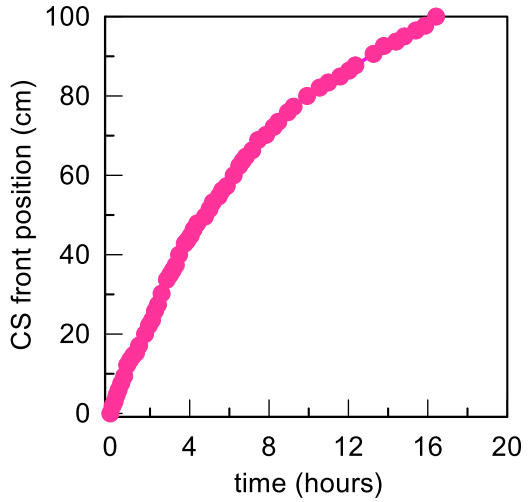

Figure 5.44 *Test No3SW: Recorded CS front position versus time.*

From the tests exexuted within sea water saturated sand columns it is concluded that the viscosity of the CS solution seems to be slightly only affected if the solution has been prepared with salt addition (Test No1SW). Moreover, even for tests where no salt eas added in the CS solution preparation (2SW, 3SW), the marine environment does not seem to affect considerably the CS viscosity, at least for the travelled distances (up to 1m) and the injection

durations (up to 16.4hrs) used in these tests. Caution is necessary for CS solutions having very high pH values (8-10) since these may be more intensely affected when injected in a marine environement. However, in practice, such options for the CS solutions are not expected to be commonly selected.

5.4 Comparative evaluation of injection test results

5.4.1 Pore fluid sampling results

As shown in the previous paragraphs, in all tests (where pore fluid sampling was performed) the CS(%) equals to zero at locations downstream from the CS front (measurements for positions with negative values). On the contrary, for measurements conducted exactly at the point of the sampling port, this concentration increases to 3.5-4% (for nominal CS_{nom} concentration of 10%), 2% (for CS_{nom} =5%), 2-3% (for CS_{nom} =7.5%). This percentage is increased further to 90% of the CS_{nom} value, when the CS front is 1cm higher than the sampling port and finally reaches the CS_{nom} when it is 2cm higher (at least) than the sampling port. In order to clarify if this behavior remains the same for all injection tests, Figure 5.45 shows the cumulative results of CS(%) measurements for all tests presented herein. These results are presented in Figure 5.45 in terms of the CS(%) concentration versus the distance of the sampling port position from the CS front position. The same results are presented in plot (b) normalized with the source concentration of CS, namely the initial concentration chosen for each test. Note that the CS_{nom} of each test is the actually measured value of CS(%) in the beginning of the injection test, which was not necessarily an integer value (see Table 5-1 for CS(%) values of each test, where, for example, the target CS=10% could actually be 10.1% or 10.3%). This explains why the CS/CS_{nom} values are practically all smaller or equal to 1.0 in Figure 5.45(b), while the scatter around the target CS(%) seems larger in Figure 5.45(a).

Based on Figure 5.45 the following conclusions can be drawn:

- An S-shaped curve can describe the relation between sampling port position (as compared with CS front position) and the CS(%) concentration in the pore fluid. If more tests are taken into account, the scatter of the curve becomes larger, without qualitatively changing its shape. Values slightly higher than the nominal CS concentration can be attributed to the (small) mass of salt and color in the samples extracted from the ports, but the deviations are considered insignificant for practical applications.
- At sampling ports before the CS front position (≤ -2cm) there is a small (if any) amount of CS in the pore fluid, which becomes zero at -4cm.

- At sampling ports after CS front position (≥+2cm) the CS concentration in the pore fluid is approximately equal to the nominal CS concentration (differences of maximum 20% from CS_{nom}), but a distance of almost 10cm is required in order to achieve a difference smaller than 10% from CS_{nom}.
- A region of 4cm (2cm before and after the CS front) exists where a transition zone is observed with intermediate CS(%) values (from zero up to 80% at least of CS_{nom}) with the smaller values downstream from the CS front and the opposite for the relatively higher values.
- Based on these conclusions, it may be safely concluded that an upward 1-D injection of CS with low hydraulic gradient essentially displaces the preexisting water in soil pores with a small thickness transition zone, especially downstream from the horizontal CS front. This last basic conclusion agrees well with the literature (e.g. Gallagher and Lin, 2009).

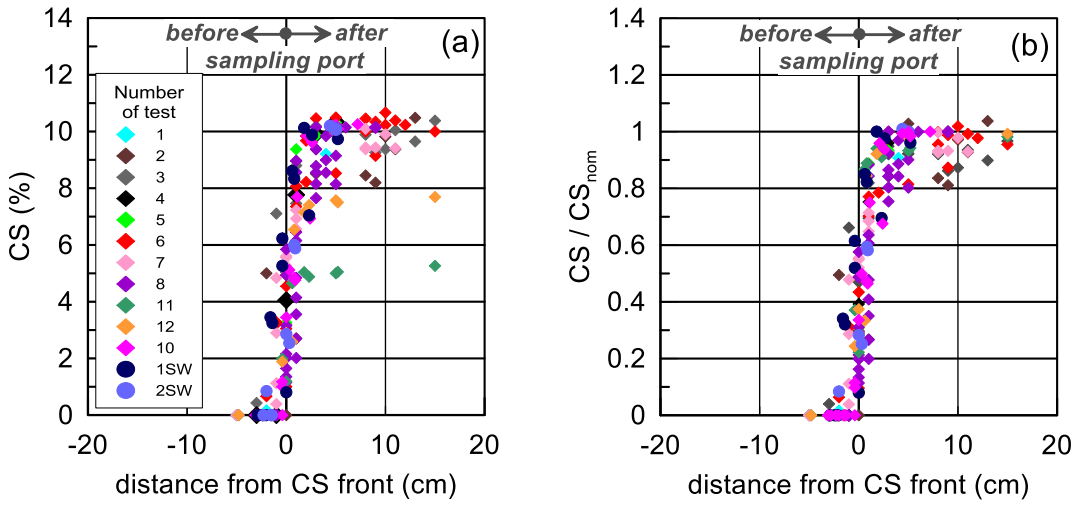

Figure 5.45 *(a) CS concentration extracted from the sampling ports for all tests, (b) Normalized CS concentration extracted from each sampling port with initial concentration (CS/CSnom) in relation with distance of CS front from the sampling ports.*

5.4.2 Flow rate and CS travel distance results

In order to better understand the effects of different parameters on CS injection the measurements of flow rate, viscosity and travel distance (CS front location) with time from different tests will be compared in the sequel.

Effect of initial hydraulic gradient i_0 (Test No4 vs Test No8)

Figure 5.46 presents the effect of different initial hydraulic gradients, i_0 on the measured flow rate and travel distance of CS. Test No 4 was performed using a low initial hydraulic gradient of 0.05, whereas Test No8 uses a quite higher initial gradient of 0.23, while the CS solutions in

the 2 tests had similar gel time. Note that in Figure 5.46a the flow rate and CS viscosity curves (with time) of the 2 tests are compared, by using different y-axes for the 2 different physical measures, but the same time scale (in the x-axis). The 2 tests are presented with different types of notation (dashed and solid lines). Figure 5.46b compares directly the two (2) tests in terms of the progression of the CS front with time, by using again dashed and solid lines. As illustrated in Figure 5.46, at the initial stage of injection, a higher gradient leads to increased flow rate, which stops when the viscosity of the CS solution reaches a value of 5-7cP, regardless of the i_0. Overall, the travel distance is much longer for the higher i_0. These results agree with the literature data of Gallagher and Lin (2009) who performed 1D column injection tests with different hydraulic gradients and found that the speed of CS transport is proportional to the hydraulic gradient used. Particularly, their results showed that, for a given distance, the travelling time decreases linearly with increasing hydraulic gradient.

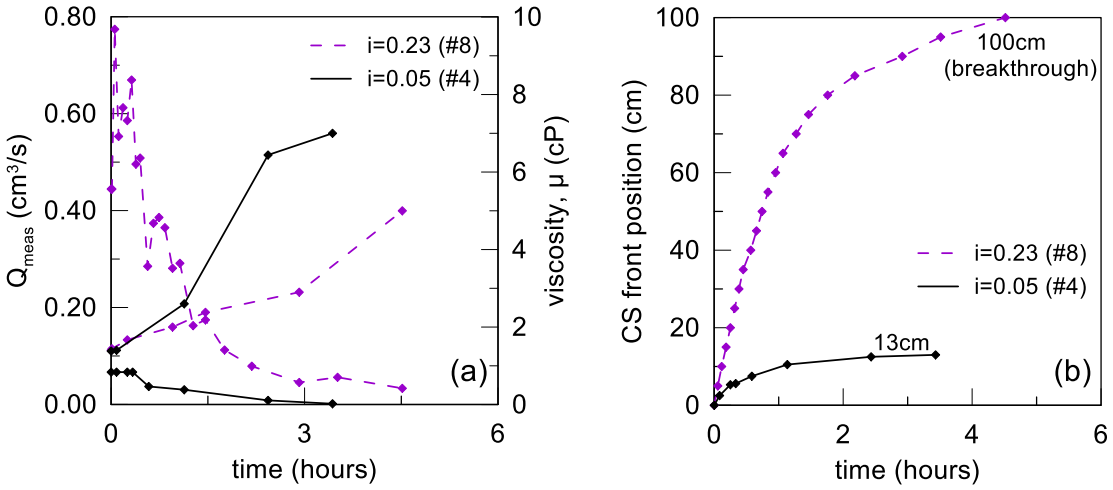

Figure 5.46 *Effect of initial hydraulic gradient i_0 on (a) measured flow rate with time (b) travel distance with time for injection tests in sand with CS of similar gel times (tests 4 and 8)*

Effect of time increasing viscosity resulting from different normality and pH (Test No4 vs Test No9)

For almost all injection tests, the flow is hindered by two different mechanisms; namely the increase of viscosity and the different density of the two fluids, CS and water. In order to eliminate one of these factors and more specifically to exclude the viscosity effect, in Test No9 the viscosity was held constant at the initial value of 1.47cP by adjusting the NaCl normality and pH of the CS solution. Figure 5.47, shows the effect of time-increasing viscosity of CS resulting from different NaCl normality and pH on the flow rate and the CS travel distance in the format of the Figure 5.46. For Test No9 the flow rate decreases due to the density

difference of CS and water, whereas for Test No4 both time-increasing viscosity and different densities affect the flow rate. Both tests have the same initial hydraulic gradient (i_0=0.05) and the same hydraulic conductivity and so, their initial values of Q_{meas} practically coincide. However, the flow rate for Test No4 decreases faster and finally stops after 3.4h when the CS viscosity has reached a value of 7cP, while for Test No9 the injection continues further, but at a much reduced flow rate which eventually leads to a slightly higher travel distance.

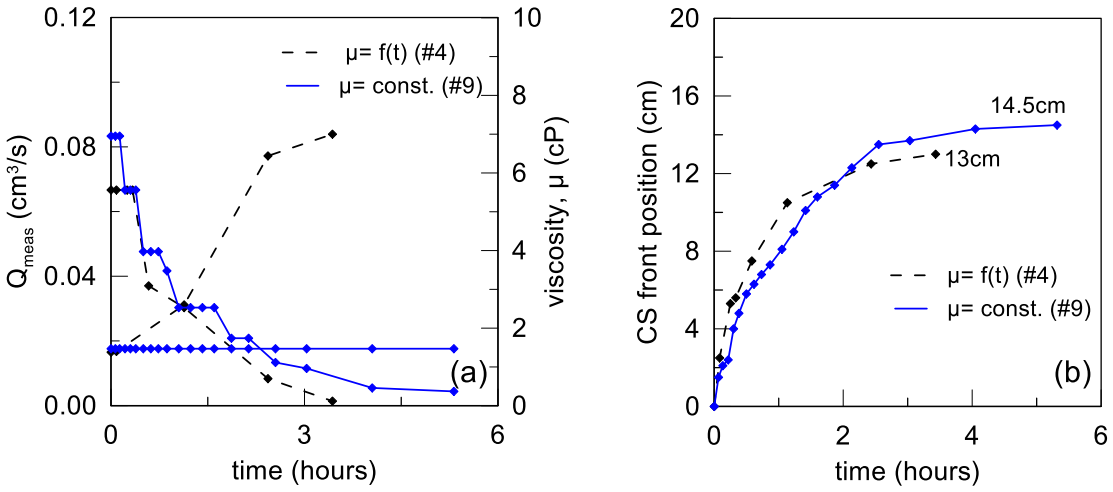

Figure 5.47 *Effect of time increasing CS viscosity on (a) measured flow rate with time, (b) travel distance with time for injection tests in sand with CS solutions with very different rheology due to different NaCl normality and pH (tests 4 and 9)*

Effect of time increasing viscosity resulting from different CS(%) (Test No4 vs Test No11)

The two flow rate affecting effects can also be disassociated by altering the CS(%) in the solution, thus altering again its gel time. This is illustrated on Figure 5.48 where 2 injection tests using 2 solutions with different CS(%) are compared in the known format of Figure 5.46. Test No4 has a solution with CS(%)=10 and its viscosity reaches a value of 7cP after 3.4hrs, whereas Test No11 uses a solution with CS(%)=5 whose viscosity does not increase, but remains constant at a value of 1.14cP (within a 4hr time window tested). Observe that the flow rate reduces due to the density-driven flow despite the fact that the CS viscosity remains constant similarly to what is shown in Figure 5.47 for tests where the viscosity does not change due to other solution properties (NaCl normality and pH, versus CS(%) here). However, in this test the flow rate remains large for enough time to allow for breakthrough of the 20 cm sand column, even though the initial hydraulic gradient of Test No11 is slightly smaller than this of Test No4. This is attributed to CS=5%, which leads to a much lower constant CS viscosity (1.14cP here, versus 1.47cP in Figure 5.47 for Test No9) but also to the smaller difference in

density between the CS=5% and water here (as opposed to CS=10% and water in Figure 5.47 for Test No9).

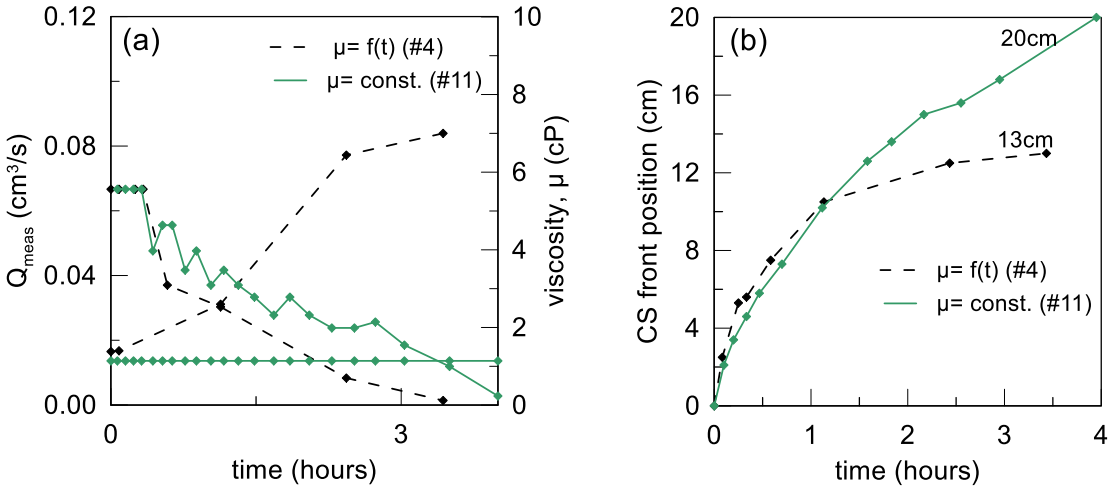

Figure 5.48 *Effect of time increasing CS viscosity on (a) measured flow rate with time, (b) travel distance with time for injection tests in sand with CS solutions with very different rheology due to different CS(%) (tests 4 and 11)*

Effect of gel time (Test No4 vs Test No6)

Figure 5.49 shows the effect of different gel time, resulting from different pH values in the solution, on the measured flow rate and the travel distance under similar (low) initial hydraulic gradients in the well-known format of Figure 5.46. Observe that the slower increase of viscosity (related to longer gel time) leads to a slower decrease of Q_{meas}, despite that the initial flow rate is the same due to the same initial hydraulic gradient and viscosity values. For both tests the flow rate ends when the CS viscosity has reached a value of 4-7cP, which occurs at different times leading to quite different travel distances. The same conclusions were drawn by Gallagher and Lin (2009) who observed that as the viscosity increased, CS transport decreased dramatically, and so decreased travel times were observed. Particularly, they show that in a column test with low initial gradient and a CS solution with a gel time equal to 3.2 days, the CS delivery was completed (breakthrough) in about 45 hours, because the viscosity was still less than 3 cP at that time. In contrast, the CS delivery lasted only 18 hours in another test with ithe same initial gradient but a gel time equal to almost 1 day, because the viscosity increased faster and finally the CS covered a distance of 85% the column length (no breakthrough).

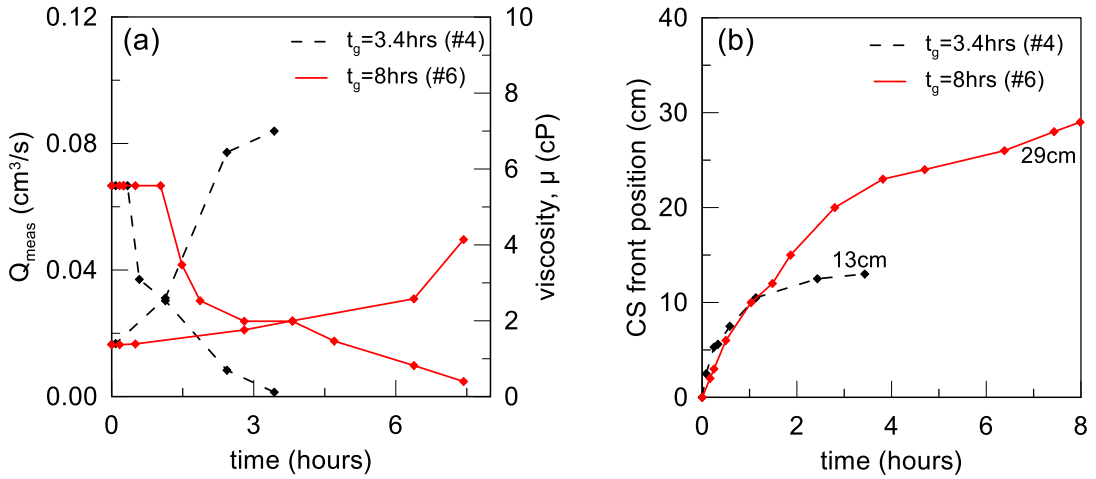

Figure 5.49 *Effect of time increasing CS viscosity on (a) measured flow rate with time, (b) travel distance with time for injection tests in sand with CS solutions with very different rheology due to different pH (tests 4 and 6)*

Effect of hydraulic conductivity (Test No4 vs Test No1S)

Injection test results from sand and silty sand samples with the same CS solution properties, and initial hydraulic gradient are compared in Figure 5.50 which employs the known format of previous figures. The difference in the consistency of the soil is considered to be fully reflected for these tests on the difference in the hydraulic conductivity k of the two samples, which causes an expected different flow rate according to Darcy's law.

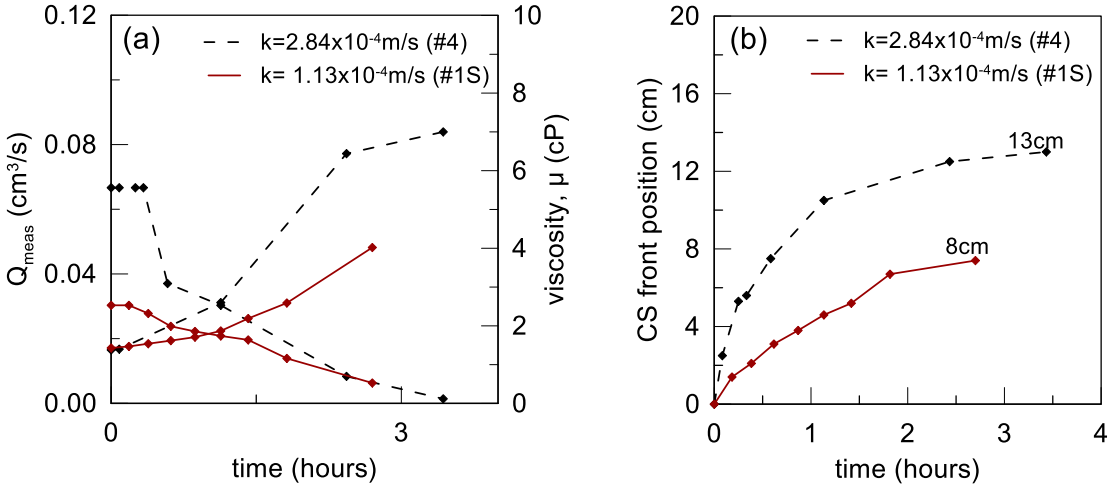

Figure 5.50 *Effect of hydraulic conductivity on (a) measured flow rate with time, (b) travel distance with time for injection tests in different sandy samples with the same CS solutions (tests 4 and 1S)*

This is approximately measured on the initial flow rate, however the Q_{meas} decreases asymptotically with time for both tests and finally the flow ends at the same time, i.e. when

the CS viscosity has reached a value of 4-7cP. It should be stated here that the CS front in Test No1S (silty sand) was not easily observed despite the dye, however the difference in k values is clearly reflected on the different travel distances. This does not mean that the injection is impossible for silty sands. On the contrary, this test shows that it may be performed but it requires higher initial hydraulic gradients (e.g. see this effect in Figure 5.46) and/ or CS solutions with larger gel times (e.g. see this effect inFigure 5.49). Gallagher and Lin (2009) conducted 1D column injection tests on samples of Nevada and Ottawa sand which have $k=8.9x10^{-5}$cm/s and $k=220x10^{-5}$cm/s respectively. They found that the flow rate was directly proportional to the hydraulic conductivity of the soil and the traveling distance through the Ottawa sand column was nearly two orders of magnitude lower than through the Nevada sand column. Hence, our findings are compatible with the literature although we performed tests with much smaller difference in hydraulic conductivity k.

Effect of salt content in sand pores (Test No6 vs Test No1SW)

In order to investigate the potential of CS injection in marine sands, i.e. when the saturation of the pores is performed with sea water, Figure 5.51 compares the flow rates and CS travel distances for two otherwise identical tests in terms of soil type, CS solution and hydraulic gradient, by employing the format of Figure 5.46 once again. Test No 1SW was conducted with a CS solution, consisted of deionized water and salt and its pH was not large (7.03). Consequently, the effect of sea water on viscosity evolution is expected to be quite small and this is obvious by the fact that the flow rate becomes zero faster than in Test No6. The effect of the marine environment on CS viscosity is expected to be gradual and that is why the flow rate becomes systematically lower in Test No1SW after 3h. Because of this fact, the CS front in Test No1SW finally stops a little lower than in Test No6. Observe in Figure 5.51 that the viscosity of the two CS solutions is almost identical outside the soil column, since the solutions were produced with deionized water and the viscosity measurement was performed in the container of CS, which is not exactly relevant to the viscosity of the CS in the pores.

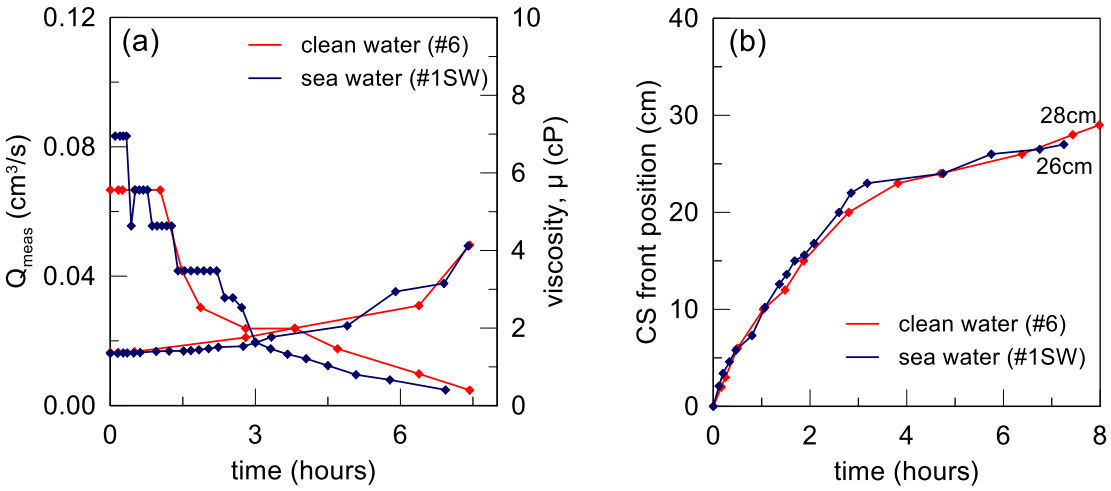

Figure 5.51 *Effect of salt content in sand pores on (a) measured flow rate with time, (b) travel distance with time for injection tests on sand samples saturated with clean and sea water (tests 6 and 1SW)*

Finally, apart from the vertical 1-D injection tests, a horizontal pseudo 2-D test was also performed in an attempt to investigate basic aspects of the multi- dimensional problem of CS injection in practice. The equipment used was the same as before, but it was placed horizontally, while the levels of CS and water in the outlet and inlet chambers were kept constant during the whole test (as in the vertical 1D injection tests). The CS solution characteristics were chosen so that its viscosity would remain constant and would thus not affect the flow rate. It was observed that despite the higher density of CS compared to water, the flow rate practically retained its initial value throughout the injection. This shows that the difference in (pore fluid) density does not essentially affect the flow rate of a horizontally travelling CS solution under a constant hydraulic gradient flow. Nevertheless, the higher density of CS in comparison with water made the front of the horizontally travelling CS not to be vertical, but with a small inclination at the beginning of the test (Figure 5.52) that became larger as the injection progressed (Figures 5.53 and 5.54). This is an effect of gravity on the denser CS, which has also been demonstrated in real 2D injection tests. More specifically, Gallagher and Koch (2003) performed a 2D injection test and state that due to the density difference between the CS solution and the water, there was a tendency for the stabilizer to treat the bottom half of the formation first. The same holds in our test, where the bottom half of the container is more fully filled with CS, due to the observed inclination of the CS front.

Figure 5.52 *View of CS front in the beginning of the horizontal injection test.*

Figure 5.53 *View of CS front location during the horizontal injection test.*

Figure 5.54 *View of CS front location at the end of the horizontal injection test.*

5.5 Analytical simulation of 1D column injection tests

This paragraph attempts an analytical simulation of this multi- variable CS delivery problem that was studied via the shown 1D column injection tests. Figure 5.6 presented a schematic illustration of the test variables at a random time during the CS injection. Particularly, as the CS solution is delivered from the inlet chamber, it moves upwards within the soil column displacing pore water. Thus, over time the CS solution occupies a region of the soil column with height equal to L_g; this region is defined by the bottom layer of the soil column and the (horizontal) front of the CS solution. In this region, the pore space is filled with the CS solution, which is heavier (stabilizer density, $\rho_g > 1000$ kg/m^3) and more viscous than water (stabilizer viscosity, $\mu_g > 1.00$cP from the beginning of the injection) it displaces. For usual CS percentages its properties vary as: ρ_g = 1024- 1048kg/m^3, $\mu_g \geq 1.24$cP – 1.39cP for CS = 5-10% respectively (these values correspond to average initial viscosities for T=25^{o}C). In other words, the injection of a CS solution into a saturated porous medium constitutes a flow problem under viscosity and density varying conditions.

It is common for many mainstream numerical codes (e.g. MOCDENSE, SEAWAT) to assess the variable-density flow with the concept of equivalent fresh water heads. According to this concept, every measured hydraulic head is expressed in terms of an equivalent fresh water hydraulic head (h_f) according to:

$$h_f = z + \frac{P}{\rho_w g} \tag{5.1}$$

where z is the elevation head (m), P is fluid pressure (Pa), ρ_w is fresh water density (kg/m^3) and g is the gravitational acceleration (m/s^2). However, the concept of equivalent fresh water heads may produce erroneous flow rate estimates, especially in cases of vertical flow (Simmons 2005). Fresh water head analyses can misinterpret water flow calculations, if density variations are not properly taken into account (Post et al. 2007). To avoid such misinterpretations, Post et al. (2007) suggest the application of the more general form of Darcy's law for fluid flow in a porous medium:

$$Q_{calc} = -\frac{k_i}{\mu}\left(\frac{\partial P}{\partial z} + \rho g\right) A \tag{5.2}$$

where k_i is intrinsic hydraulic conductivity (m^2), μ is the fluid dynamic viscosity (kg/m/s), ρ is the fluid density (kg/m^3) and A is the cross-sectional area to flow direction (m^2), while Q_{calc} is the calculated value of the flow rate (m^3/s), that is to be compared to the measured values

Q_{meas} in the previous paragraphs. This form of Darcy's law explicitly demonstrates the two driving forces of flow, i.e. the pressure gradient (∇P) and the gravity force per unit volume (ρg). By differentiating and rearranging in order to be combined with Equation (5.1) Equation (5.2), the latter becomes equivalent to the following expression:

$$Q_{calc} = -\frac{k\rho_w g}{\mu}\left[\frac{\partial h_f}{\partial z} + \left(\frac{\rho - \rho_w}{\rho_w}\right)\right]A \tag{5.3}$$

For the assessment of variable-density flow, Post et al. (2007) suggest the application of Equation (5.3) with an average fluid density that is given by:

$$\rho_\alpha = \frac{1}{z_2 - z_1}\int_{z_1}^{z_2}\rho dz \tag{5.4}$$

where z_1 and z_2 are any two different heights within the soil column with $z_2>z_1$, while the calculated ρ_α corresponds to the average fluid density for the area between z_1 and z_2.

In the case of CS injection, the spatial variation of viscosity cannot be neglected. Hence, as proposed by Agapoulaki et al (2015) the calculation of an average viscosity term is required, that may be similarly estimated by:

$$\mu_\alpha = \frac{1}{z_2 - z_1}\int_{z_1}^{z_2}\mu dz \tag{5.5}$$

where the μ_α corresponds to the average fluid viscosity in the area between z_1 and z_2. Based on the spatial distributions of density and viscosity depicted in Figure 5.6, the average rheological properties described in Equations (5.4) and (5.5) may be simply expressed by:

$$\rho_\alpha = \frac{\left(\rho_g L_g + \rho_w L_w\right)}{L} \tag{5.6}$$

$$\mu_\alpha = \frac{\left(\mu_g L_g + \mu_w L_w\right)}{L} \tag{5.7}$$

Where ρ_g and μ_g are the density and the viscosity of CS, L, L_g and L_w are lengths defined in Figure 5.6, with L being the total length of the soil sample, L_g being its fraction that is saturated with CS in the pores and L_w being the remainder of Lthat is still saturated with water (L_w=L-L_g).

Note that these average quantities are functions of time, since L_g increases over time thus leading to a decrease of L_w. Furthermore, μ_α is dependent on μ_g, which also increases over

time due to the gelling process of the CS solution. Hence, both ρ_α and μ_α increase over time, with the latter increasing more intensely due to the concurrent increase of μ_g and L_g.

Finally, if one substitutes Equations (5.6) and (5.7) into Equation (5.3), the flow rate can be estimated by the following analytical equation (Agapoulaki et al, 2015):

$$Q_{calc} = \frac{k\rho_w g}{\left(\mu_g L_g + \mu_w L_w\right)}\left\{\left[\left(\frac{\rho_g}{\rho_w}\right)h_1 - h_2\right] - \left(\frac{\rho_g}{\rho_w} - 1\right)L_g\right\}A \quad (5.8)$$

where h_1 and h_2 are the measured hydraulic heads corresponding to the inlet and the outlet chambers of the test, respectively (see Figure 5.6). The initial equilibrium levels of the inlet and outlet chambers (for no-flow conditions) can be estimated from Equation (5.8) by considering L_g=0, i.e. when the CS has not yet entered the soil column. For example, if h_1=1m, then the level of water should be adjusted slightly higher to $h_2=h_1\rho_g/\rho_w$= 1.05m for an initial equilibrium state of flow (for ρ_g =1.048t/m^3 corresponding to CS=10%).

In order to use Equation (5.8) constant parameters h_1, h_2, ρ_g, ρ_w, k, L and evolution of μ_g and L_g are required as input. The values of the constant parameters are shown in Table 5-2 for each 1D injection test that had measurements of flow rate, except for the values of L and k which are already presented in Table 5-1. Note that ρ_w=1000 kg/m^3, but when sea water was used in the injection test, the density of the sea water was measured equal to 1021kg/m^3. Viscosity of water is always equal to 1cP, while sea water viscosity equals to 1.002cP. The density of CS (ρ_g) differs at each test depending on the initial concentration CS(%) used, with this variation being: ρ_g = 1024- 1048kg/m^3 for CS(%)=5-10 respectively.

Note that Equation (5.8) refers to the injection of the CS solution before its breakthrough. Furthermore, for given values of the constant parameters this equation can predict the maximum L_g where the injection ends because of the density difference between CS and water. Specifically, if the equation yields negative values of Q_{calc}, this means that the injection has ended because of this fluid density difference, and as a result the accurate value of Q_{calc}=0 thereafter. Hence, if the maximum L_g (provided by Eq. 5.8 by solving for Q_{calc}=0) is smaller than the L of the column, then breakthrough is not possible in this injection. This value of maximum L_g (denoted by $L_{g,max}$) is this given by:

$$L_{g,max} = \frac{\rho_g h_1 - \rho_w h_2}{\rho_g - \rho_w} \quad (5.9)$$

Moreover, Eq. (5.8) can also be modified to predict the Q_{calc} values after breakthrough. Based on the above, this can only occur if $L_{g,max}>L$. In such a case, one can set $L_g=L$ (and $L_w=0$) in Eq. (5.8), which leads to the following equation for estimating Q_{calc} after breakthrough:

$$Q_{calc}=\frac{k\rho_w g}{\left(\mu_g L_g\right)}\left\{\left[\left(\frac{\rho_g}{\rho_w}\right)(h_1-L)-(h_2-L)\right]\right\}A \tag{5.10}$$

This equation (5.10) predicts a decreasing Q_{calc} due to the increasing μ_g, while if μ_g is kept constant then Q_{calc} will also remain constant. In general, for the successful application of Equations (5.8) and (5.10) the evolution of L_g with time (before breakthrough) is necessary, as well as the values of μ_g which can be either the measured ones in the laboratory, or the predicted ones as expressed by Equation (4.1).

In order to test the predictive abilities of Equation (5.8), its predictions are compared with the corresponding data of the various CS injection tests presented above. There are no estimates of Q_{calc} after breakthrough (Eq. 5.10), since no pertinent Q_{meas} measurements were performed in the few tests that did show breakthrough. The analytical predictions of flow rate in these tests are compared herein with the pertinent data in Figures 5.55-5.67 (13 injection tests in Table 5-2). Particularly, these figures present the prediction of Q_{calc} on the basis of Eq. (5.8) by taking into account the values of h_1, h_2, ρ_w and ρ_g from Table 5-2, the values of k and L from Table 5-1, the measurements of L_g and μ_g with time for each test. This prediction is denoted by $Q_{calc}(\mu_{meas})$. In addition, an alternative prediction of the flow rate is presented for which the calculated μ_g (via Eq. 4.1) is used and this is denoted by $Q_{calc}(\mu_{calc})$, and both these predictions of Q_{calc} are compared to the measured values Q_{meas}. The values of measured flow rate (Q_{meas}) are shown with the hollow symbols whereas the predicted values of flow rate where the CS viscosity takes the measured values from the experiments [$Q_{calc}(\mu_{meas})$] are depicted with line-connected solid symbols. Similarly, the predicted values of $Q_{calc}(\mu_{calc})$ are depicted with the dashed black lines. It should be noted that the predictions of μ_g (via Eq. 4.1) are not always in full agreement with the pertinent experimental measurements since temperature could not be kept constant during the injection tests, especially those of long duration. Hence, it is expected that the use of the measured μ_g values will lead to slightly more accurate results.

It is noted that Eq. (5.8) first appeared in Agapoulaki et al. (2015) who demonstrated its applicability on the basis of selected injection tests as part of a related research project (see nanoliq.org) conducted concurrently with this Thesis. In this Thesis, a thorough investigation of the reliability of this equation is performed on the basis of all conducted injection tests,

while this equation is also extended for estimating the flow rate even after breakthrough (Eq. 5.10). In addition, Eq. (5.8) is also used by accounting for the calculated values of viscosity (μ_{calc}, via Eq. 4.1), as a means to test its predictive ability without rheological measurements.

Table 5-2 *Values for a subset of the constant parameters of Eq. (5.8), that are used for predicting Q_{calc} for each injection test based on the laboratory measurements.*

Test (#)	h_1 (cm)	h_2 (cm)	ρ_w (kg/m^3)	ρ_g (kg/m^3)
4	57	58.6	1000	1048
5	57.6	59.3	1000	1048
6	120	123.7	1000	1048
8	130	113	1000	1048
9	55	56.6	1000	1048
10	120.3	124.3	1000	1048
11	56	56.7	1000	1024
12	57.6	58.4	1000	1036
13	120.1	124.1	1000	1048
1S	57.7	59.5	1000	1048
1SW	120.1	121.5	1021	1048
2SW	120.1	121.5	1021	1048
3SW	120	119.3	1021	1048

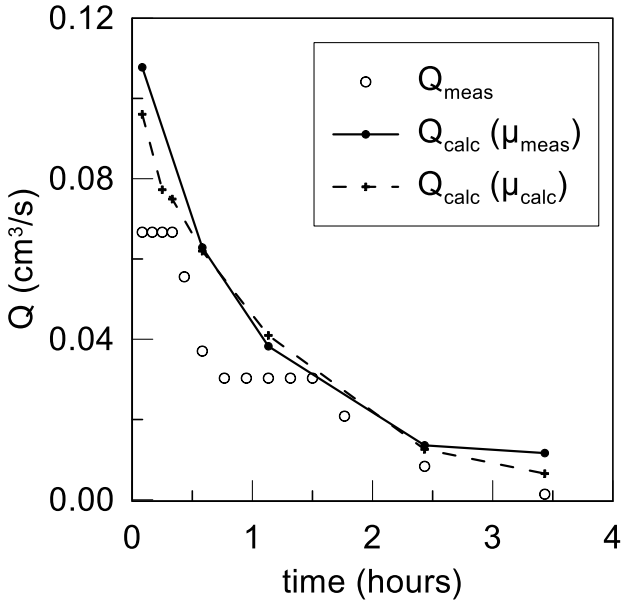

Figure 5.55 *Measured Q_{meas} vs calculated Q_{calc} flow rates [using the measured CS viscosity, (μ_{meas}), as well as the calculated CS viscosity from Eq(4.1) (μ_{calc})) versus time for CS injection Test 4.*

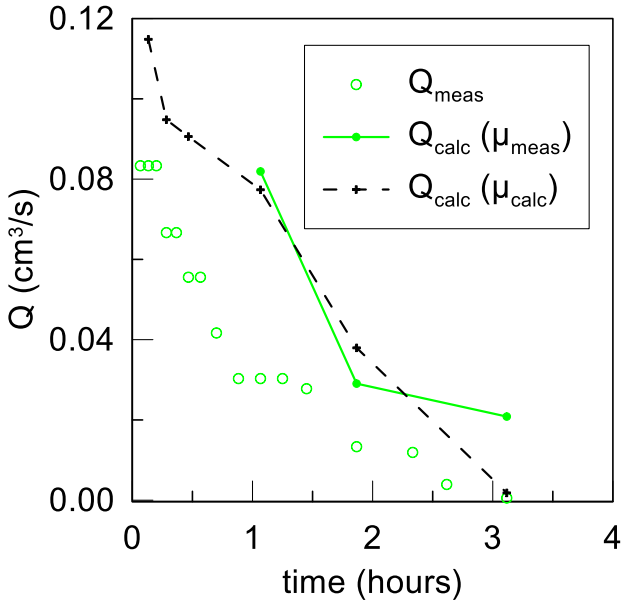

Figure 5.56 *Measured Q_{meas} vs calculated Q_{calc} flow rates [using the measured CS viscosity, (μ_{meas}), as well as the calculated CS viscosity from Eq(4.1) (μ_{calc})) versus time for CS injection Test 5.*

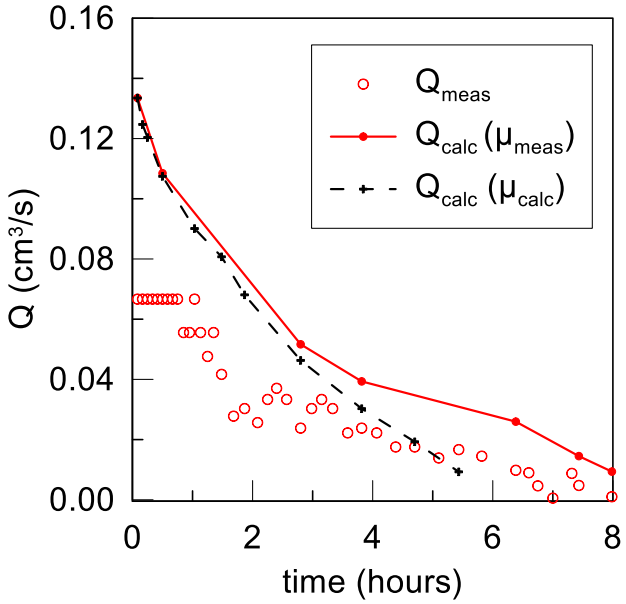

Figure 5.57 *Measured Q_{meas} vs calculated Q_{calc} flow rates [using the measured CS viscosity, (μ_{meas}), as well as the calculated CS viscosity from Eq(4.1) (μ_{calc})) versus time for CS injection Test 6.*

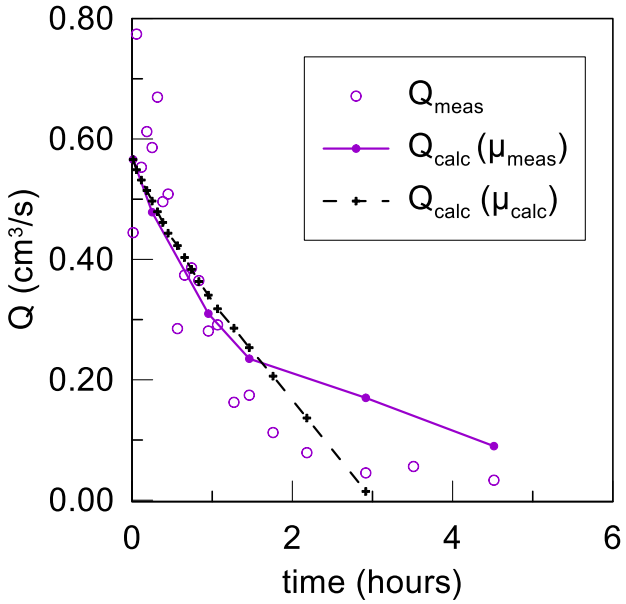

Figure 5.58 *Measured Q_{meas} vs calculated Q_{calc} flow rates [using the measured CS viscosity, (μ_{meas}), as well as the calculated CS viscosity from Eq(4.1) (μ_{calc})) versus time for CS injection Test 8.*

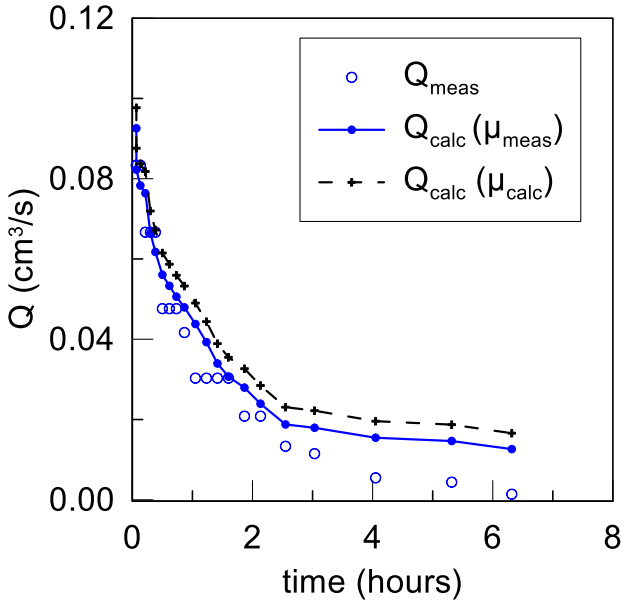

Figure 5.59 *Measured Q_{meas} vs calculated Q_{calc} flow rates [using the measured CS viscosity, (μ_{meas}), as well as the calculated CS viscosity from Eq(4.1) (μ_{calc})) versus time for CS injection Test 9.*

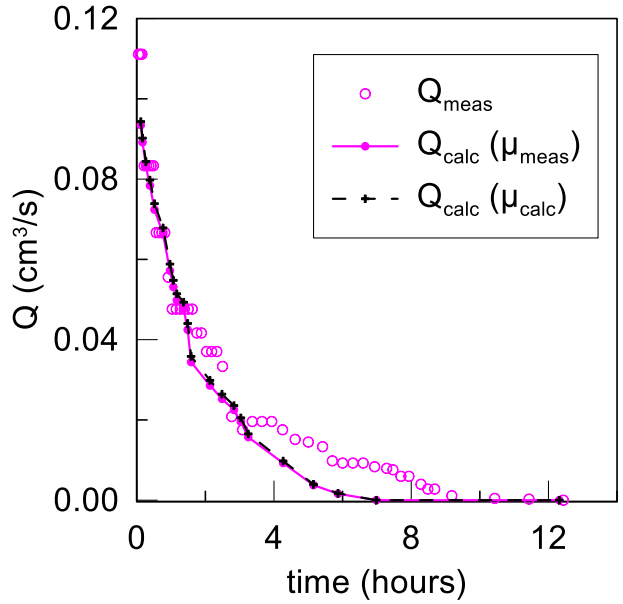

Figure 5.60 *Measured Q_{meas} vs calculated Q_{calc} flow rates [using the measured CS viscosity, (μ_{meas}), as well as the calculated CS viscosity from Eq(4.1) (μ_{calc})) versus time for CS injection Test 10.*

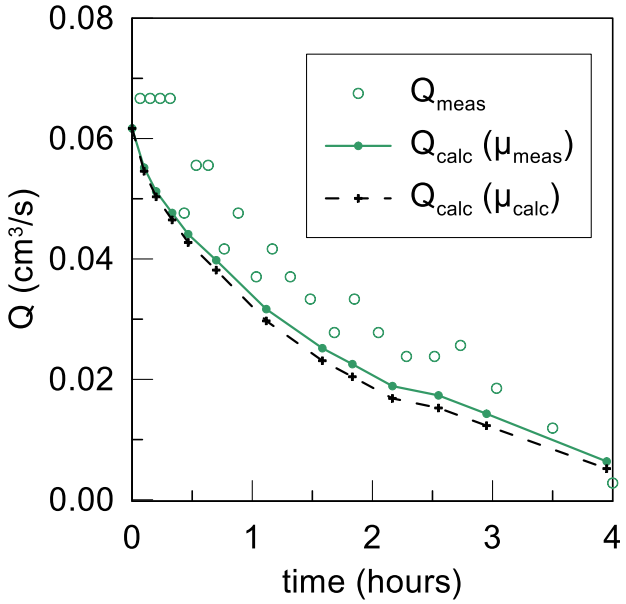

Figure 5.61 *Measured Q_{meas} vs calculated Q_{calc} flow rates [using the measured CS viscosity, (μ_{meas}), as well as the calculated CS viscosity from Eq(4.1) (μ_{calc})) versus time for CS injection Test 11.*

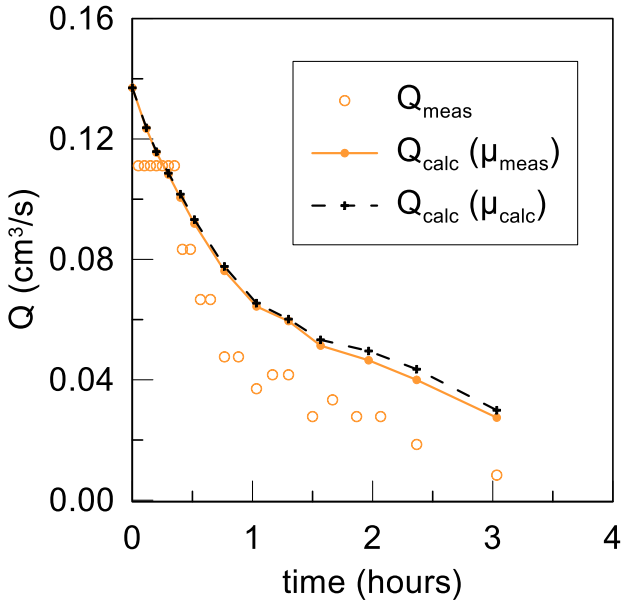

Figure 5.62 *Measured Q_{meas} vs calculated Q_{calc} flow rates [using the measured CS viscosity, (μ_{meas}), as well as the calculated CS viscosity from Eq(4.1) (μ_{calc})) versus time for CS injection Test 12.*

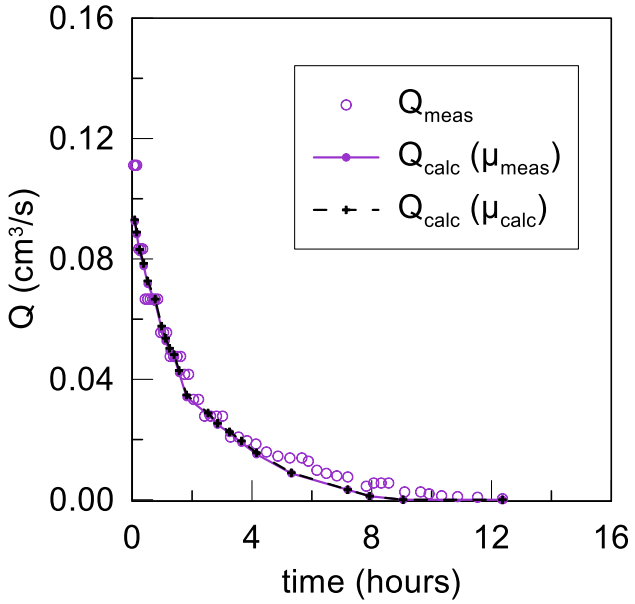

Figure 5.63 *Measured Q_{meas} vs calculated Q_{calc} flow rates [using the measured CS viscosity, (μ_{meas}), as well as the calculated CS viscosity from Eq(4.1) (μ_{calc})) versus time for CS injection Test 13.*

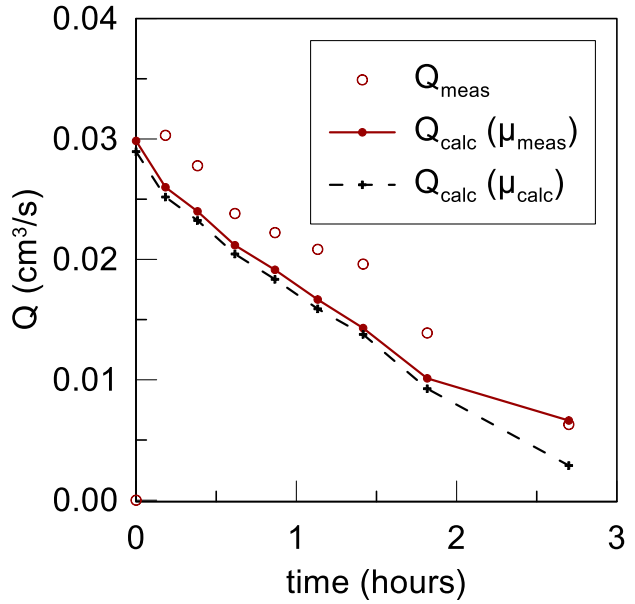

Figure 5.64 *Measured Q_{meas} vs calculated Q_{calc} flow rates [using the measured CS viscosity, (μ_{meas}), as well as the calculated CS viscosity from Eq(4.1) (μ_{calc})) versus time for CS injection Test 1S.*

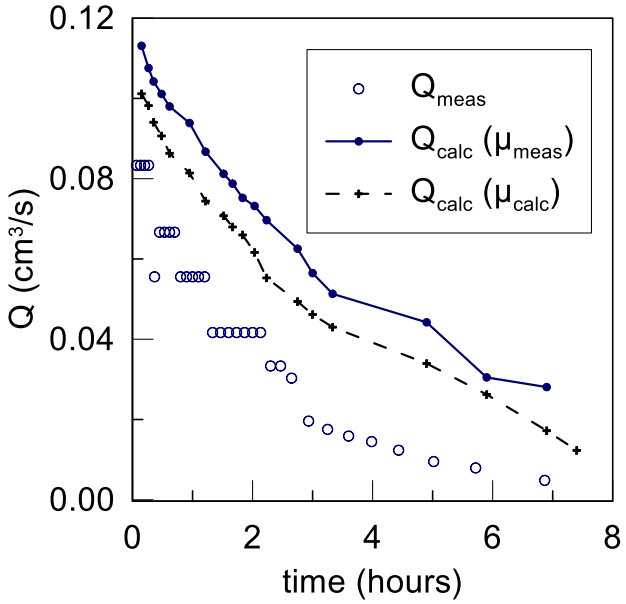

Figure 5.65 *Measured Q_{meas} vs calculated Q_{calc} flow rates [using the measured CS viscosity, (μ_{meas}), as well as the calculated CS viscosity from Eq(4.1) (μ_{calc})) versus time for CS injection Test 1SW.*

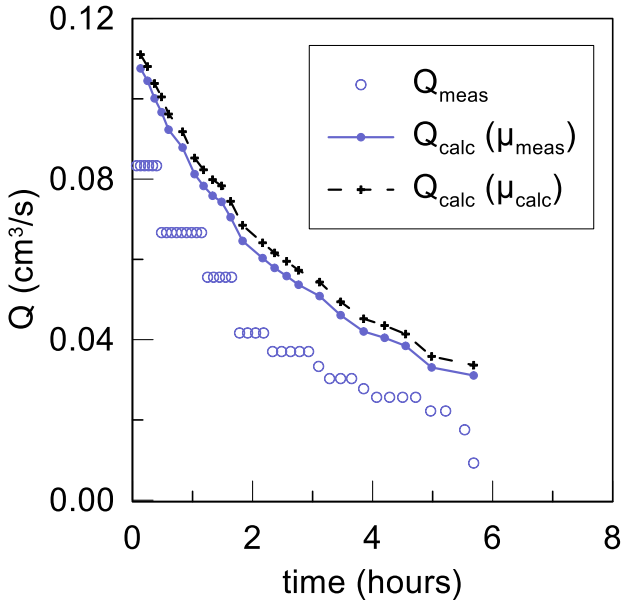

Figure 5.66 *Measured Q_{meas} vs calculated Q_{calc} flow rates [using the measured CS viscosity, (μ_{meas}), as well as the calculated CS viscosity from Eq(4.1) (μ_{calc})) versus time for CS injection Test 2SW.*

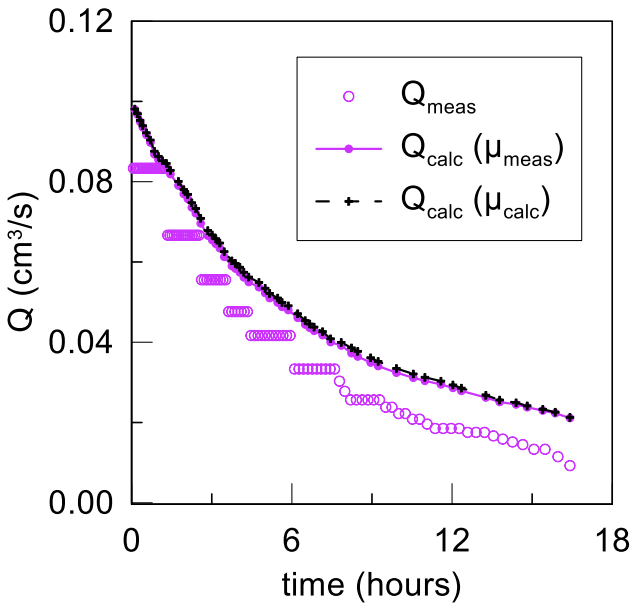

Figure 5.67 *Measured Q_{meas} vs calculated Q_{calc} flow rates [using the measured CS viscosity, (μ_{meas}), as well as the calculated CS viscosity from Eq(4.1) (μ_{calc})) versus time for CS injection Test 3SW.*

As a whole, Figures 5.55 through 5.67 show that the analytical solution developed by Post et al. (2007), as modified by Agapoulaki et al (2015), reproduces satisfactorily the measured pattern of flow rates decreasing with time. This reduction of the flow rates with time results from: (a) the increase of the height of the CS front within the sample (L_g in Figure 5.6), and (b) the increase of the CS viscosity. From a quantative point of view, a differentiation may be considered between the 10 injection tests using deionized water as pore fluid (Figures 5.55 through 5.64) and the 3 injection tests with sea water as pore fluid (Figures 5.65 through 5.67).

Particularly, for 5 of the former set of 10 injection tests, the calculated flow rates accurately (or slightly over-) predict the measured ones (Tests 4, 8, 9, 10, 13). For the remaining 5 tests in this set, in 3 tests the calculated flow rates overestimate the measured ones (Tests 5, 6 and 12), while in the remaining 2 tests (Tests 11, 1S) the opposite occurs. Hence, an overall satisfactory prediction of the measured flow rates is obtained by the hereby employed analytical tool, when deionized water is used as pore fluid. The discrepancy between calculated and measured flow rates is not systematic and may be attributed partly to the objective difficulty in accurately determining the height of the treated region (L_g) by mere visual inspection. More specifically, the calculated flow rate depicts breakthrough of the CS in Tests 8, 11 and 12, exactly as the measurements showed, while the essential zeroing of the flow rate (within the time frame of the test) measured in the remaining 7 tests was also accurately predicted, with the possible exception of Test 9. In more detail, in 8 of the 10 tests,

the use of the calculated CS viscosity with time (via Eq. 4.1) instead of the measured one leads to insignificant differences in the predicted flow rates, thus underlining the accuracy of Eq.4.1, as well its practical usefulness. In only 2 of the 10 tests (Tests 6 and 8) the calculated CS gel times are smaller than the measured ones (see Figures 5.18 and 5.20), thus leading to calculation of zero flow rate in advance of what the measured flow rates show.

On the other hand, for the 3 injection tests with sea water as pore fluid, an over-prediction of the measured flow rate is obtained (Tests 1SW, 2SW, 3SW). This over-prediction is not more significant than in Tests 5, 6 and 12 that were performed with deionized water and also showed an over-prediction of the flow rate. In addition, as was deduced in the previous paragraph, the CS viscosity is not considered to be considerably affected by its injection in sea water saturated sands, at least for the travel distances (up to 1m) and the injection durations (up to 16.4hrs) used in Tests 1SW, 2SW, 3SW. Anyway, the depicted over-prediction (up to a factor of 3) in these latter tests may be partly attributed to an under-estimation of the CS viscosity, since this was measured in the solution of the inlet chamber (that retained a constant NaCl normality) and not in the CS solution in the pores of the sandy columns (which is exposed to additional NaCl). The same holds when Eq. (4.1) is used for predicting the CS viscosity versus time curve, since this was based on measurements using deionized water for preparing the solution (in *Chapter 4*). Thus, both calculated flow rates (with μ_{meas} and μ_{calc}) are expected to slightly (at least) over-predict the measured flow rates in tests with sea water as pore fluid. Despite these over-estimations, the calculated flow rates depict breakthrough of the CS in Tests 2SW and 3SW, exactly as the measurements showed, while the essential zeroing of the flow rate measured in Test 1SW would also be predicted, but at a slightly increased amount of time.

Based on all the above, it is concluded that the employed analytical tool provides sufficient accuracy in predicting the measured flow rates in 1D vertical CS injection tests, especially when deionized water is used as pore fluid before stabilization of the sand. The relative error in the flow rate prediction is not systematic and may reach a factor of 3. It should be underlined here that for the presented predictions of flow rate unified set of water ρ_w and CS solution ρ_g densities was used in all tests depending on a nominal values of the materials (see Table 5-2) and not the slightly more accurate test-specific values, and this is in order to simulate an application of the analytical tool in practice.

Chapter 6

NUMERICAL SIMULATION OF THE MECHANICAL BEHAVIOR OF STABILIZED SANDS AT THE ELEMENT LEVEL

6.1 General

Based on *Chapter 3*, the mechanical behavior of stabilized sands has several similarities with that of natural sands, but also some distinct differences. Stabilized sand, as a new geomaterial, has been only macroscopically investigated in the literature and only Kodaka et al. (2005) made an effort to create a specialized constitutive model for its mechanical behavior. This Chapter attempts the use of an existing constitutive model for sands after appropriate modifications in order to simulate the depicted differences in the mechanical behavior. Specifically, the use of NTUA-SAND model (Andrianopoulos et al. 2010a; b) is explored herein, since it is a state-of-the-art constitutive model which can satisfactorily simulate the monotonic and cyclic response of non cohesive soils. Emphasis is given on the different modifications that can be used to simulate the behavior of stabilized sands. The equations of the NTUA-SAND model are briefly presented in paragraph 6.2, while paragraph 6.3 presents its calibration for untreated sands. Then, paragraph 6.4 presents the numerical simulation of cyclic element tests by assuming modifications related to the sand skeleton, while in paragraph 6.5 the numerical simulation of the same tests is performed by assuming modifications related to the pore fluid.

6.2 The NTUA-SAND constitutive model

NTUA-SAND (Andrianopoulos et al. 2010a; b) is a constitutive model for non cohesive soils, which belongs to the bounding surface elastoplastic models. It employs plasticity theory principals and it incorporates the complete soil behavior framework known as Critical State Soil Mechanics (CSSM). It is based on the elastoplastic constitutive model proposed by Papadimitriou (1999) and especially its final form presented by Papadimitriou et al. (2001) and Papadimitriou and Bouckovalas (2002). The NTUA-SAND model maintains the philosophy, the main assumptions and equations of the initial model, but adopts some modifications in order to be implemented in a numerical analysis software. One of the most important modifications

is the conversion of the yield surface to a point, thus adopting a potentially elastoplastic behavior at all loading steps. Briefly, the key ingredients of the NTUA SAND model are:

- The interrelation of the bounding surface, critical state surface and the dilatancy surface with parameter ψ (Been and Jefferies 1985), as first proposed by Manzari and Dafalias (1997).
- A modified expression of the nonlinear hysteretic Ramberg- Osgood (Ramberg and Osgood 1943) formulation for the "elastic" strain rate, which defines the response at small and large cyclic shear strains.
- A projection center of the deviatoric stress ratio tensor which is used as a reference point for defining the image point of the current stress on each of the three (3) surfaces of the model, a projection center which is updated upon load reversal, thus employing the concept of stress reversal surfaces of Mroz et al. (1999).
- An empirical macroscopic index for the effect of sand fabric evolution on sand response under shear loading which alters the plastic modulus value.

The NTUA-SAND model can satisfactorily simulate the response of non-cohesive soils under both monotonic and cyclic loading for any cyclic shear strain at the element level with the same set of model constants that are independent of the initial conditions (initial effective stress, void ratio), the loading direction and the drainage regime. The NTUA-SAND model has been successfully implemented in FLAC (Itasca 2011), a finite difference software for the simulation of geotechnical boundary value problems. The basic equations of the model are presented below, so that the numerical simulations presented herein can be better understood. A full presentation of the NTUA-SAND model can be found in (Andrianopoulos et al. 2010a; b), and is beyond the scope of this Thesis.

Model surfaces

The NTUA-SAND constitutive model employs three (3) surfaces in stress space: (a) the bounding surface which defines the peak deviatoric stress ratio, (b) the critical state surface, on which shear strain accumulation takes place under constant volume and stresses and (c) the dilatancy surface which is a generalized form of the phase Transformation Line (PTL) proposed by Ishihara et al. (1975), and defines whether the sand has contractive or dilative response during shearing. Figure 4.1 shows the model surfaces on the q – p space, where p is the mean effective stress and $q=\sigma_1-\sigma_3$ the deviatoric stress in the triaxial space. Note that r_{ij} is the deviatoric stress ratio tensor, while r_1, r_2 and r_3 are the principal stress ratio values in

Figure 6.2. Their projection on the π plane of the deviatoric stress ratio space is shown in Figure 6.2, along with the mapping rule of the model described below.

In NTUA-SAND, the Critical State Line (CSL) is a straight line in the e-ln(p) space where e is the void ratio. The form of CSL is illustrated on Figure 6.3 and is described by:

$$e_{cs} = (e_{cs})_a - \lambda \left(\frac{p}{p_a} \right) \quad (6.1)$$

where:

- e_{cs} the void ratio at Critical State for mean effective stress *p*,
- p_a atmospheric pressure (e.g. p_α = 98.1 kPa),
- $(e_{cs})_a$ the void ratio at Critical State for $p=p_\alpha$, a model constant
- λ the inclination of Critical State Line (CSL) at e – ln(p) space, a model constant.

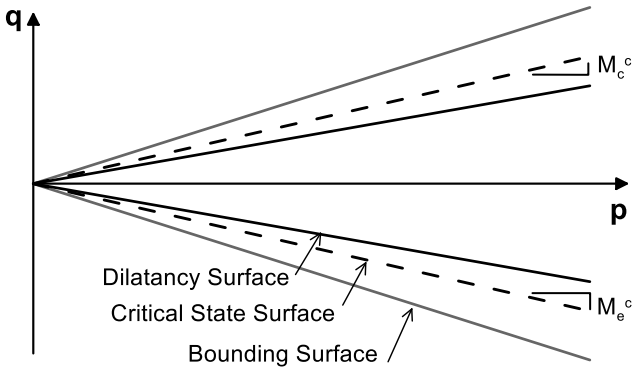

Figure 6.1 *NTUA-SAND surfaces on the p-q space (Andrianopoulos et al, 2010).*

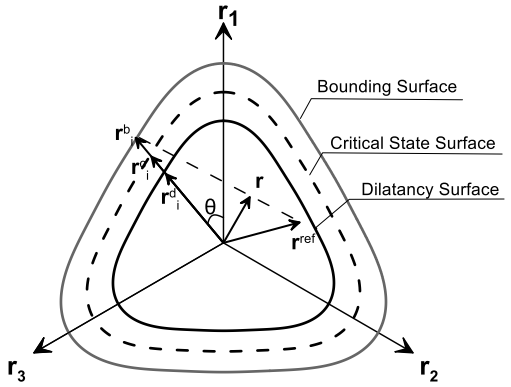

Figure 6.2 *NTUA-SAND surfaces on the π-plane of the deviatoric stress ratio space and definition of mapping rule (Andrianopoulos et al., 2010).*

Based on Figure 6.3, the state parameter ψ can be defined by (Been and Jefferies, 1985) as:

$$\psi = e - e_{cs} \tag{6.2}$$

where e, e_{cs} the void ratio of the current state of stress and at the Critical State respectively, under the same mean effective stress p. The state parameter ψ combines the effects of density (via void ratio, e) and effective stress level (via mean effective stress, p), i.e. for ψ<0 the response is dilative (dense sand under low stresses), while the response is contractive (loose sand under high stresses) for ψ>0. Finally for ψ=0 the sand is potentially at critical state. The Critical State stress ratios for triaxial compression M_c^c and triaxial extension M_e^c on q-p space are also model constants and are shown in Figure 4.1. On the contrary, the Dilatancy and Boundary stress ratios do not remain constant during loading, but are defined on the basis of the current value of the state parameter ψ and the corresponding values of either M_c^c or M_e^c, based on the equations proposed by Dafalias and Manzari (1997):

$$M_{c,e}^{\ d} = M_{c,e}^{\ c} + k_{c,e}^{\ d}\,\psi \tag{6.3}$$

$$M_{c,e}^{\ b} = M_{c,e}^{\ c} + k_{c,e}^{\ b}\left\langle -\psi \right\rangle \tag{6.4}$$

where $k_{c,e}^{\ b}$, $k_{c,e}^{\ d}$ are positive model constants. Note that for triaxial compression subscript c is used in Equations 6.3 and 6.4 and the included model constituents, while for triaxial extension subscript e. The symbol $\langle\ \rangle$ denotes the Maucaley brackets, and <A>=A for A>0 and <A>=0 for A<0.

It should be clarified that ψ<0 corresponds to dilative response, and hence $M_{c,e}^{\ d} < M_{c,e}^{\ c} < M_{c,e}^{\ b}$ based on Equations (6.3) and (6.4). Respectively, ψ>0 corresponds to contractive response and hence $M_{c,e}^{\ b} = M_{c,e}^{\ c} < M_{c,e}^{\ d}$ based on Equations (6.3) and (6.4).

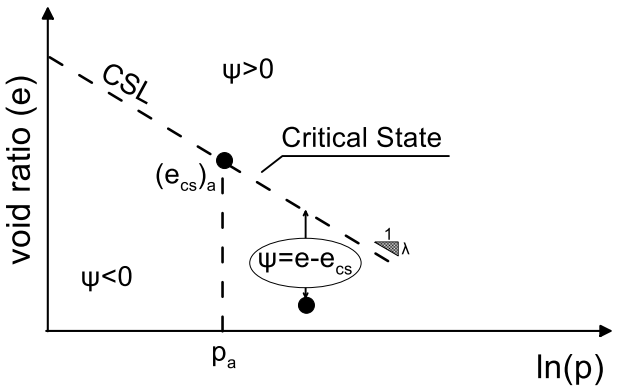

Figure 6.3 *Critical State Line on the e-lnp space and definition of state parameter ψ* (Been and Jefferies 1985)

Mapping rule

NTUA-SAND uses a mapping rule on the π-plane of the deviatoric stress ratio space which is illustrated in Figure 6.2. Observe that the image point r_i^b is estimated as the intersection point of the bounding surface with the straight line defined by the (r-r^{ref}) vector on the π plane. The r^{ref} point is the (so-called) projection center of the mapping rule, which corresponds to the value of the deviatoric stress ratio tensor r at the last load reversal. Given the position of the image point is determined via the mapping rule, the unit-deviatoric loading direction n can be estimated, which defines the deviatoric component of loading at each incremental step. It is the unit-deviatoric tensor ($\underline{n}$:$\underline{n}$=1, trace($\underline{n}$)=0) that has the Lode angle θ depicted in Figure 6.2.

Elastoplastic stress increment

The effective stress increment $\Delta\sigma$ for any given strain increment $\Delta\varepsilon$ ($= \Delta e + \Delta\varepsilon_p/3\ I$) is expressed by:

$$\Delta\sigma = 2\,G_t\,\Delta e + K_t\,\Delta\varepsilon_p\,I - \langle\Lambda\rangle\,(2\,G_t\,n + K_t\,D\,I) \qquad (6.5)$$

where:

G_t	tangential (elastic) shear modulus
K_t	tangential (elastic) bulk modulus
n	unit deviatoric loading direction (deviatoric plastic strain rate direction)
D	dilatancy coefficient
$\Delta\varepsilon_p$	volumetric component of strain increment $\left(\Delta\varepsilon_p=\Delta\varepsilon_{11}+\Delta\varepsilon_{22}+\Delta\varepsilon_{33}\right)$

I the second-order identity tensor

Δe deviatoric component of strain increment $\{\Delta e=\Delta\varepsilon-\left(\frac{1}{3}\right)\Delta\varepsilon_p I\}$, and

Λ loading index in terms of applied strain increment described by:

$$\Lambda = \frac{L : \Delta\sigma}{K_p} = \frac{2\,G_t\,n : \Delta e - (n : r)\,K_t\,\Delta\varepsilon_p}{K_p + 2\,G_t - (n : r)\,K_t\,D} \tag{6.6}$$

In more detail, for loading with Λ>0 non-zero plastic strain occurs, for Λ=0 neutral loading with zero plastic strain occurs and finally for Λ<0 load reversal is defined, a condition which occurs momentarily since there is no yield surface (or non-zero elastic region). Particularly, at load reversal the r^{ref} is updated, thus changing the direction of n and making the Λ non-negative again, so that plastic strain can be estimated (Andrianopoulos et al. 2010).

Elastic strain rate

For the simulation of the nonlinear hysteretic sand response at small and medium cyclic strains a Ramberg – Osgood type formulation is used. Hence, NTUA-SAND uses a tangential (elastic) shear modulus expressed by:

$$G_t = G_{max} / T \tag{6.7}$$

In Equation (6.7) G_{max} is the initial shear modulus, which is expressed by Equation (6.8) based on the proposal by Hardin (1978):

$$G_{max} = \frac{B\,p_a}{0.3 + 0.7\,e^2}\sqrt{\frac{p}{p_a}} \tag{6.8}$$

where p_a atmospheric pressure (e.g. p_a= 98.1 kPa), and B a positive model constant. The scalar variable T is greater or equal to 1.0 in order to introduce G_t degradation due to change in the deviatoric stress ratio r in relation to its value at the last load reversal r^{ref}, and is given by:

$$T = 1 + \left(\frac{1}{\alpha_1} - 1\right)\left(\frac{\sqrt{1/2\left(r - r^{ref}\right) : \left(r - r^{ref}\right)}}{\alpha_1\left(\frac{G_{max}^{ref}}{p^{ref}}\right)^{\gamma_1}}\right) \tag{6.9}$$

Where α_1 and γ_1 are positive model constants. Note that upon load reversal T=1, i.e. the $G_t=G_{max}$ and also the Λ<0 momentarily. Thereafter, T<1 and Λ≥0 thus leading to plastic straining with $G_t<G_{max}$ until the next load reversal occurs.

The elastic deviatoric strain rate is given by:

$$\Delta e^{e} = \frac{\Delta s}{2\,G_t} \tag{6.10}$$

while the elastic volumetric strain rate is estimated as:

$$\Delta \varepsilon_p^{e} = \frac{\Delta p}{K_t} \tag{6.11}$$

The elastic moduli G_t and K_t are interrelated using the constant Poisson ratio ν, which is a model constant, based on elasticity theory via:

$$K_t = \frac{2\,(\nu + 1)}{3\,(1 - 2\nu)}\,G_t \tag{6.12}$$

Plastic strain rate

The plastic strain increment is estimated on the basis of a non-associated flow rule, according to:

$$\Delta \varepsilon^{pl} = \langle \Lambda \rangle R \tag{6.13}$$

where R is the plastic strain rate direction described by:

$$R = n + \frac{D}{3} I \tag{6.14}$$

Note that n is the unit-deviatoric loading direction defined via the mapping rule, but is also the deviatoric plastic strain rate direction according to Equations (6.13) and (6.14). D is the dilatancy coefficient, which is explicitly defined as:

$$D = A_0\, d^{d} \left[2.0 - \sqrt{\frac{\langle d^{d} \rangle}{d^{d}_{ref}}} \right] \tag{6.15}$$

where A_0 is a positive model constant and d^d the scalar distance of the current state of stress from the image point on the dilatancy surface. By definition, the dilatancy coefficient affects only the volumetric component of the plastic strain increment and its dependence from the sign of d^d ensures negative plastic volumetric strain rates for negative values of d^d, and the opposite.

Plastic modulus

The plastic modulus K_p is defined as the product of four factors:

$$K_p = p\, h_b\, h_f\, d^b \tag{6.16}$$

where

- p mean effective stress
- h_b positive scalar function, which introduces a nonlinear interpolation rule
- h_f positive scalar function, which acts as an empirical indicator of the effect of sand fabric evolution during loading
- d^b the scalar distance of the current state of stress from the image point on the bounding surface

Apart from the distance d^b, all the factors affecting K_p have positive values. As a result, the sign of the distance d^b defines the sign of K_p. When K_p takes negative values $\left(K_p<0\right)$ then the current state of stress is outside the bounding surface ($d^b<0$) indicating softening response, while $d^b>0$ reflects a current stress state inside the bounding surface, thus leading to hardening response (with $K_p>0$).

The interpolation rule is introduced by:

$$h_b = h_0 \frac{\left|d^b\right|^3}{< d^b_{ref} - \left|d^b\right| >} \tag{6.17}$$

where h_0 is a positive model constant, while $d^b{}_{ref}$ acts like a reference value of d^b which corresponds to the "diameter" of the bounding surface along the direction of n. Finally, the distances d^b and d^d (collectively $d^{b,d}$) entering Equations 6.15 - 6.17 are defined as:

$$d^{b,d} = (r^{b,d} - r) : n \tag{6.18}$$

According to Equation (6.16), the effect of fabric evolution during loading on the response is taken into account with a positive scalar function h_f, which affects the value of K_p. Results from laboratory data on non-cohesive soils indicate that successive loading and unloading cycles at small cyclic shear strains lead to continuously stiffer response (Ladd et al. 1977). On the contrary, at large cyclic shear strains the soil response is much softer. This softer behavior is mainly observed when load reversal occurs after dilation of the soil or negative excess pore pressure development. This different response is caused by the sand fabric change and occurs

both under drained and undrained conditions. All the observations are reflected on the form given to h_f, which is beyond the scope of this Thesis. Details on this, as well as all model equations may be found in (Andrianopoulos et al. 2010a; b).

6.3 Calibration of NTUA-SAND for (untreated) sands

Calibration of the NTUA-SAND model has been performed by Andrianopoulos et al. (2010) for Nevada sand. For this purpose, laboratory results from resonant column, simple shear and triaxial compression tests for (fine grained) Nevada sand were used. These laboratory tests were conducted within the framework of the VELACS (Verification of Liquefaction Analysis by Centrifuge Studies, Arulmoli et al., 1992) project. Table 6-1 presents the physical properties of Nevada sand, while the values of the NTUA-SAND model constants for the same sand (as they were estimated from the calibration procedure) are shown in Table 6-2 (Andrianopoulos 2006).

Table 6-1 *Physical properties of Nevada sand (Arulmoli et al, 1991)*

Density of soil solid[(1)] ρ_σ	2.67 Mg/m^3
Maximum dry density[(2)] $\rho_{d,max}$	1.77 Mg/m^3
Minimum dry density [(3)] $\rho_{d,,min}$	1.41 Mg/m^3
Maximum void ratio [(3)]e_{max}	0.887
Minimum void ratio [(2)]e_{min}	0.511
Mean grain size diameter [(4)]d_{50}	0.10mm
Uniformity coefficient[(4)]$C_u = d_{50}/d_{10}$	1.41
Percent of fines per weight [(4)]	7.7%

(1) Determined by ASTM-854-83

(2) Determined by ASTM-4253-83

(3) Determined by ASTM-4254-83

(4) Determined by ASTM-422-63

Table 6-2 *Model constants values for Nevada sand* (Andrianopoulos 2006)

Physical meaning	Constant	Value
Critical State	M_c^c	1.25
	M_c^e	0.90
	$(e_{cs})_a$	0.809
	λ	0.022
Elastic strain rate	B	600 (180 for monotonic loading)
	ν	0.33
	γ_1	0.00025
	α_1	0.6 (1.0 for monotonic loading)
Model Surfaces	k_c^b	1.45
	$k_e^b(=ck_c^b)$	1.044
	k_c^d	0.30
	$k_e^d(=ck_c^d)$	0.216
Plastic strain rate	A_0	0.8
	h_0	15000
Fabric evolution	N_0	40000

Observe that the model requires the calibration of thirteen (13) dimensionless and positive constants for cyclic loading, and only eleven (11) for monotonic loading (when α_1=1.0 and γ_1 is irrelevant). Note that k_e^b and k_e^d are not independently estimated and that is why the constants are a total of 13. Ten (10) out of the thirteen (13) model constants may be directly estimated on the basis of monotonic and cyclic element tests, while the remaining three (3) constants (A_0, h_0, H_0) require trial-and-error simulations of element tests.

6.4 Simulation of cyclic element tests assuming modifications related to the sand skeleton

In general at large cyclic shear strains, loose non cohesive saturated sands have low liquefaction resistance. As a result, shear strains are accumulated, pore pressures increase rapidly and finally the stiffness of the sand decreases significantly. Contrary to natural sands, results from cyclic tests on sands passively stabilized with CS solutions, show significant increase of liquefaction resistance for the same initial and loading conditions (see *Chapter 3*).

It should be mentioned here, that liquefaction can be defined as the state where pore pressures equal the initial effective stress, or alternatively when the soil has reached a predefined strain level. During cyclic triaxial tests, this strain level is usually measured in terms of double amplitude axial strain (DA), namely the maximum strain variation developed during a full compression – extension loading cycle. For stabilized soils, where the increase of CS viscosity causes significant reduction of the hydraulic conductivity of the soil, pore pressure measurement is quite difficult and its values are questionable (e.g. Conlee et al. 2012). Hence, many researchers in the literature use the strain level criterion as the most appropriate factor for defining liquefaction.

More specifically, Figures 6.4-6.10 present such results in terms of cyclic stress ratio (CSR) versus number of cycles required for liquefaction (N_L), taken from the literature. These results include cyclic triaxial tests (Gallagher and Mitchell, 2002), cyclic simple shear tests (Díaz-Rodríguez et al., 2008) and cyclic torsional shear tests (Kodaka et al., 2005).

These results from different sands, test types and CS(%) concentrations indicate that stabilized soils reach a level of maximum strain amplitude (DA=1%, 2% or 5%), after many loading cycles, much more than the cycles required for liquefaction of the same sands without stabilization. Careful examination of these liquefaction curves show a beneficial effect of stabilization in terms of CSR increase for a given number of cycles N_L for the stabilized sands, which ranges from 0.1 to 0.28.

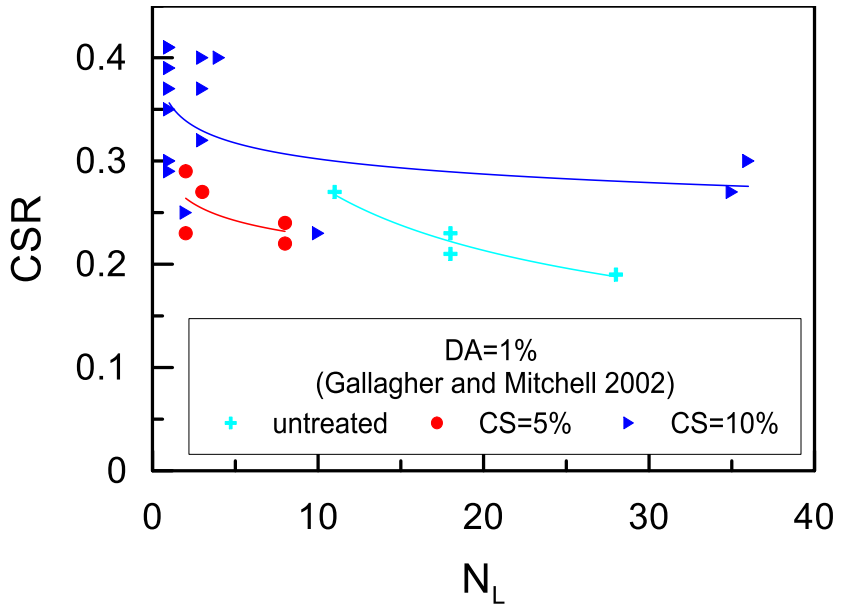

Figure 6.4 *Effect of CS(%) on the liquefaction resistance curves of Monterey sand, where liquefaction is defined when DA=1%, on the basis of cyclic triaxial data from Gallagher and Mitchell (2002).*

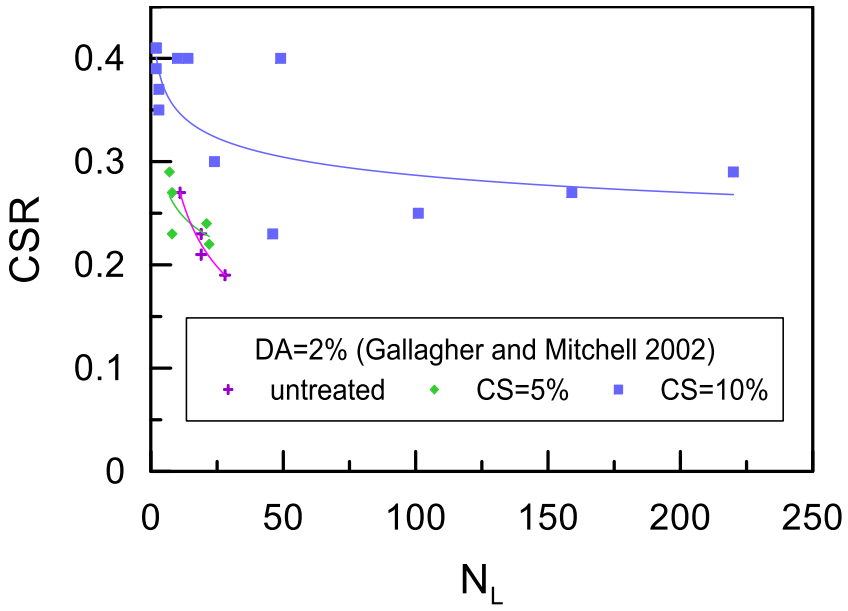

Figure 6.5 *Effect of CS(%) on the liquefaction resistance curves of Monterey sand, where liquefaction is defined when DA=2%, on the basis of cyclic triaxial data from Gallagher and Mitchell (2002).*

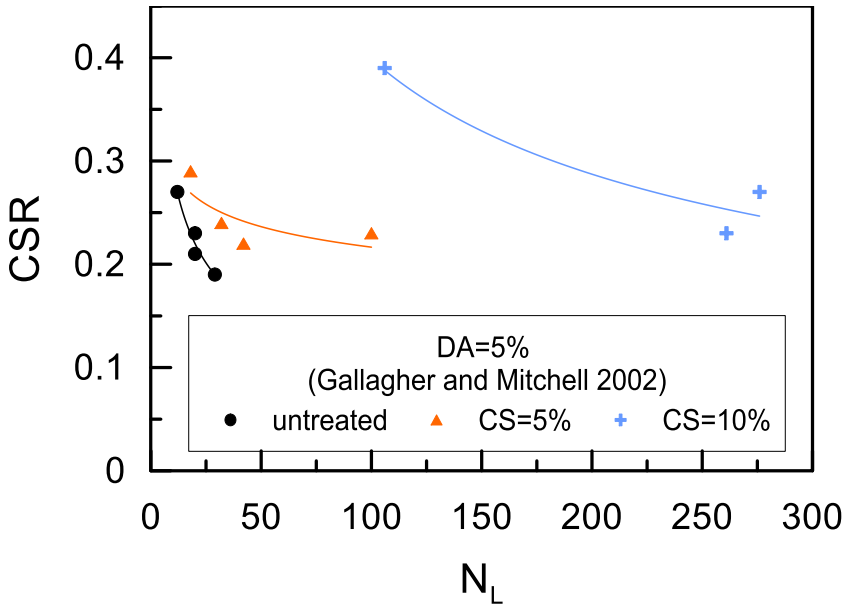

Figure 6.6 *Effect of CS(%) on the liquefaction resistance curves of Monterey sand, where liquefaction is defined when DA=5%, on the basis of cyclic triaxial data from Gallagher and Mitchell (2002).*

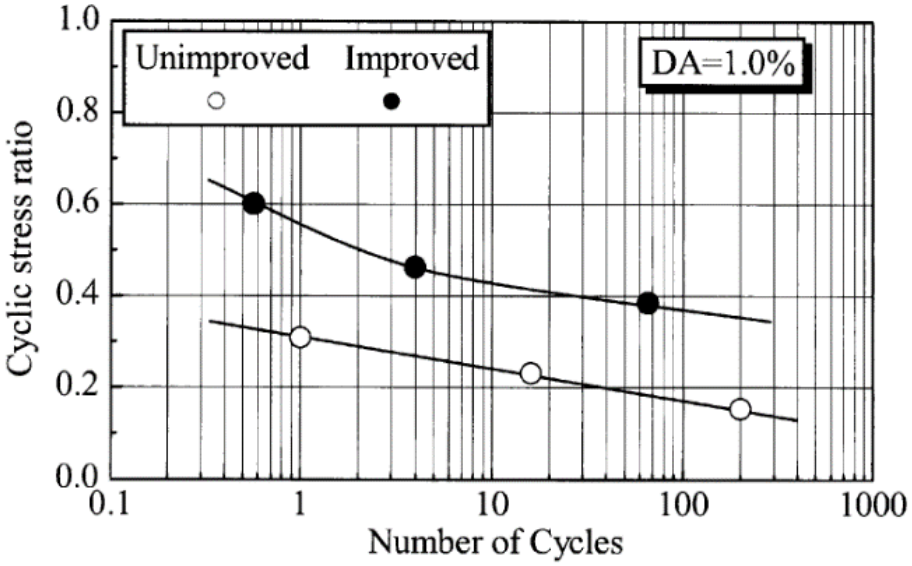

Figure 6.7 *Effect of CS(%) on the liquefaction resistance curves of Toyoura sand, where liquefaction is defined when DA=1%, on the basis of cyclic torsional shear tests from Kodaka et al (2005).*

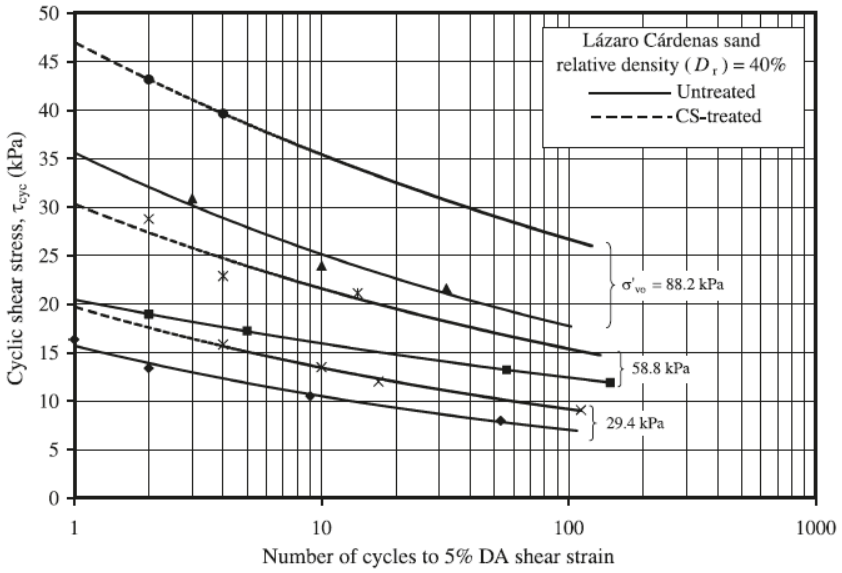

Figure 6.8 *Liquefaction resistance curves for untreated and treated with CS(%)=14.5 Lazaro-Cardenas sand from cyclic simple shear tests with σ'_{v0}=29.4, 58.8, 88.2kPa, DA=5% and D_r=40% (Diaz-Rodriquez et al, 2008)*

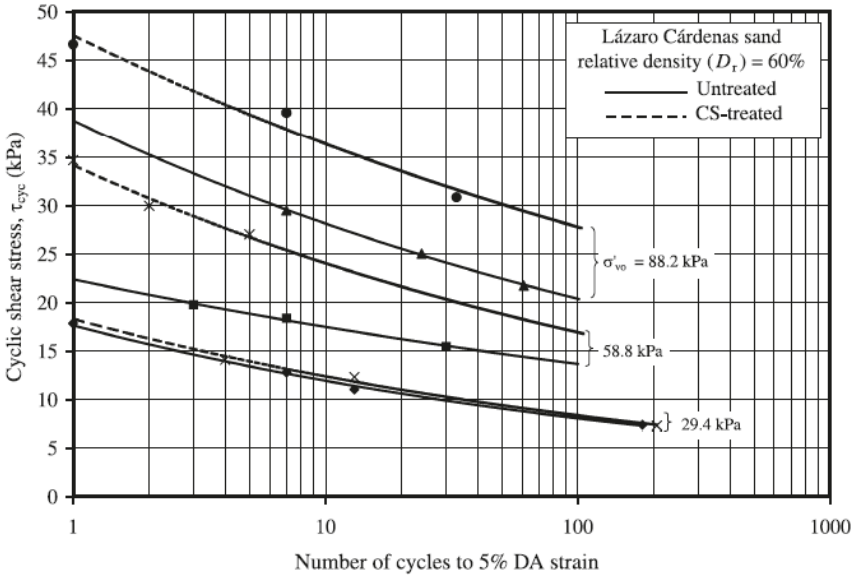

Figure 6.9 *Liquefaction resistance curves for untreated and treated with CS(%)=14.5 Lazaro-Cardenas sand from cyclic simple shear tests with σ'_{v0}=29.4, 58.8, 88.2kPa, DA=5% and D_r=60% (Diaz-Rodriquez et al, 2008)*

To further study this effect, Figure 6.10 presents the relative increase of liquefaction resistance in terms of CSR for given loading cycles (N_L) between untreated and stabilized soils based on all pertinent data from the literature. Note that the maximum increase of liquefaction resistance occurs for CS(%)=10 and a double amplitude of shear strength DA=5%

(Gallagher and Mitchell, 2002). A considerable effect of stabilization is indicated by the experimental data of Kodaka et al. (2005) for a much lower CS(%) concentration (4%), without though specifying the type of CS used (Ludox-SM® or other). From all the other testing results the gain offered by stabilization in terms of CSR (for the same N_L number) takes values up to 0.13, while the effect of initial conditions is not found so important. Note that, Figure 6.10 does not include the tests conducted by Gallagher and Mitchell (2002) for CS(%)=5 and for DA=1% and 2%, because the gain from stabilization is not obvious (in terms of CSR), since according to the authors themselves, such low CS(%) concentration does not produce a firm gel and hence the benefit of stabilization becomes obvious only for large DA=5% (see also Figures 6.4 and 6.5).

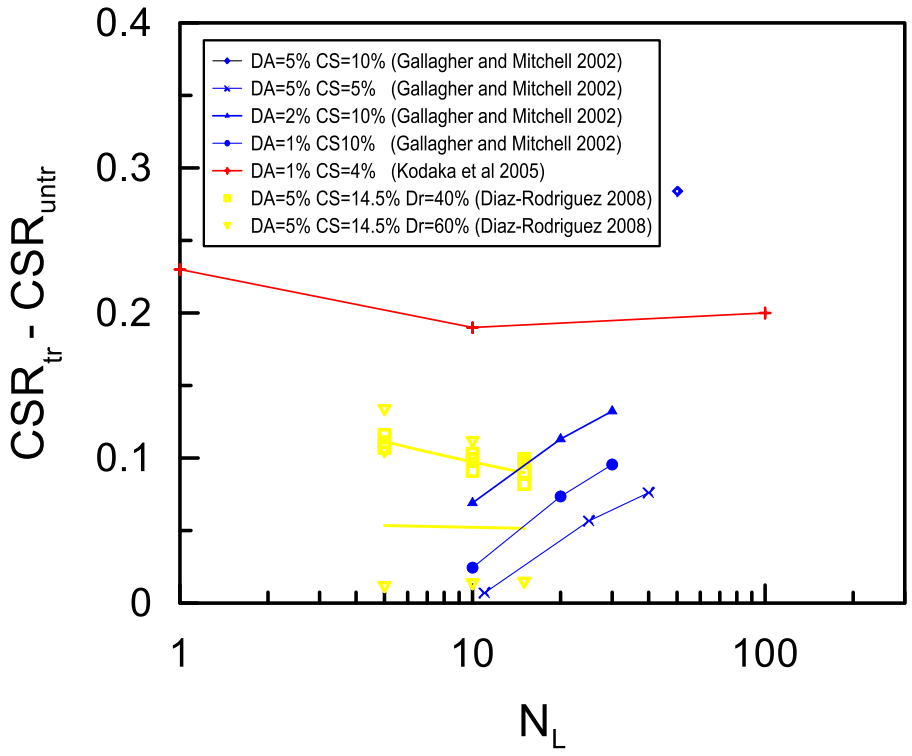

Figure 6.10 *CS(%) effect on CSR required for liquefaction for given number of cycles N_L (data from: Gallagher and Mitchell, 2002; Diaz-Rodriquez et al, 2008; Kodaka et al, 2005)*

For the numerical simulation of stabilized sands using NTUA-SAND, the main goal is to simulate the foregoing increase of CSR. This increase may be attained by modifying the response of the sand skeleton. For this approach, two alternatives are followed:

- An increase of constant h_0 of the plastic modulus K_p (see Eq.6.16), which can lead to a stiffer response.

- A decrease of the dilatancy coefficient A_0 of the dilatancy D (see Eq.6.16) which can lead to smaller volumetric change during shear and thus less intense excess pore pressure development.

Figure 6.11 presents the comparison of the experimental results of Díaz-Rodríguez et al. (2008) with a relative density of D_r=40% with the numerical simulation results for different h_0 values (h_0=45000, h_0=60000, h_0=75000 and h_0=150000), which are all arger than h_0=15000 that corresponds to the untreated sand (see Table 6-2). The hatched region in the figure depicts the previously mentioned range of gain due to stabilization, as this is taken from the literature (Figure 6.10). It is observed that all numerical results are within this range, with the constant value of h_0=60000 leading to the best simulation of the targeted data of (Díaz-Rodríguez et al. 2008).

Similarly, Figure 6.12 presents the comparison of the same experimental results with the numerical results adopting the second approach, namely the decrease of constant A_0 (A_0=0.1, A_0=0.2, A_0=0.3 and A_0=0.4), which are all smaller than A_0=0.8 that corresponds to the untreated sand (see Table 6-2). These predictions are also within the range of laboratory data and the corresponding best simulation occurs with a value of A_0 equal to 0.3.

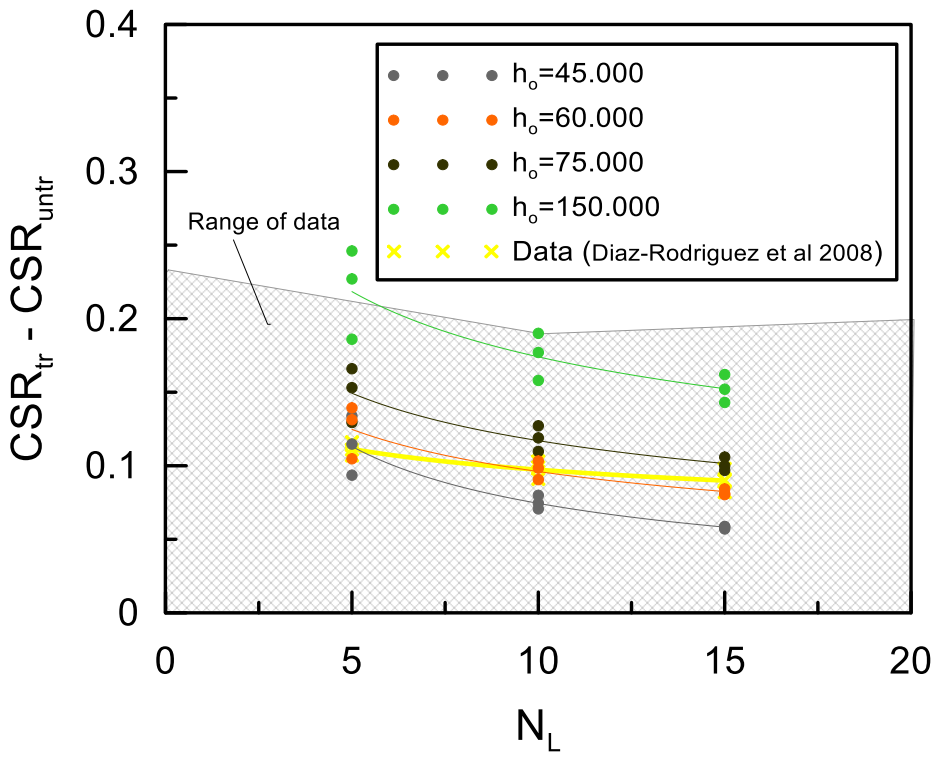

Figure 6.11 *Numerical simulation of CS(%) effect for different values of h_0 constant of NTUA-SAND model (data: Diaz-Rodriquez et al, 2008)*

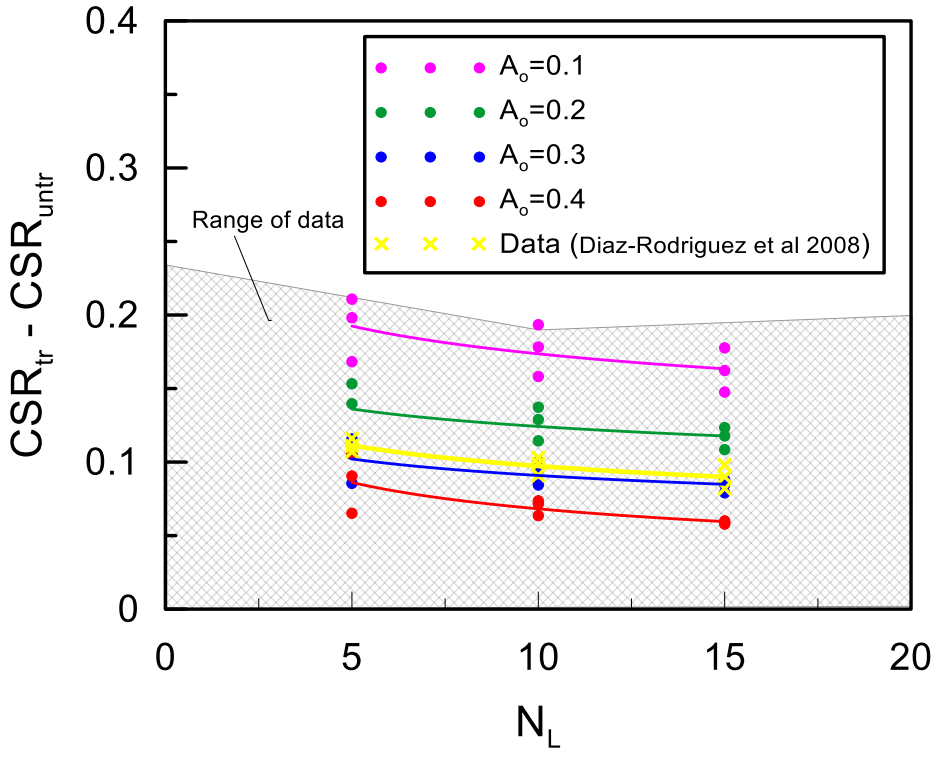

Figure 6.12 *Numerical simulation of CS(%) effect for different values of A_0 constant of NTUA-SAND (data: Diaz-Rodriquez et al, 2008)*

Then, Figure 6.13 shows the shear stress (τ) – shear strain (γ) relation and the related shear stress (τ) – mean effective stress (p) relation as resulted from the numerical simulation of undrained cyclic simple shear tests with a specific number of cycles to liquefaction equal to N_L=10 for: i) the untreated soil (Figure 6.13 (a) and (b)), ii) the stabilized soil for the optimum value A_0=0.3 (Figure 6.13 (c) and (d)) and iii) the stabilized for the optimum value h_0=60000 (Figure 6.13 (e) and (f)), all initiating from the same initial conditions (D_r=40% and σ'_{v0}=60kPa). Observe that for the stabilized soil, a significantly increased value of cyclic shear stress (CSR) is required for initial liquefaction (p=0kPa) at the same N_L, which indicates the beneficial effect of stabilization on soil strength as this is obtained by considering the two (2) different approaches for modification of the sand skeleton response. Note that this increase of CSR depicted in Figure 6.13 corresponds to approximately 0.1 difference in the CSR value for N_L=10, consistent with the optimal liquefaction curves of Figure 6.12 and Figure 6.11 respectively.

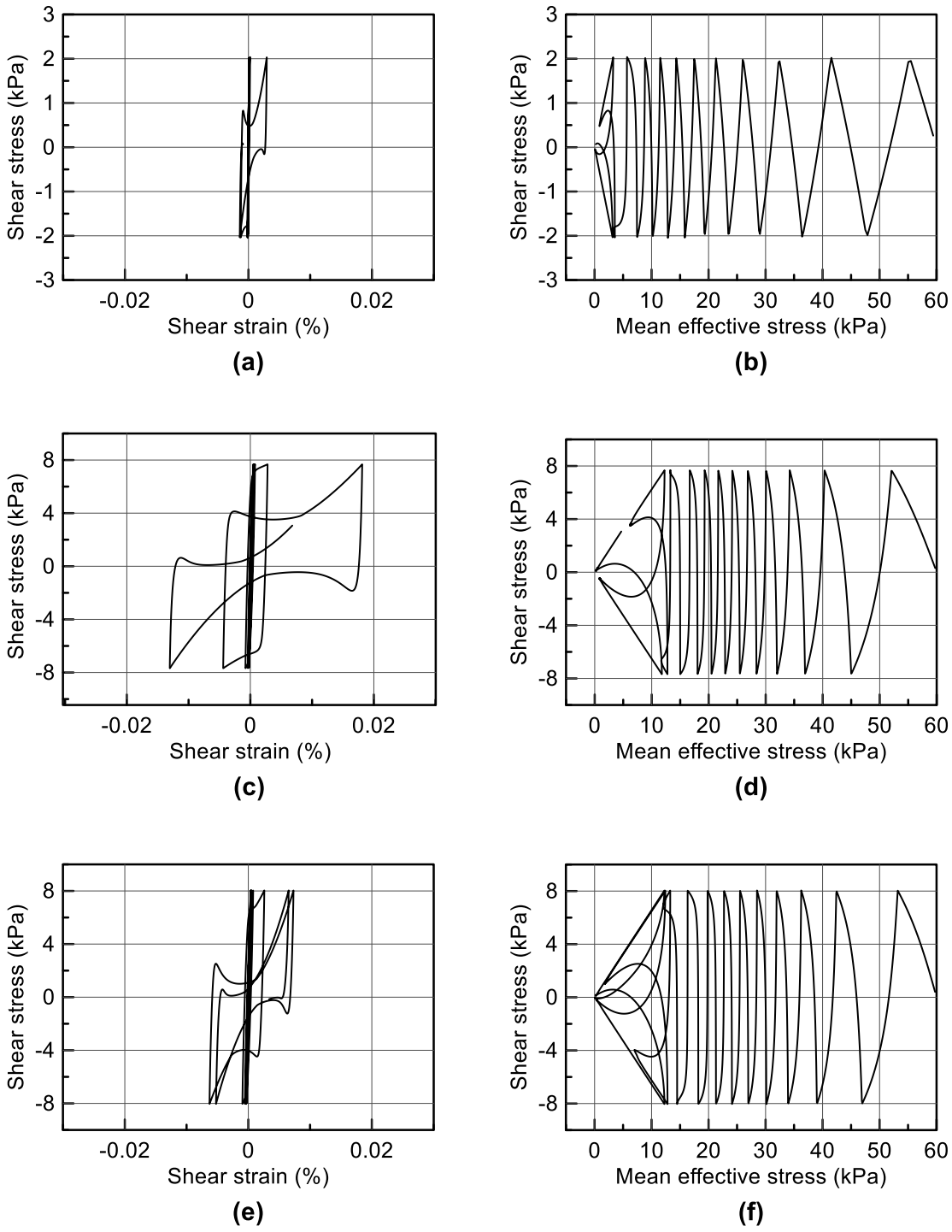

Figure 6.13 *Stress-strain relationship and effective stress paths from numerical simulation for clean sand (a) and (b) and for treated sand for the best values A_0=0.3 (c) (d) and h_0=60000 (e) and (f) and for the same initial conditions (D_r=40%, σ'_{v0}=60kPa).*

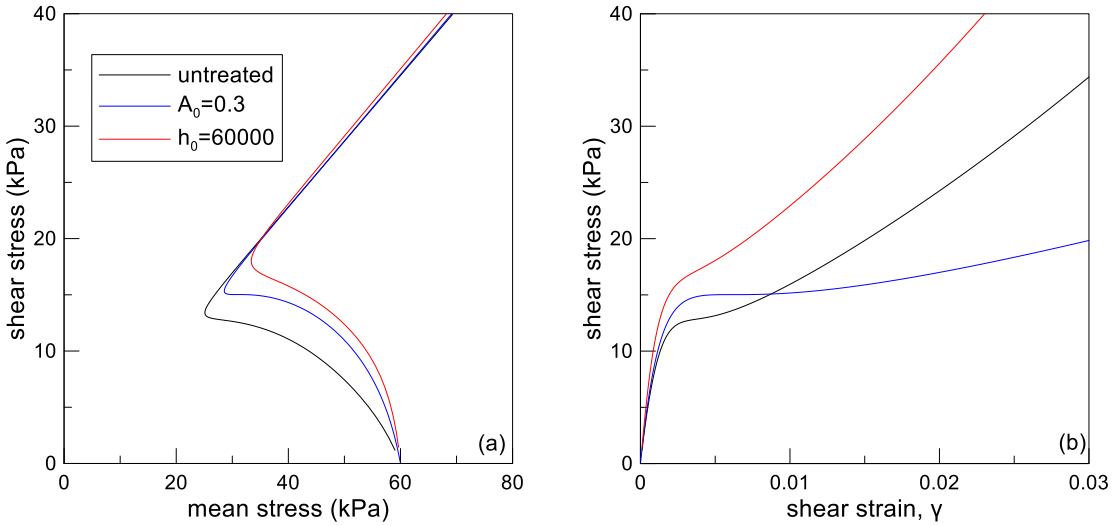

Figure 6.14 *Comparison of numerical simulations of undrained monotonic simple shear tests for untreated soil and for stabilized soil for the optimal values A0=0.3 and h0=60000, when starting from the same initial conditions (Dr=40%, σ'v0=60kPa), in terms of: (a) Shear stress – mean effective stress relation and (b) shear stress – shear strain relation*

For completeness, Figure 6.14 compares the numerical predictions of the monotonic response during undrained simple shearing for the untreated soil (black curves) and the stabilized soil for the optimal values A_0=0.3 (blue curves) and h_0=60000 (red curves), all initiating from the same initial conditions (D_r=40% and σ'_{v0}=60kPa). These optimal values of A_0 and h_0 were calibrated on the basis of cyclic undrained tests alone, and gave similar results for the stabilized sand (see Figure. 6.13). Such similar predictions for the stabilized sand continue to appear for the initial parts of the monotonic tests, where the stabilized soil predictions show a stiffer and less contractive response in comparison to that of the untreated soil. This agreement is expected, since the maximum shear stress values during cyclic loading are relatively small (e.g. up to 8 kPa, in the related Fig. 6.13) and the stress point remains in the initial part of the loading. However, when the monotonic shearing continues to greater shear strain values and the stabilized soil stress state exceeds the Phase Transformation Line (Ishihara et al. 1975), the stabilized sand predictions deviate from one another. As a result, it is only the h_0=60000 curves that continue to show a response which remains stiffer and less contractive than that of the untreated soil throughout the monotonic loading, thus remaining in qualitative agreement with the few available monotonic tests in the literature (Kodaka et al. 2005). However, cyclic loading is of primary interest in this Thesis, and hence the choice of a reduced dilatancy coefficient A_0 remains a valid alternative.

6.5 Simulation of cyclic element tests assuming modifications related to the pore fluid

6.5.1 General

Coupled response mechanisms in porous media (like soil) with presence of pore fluid are based on the interaction between the mechanical behavior of the soil skeleton and the flow of the pore fluid. When a saturated soil is subjected to loading, the deformation of its skeleton not only causes volume change in the pores, but also induces flow of the pore fluid from high to low pressure regions.

At first, this theory was developed to explain problems in soil mechanics, such as consolidation, but it was quickly extended to several other applications. In its original expression, a simple mathematical equation describes the two basic forms of soil skeleton and pore fluid interaction. These equations relate the strain development and the change of fluid mass with the change in stresses (at the soil skeleton) and the pore fluid pressure. In practice, these equations reflect the fact that pore fluid pressure affects the strain – stress relation of the soil skeleton. Hence, in porous media like soil, any change of the fluid mass or the fluid pressure leads to deformation of the soil skeleton. Moreover, a uniform change of pore fluid pressure in a porous skeleton, the movement of which has been laterally restrained, leads to the so-called poroelastic stress development. These poroelastic stresses cause a non-uniform pore fluid pressure distribution leading to a time dependent fluid flow through the pores (Darcy's Law). In turn, the pore fluid pressure change affects effective stresses, which cause deformation of the porous medium according to the effective stress principal.

When loadings are applied to saturated soils they cause an increase in the pore fluid pressure. This will cause an immediate deformation of the soil skeleton with a corresponding pore fluid pressure generation. As time passes, the excess pore pressure dissipates as the pore fluid flows due to pore pressure gradients within the soil. As the excess pore pressures change, the stresses and strains in the soil skeleton also change in order to maintain the system in equilibrium, thus leading to further deformation of the soil skeleton. The coupled nature of the problem ensures that deformation of soil skeleton will have an effect on the excess pore fluid pressures and vice versa.

The theory was firstly developed by Terzaghi (1923, 1925) for the one-dimensional consolidation, and extended to three dimensions by Biot (1941). In his original theory, Terzaghi stated that the deformations of a soil are governed only by the rearrangement of the

soil particles, and not by the compression of the pore fluid and the solid particles. In a saturated soil this means that a volume change of an element of soil can only occur by a net flow of the pore fluid with respect to the solid particles, which is related to their rearrangement. This assumption is often a good approximation of the real behavior of soft soils, especially clay. Such soils are highly compressible (deformations may be as large as several percents), whereas the constituents, particles and fluid, are comparatively very stiff. In more recent presentations of the theory, starting with those of Biot, compression of the pore fluid and compression of the particles has been also taken into account (Verruijt, 2013). Particularly, in Biot's theory of 3D poroelasticity, the saturated soils are modeled as deformable, linear, porous, elastic materials saturated with compressible fluids.

According to Wang (2000), the coupled mechanical response phenomena of soil skeleton and pore fluid flow have two main characteristics. The first is the coupling of the solid with the liquid phase, which occurs when a change of the applied stresses causes a change of the pore fluid pressures. The second is the coupling of the liquid with the solid phase, where a change in the pore fluid pressures and/ or the mass (or the volume) of the pore fluid causes a change in the total porous medium volume. Both these two coupling phenomena take place at the same time.

According to Minkoff et al. (2003) there are three ways to include these coupling effects in the analysis: "one way" coupling, "loose" coupling and "full" coupling. "One way" coupling uses a fixed porosity value for the entire time interval. The mechanical simulator will use the pore fluid pressures as periodic inputs to determine displacement and stress updates during the same time interval. No effects of the mechanical behavior are taken into account in the flow simulation. "Loose" coupling is an intermediate analysis, where the two conditions are solved separately and interact with each other, but no complex nonlinear phenomena are taken into account. "Full" coupling proposes that a change of pore fluid pressures, which is estimated for a specific time interval by the flow simulator, is then used by the mechanical simulator. The resulting stresses, correspond to porosity changes which are sent as input for the flow calculations. All the coupling effects are included in the analysis based on Biot's theory (Biot 1941). It becomes obvious that a soil – pore fluid interaction is an important parameter which cannot be ignored to simplify the physics of the problem as it can greatly affect the analysis results, especially for liquefaction phenomena, which are of interest here.

More specifically, the present study uses the finite difference code FLAC (Itasca 2011). In this code the steps for estimating the flow and mechanical behavior are performed alternately. At

the beginning of solving, even one flow loop can set the system out of balance and thus many mechanical loops are required in order to establish system equilibrium. Starting from a mechanical equilibrium condition, a coupled analysis requires a specific number of steps (loops). Each loop includes one or more flow loops, which are followed by several mechanical loops until (quasi)static equilibrium. The increase of pore pressures due to the fluid flow is calculated in the flow loops, whereas the contribution of the volumetric deformation is calculated in the mechanical loops as a grid zone ("element") value, which is then distributed to the four (4) nodes of the grid zone. The correction of total stresses, due to the pore pressure changes caused by the mechanical volume deformation or by the fluid flow, takes place in the mechanical and flow loops respectively. The total pore pressure value is used to estimate effective stresses and as a result the strain accumulation through the effective stress – strain relation, which can be either elastic or elasto-plastic (like in the case of the NTUA-SAND model).

In general, the fully coupled analysis outlined above refers to both fully saturated soil formations and to formations with a lowered water table. However, the former is for interest here for use in the analysis of liquefaction phenomena.

6.5.2 Pore pressure- volumetric strain interaction under coupled analysis

According to Biot's theory (1955, 1956) a new dimensionless variable ζ is introduced which represents the increase of fluid volume per unit volume. The increment of ζ over time is estimated on the basis of the mass balance equations:

$$\frac{\partial \zeta}{\partial t} = -\frac{q_i}{x_i} + q_v \qquad (6.19)$$

where:

q_i is the apparent velocity of the pore fluid [m/s] along direction i over distance x_i [m] and q_v the specific discharge vector or the ratio of fluid volume injection to the porous medium volume over time [1/s].

Fluid transport can be described by the well-known Darcy's law, which is an empirical expression for the apparent velocity q_i through a non-deformable porous medium. Using a small deformation assumption, Darcy's law can be written as:

$$q_i = -\frac{k}{\mu}\left(\frac{\partial P_f}{\partial x_j} - \rho_f g_i\right) \qquad (6.20)$$

where

P_f is the pore pressure [Pa], k is the hydraulic conductivity (assumed isotropic) [m/s], μ is the pore fluid viscosity [Pa*s], ρ_f is the pore fluid density [kg/m^3] and g_i is the gravitational force [m/s^2]

Finally, the pore pressure P_f and its change over time can be expressed by:

$$\frac{\partial P_f}{\partial t} = K\left(\frac{\partial \zeta}{\partial t} - \alpha \frac{\partial \varepsilon}{\partial t}\right) \quad (6.21)$$

Where

K: the pore fluid bulk modulus [Pa], α is Biot's (dimensionless) coefficient (α=1 when compressibility of grains can be neglected), ε is the volumetric strain, and ζ is the dimensionless variable introducing the coupling of volumetric strain with pore fluid pressure development (see Equation (6.19).

An important characteristic of saturated soils is the totally different response under drained and undrained conditions. Undrained behavior corresponds to ζ=0, as the pore fluid cannot escape while no flow is observed without discharge. Hence, assuming incompressible grains (α=1) Equation (6.21) is transformed to:

$$\frac{\partial P_f}{\partial t} = K\left(\frac{\partial \varepsilon}{\partial t}\right) \quad (6.22)$$

This expression indicates that, if the fluid bulk modulus K is decreased then for the same volumetric strain the developed pore pressures P_f will be smaller and the opposite. This characteristic of coupled response enabled the alternative simulation of stabilized sands by modification related to the pore fluid.

In particular, experimental results presented by Towhata (2007, 2008) from unconfined compression tests on pure colloidal silica samples, indicate that colloidal silica may be relatively compressible in comparison with practically incompressible water. In more detail, these results show that CS strength is of the order of a few kPa (see Figure 6.15), but the lateral to axial deformation ratio, or else the Poisson's ratio, is equal to 0.3 and not 0.5 (implying incompressibility) as resulting from Figure 6.16. Therefore, it is possible that liquefaction resistance increases due to this pore fluid compressibility, which according to Equation (6.22) may lead to reduced pore pressures. This fact can be introduced in the analysis

by increasing the compressibility of the pore fluid, or by decreasing the bulk modulus K in Equations (6.21) and (6.22), which will affect the pore pressure values and as a result the overall response of stabilized soil under undrained loading prevailing in the few seconds of an earthquake shaking. The existence of undrained conditions is also backed by the dramatic decrease of the hydraulic conductivity values for stabilized sands (Persoff et al., 1999).

Following this approach, for the simulation of the Díaz-Rodríguez et al. (2008) data, numerical analyses were conducted using the NTUA-SAND model, without altering the values of model constants (Table 6-2) but after modifying the value of the pore fluid compressibility by assuming a 50 times smaller pore fluid bulk modulus ($K=K_w/50$, where K_w is the bulk modulus of clean water equal to $2x10^6$ kPa). Figure 6.17 presents the comparison of the data to simulations in the known form at Figures 6.11 and 6.12. Note that the effect of K reduction seems to be qualitatively in the right direction, as it leads to an increase of the CSR required for liquefaction, in compatibility with the literature data, while the value of $K_w/50$ seems quantitatively sufficient for simulating the experimental data.

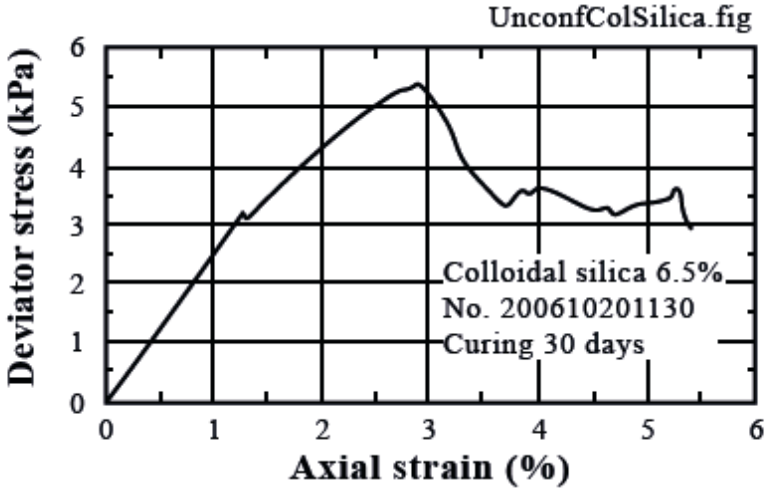

Figure 6.15 *Deviatoric stress- axial strain curve of CS under unconfined compression strength test (Towhata, 2007, 2008)*

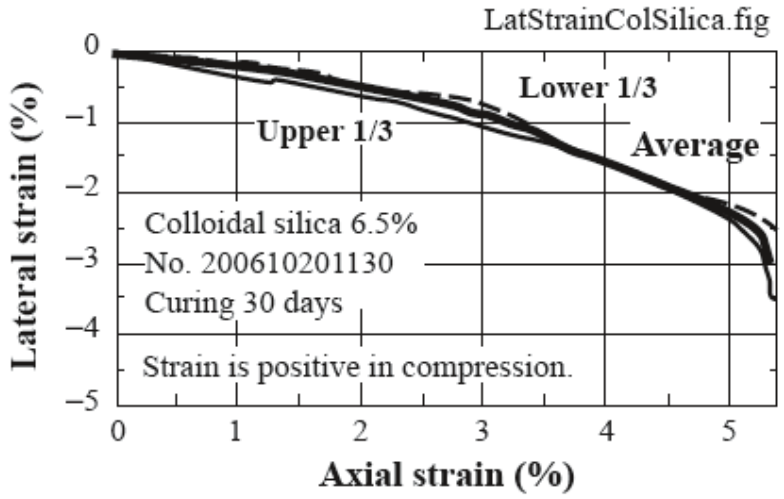

Figure 6.16 *Lateral strain versus axial strain of CS under unconfined compression test (Towhata, 2007, 2008)*

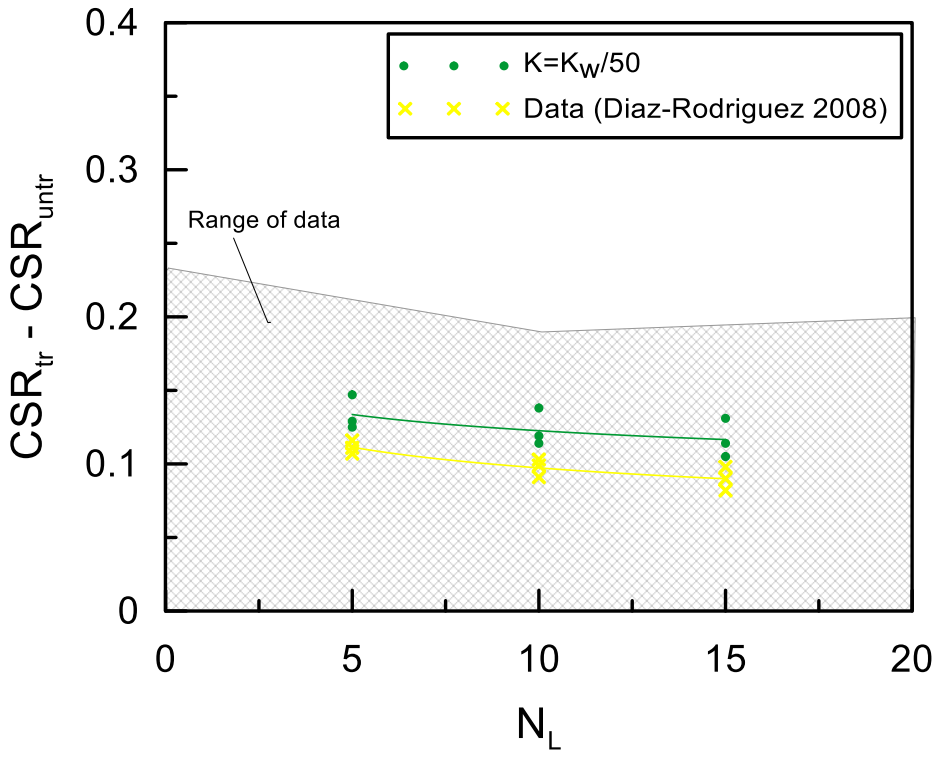

Figure 6.17 *Numerical simulation of CS(%) effect on CSR required for liquefaction using NTUA-SAND with reduced pore fluid modulus K=Kw/50 (data: Diaz-Rodriquez et al, 2008; Andrianopoulos et al, 2015)*

6.6 Simulation of resonant column tests assuming modifications related to the sand skeleton and/or the pore fluid

After calibrating the modifications related to the sand skeleton and/ or the pore fluid on the basis of cyclic element tests in paragraphs 6.4 and 6.5 above, the NTUA-SAND model employs them here for simulating the resonant column tests on stabilized sands conducted by Spencer et al. (2008). The results of these numerical simulations are shown in Figure 6.18 and emphasize on the normalized shear modulus G/G_{max} degradation and hysteretic damping D increase curves with cyclic shear strain. Particularly, subplots (b) and (d) present the simulations for untrated sand (h_0 = 15000) and two (2) simulations for treated sand with CS (h_0 = 150000 and K_w/50). These are compared to the resonant column data of Spencer et al. (2008) in subplots (a) and (c), respectively. Observe that similarly to the test data, the effect of stabilization is not significant for the stabilized sand response for small and medium cyclic shear strains.

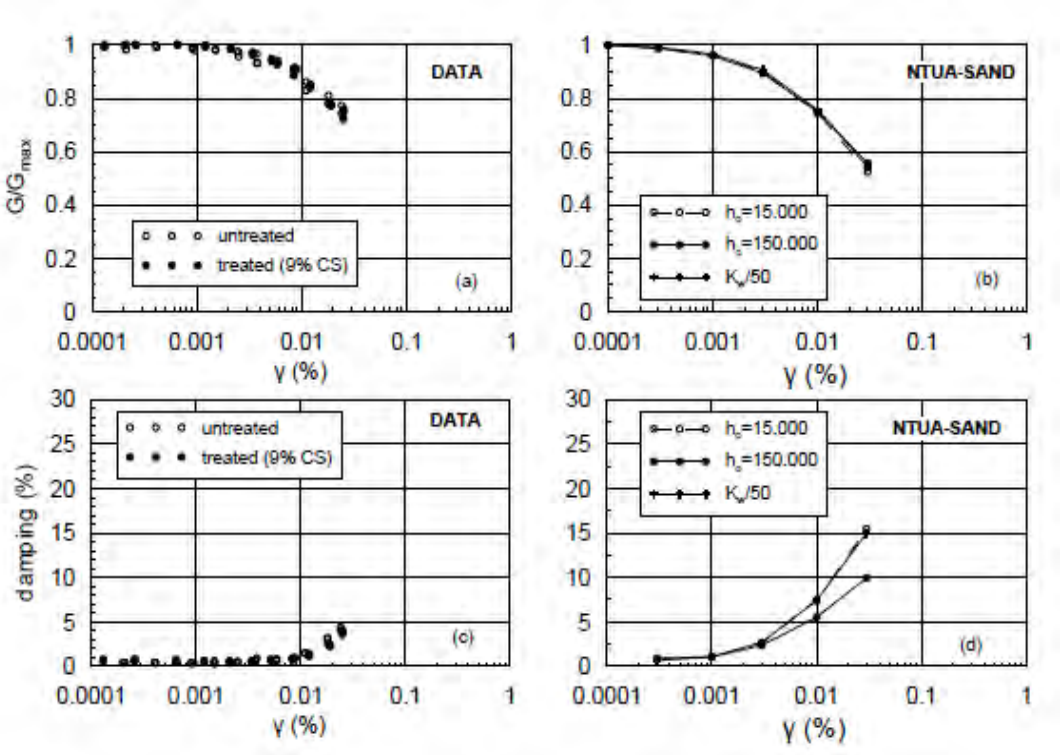

Figure 6.18 *The effect of stabilization on the normalized shear modulus G/G_{max} degradation and damping increase curves with cyclic shear strain on the basis of data of Spencer et al (2008) and comparison with numerical simulation results with the NTUA-SAND model for untreated and stabilized sand (Andrianopoulos et al, 2015)*

Figure 6.19 compares the effect of stabilization on the small strain (elastic) modulus G_{max} values from data (Spencer et al. 2008) and a series of simulations. The effect of stabilization is

particularly simulated by employing the three aforementioned simulation approaches: i) an increase in h_0 by ten times (h_0=150000), ii) a decrease in A_0 by ten times (A_0=0.08) and iii) a reduction in K by 50 times in comparison with that of water. The simulations show that the last two approaches produce negligible effects on the value of G_{max} due to stabilization, whereas the increase in h_0 leads to an increase of 15–22%, which is higher than the 10% of the shown data and lower than 25%, which is the average increase estimated in *Chapter 3* on the basis of in-flight measurements of shear wave velocity in the centrifuge tests of Conlee (2010). Hence, overall, it may be concluded that all three simulation approaches for stabilization lead to relatively small effects on the G_{max} value, in general accordance with the test data for the small cyclic shear strain regime.

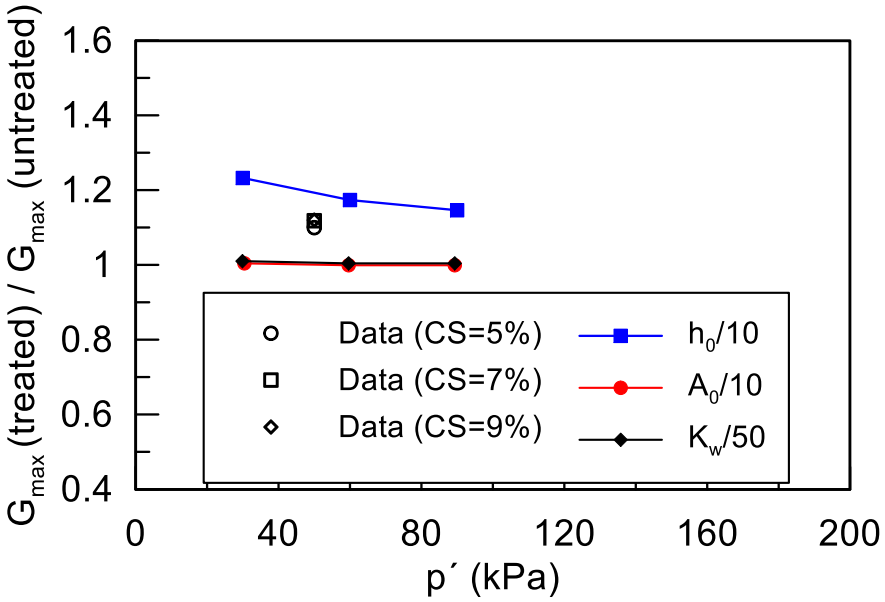

Figure 6.19 *Effect of CS (of different percentages per weight) on maximum shear modulus G_{max} (data from Spencer et al., 2008) and comparison with pertinent numerical simulations with the NTUA-SAND model.*

Chapter 7

NUMERICAL SIMULATION OF THE ONE DIMENSIONAL SEISMIC RESPONSE OF A HORIZONTAL STABILIZED SAND LAYER

7.1 General

Chapter 6 presented a numerical methodology for simulating stabilized sand response on the basis of cyclic element test results. This Chapter investigates the accuracy of this methodology (and its variants) when used in boundary value problems. For this purpose, emphasis is given on the simulation of a dynamic centrifuge test of a horizontal stabilized sand layer under base excitation (Gallagher et al. 2007a) which corresponds to free field seismic shaking conditions insitu. First, the experimental set up and the testing results are presented in detail in order to fully comprehend the response mechanisms of stabilized soils, and this as a basis for selecting the appropriate assumptions for the numerical analyses. The reliability of the suggested numerical methodology is evaluated via comparison with recordings from the foregoing dynamic centrifuge test aiming to draw general conclusions about its accuracy and appropriateness for practical applications.

7.2 Presentation of dynamic centrifuge test

This paragraph presents the dynamic centrifuge test that was selected for verifying the methodology of *Chapter 6* and refers to the 1D dynamic response of a uniform sand layer under sinusoidal base motion. The test replicates the 1D test performed during the VELACS project (Taboada, 1995) using loose Nevada sand (D_r = 40%), with the difference being that the Nevada sand in the current test is treated with colloidal silica grout with CS(%) = 6. Particularly, in prototype scale, the experiment refers to a 10m deep layer and is excited by 20 cycles of a 2Hz sinusoidal shaking parallel to its base, with uniform peak base acceleration of 0.2g.

More specifically, the test was performed by Gallagher et al. (2007a) at Rensselaer Polytechnic Institute (RPI) using Nevada No120 sand treated with Ludox-SM® colloidal silica with a concentration of CS(%)=6 per weight. Nevada No120 is a poorly graded silica sand which is categorized as SW-SM according to USCS and its properties are presented in Table 4-2. A

laminar box with flexible walls was used, which consisted of rectangular aluminum rings. These rings are separated by linear roller bearings in order to permit the relative movement between the rings with minimum friction. The dimensions of the box were 460mmx370mmx260mm. Figure 7.1 presents the cross section of the laminar box along with the locations of the displacement and acceleration transducers. For horizontal acceleration measurements five (5) pairs of accelerometers (AH) were placed at different heights, whereas for the vertical and horizontal displacements five (5) LVDTs were placed, four (4) LH (for horizontal displacements) and just one (1) LV on the layer surface measuring settlement, assuming that is uniform.

Table 7-1 *Properties of Nevada No120 sand (Gallagher et al., 2007a).*

Property	Value
Specific gravity	2.64
Maximum dry unit weight	17.5 kN/m^3
Minimum dry unit weight	14.5 kN/m^3
Maximum void ratio	0.821
Minimum void ratio	0.631
Mean grain size	0.17 mm
Coefficient of uniformity	1.64

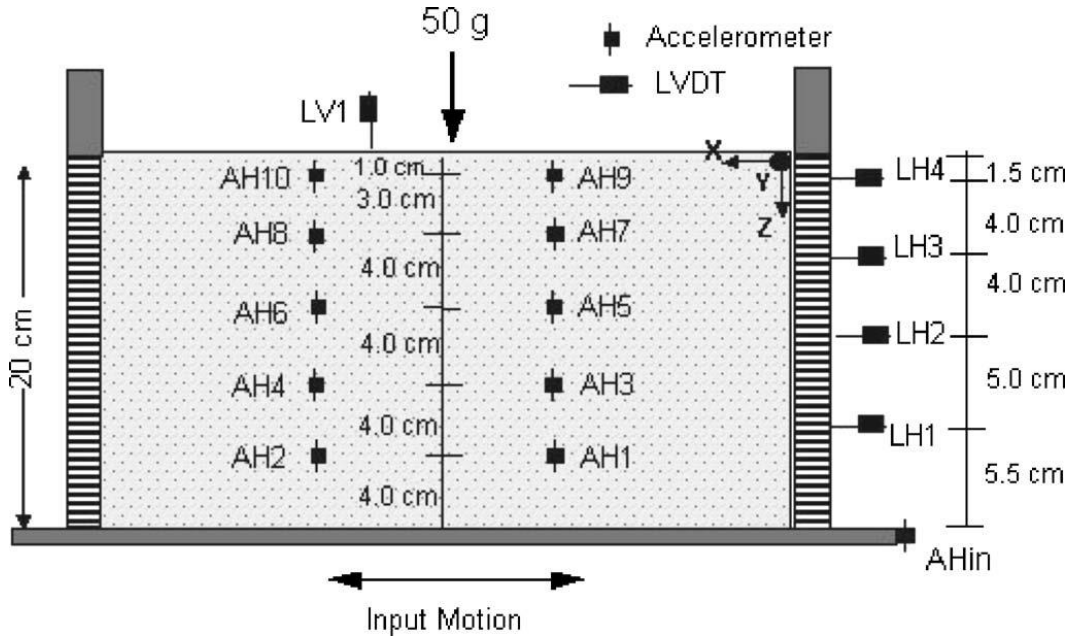

Figure 7.1 *Experimental set up and instrumentation for the dynamic centrifuge test (Gallagher et al. 2007a)*

Dry sand was placed with pluviation in the laminar box in order to achieve a uniform relative density of D_r=40%. The CS solution used had a volume of 1.5 times the pore volume so that full replacement of water with CS solution could be ensured. Figure 7.2 presents the procedure used for the CS injection into the soil, where the grout was injected from the base of the box and drawn upwards under a vacuum.

During the injection, the CS viscosity increased from 1.5 to 1.7cP and the CS solution formed a firm gel 56 hours after mixture. The solution, after its injection and before testing began, was left to cure for 240 hours, i.e. a time which corresponds to four times the gel time. The centrifugal acceleration to which the model was subjected was 50g and therefore the 200mm tall model simulates in prototype units a soil layer of treated liquefiable Nevada sand with a height of 10m.

The layer was subjected to two (2) seismic events, which consisted of twenty (20) cycles with uniform peak acceleration 0.20g and 0.25g respectively and both had a frequency of 20Hz (T=0.5s). The acceleration time-histories recorded at different depths of the soil layer during the test are illustrated in Figure 7.3 .Observe that on the basis of the recorded data, amplification of the ground motion (accelerations) takes place through the soil layer at both seismic events with higher values occurring for the 0.25g excitation and this amplification seems more intense at depths of 2m and 4m and not at the layer surface. Gallagher et al. (2007a) state that a possible explanation for this behavior might be the partial and incomplete gelation of colloidal silica solution or the degradation in the particles adhesion provided by the cementation from the colloidal silica grout, which can be potentially improved by increasing the CS concentration used. Pore pressures were not measured, but according to the acceleration recordings the treated sand did not liquefy during the two seismic events, since nullification (or at least intense de-amplification) of acceleration was not observed.

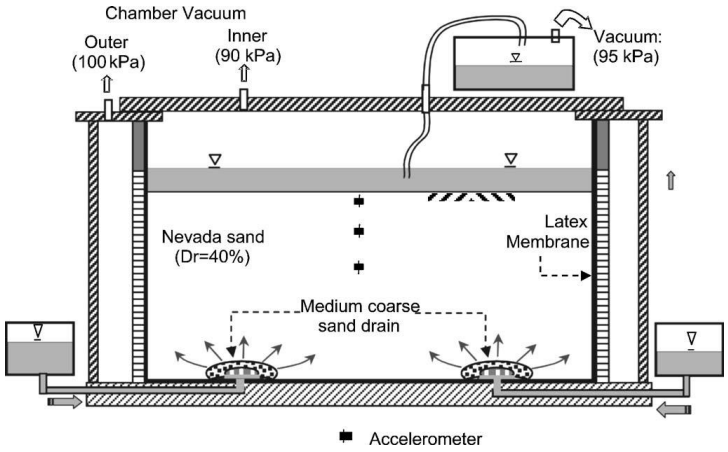

Figure 7.2 *Injection procedure of CS solution (Gallagher et al. 2007a)*

Figure 7.4 presents the lateral displacements with depth for the two shaking events as they evolved with time. It is obvious that displacements increase significantly as peak base acceleration increases from 0.2g to 0.25g. Figure 7.5 shows that vertical displacements recorded were approximately 30mm (0.3% vertical/ volumetric strain) during the first shaking event and less than 10mm during the second. This means that the settlements recorded during the first event were larger than those during the second, despite that the first event (0.20g) had lower intensity than the second one (0.25g).

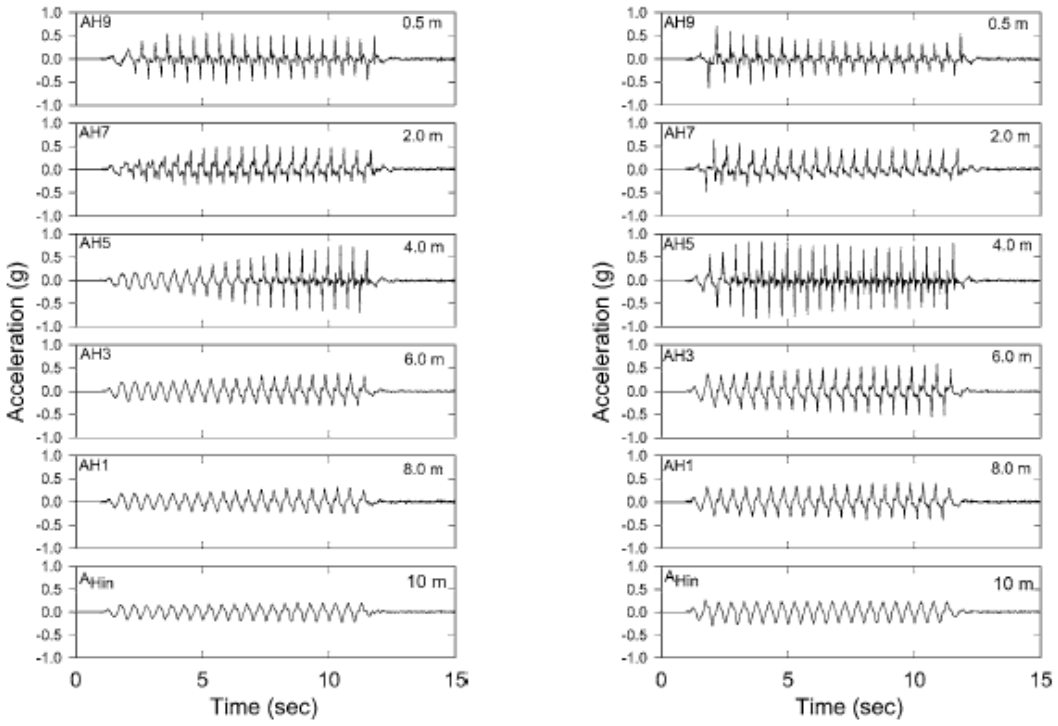

Figure 7.3 *Measured acceleration timehistories at different depths: (a) for the first (0.2g at base), and the (b) the second (0.25g at base), shaking event (Gallagher et al. 2007a)*

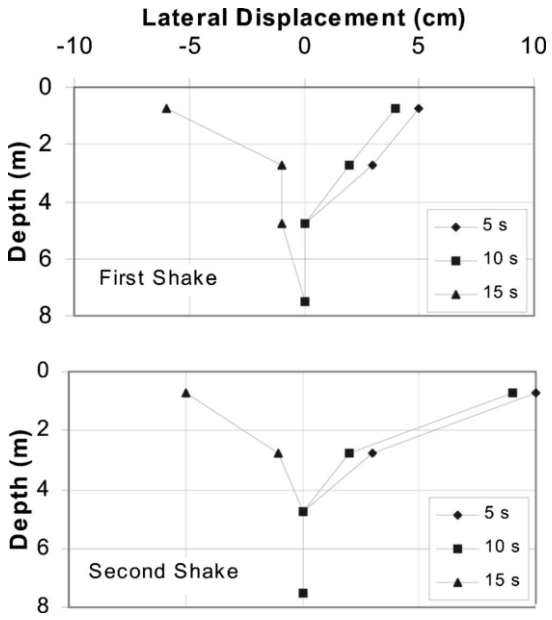

Figure 7.4 *Measured horizontal displacements at different depths and different times: (a) for the first (0.2g at base) and (b) the second (0.25g at base) events (Gallagher et al. 2007a)*

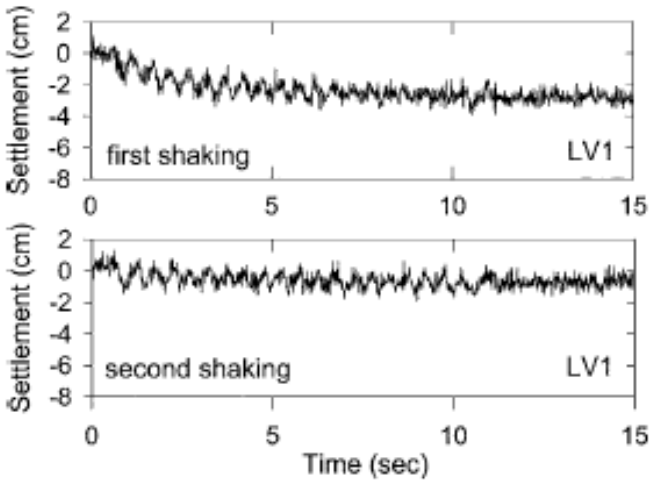

Figure 7.5 *Measured surface settlements : (a) for the first (0.2g at base) and (b) the second (0.25g at base) events (Gallagher et al. 2007a)*

7.3 Numerical simulation of dynamic centrifuge test

The numerical simulation of the foregoing centrifuge test, was performed with the finite difference code FLAC (Itasca 2011). It employed the NTUA-SAND constitutive model (Andrianopoulos et al., 2010a, b), which was appropriately calibrated for Nevada sand. The values of the model constants and state variables related to D_r=40% used are presented in Table 7-2. Interestingly, this model, which has been proven capable of simulating various

boundary value problems involving earthquake- induced liquefaction, has been made readily available for potential FLAC users in: http://www.itasca-udm.com/pages/NTUA.html .

The simulation is performed in prototype scale. Hence, the grid used for the numerical simulation had dimensions 23x10m with zones of 1x1m. The water table was set 1m over the saturated soil surface by applying pressure of 9.81kPa on the surface in order to ensure that the soil layer will remain saturated during the seismic excitation (this assumption does not change the effective stress regime). In all cases, tied node boundary conditions were imposed at the lateral boundary grid-points of the mesh, along the x and y-direction, in order to ensure the same horizontal and vertical displacements at its two lateral boundaries. The particular type of boundary conditions proves very efficient in reproducing the deformation pattern of a laminar box (e.g. Andrianopoulos et al., 2010a, b, among many). The numerical simulation of the treated layer was performed using the methodology presented in Chapter 6, i.e. by considering all three (3) approaches mentioned there. More specifically by assuming: (a) an increase of the constant h_0 of the plastic modulus of the constitutive model for the soil skeleton of the sand, (b) a decrease of the dilatancy constant of the constitutive model A_0, and (c) a decrease of the bulk modulus $K=K_w/n$ of the pore fluid by assuming different denominator n values (where K_w is the bulk modulus of water). Firstly, the parameter values which simulated best the stabilized soil behavior at element level were tested (A_0=0.3, h_0=60000, and K_w/50) in order to investigate their adequacy in simulating the dynamic response of a stabilized soil layer. The hydraulic conductivity value of the treated sand for silica concentration of CS(%)=6 was based on the work of Persoff et al (1999) and is set equal to 10^{-9}m/s for all three approaches.

At the base of the grid a sinusoidal horizontal excitation was applied with peak base acceleration of 0.20g and frequency of 2Hz, aiming at the simulation of the first event. A cycle of smaller amplitude was also added at the beginning and at the end of the time history to ensure a gradual increase and decrease of the input acceleration and eliminate numerical inertial effects related to abrupt change in loading conditions. Local damping of 2% was used in the analysis but for medium and large cyclic shear strain amplitudes increased hysteretic damping is simulated via the elastoplastic formulation of the NTUA-SAND constitutive model.

Before proceeding to comparing data to simulations, note that contrary to the original experiment for the excitation with peak base acceleration (PBA) equal to 0.20g for the untreated sand (Taboada 1995), the stabilized sand did not liquefy during shaking (Gallagher et al. 2007a). Moreover, the stabilized sand did not depict de-amplification of the ground

motion; rather it even showed significant amplification after the first 3-4 cycles, with peak accelerations reaching 0.55g (in comparison to 0.2g at the base) in Figure 7.3. The measured acceleration response also included, what seems to be, significant dilation spikes, which are essentially the cause for the foregoing amplification.

The following figures present the comparison of recordings with results from the numerical simulation in terms of accelerations, excess pore pressure ratio and settlement time histories. More specifically, the measurements recorded from the accelerometers at the left side of the laminar box (denoted as AH10, AH8, AH6, AH4, AH2) are compared with the acceleration time-histories resulting from the numerical analyses at the same locations of the mesh. Also, the measured settlements on the soil surface from transducer LV1 are compared with the settlements resulting from the analysis at the same location. Finally, the excess pore pressure ratio time-histories are also included in the figures at different depths only as they resulted from the numerical simulation since there are no corresponding recordings from the centrifuge test.

It should be clarified here that the pore pressure development mechanism in stabilized with CS soils has not been microscopically investigated yet (e.g. Conlee et al., 2012). Hence, the numerical results that refer to r_u are presented here merely as a means for better understanding the simulation mechanisms in terms of accelerations and settlements.

In the following figures, the results of the numerical analyses for parameter values A_0=0.3 (Figure 7.6), h_0=60000 (Figure 7.7) and K=40MPa (Figure 7.8), which correspond to $A_0/2.67$, $4h_0$ and $K_w/50$ are presented. It is noted that analyses for A_0=0.3 and/ or h_0=60000 use all the other NTUA-SAND constants as calibrated for Nevada sand (Table 7-2) while in the analysis with $K_w/50$ all model constants retain their Nevada sand values. Observe that, even though these approaches were able to simulate the laboratory results at the element level (e.g. for the available data recorded from Díaz-Rodríguez et al., 2008) in Chapter 6, none of the aforementioned simulations was able to satisfactorily simulate the dynamic response of the treated soil layer. More specifically, all analyses predict liquefaction of the stabilized layer in contrast to the recordings. Liquefaction herein is related to a value of r_u=1.0 and intense de-amplification of the acceleration after the first 2-3 cycles. In addition, all these simulation efforts produce zero surface settlements (Figure 7.9), an outcome also related to the formulation of NTUA-SAND which produces very small volumetric strains in consolidation loadings (Andrianopoulos et al. 2010).

Table 7-2 *Values of model constants and state variables for D_r=40% of NTUA-SAND model for untreated Nevada sand (Andrianopoulos et al.2010)*

Nevada sand	
Dry density (Mgr/m^3)	1.52
Porosity	0.424
e	0.737
M_c^c	1.25
M_c^e	0.72
$(e_{cs})_a$	0.809
λ	0.022
B	600
v	0.33
k_c^b	1.45
k_c^d	0.30
γ_1	0.00025
α_1	0.6
A_o	0.8
h_o	15000
N_o	40000

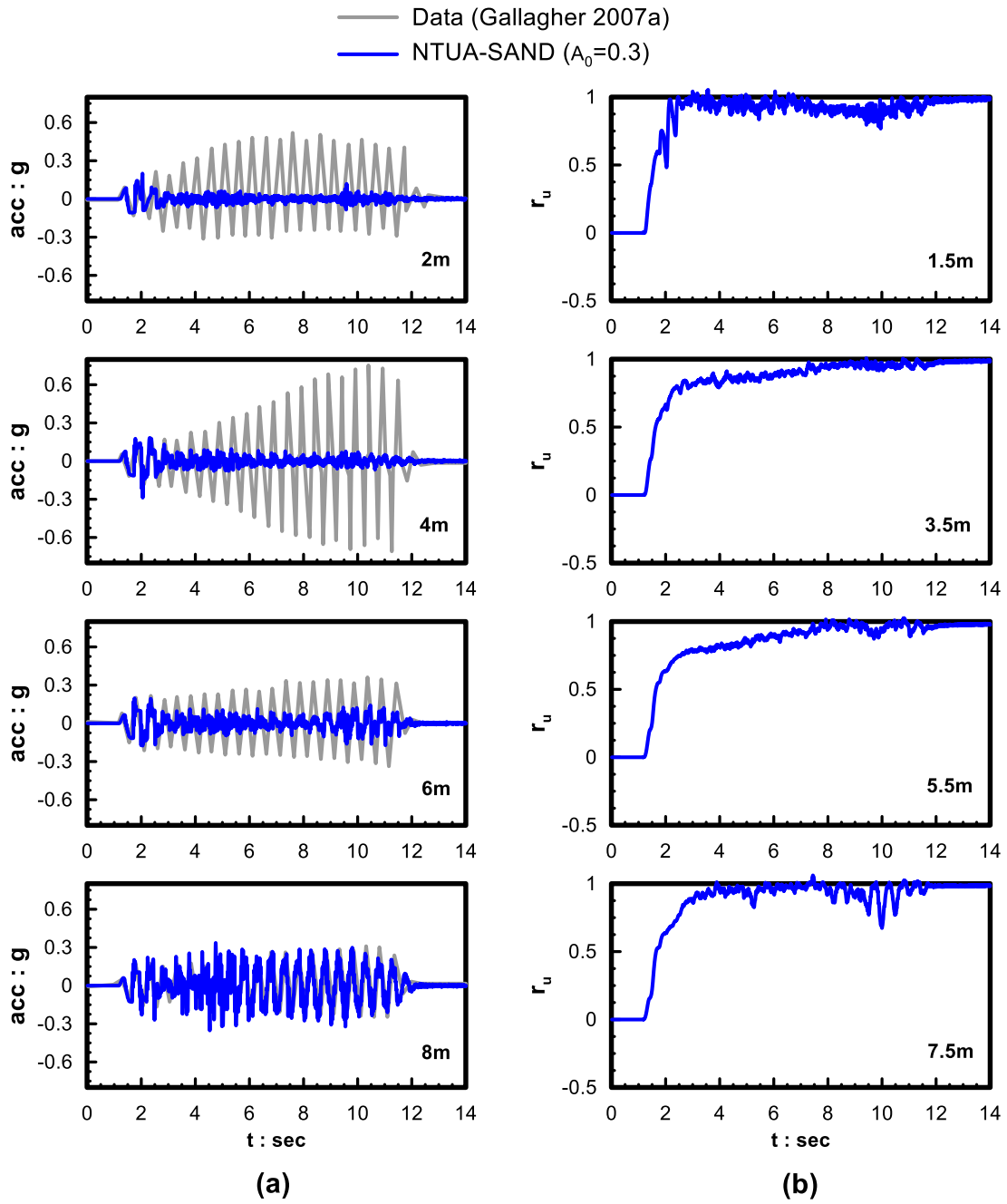

Figure 7.6 *(a) Comparison of measured acceleration time histories at different depths with their numerical counterparts, (b) Excess pore pressure ratio time histories at different depths resulting from the numerical analysis. (data: Gallagher et al., 2007a; analyses: using NTUA-SAND with values of constants in Table 7-2, but A_0=0.3)*

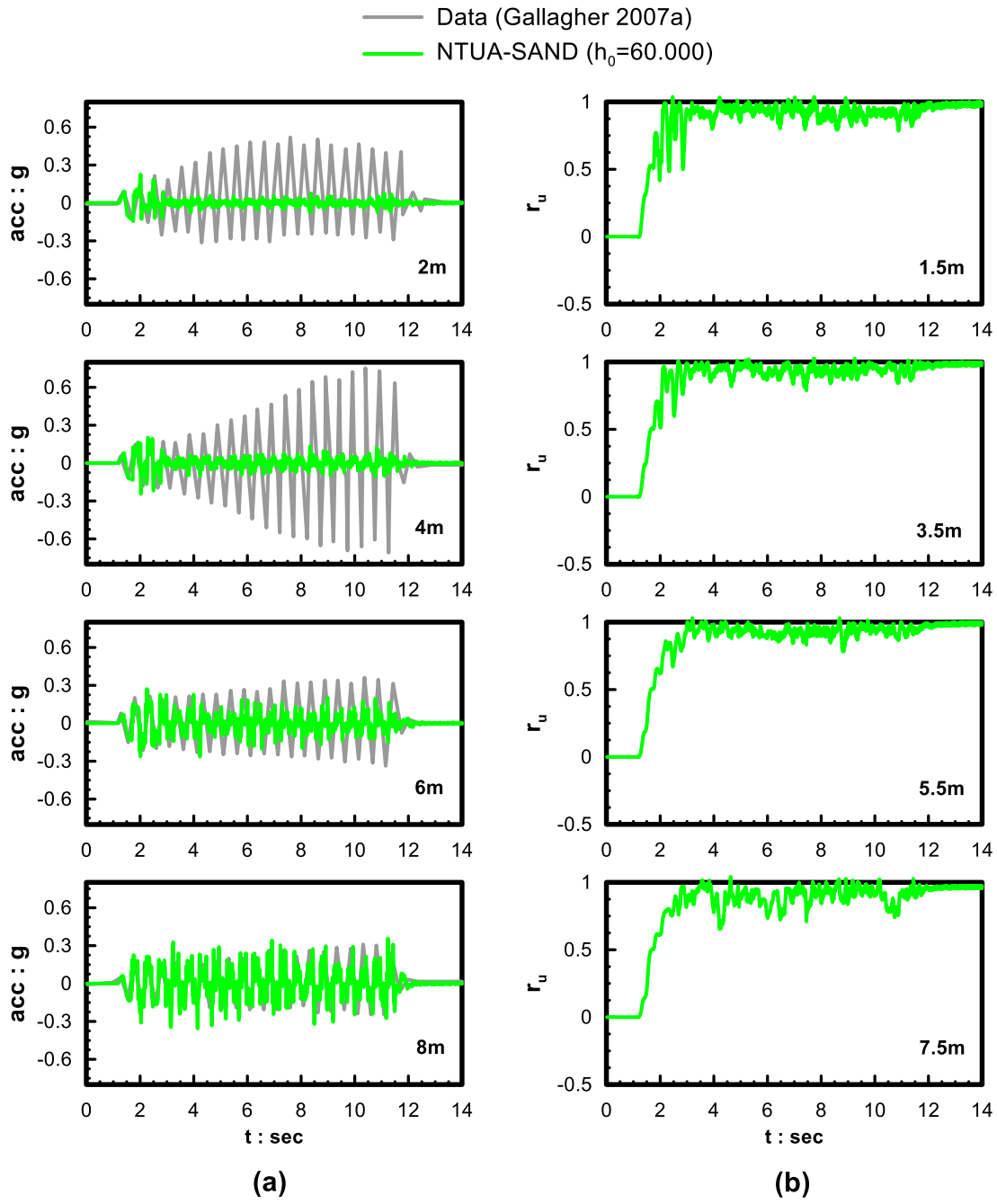

Figure 7.7 *(a) Comparison of measured acceleration time histories at different depths with their numerical counterparts, (b) Excess pore pressure ratio time histories at different depths resulting from the numerical analysis. (data: Gallagher et al., 2007a; analyses: using NTUA-SAND with values of constants in Table 7-2, but h_0=60000)*

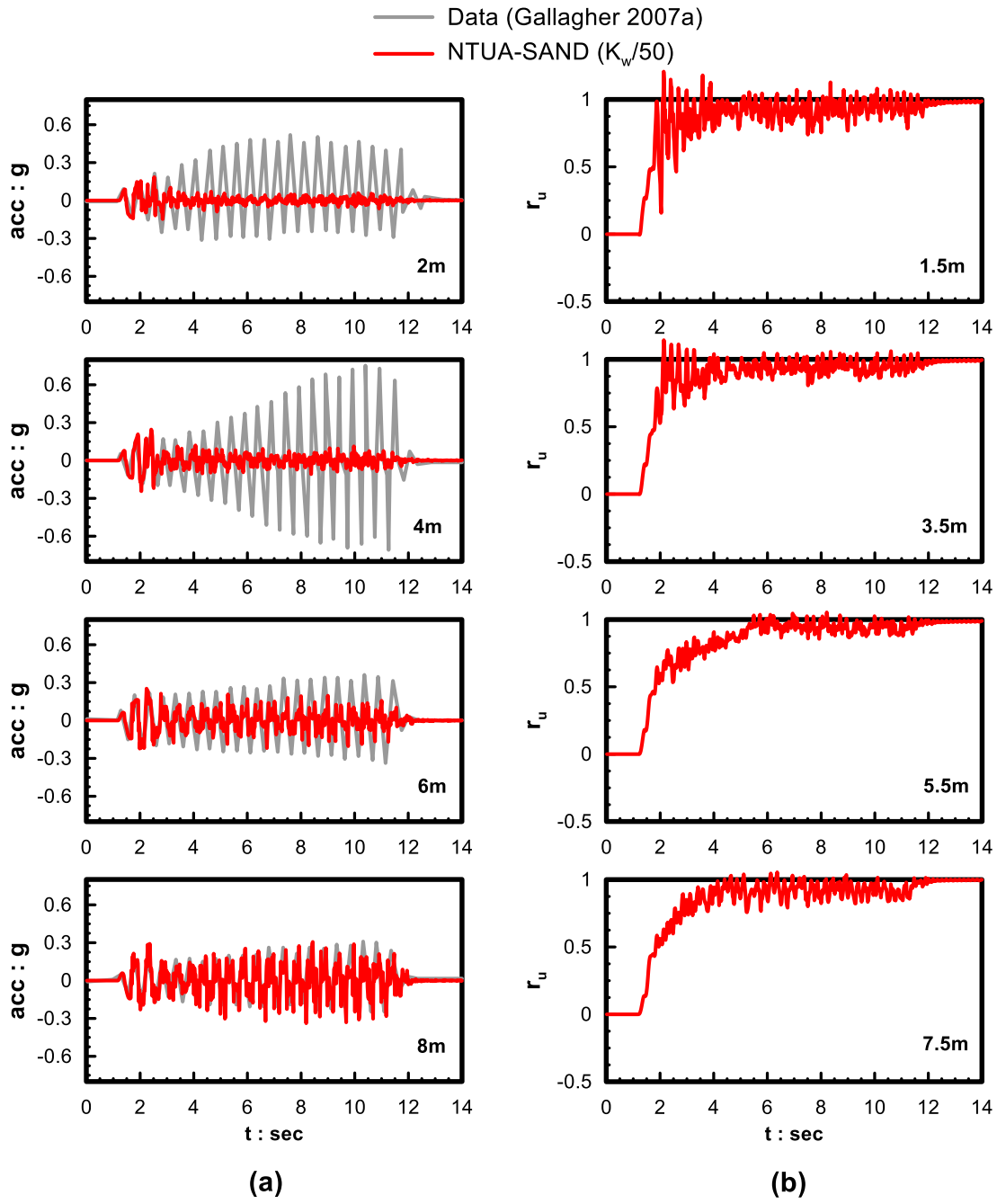

Figure 7.8 *(a) Comparison of measured acceleration time histories at different depths with their numerical counterparts, (b) Excess pore pressure ratio time histories at different depths resulting from the numerical analysis. (data: Gallagher et al., 2007a; analyses: using NTUA-SAND with values of constants in Table 7-2 and K=40MPa=K_w/50)*

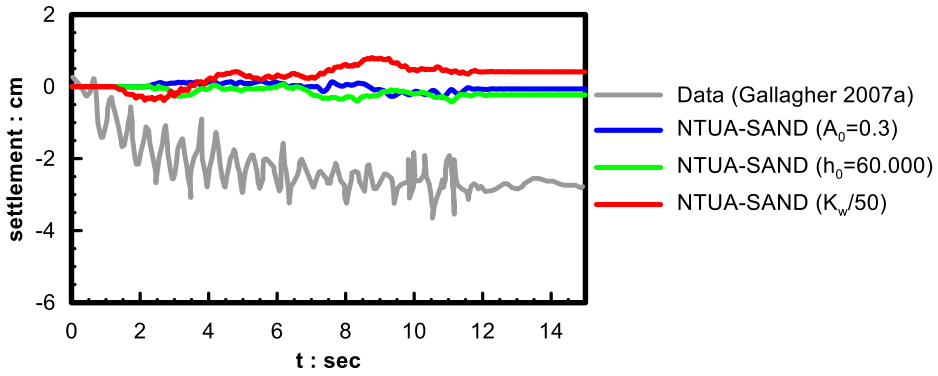

Figure 7.9 *Comparison of surface settlement time history as measured in centrifuge test with its numerical simulations (data: Gallagher et al., 2007a; analyses: using NTUA-SAND with values of constants in Table 7-2 but A_0=0.3, either h_0=60000, or K=40MPa=K_w/50)*

It has to be underlined that although the parameter values of A_0/2.67, 4h_0 and K_w/50 were not able to quantitatively depict the seismic response of stabilized soil in this centrifuge test, their use led to qualitatively accurate response. Hence, analyses were repeated, this time by modifying 10 times further the values of the parameters, namely using A_0=0.03, h_0=600000 and K=K_w/500 and these results were again compared with the recordings in terms of the acceleration time history at a shallow depth of 2m and in terms of the surface settlement time history. The time history of excess pore pressure ratio r_u is also presented in Figure 7.10 for each numerical simulation at a depth of 1.5m for the sake of completeness, despite that there is no pertinent recording. The results indicate that the new proposed values for all three parameters simulate significantly better the response of the stabilized soil layer in terms of accelerations since all pertinent indications of liquefaction disappear, and this is also evident in the simulated r_u time histories where r_u=1.0 only at the end of the excitation, if at all. This is a completely different response than in Figures 7.6-7.8, where r_u=1.0 appears from the beginning of the excitation. However, as deduced from Figure 7.11, the additional modification of model constants (h_0 and A_0) does not lead to an ameliorated simulation of the settlement time history. On the contrary, a further modification related to the pore fluid modulus (K_w/500) seems to be the most accurate approach among the three.

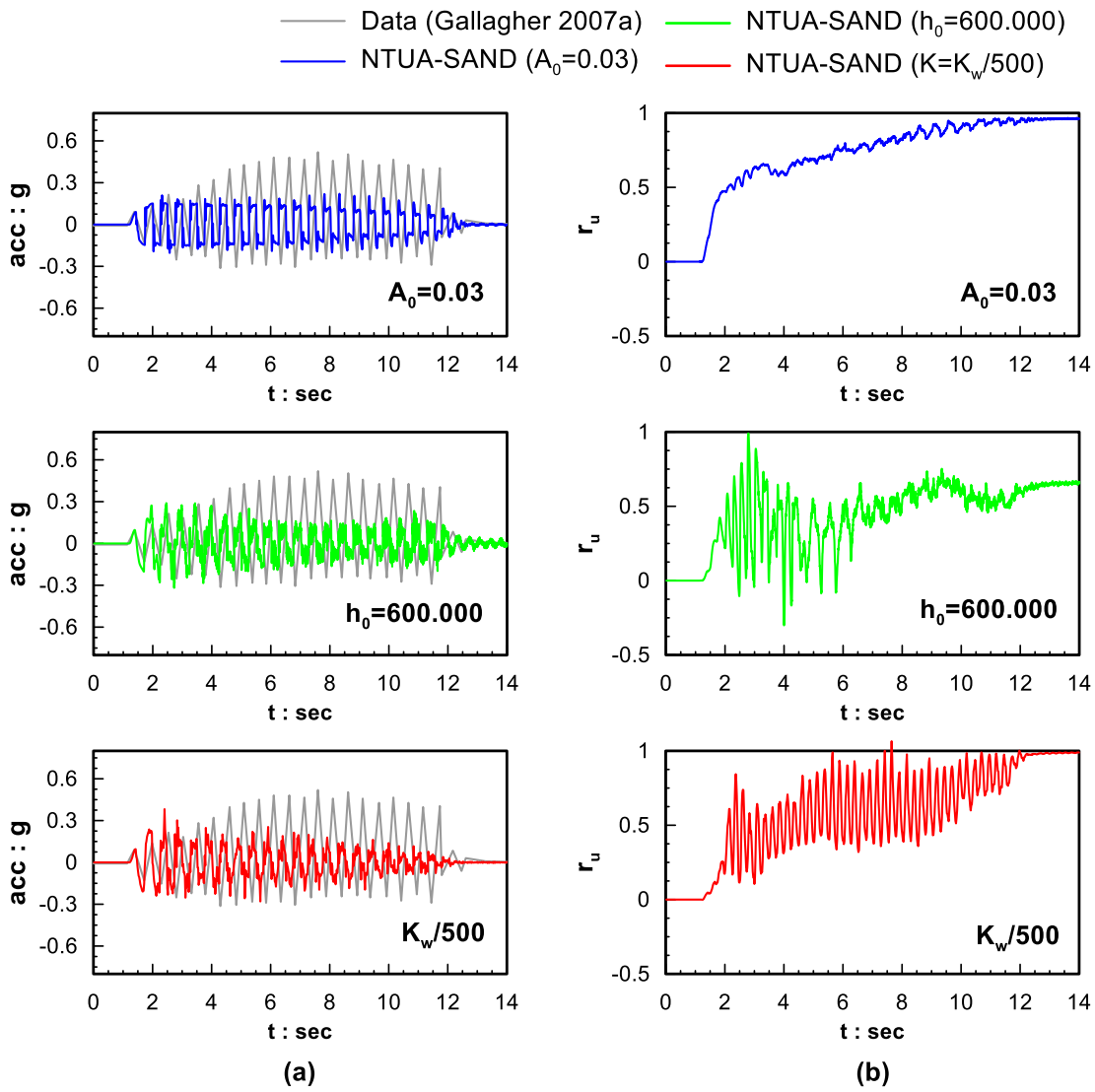

Figure 7.10 *(a) Comparison of measured acceleration time history at 2m depth with its numerical counterparts (b) Excess pore pressure ratio time history at 1.5m depth resulting from the numerical analyses. (data: Gallagher et al., 2007a; analyses: using NTUA-SAND with values of constants in Table 7-2, but A_0=0.03, either h_0=600.000 or K=4000kPa=K_w/500)*

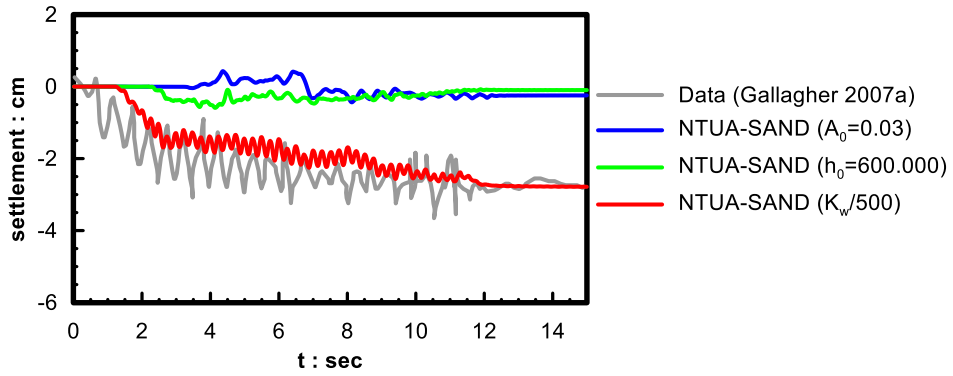

Figure 7.11 *Comparison of surface settlement time history as measured in centrifuge test with its numerical simulations (data: Gallagher et al., 2007a; analyses: using NTUA-SAND with values of constants in Table 7-2 but A_0=0.03, either h_0=600.000 or K=4000kPa=K_w/500)*

Overall, it is observed that modifying the sand skeleton component of the soil – fluid system seems less accurate and so, one could consider modifying the pore fluid component of the analysis as proposed. In reality, given that passive stabilization affects the pore fluid (it becomes a firm resonating gel after enough time) and not the sand skeleton, this approach seems even more realistic. Hence, one could use the properties of colloidal silica for the pore fluid component in any finite element or finite difference analysis, instead of the (default) values for water. This is especially true in large scale boundary value problems where the conditions are not fully controlled as in element tests. The same concerns were raised by Towhata (2007, 2008) as mentioned previously, who, based on results from unconfined compression tests of pure gelled colloidal silica samples, concluded that this material has significant volume compressibility in comparison to that of water (which is practically incompressible). In other words, while any tendency for volume reduction (e.g. due to seismic shaking) translates to excess pore pressure development in saturated untreated sand, any similar loading in treated (stabilized) sand is not expected to generate (significant) excess pore pressures no matter its intensity.

In conclusion, taking into account all the above observations, the approach that assumes a reduction of the fluid bulk modulus K (in comparison to that of water: K_w=2x10^{-6}kPa) seems to offer the best simulation of the 1D seismic response of a stabilized soil layer, because of its clearly improved simulation in terms of settlements. However, a value of 500 for the divider of the fluid bulk modulus (K=K_w/500) is not necessarily the best value to simulate the overall response in terms of both settlements and accelerations. For this purpose, more appropriate values of K_w dividers were investigated. Particularly, a possible relation between the K_w divider and the concentration of CS solution per weight CS(%) was investigated. After a large number

of parametric analyses and through a trial and error procedure, for both the 1D ground shaking centrifuge test conducted by Gallagher et al. (2007a) and the 2D ground shaking centrifuge test conducted by Conlee et al. (2012) which will be presented in Chapter 8, the following simple expression was devised, which offers appropriate estimates for K, as a fraction of K_w, on the basis of the CS(%) of the treated soil. This expression reads:

$$K = K_w / \left[\left(CS(\%) + 2.25 \right) \cdot 100 \right] \quad (7.1)$$

where:

K is the fluid bulk modulus, K_w is the bulk modulus of water and CS(%) is the concentration per weight of colloidal silica in the pore fluid.

For a concentration of CS(%)=6 used by Gallagher et al. (2007a) the above expression leads to a divider value equal to 825. i.e. $K=K_w/825$. Apart from this value the appropriateness of a divider equal to 975 is also investigated, which results from a silica concentration of CS(%)=7.5, the average value of CS(%)=5 and 10%, which are the minimum and maximum values of CS(%) for use in passive stabilization against liquefaction, in terms of effectiveness and cost. The following figures explore the appropriateness of these pore fluid modulus K values in terms of the time histories of acceleration and excess pore pressure ratio (Figure 7.12), as well as settlement (Figure 7.13) by comparison to the recordings (wherever available). It is evident that these values of K lead to better simulations of the response of the stabilized soil layer in terms of accelerations and excess pore pressures when compared to previous analyses in this Chapter, while their relative differences are small. This fact provides evidence of the adequacy of the abovementioned Equation (7.1) for quantitative accuracy in simulating the 1D seismic response of stabilized sand layers.

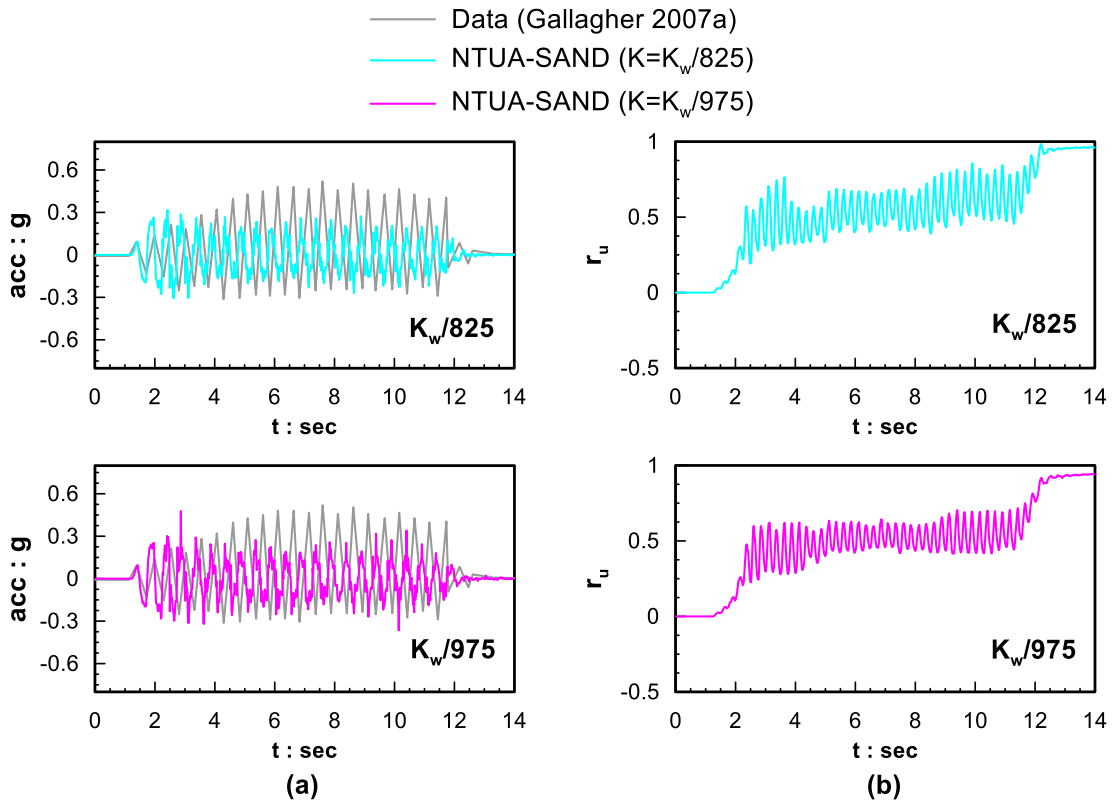

Figure 7.12 *(a) Comparison of measured acceleration time history at 2m depth with its numerical counterparts (b) Excess pore pressure ratio time history at 1.5m depth resulting from the numerical analyses. (data: Gallagher et al., 2007a; analyses: using NTUA-SAND with values of constants in Table 7-2 and K=Kw/825 or K=Kw/975)*

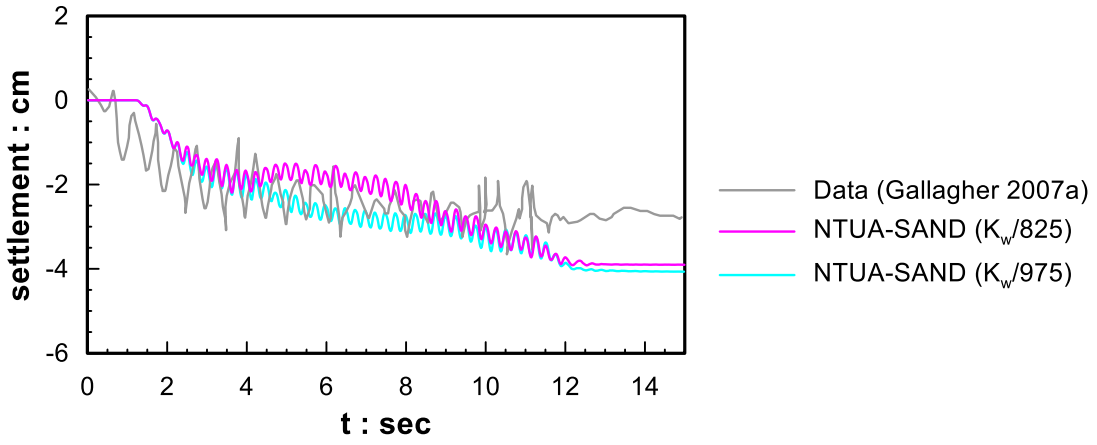

Figure 7.13 *Comparison of surface settlement time history as measured in centrifuge test with its numerical simulations (data: Gallagher et al., 2007a; analyses: using NTUA-SAND with values of constants in Table 7-2 and K=Kw/825 or K=Kw/975)*

7.4 Effect of hydraulic conductivity of untreated sand on its seismic response

This paragraph investigates the value of hydraulic conductivity, k, which should be adopted in cases where the sand is not stabilized and liquefaction occurs. More specifically, in cases of dynamic loading and especially when liquefaction occurs, the use of the hydraulic conductivity k value which is measured in laboratory experiments (e.g. permeability testing) is considered questionable in the literature. The reason is that when the soil is subjected to dynamic loading, some of the basic assumptions of Darcy's law –steady state constant direction flow through the pores of a stable soil – are not fulfilled. In more detail, dynamic loading is characterized by a rapid change of flow direction and concurrently excess pore pressure develop, which lead to an unstable soil skeleton especially if liquefaction is observed.

For this purpose, in the literature, three different ways of incorporating the hydraulic conductivity coefficient k in numerical analyses has been reported. These ways are outlined by Chaloulos et al. (2013) and are presented below with reference to Nevada sand, the sand used in the centrifuge experiments of Gallagher et al. (2007a) simulated above after its stabilization. Specifically, one could use:

- The "static" value as measured from (constant head) permeability tests under 1g gravitational acceleration ($k=6.6*10^{-5}$m/s for Nevada sand with relative density D_r=40%; Arulmoli et al. 1992, Arulanandan K. & Scott R. F 1994), or
- The "dynamic" value, as proposed by Liu and Dobry (1997) considering the alternating flow direction in the pores of the soil ($k=2.1*10^{-5}$m/s, for Nevada sand with D_r=40%, which is approximately 3 times lower than the "static" value), or
- The "variable" value, which takes into account the dislocations of soil grains during liquefaction and the creation of "flow channels" within the soil skeleton. This value changes as a function of either the excess pore pressure ratio r_u, or as a function of time.

More specifically, Arulanandan and Sybico (1993) proposed a triangular distribution of k with time, which initiates from a value of k_{ini} and takes its maximum value when initial liquefaction (r_u=1) first appears, or alternatively the use of an equivalent average value equal to $3.67k_{ini}$. The rationale behind this triangular distribution is also adopted by Manzari and Arulanandan (1994). More recently, Shahir et al. (2012) suggest the change of k as a function of r_u following the expression below:

$$k = k_{ini}\left[1+(\alpha-1)r_u^{\,b}\right] \tag{7.2}$$

where α and b are soil constants, calibrated for Nevada sand equal to α=20 and b=1.

Following this expression, the maximum hydraulic conductivity has a value of $20k_{ini}$ with an equivalently average value of $10k_{ini}$. Taiebat et al. (2007) propose the use of a simplified equivalent average value equal to $4k_{ini}$, for simplicity.

Similarly, Andrianopoulos (2006) performed a literature review of the different k values used in order to simulate the response of untreated Nevada sand during the VELACS (Verification of Liquefaction Analyses by Centrifuge Studies) research program. In most of the numerical simulations, the hydraulic conductivity coefficient used in the analyses was 50 times higher than the value measured in the laboratory ("static" value), so that the effect of the centrifugal acceleration is taken into account since water was used as a pore fluid in the centrifuge tests that were simulated. Only two researchers used a decreased value of k, namely Bardet and Huang (1994) adopted a smaller value of k during the whole test simulation, while Popescu and Prevost (1994) also adopted a reduced value of k during the seismic excitation implying a "dynamic" value of k. Note that all simulation efforts led to settlements clearly smaller than those measured in the centrifuge test.

In the present study, an effort was made to simulate the response of untreated Nevada sand, using some of the suggestions proposed for the "static", "dynamic" and "variable" values of k. This procedure aims at establishing the relative importance of these assumptions on the predicted response of the 10m-thick layer in the test of Gallagher et al. (2007a) if it hadn't been passively stabilized. The approaches used for the value of k are the following:

1. $k=k_{ini}=6.6x10^{-5}$m/s, according to Arulmoli et al. (1992)
2. $k=k_{ini}$ $k=2.1x10^{-5}$m/s, according to Liu and Dobry (1997)
3. $k=10xk_{ini}$, according to the simplified coefficient proposed by Shahir et al. (2012). For the simulations that used this approach two (2) cases were investigated: (3a) $10xk_{ini}$, with $k_{ini}=6.6x10^{-5}$m/s and (3b) $10xk_{ini}$, with $k_{ini}=2.1x10^{-5}$m/s.
4. $k=4xk_{ini}$, according to the simplified coefficient proposed by Taiebat et al. (2007) For the simulations that used this approach two cases were investigated: (4a) $4xk_{ini}$, with $k_{ini}=6.6x10^{-5}$m/s and (4b) $4xk_{ini}$, with $k_{ini}=2.1x10^{-5}$m/s.
5. $k=3.67xk_{ini}$, according to the simplified coefficient proposed by Arulanandan and Sybico (1993) For the simulations that used this approach two cases were investigated: (5a) $3.67xk_{ini}$, with $k_{ini}=6.6x10^{-5}$m/s and (5b) $3.64xk_{ini}$, with $k_{ini}=2.1x10^{-5}$m/s.
6. Time – variable *k*, as proposed by Manzari and Arulanandan (1994) as presented qualitatively in Figure 7.14. Observe that the *k* returns to its initial value k_{ini} after the end of excitation and takes its maximum value of $6.7xk_{ini}$ when initial liquefaction ($r_u=1$) occurs

for the first time. For the simulations that used this approach two (2) cases were investigated: (6a) where k_{ini}=6.6x10^{-5}m/s and (6b) where k_{ini}=2.1x10^{-5}m/s.

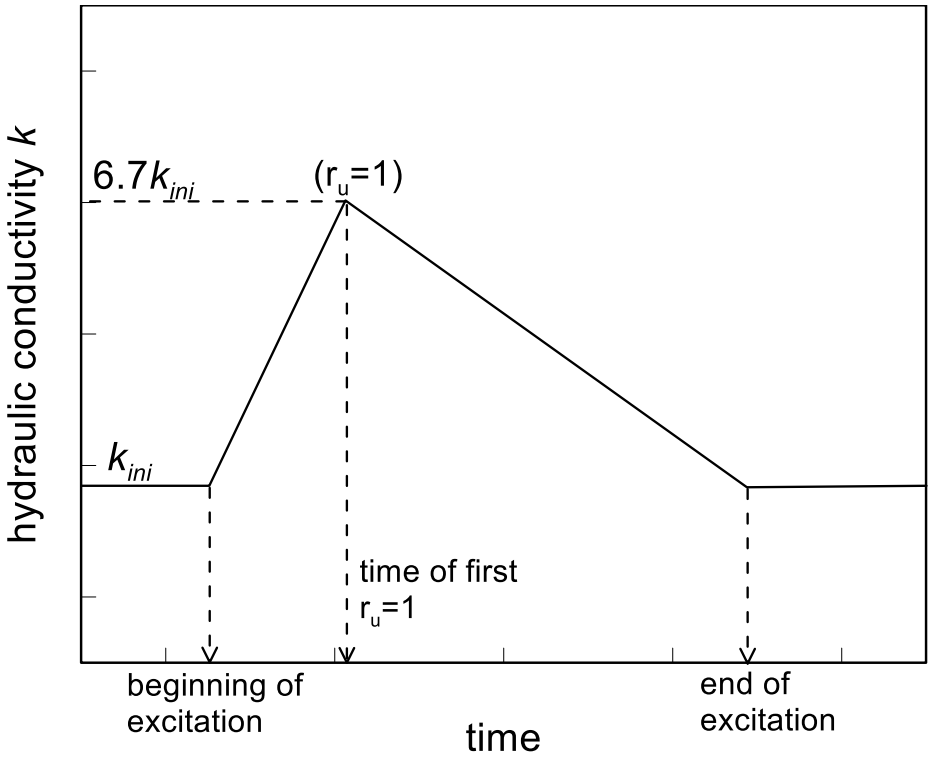

Figure 7.14 *Time dependent hydraulic conductivity , for numerical analyses in a liquefaction regime as proposed by Manzari and Arulanandan (1994)*

It becomes obvious that in cases 3 to 6, the two sets of analyses correspond to the "static" and "dynamic" values of k used as k_{ini}. Figures 7.15 and 7.16 present the results of all ten (10) analyses outlined above, and each color represents one of the above approaches in terms of settlement and excess pore pressure ratio histories respectively. It should be mentioned that in all numerical simulations a 50-fold higher k value was used (from the values outlined above) so that centrifugal effects are taken into account. The reason for this selection is that the emphasis here is to compare with what the centrifuge test of Gallagher et al. (2007a) would give if the soil hadn't been passively stabilized and pure water was used as the pore fluid (as was done in the VELACS project). This also allows for a direct comparison with what the settlements that the VELACS project test showed and what different researchers had predicted (see overview in Andrianopoulos 2006).

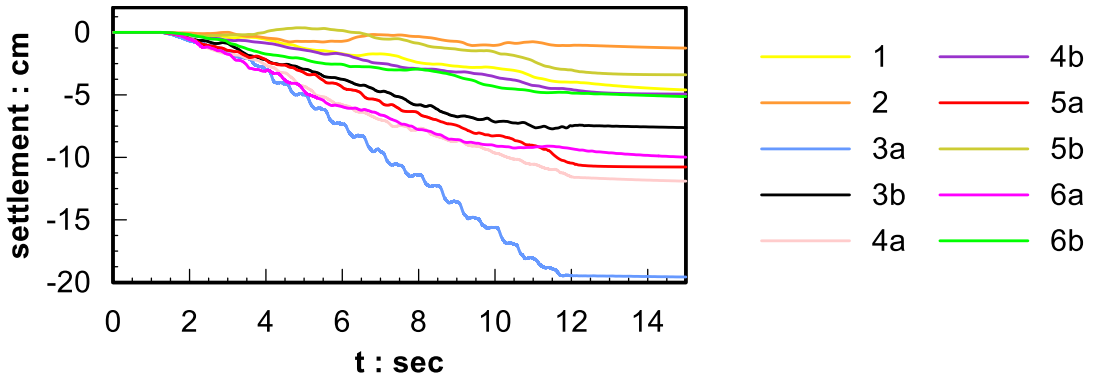

Figure 7.15 *Comparison of computed time histories of surface settlement for different approaches for the hydraulic conductivity k if the test of Gallagher et al. (2007a) was performed on untreated Nevada sand with water as pore fluid and 50g centrifugal acceleration.*

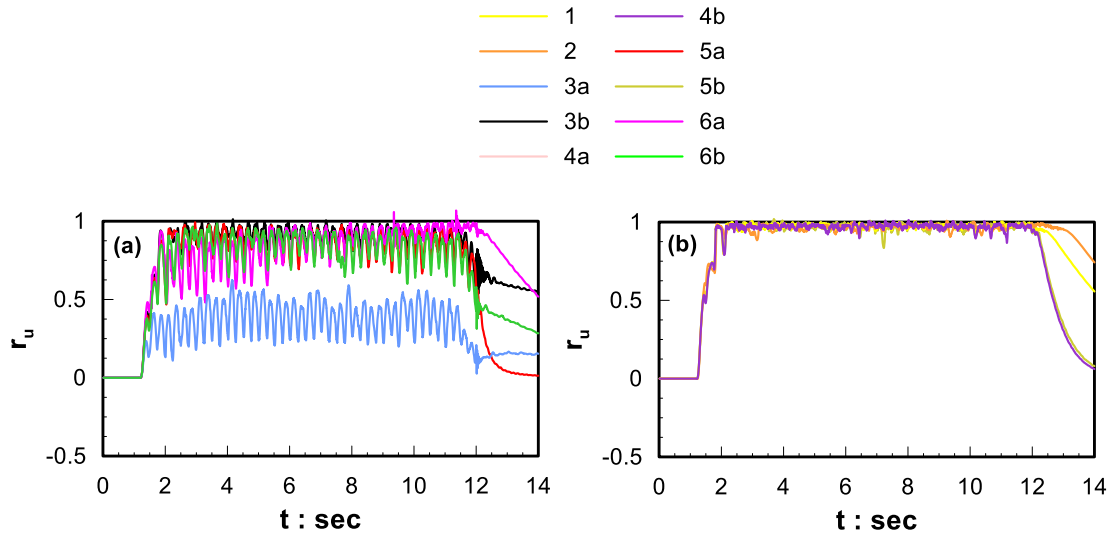

Figure 7.16 *Comparison of computed time histories of excess pore pressure ratio r_u at a depth of 1.5m for different approaches for the hydraulic conductivity k if the test of Gallagher et al. (2007a) was performed on untreated Nevada sand with water as pore fluid and 50g centrifugal acceleration.*

Based on Figure 7.15 two groups of results are observed: one that leads to settlements of 2-5 cm (analyses 2, 5b, 1, 6b, 4b) and one that leads to settlements larger than 5cm (analyses 3b, 5a, 6a, 4a, 3a). The pertinent test in the VELACS project showed settlements higher than 15-20cm, so is more compatible with the latter set of analyses. Interestingly, in the numerical simulation results, this behavior is related to analyses 3a and 4a, that correspond to $k=(4\text{-}10)xk_{ini}$ with $k_{ini}=6.6x10^{-5}$m/s, i.e. the "static" value. In addition, practically all cases led to settlements higher than those observed at the stabilized soil layer, as expected.

The results in terms of r_u are presented in Figure 7.16 in the two different subplots, which correspond to the two different groups of seismic settlements (a)2-5cm, (b)>5cm. It becomes obvious that most of the approaches predict liquefaction which can be expected considering previous analyses for similar soil types. However, it is clear that large settlements (higher than 5cm) are related to complete liquefaction, i.e. for values of r_u=1 throughout the shaking (as shown in Figure 7.16b).

Chapter 8

NUMERICAL SIMULATION OF THE TWO DIMENSIONAL SEISMIC RESPONSE OF A GENTLY SLOPING STABILIZED SAND LAYER

8.1 General

The previous *Chapter* presented the numerical simulation of the 1D seismic response of a horizontal stabilized sand layer. This *Chapter* investigates the ability of the same numerical methodology to simulate the seismic response of a gently sloping stabilized sand layer, namely a 2D boundary value problem. Hence, the simulation of a series of dynamic centrifuge tests on gently sloping stabilized sand layers (Conlee et al. 2012) are presented herein and evaluated versus the pertinent measurements. The purpose of this evaluation is to further explore the reliability to the employed numerical methodology by highlighting its merits and limitations for different boundary value problems. Hereafter, paragraph 8.2 presents the experimental set up and the centrifuge testing results, in order to illustrate the pertinent response mechanisms, while paragraph 8.3 presents the assumptions of the conducted numerical analyses aiming to simulate these tests. The reliability of the proposed numerical methodology is evaluated via comparison with the centrifuge test results in paragraph 8.4.

8.2 Presentation of dynamic centrifuge experimental set up

The tests that will be examined here were performed on the 9-m-radius centrifuge at the Center for Geotechnical Modelling (CGM) at the University of California, Davis (NEES@UCDavis) and were presented in detail by Conlee (2010) in her PhD thesis. Their goal was to evaluate the effectiveness of CS solutions as possible stabilizers for mitigating liquefaction and lateral spreading displacements of gently sloping layers towards a free face, as well as to compare the lateral spreading response of two similar slopes during seismic excitations of different amplitude with and without stabilization or with stabilization with different CS(%). The typical model consisted of two symmetrical slopes with a 3^o inclination towards a central channel of 3m width (in prototype units) as presented in Figure 7.1. The slope consisted of three layers with the following properties: (a) a 0.75m thick bottom layer of dense Monterey No0/30 sand, (b) a 4.8m thick layer of liquefiable Nevada No120 sand and (c) a top 1m thick layer of compacted, practically impermeable silty clay named Yolo loam.

A total of two (series of) tests were performed, denoted hereafter as CTC01 and CTC02. During the first test series (CTC01) which will be examined extensively herein, Monterey and Nevada sand layers on the left slope were stabilized with Ludox-SM® colloidal silica at a concentration of CS(%)=9 and the right slope was left untreated. During the second test series (CTC02) the same layers of the left slope were stabilized with Ludox-SM® colloidal silica at a concentration of CS(%)=4 and the right slope was also stabilized with CS(%)=5.25. The reference to a "series" of tests is related to the fact that each model (CTC01, CTC02) was shaken with a series of excitations of different amplitude. The model geometry of the two tests series is the same and is shown in Figure 7.1, while the physical properties of the soils used are presented in Table 8-1.

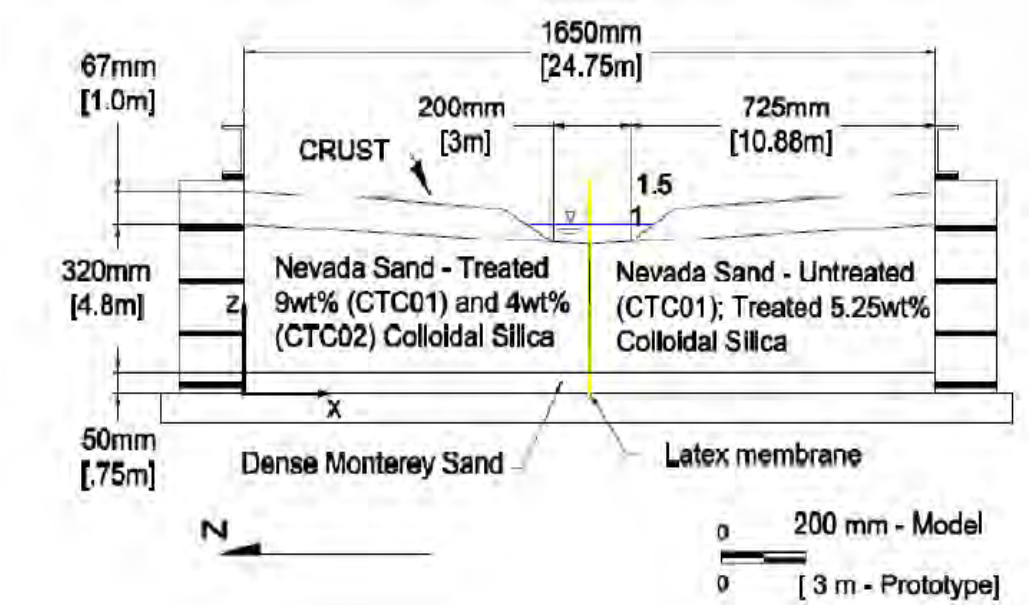

Figure 8.1 *Model geometry for the centrifuge tests CTC01 and CTC02* (Conlee 2010)

In order to perform the test, a flexible box was used (Equivalent Shear Beam, ESB-Container) where the sand layers were placed via pluviation, so that the desirable values of relative density could be achieved. The stabilized slope was saturated with colloidal silica solution and the untreated slope was saturated with deionized water. The top layer of Yolo loam was placed after saturation with colloidal silica, in order to avoid creation of flow channels through the material which could lead to weak (and possibly permeable) zones. Ten accelerometers, nine pore pressure transducers, horizontal (LP/LVDT) and vertical (vertical LP/LVDT) displacement transducers were placed to record the time-histories of acceleration, pore pressure, lateral spreading and surface settlement respectively. Figure 8.2 presents the instrumentation set up for CTC01 test series. Colloidal silica grout was injected from the

bottom of the box using a vacuum. The gel time selected was large enough to fully saturate the liquefiable sand layer, and adequate curing time was retained before conducting the experiment.

Table 8-1 *Physical properties of soils used at the centrifuge tests (based on Conlee et al., 2010)*

Parameter	***Dense sand***	***Loose sand***	***Crust***
Soil type	Monterey 0/30	Nevada No120	Yolo loam
Density of solid skeleton ρ_s (Mg/m^3)	2.64	2.64	-
Maximum dry unit weight $\gamma_{d,max}$ (kN/m^3)	16.81	17.5	-
Minimum dry unit weight $\gamma_{d,min}$ (kN/m^3)	13.96 (CTC01) 13.74 (CTC02)	14.5	-
Relative density (%)	95 (CTC01) 98 (CTC02)	35 (CTC01) 45 (CTC02)	-
Mean grain size d_{50} (mm)	0.4	0.17	0.32
Coefficient of uniformity $C_u = d_{50}/d_{10}$	-	1.64	10
Wet unit weight γ_{sat} (kN/m^3)	23.4 (CTC01) 19.9 (CTC02)	19	
Permeability (cm/s)		0.002	
PL			20
LL			33
OCR			1
Water content			15% (CTC01) 12% (CTC02)

The model was subjected to nine successive seismic events along the longitudinal x-direction as defined in Figure 7.1 and Figure 8.2 at a centrifugal acceleration of 15g. Each shaking event consisted of twenty (20) sinusoidal cycles of 2Hz frequency (period T=0.5s). The sequence of the excitations and their corresponding peak base accelerations (PBA) are shown in Table 8-2. This study emphasizes on the medium intensity excitations (Shakes 3 and 4) for CTC01 which take place after two low intensity excitations (Shakes 1 and 2) with no practical interest. Furthermore, these latter 2 excitations are considered too weak to produce permanent

displacements and thus the initial model geometry is considered as representative for the former 2 medium intensity excitations.

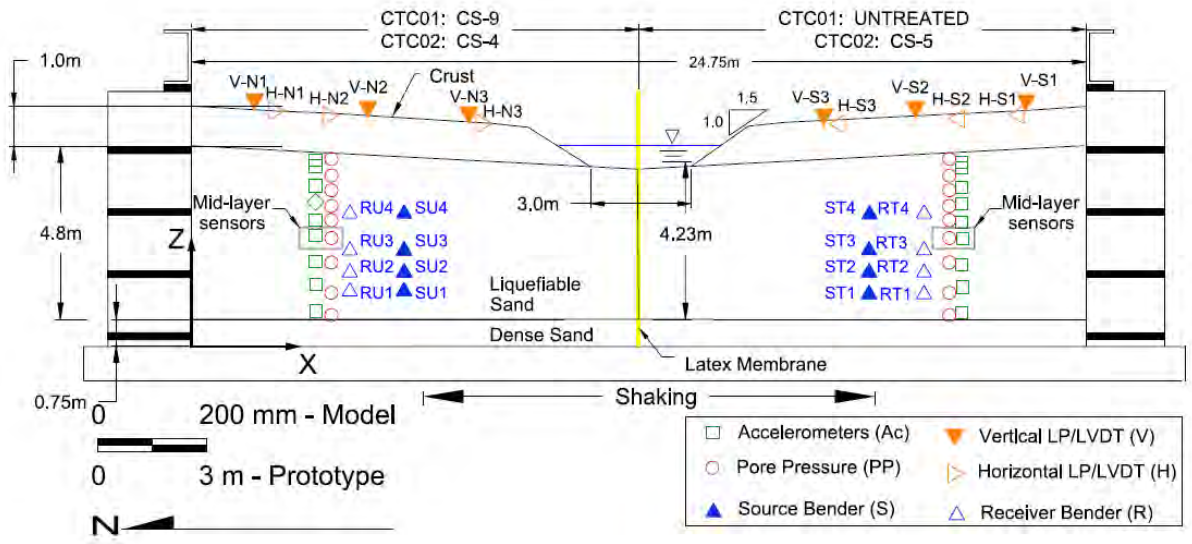

Figure 8.2 *Instrumentation set up for centrifuge test CTC01* (Conlee et al. 2012)

Table 8-2 *Sequence of seismic events for centrifuge tests CTC01 and CTC02 (based on Conlee 2010)*

Seismic event sequence			
CTC01		**CTC02**	
Event ID	PBA	Event ID	PBA
CTC01_01	0.007	CTC02_01	0.007
CTC01_02	0.03	CTC02_02	0.03
CTC01_03	0.1	CTC02_03	0.15
CTC01_04	0.19	CTC02_04	0.25
CTC01_05	0.56	CTC02_05	0.69
CTC01_06	0.03	CTC02_06	0.03
CTC01_07	0.18	CTC02_07	0.24
CTC01_08	1.28	*CTC02_08*	0.89
CTC01_09	0.03	CTC02_09	1.37

Simulation of the remaining excitations of the CTC01 series were not executed, since the initial geometry of the model for these shakes was no longer the initially constructed one (e.g. Figure 7.1), while some of these shakes were extremely intense and of small practical interest (e.g.

1.28g!). Figure 8.3 and Figure 8.4 present the cummulative settlement and horizontal displacement time histories respectively for untreated and treated with CS(%)=4, 5.25 and 9 sand, as recorded by the transducers of CTC01 and CTC02. It should be noted that positive values for horizontal displacements suggest movement towards the central channel. Observe that surface settlements were significantly reduced after stabilization. Interestingly the large settlements of the untreated slope were primarily detected near the boundaries (walls) of the model and not near the central channel. This can be explained assuming that the entire surficial layer moved towards the central channel and led to slope failure after liquefaction occurred. Indicatively, at the end of the fifth shaking event (CTC01) surface settlements for the untreated soil layer ranged from 0.2m to 0.9m and the corresponding settlements for the treated soil layer were 0.05m up to 0.07m (4 to 13 times lower). Additionally, horizontal displacements were remarkably reduced after stabilization. For example, after the fifth excitation (CTC01) measured lateral spreading reached 0.9m for the untreated sand near the channel and just 0.15m for the stabilized soil layer (6.7 times lower).

In order to determine the time of initial liquefaction at the loose untreated Nevada sand layer, the developed pore pressures during excitation were measured. Figure 8.5 and Figure 8.6 show the excess pore pressure ratio, r_u, along with the acceleration time history in the middle of both untreated and treated slopes for the shaking events No3 and No4 of CTC01 respectively. It should be clarified that for untreated sand a value of r_u=1 suggests initial liquefaction, but this does not necessarily have the same meaning for the treated formations where r_u<1 was retained. It is observed that the untreated soil layer liquefied during the third seismic event (PBA=0.1g) after the first 3 seconds and at the same time transient amplification of ground motion followed by de-amplification was observed. This response was much more intense during the fourth (PBA=0.19g) shaking event. On the contrary, stabilized sand seems to retain its strength and stiffness during the third and fourth excitations showing a more uniform response in terms of accelerations, without dramatic amplifications or de-amplifications (see Figure 8.5 and Figure 8.6).

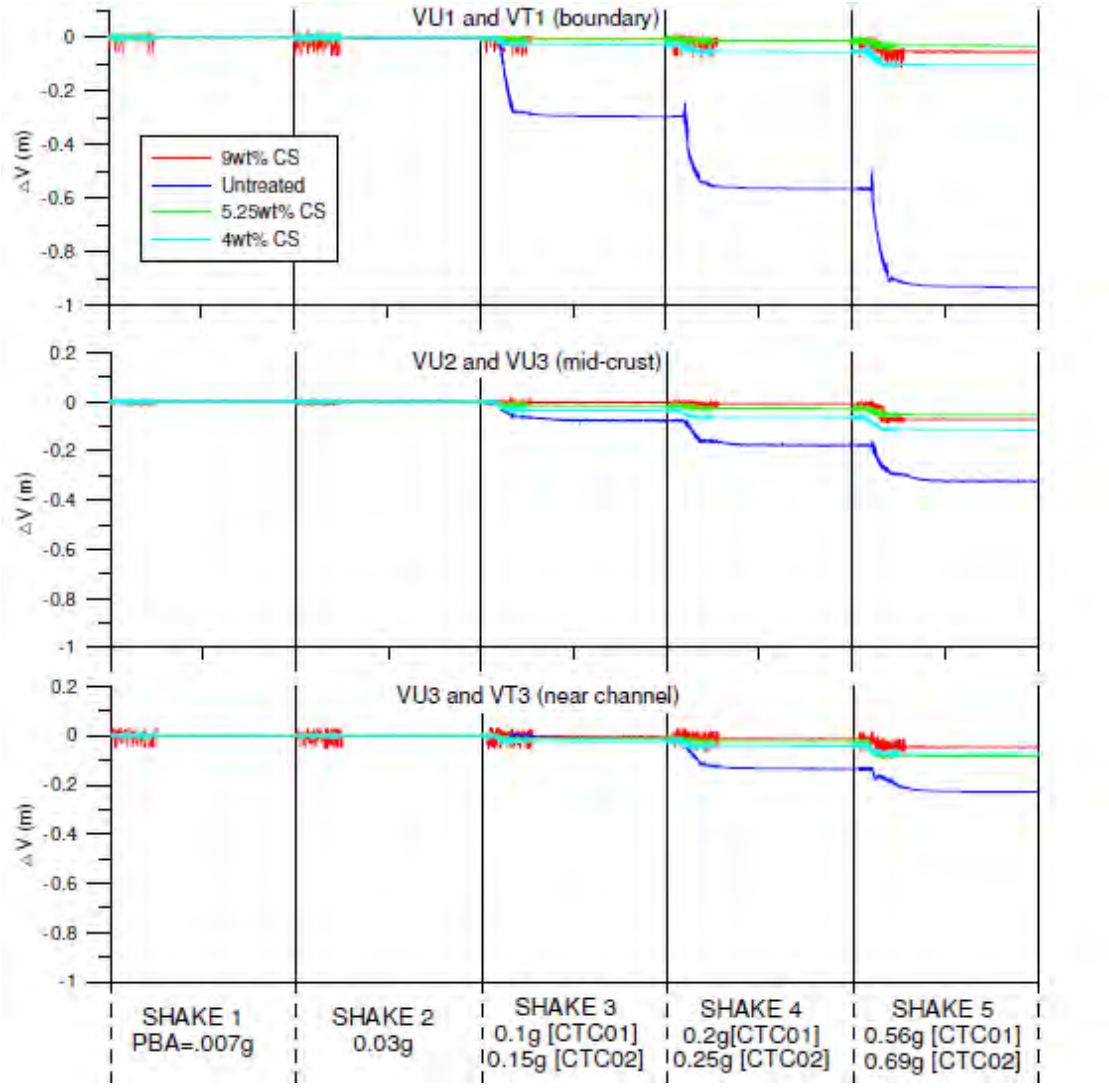

Figure 8.3 *Cumulative surface settlements at different distances from the channel for the seismic events 1 through 5 for CTC01 (treated with CS(%)=9 and untreated slope) and CTC02 (treated with CS(%)=4 and CS(%)=5.25 slope) tests series* (Conlee 2010)

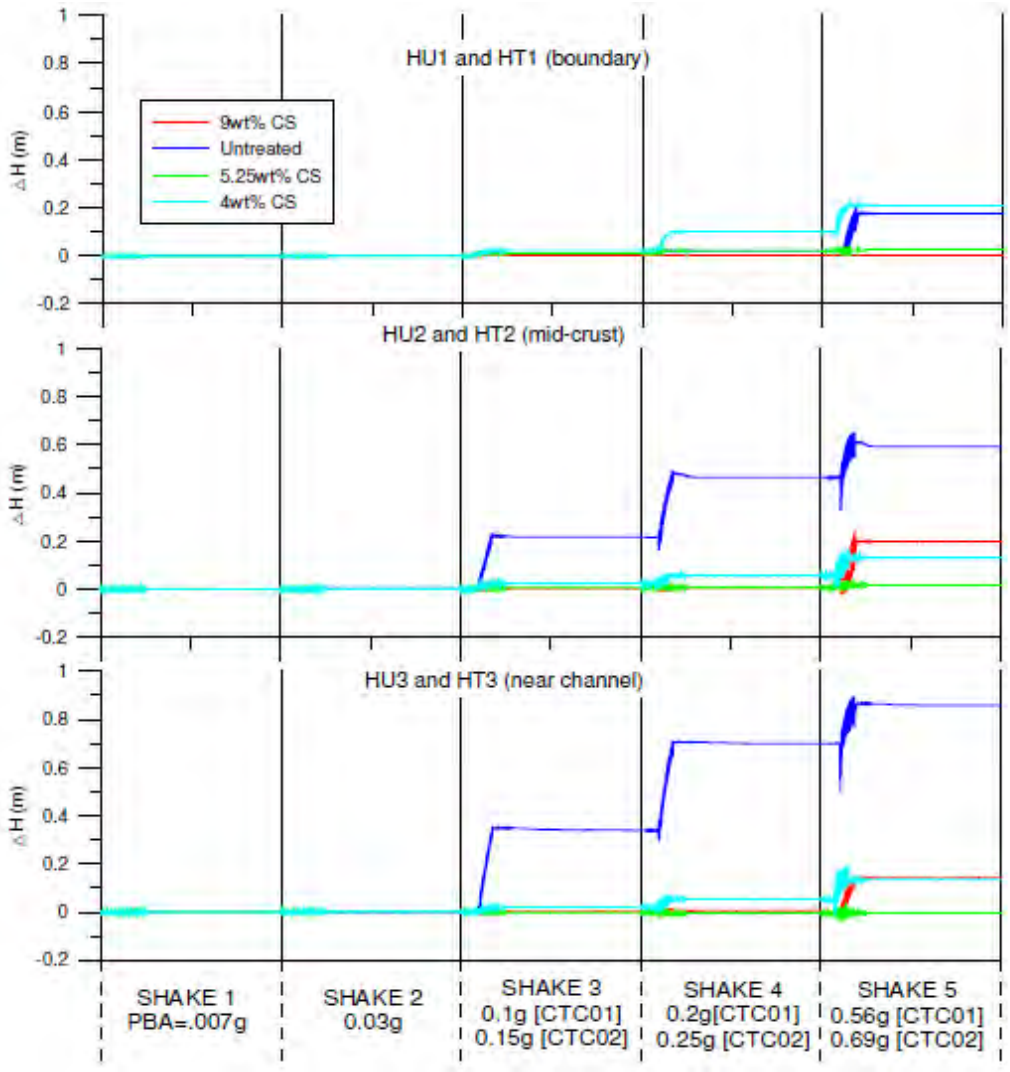

Figure 8.4 *Cumulative surface horizontal displacements (towards the channel) at different distances from the channel for the seismic events 1 through 5 for CTC01 (treated with CS(%)=9 and untreated slope) and CTC02 (treated with CS(%)=4 and CS(%)=5.25 slope) test series* (Conlee 2010)

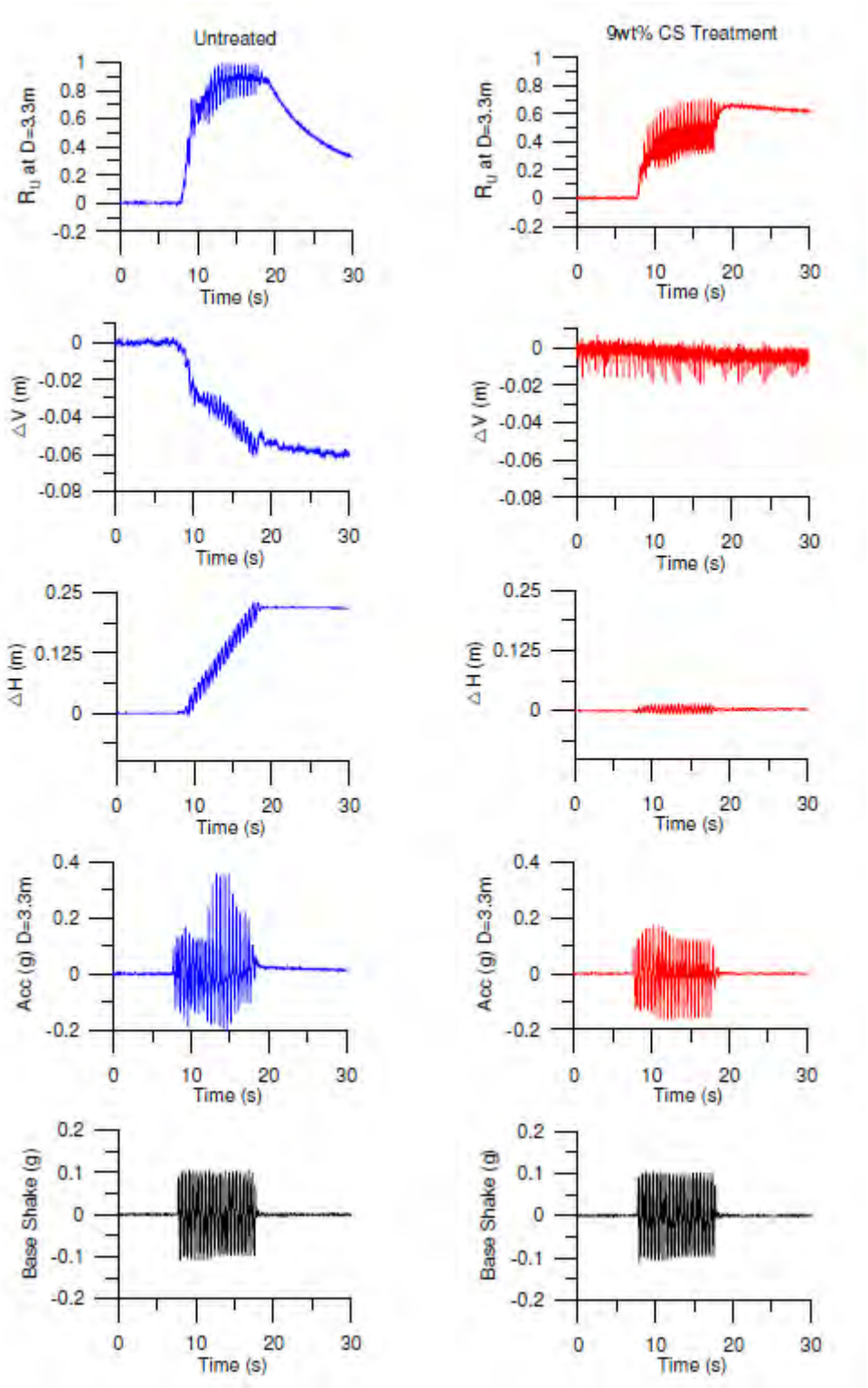

Figure 8.5 *Excess pore pressure ratio (R_u), settlement (ΔV), horizontal displacement (ΔH), and acceleration time histories in the middle of the untreated (left) and treated (right) sand layer for the third seismic event (PBA=0.1g) of CTC01 test series* (Conlee 2010)

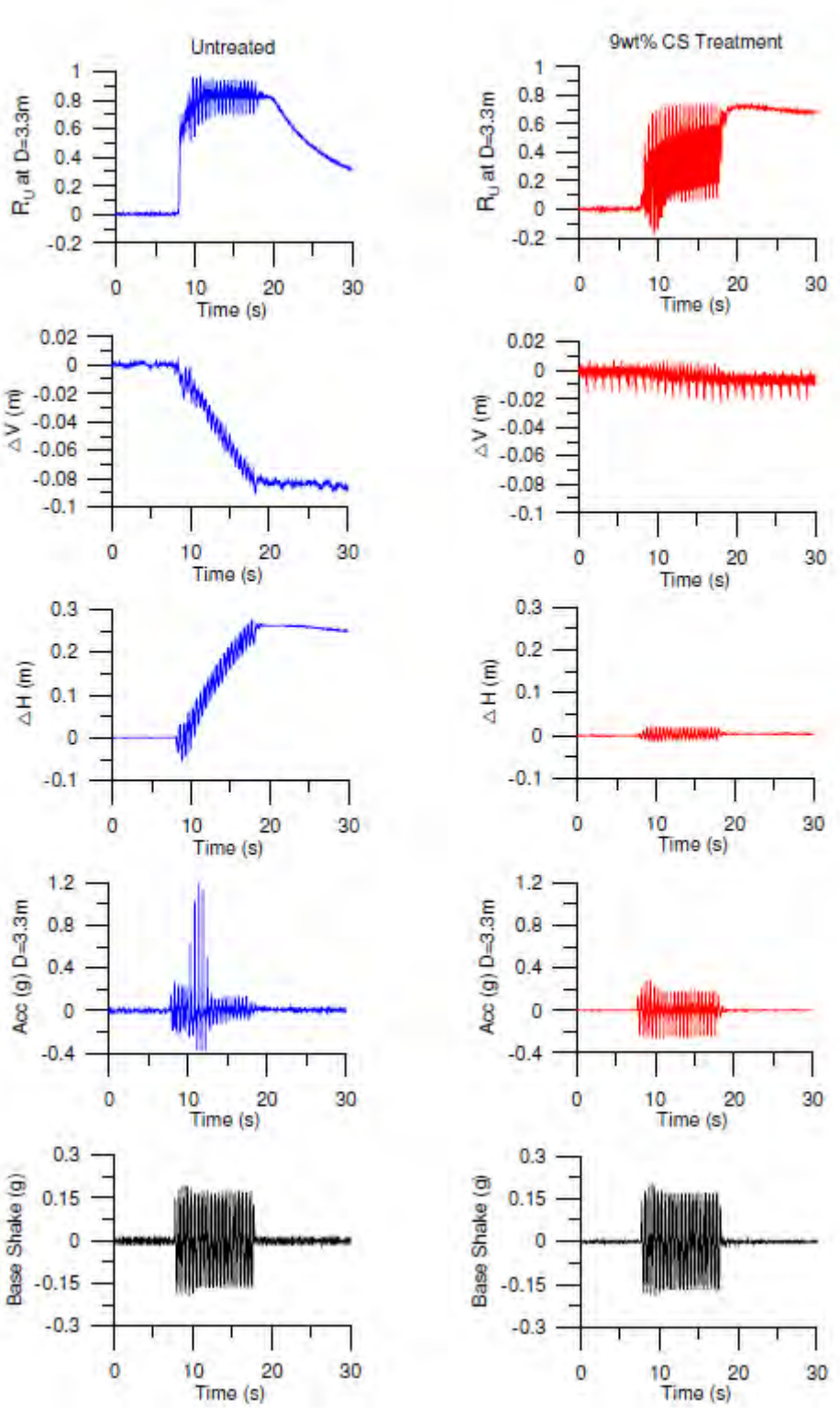

Figure 8.6 *Excess pore pressure ratio (R_u), settlement (ΔV), horizontal displacement (ΔH), and acceleration time histories in the middle of the untreated (left) and treated (right) sand layer for the fourth seismic event (PBA=0.19g) at CTC01* (Conlee 2010)

Based on Conlee et al. (2012), a second centrifuge test series (named CTC02) was executed using the same model (Figure 7.1). In CTC02 both slopes were stabilized with colloidal silica at concentrations of CS(%)=4 and CS(%)=5.25 for the left and right slope respectively. The goal of this centrifuge test was to investigate the effectiveness of colloidal silica to mitigate liquefaction using smaller concentrations than CS(%)=9 (used in CTC01). According to cyclic triaxial compression results performed by Gallagher and Mitchell (2002), a minimum concentration of CS(%)=5 (of Ludox-SM) is able to satisfactorily increase the liquefaction resistance. Hence, an additional reason of choosing smaller CS concentrations was to confirm again the minimum required concentration of colloidal silica that is able to successfully stabilize a liquefiable soil. Note that results from tests performed before the centrifuge tests of Conlee et al. (2012) had shown that a solution with CS(%)=4 forms an unstable gel whereas higher concentrations (CS≥5%) lead to the formation of a firm gel. Therefore, the concentration of CS(%)=4 was used to additionally compare the response of a relatively unstable gel with a properly formed, firm gel (that of CS(%)=5.25). Figure 8.7 and Figure 8.8 present the response of the treated layer with CS(%)=4 and 5.25 in terms of acceleration, settlement, horizontal displacement and excess pore pressure ratio for the third and fourth seismic events of CTC02 respectively, following the format and rationale of Figure 8.5 and Figure 8.6 for CTC01. Overall, observe that the sand treated with CS(%)=5.25 shows clearly smaller settlements and horizontal displacements and also smaller ground motion amplification compared with the threated with CS(%)=4 soil. Indicatively, at the end of the fifth excitation (Shake 5) settlement ranged from 0.05m to 0.08m for the slope stabilized with CS(%)=5.25 and from 0.07m to 0.1m for the slope treated with CS(%)=4. However, the response for both slopes was significantly improved in comparison with the untreated soil response, since liquefaction did not occur at neither of the two slopes and thus the displacements were kept quite lower.

To sum up, results from both CTC01 and CTC02 lead to the conclusion that stabilization of a loose sand layer with colloidal silica can offer an improved soil behavior under cyclic shearing. Also, it is concluded that by increasing the CS concentration in the solution, soil liquefaction resistance increases, a fact that is compatible with laboratory test results at the element level (e.g. Gallagher and Mitchell 2002). It is noted here, that Conlee (2010) uses a concentration of CS(%)=5.25 for the treatment of the right slope. Note that, in this study a concentration of CS(%)=5 will be assumed for the left slope of CTC02, in agreement with the publication of Conlee et al. (2012), which appeared more recently in the literature.

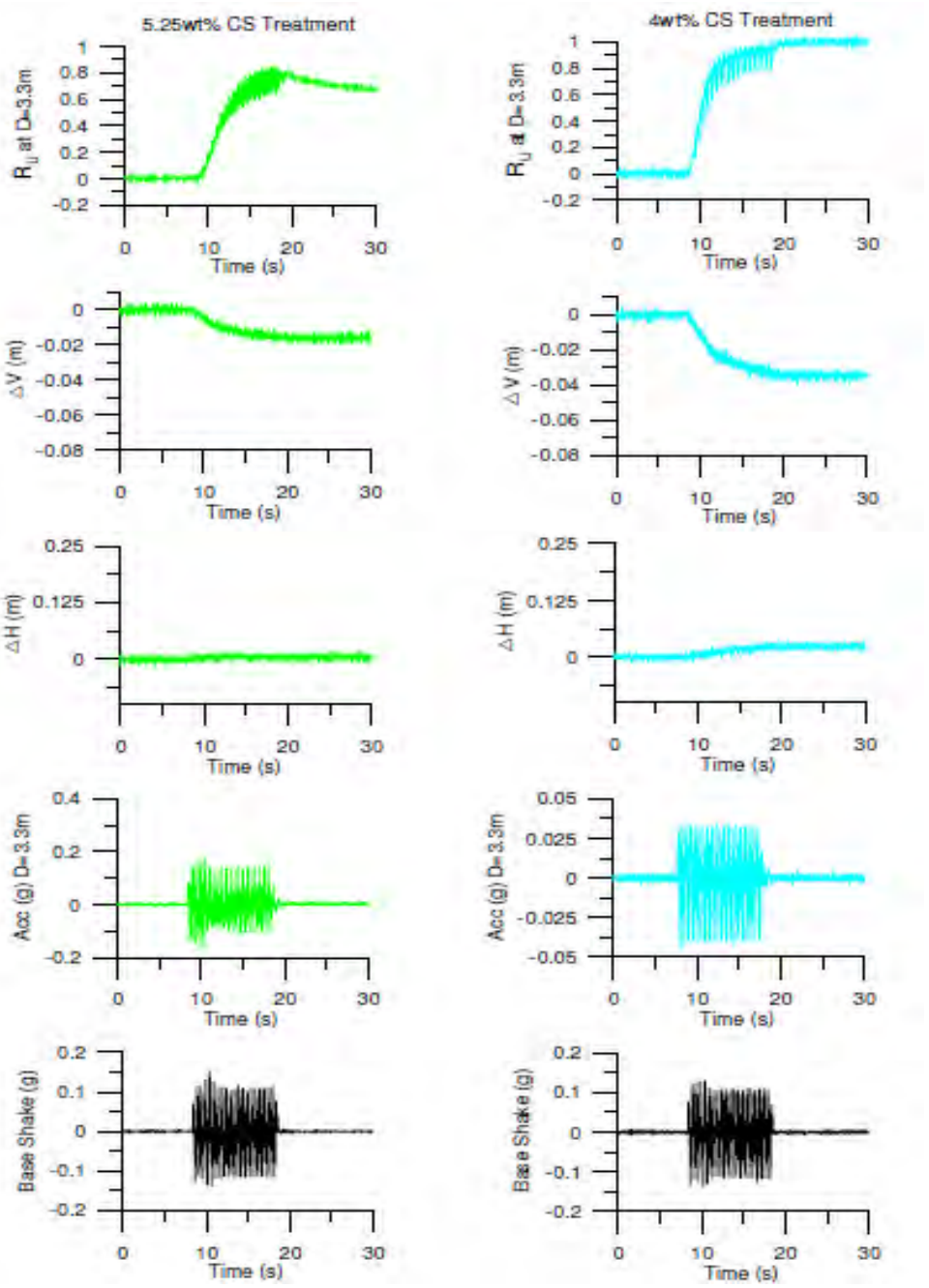

Figure 8.7 *Excess pore pressure ratio (R_u), settlement (ΔV), horizontal displacement (ΔH), acceleration time histories in the middle of the untreated (left) and treated (right) sand layer for the third seismic event (PBA=0.15g) at CTC02* (Conlee 2010)

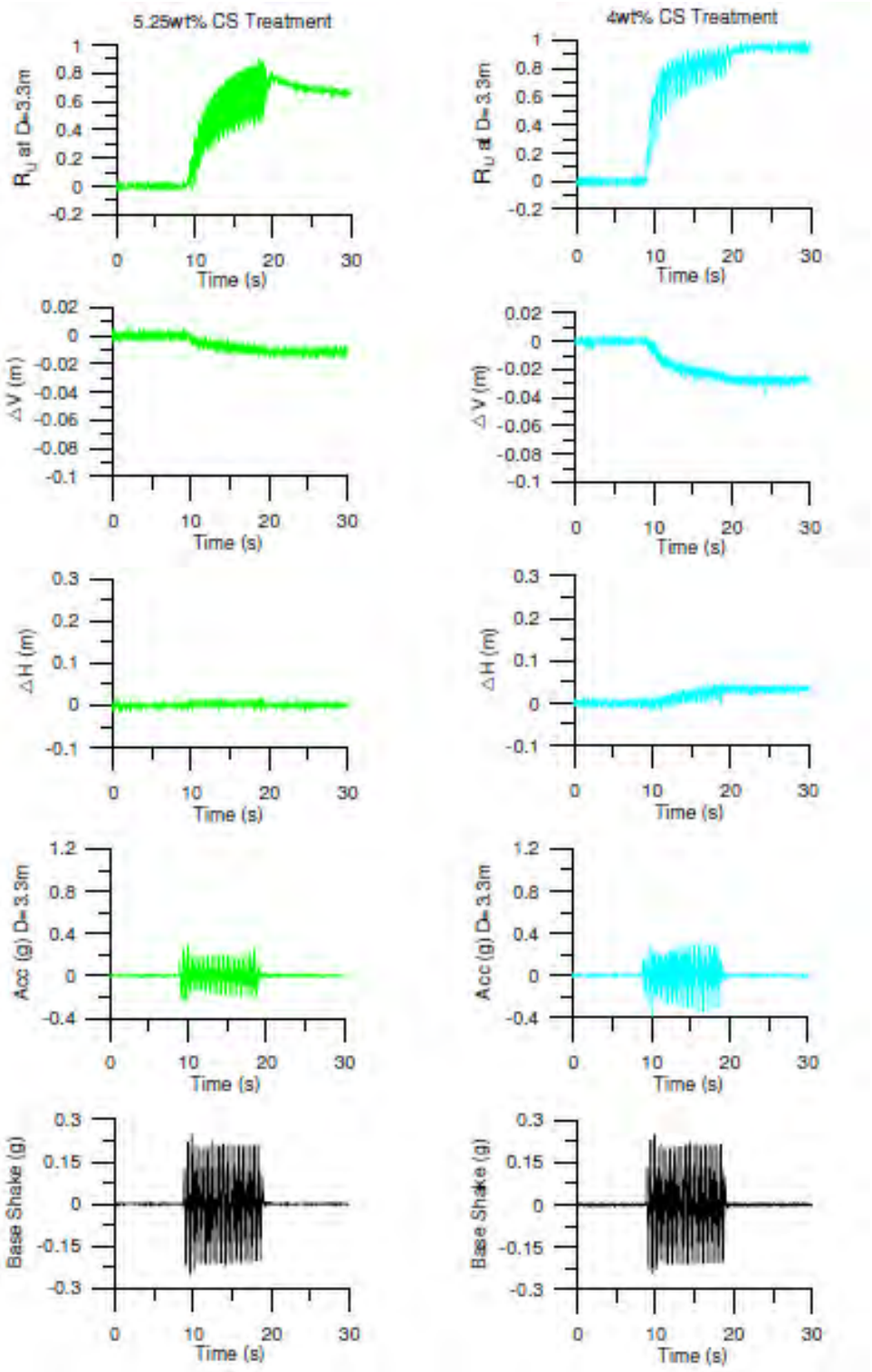

Figure 8.8 *Excess pore pressure ratio (R_u), settlement (ΔV), horizontal displacement (ΔH), acceleration time histories in the middle of the untreated (left) and treated (right) sand layer for the fourth seismic event (PBA=0.25g) at CTC02* (Conlee 2010)

8.3 Numerical simulation of the dynamic centrifuge test CTC01

The validity of the numerical methodology proposed in Chapter 7 for the 1D seismic response of a horizontal soil layer is checked here via the analysis for the centrifuge test CTC01 presented in Conlee (2010) and Conlee et al. (2012). The numerical simulation is achieved using FLAC (Itasca 2011), and the grid presented in Figure 8.9. The mesh consists of 676 elements of variable area in order to successfully simulate the geometry of the experimental set up presented in Figure 7.1 (symmetrical slopes with 3^o inclination). The grid has a total length of 24.75m in prototype units and the maximum height is 6.73m. These dimensions were chosen as the best possible simulation approach, because there were small differences in the model geometry presented in Conlee (2010) and Conlee et al. (2012). The overall results of the test were downloaded from the website: https://nees.org/data/get/NEES-2005-0086/Experiment-2/Documentation_/Data%20Report/_CTC01_DR1.pdf. The left side of the grid represents the stabilized slope, whereas the symmetrical right side refers to the untreated slope. The soil profile used for the simulation is shown in Figure 8.10. Grid elements are divided into groups with different properties: the bottom 0.81m correspond to dense Monterey sand (pink for the treated and yellow for the untreated slope), the upper 4.92m correspond to the middle liquefiable loose Nevada sand (green for the treated and red for the untreated slope) and the top layer of Yolo loam which remains the same for both slopes (purple). The water table into the channel is set on the free surface of Nevada sand and saturation of both sand layers of untreated slope is simulated.

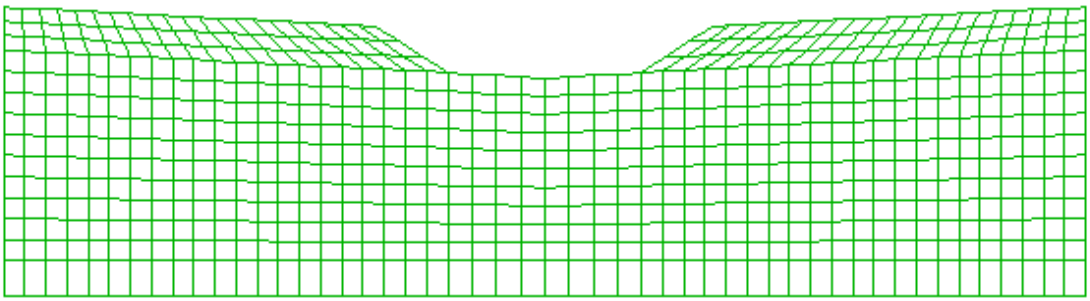

Figure 8.9 *Grid used for the numerical simulation of centrifuge tests CTC01 and CTC02 in FLAC.*

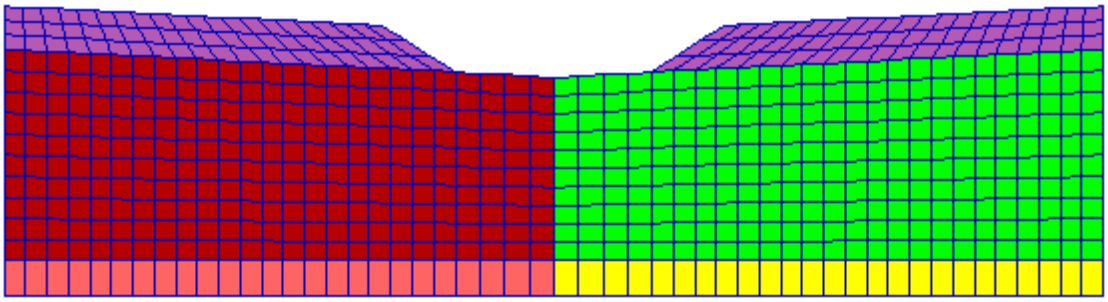

Figure 8.10 *Soil types (within the grid) used for the simulation of centrifuge test CTC01: dense Monterey sand (pink for the treated and yellow for the untreated slope), loose Nevada sand (green for the treated and red for the untreated slope) and Yolo loam (purple in both slopes)*

The latex membrane in the middle of the model was simulated with extremely flexible beam elements of zero width disallowing flow through it. Hence, the interface was impermeable, but interaction between the two slopes was allowed. Tied nodes were considered for the lateral boundaries, which are achieved by connecting grid points at the same elevation through rigid elements in order to develop equal horizontal displacements. This type of boundary condition can effectively simulate the response of a laminar (flexible) box during dynamic base loading.

The constitutive model NTUA-SAND (Andrianopoulos et al. 2010b) was used to simulate the response of the sand layers (dense Monterey and loose Nevada sand) with the values of constants presented in Table 8-3. Observe that NTUA-SAND is considered able to simulate the seismic response of Monterey sand (placed at the bottom of both slopes) by using the same values of the model constants which result from the calibration of the model for Nevada sand. Only the void ratio (and/ or porosity) was changed to account for the higher density of this layer. In order to simulate the top layer of Yolo loam, the Mohr Coulomb constitutive model was used with the values of its constants that are presented in Table 8-4 and are compatible with the soft character of this soil (see also Kamai and Boulanger, 2013).

For the simulation of the CS treatment parameters A_0, h_0 and $K=K_w/n$ were altered following the rationale proposed in Chapter 6. According to Persoff et al. (1999) the hydraulic conductivity value of a stabilized sand with CS(%)= 9 is equal to $3x10^{-10}$m/s. For the untreated sand layers, the hydraulic conductivity was assumed equal to $2.94x10^{-6}$m/s and for the Yolo loam equal to $1.97x10^{-9}$m/s. Finally, a base excitation was applied at the bottom of the grid, which corresponds to the third shaking event (Shake 3) and for both slopes local damping

(independent of frequency) was used with a value of 2% for the non-cohesive soils and 10% for the top layer of Yolo loam.

Table 8-3 *Values of constants used for the simulation of granular materials with NTUA-SAND (based on the calibration by Andrianopoulos et al. (2010) as included in centrifuge tests CTC01* (Conlee et al. 2012)

Parameter	***Dense Monterey sand***	***Loose Nevada sand***
Dry density (Mgr/m^3)	1.52	1.66
Porosity	0.42	0.33
e	0.72	0.49
M_c^c	1.25	
M_c^e	0.72	
$(e_{cs})_a$	0.809	
λ	0.022	
B	600	
ν	0.33	
k_c^b	1.45	
k_c^d	0.30	
γ_1	0.00025	
α_1	0.6	
A_o	0.8	
h_o	15000	
N_o	40000	

Table 8-4 *Values of constants used for the simulation of the Yolo loam layer with Mohr- Coulomb model, as included in centrifuge tests CTC01 and CTC02*

Bulk modulus (kPa)	18000
Shear modulus (kPa)	8300
Dry density (Mgr/m^3)	1.90
Poisson ratio	0.30
Cohesion (kPa)	10
Friction angle (deg)	0

Following the rationale of *Chapter 7*, the following figures compare numerical results for the three (3) different simulation approaches, namely altering the values of A_0, h_0 and $K=K_w/n$ respectively. The numerical simulations are compared in Figures 8.11- 8.13 in terms of acceleration time-histories: (a) at depths from the surface equal to z=0.6m, 3.5m, 5.7m and at the base of the model as recorded from accelerometers T21, T4, T1 and C49 of the left treated slope and (b) at depths from the surface equal to z=0.5m, 3.4m, 5.5m and at the base of the model as recorded from accelerometers U45, U28, U25 and U49 of the right untreated slope. Figure 8.14 shows the comparison of numerical simulation results with recordings in terms of vertical and horizontal displacements, as they were recorded from transducers (a) VT1, VT3 and (b) HT1, HT3 at distances of x=10.8m and 4.8m from the central membrane (axis of symmetry of the model) respectively for the treated slope For the untreated slope the corresponding transducers are VU1 and VU3 (settlement) and HU1, HU3 (horizontal displacements) at distances of x=10.4m and 4.4m from the membrane. The locations of all these recorders can be seen in Figure 8.2.

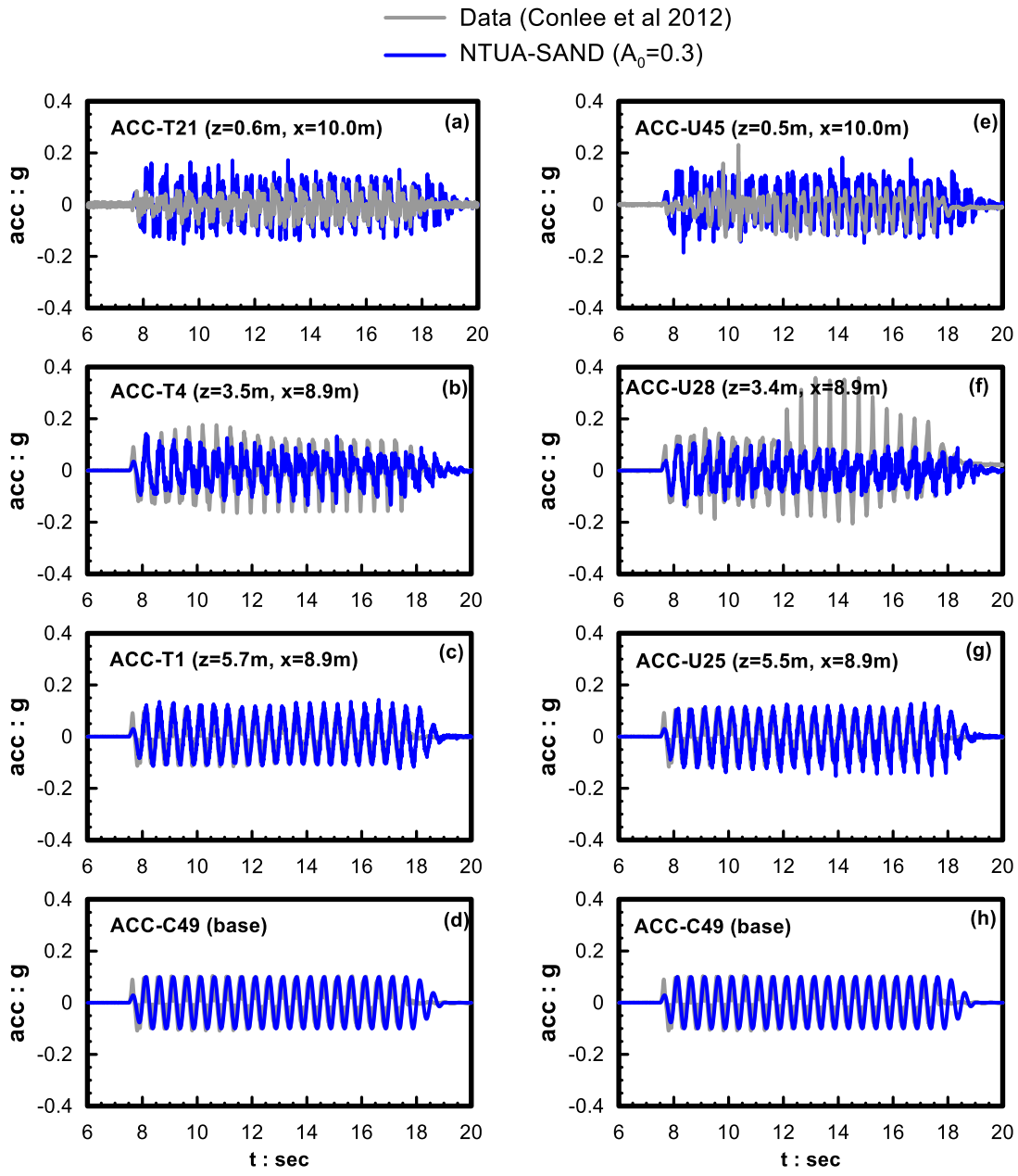

Figure 8.11 *Comparison of recorded acceleration time-histories at different depths z and horizontal distances x from the central membrane x during CTC01 Shake 3* (Conlee et al. 2012) *with the corresponding numerical analyses results for A_0=0.3 (2.67 times lower than for untreated sand).*

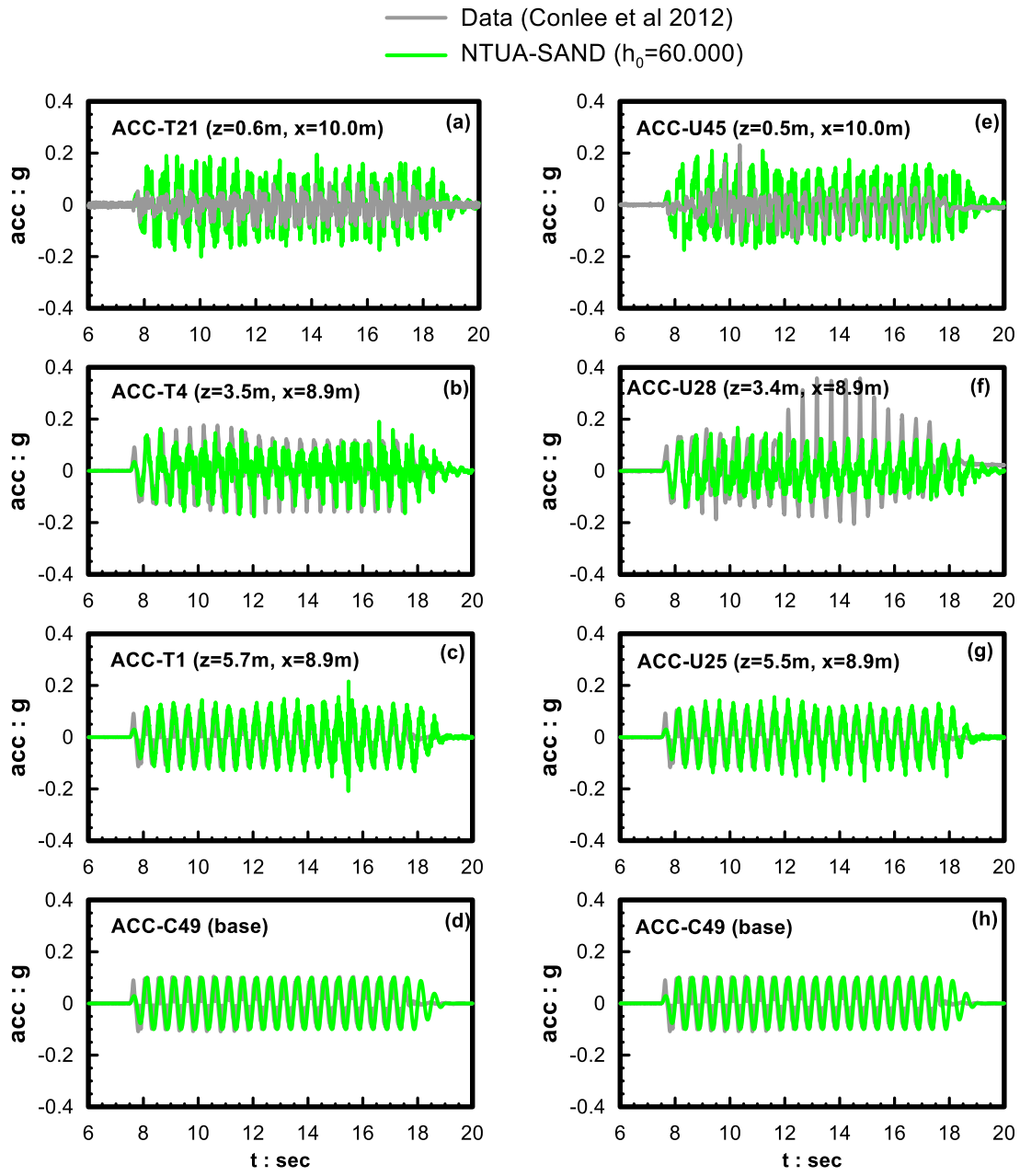

Figure 8.12 *Comparison of recorded acceleration time-histories at different depths z and horizontal distances x from the central membrane x during CTC01 Shake 3* (Conlee et al. 2012) *with the corresponding numerical analyses results for h_0=60000 (4 times higher than for untreated sand).*

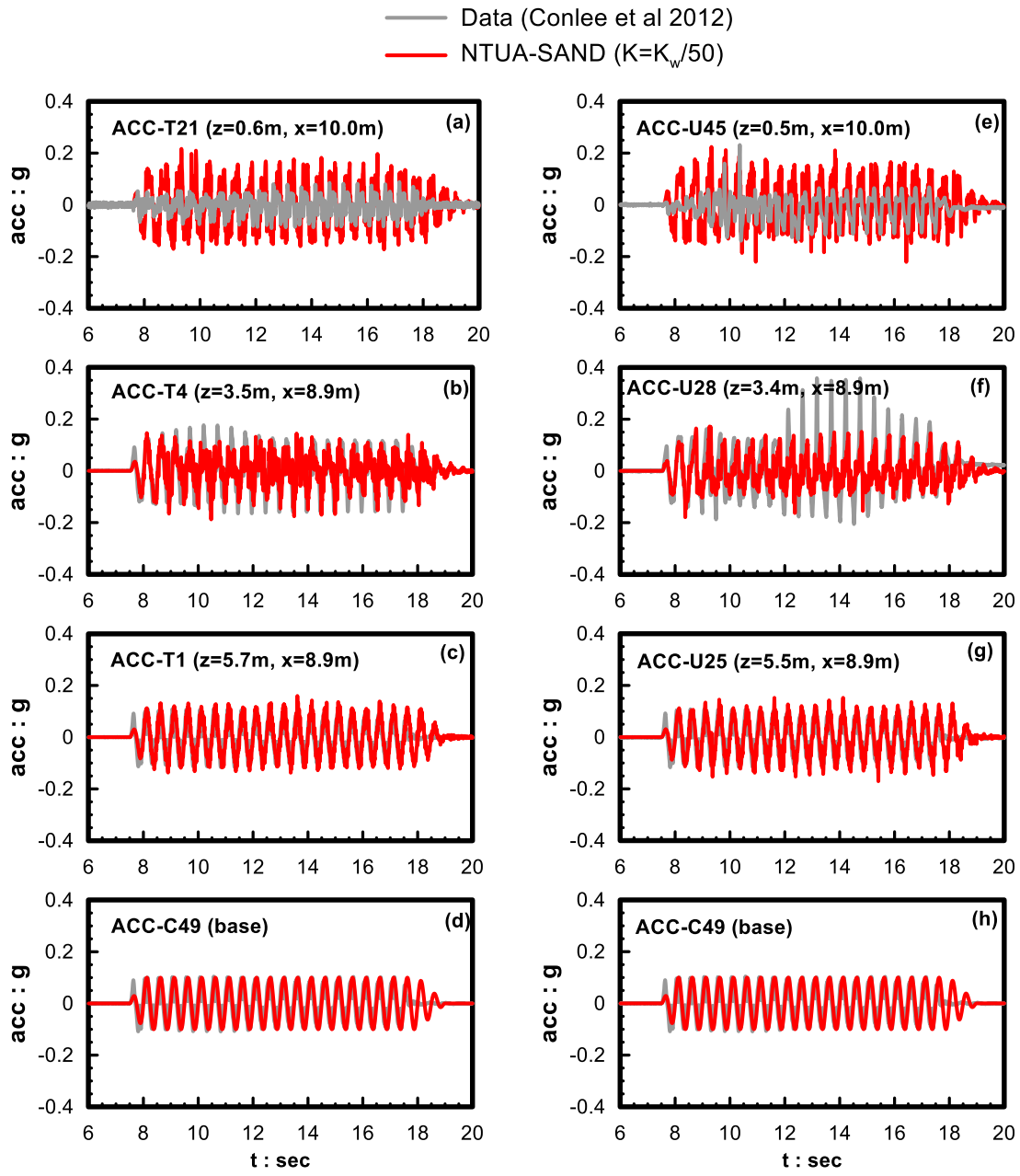

Figure 8.13 *Comparison of recorded acceleration time-histories at different depths z and horizontal distances x from the central membrane x during CTC01 Shake 3* (Conlee et al. 2012) *with the corresponding numerical analyses results for K=K_w/50 (where K_w is bulk modulus for water).*

Additionally, Figure 8.15 presents the excess pore pressure ratio r_u time-history for both treated and untreated slopes at different depths from the model surface (z) and at different horizontal distances from the central membrane as recorded in CTC01 test and as predicted by numerical analyses. The comparison in terms of r_u is not considered as reliable as for the other measurements, because the pore pressure transducers are designed to measure pore pressures of water (with viscosity value equal to 1cP) and not for more viscous pore fluid. It is

noted that the transducer recordings presented in this study were selected from the whole instrumentation set of Figure 8.2 in order to fully illustrate the response of the two slopes without taking into account the faulty measurements or misplaced instrumentation which have been detected by the researchers themselves (Conlee 2010; Conlee et al. 2012).

Similarly to *Chapter 7*, firstly the adequacy of the values of the parameters which best simulate the results of cyclic tests at element level (A_0=0.3, h_0=60000, $K=K_w/50$) is investigated via the simulation of the 2D seismic response of the model CTC01 configuration. A comparison in terms of acceleration time histories (Figures 8.11 – 8.13) indicates that all 3 approaches above can simulate satisfactorily the response of the treated side (left column), except for the model surface (z=0.6) where an underestimation of the measured acceleration values is systematically observed (note that this location is within the Yolo loam crust).

Based on Figure 8.14, the 3 numerical analyses do not lead to particular differences in terms of vertical displacements, since they systematically predict significant settlements on the stabilized layer surface, contrary to the recordings which show practically zero settlements. Additionally, horizontal displacements resulting from the above numerical simulations are also non-zero, contrary to the measured ones. Finally, Figure 8.15 presents similar comparisons in terms of excess pore pressure ratio r_u time histories at the treated slope (right column) and at the untreated slope (left column). In this case, the numerical analyses show similar results that overestimate the measured values in the treated slope.

Despite the qualitatively accurate simulations, the overall quantitative accuracy is not considered satisfactory. Having in mind this observation, additional numerical analyses were conducted by further altering the values of A_0, h_0 and $K=K_w/n$. More specifically, a 10 fold change of these parameters was investigated, namely values of A_0=0.03, h_0=600000 and $K=K_w/500$ were assumed following the same rationale introduced in *Chapter 7*.

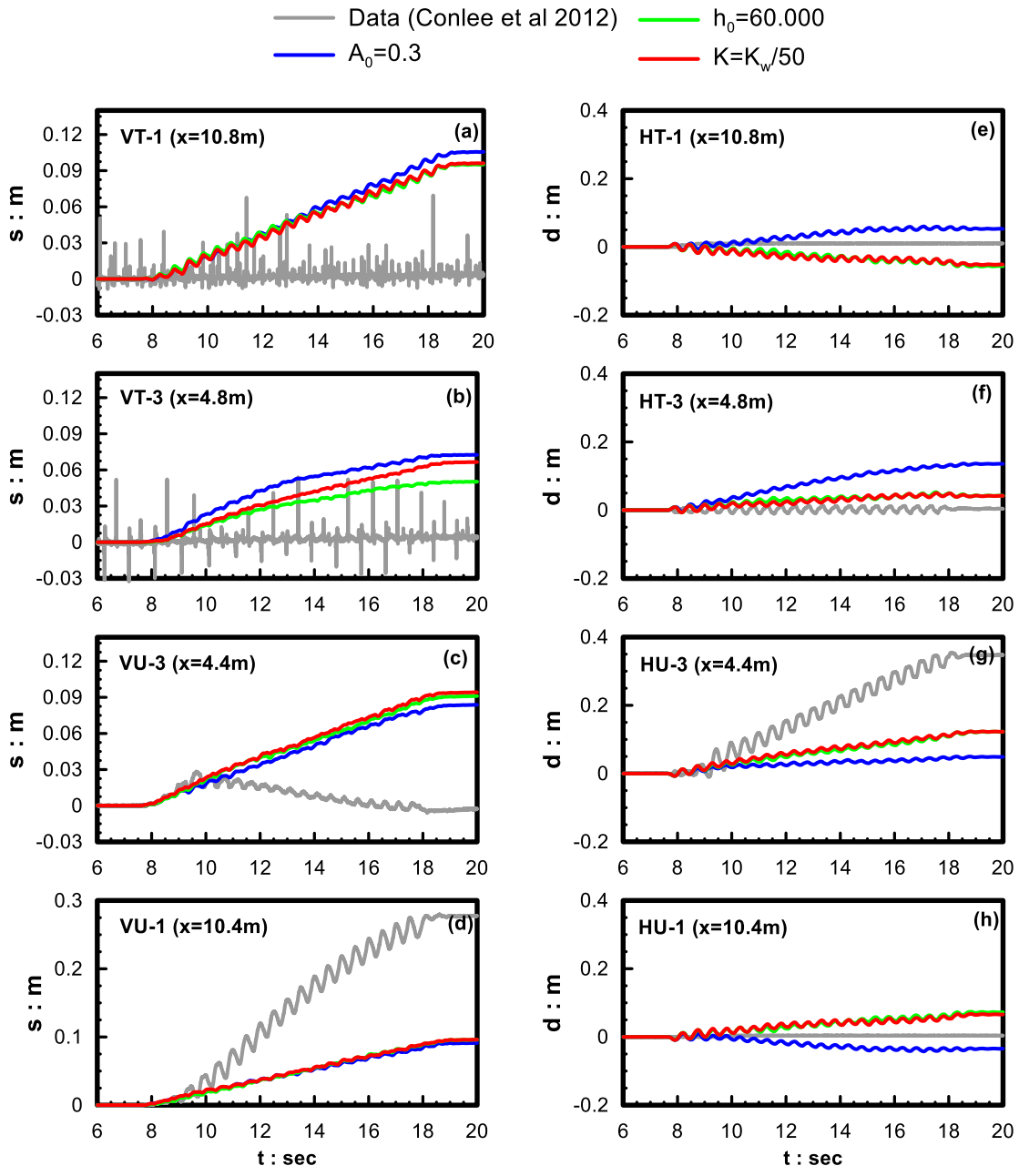

Figure 8.14 *Comparison of recorded surface settlement time-histories (a to d) and horizontal surface displacements (e to h) at different horizontal distances x from the central membrane during CTC01 Shake 3* (Conlee et al. 2012) *with the corresponding numerical analyses results for* A_0*=0.3,* h_0*=60000 and* $K=K_w/50$.

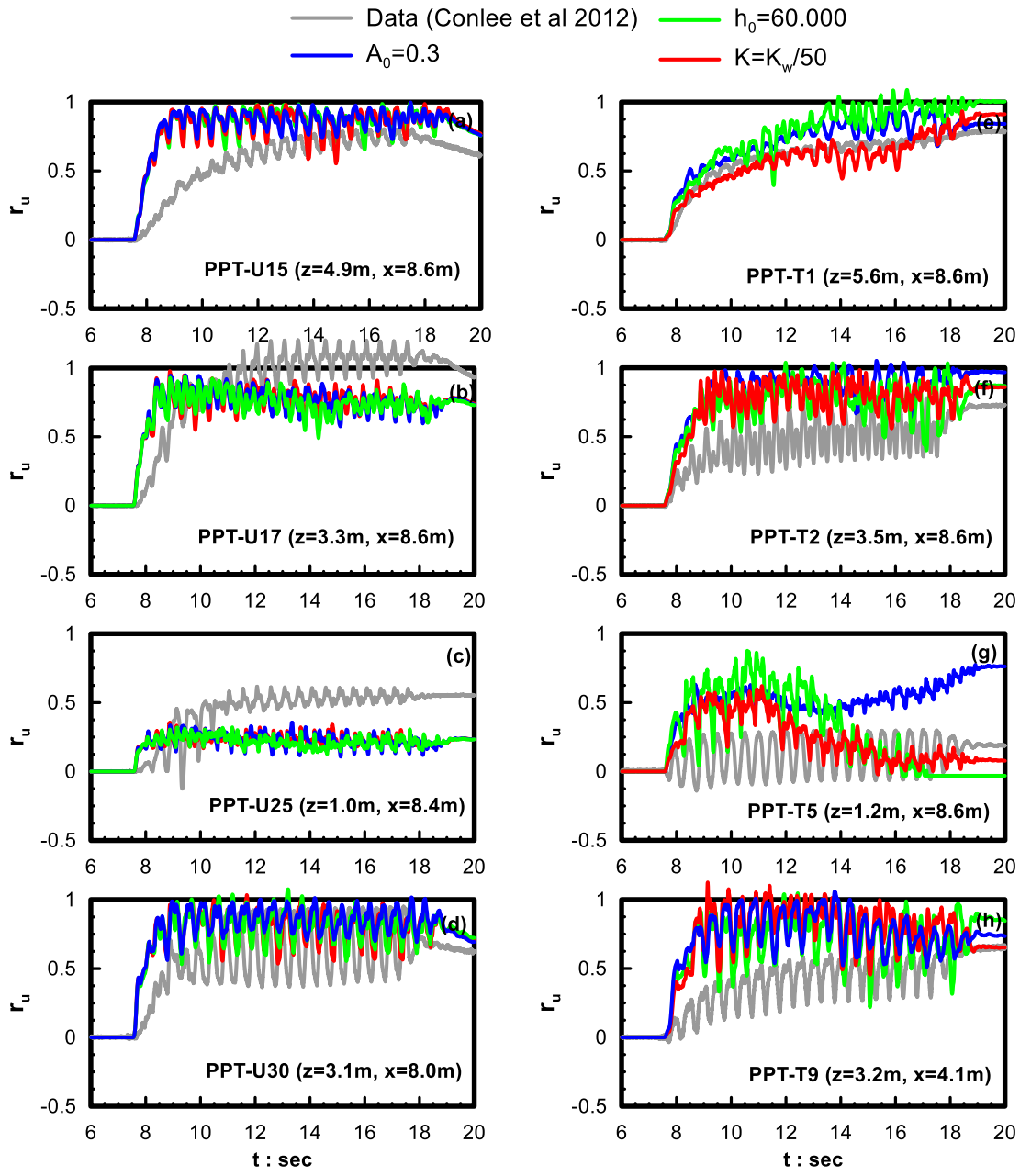

Figure 8.15 *Comparison of recorded excess pore pressure ratio r_u time-histories at different depths z and horizontal distances x from the central membrane during CTC01 - Shake 3* (Conlee et al. 2012) *with the corresponding numerical results for A_0=0.3, h_0=60000 and K=K_w/50: (a to d) for untreated and (e to h) for treated side.*

Comparison of the new predictions with the centrifuge recordings are presented in Figures 8.16 through 8.20 and follow the format of Figures 8.11 through 8.15, respectively. More specifically, comparison in terms of accelerations is presented in Figures 8.16 to 8.18 and shows similarly successful simulations for the stabilized slope (left column), but an amelioration of predictive ability is observed for the untreated soil as an effect of the interaction of the two slopes. On the contrary, comparison in terms of displacements (Figure

8.19) shows that the simulation results for the new parameter values, h_0=600000 and $K=K_w/500$ approach better the recordings with the $K=K_w/500$ approach offering the best results. In terms of excess pore pressure ratio (Figure 8.20) all three numerical simulation approaches lead to similar predictions and indicate significantly lower r_u values at the stabilized slope in comparison with the treated slope, in agreement with the recordings (at least quantitatively).

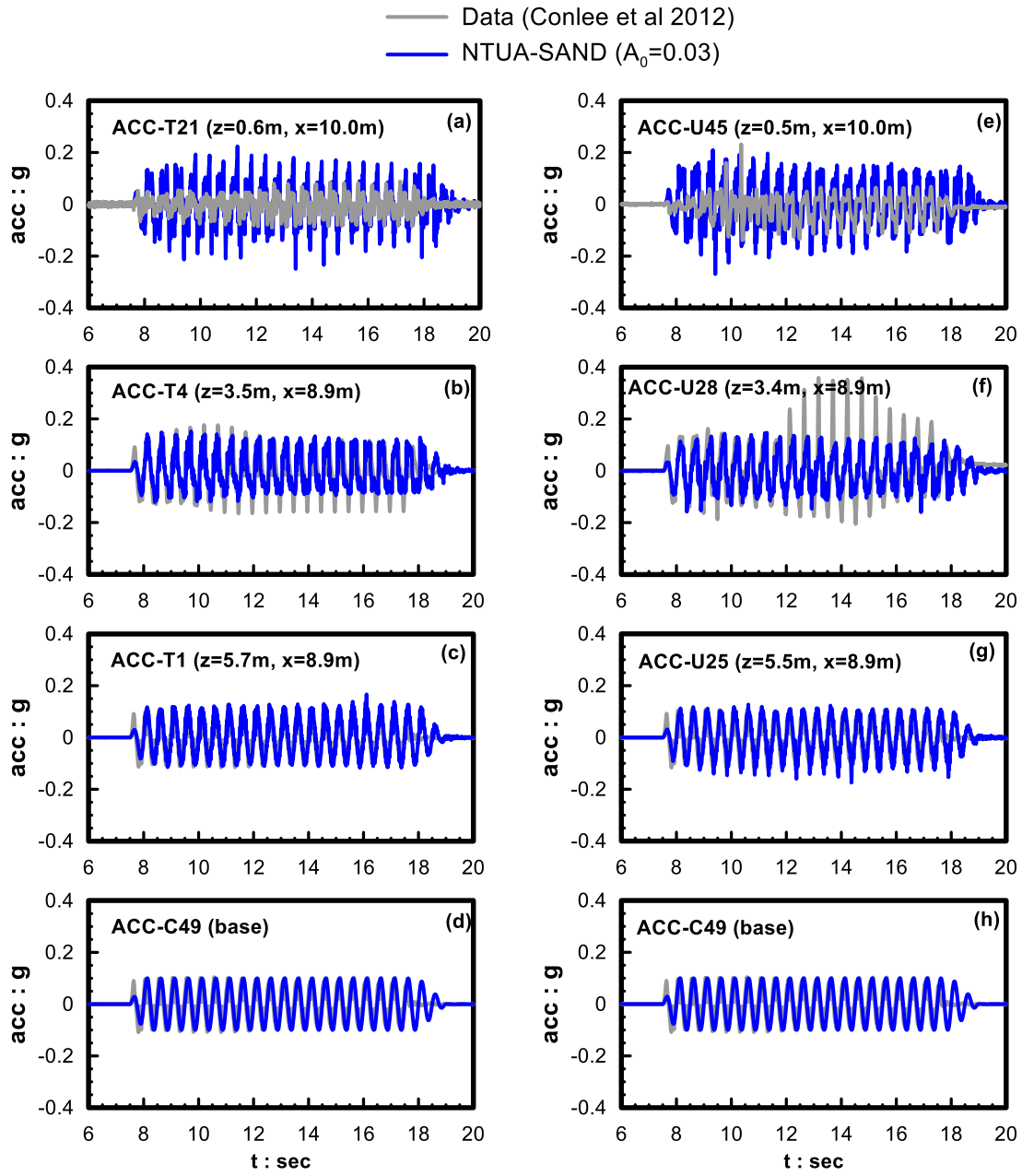

Figure 8.16 *Comparison of recorded acceleration time-histories at different depths z and horizontal distances x from the central membrane x during CTC01 Shake 3* (Conlee et al. 2012) *with the corresponding numerical analyses results for A_0=0.03 (26.7 times lower than for untreated sand).*

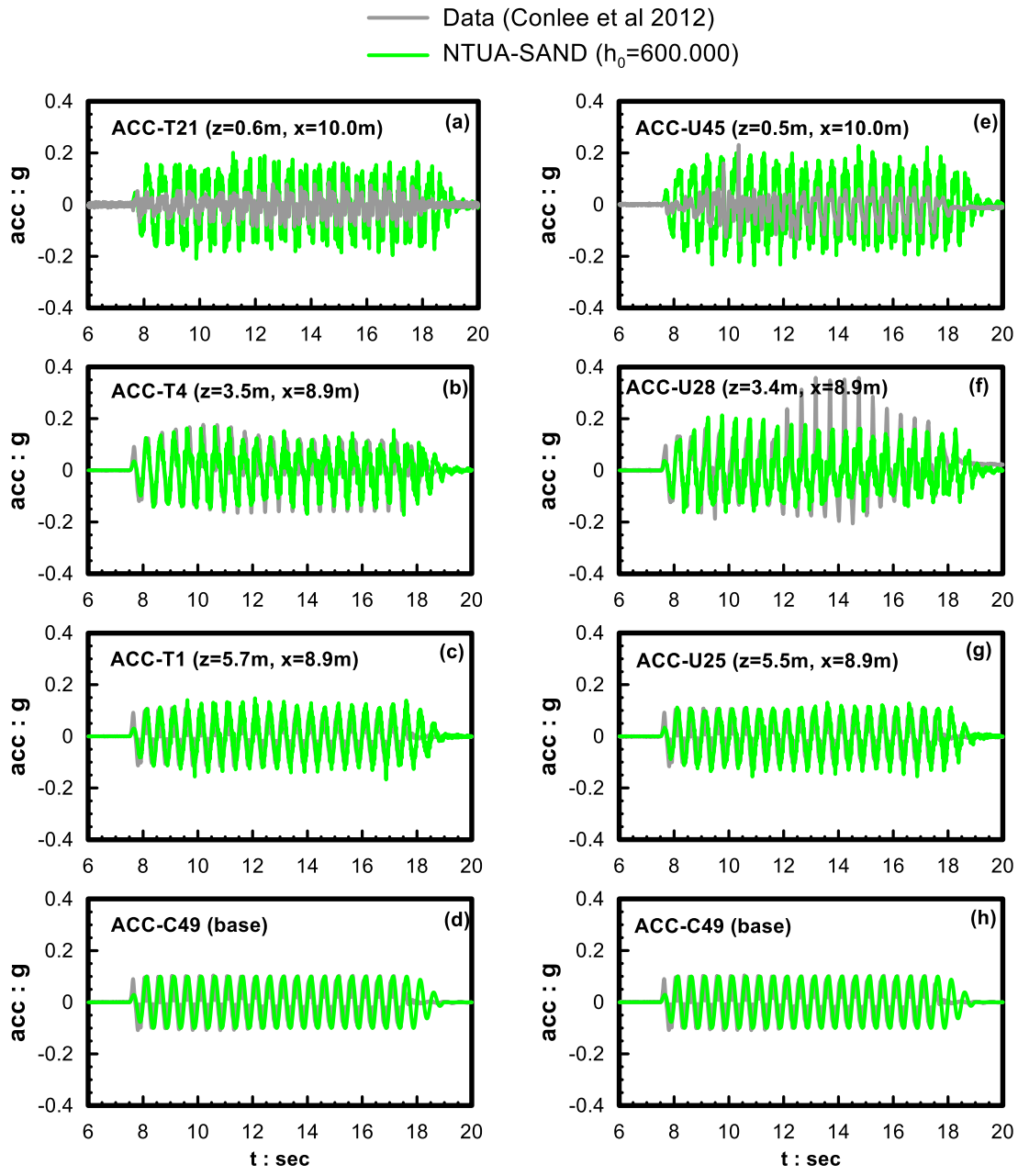

Figure 8.17 *Comparison of recorded acceleration time-histories at different depths z and horizontal distances x from the central membrane x during CTC01 Shake 3* (Conlee et al. 2012) *with the corresponding numerical analyses results for h_0=600000 (40 times higher than for untreated sand).*

In conclusion, the numerical simulation which assumes a reduced fluid bulk modulus (K) by 500 times compared with that of water (K_w) is considered to be the most appropriate of the three. Having in mind that this approach also offered the best results for the 1D seismic response of a horizontal treated layer (presented in *Chapter 7*) it may be concluded that the modification of pore fluid compressibility could be adopted as a simulation tool for the effect of passive stabilization on soil response in boundary value problems. However, quantitatively,

the value of K_w/500 may not offer the best approach for both boundary value problems, because it predicts successfully the settlements for the centrifuge test of Gallagher et al. (2007a) with CS(%)=6 (in *Chapter 7*) but overestimates the measured data of Conlee et al. (2012) with CS(%)=9 here.

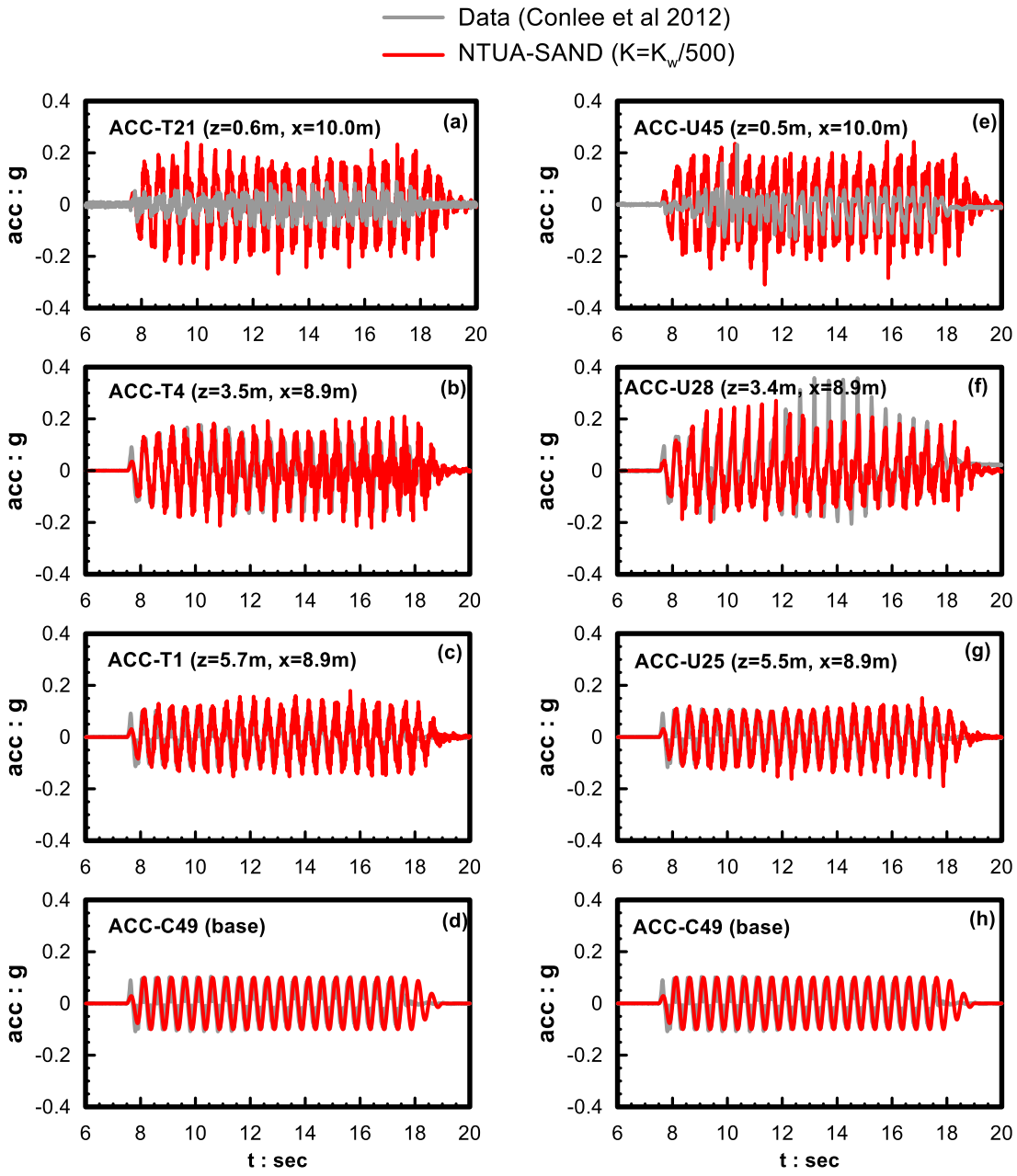

Figure 8.18 *C omparison of recorded acceleration time-histories at different depths z and horizontal distances x from the central membrane x during CTC01 Shake 3* (Conlee et al. 2012) *with the corresponding numerical analyses results for K=K_w/500 (where K_w is bulk modulus for water).*

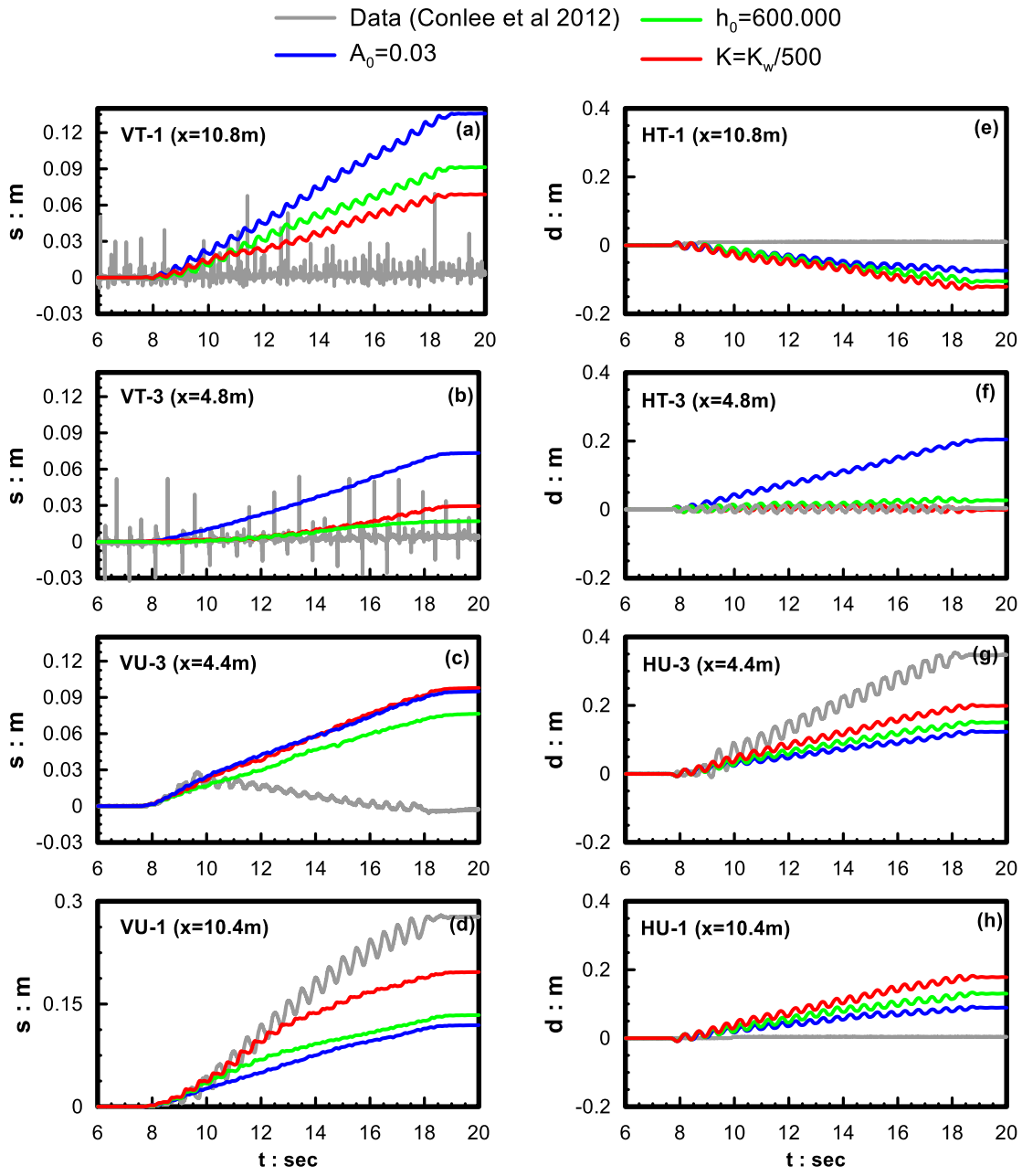

Figure 8.19 *Comparison of recorded surface settlement time-histories (a to d) and horizontal surface displacements (e to h) at different horizontal distances x from the central membrane during CTC01 Shake 3* (Conlee et al. 2012) *with the corresponding numerical analyses results for* A_0*=0.03,* h_0*=600000 and* $K=K_w/500$.

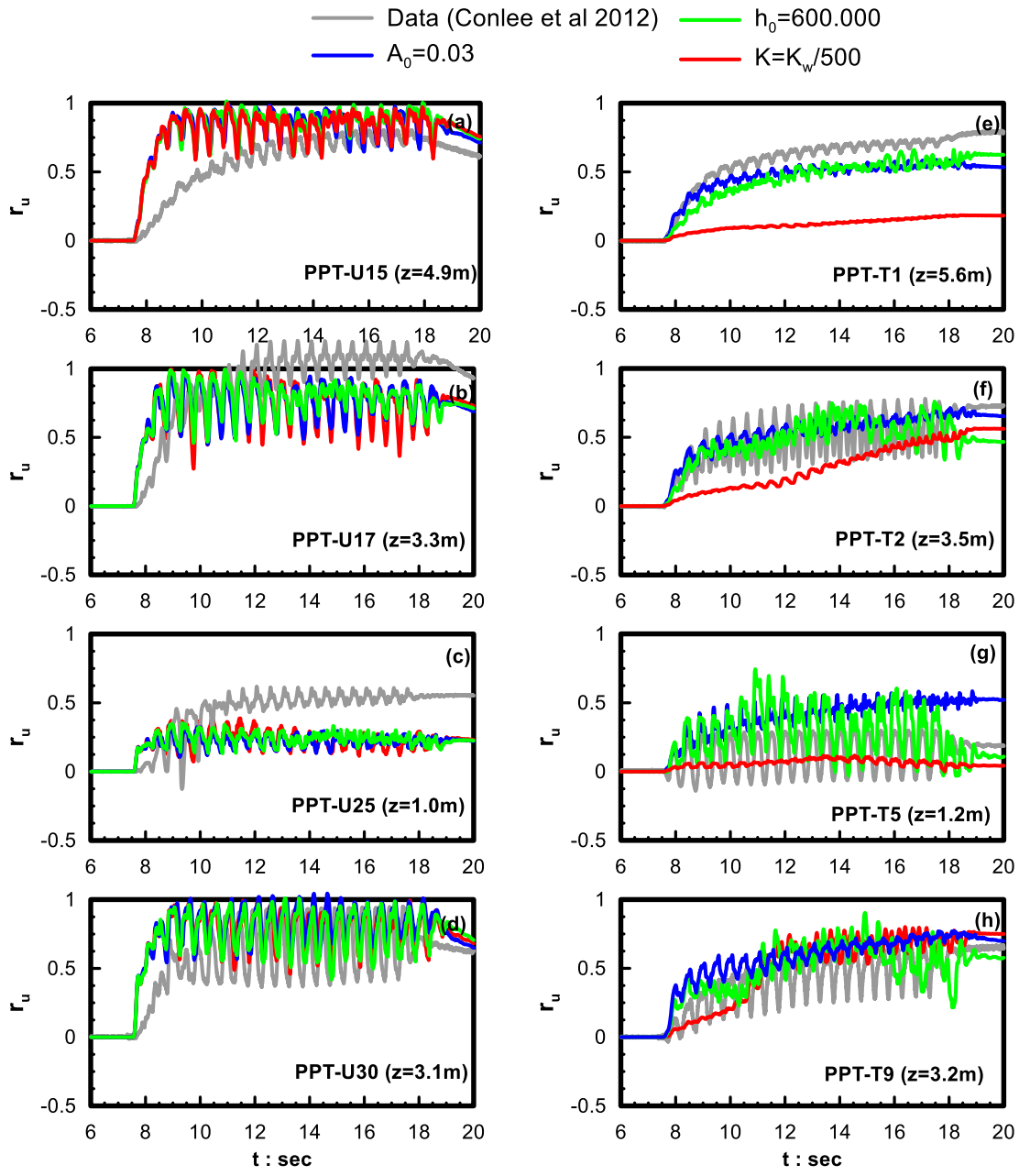

Figure 8.20 *Comparison of recorded excess pore pressure ratio r_u time-histories at different depths z and horizontal distances x from the central membrane during CTC01 - Shake 3* (Conlee et al. 2012) *with the corresponding numerical results for A_0=0.03, h_0=600000 and K=K_w/500: (a to d) for untreated and (e to h) for treated side.*

For this purpose, the appropriate value of the divider n of the bulk modulus K (=K_w/n) will be investigated here as in *Chapter 7*, based on its correlation with the concentration per weight of CS(%). This investigation is performed for the centrifuge test (CTC01), and the two values that were investigated are n=1125 for CS(%)=9 as resulting from Equation (7-1) and n=975 estimated from the same equation for CS(%)=7.5, which corresponds to the average value of the usually used CS concentration between 5% and 10%. Figure 8.21 and Figure 8.22 present

the comparison of the measured acceleration time-histories with depth to their numerical counterparts resulting from the simulations with $K=K_w/975$ and $K=K_w/1125$ respectively. In addition, in Figure 8.23 the comparison of recordings and simulations is presented in terms of settlements and horizontal displacements at different surface locations, and in Figure 8.24 this is performed in terms of excess pore pressure ratio.

The foregoing figures indicate that predictions using a fluid bulk modulus equal to $K=K_w/1125$ and $K=K_w/975$ approach generally better the recordings in comparison to what was observed for $K=K_w/500$ above. The value of $K=K_w/1125$ slightly overestimates the measured surface acceleration time-histories (z=0.6m, x=10.0m), settlements (x=10.8m) and horizontal displacements near the boundaries (x=10.8m) but leads to the best overall qualitative and quantitative simulation of the treated slope. It should be also noted here that, this parameter value ($K=K_w/1125$) expresses satisfactorily the response of the untreated slope as well, in terms of both accelerations and displacements. Note that the untreated slope was simulated using the same parameter values in all analyses (A_0=0.8, h_0=15000 and K_w, namely the parameters for Nevada sand according to Andrianopoulos et al. 2010), but its simulated response changes because of the interaction between the two slopes which seems significant based on all performed analyses.

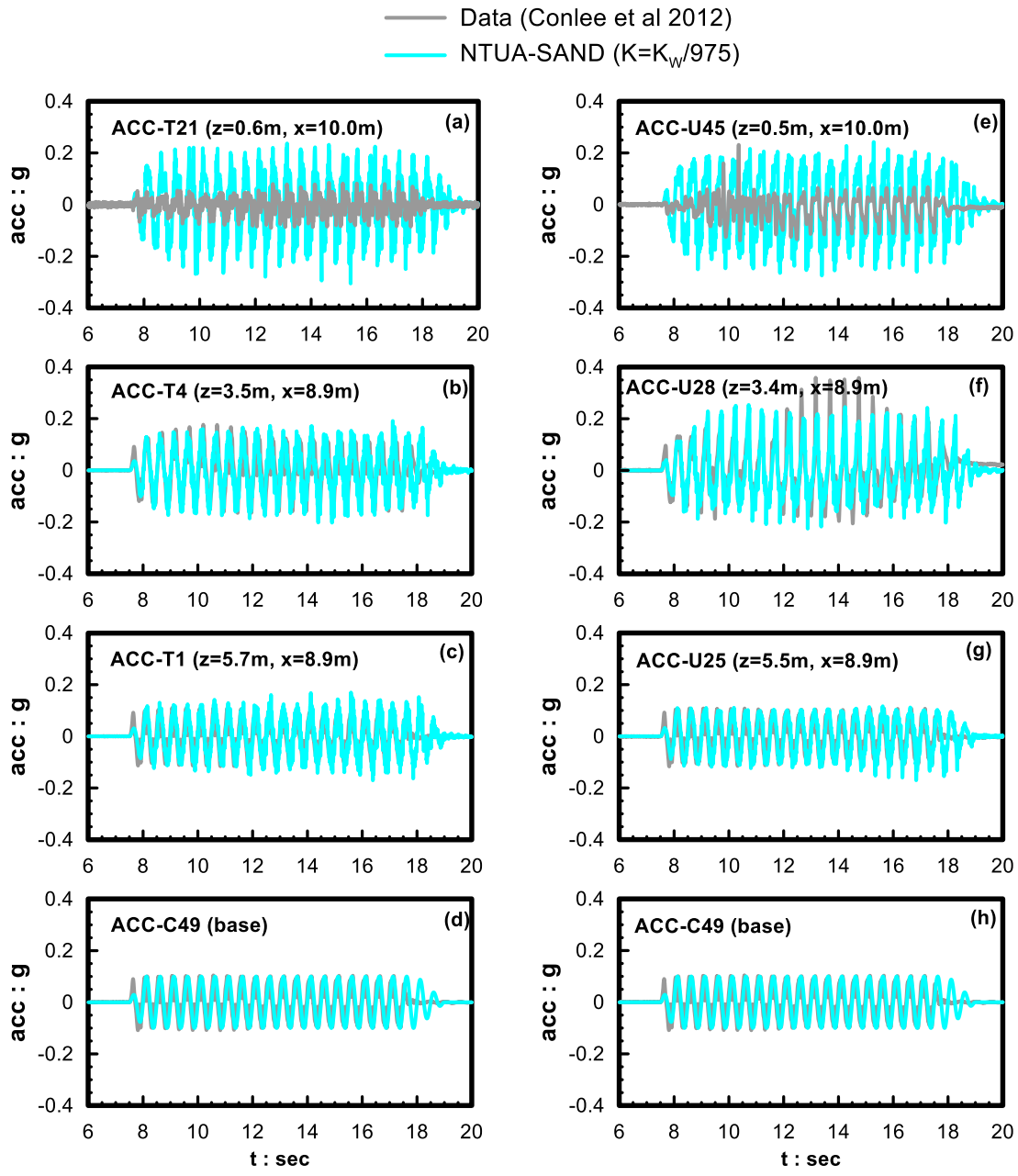

Figure 8.21 *Comparison of recorded acceleration time-histories at different depths z and horizontal distances x from the central membrane x during CTC01 Shake 3* (Conlee et al. 2012) *with the corresponding numerical analyses results for* $K=K_w/975$ *(where* K_w *is bulk modulus for water).*

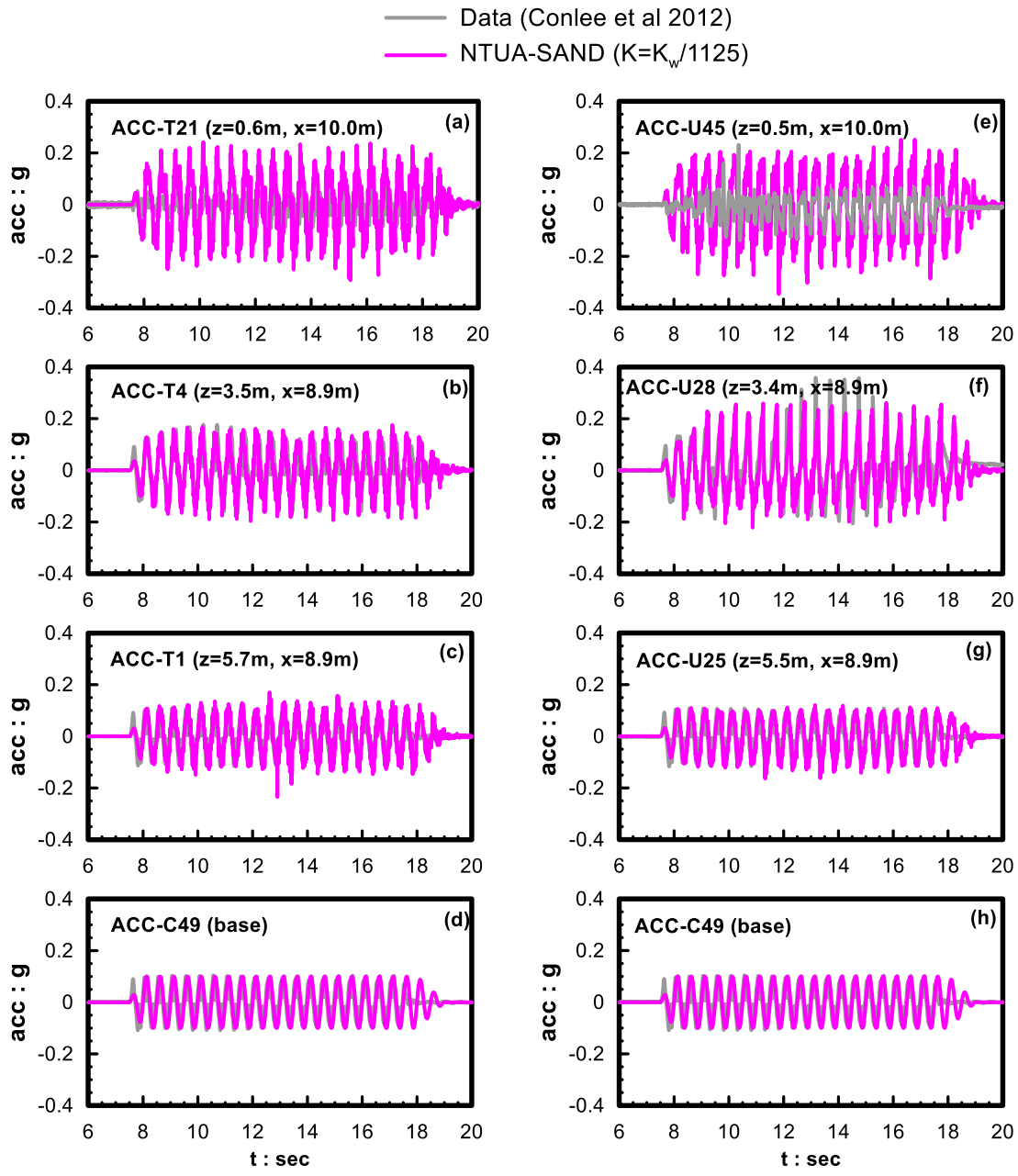

Figure 8.22 *Comparison of recorded acceleration time-histories at different depths z and horizontal distances x from the central membrane x during CTC01 Shake 3* (Conlee et al. 2012) *with the corresponding numerical analyses results for* $K=K_w/1125$ *(where* K_w *is bulk modulus for water).*

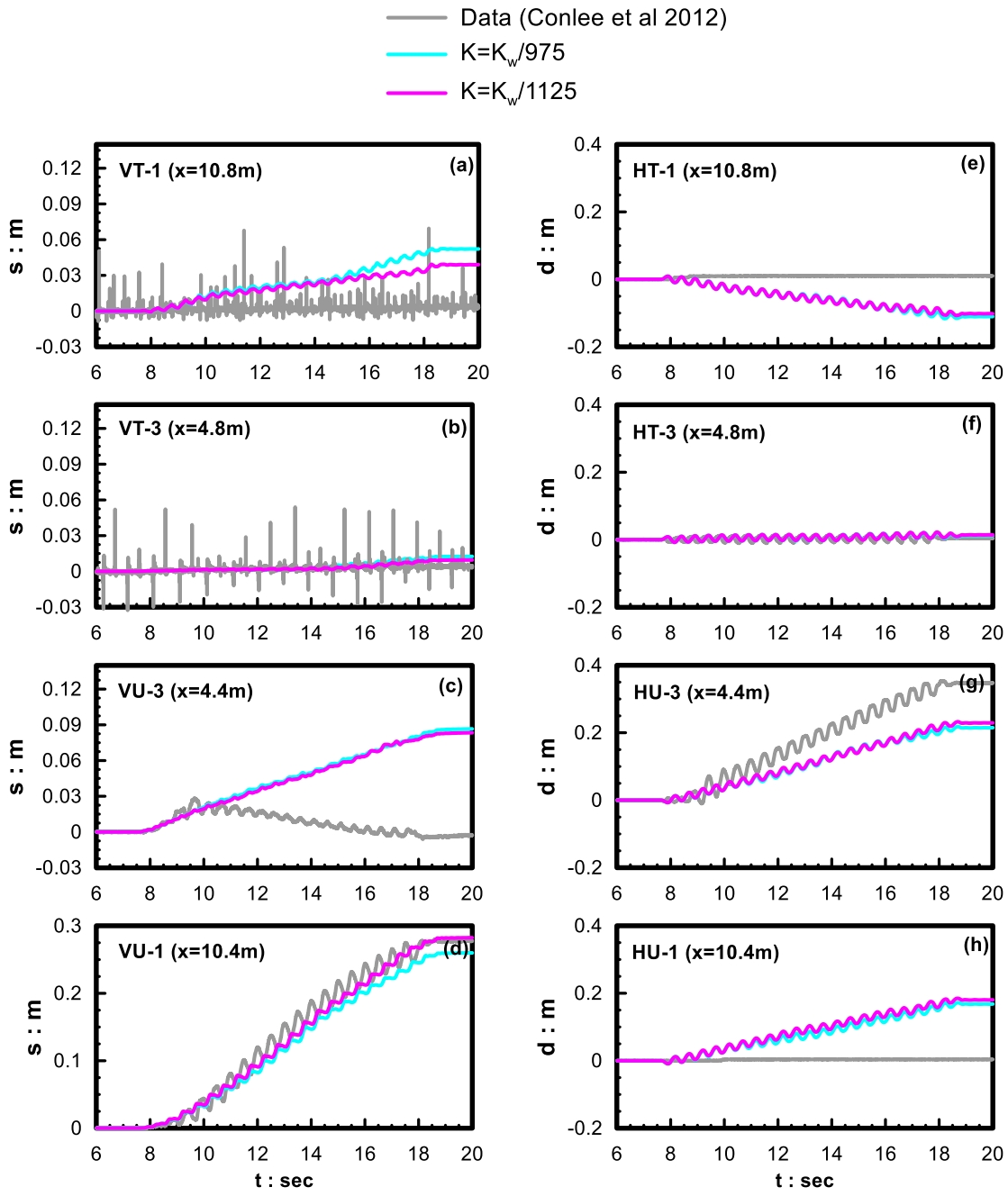

Figure 8.23 *Comparison of recorded surface settlement time-histories (a to d) and horizontal surface displacements (e to h) at different horizontal distances x from the central membrane during CTC01 Shake 3* (Conlee et al. 2012) *with the corresponding numerical analyses results for* $K=K_w/975$ *and* $K=K_w/1125$

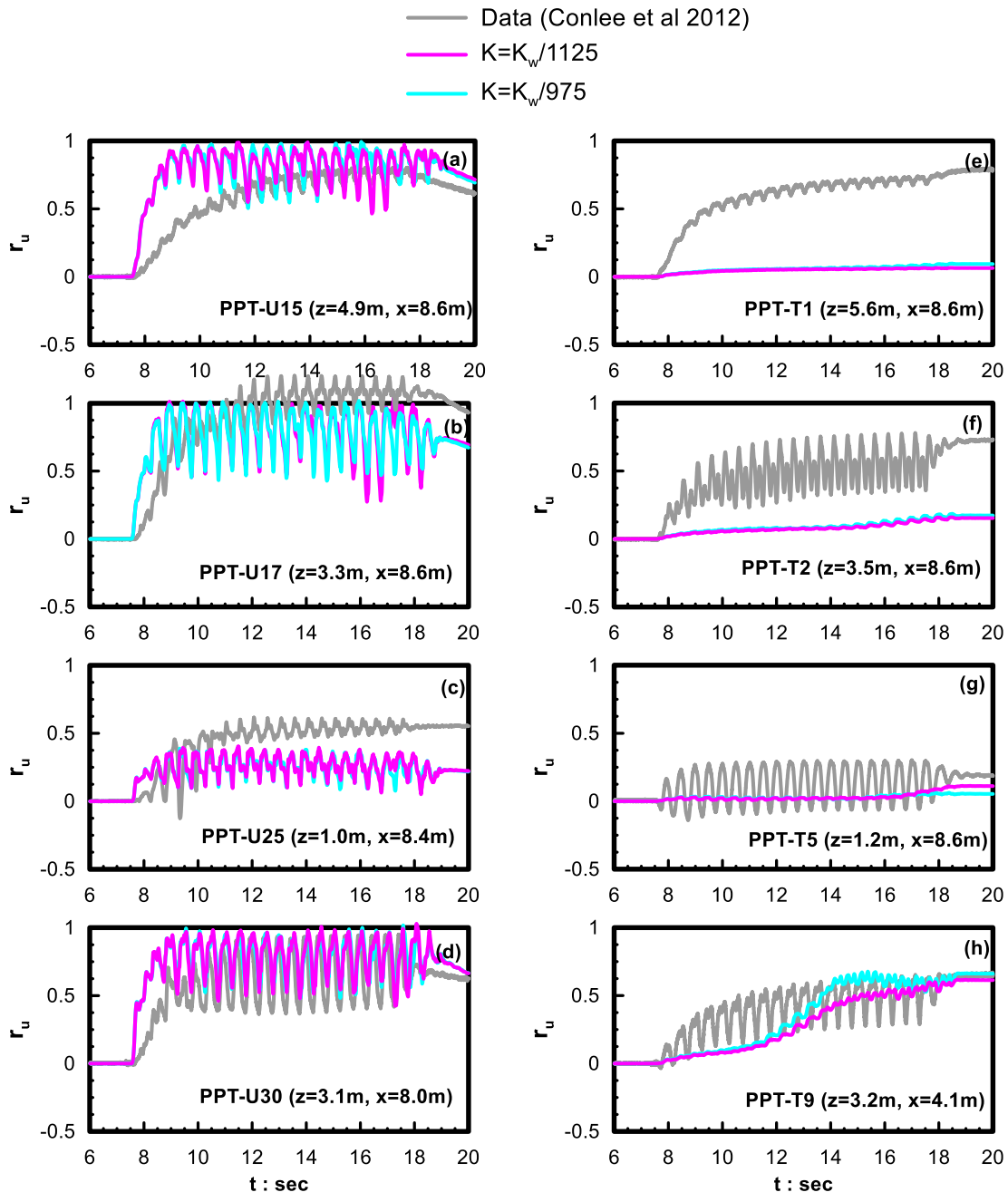

Figure 8.24 *Comparison of recorded excess pore pressure ratio r_u time-histories at different depths z and horizontal distances x from the central membrane during CTC01 - Shake 3* (Conlee et al. 2012) *with the corresponding numerical results for $K=K_w/975$ and $K=K_w/1125$ (a to d) for untreated and (e to h) for treated side.*

To conclude, all the analyses presented in *Chapters 7* and *8* indicate that the use of Equation (7-1) can be generally adopted in order to numerically simulate the dynamic response of a stabilized soil in a boundary value problem. This can be performed either for the ever current CS(%) concentration, or for an average value ($K_w/975$) which corresponds to CS(%)=7.5, i.e. the average value of the usually applied range of CS(%)=5-10 in practice. For this purpose, the

Equation (7-1) will be further investigated in paragraph 8.4 by performing "blind" prediction of other boundary value problems, as a means of estimating the overall reliability of this simulation approach.

8.4 Evaluation of reliability of the numerical simulation methodology for stabilized soils

Previous paragraphs of this *Chapter* as well as *Chapter 7*, present a numerical simulation methodology for stabilized soils based on two dynamic centrifuge tests: Gallagher et al. (2007a) for a horizontal stabilized layer with PBA=0.20g and Conlee et al. (2012) for a gently sloping stabilized layer subjected to an excitation with PBA=0.15g (CTC01, Shake 3). In this paragraph, the reliability of this methodology is investigated via "blind" predictions of the recordings of other centrifuge tests, namely the CTC01 test at a higher intensity excitation (CTC01, Shake 4: Conlee et al. 2012), as well as the CTC02 test which employs the same geometry but stabilized with different CS(%) concentrations (CTC02, Shake 3, Conlee et al. 2012). Hence, the same test (CTC01) was examined with the same properties, but with PBA=0.19g (Shake 4). This particular shaking event was selected because all other excitations had either very low intensity (e.g. Shakes 1, 2) and were therefore inappropriate to illustrate the effect of passive stabilization, or had extremely high intensity (Shakes 5, 6) with small practical interest. The comparison of acceleration time-histories with depth is presented in Figure 8.25 and Figure 8.26 (left column for stabilized slope) suggests that the results of the analyses for $K=K_w/975$ and $K=K_w/1125$ are able to successfully simulate the measured time-histories at different depths of the stabilized slope, showing a slight overestimation at the soil surface, which was also observed at CTC01 (Shake 3) and is probably caused by the fact that these measurements are recorded on the Yolo loam top layer which is simulated using a less sophisticated constitutive model (Mohr – Coulomb) that was calibrated without available laboratory element tests (based on the literature, e.g. Kamai and Boulanger, 2013).

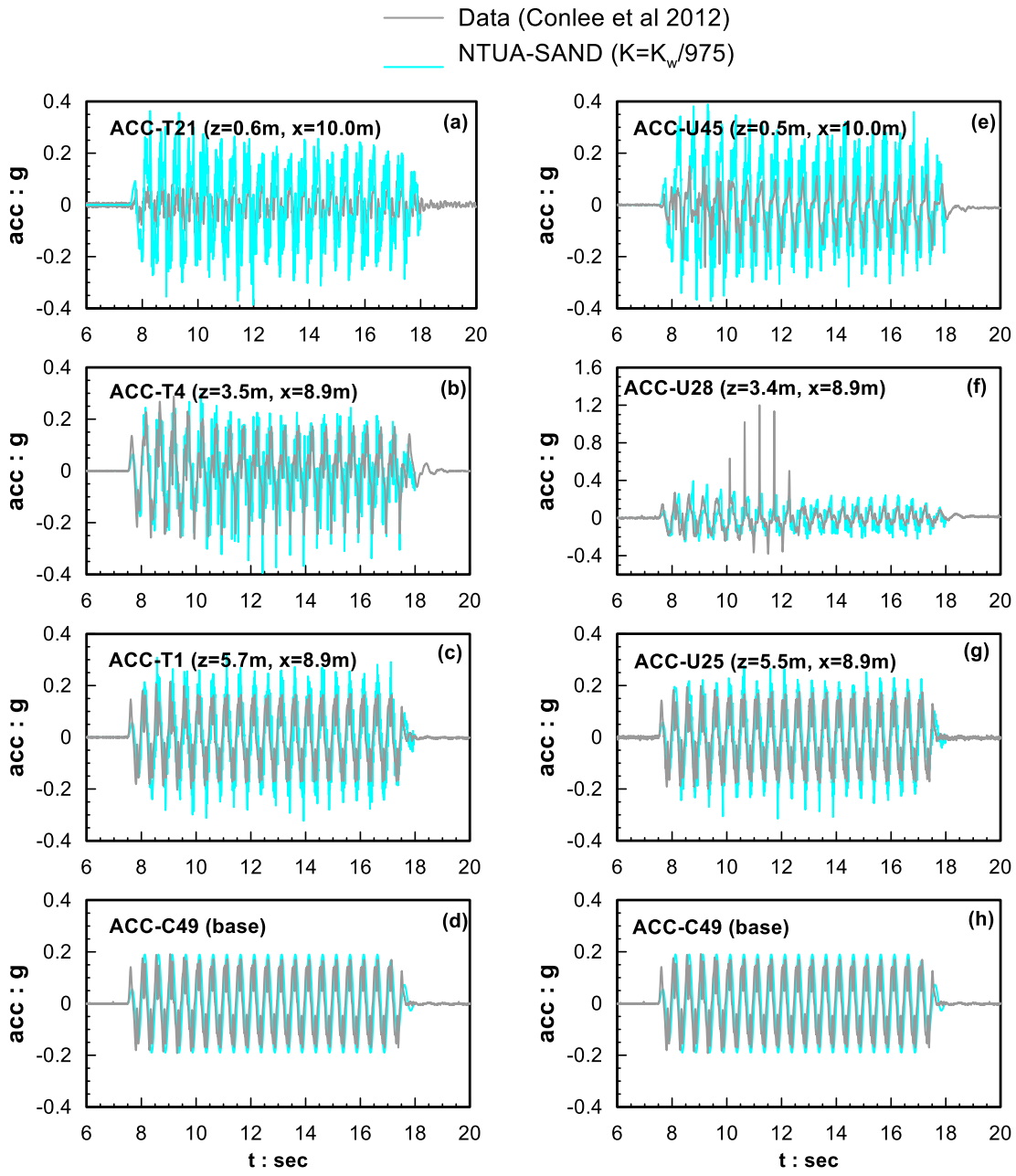

Figure 8.25 *Comparison of recorded acceleration time-histories at different depths z and different horizontal distances x from the central membrane during CTC01- Shake 4* (Conlee et al. 2012) *with the corresponding numerical analyses results for* $K=K_w/975$.

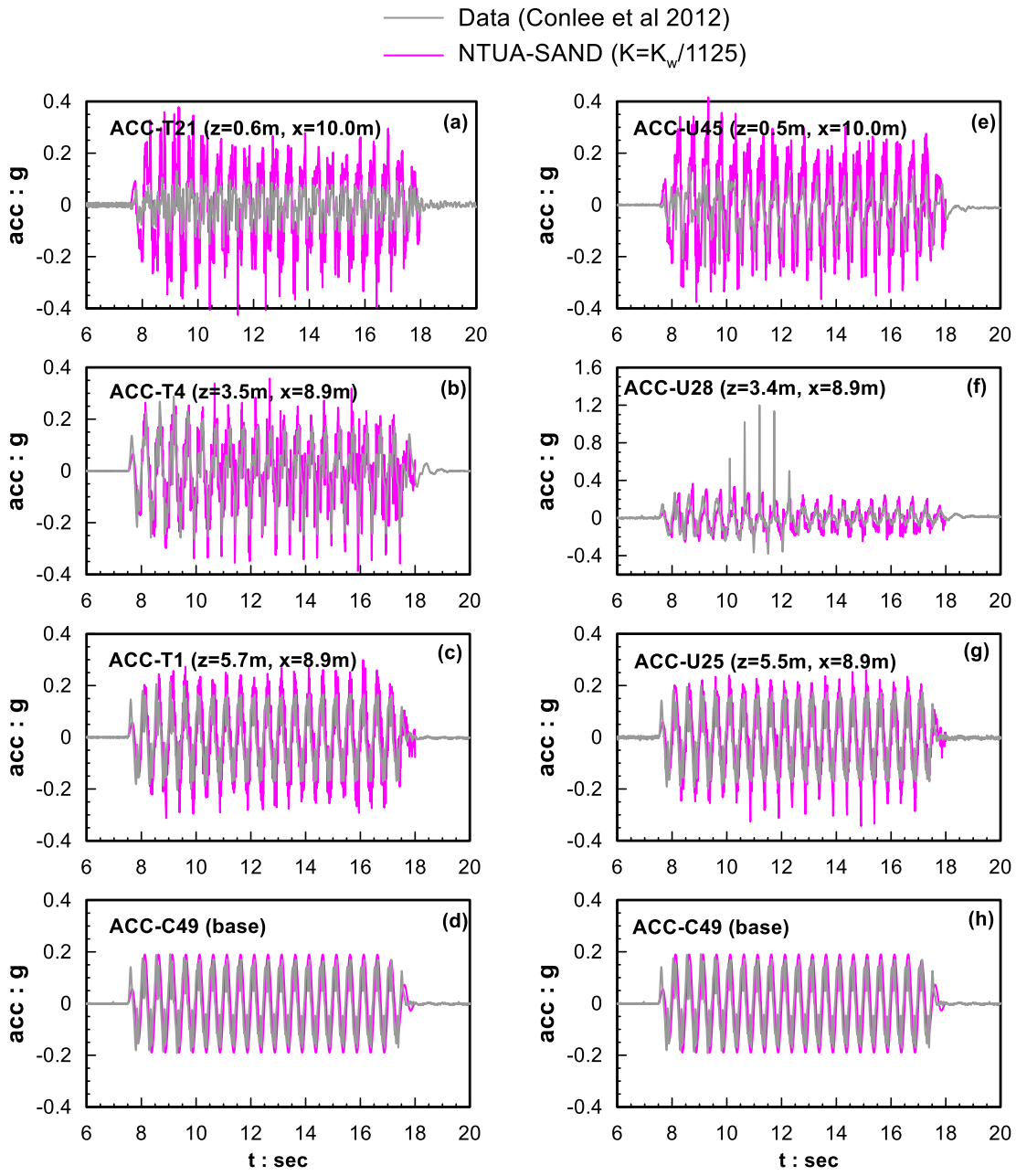

Figure 8.26 *Comparison of recorded acceleration time-histories at different depths z and horizontal distances x from the central membrane x during CTC01 - Shake 4* (Conlee et al. 2012) *with the corresponding numerical analyses results for K=K$_w$/1125 (where K$_w$ is bulk modulus for water).*

A comparison in terms of displacements (Figure 8.27) shows that as PBA increases (from Shake 3 to Shake 4), the numerical analyses are less able to satisfactorily simulate the measured settlement time-histories, since they predict non-zero settlements at the soil surface and finite horizontal displacements near the walls of the model contrary to what the recordings show. This simulation inability seems less important in terms of excess pore pressure ratio r_u and is thus hardly noticeable in Figure 8.28.

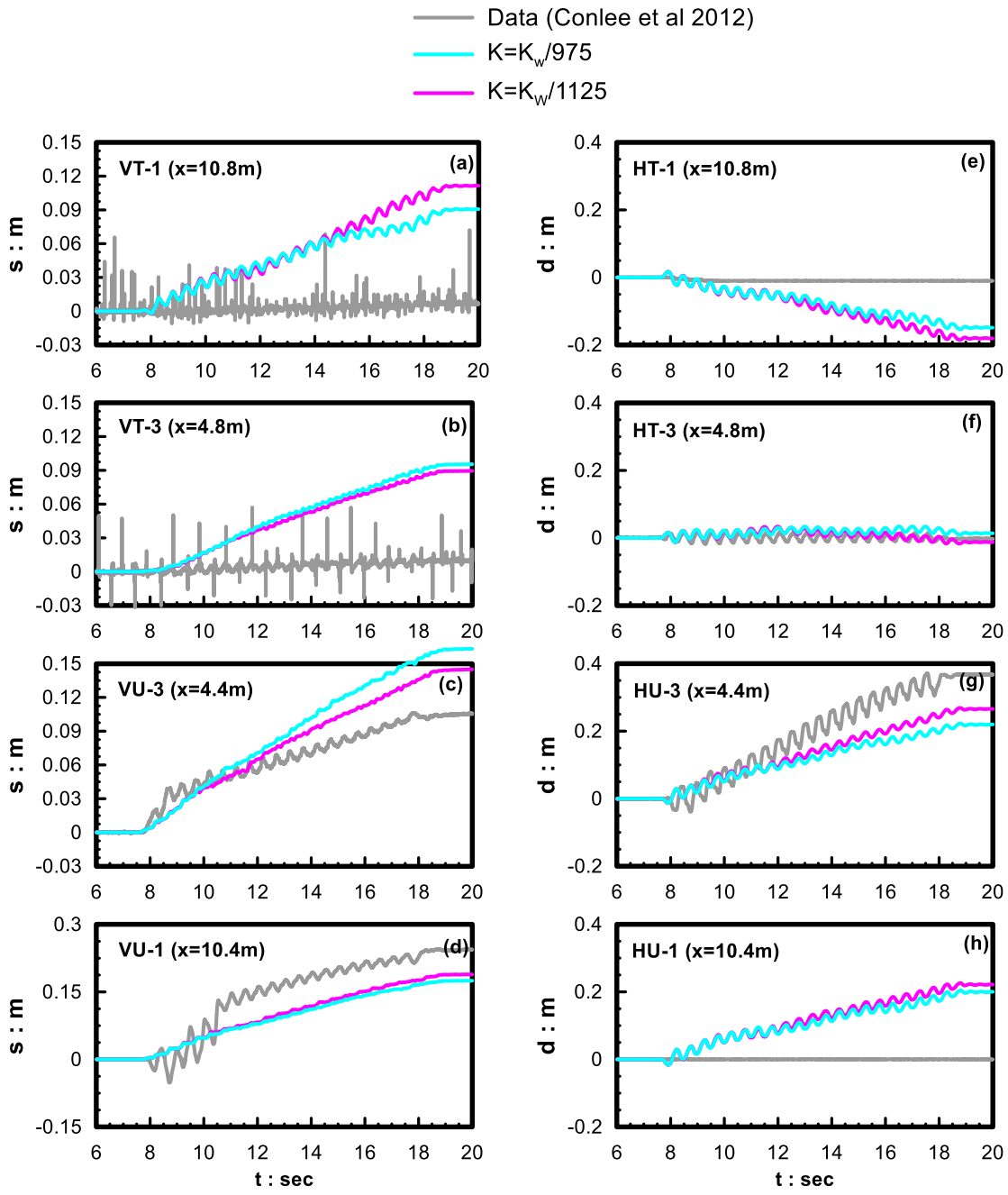

Figure 8.27 *Comparison of recorded surface settlement time-histories (a to d) and horizontal surface displacements (e to h) at different horizontal distances x from the central membrane during CTC01 Shake 4* (Conlee et al. 2012) *with the corresponding numerical analyses results for K=K$_w$/975 and K=K$_w$/1125.*

A general conclusion that can be drawn based on the results of numerical analyses for the high intensity excitation, is that an underestimation of the effectiveness of the stabilization can be observed in comparison with the recordings. However, it must be clarified here that the higher intensity excitation (Shake 4) was subjected to the model after Shake 3 and this fact may have caused a change in the overall geometry (especially of the untreated side) and/

or the position of the transducers within the model. On the contrary, the numerical analyses assumed that each excitation was imposed separately, namely with the same initial overall geometry and the same initial transducer positions, without the effects of the preceding shaking events. This does not hold for Shake 3, which also follows two lower intensity excitations (Shakes 1 and 2), but its results are not expected to have been affected by these excitations due to their very low intensity.

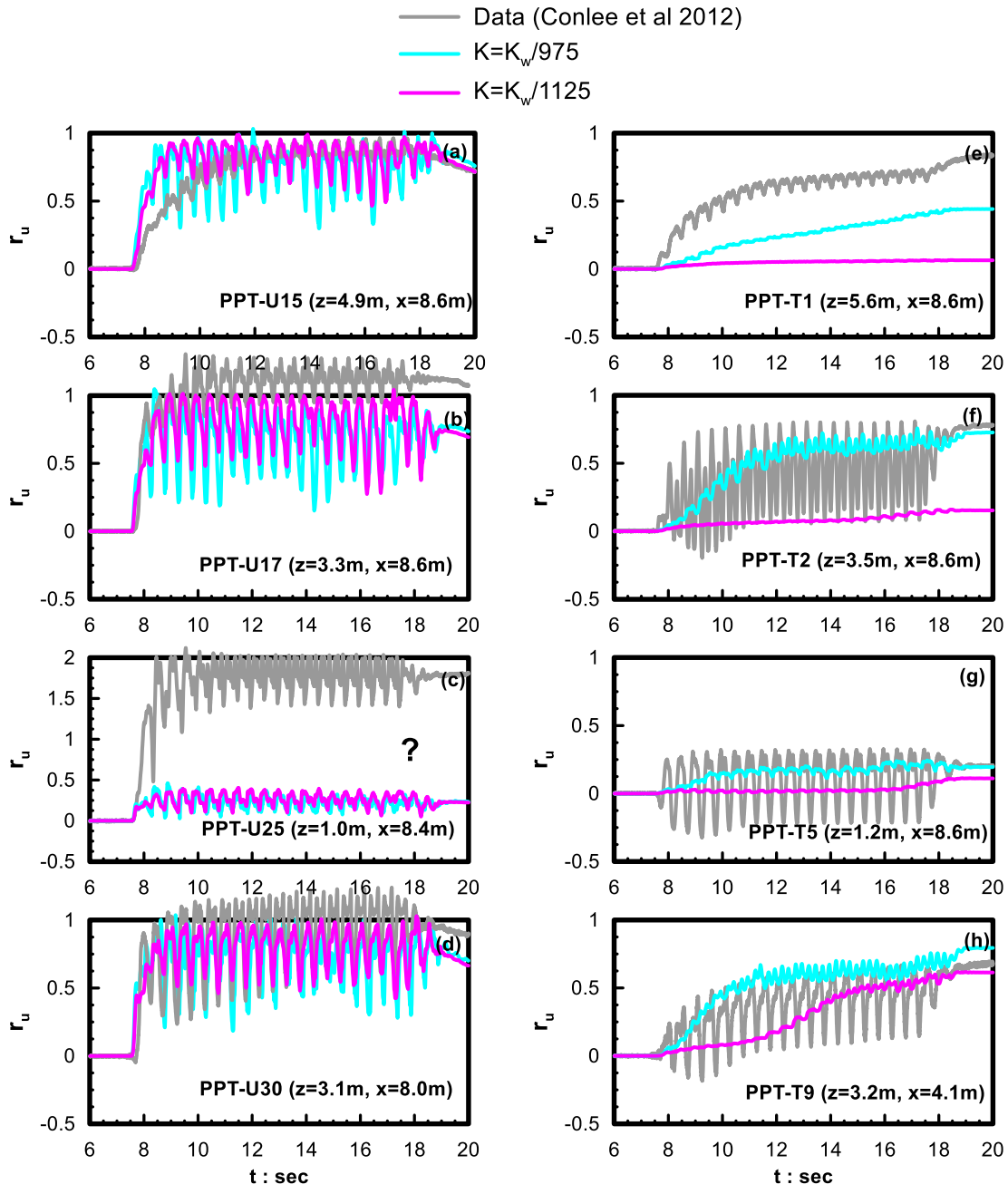

Figure 8.28 *Comparison of recorded excess pore pressure ratio r_u time-histories at different depths z and horizontal distances x from the central membrane during CTC01 - Shake 4* (Conlee et al. 2012) *with the corresponding numerical results for K=K$_w$/975 and K=K$_w$/1125: (a to d) for untreated and (e to h) for treated side*

For the sake of completeness, the accuracy of the numerical simulation methodology will be also investigated for treatment with different concentrations of CS grout. To do so, the second test series conducted by Conlee et al. (2012) will be simulated (CTC02). This test retains the same model geometry (Figure 8.2), but in comparison with CTC01 both slopes are treated with CS: the left with CS(%)=4 and the right with CS(%)=5. The sinusoidal base excitation (CTC02-Shake 3) had a peak base acceleration equal to 0.15g and a frequency of 2Hz, i.e. it has an intermediate shaking intensity between Shake 3 of CTC01 and Shake 4 of CTC01. FLAC (Itasca 2011) was also used for the numerical simulation of CTC02 and the stabilization was introduced in the simulation by reducing the bulk modulus of the pore fluid K (compared to water) taking into account the concentration of CS used for each slope according to Equation (7-1). Based on this expression, values of $K=K_w/625$ and $K=K_w/725$ were used for the left and right slope, respectively. The hydraulic conductivity coefficients were estimated equal to 10^{-8}m/s and $5.1x10^{-9}$m/s for CS(%)=4 and 5 respectively, based on Persoff et al. (1999).

Figures 8.29 through 8.31 compare acceleration, (horizontal and vertical) displacement and excess pore pressure ratio time-histories recordings, respectively, with the corresponding results of the abovementioned numerical analyses. Unfortunately, in respect with CTC02 the full presentation of the measurements (recordings) from the whole instrumentation set up was not possible (as in CTC01), because the data in the literature are not provided with full documentation (as in CTC01).

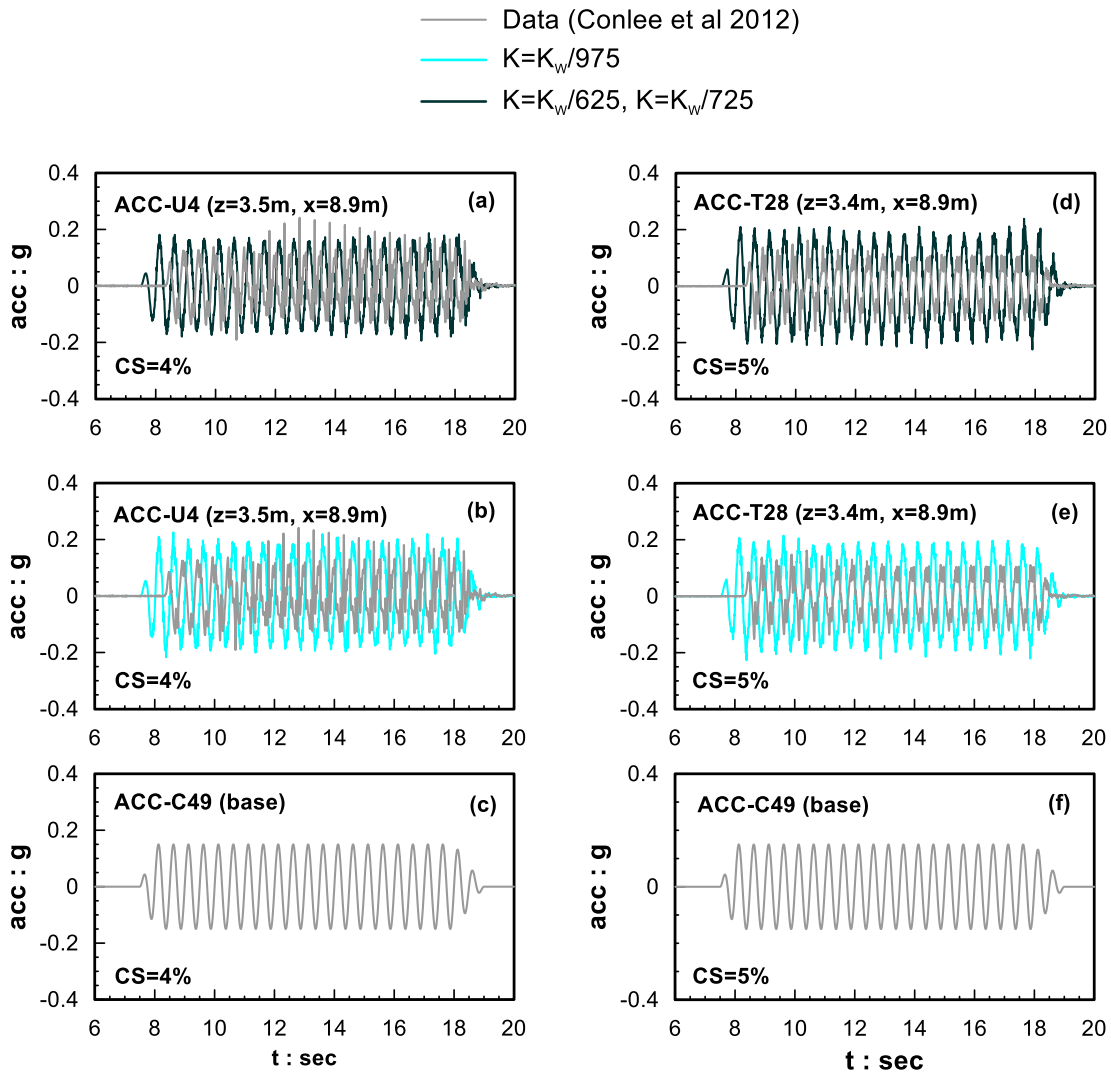

Figure 8.29 *Comparison of recorded acceleration time-histories at different depths z and horizontal distances x from the central membrane during CTC02- Shake 3* (Conlee et al. 2012) *with the corresponding numerical results for (a) $K=K_w/625$ for the left slope and. $K=K_w/752$ for the right slope, (b) for average fluid bulk modulus value. $K=K_w/975$ for both slopes.*

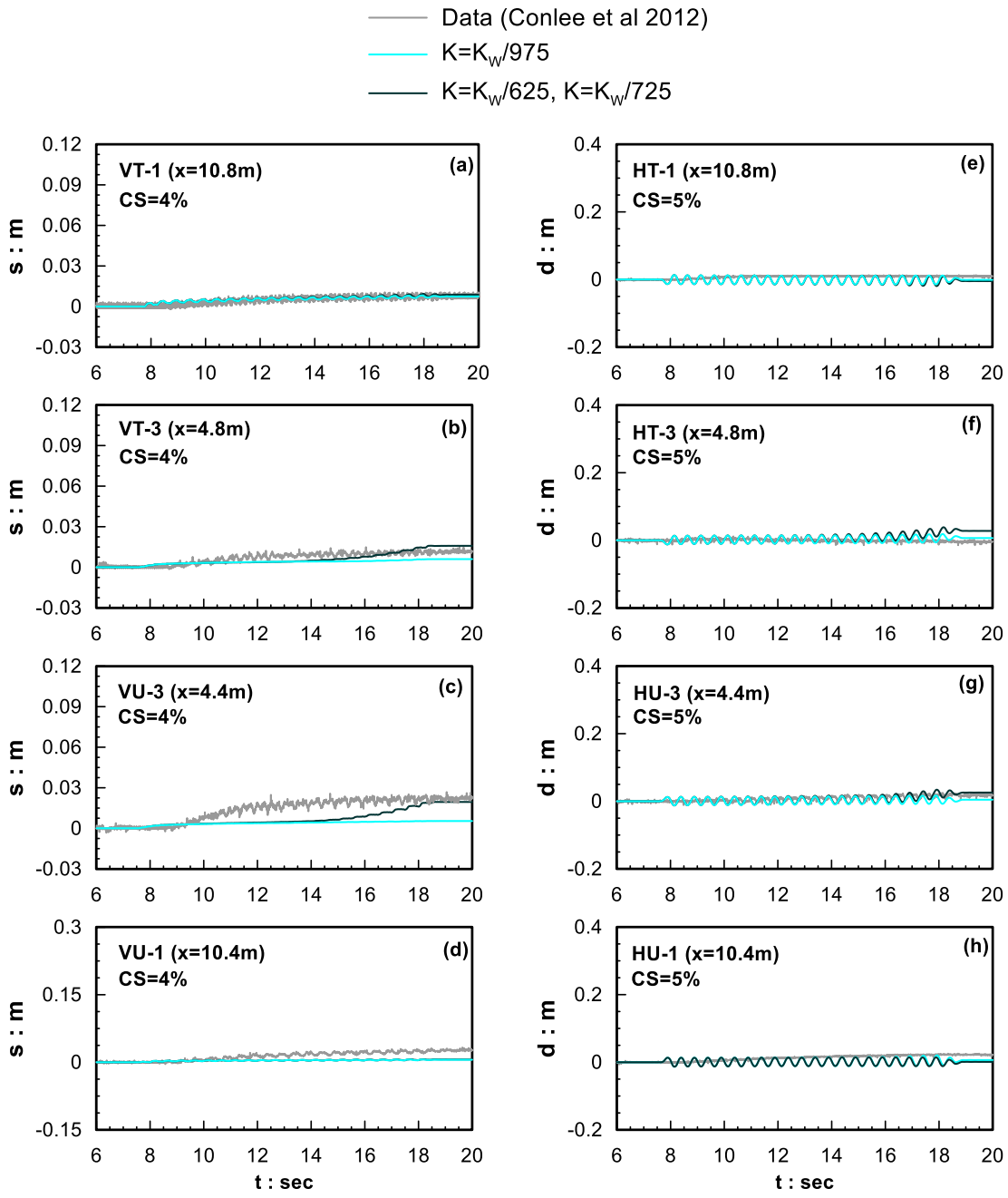

Figure 8.30 *Comparison of recorded vertical and horizontal displacement time-histories on the model surface and different horizontal distances x from the central membrane during CTC02- Shake 3* (Conlee et al. 2012) *with the corresponding numerical results for (a) $K=K_w/625$ for the left slope and. $K=K_w/752$ for the right slope, (b) for average fluid bulk modulus value. $K=K_w/975$ for both slopes*

Transducers ACC-U4, VU-1, VU-3, HU-1, HU-3 and PPT-U1 refer to the left slope treated with CS(%)=4 and the rest (ACC-T28, VT-1, VT-3, HT-1, HT-3, PPT-T15 and PPT-T17) refer to the right slope treated with CS(%)=5. Briefly, Figure 8.29 indicates that an average value of the pore fluid bulk modulus *K* for both slopes, as well as the variation of *K* by taking into account the

exact CS(%) concentrations, can simulate satisfactorily the response in terms of accelerations despite a general small overestimation in both cases (as in CTC01). However, a careful observation of the numerical simulation results in the case of the average K value, illustrates a symmetrical response of the model, namely the same values of horizontal and vertical displacements, accelerations, excess pore pressure ratios at the same depths for the two slopes. These results are expected, but are not compatible with the recording which show a small variability (the CS=4% performs less satisfactorily than CS=5%).

Especially in terms of displacements (Figure 8.30) both analyses satisfactorily predict the response of stabilized soil, but the approach which correlates the reduction of the fluid bulk modulus K with CS(%) concentration seems to be in better agreement with the recordings at both slopes. In addition, as resulted from Figure 8.31, the numerical analyses systematically underestimate the pore pressure development with or without taking into account the different percent of CS used in the treated slopes.

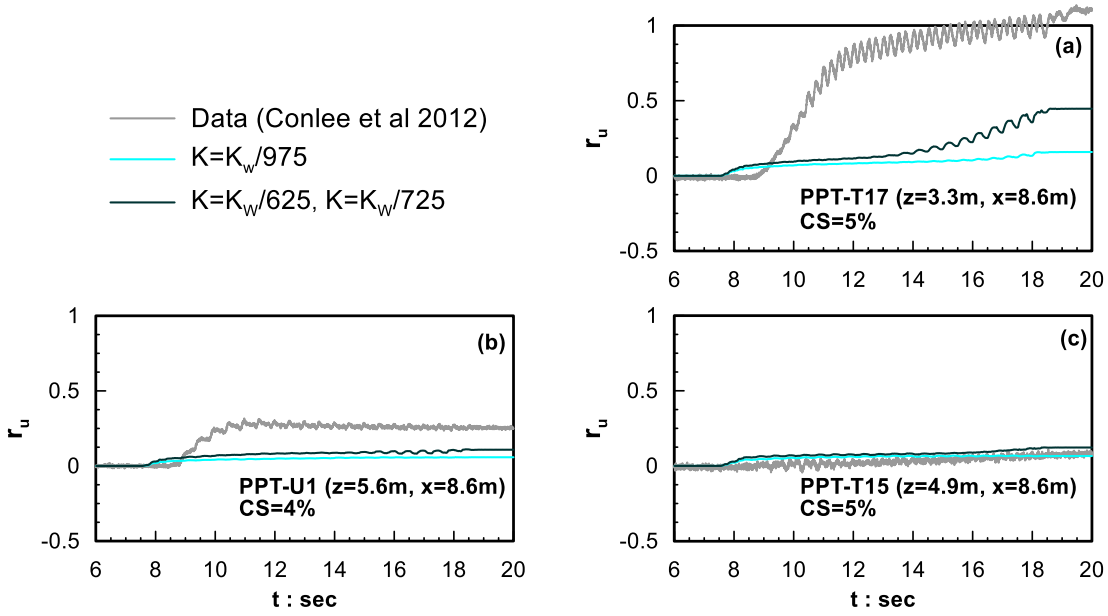

Figure 8.31 *Comparison of recorded excess pore pressure ratio time-histories at different depths z and horizontal distances x from the central membrane during CTC02- Shake 3* (Conlee et al. 2012) *with the corresponding numerical results for (a) K=K$_w$/625 for the left slope and. K=K$_w$/752 for the right slope, (b) for average fluid bulk modulus value. K=K$_w$/975 for both slopes*

Based on all the findings in *Chapters 7* and *8* it is considered that employing a reduced pore fluid modulus K as a function of CS(%) in combination with a constitutive model for untreated sands (like NTUA-SAND of Andrianopoulos et al., 2010a) offers a reliable means for simulating the response of stabilized soils at least for small and medium intensity excitations.

Chapter 9

AMPLIFICATION OF ELASTIC RESPONSE SPECTRA IN STABILIZED SAND LAYERS

9.1 Introduction

This Chapter studies the elastic response spectra at the surface of stabilized soil layers, which could be used to design civil engineering structures. Specifically, an effort is made to estimate the amplification of elastic response spectra in stabilized soil layers based on coupled dynamic elastoplastic analyses. This work will prove useful for the practical application of passive stabilization, as the execution of such analyses from non-specialized engineers may prove a difficult task and will be time consuming.

For this purpose, the calibrated numerical methodology presented in previous *Chapters* is used, namely a parametric investigation using NTUA-SAND (Andrianopoulos et al. 2010a, b) with the proper reduction of the fluid bulk modulus K to account for CS in the sand pores. For this purpose, a sand column of 9m total thickness and four different stabilization thickness with depth is considered, and is subjected to 11 different seismic excitations. These excitations have different frequency content and intensity as they were recorded from earthquakes with different magnitudes (M). Hence, in order to homogenize the database of the recordings, the 11 recorded acceleration time histories are processed so as to correspond to the same effective acceleration value (a_{eff}), thus yielding comparable amounts of energy at the base of the layer. To do so, the acceleration time-histories were uniformly multiplied with a coefficient factor λ, which is expressed by:

$$\lambda = \frac{a_{max,req}}{a_{max}} \tag{9.1a}$$

with:

$$a_{max,req} = a_{eff}\,\frac{10}{M-1} \tag{9.1b}$$

where a_{max} is the recorded maximum acceleration value (per recording) and $a_{max,req}$ is the final maximum acceleration value (per recording) based on homogenization of the database so as

to have the same effective acceleration a_{eff}, regardless of magnitude M, for all recordings in the database.

Table 9-1 presents the names of the 11 selected recordings (with their year of occurrence), their recorded maximum values of acceleration (a_{max}), their predominant period (T_e), the magnitude of the corresponding earthquake (M), the value of the coefficient factor (λ) and the final maximum acceleration value for a_{eff}=0.25g (as an example) for all 11 excitations. Moreover, Figure 9.1 illustrates the elastic response spectra of the 11 excitations after normalization to the spectral acceleration for T=0sec and their comparison to the elastic design spectrum proposed by Eurocode 8 (EC8) for soil type A (bedrock). Figure 9.1 indicates that the chosen excitations securely cover the range of the expected excitation spectra, at least for Europe, and also extend to lower frequencies (e.g. Lefkada, Aigio) so as to also cover relatively extreme cases. The excitations with their elastic response spectra, and their time-histories of acceleration, velocity and displacement for the 11 recordings can be found in Appendix B.

Table 9-1 *Properties of the 11 excitations used in the numerical analyses.*

Excitation name (Date)	$a_{max}(m/s^2)$	T_e***(sec)***	***M***	***λ***	$a_{max,req}(m/s^2)$, ***(for*** a_{eff}***=0.25g)***
Aigio (1995)	3.8	0.52	6.2	1.2	4.7
Coyote Lake (1979)	1.0	0.42	5.7	5.3	5.2
Kefalonia (1983)	2.4	0.18	6.2	2.0	4.7
Kobe (1995)	8.0	0.20	7.2	0.5	4.0
Lefkada (2003)	4.1	0.46	6.3	1.1	4.6
Loma Prieta (1989)	1.1	0.20	6.9	3.9	4.2
Northridge (1994)	8.6	0.36	6.7	0.5	4.3
Northridge 265 (1994)	4.2	0.40	6.7	1.0	4.3
Parkfield (2004)	2.6	0.27	6.2	1.8	4.7
Pyrgos (1993)	4.4	0.30	4.9	1.4	6.3
Sepolia (1999)	3.0	0.25	5.8	1.7	5.1

It should be mentioned that all acceleration time-histories at the surface, base and soil layer interfaces presented herein, have been filtered. This procedure was considered necessary

because the output acceleration time-histories from FLAC (Itasca Inc., 2011) showed high frequency numerical noise. This noise made the interpretation of time-histories difficult, and showed high frequency content which is unrealistic and unimportant for civil engineering projects.

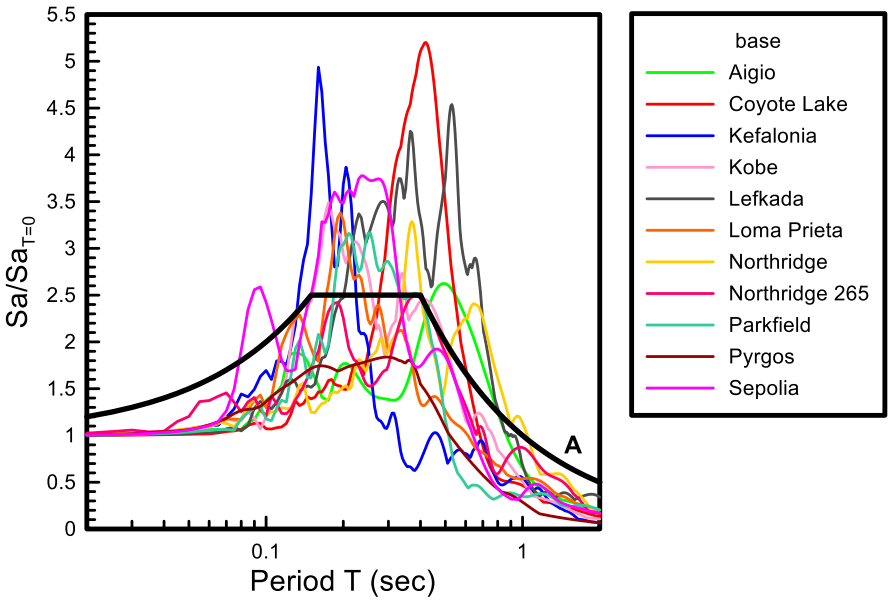

Figure 9.1 *Normalized elastic response spectra (5% damping) of the 11 excitations compared to the elastic design spectrum proposed by EC8 for soil type A and large magnitude events (M>5.5).*

The filtering process was executed with SeismoSignal (Seismosoft, 2016) using the Butterworth method of order 8 to limit frequencies greater than 12Hz. This value was chosen after a trial-and-error procedure as it does not distort the base acceleration time-history energy content. As an example, Figure 9.2 presents the acceleration time-history for the Kobe excitation filtered with different upper frequency limits and unfiltered, whereas Figure 9.3 presents the corresponding elastic response spectra. It is obvious that the filtering process for the reduction of frequency content over 12Hz eliminates the unimportant (and erroneous) amplification of the acceleration at low periods and does not alter the critical information of the original (initial) spectrum (e.g. predominant period, maximum spectral acceleration region). Furthermore, the filtered acceleration time-histories were further corrected using the SeismoSignal software, so that the residual displacement at the end of the excitation will be equal to zero (baseline correction).

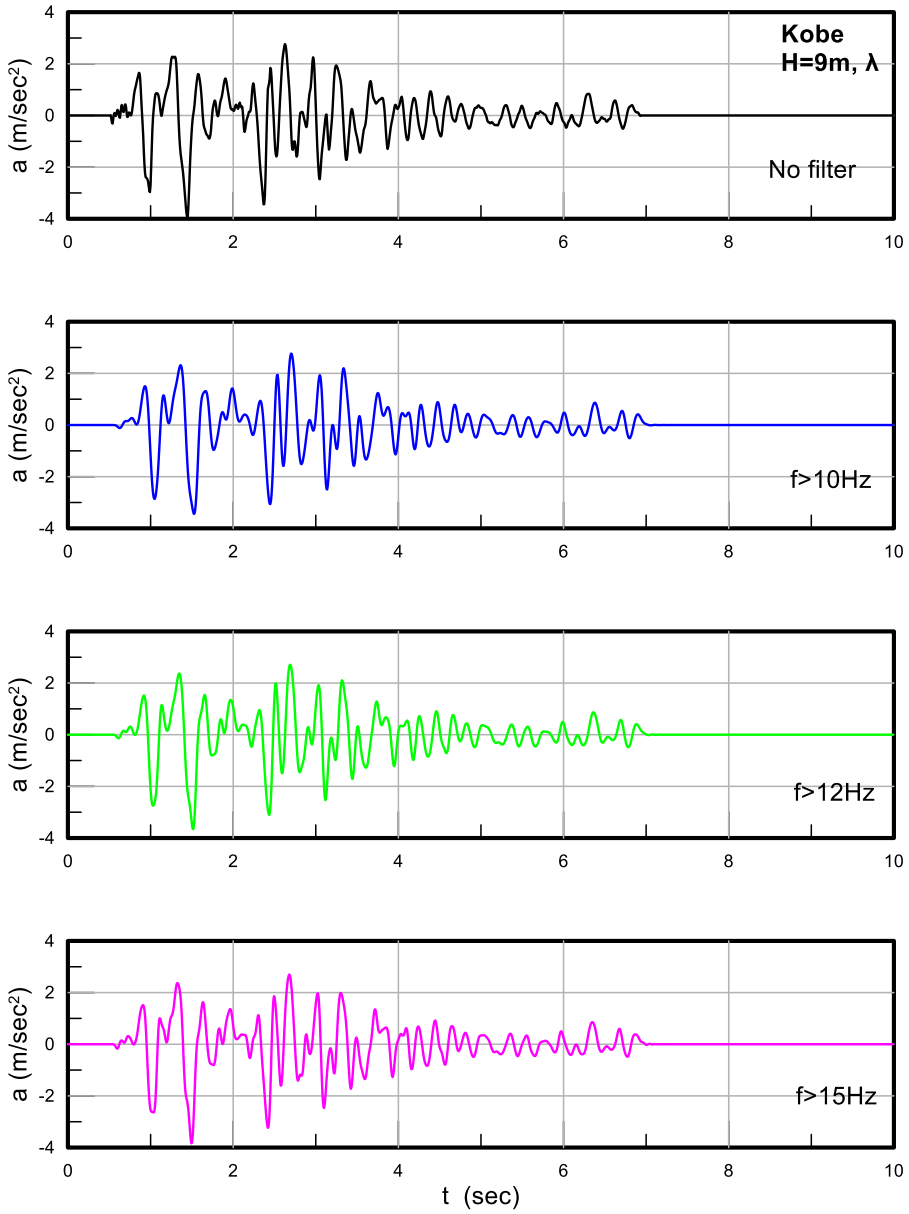

Figure 9.2 *Acceleration time-histories for Kobe excitation (a) unfiltered and filtered with lower frequency limit of (b) 10Hz, (c) 12Hz and (d) 15Hz respectively.*

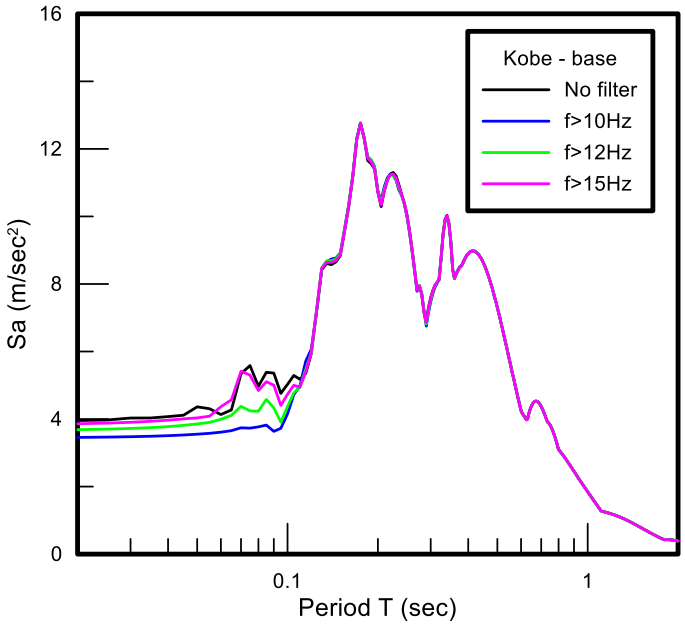

Figure 9.3 *Comparison of filtered (f>10, 12, 15Hz) and unfiltered elastic response spectra (5% damping) for the Kobe excitation.*

Four (4) soil profiles of 9m total thickness over bedrock were investigated: (a) 9m of (fully) untreated soil, (b) 9m of treated soil (c) 6m of treated soil overlaying 3m of untreated soil and (d) 3m of treated soil overlaying 6m of untreated soil. It is noted here, that the response of the soil profile (a) is to be compared to the response of the soil profile (b) while the soil profiles (c) and (d) are investigated in order to simulate a partially treated soil layer. For the numerical simulation of the seismic response of the 9m column with FLAC (Itasca 2011) a grid of 3m x 9m with zones of 1m length and 0.5m height was used. At the area of the interfaces of the untreated and treated layer (at depths of 3m and 6m) the grid was densified with zones of 1m x 0.25m.

Figure 9.4 illustrates the grid used for the simulation of the abovementioned soil profile (d), as an example. The term $S_{a,surf}$ refers to the elastic response spectrum (with 5% damping) of the illustrated node at the layer surface, whereas the terms $S_{a,int}$ and $S_{a,bas}$ refer to the elastic response spectra (with 5% damping) of the illustrated nodes at the interface and the base, respectively. For the simulation of the 3m and 6m treated sand columns (which will be presented in paragraph 9.3) a grid of 3m and 6m height was used, which retained the same zone dimensions as presented above. The water table was simulated by applying a (water) pressure equal to 9.81kPa on the surface, which corresponds to 1m-height water above ground, in order to retain saturation of the underlain grid zones during the seismic oscillation. Furthermore, the nodes on the left side of the grid were tied to the corresponding ones on

the right side (tied nodes) in order to ensure identical horizontal displacements at each depth, thus simulating 1D shaking conditions.

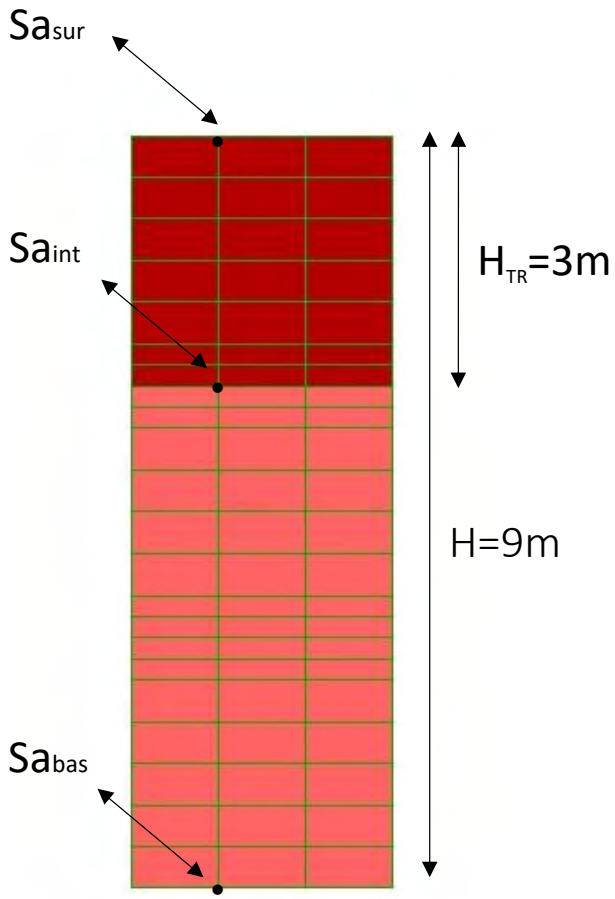

Figure 9.4 *Grid used for the 1D numerical analyses with FLAC* (Itasca 2011) *of the partially treated soil column.*

The constitutive simulation of the response of the geomaterial was performed with NTUA_SAND (Andrianopoulos et al. 2010b), which is calibrated for Nevada sand with the parameter values shown in Table 9-2. The simulation of the treated layers was done by applying the numerical methodology presented and calibrated in the previous *Chapters*, namely the fluid bulk modulus, K, was reduced in comparison with that of water K_w, using a divider of 975 which corresponds to a concentration equal to CS=7.5% (average value of the commonly used CS concentrations range: 5-10%). The hydraulic conductivity k of the stabilized sand was estimated based on the results of Persoff et al. (1999) as equal to $8*10^{-10}$m/s, while the pertinent value for the untreated layers was assumed equal to $3.3*10^{-4}$m/s. the sand was

considered equal to D_r=40%, and this is illustrated by the values of void ratio e, porosity and density (state variables).

Table 9-2 *Values of constants of NTUA-SAND model calibrated for untreated Nevada sand* (Andrianopoulos et al. 2010b) *and state variables for D_r=40% relative density.*

	Nevada sand
Density (Mgr/m^3)	1.52
Porosity	0.424
e	0.737
M_c^c	1.25
M_c^e	0.72
$(e_{cs})_a$	0.809
λ	0.022
B	600
v	0.33
k_c^b	1.45
k_c^d	0.30
γ_1	0.00025
α_1	0.6
A_o	0.8
h_o	15000
N_o	40000

9.2 Effect of passive stabilization, excitation intensity and drainage conditions

The beneficial effect of stabilization with CS on the seismic response of a liquefiable sand layer was studied via analyzing three (3) cases of a 9m Nevada sand column at a relative density of D_r=40%: (a) untreated sand, (b) fully treated sand with CS=7.5%. and (c) untreated sand assuming fully drained conditions (i.e. with an unrealistically large k value). All three cases were subjected to the 11 aforementioned excitations, but here only the results of the low frequency Northridge excitation with a_{eff}=0.25g will be presented (namely, a value of λ, according to Table 9-1). Figure 9.5 presents the acceleration time-histories at the surface and base of the 9m column: (a) for untreated sand, (b) for fully treated sand and (c) for untreated sand under fully drained conditions. It is obvious that the treated layer vibrates by retaining

the characteristics of the base motion as opposed to the untreated sand, which after the first cycle shows severe de-amplification of the seismic motion, possibly due to liquefaction.

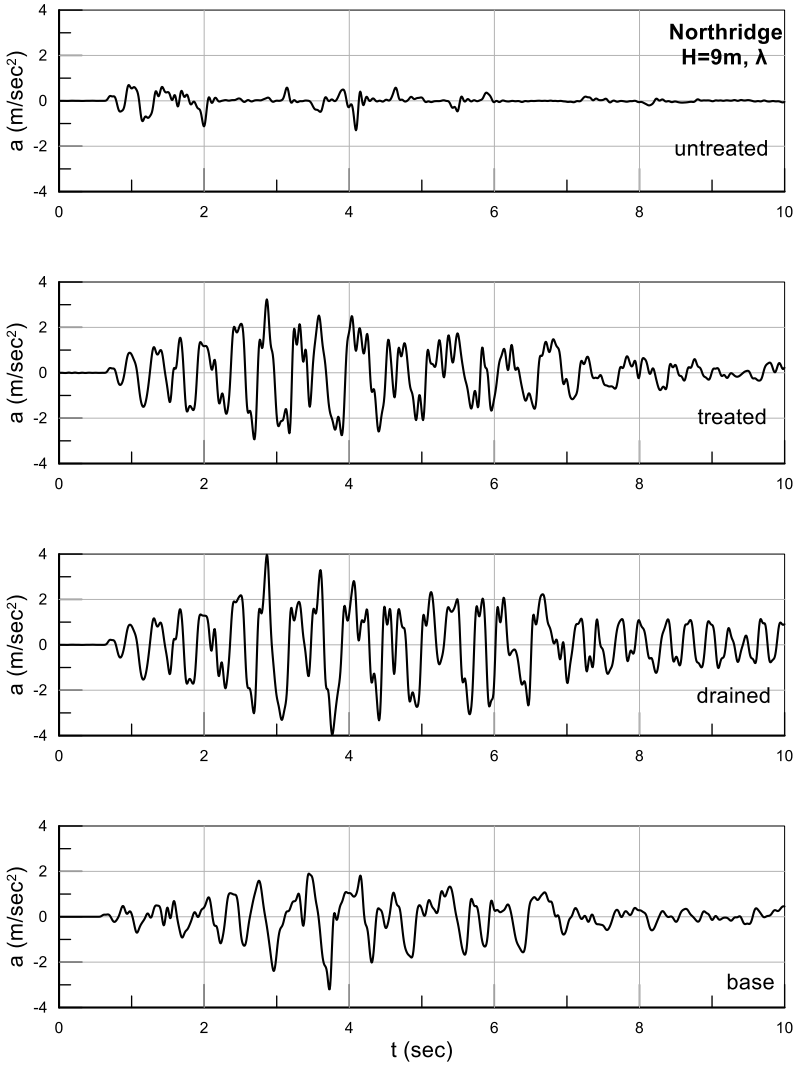

Figure 9.5 *Acceleration time-histories at the surface of the 9m column with (a) untreated sand, (b) treated sand, (c) untreated sand under fully drained conditions and (d) at the base of all columns subjected to Northridge excitation with a_{eff}=0.25g (intensity level λ).*

Moreover, amplification of the acceleration is observed at the top of the stabilized layer (as compared to the base acceleration), which however is less pronounced than the amplification taking place under fully drained conditions. It is thus clear that the response of the stabilized layer (case b) is intermediate between the response in cases (a) and (c). In addition it seems much more similar to the seismic response under full drainage at least in terms of accelerations. This fact becomes more obvious by observing the corresponding elastic response spectra of acceleration (with 5% damping ratio) which are presented in Figure 9.6. Particularly, the elastic spectrum at the surface of the untreated sand appears to be

significantly de-amplified in comparison with that at the base, implying that the untreated sand is liquefied, whilst the surface spectra of the treated and the untreated sand under fully drained conditions are considerably amplified, indicating a more stable response.

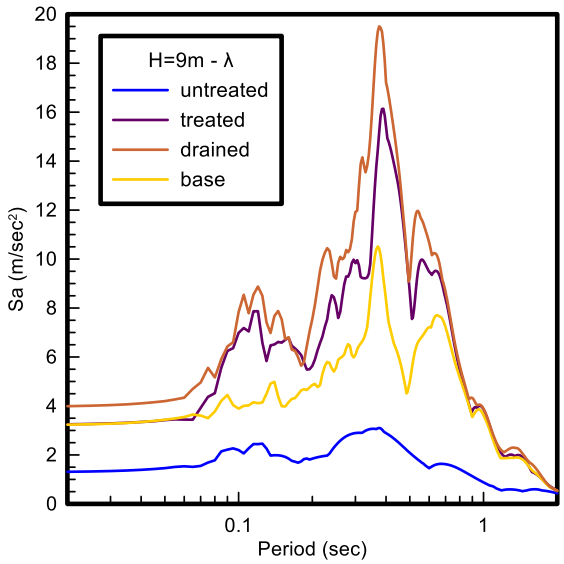

Figure 9.6 *Elastic response spectra (5% damping) at the base and at the surface of the 9m column with untreated sand, treated sand, untreated sand under fully drained conditions subjected to Northridge excitation with a_{eff}=0.25g (intensity level λ).*

In the following figures, the results of the numerical analyses are presented in terms of surface-to-base spectrum ratios, denoted hereafter as AS_a, which is used to emphasize on the effect of the soil layer on the elastic response spectrum, regardless of the excitation properties. This ratio is expressed by:

$$AS_a = \frac{S_{a,sur}}{S_{a,bas}} \tag{9.2}$$

Figure 9.7 shows the results of the analyses described before, but this time expressed in terms of AS_a for the three abovementioned cases (a), (b) and (c). it is observed that spectral ratios for T=0, denoted by A_α for brevity, the untreated layer under fully drained conditions, the treated layer and the untreated layer are equal to 1.2, 1.0 and 0.4 respectively, namely the peak ground acceleration of the untreated layer is intensely reduced, of the treated one remains practically unchanged and of the untreated layer under full drainage increases slightly. Moreover, in terms of the fundamental column periods, the stabilized sand column has T_s=0.47sec which is practically the same and only slightly increased if compared to this of the untreated layer under fully drained conditions (T_s=0.45sec). These results imply that stabilized sand seems to generate practically zero excess pore pressures, and its non-linear

response is very similar to that of soil under full drainage. On the contrary, in the case of the untreated sand, considerable excess pore pressures and liquefaction is implied in addition to intensely non-linear response, especially for base excitations of high intensity (a_{eff}=0.25g, intensity level λ).

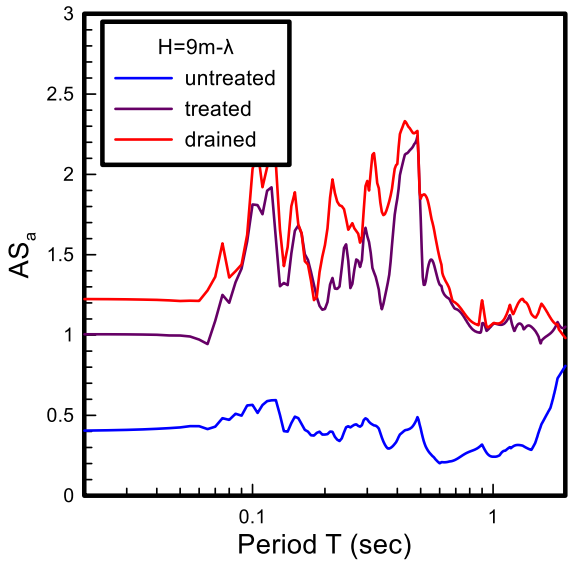

Figure 9.7 *Surface-to-base spectral ratios of the 9m column with untreated sand, treated sand, untreated sand under fully drained conditions, subjected to the Northridge excitation with a_{eff}=0.25g (intensity level λ).*

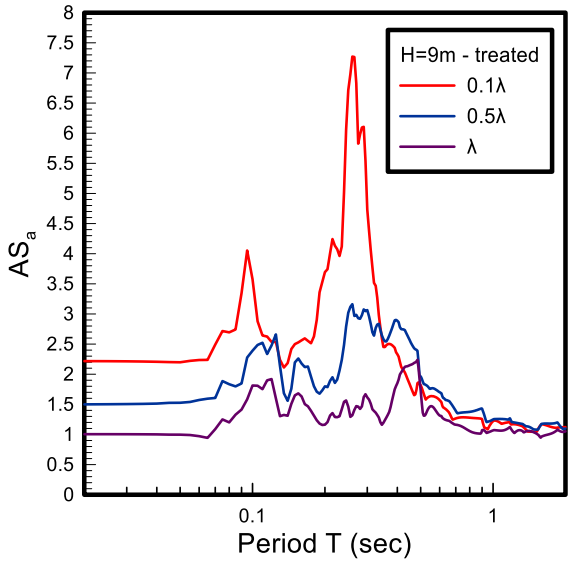

Figure 9.8 *Surface-to-base spectral ratios of the 9m column with treated sand subjected to the Northridge excitation with intensity levels equal to λ, 0.5λ, 0.1λ.*

The effect of the excitation intensity on the seismic response of stabilized sands was also studied, by altering the multiplying coefficient λ which sets the intensity level. Hence, Figure

9.8 shows the comparison of the surface-to-base spectral ratios AS_a for the 9m stabilized sand column subjected to the Northridge excitation with intensity levels equal to λ, 0.5λ and 0,1λ, which correspond to a_{eff}=0.25g, 0.125g and 0.025g respectively.

As it is obvious, the value of $AS_a(T=0)=A_\alpha$ decreases when the intensity of the excitation increases. More specifically, it takes the value of 2.2 for coefficient value equal to 0.1λ, a value of 1.5 for 0.5λ and a value of 1.0 for λ. This behavior can be explained by the fact that at lower intensity excitations the stabilized soil generates smaller excess pore pressures (even equal to zero for 0.1λ), as well as less intense nonlinearity, and as a result, its stiffness is not reduced. This conclusion is also confirmed by the decrease of the fundamental period of the 9m stabilized sand column from a value of T_s=0.47sec for λ to a value of T_s=0.33sec for 0.5λ and finally to a value of T_s=0.26sec for 0.1λ. Furthermore, a significant spectral amplification of the acceleration (for all periods T) at the surface of the stabilized layer with a decrease of the excitation intensity (a_{eff} or equivalently the percentage of λ) can also be observed, indicating the increasingly linear behavior of the stabilized soil.

It is also considered necessary to investigate the correlation between the seismic behavior of the treated sand and this of the untreated sand (with or without drainage) for a much lower excitation intensity, namely for 0.1λ which corresponds to a_{eff}=0.025g. Figure 9.9 refers to the Northridge excitation with an intensity level of 0.1λ, where the response of the treated sand layer and that of the untreated one under fully drained conditions are identical, exactly because zero excess pore pressures are generated in both cases. More specifically, the spectral ratio for T=0 ($AS_a(T=0)$) has a value of 2.2 for both the stabilized layer and the untreated layer under fully drained conditions, whereas for the untreated layer it takes a value of 1.4. Observe that even though the untreated sand does not liquefy at the low intensity excitation, its reduced stiffness can be clearly observed by the increased fundamental period of the 9m column of T_s=0.48sec, compared to that of the other two cases: T_s=0.26sec.

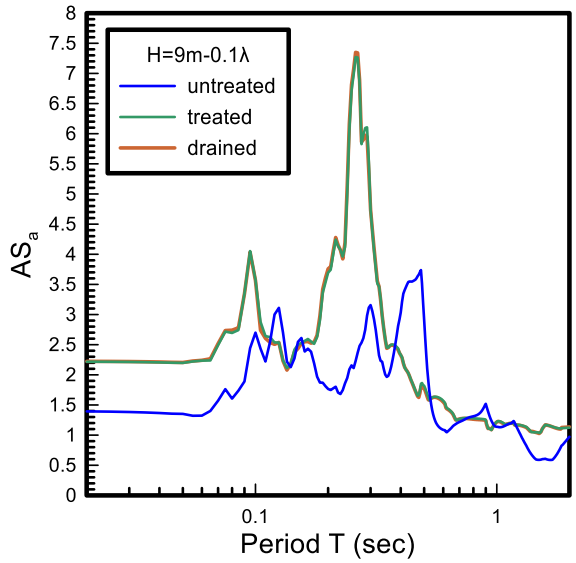

Figure 9.9 *Surface-to-base spectral ratios of the 9m column with untreated sand, treated sand, untreated sand under fully drained conditions subjected to the Northridge excitation with* a_{eff}*=0.025g (intensity level of 0.1λ).*

9.3 Effect of thickness of the stabilized soil layer

In order to investigate the effect of thickness of the stabilized layer on its seismic response, three fully treated sand columns of 3m, 6m and 9m thickness were examined. The selection of these particular thickness values was made with respect to cost efficiency, since the application of passive stabilization is considered too costly for thicker than 9m layers. The recording of the Northridge earthquake was imposed at the base of each column so the results can be compared with those presented in the previous paragraphs of this *Chapter*. These analyses were repeated for intensity levels λ and 0.1λ (a_{eff}=0.25g and 0.025g) in order to take into account the effect of seismic intensity, as well.

Figure 9.10 and 9.11 present the comparison of the seismic response of the three (3) soil profiles in terms of surface-to-base spectral ratio AS_a for the excitations with intensity levels λ and 0.1λ respectively. Although the picture is more complex in the case of the high intensity excitation (λ) due to intense non-linear response, in comparison with that of low intensity (0.1λ) where more linear response is observed, both figures lead to the general conclusion that the fundamental period T_s of stabilized layers increase with layer thickness, similarly to non-liquefiable layers.

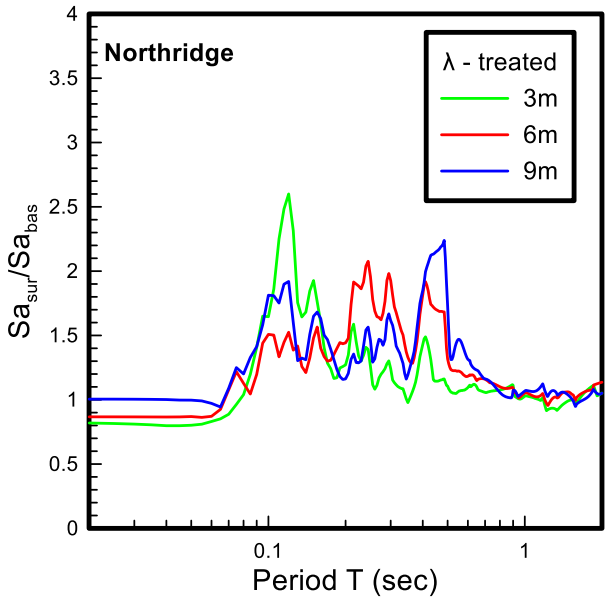

Figure 9.10 *Surface-to-base spectral ratios of fully treated sand layers of 3m, 6m, 9m thickness subjected to the Northridge excitation with a_{eff}=0.25g (intensity level λ).*

Table 9-3 presents the values of fundamental periods T_s for each case studied, where this distinction between the three layers is more notable for the strong shaking event (λ) because of the significant effect of non-linearity. Another conclusion that can be drawn from Figure 9.10 and Figure 9.11 is that the values of A_α increase with layer thickness, from the H_{tr}=3m up to 9m, regardless of intensity level. This conclusion cannot be generalized, as this behavior is expected only for low frequency excitations (like the Northridge one depicted in these figures). It should be clarified at this point, that for the high intensity excitation, these initial values of A_α are slightly smaller than unity (de-amplification), which indicates a reduction of the acceleration at the column surface with respect to the base due to intense non-linearity, contrary to the low intensity excitation which appears amplified at the surface (compared to the base).

Table 9-3 *Fundamental period T_s values of 3m, 6m and 9m –thick stabilized sand layers for excitations with intensity levels 0.1λ and λ.*

	T_s (sec)		
$H=H_{tr}$	3m	6m	9m
Excitation 0.1λ (a_{eff}=0.025g)	0.11	0.19	0.26
Excitation λ (a_{eff}=0.25g)	0.12	0.25	0.47

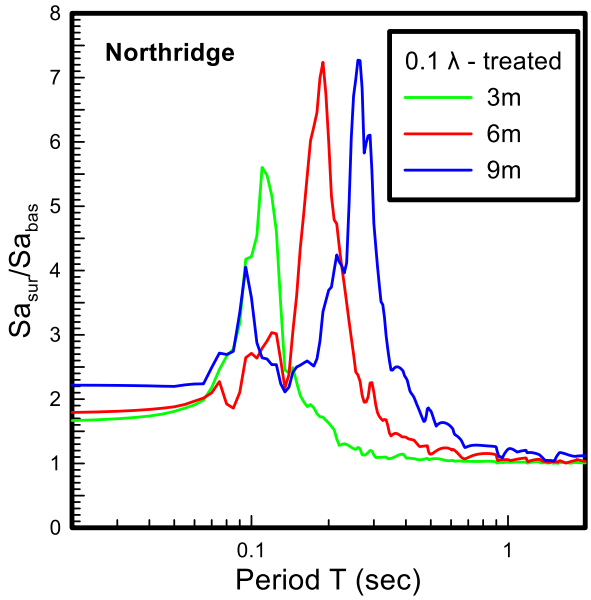

Figure 9.11 *Surface-to-base spectral ratios of fully treated sand layers at 3m, 6m, 9m thickness subjected to the Northridge excitation with a_{eff}=0.025g (intensity level 0.1λ).*

9.4 Effect of surficial (only) stabilization

As previously mentioned, passive stabilization of a thick soil layer is rather too costly. For this purpose, this paragraph studies the potential of surficial only stabilization of the 9m sand column used in previous analyses. More specifically, two cases are investigated: (a) 9m sand layer with the three (3) upper meters stabilized only, (b) 9m sand layer with the six (6) upper meters stabilized only. Stabilization of only the underlain layers has no practical meaning, since civil engineering structures cannot be founded on a liquefiable layer. Figure 9.12 presents the comparison of the results for the four different soil profiles, imposed to the Northridge excitation at the base of each column with intensity level λ (a_{eff}=0.25g). Note that besides the two cases of surficial only stabilization, this figure also includes the reference cases of H_{tr}=0 (untreated) and H_{tr}=9m (fully treated) sand layer. It can be observed that for the case of stabilization at the upper 3m, the partially stabilized column response approaches the response of the untreated layer, showing significant de-amplification of acceleration at the surface. However, for the case of stabilization at the upper 6m the response of the column is much more similar to that of the fully stabilized layer.

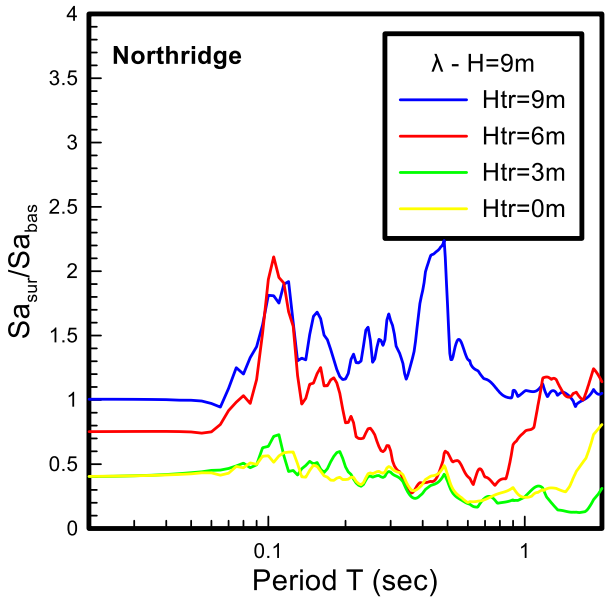

Figure 9.12 *Surface-to-base spectral ratios of a 9m sand column: fully treated (H_{tr}=9m), partially treated with the upper 6m stabilized (H_{tr}=6m), partially treated with the upper 3m stabilized (H_{tr}=3m) and untreated (H_{tr}=0m), subjected to the Northridge excitation with a_{eff}=0.25g (intensity level λ).*

The value of $AS_a(T=0)=A_\alpha$ increases as the stabilized layer thickness increases, with only exception the partial stabilization of the upper 3m, where the effects from stabilization are practically zero (at least for periods up to 1sec). More specifically, A_α has a value of 0.4 for the untreated layer and the partially treated layer at the upper 3m, the value of 0.75 for the partially treated layer at the upper 6m and the value of 1.0 for the fully treated column. From all the above, it can be deduced that only the case of fully stabilized sand layer does not present de-amplification of acceleration at the surface for this high intensity level λ. Moreover, in terms of surface-to-base spectral ratio, partial stabilization of the upper 6m seems to provide an intermediate amplification between that of full stabilization and the stabilization of the upper 3m.

However, stabilization of the upper 6m does not always lead to the above described seismic response. Figure 9.13 shows the comparison of the response of these same four (4) soil profiles for the Kefalonia excitation with an intensity level λ (a_{eff}=0.25g). The response of the layer with partial stabilization of the upper 6m approaches the response of the layer with partial stabilization of the upper 3m and the untreated column. This indicates that for this specific excitation, a surficial only stabilization (either of the upper 3m or 6m) does not essentially alter the vibration at the surface compared to the untreated layer (H_{tr}=0) and only the fully stabilized layer (H_{tr}=H) changes the vibration at the ground surface.

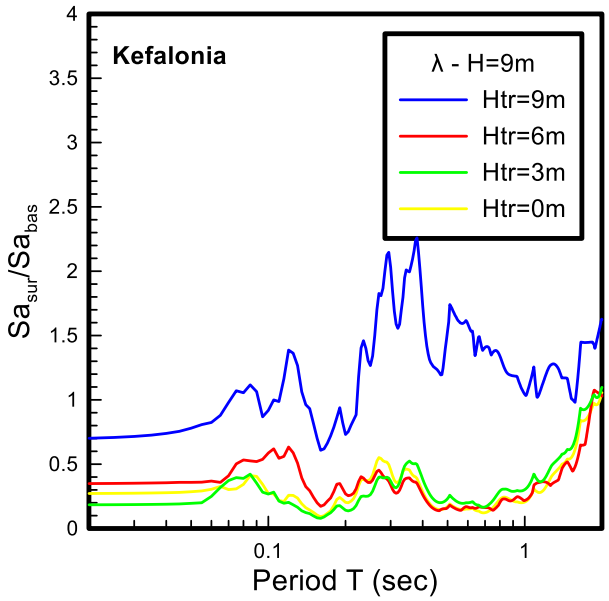

Figure 9.13 *Surface-to-base spectrum ratios of a 9m sand column: fully treated (H_{tr}=9m), partially treated with the 6 upper meters stabilized (H_{tr}=6m), partially treated with the 3 upper meters stabilized (H_{tr}=3m) and untreated (H_{tr}=0m), subjected to Kefalonia excitation with a_{eff}=0.25g.*

The reason for this differentiation in the effect of passive stabilization on ground vibration becomes evident in Figure 9.14 and Figure 9.15, which demonstrate the surface-to-base, surface-to-interface (between treated and untreated layers) and interface to base spectral ratios for these cases of surficial only stabilization for the two excitations respectively. In all cases, the underlain untreated layer develops large excess pore pressures and their dissipation becomes difficult because of the existence of a practically impermeable overlain stabilized layer. This possibly leads this underlain layer faster to liquefaction than in the case of a fully untreated layer. Observe that, the underlain liquefied layer is responsible for the significant de-amplification of acceleration from the base to the interface, while the stabilized layer leads to the amplification of acceleration from the interface to the surface. The final surface-to base spectral ratio results from the multiplication of these two spectral ratios and in the case of surficial only stabilization, the liquefied layer acts as a damper of the acceleration. It is interesting to note that as the thickness of the underlain liquefiable layer increases, the de-amplification of acceleration becomes more intense. Moreover, for the Northridge excitation, the de-amplification of the ground motion in the underlain untreated layers is less intense than that for the Kefalonia excitation and this explains the difference in the response of the case with the upper 6m stabilized for these two seismic events,

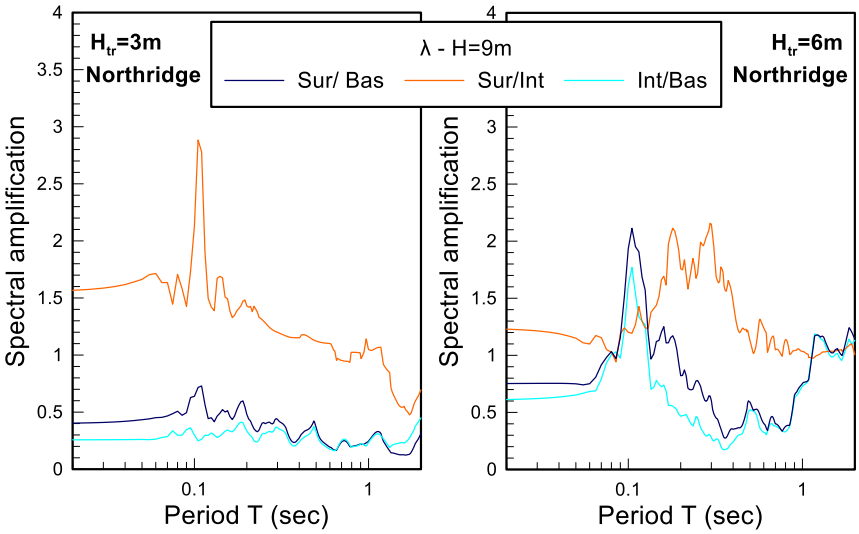

Figure 9.14 *Surface-to-base, surface-to-interface and interface-to-base spectral ratios of a 9m sand column: (a) partially treated with the upper 3m stabilized (H_{tr}=3m), (b) partially treated with the upper 6m stabilized (H_{tr}=6m), subjected to the Northridge excitation with a_{eff}=0.25g (excitation level λ).*

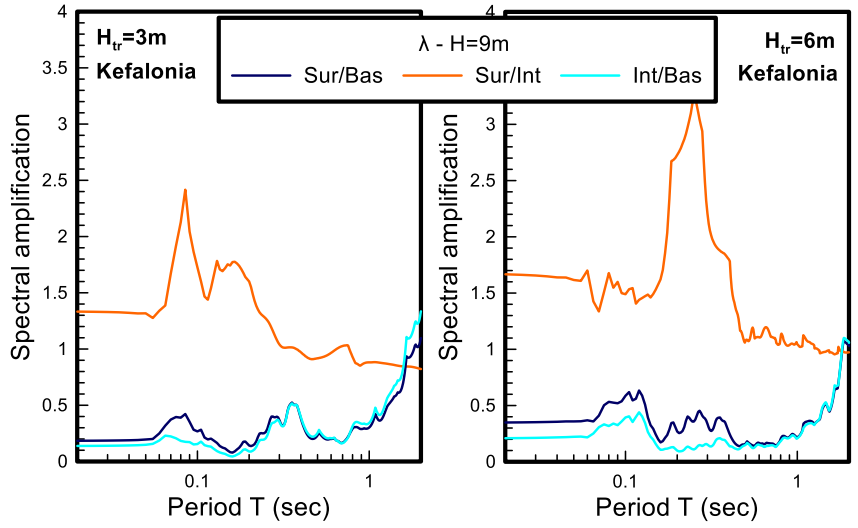

Figure 9.15 *Surface-to-base, surface-to-interface and interface-to-base spectral ratios of a 9m sand column: (a) partially treated with the upper 3m stabilized (H_{tr}=3m), (b) partially treated with the upper 6m stabilized (H_{tr}=6m), subjected to the Kefalonia excitation with a_{eff}=0.25g (excitation level λ).*

In order to further investigate the effect of intensity for a surficially only stabilized sand layer, an intensity level of 0.1λ (a_{eff}=0.025g) was studied for the Northridge excitation. From Figure 9.16 one can observe, that in terms of surface-to-base spectral ratio AS_a, the acceleration at the surface is amplified compared to the base for all four (4) soil profiles. Particularly, the untreated soil does not seem to liquefy due to the low intensity excitation and generally shows similar spectral amplification with the partially stabilized soil at the upper 3m. Non-linearities

due to high excitation intensity are eliminated and especially in the case of 6m surficial only stabilization and full stabilization behavior seems to be more linear hence leading to amplification of the motion. Figure 9.17 presents the surface-to-base spectral ratio AS_a, for both cases of partial stabilization for 0.1λ intensity level. Similarly with the case of the excitation with intensity level λ, the interface-to-base spectral ratio, which refers to the underlain untreated soil layer is the one that defines the final value of AS_a ratio, but this time there is no amplification of the motion, since the underlain untreated soil layer does not liquefy. In any case, the results in terms of the effect of H_{tr} thickness are qualitatively similar with those related to the Northridge excitation, but an intensity level of λ. The differentiation was more intense when the characteristics of the excitation changed from Northridge to Kefalonia excitation.

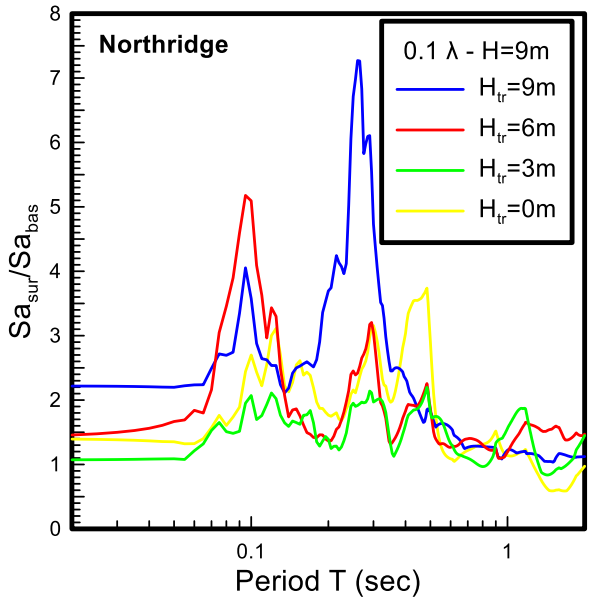

Figure 9.16 *Surface-to-base spectral ratios of a 9m sand column: fully treated (H_{tr}=9m), partially treated with the upper 6m stabilized (H_{tr}=6m), partially treated with the upper 3m stabilized (H_{tr}=3m) and untreated (H_{tr}=0m), subjected to the Northridge excitation with a_{eff}=0.025g (intensity level 0.1λ).*

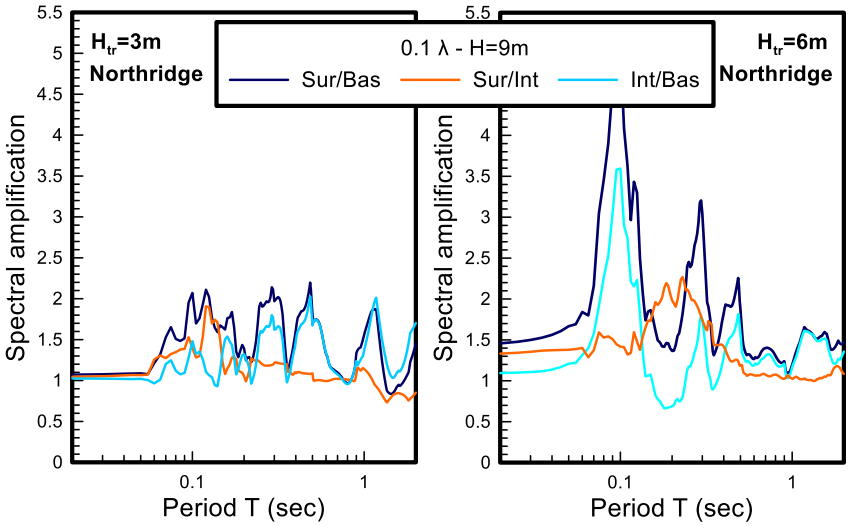

Figure 9.17 *Surface-to-base, surface-to-interface and interface-to-base spectral ratios of a 9m sand column: (a) partially treated with the upper 3m stabilized (H_{tr}=3m), (b) partially treated with the upper 6m stabilized (H_{tr}=6m), subjected to the Northridge excitation with a_{eff}=0.025g (intensity level 0.1λ).*

Finally, in Figure 9.18 and Figure 9.19 the spectral ratios for different excitation intensities are compared, which were imposed either directly at the base of the column of H=H_{tr}=3m or H=H_{tr}=6m (AS_a) respectively or resulted from the analyses of surficial only treated soil as the surface-to-interface spectral ratio of a treated over untreated layer profile. More specifically, the surface-to-base spectral ratios (AS_a) for the fully stabilized layers of 3m and 6m thickness with excitation intensity levels λ and 0.1λ are included, as well as the surface-to-interface spectral ratios of the H_{tr}=3m (in Figure 9.18) and H_{tr}=6m (in Figure 9.19) where the interface intensity is a percentage of λ between 0.1λ and λ.

Particularly, in Figure 9.18 the 0.26λ intensity stems from surficial stabilized layer (H_{tr}=3m) analysis with a base excitation of intensity λ, whereas the 0.103λ results from the analysis with a base excitation of intensity 0.1λ. Similarly, for H_{tr}=6m (Figure 9.19) the interface coefficients 0.61λ and 0.11λ result from base excitations with intensities λ and 0.1λ, respectively. These figures indicate that for base excitation of 0.1λ and H=H_{tr} the resulting spectral amplification AS_a is a conservative upper limit of spectral amplification (AS_a), regardless of whether there is an underlain untreated layer or not. However, the corresponding spectral amplification AS_a for H=H_{tr} and intensity λ is almost the lower limit of AS_a, again regardless of whether there is an underlain liquefied layer or not (for base intensities from 0.1λ to λ).

This can be explained by the fact that the case for the H=H_{tr}, implies a rigid bedrock which leads to zero radiation damping, in contrast to the case where there is an underlain soil layer.

Hence, as a first approximation, the emphasis may be given to cases where $H=H_{tr}$, and the resulting estimation of AS_a will be conservative for the cases that have an underlaying layer.

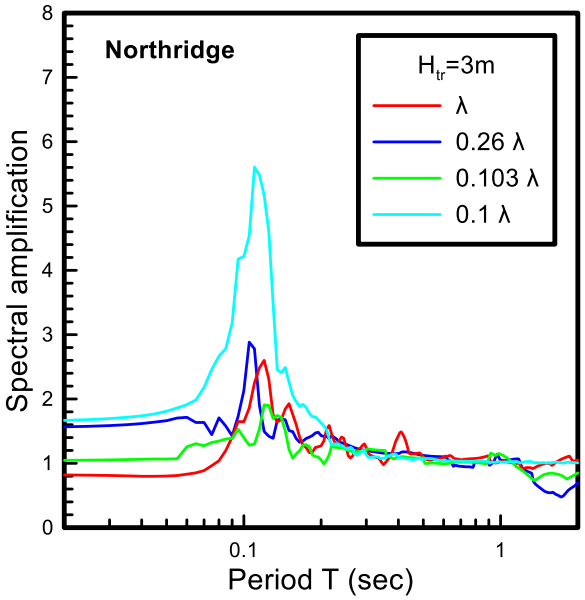

Figure 9.18 *Surface-to-base spectral ratios of a fully treated (H_{tr}=3m) sand column subjected to the Northridge excitation with excitation levels λ and 0.1λ, and of the same layer with underlain untreated layer with interface excitation intensities 0.26λ and 0.103λ.*

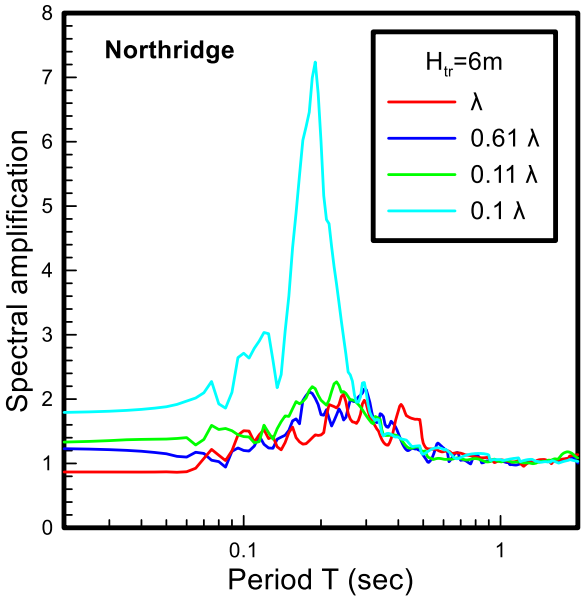

Figure 9.19 *Surface-to-base spectral ratios of a fully treated (H_{tr}=6m) sand column subjected to the Northridge excitation with excitation levels λ and 0.1λ, and of the same layer with underlain untreated layer with interface excitation intensities 0.61λ and 0.11λ.*

9.5 Average spectral amplification of stabilized soils

In the previous *Chapters*, the typical response of stabilized sands was presented, emphasizing only on the low frequency Northridge excitation for reasons of brevity. However, generalization of these results is difficult and in order to do so, all employed excitations should be studied. Table 9-1 shows that the properties of these excitations (predominant period T_e, maximum acceleration PGA, earthquake magnitude M) have a wide range as a whole which is expected to lead to a significant scatter of the seismic ground response. However, by estimating the average spectral amplifications from all excitations, the compatibility of the average response with the "typical" Northridge excitation can be studied. Figures 9.20 – 9.24 present the surface-to-base spectral ratios AS_a of the 11 excitations for all cases tested, along with their average curve. All these curves are also compared to the corresponding elastic design spectral ratios proposed by EC8 for ground categories B, C, D and E when compared to the spectrum of ground category A (for rock) for high earthquake magnitudes (M>5.5). A general conclusion that can be drawn from Figure 9.20 is that the spectral amplification of stabilized sands for low intensity excitations (0.1λ) is larger than what results from EC8 (especially for periods T<0.6sec) as expected since 0.1λ is a quite low intensity level,that may be related possibly to M<5.5 events. On the contrary, the corresponding spectral amplification for high intensity excitations (λ) is lower than this resulting from EC8 for all periods T (Figure 9.21) but this was not expected since λ is an intensity level that is typical for M>5.5 events. Figure 9.22 indicates that if an untreated layer exists, then spectral amplification converts to de-amplification if the intensity is high (λ, a_{eff}=0.25g), while for low intensity excitations (0.1λ, a_{eff}=0.025g) the amplification is generally comparable with this suggested by EC8 spectra (Figure 9.23).

Finally, Figure 9.24 presents reference case analyses related to fully drained conditions (a, b), as well as intermediate intensity 0.5λ analyses for comparison with lower 0.1λ and higher λ intensities. Moreover, this figure indicates that for fully drained conditions the spectral amplification for high intensity λ excitation is compatible with this from EC8, whereas for low intensity 0.1λ excitations is expectedly higher than what EC8 proposes. Finally, the same figure also shows that for medium intensity 0.5λ excitations the spectral amplification at thick stabilized soil layers (H_{tr}=9m) is compatible with EC8 provisions, as opposed to low intensity excitations (0.1λ, Figure 9.20) and high intensity excitations (λ, Figure 9.21) where the EC8 seems to be non-conservative and conservative, respectively.

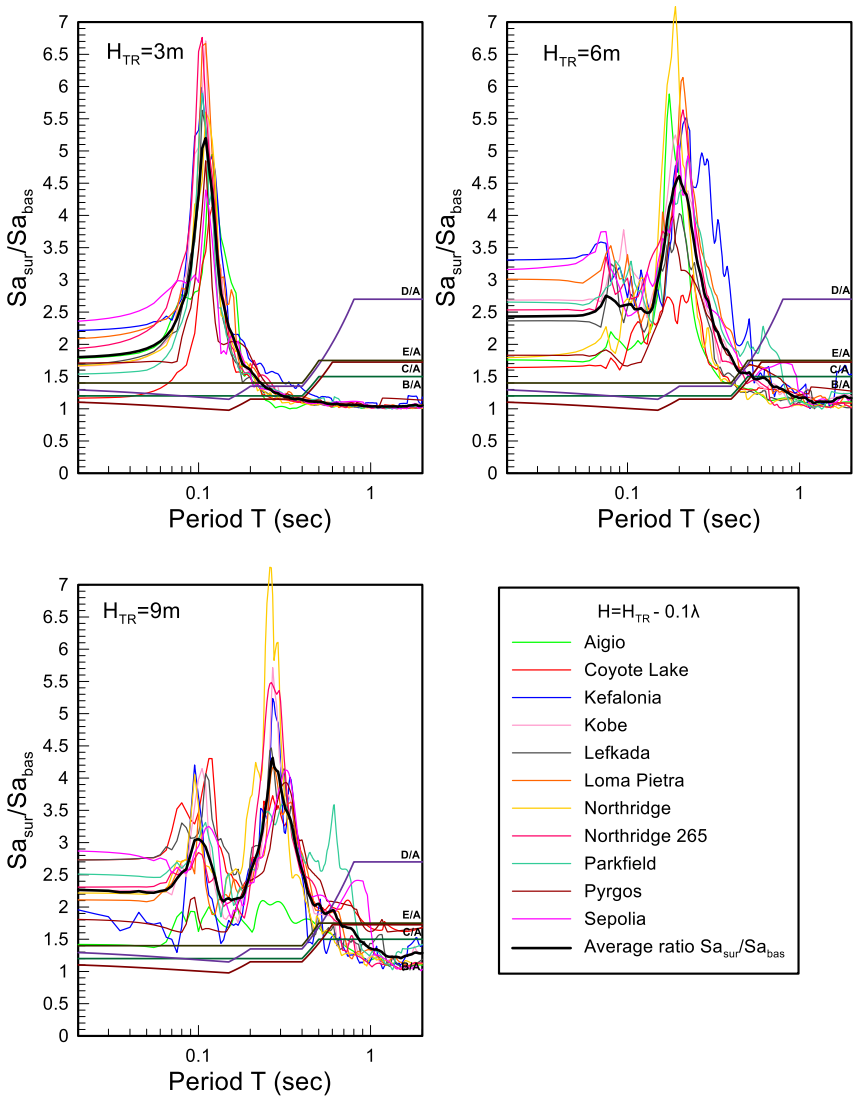

Figure 9.20 *Surface-to-base spectral ratios for all excitations with intensity 0.1λ (a_{eff}=0.025g) for fully stabilized columns with H=H_{tr}=9m, H=H_{tr}=6m, H=H_{tr}=3m in comparison with the corresponding average spectral ratios and the design spectral amplification of EC8 (M>5.5).*

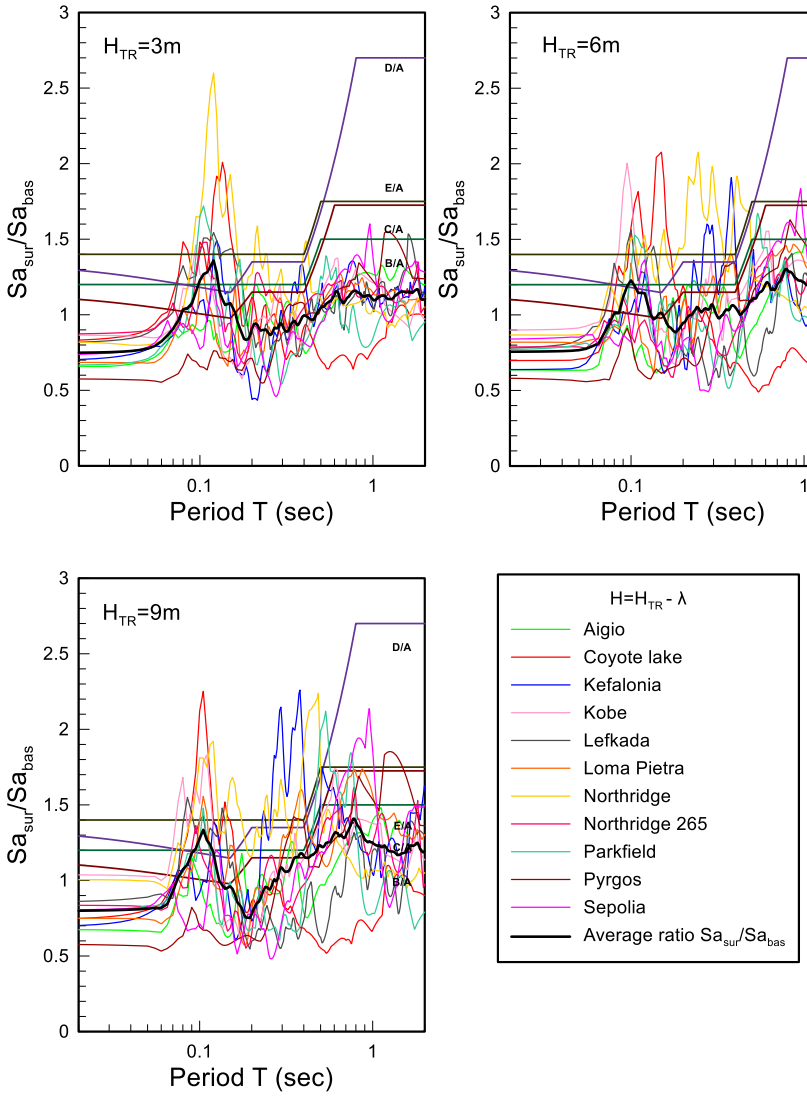

Figure 9.21 *Surface-to-base spectral ratios for all excitations with intensity λ (a_{eff}=0.25g) for fully stabilized columns with H=H_{tr}=9m, H=H_{tr}=6m, H=H_{tr}=3m in comparison with the corresponding average spectral ratios and the design spectral amplification of EC8 (M>5.5).*

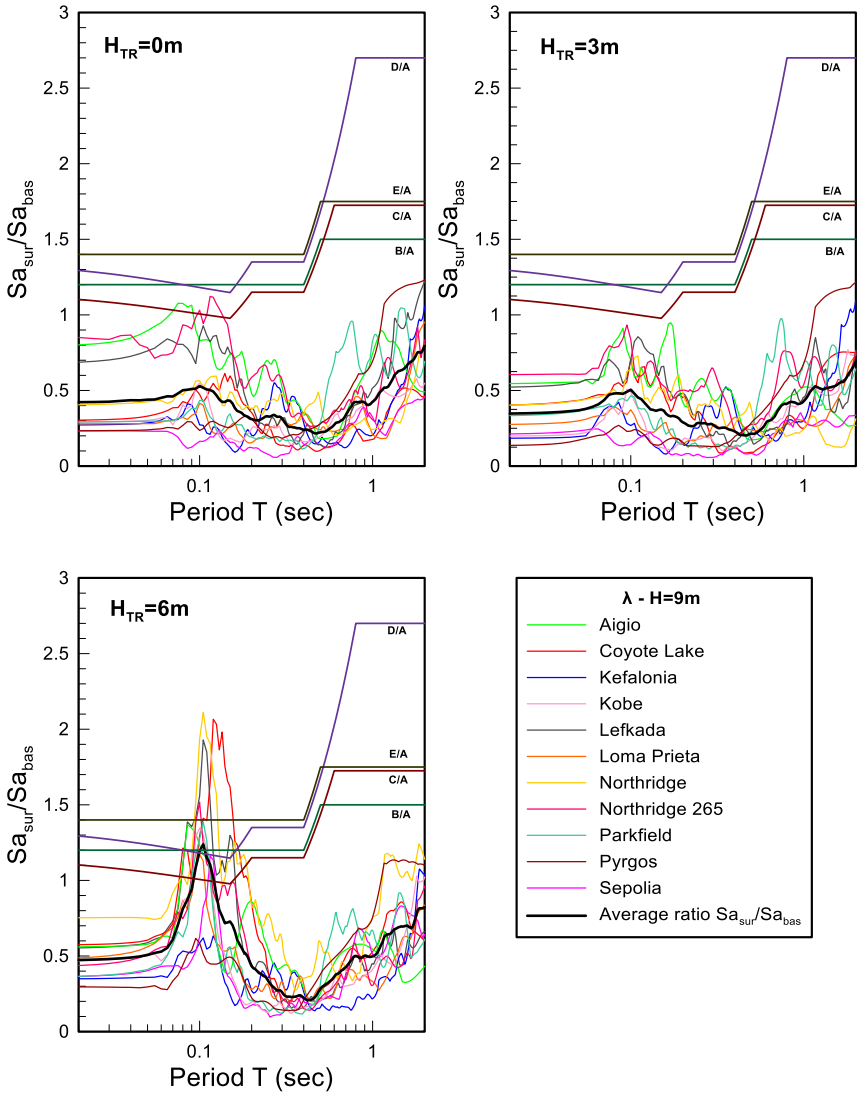

Figure 9.22 *Surface-to-base spectral ratios for all excitations with intensity λ (a_{eff}=0.25g) for a fully stabilized column with H=H_{tr}=9m and surficially only stabilized columns with H=9m and H_{tr}=6m, H=9m and H_{tr}=3m in comparison with the corresponding average spectral ratios and the design spectral amplification of EC8 (M>5.5).*

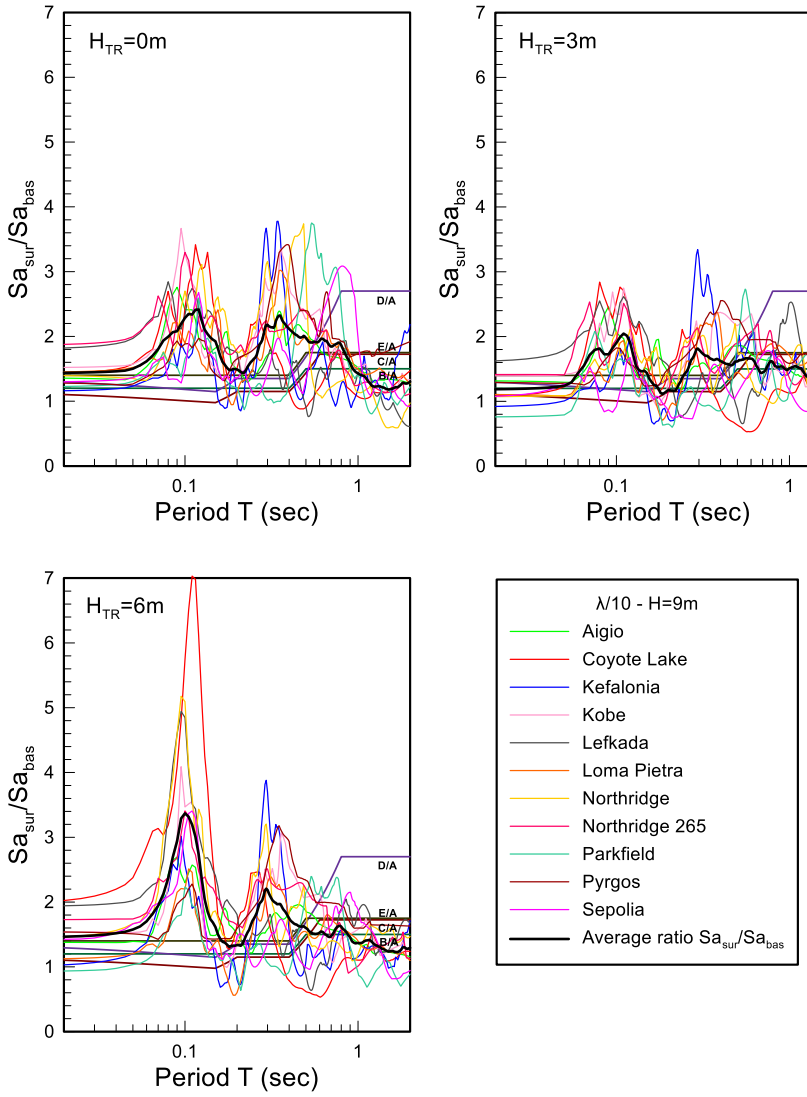

Figure 9.23 *Surface-to-base spectral ratios for all excitations with intensity 0.1λ (a_{eff}=0.025g) for a fully stabilized column with H=H_{tr}=9m and surficially only stabilized columns with H=9m and H_{tr}=6m, H=9m and H_{tr}=3m in comparison with the corresponding average spectral ratios and the design spectral amplification of EC8 (M>5.5).*

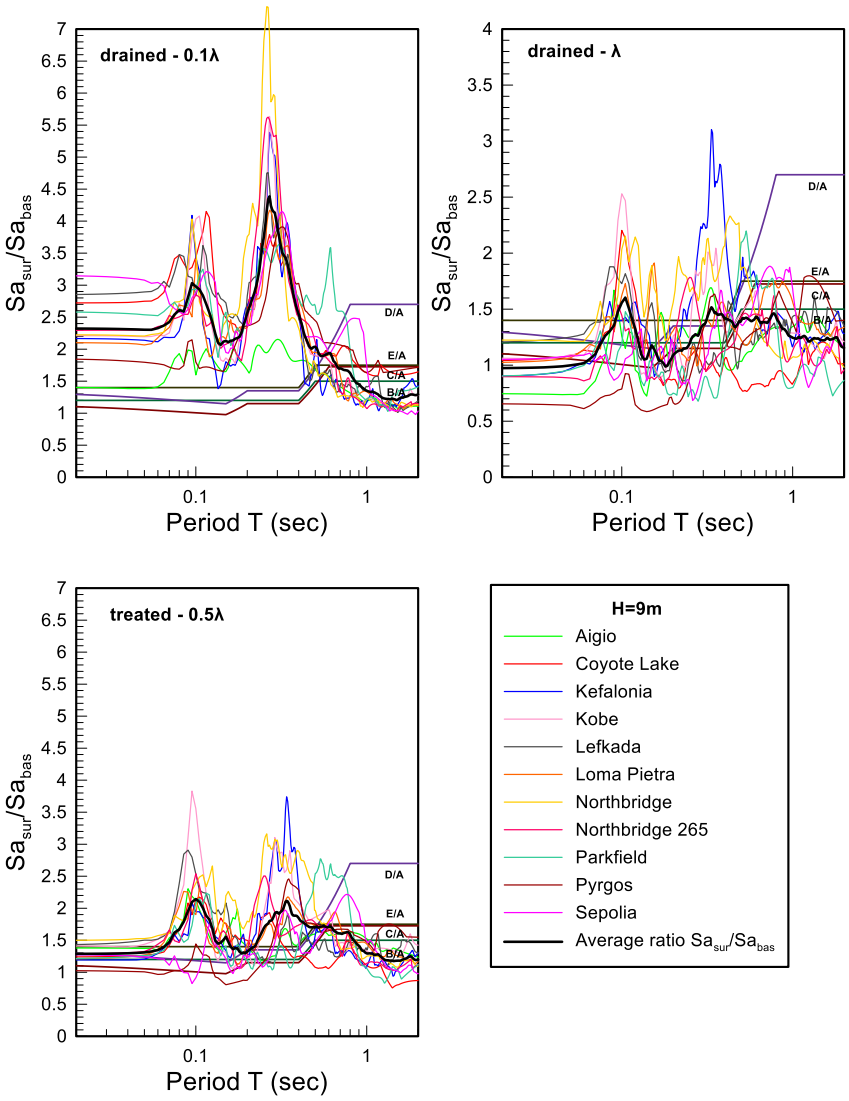

Figure 9.24 *Surface-to-base spectral ratios for all excitations: (a) for a 9m untreated column under fully drained conditions with intensity 0.1λ (a_{eff}=0.025g) and (b) λ (a_{eff}=0.25g), and (c) for a stabilized column with H=H_{tr}=9m with intensity 0.5λ in comparison with the average spectral ratios and the design spectral amplification of EC8 (M>5.5).*

In the sequel, the average spectral amplification curves of the above figures were also used in order to further investigate the effect of excitation intensity, drainage conditions, thicknesses of the stabilized layer, as in the typical case of the Northridge excitation. Figure 9.25 and Figure 9.26 which refer to the average curves of all 11 excitations lead to similar conclusions with the Northridge excitation in terms of average elastic surface spectra S_a and average spectral ratios AS_a respectively. More specifically, the fundamental period T_s of the stabilized layer remains almost the same and even slightly higher than this of the untreated soil under fully drained conditions for high intensity λ excitations. In general, the beneficial effect of stabilization is clearly observed as the stabilized soil retains its stiffness, and its response approaches that of

the untreated sand under fully drained conditions and is widely different from the response of the untreated sand (under realistic partially drained conditions) which shows significant de-amplification of the motion, due to liquefaction.

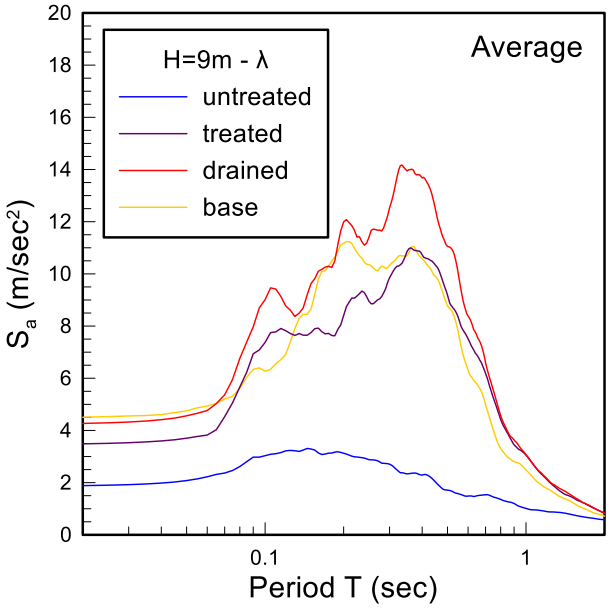

Figure 9.25 *Average surface elastic response spectra for the 11 excitations with intensity λ (a_{eff}=0.25g) of a 9m column with untreated, treated and untreated with fully drained conditions sand in comparison with the average spectrum at the base of the column.*

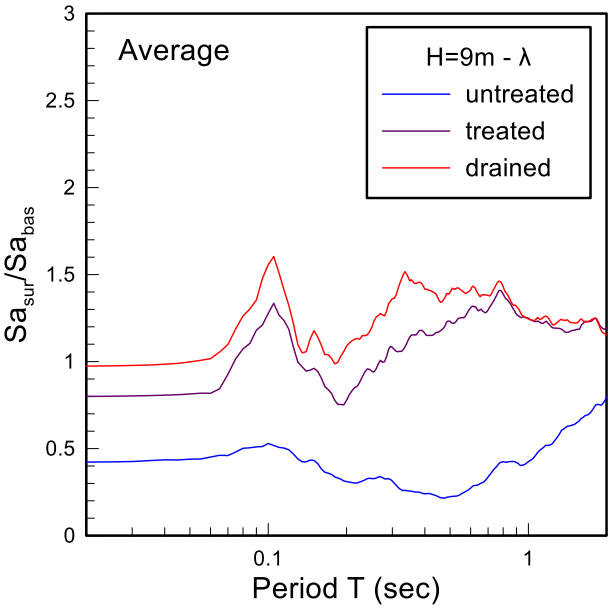

Figure 9.26 *Average surface-to-base spectral ratios for the 11 excitations with intensity λ (a_{eff}=0.25g) of a 9m column with untreated, treated and untreated under with drained conditions sand.*

The effect of intensity on the response of a stabilized $H=H_{tr}=9m$ layer is presented in Figure 9.27. It is observed that as the excitation intensity increases, the non-linearity of the geomaterial increases leading to slightly increased fundamental period T_s of the sand column along with clearly decreased amplification spectral ratios (for all T values).

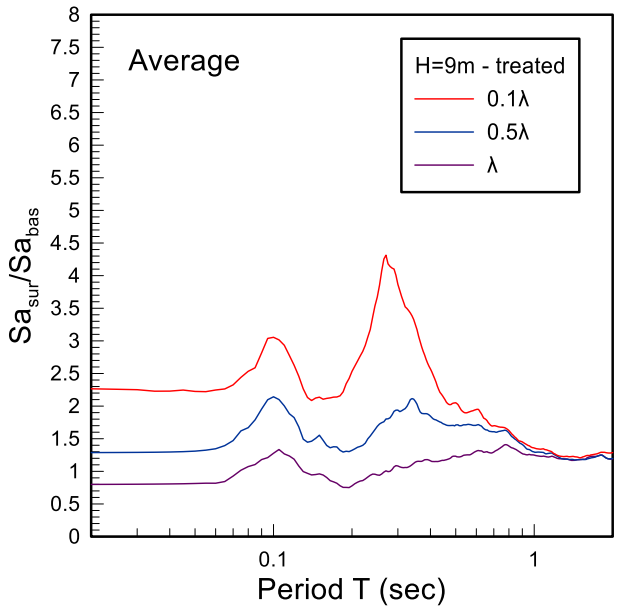

Figure 9.27 *Average surface-to-base spectral ratios for the 11 excitations with intensity of λ (a_{eff}=0.25g), 0.5λ (a_{eff}=0.125g) and 0.1λ (a_{eff}=0.025g) for a fully stabilized 9m sand column.*

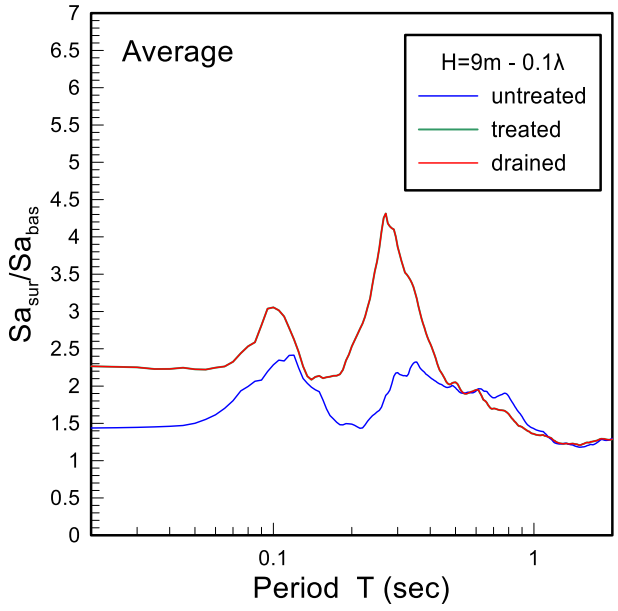

Figure 9.28 *Average surface-to-base spectral ratios for the 11 excitations with intensity of 0.1λ (aeff=0.025g) of a 9m column with untreated, stabilized and untreated under fully drained conditions soil.*

Moreover, for the low intensity excitation (0.1λ) the average response of the stabilized sand coincides with the response of that of the untreated soil under full drainage, just like in the case of the Northridge excitation. This can be explained by the fact that due to the low intensity of the excitation, the stabilized soil generates zero excess pore pressures exactly like the fully drained column. Moreover, the untreated soil does not liquefy hence slight amplification with respect to the base are observed.

The effect of thickness of the stabilization layer under low intensity excitation (0.1λ) is shown in Figure 9.29. An obvious increase of the fundamental period T_s is observed as the thickness of the stabilized layer increases. However, for a high intensity excitation (λ), Figure 9.30, the average spectral ratio for the stabilized layers of 3m, 6m and 9m thickness show negligible differences, but all of them show the expected de-amplification of the ground motion at the ground surface. More specifically, the effect of excitation intensity (and the ensuing nonlinearity) seems to overshadow the effect of the stabilized layer thickness H_{tr} resulting to negligible differences of the average spectral amplification for these cases.

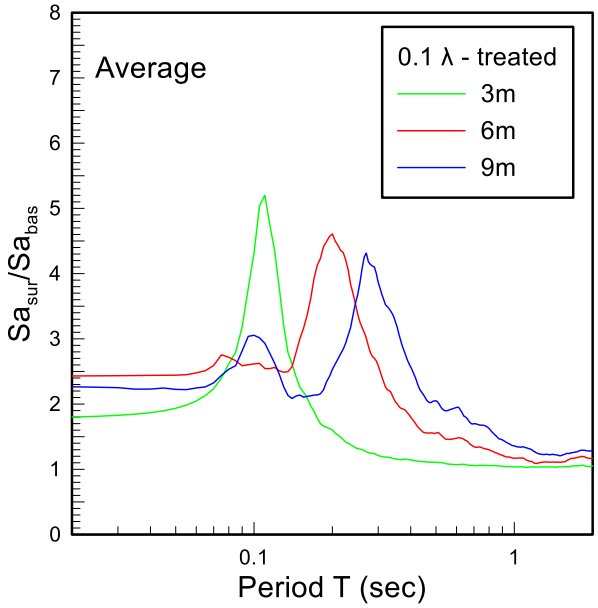

Figure 9.29 *Average surface-to-base spectral ratios for the 11 excitations with intensity of 0.1λ (aeff=0.025g) of fully treated columns with H=H_{tr}=9m, H=H_{tr}=6m and H=H_{tr}=3m.*

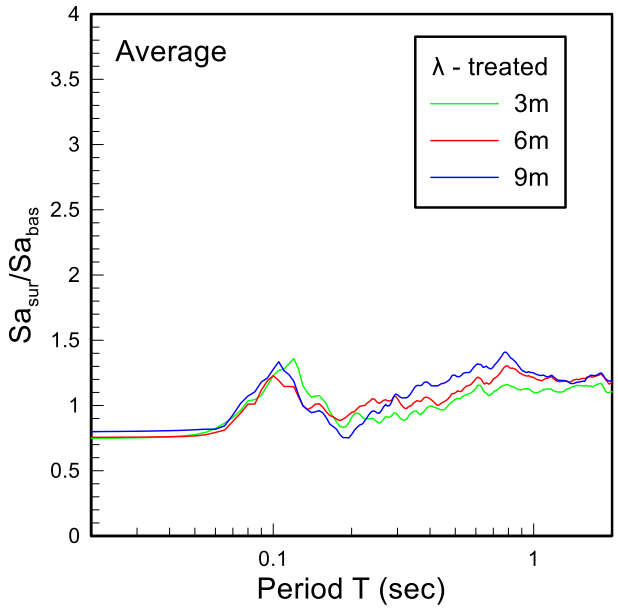

Figure 9.30 *Average surface-to-base spectral ratios for the 11 excitations with intensity of λ (aeff=0.25g) of fully treated columns with H=H$_{tr}$=9m, H=H$_{tr}$=6m and H=H$_{tr}$=3m.*

The average surface-to-base spectral ratios for the untreated (H$_{tr}$=0), fully stabilized and partially stabilized (H$_{tr}$=3m, 6m) soil columns are compared in Figure 9.31 and Figure 9.33 for excitations with intensity levels of λ and 0.1λ, respectively. It is observed that in terms of average spectral amplification, the response of the "thin" partially stabilized column (H$_{tr}$=3m) resembles the response of the untreated layer (H$_{tr}$=0m), while the response of the "thick" partially stabilized column (H$_{tr}$=6m) resembles the response of the fully stabilized column (H$_{tr}$=9m). Apparently, for the low intensity excitation (0.1λ) the differences between the abovementioned cases are smaller, but again the maximum amplification is observed for H$_{tr}$=9m. The corresponding average surface-to-base spectral ratios of the partially stabilized columns using the individual interface-to-base and surface-to-interface spectral ratios for excitation intensities of λ and 0.1λ are shown in Figure 9.32 and Figure 9.34 respectively.

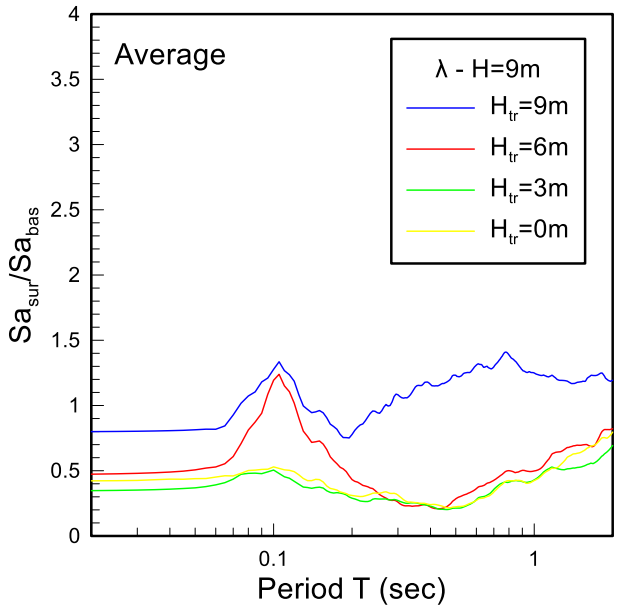

Figure 9.31 *Average surface-to-base spectral ratios for: a fully stabilized column with $H=H_{tr}=9m$, partially stabilized columns with $H=9m$ and $H_{tr}=6m$, $H=9m$ and $H_{tr}=3m$ and for an untreated column under excitation with intensity λ ($a_{eff}=0.25g$).*

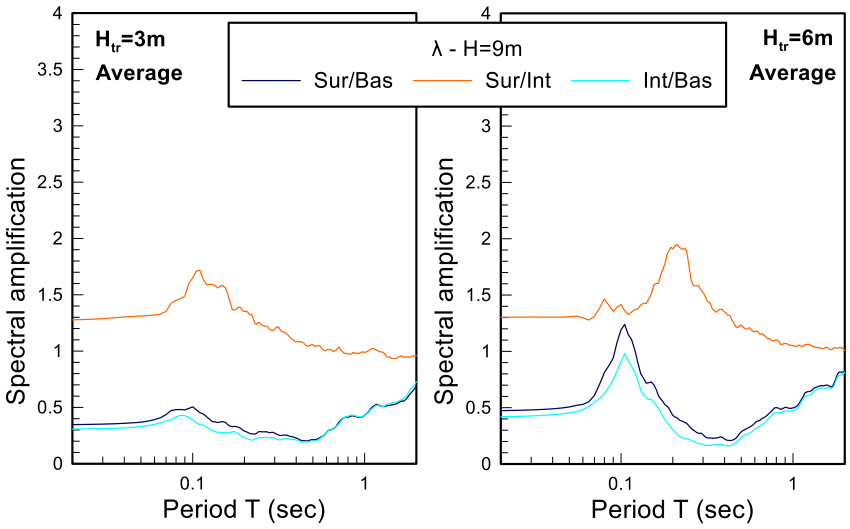

Figure 9.32 *Average surface-to-base, surface-to-interface and interface-to-base spectral ratios of a 9m sand column: (a) partially stabilized with the upper 3m stabilized ($H_{tr}=3m$), (b) partially stabilized with the upper 6m stabilized ($H_{tr}=6m$), subjected to excitation with intensity λ ($a_{eff}=0.25g$).*

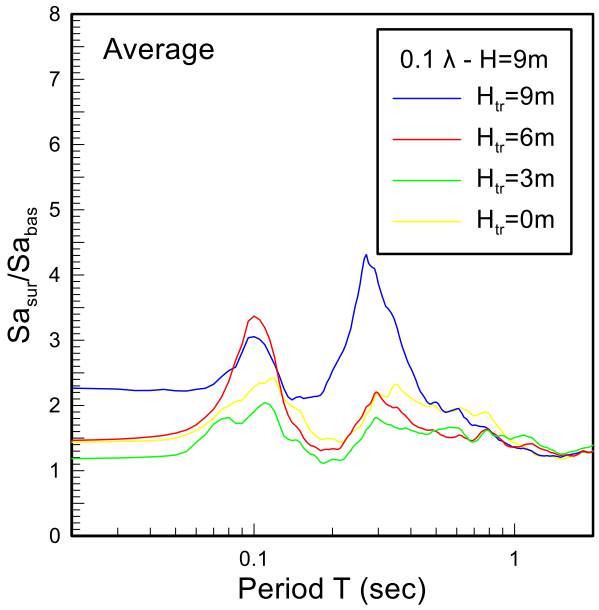

Figure 9.33 *Average surface-to-base spectral ratios for: a fully stabilized column with H=H_{tr}=9m, partially stabilized columns with H=9m and H_{tr}=6m, H=9m and H_{tr}=3m and for an untreated column under excitation with intensity 0.1λ (a_{eff}=0.025g).*

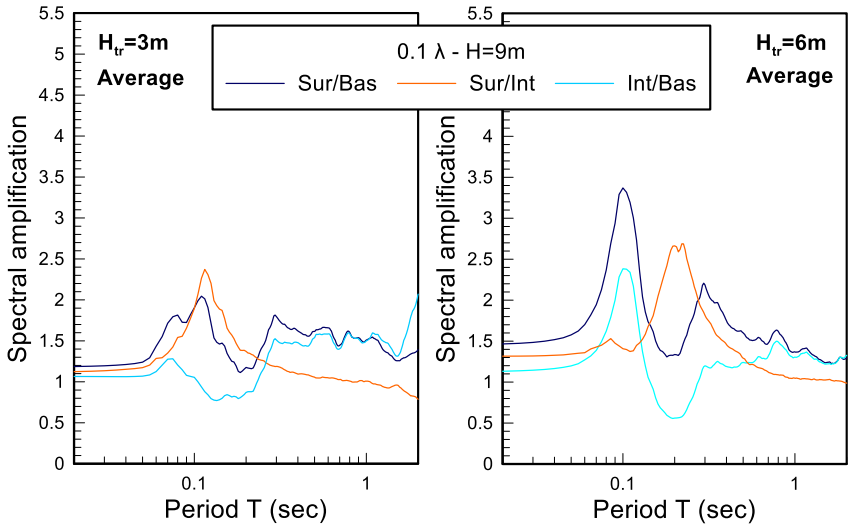

Figure 9.34 *Average surface-to-base, surface-to-interface and interface-to-base spectral ratios of a 9m sand column: (a) partially stabilized with the upper 3m stabilized (H_{tr}=3m), (b) partially stabilized with the upper 6m stabilized (H_{tr}=6m), subjected to excitation with intensity of 0.1λ (a_{eff}=0.025g).*

Consequently, the existence of a "thin" surficial stabilized layer of 3m does not seem to affect the vibration at the ground surface, which is governed by the occurrence of liquefaction (or not) at the underlain untreated layer. This conclusion remains, more or less, valid even if the surficial stabilized layer thickness increases from H_{tr}=3m to H_{tr}=6m.

Finally, Figure 9.35 and Figure 9.36 present the average surface-to-base spectral ratios for the fully stabilized columns of 3m and 6m thickness and for intensity excitations of λ and 0.1λ along with the related surface-to-interface spectral ratios for partially stabilized columns denoted by the excitation intensity which corresponds to the interface with the underlain untreated layer. More specifically, for H_{tr}=3m the average intensity level at the interface is estimated equal to 0.31λ for base excitation of intensity λ and equal to 0.11λ for base excitation of intensity 0.1λ respectively. Similarly, for H_{tr}=6m, the corresponding average intensity levels were equal to 0.42λ and 0.11λ at the interface with the underlain untreated layers. Thus, it is observed that the average spectral ratios for the fully stabilized columns under both the high and low intensity excitations (λ and 0.1λ) are the absolute lower and upper limits respectively for the surface-to-interface spectral ratios of layers with the same thickness in the cases of surficial only stabilization.

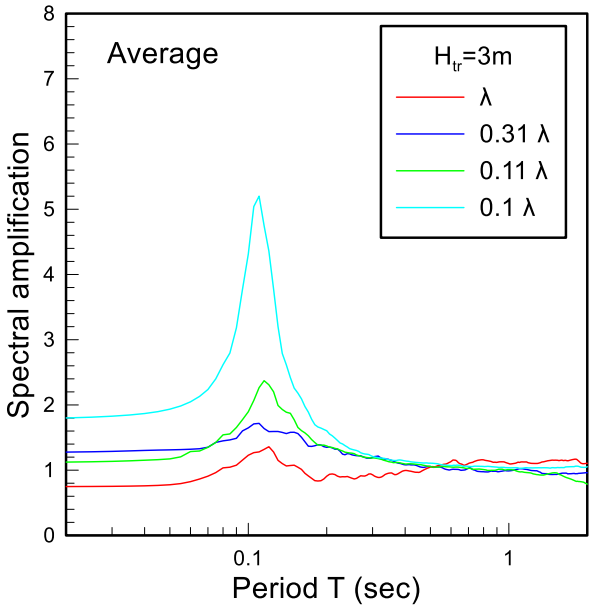

Figure 9.35 *Average surface-to-base spectral ratios of a 3m sand column fully stabilized (H=H_{tr}=3m) subjected to excitation intensities λ and 0.1λ, and of the same layer with underlain untreated layer with interface excitation intensities 0.31λ and 0.11λ.*

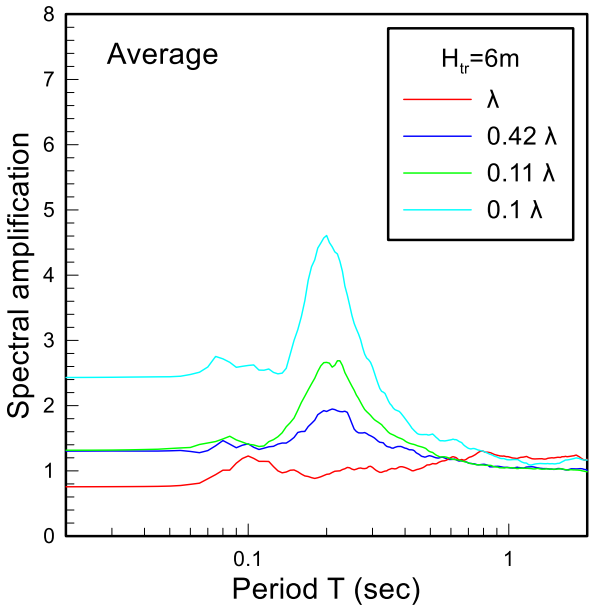

Figure 9.36 *Average surface-to-base spectral ratios of a 6m sand column fully stabilized ($H=H_{tr}=6m$) subjected to excitation intensities λ and 0.1λ, and of the same layer with underlain untreated layer with interface excitation intensities 0.42λ and 0.11λ.*

9.6 Multi-variable relations for the estimation of spectral amplification of stabilized soils

Based on the results presented in previous paragraphs, the seismic response of stabilized soil layers with H_{tr}=3m, 6m and 9m has similar qualitative characteristics with the response of stable, natural layers. However, there are some quantitative differences. In addition, based on the previous findings, the predictions which refer to fully stabilized layers with H_{tr}=3m and 6m may offer useful guidance for estimating the response of such layers even when an underlain layer exists, regardless of whether it is liquefiable or not. Hence, by emphasizing on the predictions for fully stabilized soil layers, multi-variable relations are proposed herein for estimating the spectral amplification ratio AS_a. The general form of the spectral ratio AS_a can be expressed using three parameters: the fundamental soil period T_s, the amplification of peak ground acceleration $A_a=A_{Sa}(T=0)$ and the peak spectral acceleration $A_{sap}=A_{Sa}(T=Ts)$. These parameters are indicatively defined in Figure 9.37(a) for the Loma Prieta excitation, along with an analytical prediction originating from the pertinent suggestion by Bouckovalas & Papadimitriou (2003) for stable natural layers. Particularly, this relation uses the normalized over A_α parameters: A_{Sa}*, A_{Sap}* which are defined in Figure 9.37(b) for the same excitation. This relation is expressed by Eq.(9.3) and refers to stable natural soils but will be generalized to stabilized soils herein.

$$A^{*}_{Sa} = \frac{1+\frac{1}{A_a}\left(\frac{T}{T_s}\right)}{\sqrt{\left(1-\left(\frac{T}{T_s}\right)^2\right)^2+\left(\frac{1+\frac{1}{A_a}}{A^{*}_{Sap}}\left(\frac{T}{T_s}\right)\right)^2}} \quad (9.3a)$$

$$\text{with } A^{*}_{Sap} = \frac{AS_{ap}}{A_\alpha} \quad (9.3b)$$

Based on Eq.(9.3),the estimation of AS_a for any given structural period T, requires first the definition of T_s, A_α and A_{Sap}^{*}. Hence, an effort was made to devise multivariable relations for estimating these 3 parameters.

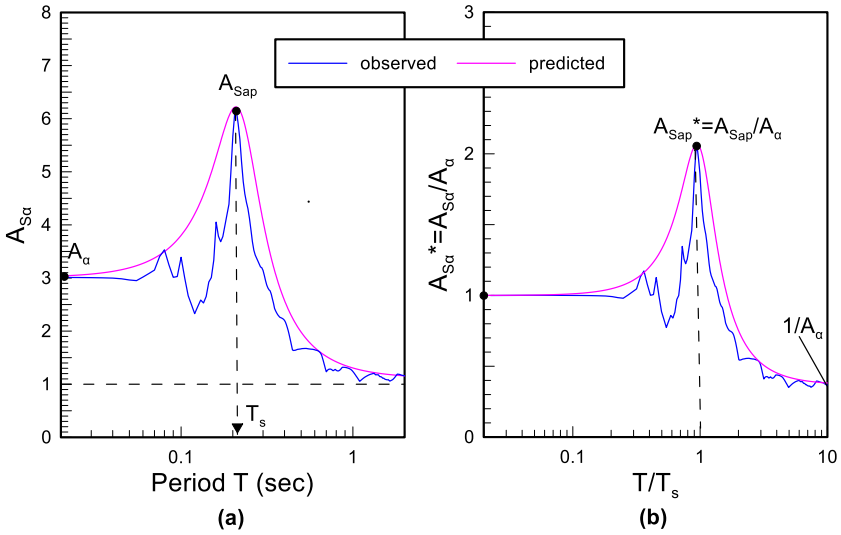

Figure 9.37 *(a)Typical surface-to-base spectrum ratio of a fully treated sand layer (observed) and approximate relation which simulates it (predicted), (b)Typical behavior of the normalized surface-to-base spectrum ratio (to A_α and T_s) A_{Sa}^{*} of a fully treated soil layer (observed) and approximate relation which simulates it (predicted)*

For this purpose, the results from the analyses conducted for fully stabilized (with CS) soil layers of 3, 6 and 9m thickness, subjected to the aforementioned 11 excitations with low (0.1λ) and intermediate (0.5λ) were used. It should be noted here that results from the high intensity analysis (λ) are excluded from this statistical analysis, since the results indicated extensive non-linearity of the stabilized soil response and the employed numerical methodology is not considered sufficiently verified for such levels of seismic intensity. This assertion is based on the fact that the simulations of centrifuge test data showed satisfactory accuracy for accelerations as high as 0.20g – 0.25g, and less so for higher intensities (see *Chapters* 7 and

8). In the following figures, results from the analyses with intensity levels of 0.1λ and 0.5λ are shown with red and blue color respectively and refer to an effective acceleration equal to a_{eff}=0.025g and a_{eff}=0.125g respectively. Note that based on Eq. (9.1), these a_{eff} values correspond to peak acceleration values 40% to 100% higher for M=6 to 8.

Processing of the data begins from Figure 9.38, where open symbols represent the T_s values of stabilized soil layers of 3m, 6m and 9m thickness, subjected to the 11 excitations for effective acceleration values equal to a_{eff}=0.025g and a_{eff}=0.125g as resulted from the analyses. Moreover, in the same figure, the approximate relation for the two different values of the effective acceleration, which predicts the fundamental period T_s of the stabilized soil layer, is illustrated with red and blue line respectively. This relation is expressed analytically by:

$$T_s(s) = \beta\left[H_{tr}(m)\right]^{0.89} \tag{9.4}$$

where:

$$\beta = 0.04\left(1+\frac{a_{eff}}{g}\right) \tag{9.5}$$

By observing Figure 9.38, it is obvious that the fundamental period T_s of the stabilized soil column depends mainly on the thickness of the stabilized layer H(m) and secondarily on the (effective) acceleration level of the excitation (a_{eff}). Interestingly, the selected form of this relation has physical meaning, in the sense that the T_s increases with H_{TR} (and T_s=0 for H_{TR}=0), while as the effective acceleration increases, the fundamental period, T_s, also increases.

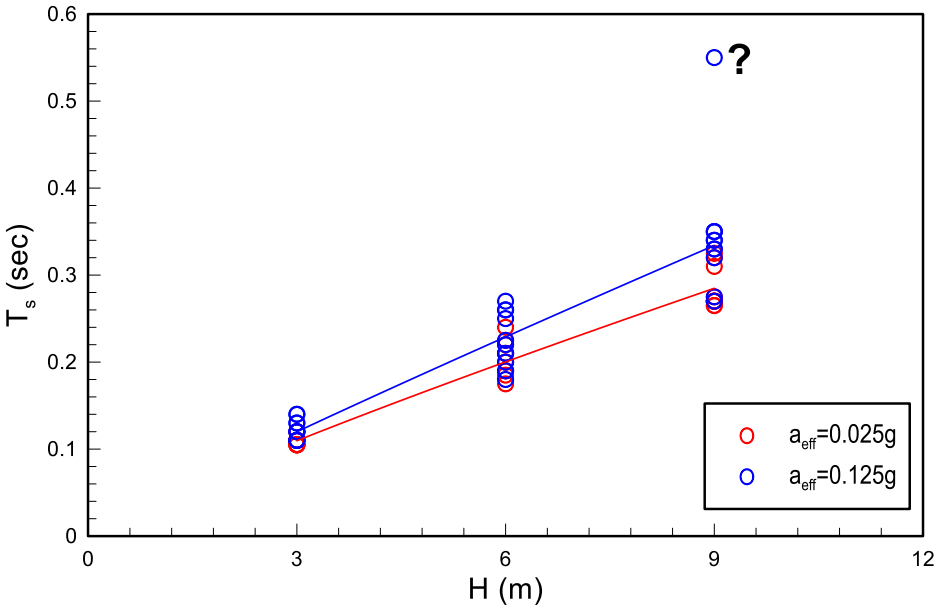

Figure 9.38 *Fundamental periods T_s of a stabilized soil layer as a function of the layer thickness H_{tr} for a_{eff}=0.025g and 0.125g as resulted from the analyses (symbols) and from approximate relation (lines) based on Eq (9.4)*

It is important here to quantify the error introduced by Eqs (9.4) and (9.5). for this purpose the relative error will be used as an index, which for any variable X is expressed by:

$$R_x = \frac{(\text{predicted\_x}) - (\text{observed\_x})}{\text{observed\_x}} \tag{9.6}$$

Namely R_x>0 corresponds to overestimation, R_x<0 to underestimation and finally R_x=0 implies a perfect prediction. The standard deviation of the relative error is calculated as the standard deviation of parameter R_x, while consistency is depicted by the average value of R_x which should converge to a zero value.

Hence, Figure 9.39 and Figure 9.40 present the relative error R_{Ts} of Equations (9.4) and (9.5) for the prediction of the T_s as a function of the thickness of the stabilized soil layer H_{tr} and the effective acceleration a_{eff} respectively. In the same figures the standard deviation of the relative error is also presented with the dashed lines. Observe that the relative error is generally small and uniformly distributed (with a standard deviation of just ±11%) without any systematic bias introduced by the parameters affecting the fundamental period T_s of the layer.

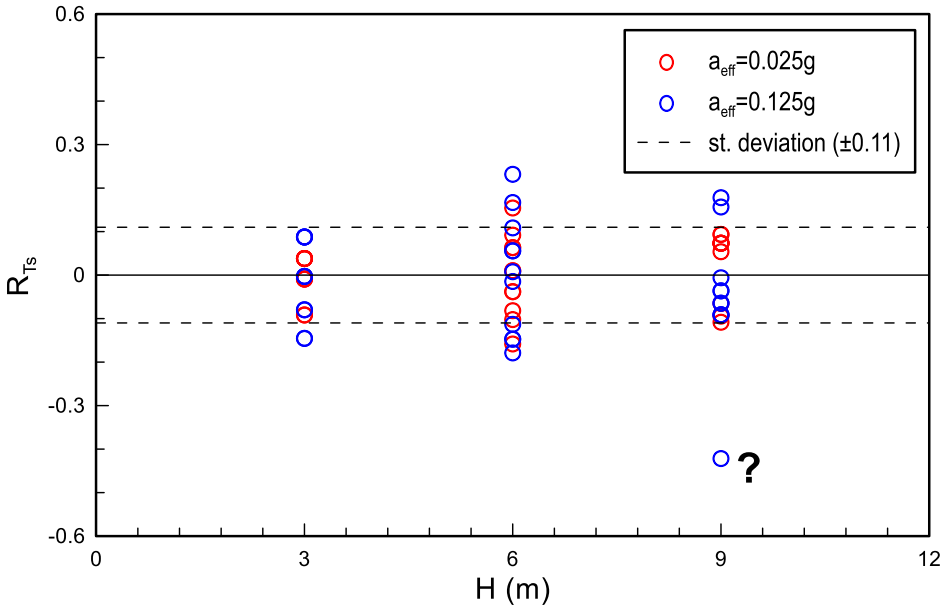

Figure 9.39 *Relative error (and standard deviation of the error) arising from (9.4) for the prediction of the fundamental period T_s in relation with the thickness of the stabilized soil layer H_{tr} for a_{eff}=0.025g and 0.125g.*

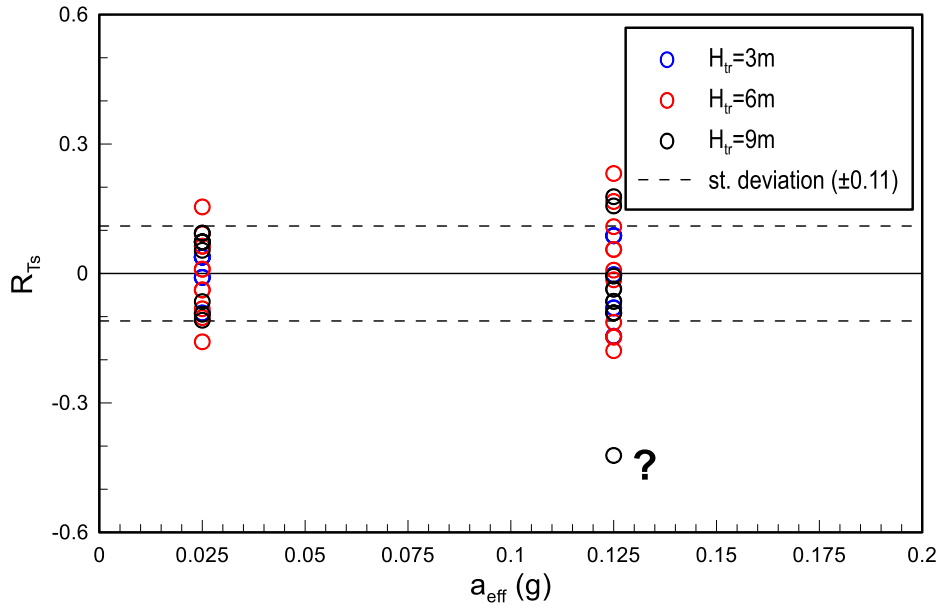

Figure 9.40 *Relative error (and standard deviation of the error) arising from (9.4) for the prediction of the fundamental period in relation with the effective acceleration a_{eff} for layer thicknesses H_{tr}=3m, 6m and 9m.*

Then, emphasis is put on the amplification of the peak acceleration $A_\alpha=A_{Sa(T=0)}$. The relationship proposed by Bouckovalas and Papadimitriou (2003) is adopted herein as a general relation for estimating the A_α of natural – stable soils. This relation will be used after re-calibration for

stabilized soils as well. Particularly, the general form of the suggested relation is (Bouckovalas and Papadimitriou, 2003):

$$A_\alpha = \frac{\left[1 + c_1\left(\frac{T_s}{T_e}\right)^2\right]}{\sqrt{\left[\left(1-\left(\frac{T_s}{T_e}\right)^2\right)^2 + \left(c_2\left(\frac{T_s}{T_e}\right)^2\right)\right]}} \quad (9.7a)$$

where the new calibrated values for c_1 and c_2 are:

$$c_1 = 0.26\left(0.1 + \frac{a_{eff}}{g}\right)^{-0.8} \quad (9.7b)$$

$$c_2 = 3.10\left(\frac{a_{eff}}{g}\right)^{0.4} \quad (9.7c)$$

Figure 9.41 compares the values of A_α, as resulted from the analyses (symbols) and from Eq. (9.7) (lines) for effective acceleration equal to a_{eff}=0.025g and a_{eff}=0.125g respectively. Observe the satisfactory overall fit. Furthermore, note that Eq.(9.7) is physically sound since the value of A_α for T_s/T_e=0 always equals to unity, because then the acceleration at the ground surface equals the acceleration at the base of the layer, either due to a very stiff/ shallow layer or due to a very high predominant period of the excitation. Moreover, for the resonance value of T_s/T_e=1, Eq.(9.7) is able to predict the maximum amplification, while it can also estimate the de-amplification of the acceleration when a_{eff} is further increased due to the very nonlinear ground response (e.g. for an excitation with intensity equal to λ, which corresponds to a_{eff}=0.25g).

Figures 9.42 up to 9.44 explore the relative error of Eq.(9.7) for the prediction of the amplification of the peak ground acceleration A_α in relation with the period ratio T_s/T_e, the effective acceleration a_{eff} and the thickness of the stabilized soil layer H_{tr}, respectively. These figures also illustrate with the dashed lines the standard deviation of the relative error, which is relatively small (±21%). It can be observed that there is no systematic bias introduced by the important parameters which affect the A_α, and that the error is relatively small and uniformly distributed with no obvious underestimation or overestimation of the numerical results.

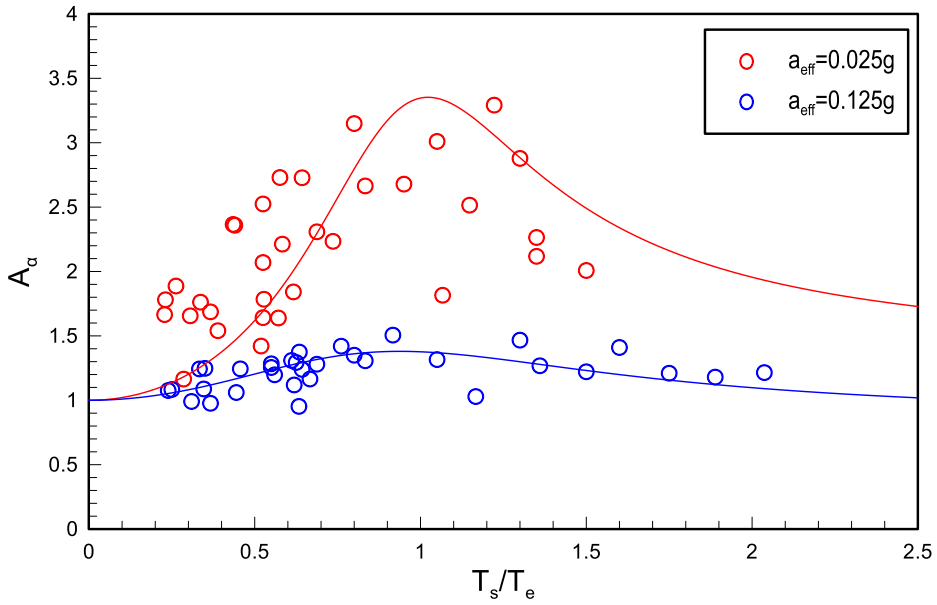

Figure 9.41 *Effect of period ratio T_s/T_e on the amplification of peak ground acceleration A_α, resulting from the analyses (symbols) and from Eq.(9.7) (lines) for effective acceleration equal to a_{eff}=0.025g and a_{eff}=0.125g*

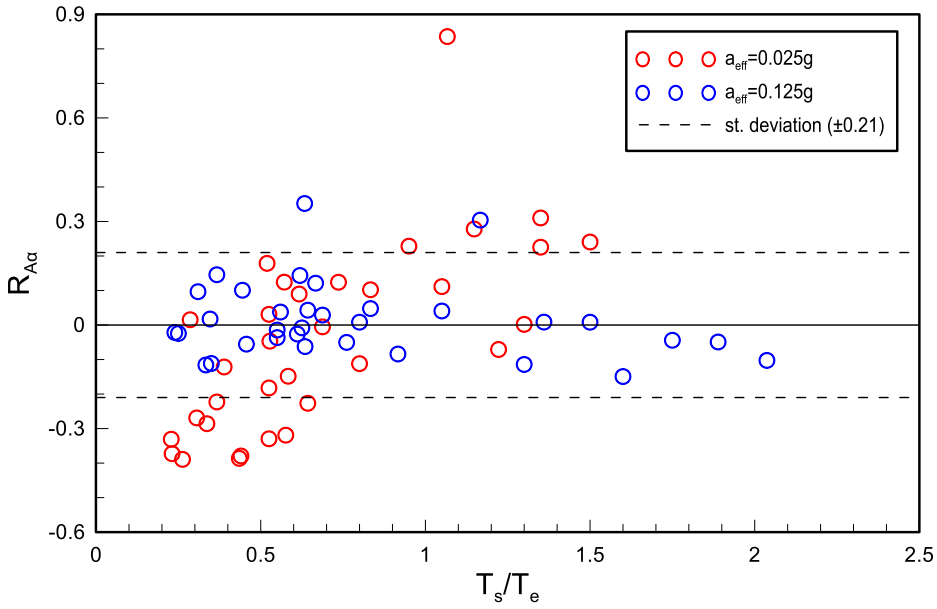

Figure 9.42 *Relative error (and standard deviation of the error) arising from Eq.(9.6) for the prediction of the amplification of the peak ground acceleration A_α in relation with the period ratio T_s/T_e for a_{eff}=0.025g and 0.125g.*

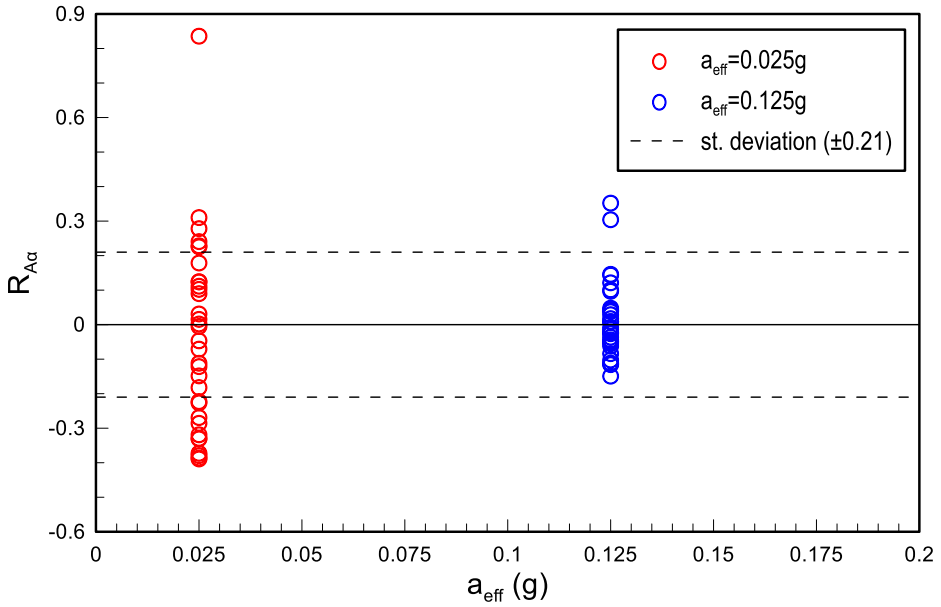

Figure 9.43 *Relative error (and standard deviation of the error) arising from Eq.(9.6) for the prediction of the amplification of the peak ground acceleration A_α in relation with the effective acceleration a_{eff}.*

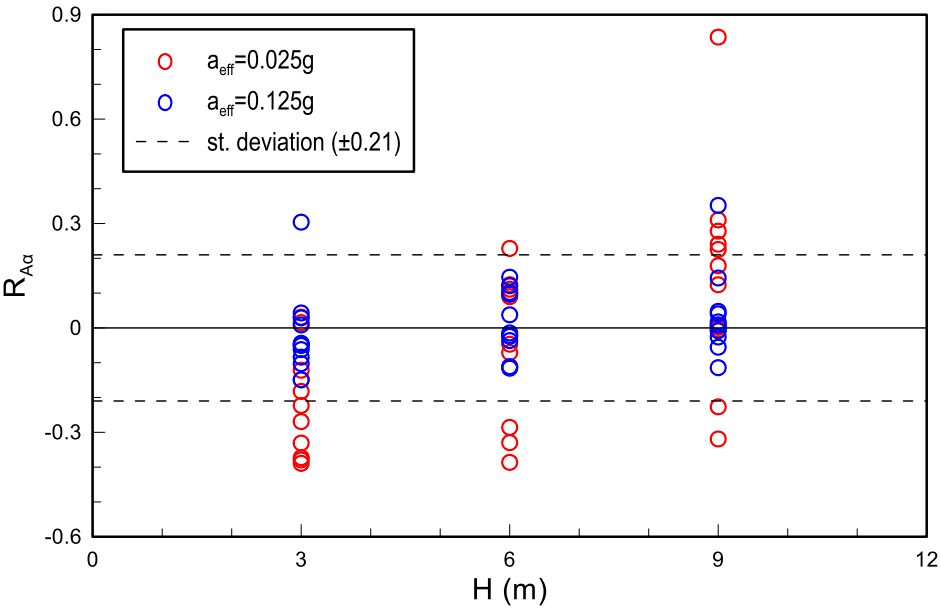

Figure 9.44 *Relative error (and standard deviation of the error) arising from Eq.(9.7) for the prediction of the amplification of the peak ground acceleration A_α in relation with the thickness of the stabilized soil layer H_{tr} for a_{eff}=0.025g and 0.125g.*

Finally, in order to propose a complete design methodology, it is still required to define the peak spectral acceleration A_{Sap}, or alternatively, to define its normalized value A_{Sap}*=A_{Sap}/A_α. The latter is hereby performed and a statistical analysis of A_{Sap}* values led to the following expression:

$$A_{Sap}{}^{*} = 1 + C_0 \left(\frac{T_s}{T_e} \right)^{C_t} H(m)^{C_h} \left(\frac{a_{eff}}{g} \right)^{C_a} \quad (9.8)$$

Where: C_0=3.97, C_h=1, C_t=0.4 and C_a=-0.2.

Figure 9.45 presents the values of A_{Sap}* in relation with the period ratio T_s/T_e as resulted from the analyses by the use of different symbols differentiating for effective acceleration (a_{eff}=0.025g and a_{eff}=0.125g) and for thickness of stabilized layer H_{tr} (3m, 6m, 9m). The included lines originate from rhe use of Eq. (9.8). As expected, the value for T_s/T_e=0 for any tested case equals to unity, as the vibration of the layer surface is identical with that at its the base (remember that A_α=1 for T_s/T_e=0 based on Eq.(9.7)). Moreover, the proposed relation considers the effect of effective acceleration, a_{eff}, and for a given stabilized layer thickness H_{tr}, as a_{eff} increases there is a corresponding decrease of A_{Sap}*, and so the reduction of amplification due to the increasing non-linearity can be successfully simulated. A similar decreasing effect on A_{Sap}* value is observed when the layer of the stabilized layer, H_{tr}, increases and the value of effective acceleration a_{eff} remains constant. All these effects are captured by the proposed Eq.(9.8).

Figure 9.46 investigates the effectiveness of the proposed methodology to predict the values of the normalized peak spectral amplification A_{Sap}*. More specifically, this figure compares the values of A_{Sap}* resulting from all analyses to their counterparts estimated from Equation (9.8) for all analyses conducted after considering the value of T_s from the analyses and not from Eq.(9.4). In this way, one can estimate the error related to Eq.(9.8) alone, without any propagation of the error from the estimation of period T_s.

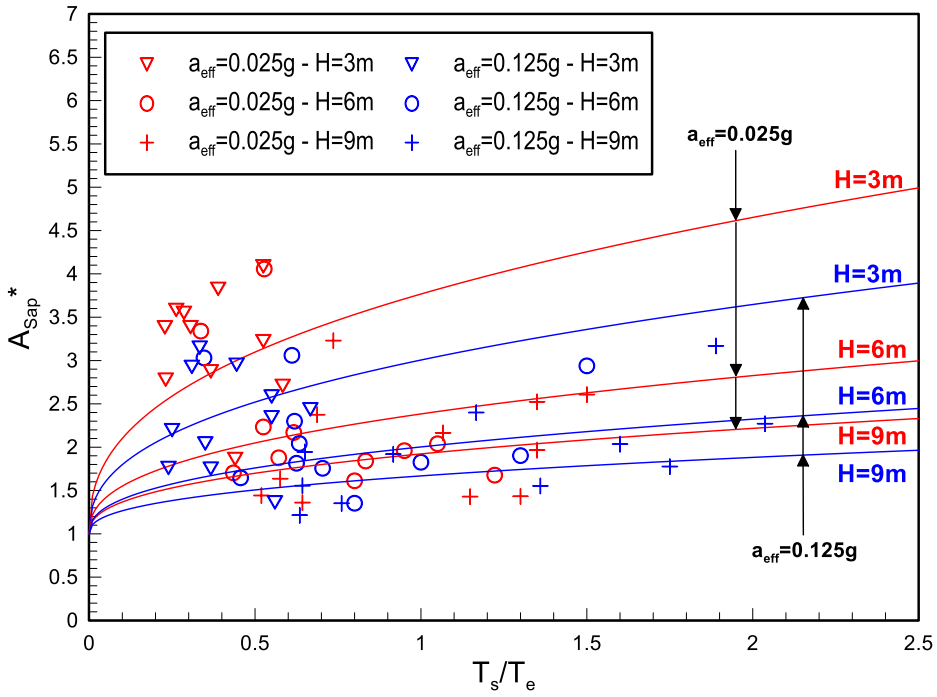

Figure 9.45 *Effects of period ratio T_s/T_e and stabilized layer thickness H_{tr} on the peak normalized spectral amplification A_{Sap}^* resulting from the analyses (symbols) and from equation (9.8) (continuous lines) for effective acceleration equal to a_{eff}=0.025g and a_{eff}=0.125g and layer thicknesses H_{tr}=m, 6m and 9m.*

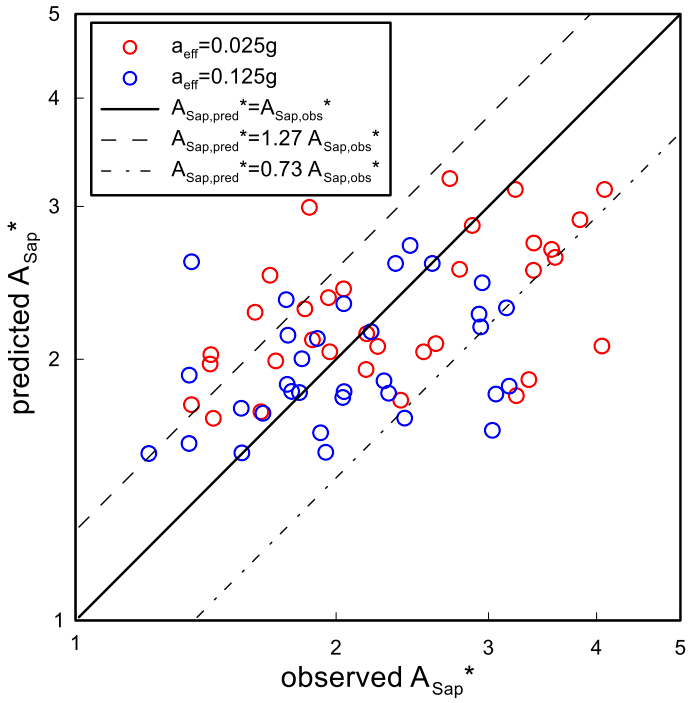

Figure 9.46 *Comparison of the values of normalized peak spectral amplification A_{Sap}* resulting from all numerical analyses (observed) and from Eq.(9.8) for the same cases (predicted), by considering the value of period T_s from the numerical analyses.*

The comparison of analytical estimates to numerical results for A_{Sap}* is satisfactory and the relative error of the prediction is investigated in Figures 9.47 up to 9.49 as a function of the period ratio T_s/T_e, the effective acceleration a_{eff} and the thickness of the stabilized soil layer H_{tr} respectively. In the same figures, with the dashed lines, the standard deviation of the relative error is also presented, which is considered satisfactory (±27%). No significant bias of the error is observed in these figures.

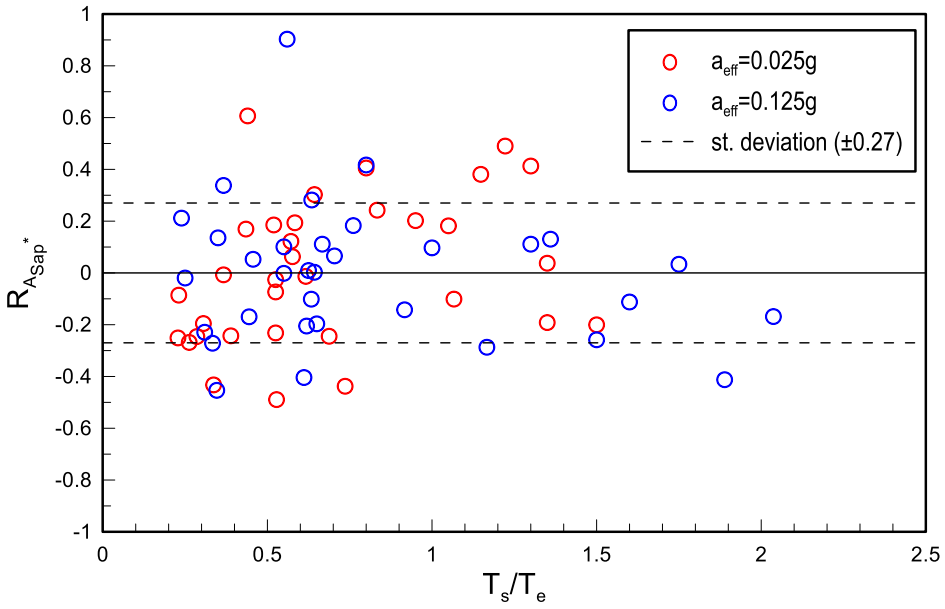

Figure 9.47 *Relative error R (and standard deviation of the error) of the normalized peak spectral amplification A_{Sap}* as a function of the period ratio T_s/T_e, for a_{eff}=0.025g and 0.125g.*

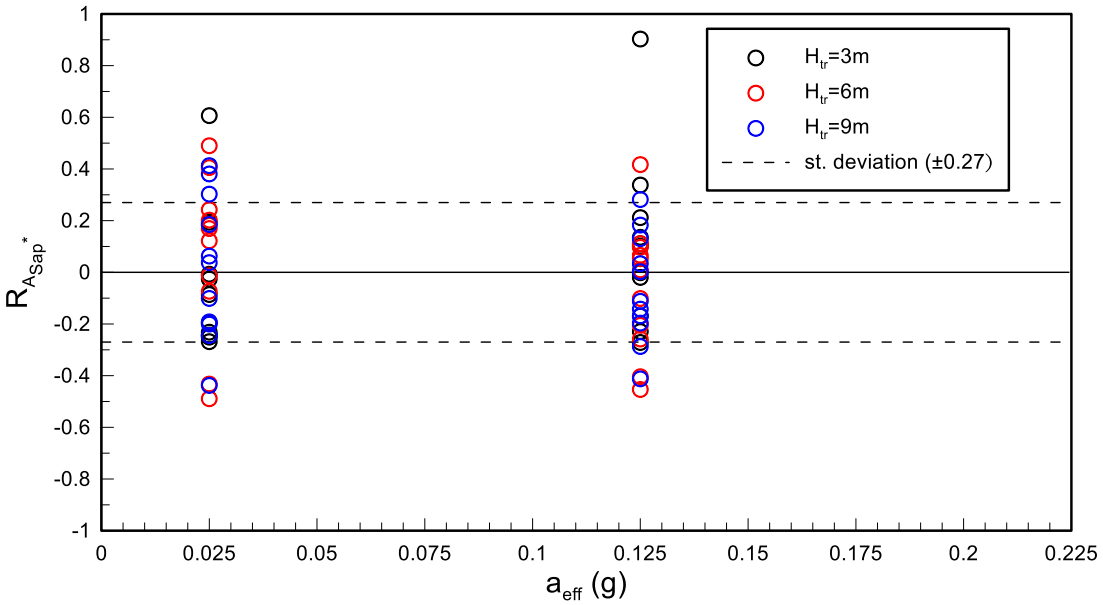

Figure 9.48 *Relative error R (and standard deviation of the error) of the normalized peak spectral amplification A_{Sap}* as a function of the effective acceleration a_{eff} stabilized layer thickness H_{tr}=3, 6, 9m.*

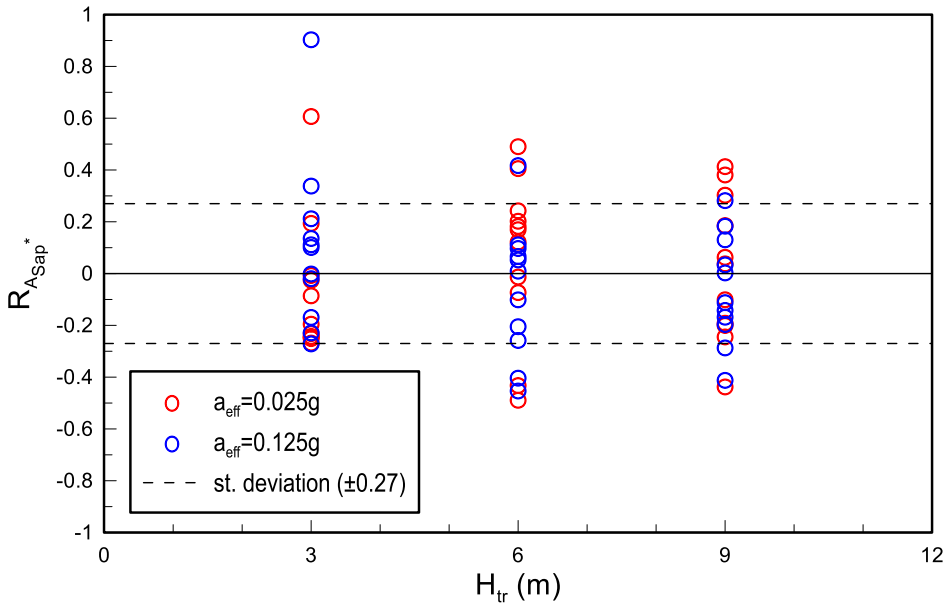

Figure 9.49 *Relative error R (and standard deviation of the error) of the normalized peak spectral amplification A_{Sap}* as a function of the layer thickness H_{tr}, for a_{eff}=0.025g and 0.125g.*

In addition, the effectiveness of the methodology to accurately predict the amplification of the peak spectral acceleration of a stabilized layer A_{Sap}, was investigated using successively all proposed multi-variable relations and comparing the analytical results with those from the numerical analyses. Firstly, the values of T_s were estimated using Eq.(9.4) and (9.5) for the stabilized layers with a layer thickness of 3m, 6m and 9m and for effective acceleration values

equal to a_{eff}=0.025g and a_{eff}=0.125g. Figure 9.50 compares directly the values of the fundamental period T_s resulting from the approximate relations (predicted) to their counterparts from the analyses (observed) and an excellent predictive accuracy is obtained.

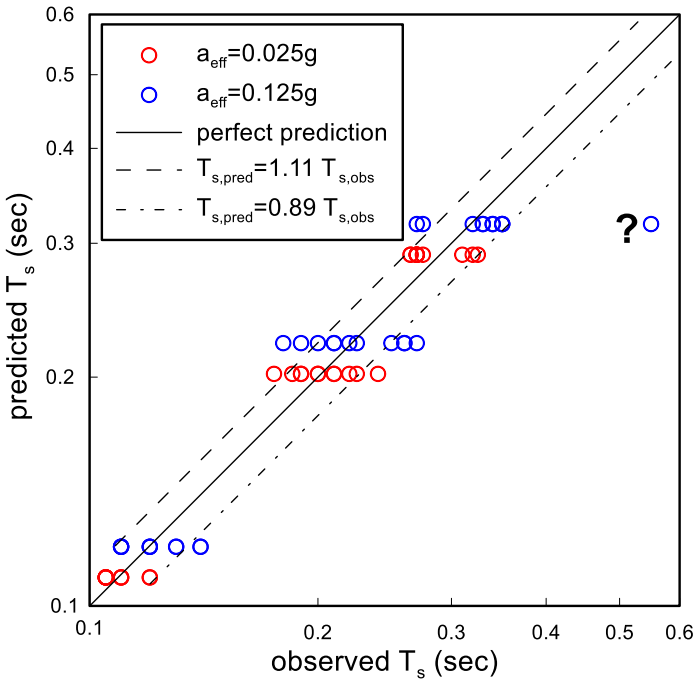

Figure 9.50 *Comparison of the values of fundamental soil period T_S resulting from all numerical analyses (observed) and from Eq.(9.4) and (9.5) for the same cases (predicted).*

Then, the estimation of the peak ground acceleration amplification A_α (via Eq.9.7) for the predicted (and not the measured) values of period T_s was obtained. Figure 9.51 shows the comparison of predicted A_α with observed A_α from the analyses for a_{eff}=0.025g and a_{eff}=0.125g. The overall accuracy is again satisfactory (as in Figures 9.41 - 9.44) and the standard deviation of the relative error remains equal to ±21-22%, given the practically excellent prediction of the period T_s.

Following the same rationale, for the same values of predicted fundamental periods T_s, the peak normalized spectral amplification values A_{Sap}* were estimated using Eq.(9.7). Figure 9.52 presents the comparison of the aforementioned predictions of A_{Sap}* with the values resulting from the numerical analyses (observed). Again, satisfactory accuracy is achieved, which is similar to the accuracy illustrated in Figures 9.45 – 9.49, since the standard deviation of the relative error remains in the range of ±27%.

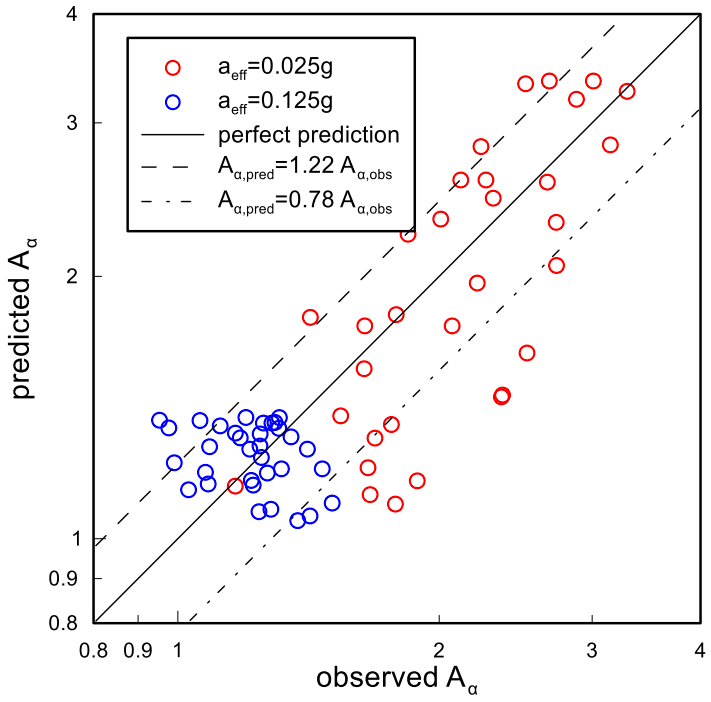

Figure 9.51 *Comparison of predicted peak ground acceleration amplification ratio A_α (Eq.9.7) versus the observed A_α values from the numerical analyses for a_{eff}=0.025g and a_{eff}=0.125g.*

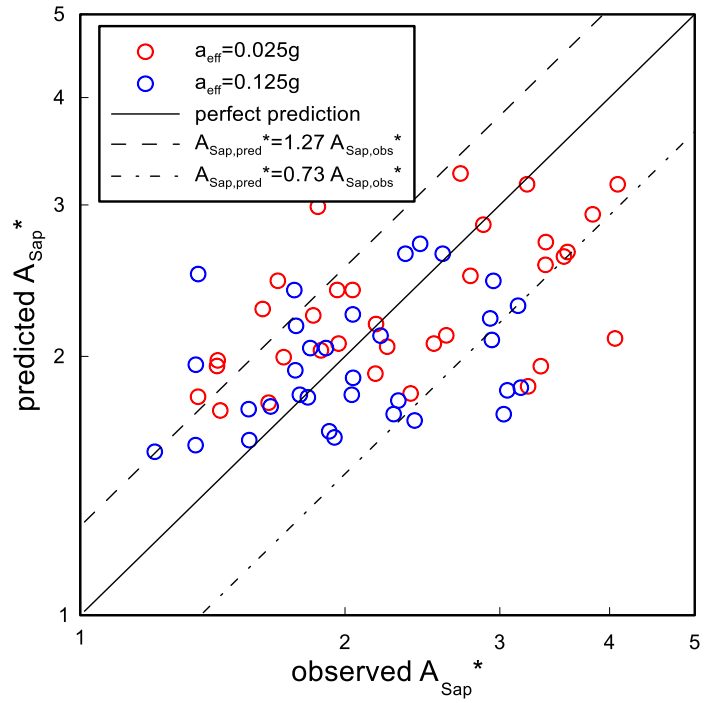

Figure 9.52 *Comparison of the values of A_{Sap}* resulting from all numerical analyses (observed) and from Eq.(9.8) for the same cases (predicted), by considering the value of T_s from Eq.(9.4).*

By multiplying the estimated values of A_α and A_{Sap}* the peak spectral amplification A_{Sap} can be calculated. Hence, Figure 9.53 shows the comparison of the abovementioned estimated

values of A_{Sap} (predicted) with the corresponding values which resulted from the numerical analyses (observed). The comparison is satisfactory and the standard deviation of the relative error is ±33%.

In order to examine if the relative error of the A_{Sap} prediction is affected by the involved parameters of the problem, Figures 9.54 – 9.56 show its values for all predictions in relation with the ratio T_s/T_e, the effective acceleration a_{eff} and the thickness of the stabilized soil layer H_{tr}, respectively. In the same figures, the standard deviation of the relative error is also presented with the dashed lines, which is still relatively small. No significant bias is observed in these figures a fact that underlines the reliability of the proposed multivariable relations for estimating the amplification of the elastic response spectra in stabilized layers.

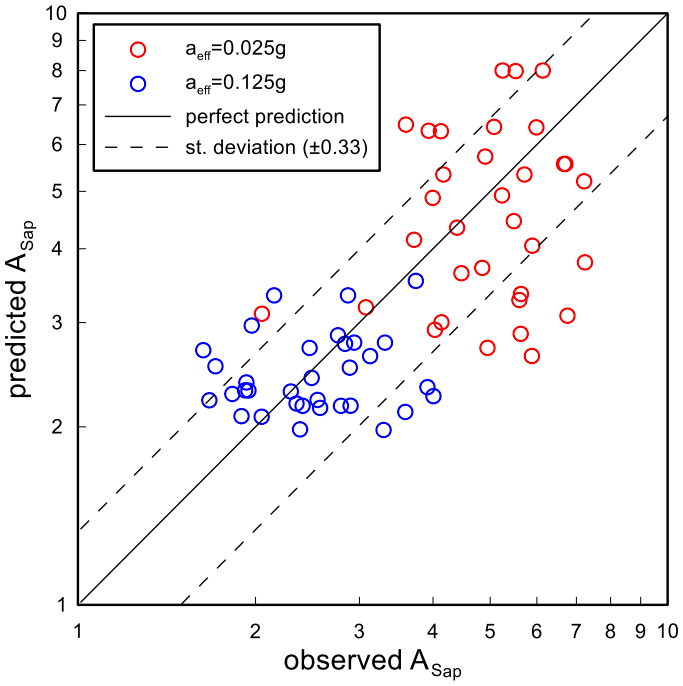

Figure 9.53 *Comparison of the values of A_{Sap} resulting from all numerical analyses (observed) versus the estimates of A_{Sap} (estimated from the values of A_α and A_{Sap}*) for the same cases (predicted).*

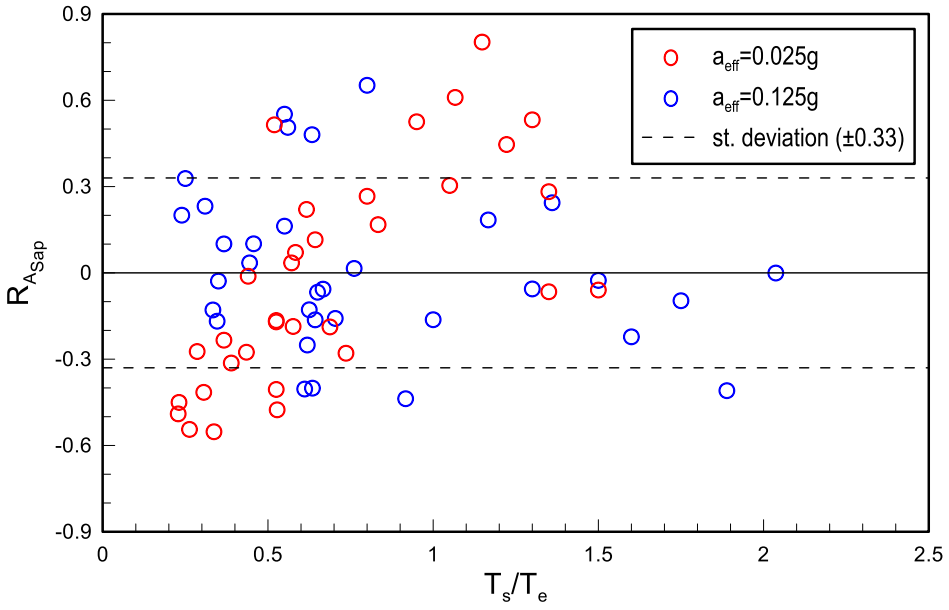

Figure 9.54 *Relative error (and standard deviation of the error) of the peak spectral amplification A_{Sap} (estimated from the values of A_α and A_{Sap}*) as a function of the period ratio T_s/T_e for a_{eff}=0.025g and 0.125g*

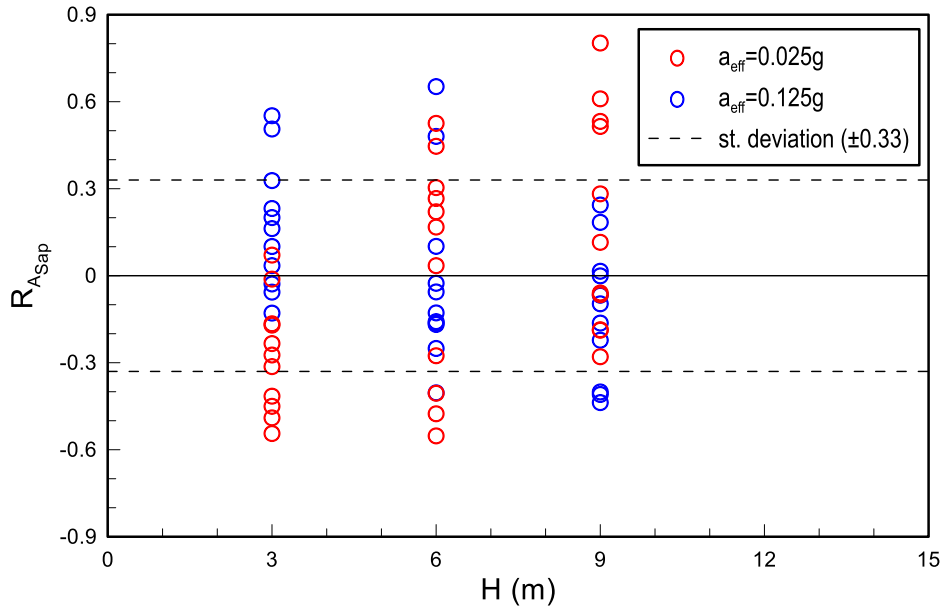

Figure 9.55 *Relative error (and standard deviation of the error) of the peak spectral amplification A_{Sap} (estimated from the values of A_α and A_{Sap}*) as a function of the layer thickness H_{tr} for a_{eff}=0.025g and 0.125g*

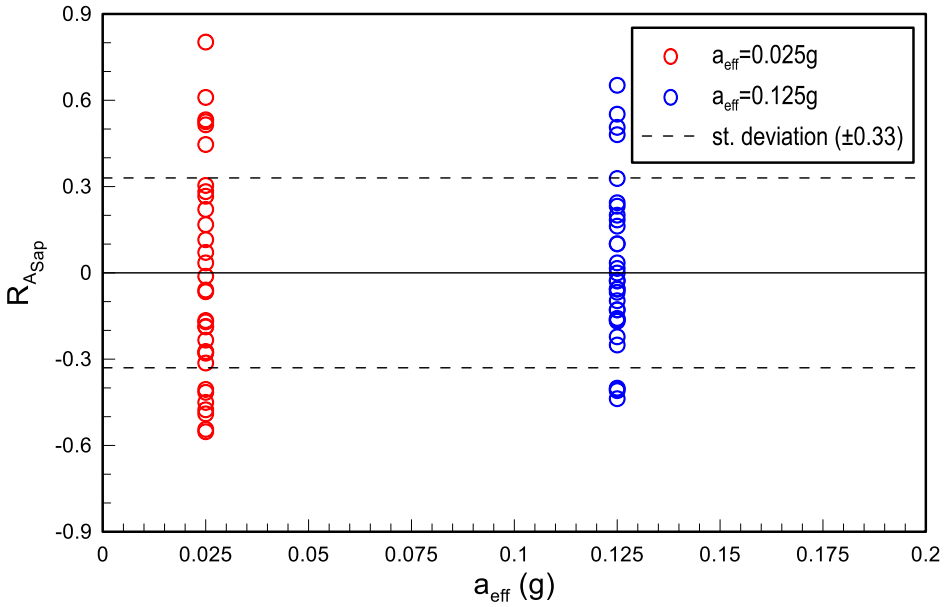

Figure 9.56 *Relative error (and standard deviation of the error) of the peak spectral amplification A_{Sap} (estimated from the values of A_α and A_{Sap}*) as a function of the effective acceleration a_{eff} for a_{eff}=0.025g and 0.125g*

In order to further understand the applicability and the reliability of the proposed set of multi-variable relations for predicting the spectral amplification of stabilized soil layers, three (3) examples are presented below where the full set of relations is applied and compared with the results of the numerical analyses. The comparison is presented in terms of surface-to-base spectral ratios of the stabilized soil column, so as to be consistent with the already presented figures from the numerical analyses.

The first example refers to the Northridge excitation for reasons of compatibility with the previously presented typical results and the other two examples refer to the Loma Prieta and Coyote Lake excitations for effective acceleration values of a_{eff}=0.025g and a_{eff}=0.125g. The followed procedure was the same for all three examples: firstly, the fundamental period T_s of the soil column, and the ratios A_α and A_{Sap}* were estimated through Eqs.(9.4), (9.5), (9.7) and (9.8) respectively for given predominant periods of these excitations : T_e=0.36sec for the Northridge excitation, T_e=0.20sec for the Loma Prieta excitation and T_e=0.42sec for the Coyote Lake excitation. The estimations are performed for the average thickness of the stabilized soil layer H_{tr}=6m (indicatively). The normalized spectral amplification A_{Sa}* was calibrated using Eq.(9.3) as a function of the normalized fundamental period of the structure T/T_s, and then the final spectral amplification $A_{Sa}(T)$ was calculated based on the predicted values of ratio A_α and period T_s. The spectral amplification curve representing $A_{Sa}(T)$ which resulted from this procedure was compared to the curve of the corresponding spectral ratio that resulted from

the numerical analyses. Hence, Figure 9.57(a) and (b) represent the comparison for the Northridge excitation, for a_{eff}=0.025g and a_{eff}=0.125g. Similarly, Figure 9.58(a) and (b) present the corresponding comparison for the Loma Prieta excitation, while Figure 9.59(a) and (b) do the same for the Coyote Lake excitation for a_{eff}=0.025g and a_{eff}=0.125g, respectively.

It is observed that for the Northridge excitation there is an underestimation of the numerical results at resonance and the contrary is observed for the Loma Prieta excitation. However, for the Coyote Lake excitation the overall predictions seem to be more accurate. As a whole, judging from the comparisons of all three (3) indicative examples, a satisfactory prediction of the spectral amplification of stabilized soil layers can be achieved via the proposed set of multivariable relations.

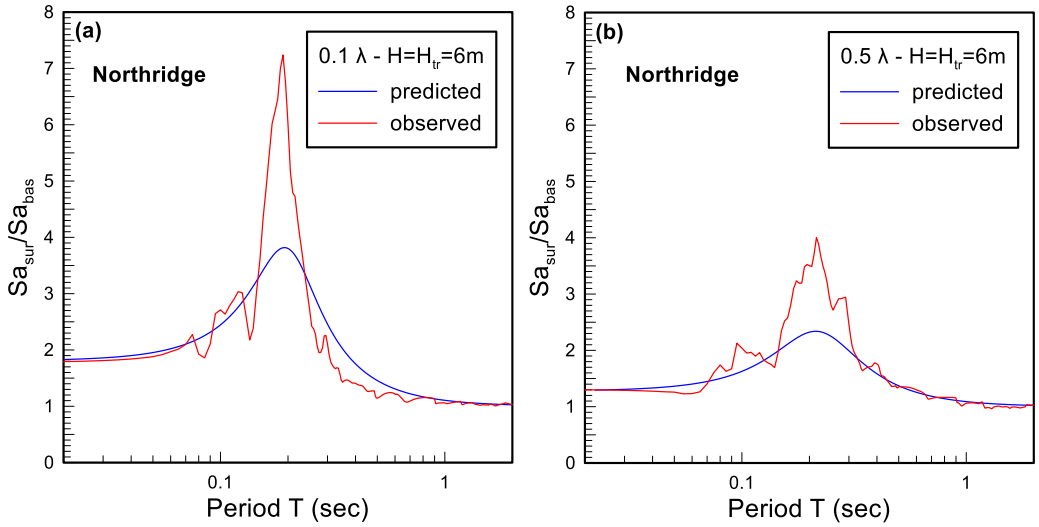

Figure 9.57 *Comparison of the estimated surface-to-base spectral ratio (blue line) with the one resulting from the analyses for the Northridge excitation (red line) for a stabilized layer of 6m thickness with (a) a_{eff}=0.025g, (b) a_{eff}=0.125g.*

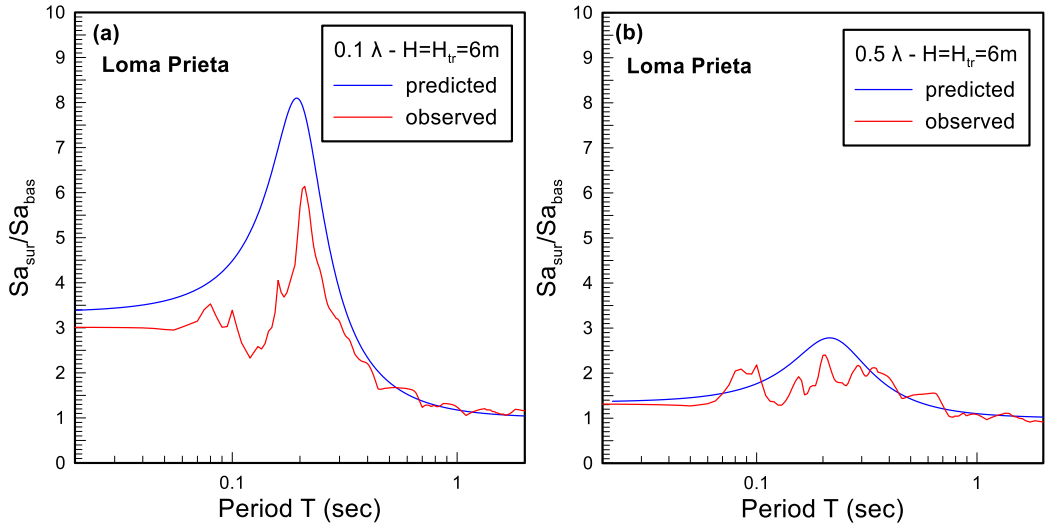

Figure 9.58 *Comparison of the estimated surface-to-base spectral ratio (blue line) with the one resulting from the analyses for the Loma Prieta excitation (red line) for a stabilized layer of 6m thickness with (a) a_{eff}=0.025g, (b) a_{eff}=0.125g.*

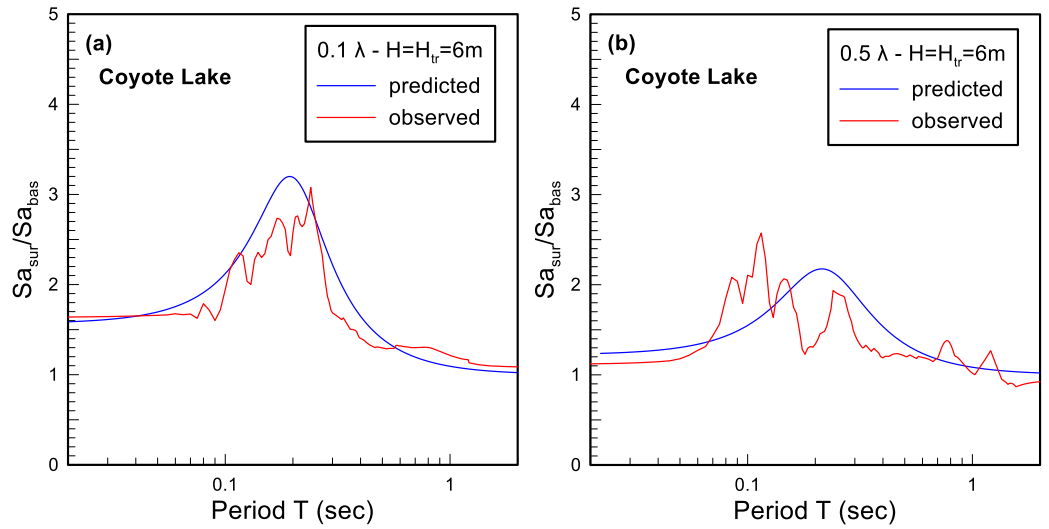

Figure 9.59 *Comparison of the estimated surface-to-base spectral ratio (blue line) with the one resulting from the analyses for Coyote Lake excitation (red line) for a stabilized layer of 6m thickness with (a) a_{eff}=0.025g, (b) a_{eff}=0.125g.*

To conclude, the proposed analytical procedure seems able to predict satisfactorily the 1D seismic response of stabilized soil with different layer thickness and for different cases of realistic excitations of small and intermediate intensity (e.g. a_{max} up to 0.25g). For this reason, this procedure is considered a useful tool for the application of passive stabilization in practice.

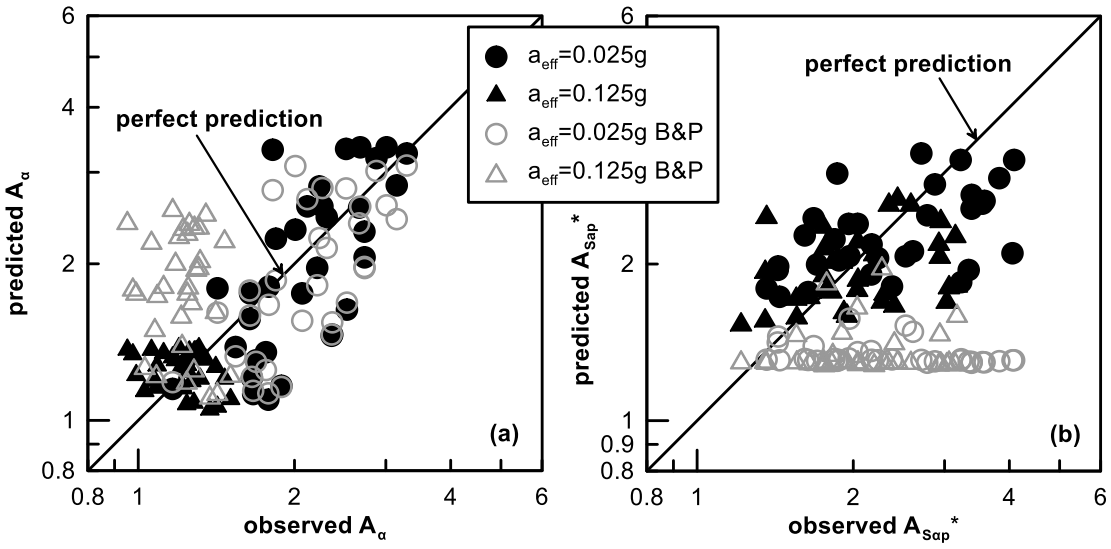

Figure 9.60. *Comparison of the values of (a) A_a and (b) A_{Sap}*, for a_{eff}=0.025g and 0.125g, resulting from all numerical analyses (observed) and from the application of the hereby proposed multi-variable equations (predicted; solid symbols) and the respective equations of Bouckovalas and Papadimitriou (2003) (predicted; hollow symbols) for $V_b = 20V_s$.*

As mentioned above, the hereby proposed multi-variable relations essentially originate from a re-calibration of the pertinent equations of Bouckovalas and Papadimitriou (2003), which were proposed for stable untreated soils and pertained to the soil-to-rock outcrop spectral amplification ratio. On the contrary, the hereby proposed equations refer to stabilized soils and pertain to the surface-to-base spectral amplification ratio, thus dictating the necessity for the re-calibration. The former difference is not expected to yield significant differences, but the latter poses a practical problem for the application of the literature relations, since they correspond to a compliant bedrock (where the bedrock wave velocity V_b is finite) whereas the hereby performed analyses (and the proposed relations) imply a rigid bedrock ($V_b \rightarrow \infty$).

However, in order to investigate the necessity for this re-calibration, the accuracy in predicting the A_a (via Eq. 9.7) and the A_{Sap}* (via Eq. 9.8) should be compared to the accuracy offered by the literature relations. To allow for this comparison, the literature relations are used beyond their range of applicability, by assuming a value of V_b equal to 20 times the average shear wave velocity V_s of the stabilized soil, and this as an approximation of a rigid bedrock. This comparison is shown in Figure 9.60, where the solid symbols present the accuracy of the hereby proposed relations and the hollow symbols that of the literature relations. Observe that the literature relations predict satisfactorily the numerical results of A_a for a_{eff}=0.025g, but they over-predict the results for a_{eff}=0.125g. In terms of A_{Sap}*, the literature relations underestimate the results for both values of the effective acceleration. Based on Figure 9.60

the necessity for the proposed re-calibration becomes obvious. Moreover, this figure underlines that the literature relations should not be used for rigid bedrock conditions, since such conditions are beyond their scope.

Chapter 10

SEISMIC RESPONSE OF SHALLOW FOOTINGS LAYING ON STABILIZED SOIL LAYERS

10.1 Introduction

According to existing anti-seismic code provisions, the construction of civil engineering structures with shallow foundations is prohibited on soils which are at risk of liquefaction, unless ground improvement is performed in advance. However, in many cases, the foundation soil is characterized as liquefiable after the construction of the structure and this is true for many structures built before 1980 or so. For such cases, an alternative technique of improvement of the foundation soil is passive (site) stabilization, which has the comparative advantage of easy application at developed sites.

As presented in *Chapter 9*, the 1D seismic response of surficially only or fully stabilized soil layer is very different from this of the natural – untreated soil. This is because liquefaction (r_u=1, and related de-amplification of the vibration) is not expected within the layer that has been stabilized. The goal of the present chapter is to investigate the seismic response of a shallow footing which rests on a stabilized layer, since shallow foundations are the most commonly used foundation types for structures, especially in previous decades (existing structures). Unfortunately, there are no experimental data available in the literature referring to this issue and so a purely numerical study will be performed, by adopting the simulation procedure presented and calibrated in the previous chapters. More specifically, stabilization of the soil is simulated with a reduction of the fluid bulk modulus K in the soil pores, while the response of the sand skeleton is simulated via an appropriate constitutive model for sands and without change in the values of its model constants.

10.2 Methodology of numerical simulation

As shown in previous Chapters, relatively accurate simulations of stabilized sand response may be attained by using existing elastoplastic constitutive models for sands, if one takes into account the seemingly increased compressibility of colloidal silica in the pores of the saturated sand (e.g. Andrianopoulos et al. 2015). Hence, here, the simulation of the shallow footing resting on a stabilized layer will be performed by adopting the boundary surface plasticity

critical state model, NTUA-SAND (Andrianopoulos et al. 2010a; b), since it has proven its ability to simulate the cyclic response of sands at both element and system level, using the same set of model constants independently of initial conditions (stress and density) and cyclic shear strain level.

The foregoing relative compressibility of colloidal silica (CS) was observed by Towhata (2007), who performed unconfined compression tests on gelled (pure) CS samples and concluded that this material has relatively increased volume compressibility in comparison to water, which is practically incompressible (it actually has a fluid modulus K_w = 2x10^6 kPa). In other words, while any tendency for volume reduction (e.g. due to seismic shaking) translates to excess pore pressure development in untreated sand, in stabilized sand any similar loading is not expected to generate (significant) excess pore pressures. This fundamental observation allowed the use of NTUA-SAND in boundary value problems of saturated media, whose fluid in the soil pores is filled by a CS dispersion, which is characterized by a decreased value for the pore fluid (bulk) modulus (in comparison to K_w).

A plane strain analysis is used for the shallow strip foundation (footing) with a 106x9m grid which is presented in Figure 10.1.The grid zones have dimensions of 084x0.41m at the free field and are densified in the area under the footing (0.5x0.41m), leading to a total number of 132x22. The soil layer is Nevada sand with relative density of D_r=40% and saturated density ρ_{sat}=1.91Mgr/m^3, which is simulated using NTUA-SAND with the model constants values in Table 10-1, which also includes the state variables of density, porosity and void ratio corresponding to D_r=40%. In all numerical simulations, the surface footing had a width of 3m. The grid height is 9m and corresponds to a 9m thick saturated sand layer over bedrock. The employed grid size is wide enough in order to provide results unaffected from any potential lateral boundary effects. To further ensure this for the seismic shaking, tied-nodes boundary conditions were assigned at the lateral boundaries, thus enforcing equal horizontal displacements of the corresponding nodes on the left and right boundaries. All boundaries were considered impermeable, apart from the top boundary where flow was allowed towards the free surface. The footing was simulated using cable elements interconnecting the corresponding surface nodes, while these nodes were also tied to one another to enforce common horizontal and vertical displacements. As such, a rough rigid (and massless) footing is simulated, on which a vertical velocity v is applied as the structural load on 6 adjacent nodes 0.5m apart (see Figure 10.2). According to Itasca (2011), this velocity varies linearly from the value at the last grid point upon which it is applied, to zero at the adjacent grid point.

Therefore, half the width of the adjacent zones should be added to the footing width, thus resulting to a 3m wide strip footing.

Table 10-1 *Values of model constants of NTUA-SAND model for Nevada sand and state variables for D_r=40% (Andrianopoulos et al. 2010a,b).*

Parameter	*Dense sand*
Density (Mgr/m³)	1.52
Porosity	0.424
Permeability (m/s)	1.02e-10
e	0.737
M_c^c	1.25
M_c^e	0.72
$(e_{cs})_a$	0.809
λ	0.022
B	600 (180 for monotonic loading)
v	0.33
k_c^b	1.45
k_c^d	0.30
γ_1	0.00025
α_1	0.6 (1.0 for monotonic loading)
A_o	0.8
h_o	15000
N_o	40000

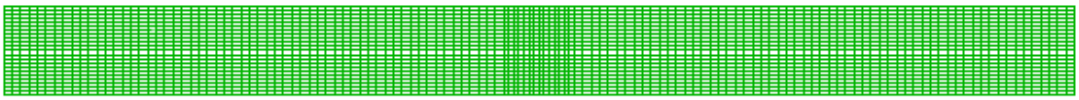

Figure 10.1 *Grid used for the simulation of the seismic response of a shallow strip footing in FLAC (Itasca, 2011).*

In order to achieve full saturation of the layer during the whole seismic shaking, the water table level was set 1m higher than the layer surface and a pore pressure equal to 9.81kPa was applied on the surface. Firstly, the bearing capacity of the footing resting on untreated Nevada sand was estimated by applying a vertical constant velocity on the 6 nodes of the footing (see Figure 10.2). The velocity used was small enough ($2.5 \cdot 10^{-6}$ m/s), so as to achieve a stable

response and minimize the unbalanced forces for this specific grid geometry. The load from the footing which corresponds to each settlement value was calculated by summing the vertical resistance forces at the tied and moving nodes related to the footing. As uniform settlement is imposed with a very low velocity, the loading is practically static and so the analysis is conducted under fully drained conditions. The bearing capacity q_{ult} of the sandy foundation soil (with D_r=40%) for the footing with width B_f=3m was estimated equal to q_{ult}=601KPa, based on the load – settlement curve presented in Figure 10.3. All analyses with stabilized sand assumed that the bearing capacity (q_{ult}) is not affected by the low-pressure injection of CS in the soil pores, since the injection takes place long after the construction and the loading of the footing with the structural load, i.e. when hydrostatic pressures have been restored. This is a reasonable assumption, considering that, during the CS injection, the soil skeleton continues to carry the load of the footing and the pore fluid (no matter its consistency) remains in a hydrostatic pressure regime.

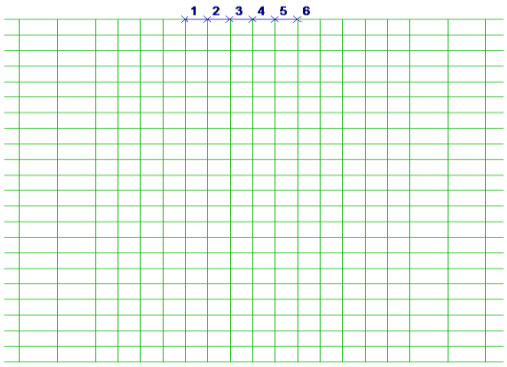

Figure 10.2 *Detail of grid used for the simulation of the seismic response of a shallow strip footing at FLAC (Itasca, 2011) with notation of the 6 nodes related to the footing location.*

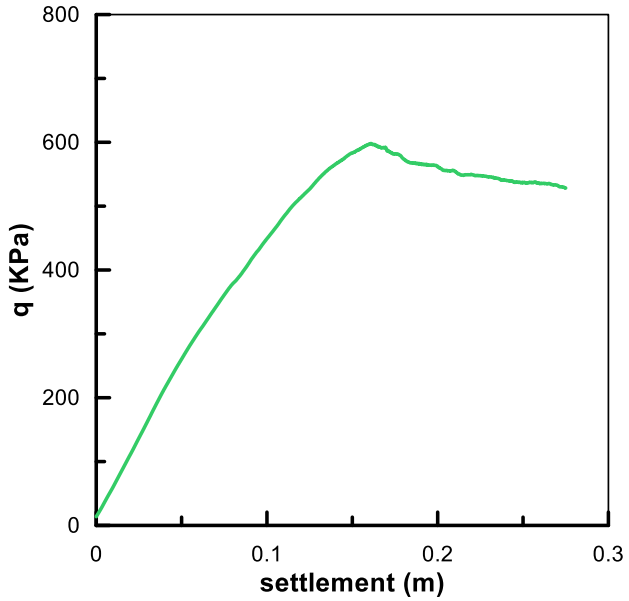

Figure 10.3 *Static load – settlement curve for 3m wide surface strip footing resting on a 9m-thick untreated Nevada sand layer with D_r=40% (loading under fully drained conditions).*

Consequently, the dynamic analysis was performed after a uniform contact pressure equal to q = 200kPa was first established via a stress-controlled analysis, i.e. when the operational load brings the footing at a static factor of safety FS = q_{ult}/q = 3 and hydrostatic pressures have been also established (see q_{ult}=601kPa in Figure 10.3). This implies that stabilization is applied to an existing structure, that rests on a liquefiable foundation soil and its loading corresponds to a static factor of safety equal to 3. It has to be mentioned here that the footing is considered an impermeable barrier for the pore fluid flow during shaking, and that the analysis does not take into account a potential increase of q_{ult} (and FS) under static conditions.

The effect of passive stabilization on the surface footing response is studied by comparing two (2) reference dynamic analyses, one for an untreated layer (with water in the soil pores) and one for a stabilized layer (with CS in the soil pores) of the same 9m thickness subjected to the same ground excitation. The untreated layer has a hydraulic conductivity equal to $k=3.31*10^{-3}$m/s, while the treated layer is considered stabilized with CS(%)=7.5 (average value of the commonly used concentrations CS(%)=5-10) and has a hydraulic conductivity equal to $k_{tr}=10^{-9}$m/s (Persoff et al., 1999). The NTUA-SAND model was used for the simulation of the seismic response of the sand skeleton with the model constant values presented in Table 10-1, while for the simulation of the seismic response of the stabilized layer the fluid bulk modulus value was reduced by dividing the water bulk modulus K_w with the factor n, using the expression n= (CS(%) + 2.25) x 100 = 975 (Equation 7.1). It is mentioned here, that the CS is assumed to have reached the desirable (very high) viscosity value before the dynamic loading is applied. The input motion consisted of 10 cycles (N=10) of sinusoidal (purely) horizontal acceleration, with uniform peak base acceleration of 0.15g at a period T_e = 0.15sec. In all analyses for the simulation of the seismic response of Nevada sand, local non-viscous, frequency independent damping was assigned having a value of 2%.

The above outline the characteristics of the basic reference analyses for the problem at hand. The paragraph that follows presents their results and the next paragraphs of this *Chapter* proceed in presenting the parametric investigation results for the effects of the excitation characteristics, as well surficial only (partial) stabilization on the footing response.

10.3 Effects of full stabilization on the seismic response of a surface footing

The results of the two (2) reference analyses for fully stabilized and untreated soil (described in paragraph 10.2) are presented herein. Figure 10.4 presents the comparison of the acceleration time-histories of the ground surface (z=0m) and at depths of 3 and 6m below the middle of the (rough rigid) surface footing, as well as for a surface location far laterally from the footing (approximately 42m from the middle of the footing), e.g. essentially at the free field. It is observed that under the footing, the sinusoidal form of the input motion is more or less retained in the shaking of both stabilized and untreated soil and only a slight de-amplification of the peak acceleration is observed in the former case.

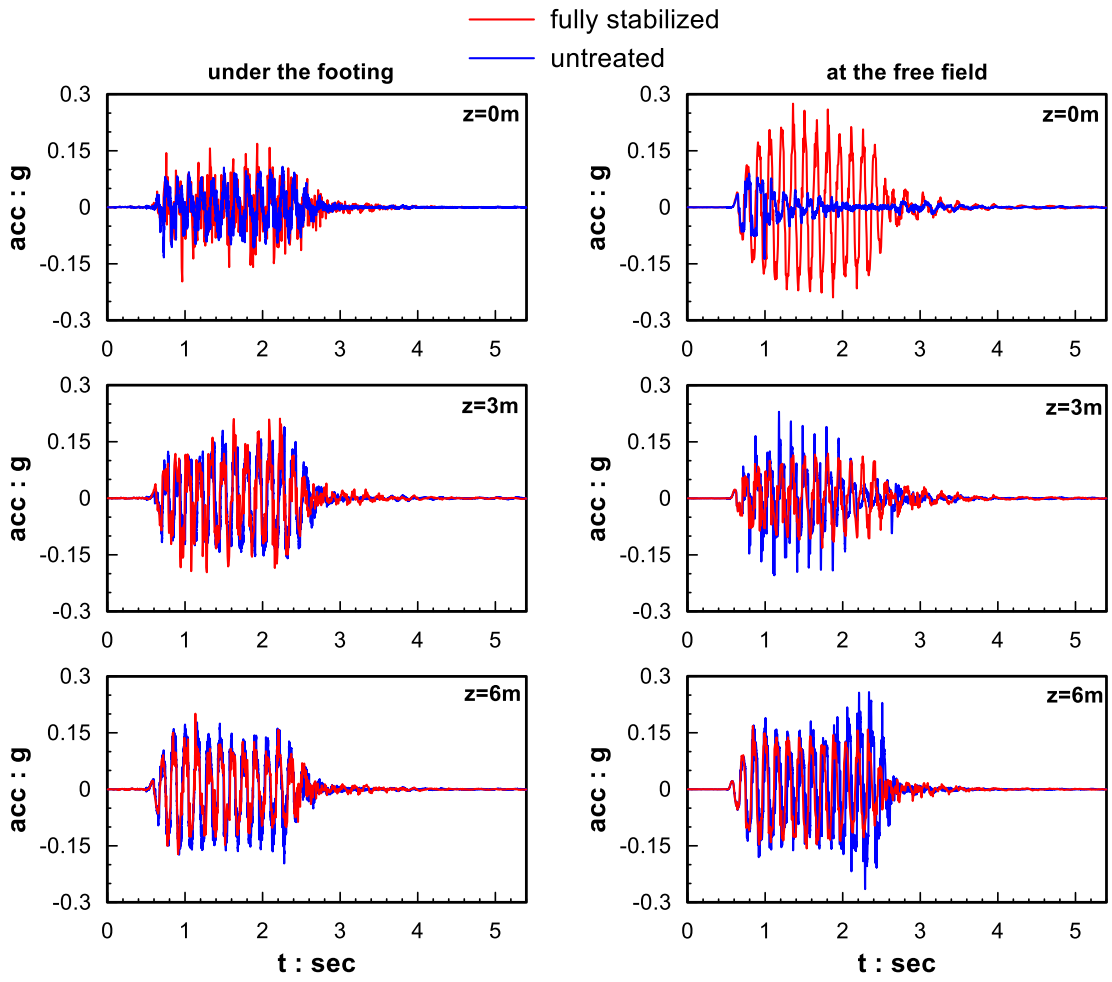

Figure 10.4 *Acceleration time-histories at different depths under the footing and at the free field for the fully stabilized and untreated 9m thick soil layers.*

On the contrary, at the free field the stabilized soil exhibits a slight amplification in comparison with the base excitation, opposite to the untreated soil which shows an intense de-amplification (especially after the first 1-2 loading cycles, or after t=1sec) typically observed response in liquefied soil formations. The amplification issues are better depicted and compared in Figure 10.5, which presents the elastic response spectra (5% damping) at the ground surface under the footing and at the free field.

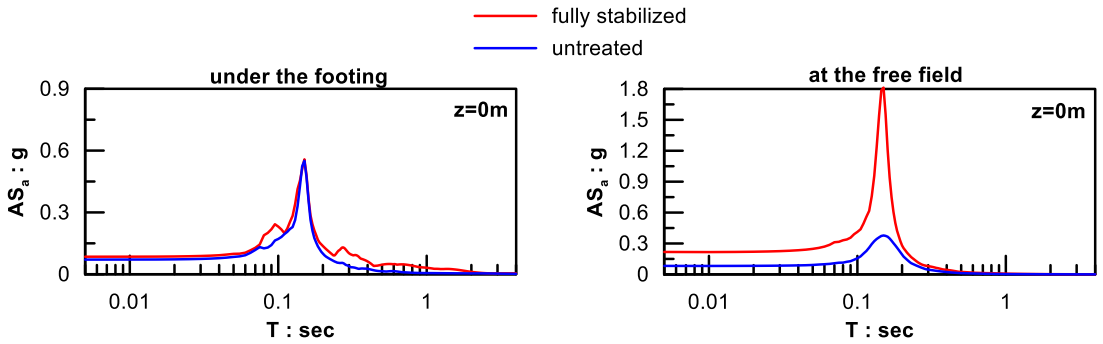

Figure 10.5 *Elastic response spectra (5% damping) at the ground surface under the footing and at the free field for the fully stabilized and untreated 9m thick soil layers.*

This difference in response can be explained by observing the excess pore pressure ratio time-histories (Figure 10.6) where liquefaction of the untreated soil at the free field occurs at depths of z≤3m (mainly near the surface), contrary to the stabilized layer where excess pore pressures are practically zero everywhere. The small values of r_u under the footing are a side-benefit of the increased vertical stresses, due to the footing loading, which increase the denominator (vertical effective stress) of the r_u ratio, thus reducing the liquefaction risk even for the untreated soil. Given the stabilization, the already small values of r_u due to the increased vertical stresses, become essentially zero under the footing. In addition, the small differences in r_u values are the reason that the accelerations under the footing are quite similar in both stabilized and untreated layers. This is not the case at the ground surface of the free-field, where even the stabilized soil shows non-zero (but small) excess pore pressures, whereas the untreated soil liquefies (r_u = 1) at t=1sec and remains so until the end of shaking, while r_u dissipates fast thereafter. Interestingly, t=1sec is the time when the intense de-amplification of accelerations is observed. Moreover, the fact that the stabilized soil does not develop significant excess pore pressures even at the free-field is the reason that slight amplification is observed (see also *Chapter 9*).

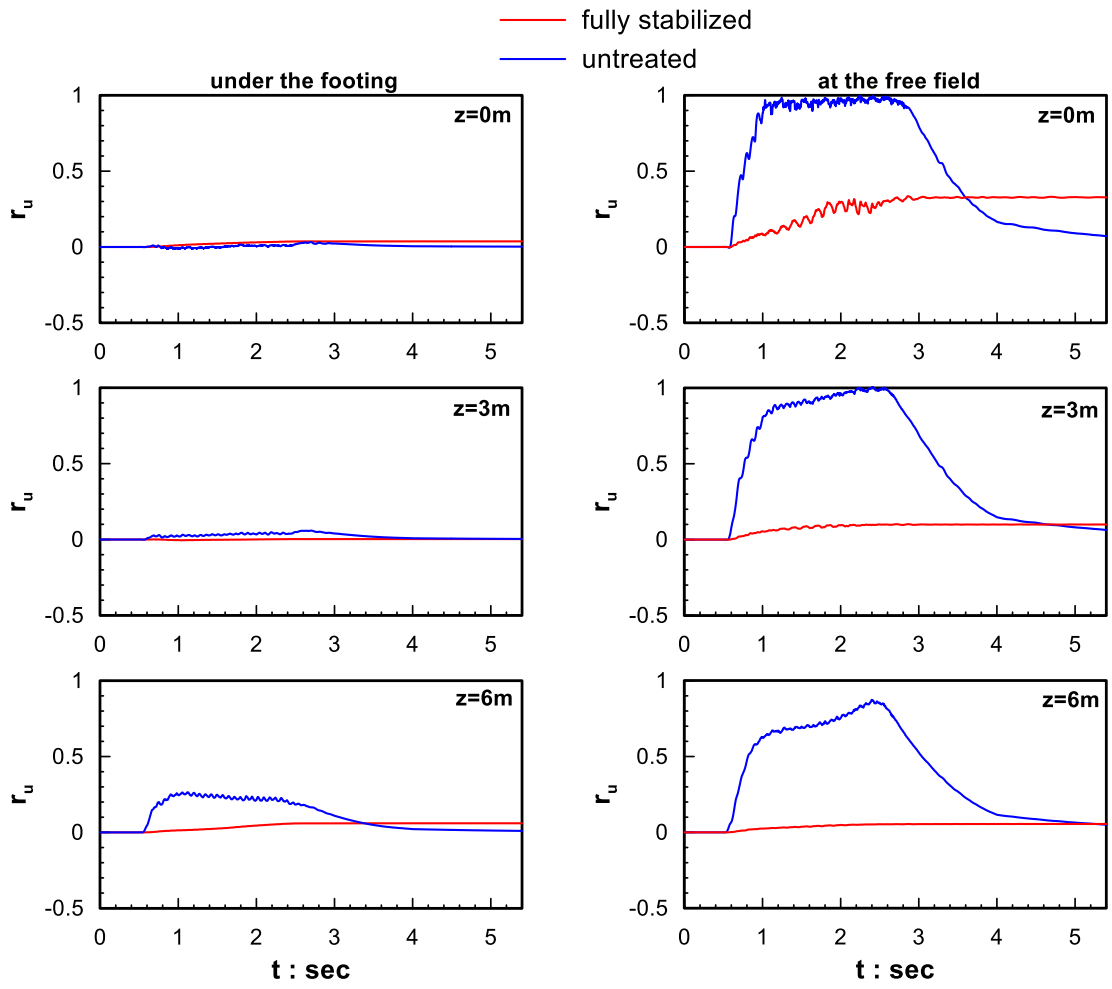

Figure 10.6 *Excess pore pressure ratio time-histories at different depths under the footing and at the free field for the fully stabilized and untreated 9m soil layers.*

Figure 10.7 presents the settlement time-histories for the ground surface under the footing and at the free field. The settlements that occur under the footing during the shaking are shear- induced, accumulate during shaking and do not result from the excess pore pressure dissipation after the end of shaking. Settlements are clearly larger for the case of the untreated layer in comparison with those of the stabilized layer, which shows a notably improved response. Indeed, the value of the final settlement in the case of the untreated layer is considered prohibitively large, and equals to almost 13cm, contrary to that in the case of the stabilized layer which is within potentially acceptable limits (almost 4cm).

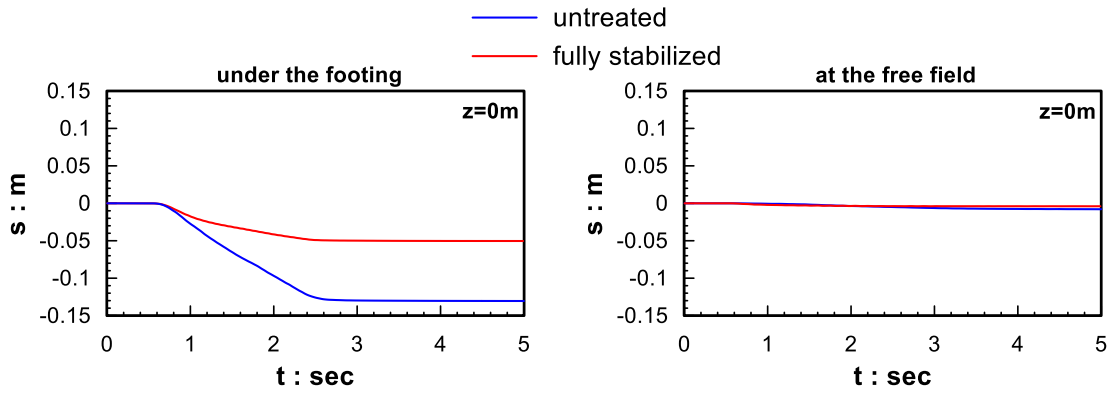

Figure 10.7 *Settlement time-histories at the ground surface under the footing and at the free field for the fully stabilized and untreated 9m soil layers.*

Moreover, at the free field, where there is no vertical loading from the footing and there are no static equilibrium shear stresses (geostatic conditions), settlements are almost zero for both cases of fully stabilized and untreated soils. The fact that settlements at the free field are insignificant compared to those under the footing is expected based on laboratory data for untreated soils (e.g. comparison of response in Velacs No1 with Velacs No12 model tests, see Andrianopoulos et al., 2010). However, the practically zero settlements predicted herein are also a consequence of the inability of the NTUA-SAND to predict large plastic volumetric strains without a significant change in the deviatoric stress ratio (n=q/p), such as in the case of a 1D (free field) seismic shaking of a horizontal soil layer.

The effect of the static factor of safety (FS) against bearing capacity on the seismic response of the surface footing resting on a fully stabilized layer was also investigated. Particularly, the values of operational loads which were additionally selected relate to: q=400kPa and 100kPa for the dynamic analyses, which correspond to factors of safety FS=1.5 and 6 respectively and were compared with the reference analysis values (q=200kPa and FS=3). Figure 10.8 presents the acceleration and excess pore pressure ratio time-histories at the stabilized layer – footing interface for the different values of factor of safety FS, while Figure 10.9 shows the corresponding settlement time-histories. It is obvious that a decrease of the factor of safety leads to an increase of acceleration amplification under the footing. Moreover, a decrease of the factor of safety FS has an increasing effect on the accumulated settlements. These effects can be related to the fact that as the FS becomes smaller, the operational load q becomes larger and thus the footing approaches bearing capacity failure and large shear induced settlements are accumulated under both static and seismic loading. It is interesting that for FS=6, the seismic settlements are practically zero after stabilization, while for FS=1.5 the value

of the settlement is increased and is equal to 16cm despite the fact that the soil has been stabilized (obviously for untreated soil and FS=1.5 the settlements are much higher, not shown here). This significant effect of FS on accumulated settlements is not related to the excess pore pressures (which are always practically zero), but to the increased amplification of the motion and the related increase of shearing loading.

Finally, the effect of the relative density D_r of the foundation soil (before stabilization) on the seismic response of the surface footing resting on a stabilized layer was investigated. In particular, two (2) additional analyses were conducted to complement the reference one related to D_r(%)=40%, one for D_r=20% which corresponds to a very loose formation and another for D_r=60% which corresponds to a quite denser sand formation. Note that the new D_r values lead to new values of the static bearing capacity, which were estimated equal to 560kPa and 720kPa respectively using the static load – settlement curves that were estimated via a displacement - controlled analysis (not shown here). Hence, in order to make a comparison for a fixed factor of safety FS=3, different operational loads were considered for the different D_r(%) values. The comparison of the results in terms of acceleration and excess pore pressure ratio r_u time-histories (Figure 10.10) does not demonstrate significant effect of the relative density D_r on accelerations, since no differences are observed in the response of the fully stabilized layer. Only a slight de-amplification of the motion is observed in the analysis of the loose sand (D_r=20%), but in terms of settlements a decreasing effect of the relative density is observed (Figure 10.11) just like for any untreated but stable soil layer. Observe, for the smaller value of D_r=20% the final value of the settlement is 10cm, which potentially could be unacceptable. However, again, the calibration of the numerical methodology has been performed for sands with medium density (Conlee et al. 2012; Gallagher et al. 2007b) and hence the response for really loose sand shown above may be an artifact of the methodology and not a drawback of passive stabilization.

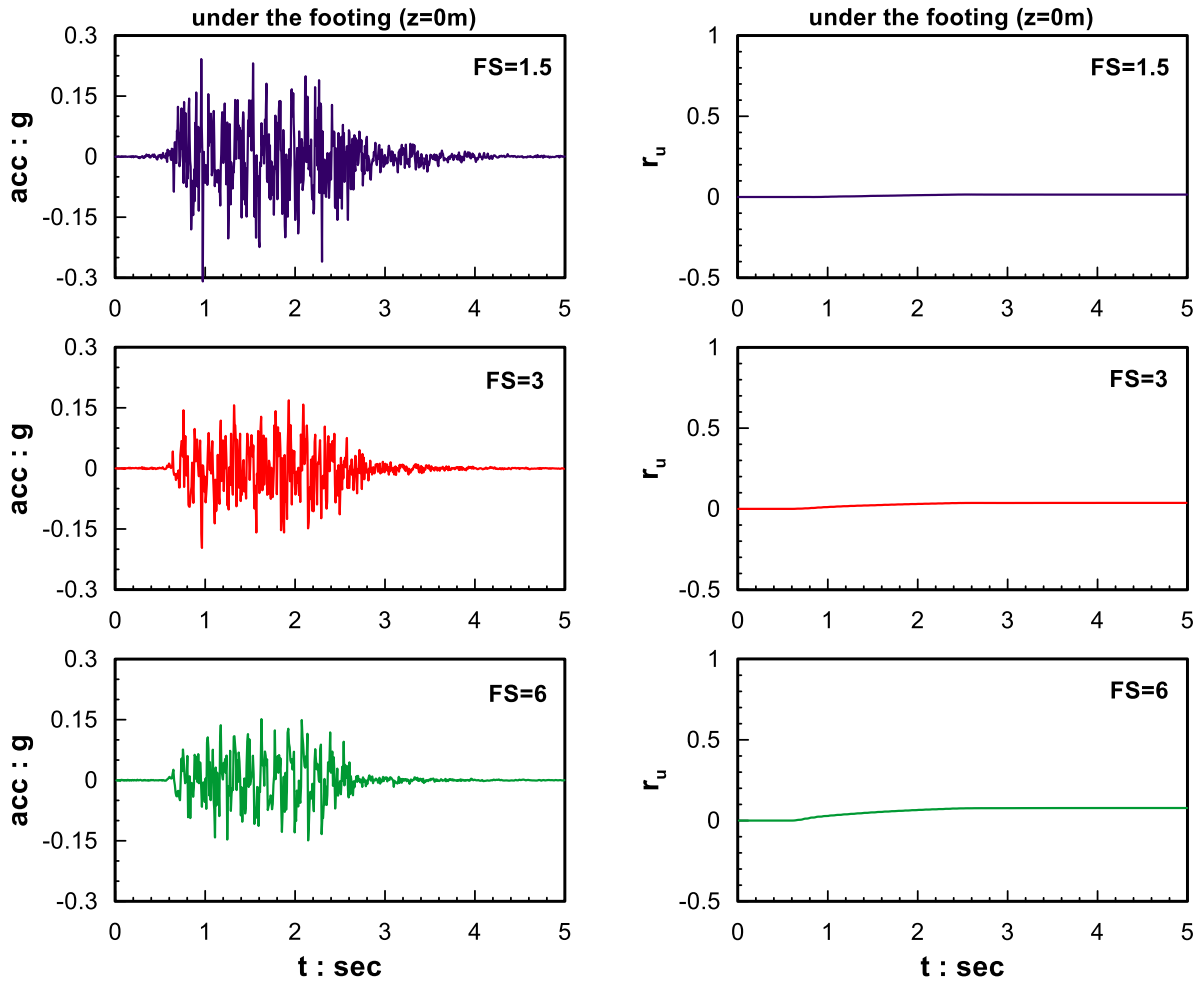

Figure 10.8 *Effect of the factor of safety (FS) against bearing capacity failure on the seismic response of a surface footing resting on a fully stabilized soil layer in terms of time-histories of acceleration (left) and excess pore pressure ratios (right).*

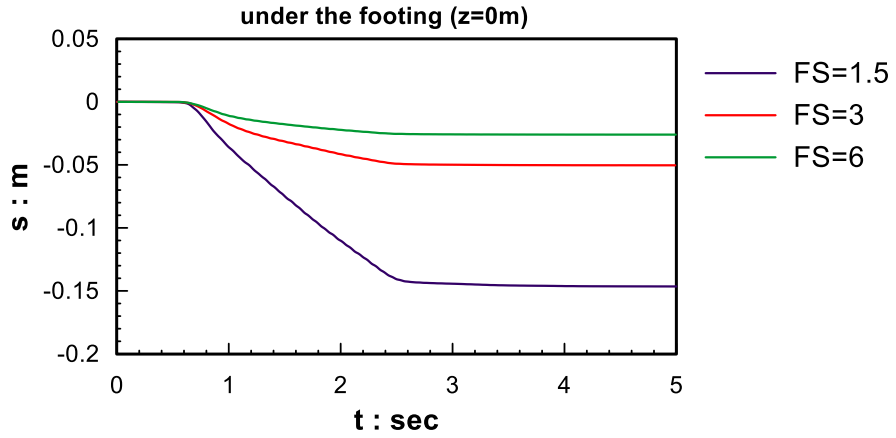

Figure 10.9 *Effect of the factor of safety (FS) against bearing capacity failure on the seismic response of a surface footing resting on a fully stabilized soil layer in terms of settlement time-histories*

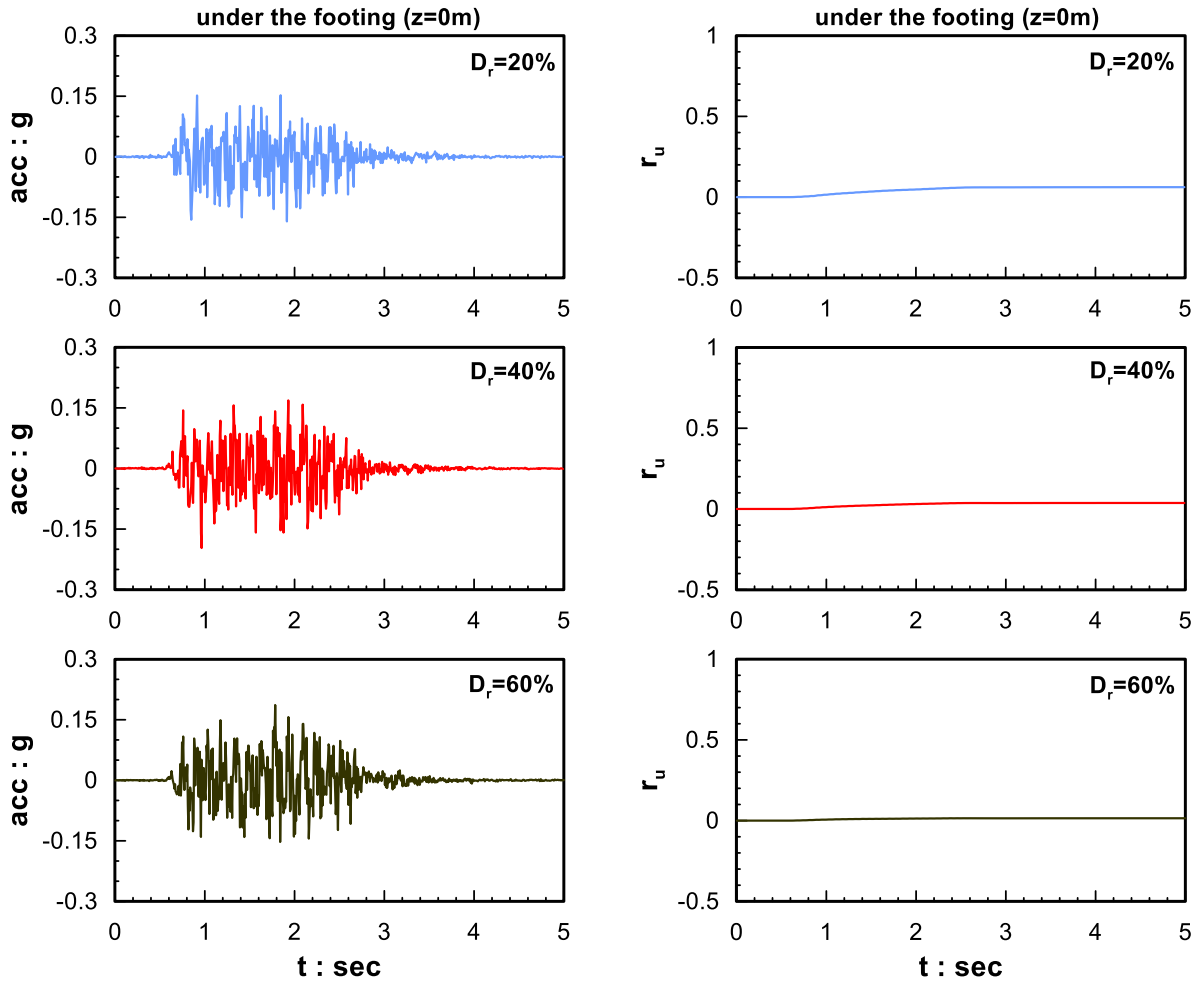

Figure 10.10 *Effect of the relative density D_r of the soil (before stabilization) on the seismic response of a surface footing resting on it after stabilization, in terms of acceleration time-histories (left) and excess pore pressure ratios (right).*

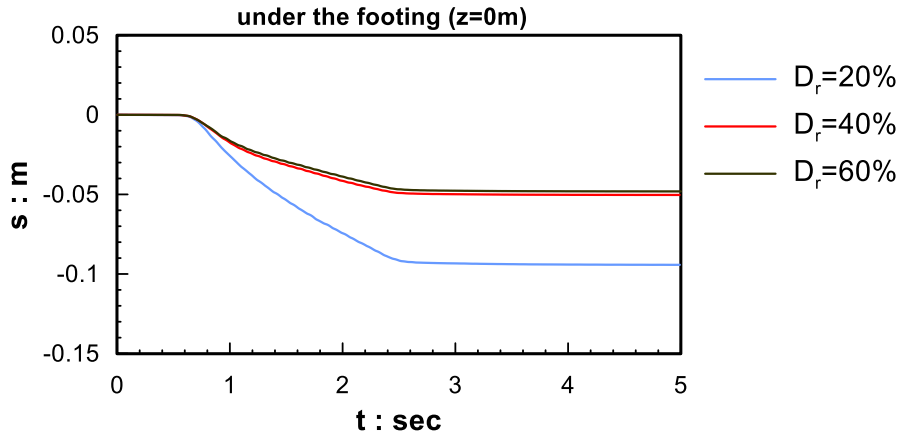

Figure 10.11 *Effect of the relative density D_r of the soil (before stabilization) on the seismic response of a surface footing resting on it after stabilization, in terms of settlement time-histories*

10.4 Effects of seismic excitation properties on the response of a surface footing resting on fully stabilized soil

In order to investigate the effects of the seismic excitation properties on the response of a surface footing resting on a fully stabilized layer, further analyses were conducted and their results were compared to those of the reference analysis for the fully stabilized layer (see paragraph 10.3). Firstly, the effect of the number of cycles N of the excitation was investigated. Figure 10.12 shows the acceleration and excess pore pressure ratio time-histories at the stabilized layer - footing interface for number of loading cycles N equal to N=2, 10 (reference analysis) and 20, while Figure 10.13 presents the corresponding settlement time-histories of the footing. As deduced from the results in terms of accelerations and excess pore pressure ratios r_u, the number of cycles N does not seem to cause significant change in the seismic response under the footing (e.g. peak acceleration remains approximately 0.2g, zero excess pore pressure ratios r_u). Moreover, as expected, the number of loading cycles N has an increasing effect on the settlement accumulation of the footing which rests on a fully stabilized layer, as would appear for untreated soils as well, in qualitative terms. However, this effect is not intense and leads to small changes in the final values of the settlements which reach a value of 7cm for the maximum studied value of loading cycles (N=20). It is interesting that the effect of loading cycles is not linear, e.g. for a fivefold increase of the number of cycles from n=2 to N=10 settlements show only a twofold increase, while for a tenfold increase from N=2 to N=20 settlements show a fourfold increase.

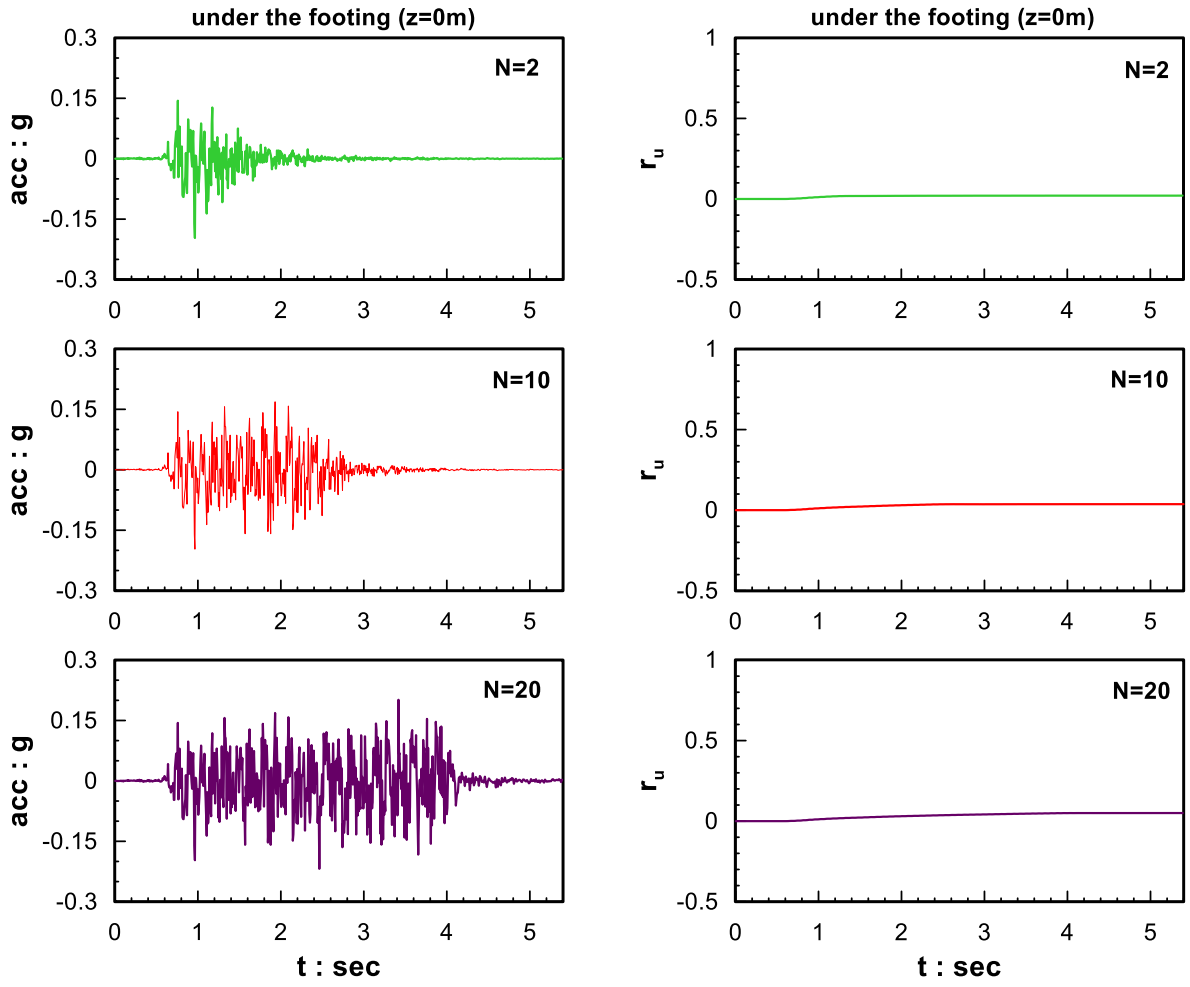

Figure 10.12 *Effect of number N of loading cycles on the seismic response of a surface footing resting on a fully stabilized soil layer in terms of time-histories of accelerations (left) and excess pore pressure ratios (right).*

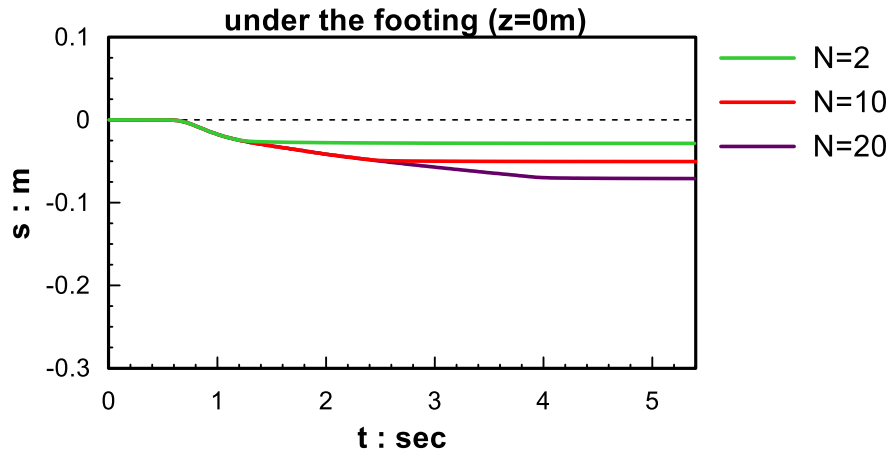

Figure 10.13 *Effect of number N of loading cycles on the seismic response of a surface footing resting on a fully stabilized soil layer in terms of settlement time-histories.*

In the sequel, the effect of excitation intensity was investigated. Figure 10.14 presents the acceleration and excess pore pressure ratio time-histories at the stabilized layer - footing interface for peak base acceleration values equal to PGA=0.10g, 0.15g (reference analysis) and 0.35g, while Figure 10.15 shows the corresponding settlement time-histories of the footing. When the excitation intensity increases, a slight de-amplification of acceleration at the layer surface (due to the increasing nonlinearity) takes place, while no substantial effect seems to exist in terms of excess pore pressure ratios, which remain approximately zero even for the maximum value of the base acceleration. However, in terms of settlements, the effect of the excitation intensity seems more intense, because as the intensity becomes higher, plastic strain accumulation becomes larger under the footing and leads to larger overall settlements. Indeed, for PGA=0.35g, the final value of settlement is equal to 12cm, which is considered excessive.

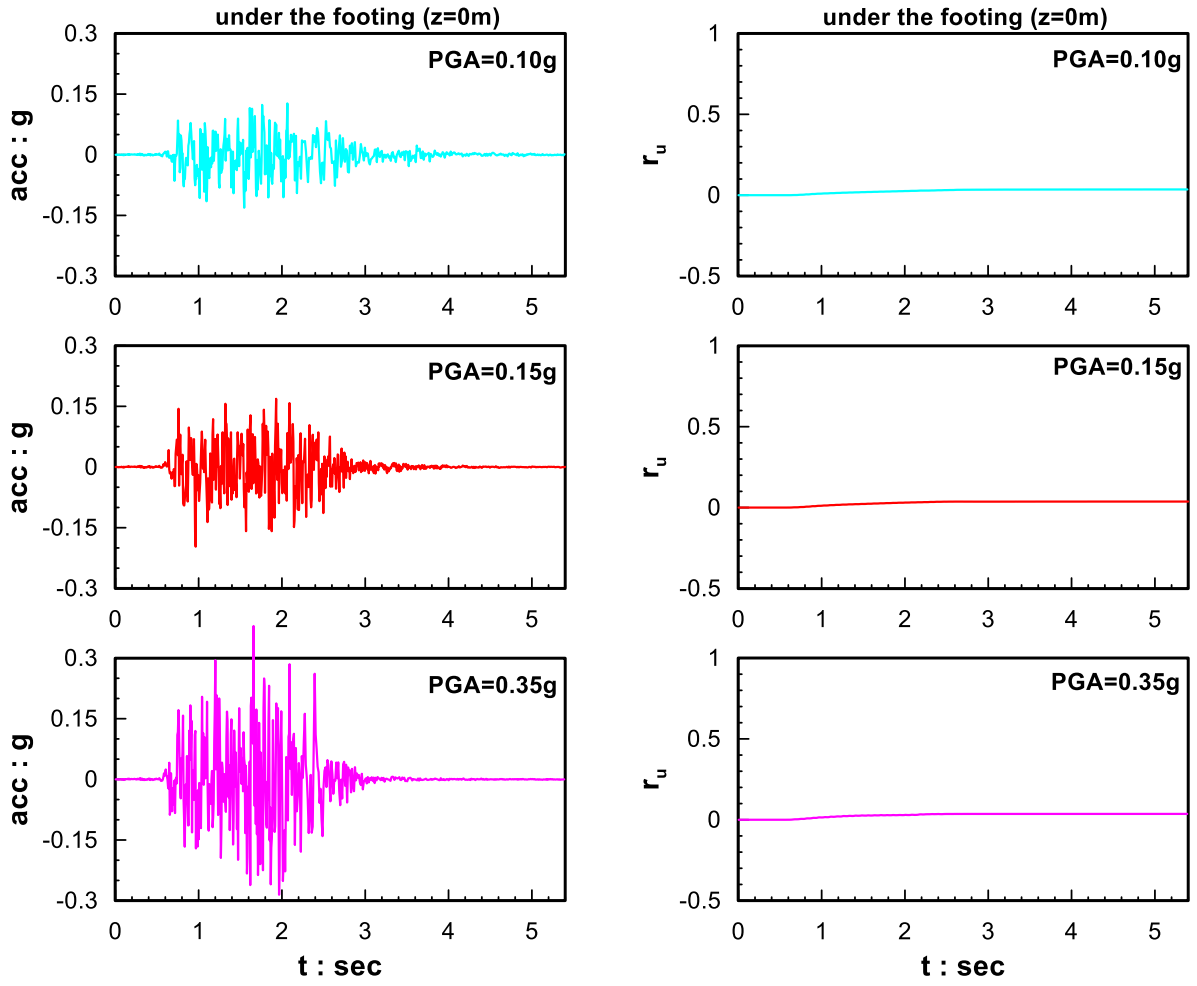

Figure 10.14 *Effect of peak ground acceleration (PGA) on the seismic response of a surface footing resting on a fully stabilized soil layer in terms of time-histories of accelerations (left) and excess pore pressure ratios (right).*

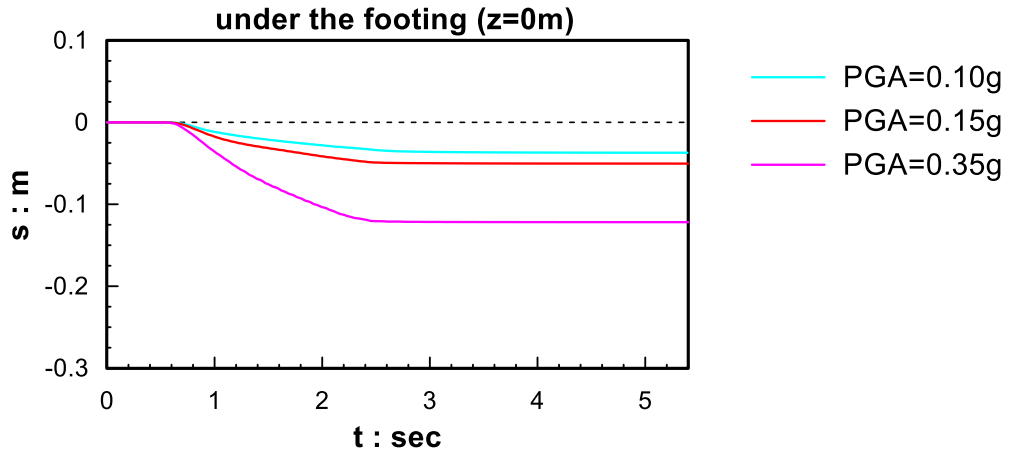

Figure 10.15 *Effect of peak ground acceleration (PGA) on the seismic response of a surface footing resting on a fully stabilized soil layer in terms of settlement time-histories*

It should be reminded here that the calibration of the methodology on the basis of centrifuge tests (Conlee et al. 2012; Gallagher et al. 2007b) is based on lower intensity excitations (010g-0.15g) if compared to the maximum value of peak base acceleration (PBA=0.35g) which led to prohibitive values of settlement (12cm). Hence, it is uncertain here if this settlement value is an artifact of the numerical methodology, or a shortcoming of the passive stabilization technique. This can only be clarified when pertinent data becomes available, but it is believed that it is an effect of the former.

Figure 10.16 presents the acceleration and excess pore pressure ratio time-histories r_u, at the stabilized layer - footing interface for different values of the predominant period: T_e=0.15sec, 0.25sec and 0.45sec of the sinusoidal motion, while Figure 10.17 shows the corresponding settlement time-histories of the footing. In terms of accelerations, the stabilized layer shows an increase of the amplification of acceleration at the footing when the predominant period of the excitation T_e increases. This increase of the amplification for lower frequencies is related to the fundamental period of the stabilized layer T_s and with the out-of-phase oscillation for T_e=0.15sec in comparison with the excitations with lower frequency which are closer to T_s. Excess pore pressure time-histories r_u retain their very low (approximately zero) values, independently of the predominant excitation period.

Taking into account that an increase of T_e leads to higher peak ground velocity values, the significant increase of settlements is expected and it is also amplified by the increased amplification of the acceleration at lower frequencies shown above. This qualitatively explains the significant increase of settlements for the low frequency excitations and leads to problematic values of settlements equal to almost 13cm even for T_e=0.25sec.

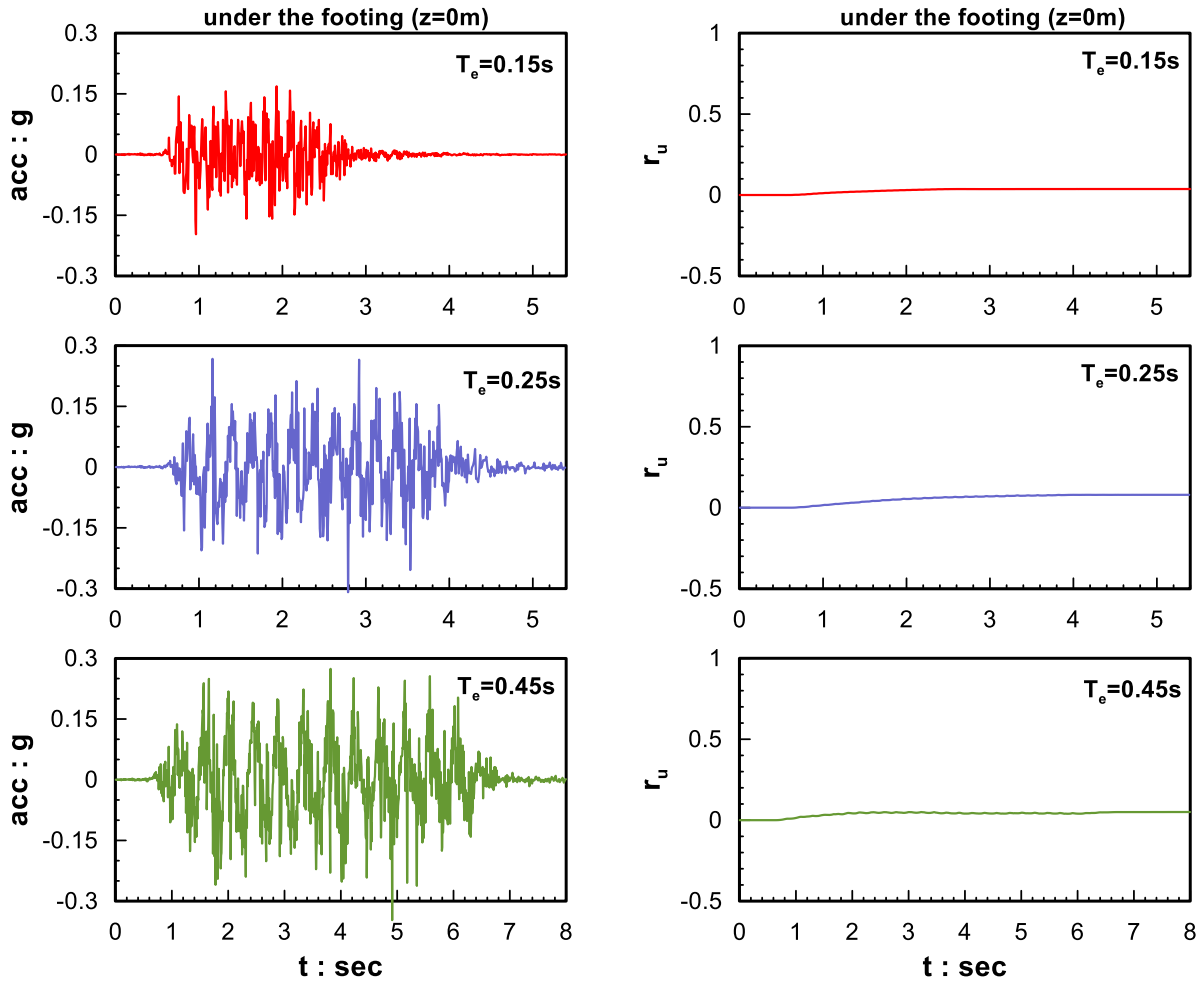

Figure 10.16 *Effect of excitation predominant period (T_e) on the seismic response of a surface footing resting on a fully stabilized soil layer in terms of time-histories of accelerations (left) and excess pore pressure ratios (right).*

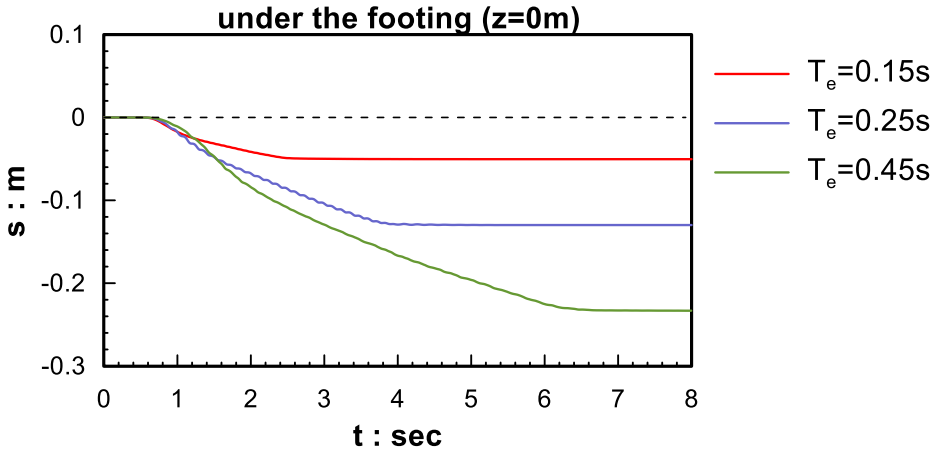

Figure 10.17 *Effect of excitation predominant period (T_e) on the seismic response of a surface footing resting on a fully stabilized soil layer in terms of settlement time-histories.*

In conclusion, judging from the results of all the aforementioned analyses, it is clear that the basic parameters which affect the response of a footing- fully stabilized foundation soil system are the predominant period of the excitation T_e, the excitation intensity (peak ground acceleration, PGA) and finally the static factor of safety, FS against bearing capacity failure. Other parameters like the number of cycles N, or the relative density D_r of the soil are of less importance.

10.5 Effects of surficial only stabilization on the seismic response of a surface footing.

This paragraph investigates the effect of surficial only (partial) stabilization on the seismic response of a 3m- wide surface footing resting on a soil layer of total thickness equal to H=9m. Two (2) cases of surficial only stabilization were analyzed, where the surficial sub-layer is stabilized having thickness H_{tr}=3m or H_{tr}=6m and the remaining underlain layer is left untreated. Figure 10.18 presents the acceleration and excess pore pressure ratio time-histories at the stabilized layer – footing interface for stabilization thicknesses equal to H_{tr}=3m and H_{tr}=6m with an underlain untreated Nevada sand layer and compares them with the corresponding response of a fully stabilized soil layer (H_{tr}=H=9m). In terms of accelerations, the partially stabilized column with H_{tr}=3m shows amplification of accelerations at the ground surface, while the opposite response is observed for the partially stabilized column with H_{tr}=6m. The effect of partial stabilization does not seem to be monotonic as far as the values of accelerations are concerned, since for the fully stabilized column with H=H_{tr}=9m, the peak acceleration at the layer surface is practically equal to that at the base of the model (PGA=0.15g). It should be clarified at this point that the response of the partially stabilized column is governed by the response of both the (surficial) stabilized and the (underlain) untreated sub-layers. If the untreated sub-layer liquefies and the stabilized sub-layer causes amplification of the ground motion, the final result of the shaking at the ground surface can be either amplification or de-amplification depending on the predominant period of the excitation T_e and the thickness of the stabilized and untreated sub-layers. However, the values of the excess pore pressure ratio r_u under the footing remain equal to zero regardless of the thickness of the surficial stabilized sub-layer. In terms of settlements, Figure 10.19 clearly depicts the benefit from passive stabilization, since the increase of the stabilization sub-layer thickness leads to significant reduction of the induced settlements. The final values of settlements are acceptable for the fully stabilized layer (H_{tr}=H=9m) and the partially stabilized with H_{tr}=6m, while for the case of partial stabilization with H_{tr}=3m the benefits of stabilization are not obvious, since the final value of the settlement reaches almost 12cm. If one considers

the results from another perspective, it may be concluded that stabilization with H_{tr}=3m is not sufficient for a 3m-width footing, while full stabilization with $H=H_{tr}$=9m is probably unnecessary because for partial stabilization with H_{tr}=6m, the settlements are practically equally reduced.

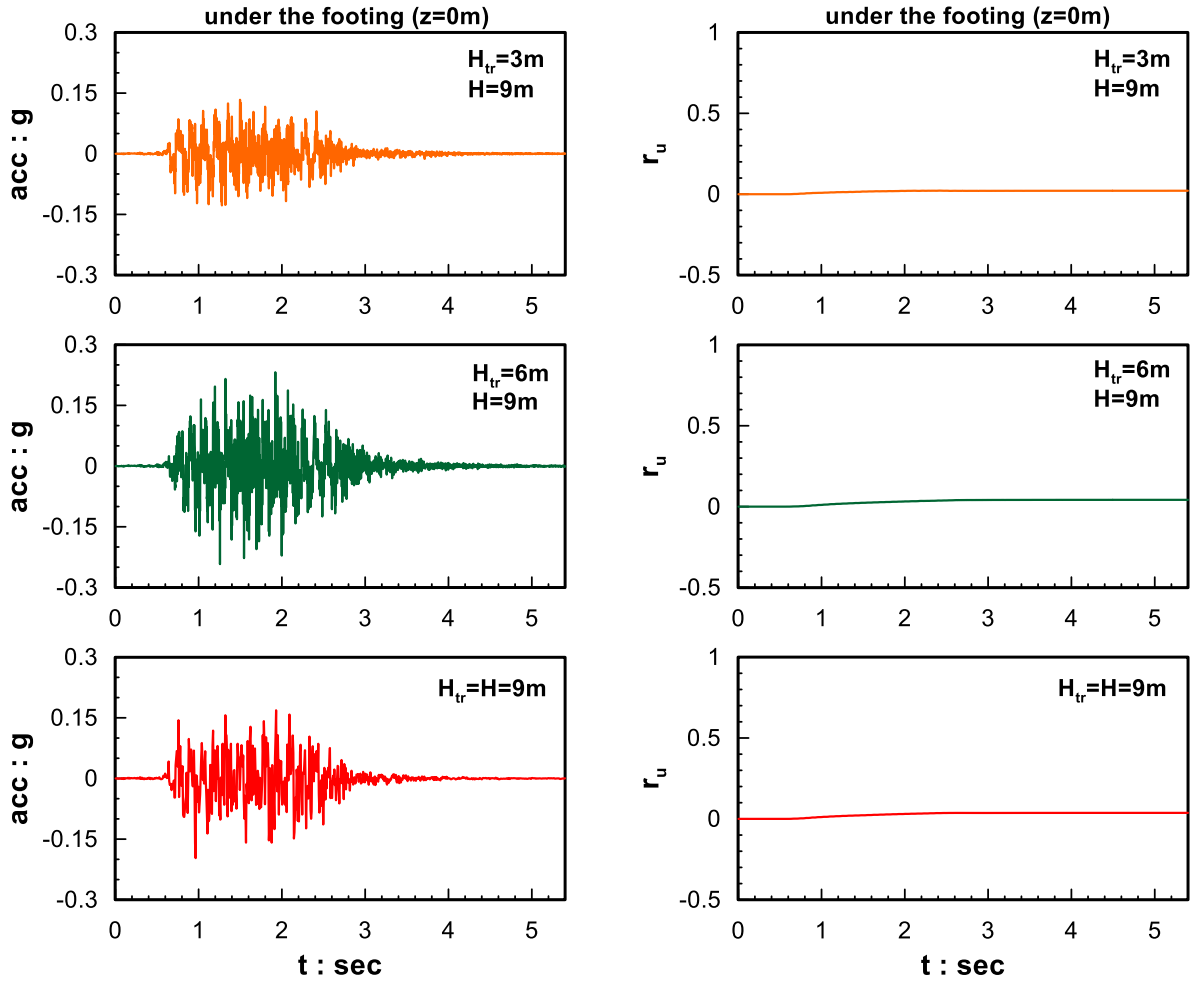

Figure 10.18 *Effect of stabilized sub-layer thickness on the seismic response of a surface footing resting on a surficially only stabilized soil layer in terms of time-histories of accelerations (left) and excess pore pressure ratios (right).*

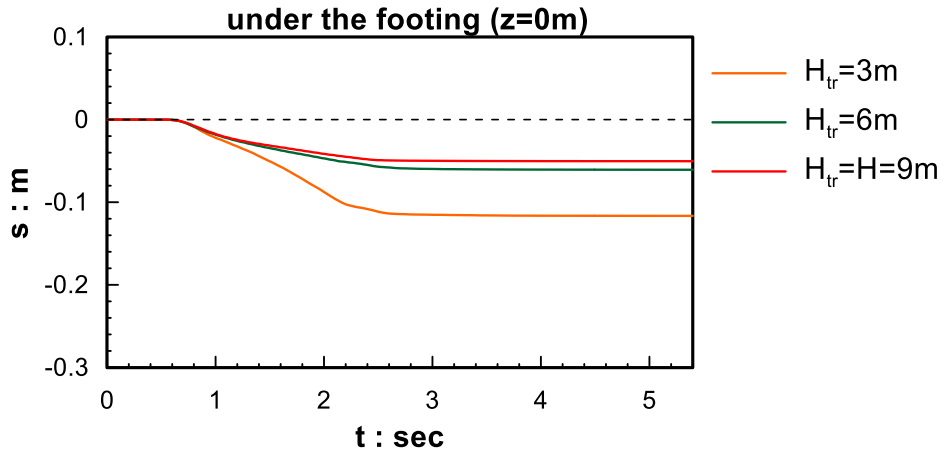

Figure 10.19 *Effect of stabilized sub-layer thickness on the seismic response of a surface footing resting on a surficially only stabilized soil layer in terms of settlement time-histories*

The effect of the permeability of the untreated soil on the seismic response of a surface footing when it rests on a fully untreated (H_{tr}=0m) or on a partially stabilized sub-layer (H_{tr}=3m) was also investigated. In particular, two (2) analyses were conducted one for the reference permeability value equal to k=3.3*10^{-3}m/s which corresponds to a coarse or gravelly sand and one with a 50 times reduced value of k/50=6.62*10^{-5}m/s which corresponds to a fine grained or silty sand. As it is obvious from Figure 10.20 where the results of the two analyses are presented in terms of acceleration and excess pore pressure ratio time-histories, the reduced permeability value (k/50), for the case of the untreated layer, leads to larger de-amplification of the motion at the soil – footing interface and also to negative excess pore pressures under the footing due to dilation. On the contrary, for the case of partial stabilization, the 50 times reduced permeability value of the underlain untreated sub-layer, does not seem to have significant effect on the response, as both the de-amplification of the accelerations at the soil – footing interface and the approximately zero excess pore pressure are practically the same in both analyses.

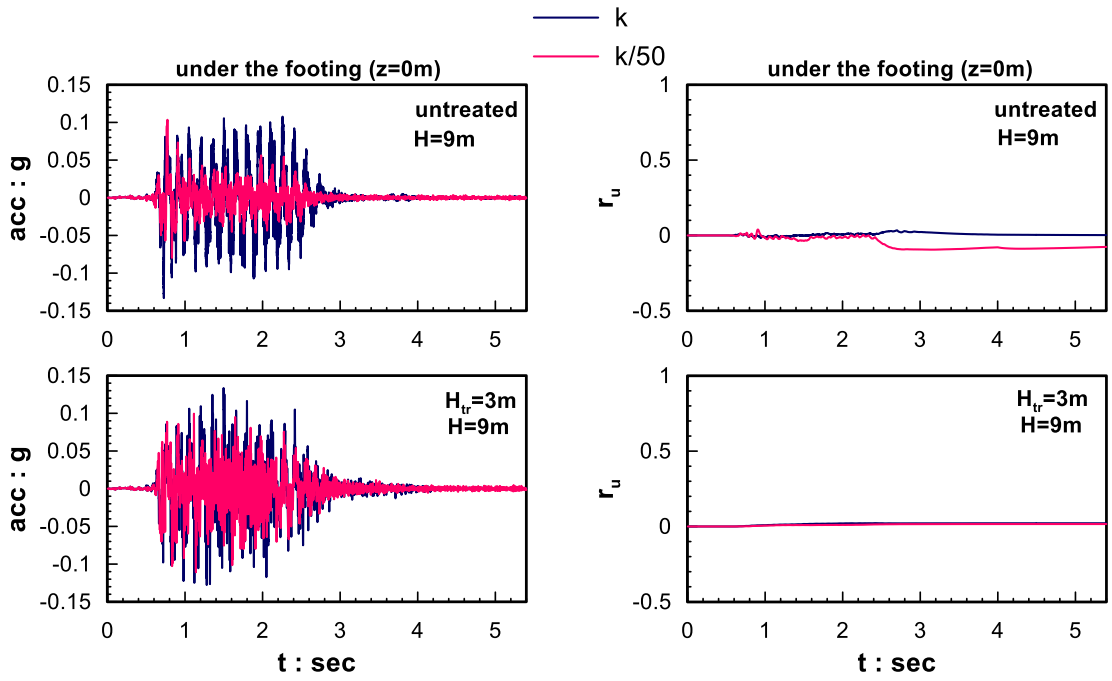

Figure 10.20 *Effect of untreated soil permeability value on the seismic response of a surface footing resting on a fully untreated (up) and a partially stabilized soil layer (down) in terms of time-histories of acceleration (left) and excess pore pressure ratios (right) at the ground surface.*

Figure 10.21 shows the results of the same comparison in terms of acceleration and excess pore pressure ratio time-histories at a depth of 3m under the footing. By comparing these results with the results at the layer surface (in Figure 10.20), it can be observed that at larger depths accelerations do not show such intense de-amplification compared to the base acceleration, while excess pore pressures in the case of partial stabilization are again practically equal to zero.

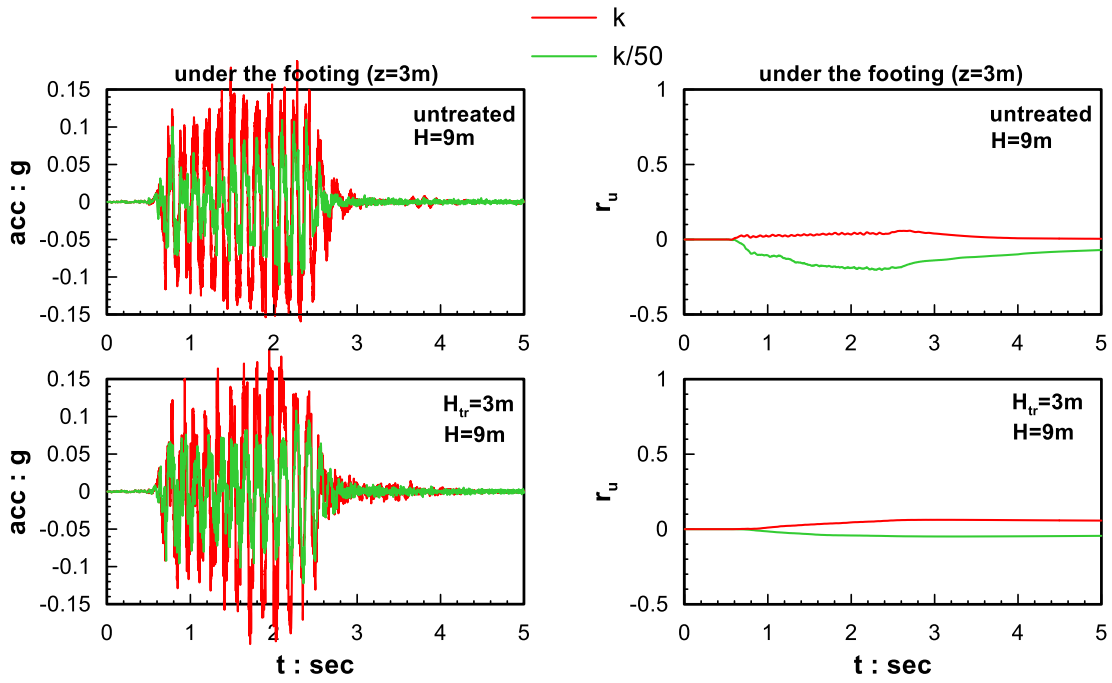

Figure 10.21 *Effect of permeability value on the seismic response of a surface footing resting on a fully untreated (up) and a surficially only stabilized soil layer (down) in terms of time-histories of accelerations (left) and excess pore pressure ratios (right) at a depth of 3m.*

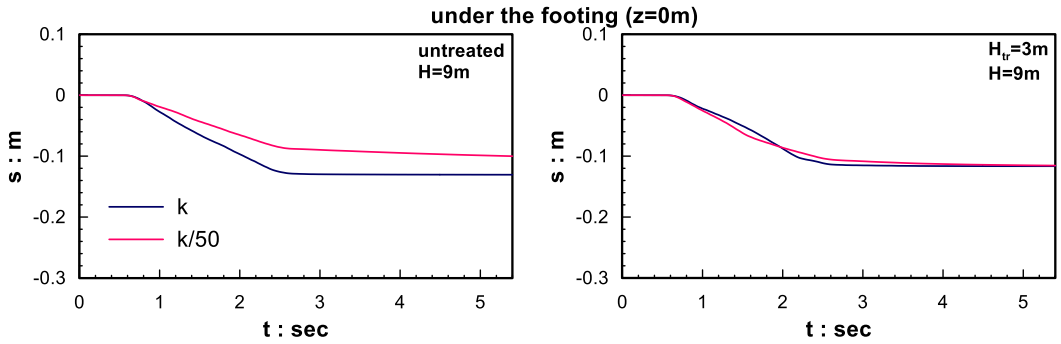

Figure 10.22 *Effect of untreated soil permeability value on the seismic response of a surface footing in terms of settlement time-histories at the ground surface when it rests on (a) a fully untreated layer of 9m thickness, (b) a surficially only (H_{tr}=3m) stabilized layer of 9m thickness.*

In terms of settlements, for the untreated layer (Figure 10.22) a decrease of settlements is observed as the permeability value decreases and this due to the anticipated dilation effects which increase rather than decrease the effective stresses during shaking. However, for the case of the partially stabilized sub-layer with H_{tr}=3m, the settlement time-histories are practically the same regardless of the permeability value of the underlain untreated sub-layer. Hence, it is clear that the permeability value of the untreated underlain sub-layer in the case

of partial stabilization is not a crucial parameter for the accumulation of the induced settlements, since they seem to depend mainly on the response of the stabilized layer.

Chapter 11

CONCLUSIONS - RECOMMENDATIONS

11.1 Summary and Conclusions

Passive (site) stabilization is a novel liquefaction mitigation technique (Gallagher 2000), with comparative advantages over existing pertinent techniques when used at developed sites, or around lifelines. It concerns the low pressure injection of a stabilizer (colloidal silica, CS) with time-increasing viscosity, at the up-gradient side of a developed site followed by delivery in place (e.g. in the foundation soil of existing structures) via enhanced groundwater flow. Once colloidal silica gels in the pores of the non-cohesive liquefiable soil, it alters the mechanical response of the soil skeleton–pore fluid system, making it less vulnerable to plastic strain accumulation related to seismic liquefaction.

This liquefaction mitigation technique is still an experimental stage worldwide and this Doctoral Thesis aids in advancing the related state-of-the-art in an attempt to make this technique practically useable by engineers. In particular, the Thesis comprises a combined experimental and computational effort studying the stabilizer properties (gel time, viscosity variation), the application procedure (injection) and the mechanical response of stabilized soil in the laboratory (element and centrifuge tests) and in the field (seismic response of stabilized soil layers, as well as of footings founded on them).

The experimental effort includes a full set of viscosity measurements with time of different CS solutions and a series of one-dimensional (1D) injection tests of CS in sandy columns aiming to complement the literature in establishing the rheological properties and the injection potential of CS. These measurements also lead to design charts and multi-variable relations for predicting the gel time and the viscosity versus time curve of CS, as well as an analytical tool for simulating the (1D) flow rate of CS, when injected in soil. In addition, the computational effort is based on a hereby proposed numerical methodology for simulating the dynamic response of CS-stabilized soils, on the basis of laboratory element tests, as well as a series of dynamic centrifuge tests. This methodology was then used parametrically for analyzing the 1D seismic response of stabilized soil layers, and the results of these analyses were used for devising a set of multi-variable relations for predicting the surface-to-base

amplification of elastic response spectra (5% damping) for such soils. The same methodology was also used parametrically for analyzing the seismic response of strip footings laying on stabilized sand layers. Emphasis was given on depicting the important problem parameters governing the footing vibration and its seismic settlements for fully or surficially only stabilized foundation soil.

The basic conclusions from this Thesis are outlined below, with references to the *Chapters* of the manuscript where these issues are addressed. In particular, the results from the literature review which refer to the rheological properties of CS (*Chapter 2*), as well as to the mechanical behavior of the CS-stabilized (*Chapter 3*) soils showed that:

- CS seems like an ideal stabilizer, since it is characterized by fairly low cost (competitive with other chemical grouts) and has appropriate chemical (environmentally inert) and rheological properties (low initial viscosity allowing for low pressure injection and rapid gelation at a well-controlled time),
- Viscosity and as a result gel time are strongly affected by pH value, the percent of CS per weight, CS(%), and the normality of cations (the concentration of an aqueous solution or how many gram equivalents of the ion are diluted into one liter of the solution) of the CS solution. As viscosity increases, the travel time of CS in sand decreases dramatically, and low-pressure injection essentially stops for viscosity values higher than very few cP. On top of viscosity, hydraulic gradient plays a significant role in CS injection, and delivery over large distances can be achieved if the viscosity of CS is retained at low values.
- Based on laboratory element test results, CS-stabilized sands have non-zero unconfined compression strength, which increases with the percent per weight of colloidal silica, CS(%), in the pore fluid, and show consistently stiffer and more dilative response, as compared to the untreated sand under the same initial and loading conditions
- Stabilization of sand with CS leads to a small increase of the elastic (small-strain) shear modulus (10% on average), but no substantial effect on the normalized shear modulus degradation and hysteretic damping increase curves with cyclic shear strain level.
- Cyclic element tests depict liquefaction (i.e. they attain a large level of cyclic strain amplitude, e.g. 2-5%) after a much increased number of cycles, as compared to the untreated sand under the same initial and loading conditions.

The results from the performed viscosity measurements at the University of Thessaly for a wide range of CS solutions (*Chapter 4*) led to the following main conclusions:

- Gel time (t_g) of CS is affected by four (4) basic factors, CS(%), cation normality, pH value, but also temperature T. The CS(%), cation normality and T have a monotonically decreasing effect on t_g, in contrast with the pH value which has a non-univocal effect. Appropriate adjustment of these 4 factors enables the control of t_g for values of a few hours to a few days or even more (as required for the application at hand).
- For all combinations of [CS(%), cation normality, T] there is a value of pH (denoted by pH_{opt}), where the minimum gel time (t_g) occurs. The value of pH_{opt} is affected by CS(%) and cation normality, but not temperature T.
- The initial CS viscosity (μ_o) is generally less than 1.5cP (for CS ≤ 10%), and proves an increasing function of CS(%). The viscosity versus time curve is qualitatively similar for all [CS(%), cation normality, T, pH] combinations and shows that a viscosity value 4 times higher than the μ_o appears at a time approximately equal to 80% of the gel time t_g.
- On the basis of the created database, a set of design charts and multi-variable relations is proposed for estimating the gel time t_g of CS solutions and the CS viscosity versus time curve, given the 4 controlling parameters [CS(%), NaCl normality, T, pH].

The 1D injection tests of CS in sand and silty sand columns of various heights performed at the University of Thessaly (*Chapter 5*) showed that:

- The ability to inject CS into sand and silty sand columns depends on the hydraulic conductivity of the soil, the properties of the CS solution and the initial gradient. The CS solution needs to be tailored to the required gel time (t_g) in order to allow delivery over the required distance, since viscosity values of 4–7cP essentially stop permeation, at least for the tested initial gradients ranging from 0.03 to 0.23.
- In order to design the injection of CS in situ, two CS characteristics need to be considered: the rate of CS viscosity increase with time (which is a function of the 4 controlling parameters [CS(%), NaCl normality, T, pH]) and the higher density of CS [which is a function of CS(%)] in comparison to the water that it displaces.
- The CS flow rate during injection may be satisfactorily simulated via an analytical tool, proposed by Agapoulaki et al (2015), that was developed in a research effort conducted concurrently with this Thesis. This tool is based on Darcy's law after appropriate adjustments for the differences in viscosity and density of CS as compared to that of water that it displaces.

Given the lack of a dedicated constitutive model of the mechanical response of stabilized sands, *Chapter 6* investigated the potential of using existing state-of-the art constitutive models for sands, after appropriate adjustments. For this purpose, the critical state NTUA-

SAND model (Andrianopoulos et al. 2010a, b) was used, following two (2) approaches for the simulation: (a) recalibration of the model constants for the soil skeleton (depicting a stiffer and less contractive response) and (b) decrease of the pore fluid bulk modulus K in comparison to the value K_w for water (denoting the seemingly increased compressibility of colloidal silica in comparison to that of water). Comparison with cyclic element tests shows that both these approaches are capable of simulating the increased liquefaction resistance of stabilized sands, as well as the related decreased dilatancy and compliance in monotonic response.

Then, *Chapter 7* and *Chapter 8* investigated the accuracy of both approaches in boundary value problems by comparing pertinent simulations (using coupled finite difference analyses) with recordings from dynamic centrifuge tests involving stabilized sand. The former Chapter emphasized the 1D seismic response of a stabilized sand layer (Gallagher et al. 2007), which does not exhibit the de-amplification of ground motion that is typically observed in liquefied layers. The latter Chapter focused on the lateral spreading response towards a free face of stabilized sand layers (Conlee et al. 2012), which shows minimal horizontal displacements and settlements. The comparisons of simulations to recordings show that:

- The recalibration of model constants and the pore fluid bulk modulus decrease that are quantified on the basis of cyclic element tests proved qualitatively accurate, but underestimated the effectiveness of stabilization in both dynamic boundary value problems.
- However, only the reduction of pore fluid bulk modulus K (via K_w/n with $n>1$) can provide quantitatively accurate predictions for both dynamic boundary value problems, and this when the denominator n increases (in comparison to its value on the basis of cyclic element tests) and is correlated to the used percentage per weight CS(%) for stabilization.
- The proposed phenomenological methodology for simulating the dynamic response of stabilized sands is applicable for the range of conditions of the experiments on which it was based, i.e. for the usual percentages per weight of CS (= 4 – 10%) and for low and intermediate intensity shakings (up to peak accelerations of 0.20g).

The foregoing proposed methodology was employed in *Chapter 9* for parametric analyses of the 1D seismic response of stabilized soil layers. These analyses showed that:

- The response of fully stabilized soil in terms of acceleration time histories is reminiscent of the pertinent response of the untreated soil under fully drained conditions, while it becomes identical to it for low intensity excitations (when zero excess pore pressures are generated in both cases).

- The surface-to-base spectral ratios for fully stabilized layers are qualitatively similar to those for stable untreated soils, like clay. For example, an increase of excitation intensity leads to an increase of the fundamental period of the stabilized soil column T_s and thus to a decrease of the spectral amplification level due to increased non-linearity, while resonance phenomena appear when the soil period T_s approaches the predominant excitation period T_e.
- In cases of surficially only stabilized soil, the seismic response at the ground surface depends mainly on the response of the underlain untreated layer, i.e. if this liquefies and its thickness is adequate, then intense de-amplification of the ground motion is observed.
- On the basis of the 66 performed parametric analyses, multi-variable relations are proposed for estimating the (surface-to-base) spectral amplification of acceleration, which require as input data: (a) the excitation properties (effective acceleration, predominant period T_e) and (b) the thickness H_{tr} of the stabilized soil layer, considering that the soil layer before stabilization is of medium density. The necessity of the new relations is dictated on the fact that currently available relations for stable untreated soils lead to considerable scatter when used for stabilized soils.

Finally, in *Chapter 10*, the seismic response of a strip (surface) footing resting on stabilized soil was also simulated with the proposed methodology, and this investigation led to the following conclusions:

- Full stabilization of the foundation soil reduces seismic footing settlements considerably, in comparison to what is expected for an untreated soil under the same excitation. However, qualitatively, for both stabilized and untreated soils, footing settlements are shear-induced and appear during shaking, i.e. they are not related to post-shaking excess pore pressure dissipation.
- The acceleration at the soil-footing interface may be significant for both fully stabilized and untreated soils, while at the free field notable differences may be observed (e.g. the untreated soil may show intense de-amplification due to liquefaction, unlike the stabilized soil).
- Seismic settlements of footings on fully stabilized soils increase with increasing acceleration, predominant period and number of loading cycles, with the effects of the first two being more significant. On the contrary, an increase of the static factor of safety against bearing capacity failure and/or the relative density of the sand prior to stabilization reduce the post-stabilization seismic settlements of the footing.
- A surficial only stabilized layer (of infinite extent) having thickness equal to the footing width does not provide adequate reduction of seismic settlements. However, if the thickness of

the stabilized layer becomes twice the width of the footing, the reduction of settlements approaches its full extent (that of a fully stabilized foundation soil).

11.2 Recommendations for future research

Based on everything outlined above, this Thesis has shed ample light to various aspects of passive (site) stabilization. However, this novel ground improvement technique is not considered yet ready for immediate application by engineers. This is due to the fact that there are still quality control and assurance issues that require further research. In particular, the following are suggested:

- The temperature T effect on gel time of CS is a newly explored parameter for passive stabilization which was introduced in this Thesis. This effect should be explored in more detail, especially in regard to actual soil temperatures in situ, as opposed to the CS solution preparation and storing temperatures.
- The injection of CS solutions prepared with low NaCl normality into marine environments should be further investigated, since in such cases the water in the sand pores already has NaCl (in relatively large amounts) and this could hinder the CS flow in great distances or long times (since increase of NaCl normality reduces the gel time).
- Large scale CS injections should be performed insitu, after establishing a procedure for designing the injection procedure. Given the higher density of CS in comparison to water, it is advised that the pressure levels are not very low so as not to allow the CS solution to migrate downwards. For injections that require more than one day, one crucial aspect is whether the CS is prepared once (and stored until injection), or if different batches are prepared each day (which have different viscosities due to the time lag in their mixing time).
- The proposed phenomenological methodology for simulating the mechanical response of stabilized sands is based on the premise of a relatively compressible CS solution, a fact that has been observed only indirectly. The actual value of the compressibility of CS has not been measured reliably yet, and this is a requirement for the methodology to gain further credibility. However, it has to be underlined here, that a dedicated constitutive model for stabilized sands is always preferable to any phenomenological simulation methodology, like the one proposed herein.
- In addition, the foregoing methodology has been calibrated and verified for medium dense stabilized sands that have undergone low and medium intensity excitations. The simulations for higher intensity excitations seem to underestimate the effectiveness of stabilization, but these observations are based on recordings which are not considered as reliable as those for lower intensities. Hence, reliable measurements on stabilized media of different

densities founding various structural types (e.g. footings of different sizes and load levels) and undergoing high intensity excitations are required, not only for verifying the proposed methodology, but mainly for verifying the effectiveness of this novel ground improvement technique under more extreme seismic hazard scenarios.

REFERENCES

Agapoulaki, G. I., and Papadimitriou, A. . (2015). “Rheological properties of colloidal silica as a means for designing passive stabilization of liquefiable soils.” *XVI European Conference on Soil Mechanics and Geotechnical Engineering*, Edinburgh, United Kingdom, 13-17 September.

Agapoulaki, G.I, Papadimitriou, A.G., Kandris, K., Pantazidou, M. (2015). “Permeation potential of colloidal silica for passive stabilization of liquefiable soils. ”, *XVI European Conference on Soil Mechanics and Geotechnical Engineering*, Edinburgh, United Kingdom, 13-17 September.

Andrianopoulos, K. I. (2006). “Numerical Modeling of Static and Dynamic Behavior of Elastoplastic Soils.” PhD Thesis, Dept of Civil Engineering, NTUA, Athens.

Andrianopoulos, K. I., Agapoulaki, G. I., and Papadimitriou, A. G. (2015). “Numerical analysis of the seismic response of sand passively stabilized against liquefaction.” *XVI European Conference on Soil Mechanics and Geotechnical Engineering*, Edinburgh, United Kingdom, 13-17 September.

Andrianopoulos, K. I., Papadimitriou, A. G., and Bouckovalas, G. D. (2010a). “Explicit integration of bounding surface model for the analysis of earthquake soil liquefaction.” *International Journal for Numerical and Analytical Methods in Geomechanics*, 34(15), 1586–1614.

Andrianopoulos, K. I., Papadimitriou, A. G., and Bouckovalas, G. D. (2010b). “Bounding surface plasticity model for the seismic liquefaction analysis of geostructures.” *Soil Dynamics and Earthquake Engineering*, 30(10), 895–911.

Arulanandan, K., and Scott, R. F. (1994). “Verification of numerical procedures for the analysis of soil liquefaction problems.” *International Conference on the Verification of Numerical Procedures for the Analysis of Soil Liquefaction Problems*, CRC Press, Davis, CA.

Arulanandan, K., and Sybico Jr, J. (1993). “Post-liquefaction settlement of sands.” *Predictive soil mechanics. Proc. of the Wroth memorial symposium, Oxford, 1992*, (H. G.T. and S. A.N., eds.), JOUR, Thomas Telford, 94–110.

Arulmoli, K., Muraleetharan, K. K., Hossain, M. M., and Fruth, L. S. (1992). “VELACS: verification

of liquefaction analyses by centrifuge studies; Laboratory Testing Program – Soil Data Report." *Research Report, The Earth. Technology Corporation*.

Axelsson, M. (2006). "Mechanical tests on a new non-cementitious grout, silica sol: A laboratory study of the material characteristics." *Tunnelling and Underground Space Technology*, 21(5), 554–560.

Bardet, J. P., Huang, Q., and Chi, S. W. (1994). "Numerical prediction for Model 1." *Int. Conf. on Verification of numerical procedures for the analysis of soil liquefaction problems*, Davis, CA, Vol I, pp 67-86.

Been, K., and Jefferies, M. G. (1985). "A state parameter for sands." *Géotechnique*, 35(2), 99–112.

Biot, M. A. (1941). "General theory of three dimensional consolidation." *Journal of Applied Physics*, 12(2), 155–164.

Bouckovalas, G. D., and Papadimitriou, A. G. (2003). "Multi-variable relations for soil effects on seismic ground motion." *Earthquake Engineering & Structural Dynamics*, 32(12), 1867–1896.

Chaloulos, Y. K., Bouckovalas, G. D., and Karamitros, D. K. (2013). "Pile response in submerged lateral spreads: Common pitfalls of numerical and physical modeling techniques." *Soil Dynamics and Earthquake Engineering*, 55, 275–287.

Conlee, C. T. (2010). "Dynamic properties of colloidal silica soils using centrifuge model tests and a full-scale field test." PhD Thesis, Drexel University.

Conlee, C. T., Gallagher, P. M., Boulanger, R. W., and Kamai, R. (2012). "Centrifuge Modeling for Liquefaction Mitigation Using Colloidal Silica Stabilizer." *Journal of Geotechnical and Geoenvironmental Engineering*, 138(11), 1334–1345.

Corral, G., and Whittle, A. (2007). "Cyclic direct shear testing." G. J. Rix and L. M. Spencer, eds., Atlanta, GA

Dafalias, Y. F., and Manzari, M. T. (1997). "A critical state two-surface plasticity model for sands." *Géotechnique*, Thomas Telford, 47(2), 255–272.

Díaz-Rodríguez, J. a., Antonio-Izarraras, V. M., Bandini, P., and López-Molina, J. a. (2008). "Cyclic strength of a natural liquefiable sand stabilized with colloidal silica grout."

Canadian Geotechnical Journal, 45(10), 1345–1355.

Drabarek, E., Bartlett, J. R., Hanley, H. J. M., Woolfrey, J. L., and Muzny, C. D. (2002). "Effect of Processing Variables on the Structural Evolution of Silica Gels." *International Journal of Thermophysics*, Kluwer Academic Publishers-Plenum Publishers, 23(1), 145–160.

Gallagher, P. M. (2000). "Passive site remediation for mitigation of liquefaction risk." PhD Thesis, Virginia Polytechnic Institute and State Univ., Blacksburg Va.

Gallagher, P.M., Pamuk, A., Abdoun. T., (2007a). "Stabilization of liquefiable soils using colloidal silica grout." *Journal of Material in Civil Engineering*, 19, p. 33-40

Gallagher, P. M., Conlee, C. T., and Rollins, K. M. (2007b). "Full-Scale Field Testing of Colloidal Silica Grouting for Mitigation of Liquefaction Risk." *Journal of Geotechnical and Geoenvironmental Engineering*, 133(2), 186–196.

Gallagher, P. M., and Finsterle, S. (2004). "Physical and Numerical Model of Colloidal Silica Injection for Passive Site Stabilization." *Vadose Zone Journal*, Soil Science Society of America, 3(3), 917–925.

Gallagher, P. M., and Koch, A. J. (2003). "Model testing of passive site stabilization: A new grouting technique." *Geotechnical Special Publication*, 1478–1489.

Gallagher, P. M., and Lin, Y. (2005). "'Column testing to determine colloidal silica transport mechanisms.'" *Innovations in Grouting and Soil Improvement*.

Gallagher, P. M., and Lin, Y. (2009). "Colloidal Silica Transport through Liquefiable Porous Media." *Journal of Geotechnical and Geoenvironmental Engineering*, ASCE - American Society of Civil Engineers, 135(11), 1702–1712.

Gallagher, P. M., and Mitchell, J. K. (2002). "Influence of colloidal silica grout on liquefaction potential and cyclic undrained behavior of loose sand." *Soil Dynamics and Earthquake Engineering,* 22_9–12_, 1017–1026.

Gallagher, P. M., Pamuk, A., and Abdoun, T. (2007b). "Stabilization of Liquefiable Soils Using Colloidal Silica Grout." *Journal of Materials in Civil Engineering*, 19(1), 33–40.

Gallagher, P. M., Pamuk, A., Koch, A. J., and Abdoun, T. H. (2002). "Centrifuge modeling of passive site remediation." *Proceedings of the 7th U.S. National Conference on Earthquake Engineering (7NCEE): Urban Earthquake Risk, Boston, MA*.

Haldavnekar, V., Bobet, A., Santagata, M., and Drnevich, V. (2004). “Soil treatment with a thixo-tropic fluid: an autoadaptive design for liquefaction prevention.” *11th International Conference on Soil Dynamics & Earthquake Engineering & 3rd International Conference on Earthquake Geotechnical Engineering*, Vol. II, 553-560.

Hardin, B. (1978). "The Nature of Stress-Strain Behaviour for Soils." *Proceedings of Earthquake Engineering and Soil Dynamics*, ASCE, Pasadena, 19-21 June 1978, 3-89.

Huang, H., You, B., Zhou, S., and Wu, L. (2007). “Rheological behavior of aqueous organosilicone resin emulsion stabilized by colloidal nanosilica particles.” *Journal of Colloid and Interface Science*, 310(1), 121–127.

Idriss, I. M., and Boulanger, R. W. (2008). "Soil Liquefaction During Earthquakes." Earthquake Engineering Research Institute, Oakland, California, USA.

Ishihara, K., Tatsuoka, F., and Yasuda, S. (1975). “Undrained deformation and liquefaction of sand under cyclic stresses.” *Soils and Foundations*, 15(1), 29–44.

Itasca. (2011). “FLAC version 7.0.” *Itasca Consulting Group Inc.*

Jurinak, J. J., and Summers, L. E. (1991). “Oilfield applications of colloidal silica gel.” *SPE (Society of Petroleum Engineers) Production Engineering; (United States)*, 6:4.

Kamai, R., and Boulanger, R. W. (2009). “Characterizing localization processes during liquefaction using inverse analyses of instrumentation arrays.” *Meso-Scale Shear Physics in Earthquake and Landslide Mechanics*.

Kamai, R., and Boulanger, R. W. (2013). “Simulations of a Centrifuge Test with Lateral Spreading and Void Redistribution Effects.” *Journal of Geotechnical and Geoenvironmental Engineering*, American Society of Civil Engineers, 139(8), 1250–1261.

Karol, R. H. Reuben H. (2003)." Chemical grouting and soil stabilization." M. Dekker, 3rd Ed. CRC, Boca Raton, Fla., 584.

Klein, L. C., Gallo, T. A., & Garvey, G. J. (1984). "Densification of monolithic silica gels below 1000°C." *Journal of Non-Crystalline Solids*, *63*(1), 23–33.

Koch, A. J. (2002). “Model testing of passive site stabilization.”. PhD Thesis, Drexel University.

Kodaka, T., Oka, F., Ohno, Y., Takyu, T., Yamasaki, N. (2005). Modelling of cyclic deformation and strength characteristics of silica treated sand. In Proceedings, 1st Japan – US

Workshop on Testing, Modelling, and Simulation (GSP 143)

Ladd, C. C., Foott, R., Ishihara, K., Schlosser, F., and Poulos, H. G. (1977). "Stress–deformation and strength characteristics, State of the art report." *Proc. 9th International Conference on Soll Mechanics and Foundation Engineering*, Tokyo, 1977, V2, P~21-494

Ladd, R. S. (1978). "Preparing test specimens using undercompaction." *Geotech. Test. J.* 1978; 1 (1): 16-23.

Liao, H. J., Huang, C. C., and Chao, B. S. (2003). "Liquefaction resistance of a colloid silica grouted sand." *Geotechnical Special Publication*, 1305–1313.

Lin, Y. (2006). "Colloidal silica transport mechanisms for passive site stabilization of liquefiable soils.", PhD Thesis, Drexel University.

Lin, Y., and Gallagher, P. M. (2006). "Three-Meter Column Testing of Colloidal Silica Transport through Porous Media." *Ground Modification and Seismic Mitigation*, American Society of Civil Engineers, Reston, VA, 417–424.

Liu, L., and Dobry, R. (1997). "Seismic response of shallow foundation on liquefiable sand." *Journal of Geotechnical and Geoenvironmental Engineering*, JOUR, ASCE, 123(6), 557–566.

Manchester, K., Zaluski, M., North-Abbott M., Trudnowski, J., Bickford, J., Wraith, J. (2001). "Grout Selection and Characterization in Support of the Colloidal Silica Barrier Deployment at Brookhaven National Laboratory." *WM'01 Conference*, Tucson, AZ.

Manzari, M. T., and Arulanandan, K. (1994). "Numerical Predictions for Model No. 1." *Int. Conf. on Verification of numerical procedures for the analysis of soil liquefaction problems*, Davis, CA, Vol. 1, pp. 179–185.

Manzari, M. T., and Dafalias, Y. F. (1997). "A critical state two-surface plasticity model for sands." *Geotechnique*, 47(2), 255–272.

Minkoff, S. E., Stone, C. M., Bryant, S., Peszynska, M., and Wheeler, M. F. (2003). "Coupled fluid flow and geomechanical deformation modeling." *Journal of Petroleum Science and Engineering*, 38(1–2), 37–56.

El Mohtar, C. S. (2008). "Pore fluid engineering: An autoadaptive design for liquefaction mitigation.", PhD Thesis, Purdue University.

El Mohtar, C. S., Bobet, A., Drnevich, V. P., Johnston, C., and Santagata, M. C. (2008a). "Effect of plastic fines on the small strain stiffness of sand." *4th International Symposium on Deformation Characteristics of Geomaterials*, IS-Atlanta.

El Mohtar, C. S., Clarke, J. P., Bobet, A., Drnevich, V. P., Johnston, C., and M.C., S. (2008b). "Cyclic response of a sand with thixotropic pore fluid." *4th International Conference on Geotechnical Earthquake Engineering and Soil Dynamics*, Sacramento.

Mollamahmutoglu, M., and Yilmaz, Y. (2009). "Pre- and post-cyclic loading strength of silica-grouted sand." *Proceedings of the Institution of Civil Engineers - Geotechnical Engineering*, Thomas Telford Ltd, 343–348.

Moradi, G., and Seyedi, S. (2015a). "Evaluation of uniform delivery of colloidal nano-Silica stabilizer to liquefiable silty sands." *International Journal of Nano Dimension*, 6(5), 501–508.

Moradi, G., Seyedi, S., Moradi, G., and Seyedi, S. (2015b). "Effect of Sampling Method on Strength of Stabilized Silty Sands with Colloidal Nano Silica." *Journal of Civil Engineering Research*, Scientific & Academic Publishing, 5(6), 129–135.

Moridis, G. J., Apps, J., Persoff, P., Myer, L., Muller, S., Yen, P., and Pruess, K. (1996). "A Field Test of a Waste Containment Technology Using a New Generation of Injectable Barrier Liquids | Welcome to The Berkeley Lab Publications System." *Spectrum'96*, Seattle, WA.

Mróz, Z., Norris, V. A., Zienkiewicz, O.C. (1999). "Application of an anisotropic hardening model in the analysis of elasto–plastic deformation of soils." *Géotechnique*, 1979, 29:1, 1-34

Mulilis, J. P., Seed, H. B., Chan, C. K., Mitchell, J. K., and Arulanandan, K. (1977). "Effects of Sample Preparation on Sand Liquefaction." *Journal of Geotechnical Engineering Division*, ASCE 103, GT2, 1977, pp. 91-108

Noll, M. R., Bartlett, C. L., and Dochat, T. M. (1992). "In situ permeability reduction and chemical fixation using colloidal silica." *Proceedings of the Sixth National Outdoor Action Conference*, National Ground Water Association, Las Vegas, NV, pp. 443-457.

Noll, M. R., Epps, D. E., Bartlett, C. L., and Chen, P. J. (1993). "Pilot field application of a colloidal silica gel technology for in situ hot spohorizontal groutingt stabilization and horizontal grouting." *7th National Outdorr Action Conference, National Groundwater Association*,

Las Vegas, NV, 207–219.

Otterstedt, J.-E., Greenwood, P. (2005). "Some important, fairly new uses of colloidal silica / silica soil." Chapter 57 in *Colloidal Silica: Fundamentals and Applications* (eds by Bergna H., Roberts W.O.), Taylor and Francis CR

Paassen, L. A. Van, Harkes, M. P., Zwieten, G. A. Van, Zon, W. H. Van der, Star, W. R. L. Van der, and Loosdrecht, M. C. M. Van. (2009). "Scale up of BioGrout: A biological ground reinforcement method." *Proc. 17th Int. Conf. Soil Mech. Geotech. Eng.* 2328–2333

Pamuk, A., Gallagher, P. M., and Zimmie, T. F. (2007). "Remediation of piled foundations against lateral spreading by passive site stabilization technique." *Soil Dynamics and Earthquake Engineering*, 27(9), 864–874.

Papadimitriou, A. G. Agapoulaki, G. I. (2013). "Mechanical response and simulation of sands stabilized with colloidal silica against seismic liquefaction." *International Conference on Earthquake Geotechnical Engineering in honour of Professor Kenji Ishihara*, Istanbul, Turkey.

Papadimitriou, A. G., and Agapoulaki, G. I. (2014). "Passive stabilization: A novel technique for seismic liquefaction at the foundation soil of existing structures." *Advances in Civil Engineering Research, Volume on the occasion of the 20th Anniversary of the Department of Civil Engineering, University of Thessaly, Volos, Greece*, 331–342.

Papadimitriou, A. G., and Bouckovalas, G. D. (2002). "Plasticity model for sand under small and large cyclic strains: A multiaxial formulation." *Soil Dynamics and Earthquake Engineering*, JOUR, 22(3), 191–204.

Papadimitriou, A. G., Bouckovalas, G. D., and Dafalias, Y. F. (2001). "Plasticity model for sand under small and large cyclic strains." *Journal of Geotechnical and Geoenvironmental Engineering*, JOUR, ASCE, 127(11), 973–983.

Persoff, P., Apps, J., Moridis, G., and Whang, J. M. (1999). "Effect of dilution and contaminants on sand grouted with colloidal silica." *Journal of Geotechnical and Geoenvironmental Engineering*, 125(6), 461–469.

Persoff, P., Moridis, G., Apps, J., and Pruess, K. (1998). "Evaluation Tests for Colloidal Silica for Use in Grouting Applications." *Geotechnical Testing Journal*, ASTM International, 21(3), 264.

Persoff, P., Moridis, G. J., Apps, J., Pruess, K., and Muller, S. J. (1994). “Designing injectable colloidal silica barriers for waste isolation at the Hanford Site.” Battelle Press, Columbus, OH (United States).

Popescu, R., and Prevost, J. (1994). “Numerical class ‘A’ predictions for Models Nos 1,2 ,3,4a, 4b, 6, 7, 11 & 12.” *Int. Conf. on Verification of numerical procedures for the analysis of soil liquefaction problems*, Vol. I, pp. 1105–1207.

Post, V., Kooi, H., and Simmons, C. (2007). “Using hydraulic head measurements in variable-density ground water flow analyses.” *Ground water*, 45(6), 664–71.

Ramberg, W., and Osgood, W. R. (1943). "Description of stress-strain curve by three parameters." *Technical note 902*, National Advisory Committee for Aeronautics.

Saiers, J. E., Hornberger, G. M., and Harvey, C. (1994). “Colloidal silica transport through structured, heterogeneous porous media.” *Journal of Hydrology*, 163(3–4), 271–288.

Scherer, G. W., Pardenek, S. A., and Swiatek, R. M. (1988). “Viscoelasticity in silica gel.” *Journal of Non-Crystalline Solids*, 107(1), 14–22.

Shahir, H., Pak, A., Taiebat, M., and Jeremić, B. (2012). “Evaluation of variation of permeability in liquefiable soil under earthquake loading.” *Computers and Geotechnics*, JOUR, Department of Engineering, Tarbiat Moallem University, P.O. Box 31979-37551, Karaj, Iran, 40, 74–88.

Simmons, C. T. (2005). “Variable density groundwater flow: From current challenges to future possibilities.” *Hydrogeology Journal*, 13(1), 116–119.

Spencer, L. M., Rix, G. J., and Gallagher, P. M. (2008a). “Colloidal silica gel and sand mixture dynamic properties.” *Proc., Conf. of Geotechnical Earthquake Engineering and Soil Dynamics IV*.

Spencer, L., Rix, G. J., and Gallagher, P. (2008b). “Colloidal Silica Gel and Sand Mixture Dynamic Properties.” *Geotechnical Earthquake Engineering and Soil Dynamics IV*, American Society of Civil Engineers, Reston, VA, 1–10.

Taboada, V. M. (1995). “Centrifuge modeling of earthquake-induced lateral spreading in sand using a laminar box.” Ph.D. thesis, Rensselaer Polytechnic Institute, Troy, N.Y.

Taiebat, M., Shahir, H., and Pak, A. (2007). “Study of pore pressure variation during

liquefaction using two constitutive models for sand." *Soil Dynamics and Earthquake Engineering*, 27(1), 60–72.

Towhata, I. (2007). Earthquake Geotechnical Engineering, Springer Series (eds K.D. Pitilakis), p 355–383.

Towhata, I. (2008). Geotechnical Earthquake Engineering, Springer Series in Geomechanics and Geoengineering, (eds. W. Wu, R. I. Borja), p 697.

Towhata, I., Kabashima, Y. (2001). "Mitigation of seismically-induced deformation of loose sandy foundation by uniform permeation grouting.", *Proc. Earthquake Geotechnical Engineering Satellite Conference*, 15th International Conference on Soil Mechanics and Geotechnical Engineering, Istanbul, Turkey, pp 313–318

Verruijt, A. (2013). "Theory and Problems of Poroelastisity." Delft University of Technology

Vranna, A., and Tika, T. (2015a). "Undrained monotonic and cyclic behaviour of a silty sand stabilized with colloidal silica.", *6th International Conference on Earthquake Geotechnical Engineering,* Christchurch, New Zealand, 1-4 November 2015.

Vranna, A., and Tika, T. (2015b). "The mechanical behaviour of a clean sand stabilized with colloidal silica.", *XVI European Conference on Soil Mechanics and Geotechnical Engineering*, Edinburgh, United Kingdom, 13-17 September.

Wang, H. (2000). "Theory of Linear Poroelasticity with Applications to Geomechanics and Hydrogeology". Princeton University Press.

Wang, M. ., Li, L., and Han, J. P. (2008). "Effective stress analysis of seismic behaviors of inclined micropiles on liquefiable soils." *14th World Conference on Earthquake Engineering*, Beijing, China.

Whang, J. M. (1995). "'Section 9 - Chemical-based barrier materials.'" Assessment of Barrier Containment Technologies for Environmental Remediation Applications (R. R. Rumer and J.K.Mitchell, eds), NTIS, Springfield, VA, 211-247.

APPENDIX A

OVERVIEW OF COLLOIDAL SILICA VISCOSITY MEASUREMENTS AT THE UNIVERSITY OF THESSALY

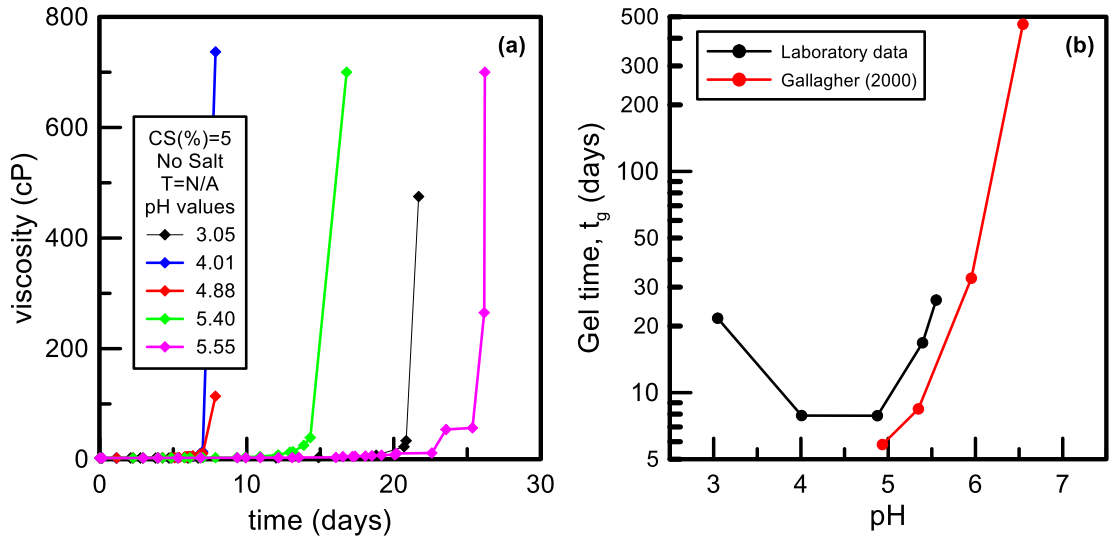

Figure A. 1 *(a) Typical CS viscosity versus time curve for CS(%)=5 with no added NaCl for different pH values, (b) Gel time curve for CS(%)=5, with no added NaCl at unknown (room) temperature and comparison with literature data of Gallagher, 2000.*

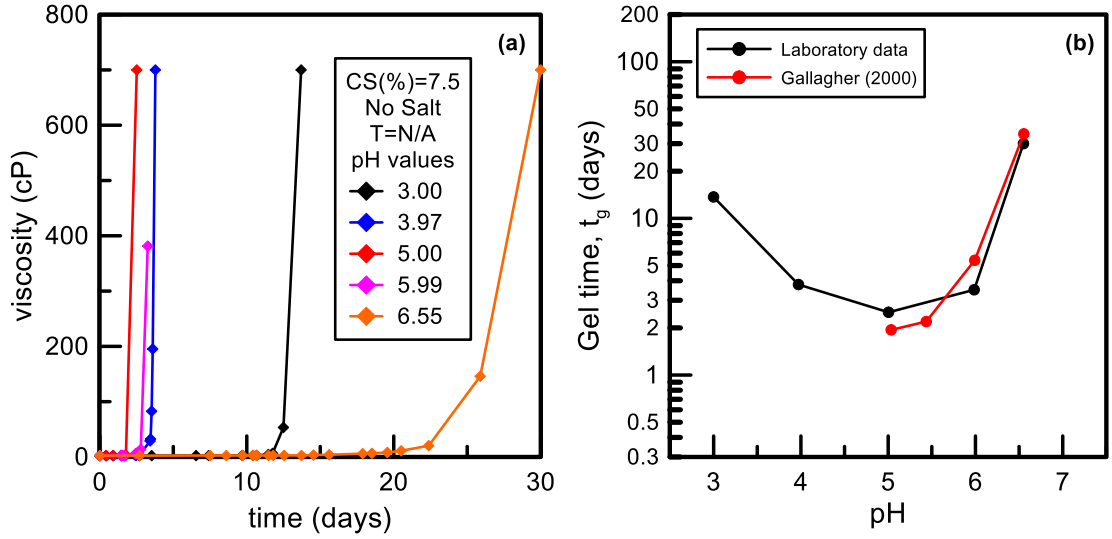

Figure A. 2 *(a) Typical CS viscosity versus time curve for CS(%)=7.5 with no added NaCl for different pH values, (b) Gel time curve for CS(%)=5, with no added NaCl at unknown (room) temperature and comparison with literature data of Gallagher, 2000.*

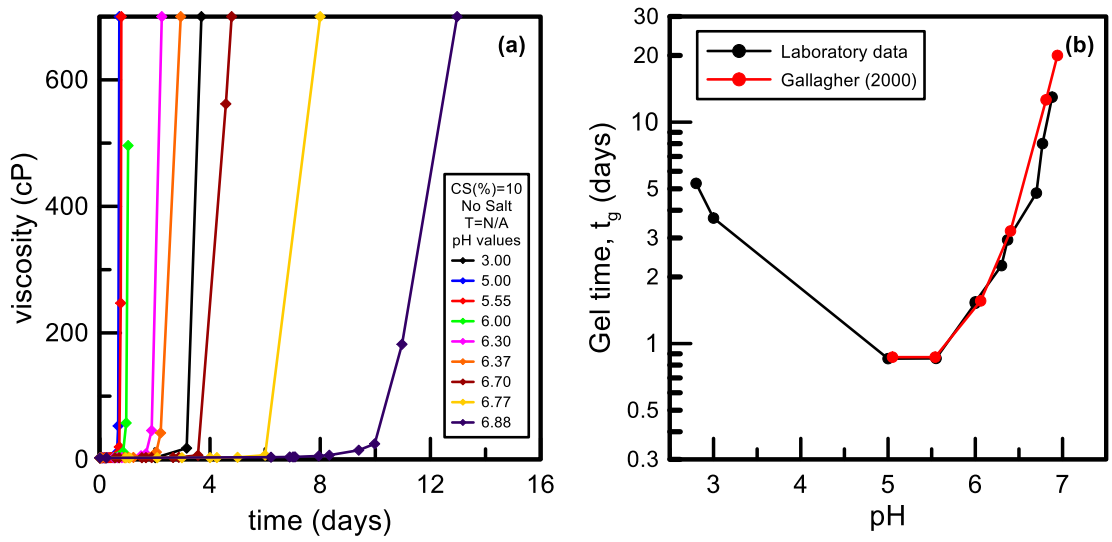

Figure A. 3 *(a) Typical CS viscosity versus time curve for CS(%)=10 with no added NaCl for different pH values, (b) Gel time curve for CS(%)=5, with no added NaCl at unknown (room) temperature and comparison with literature data of Gallagher, 2000.*

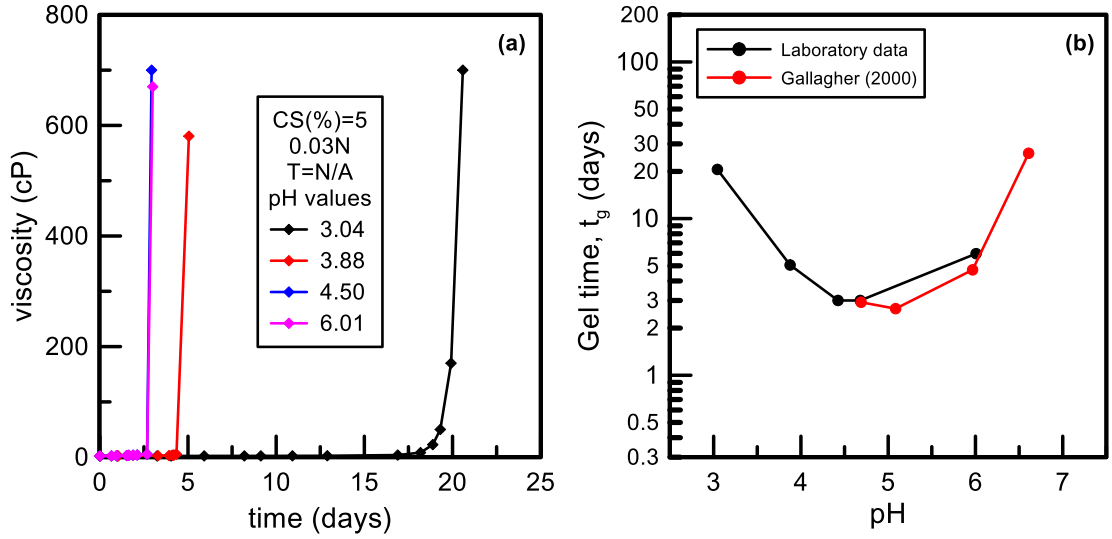

Figure A. 4 *(a) Typical CS viscosity versus time curve for CS(%)=5 with 0.03N NaCl normality for different pH values, (b) Gel time curve for CS(%)=5, with no added NaCl at unknown (room) temperature and comparison with literature data of Gallagher, 2000.*

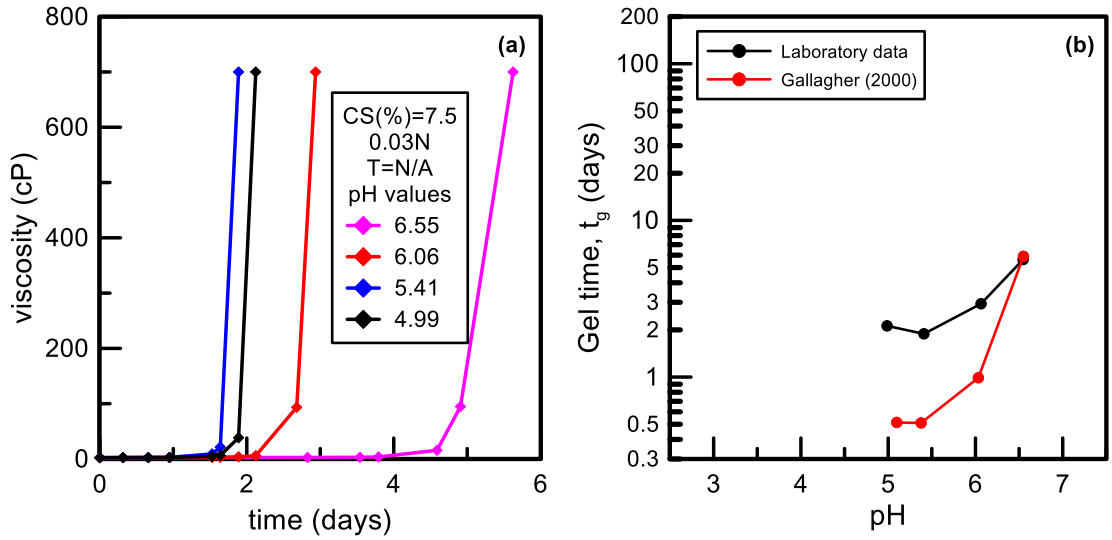

Figure A. 5 *(a) Typical CS viscosity versus time curve for CS(%)=7.5 with 0.03N NaCl normality for different pH values, (b) Gel time curve for CS(%)=5, with no added NaCl at unknown (room) temperature and comparison with literature data of Gallagher, 2000.*

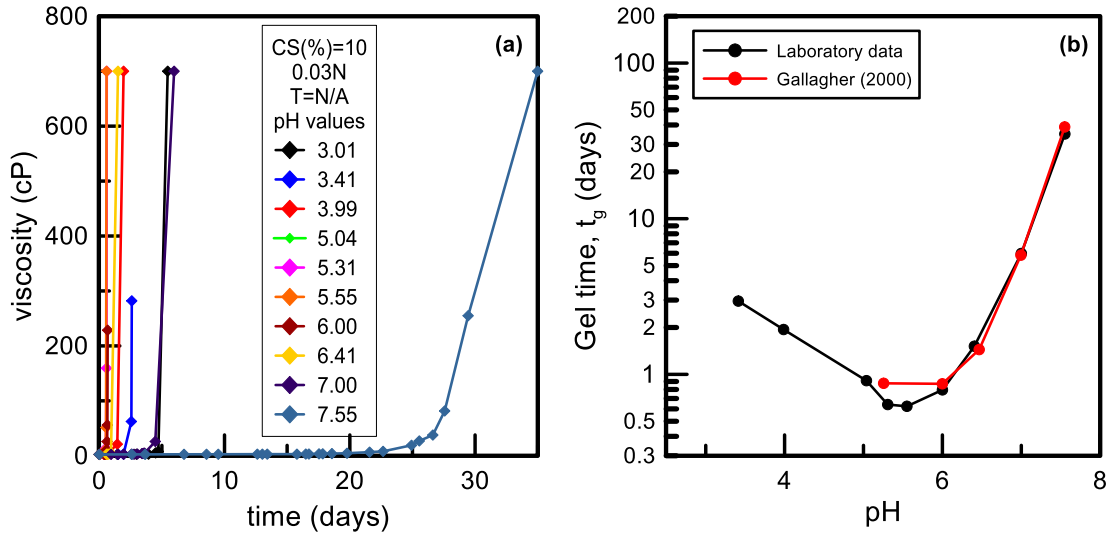

Figure A. 6 *(a) Typical CS viscosity versus time curve for CS(%)=10 with 0.03N NaCl normality for different pH values, (b) Gel time curve for CS(%)=5, with no added NaCl at unknown (room) temperature and comparison with literature data of Gallagher, 2000.*

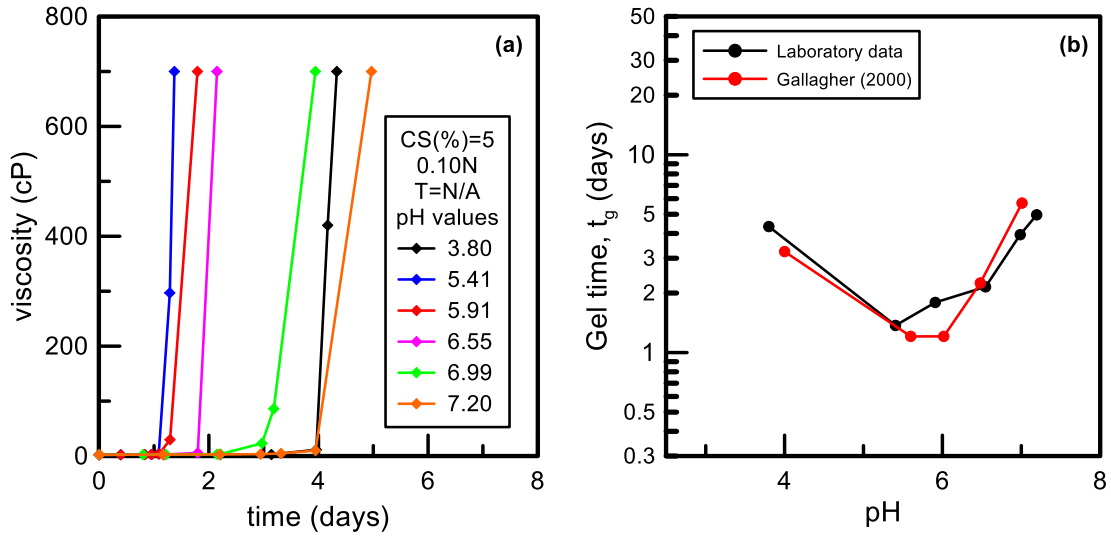

Figure A. 7 *(a) Typical CS viscosity versus time curve for CS(%)=5 with 0.1N NaCl normality for different pH values, (b) Gel time curve for CS(%)=5, with no added NaCl at unknown (room) temperature and comparison with literature data of Gallagher, 2000.*

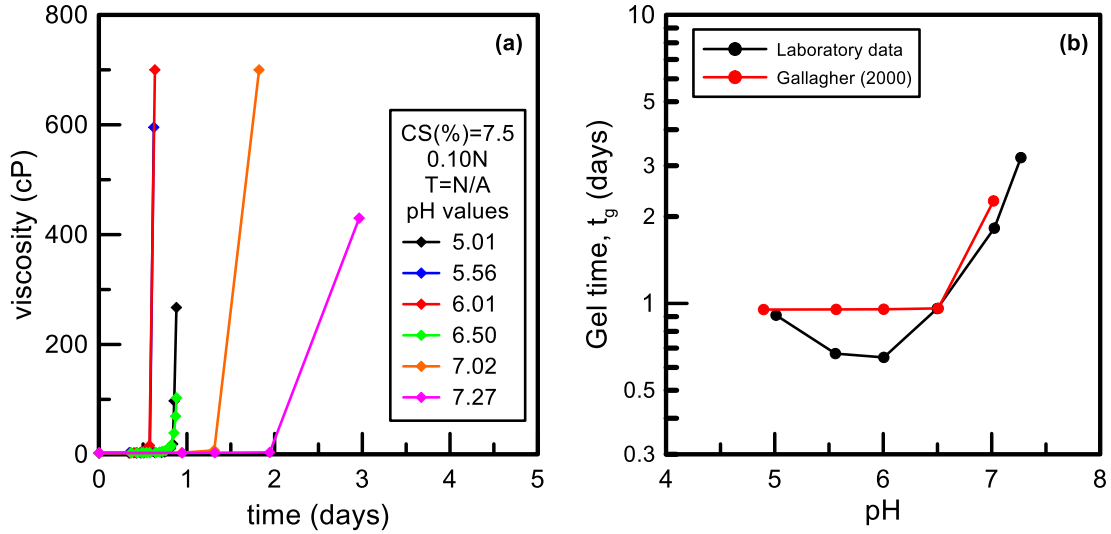

Figure A. 8 *(a) Typical CS viscosity versus time curve for CS(%)=7.5 with 0.1N NaCl normality for different pH values, (b) Gel time curve for CS(%)=5, with no added NaCl at unknown (room) temperature and comparison with literature data of Gallagher, 2000.*

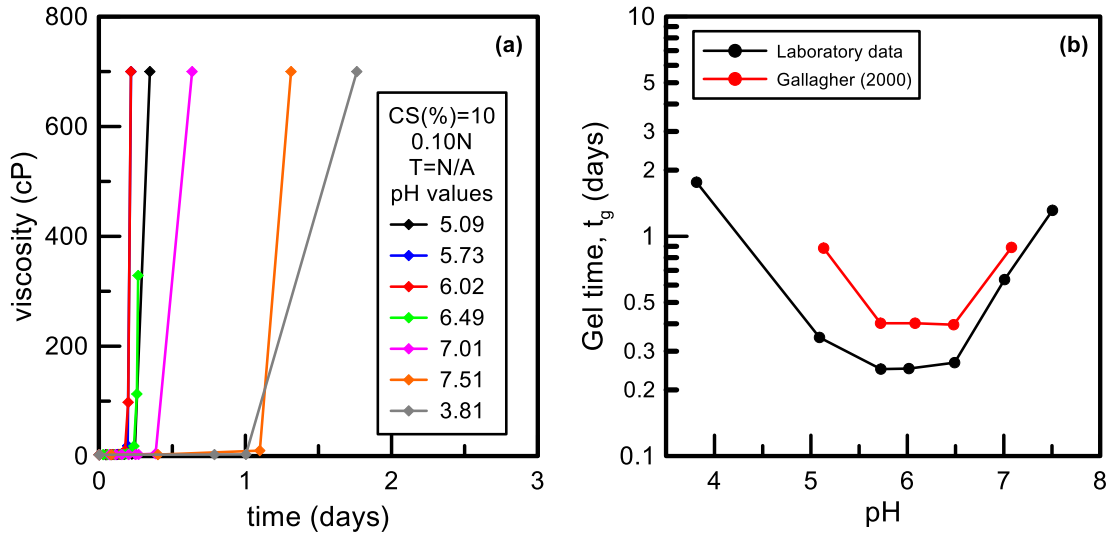

Figure A. 9 *(a) Typical CS viscosity versus time curve for CS(%)=10 with 0.1N NaCl normality for different pH values, (b) Gel time curve for CS(%)=5, with no added NaCl at unknown (room) temperature and comparison with literature data of Gallagher, 2000.*

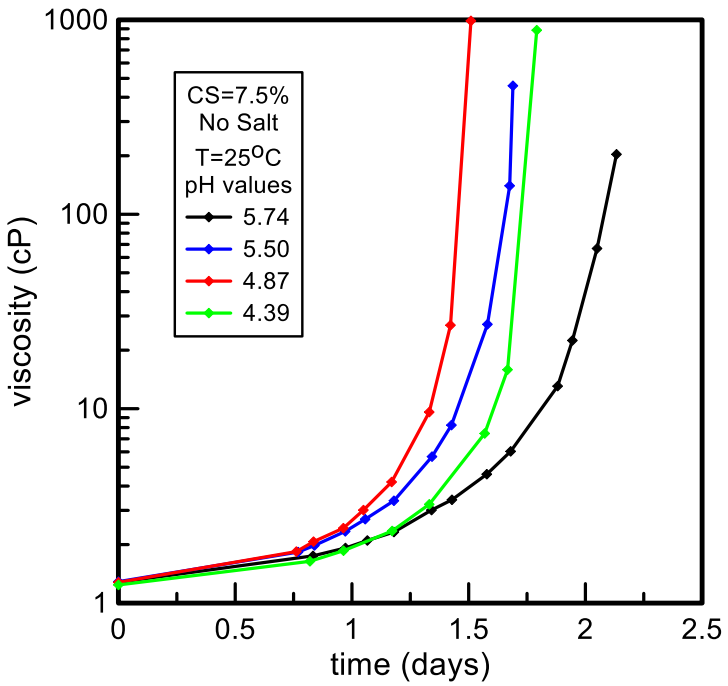

Figure A. 10 *Typical CS viscosity versus time curves for CS(%)=7.5 with no added NaCl at temperature of T=25°C and different pH values.*

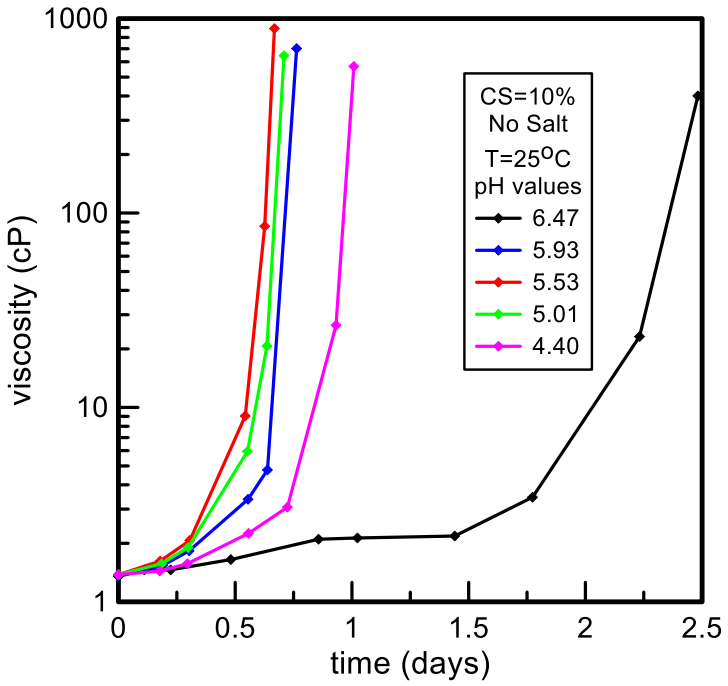

Figure A. 11 *Typical CS viscosity versus time curves for CS(%)=10 with no added NaCl at temperature of T=25°C and different pH values.*

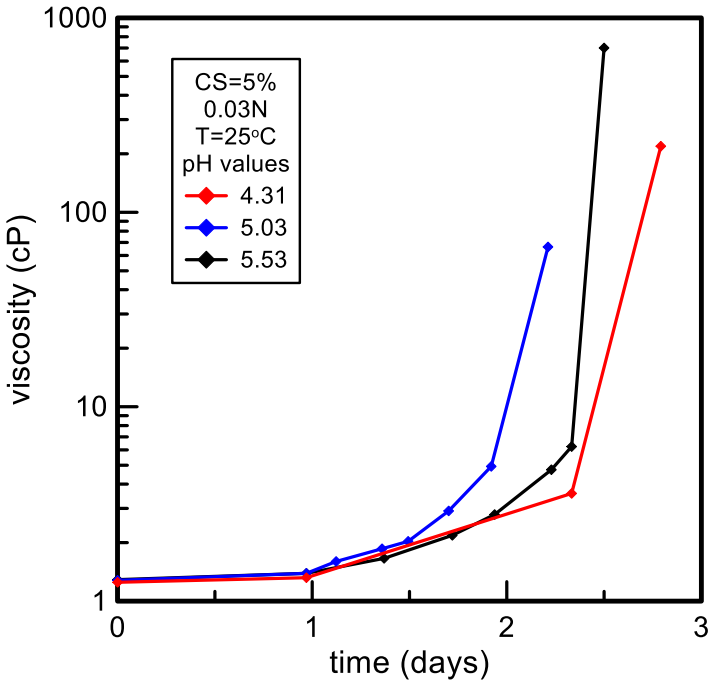

Figure A. 12 *Typical CS viscosity versus time curves for CS(%)=5 with 0.03N NaCl normality at temperature of T=25°C and different pH values.*

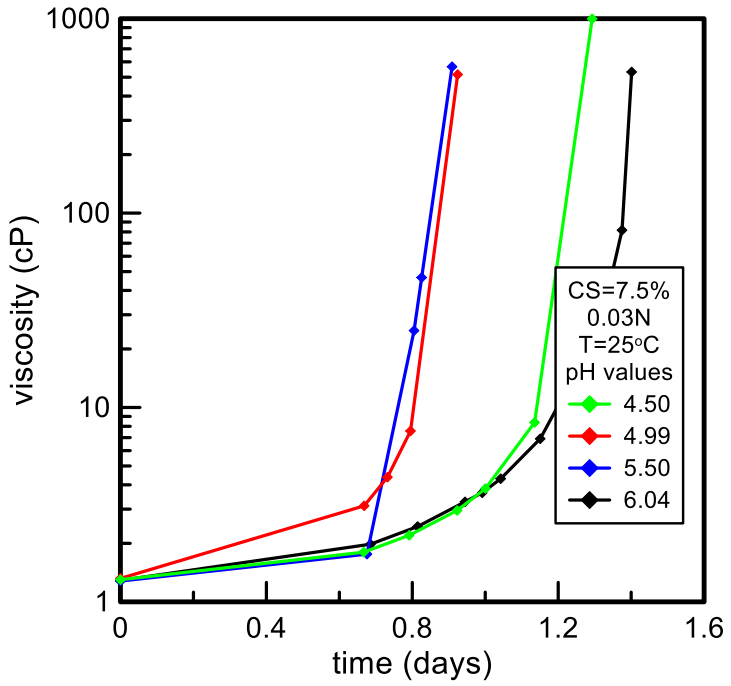

Figure A. 13 *Typical CS viscosity versus time curves for CS(%)=7.5 with 0.03N NaCl normality at temperature of T=25°C and different pH values.*

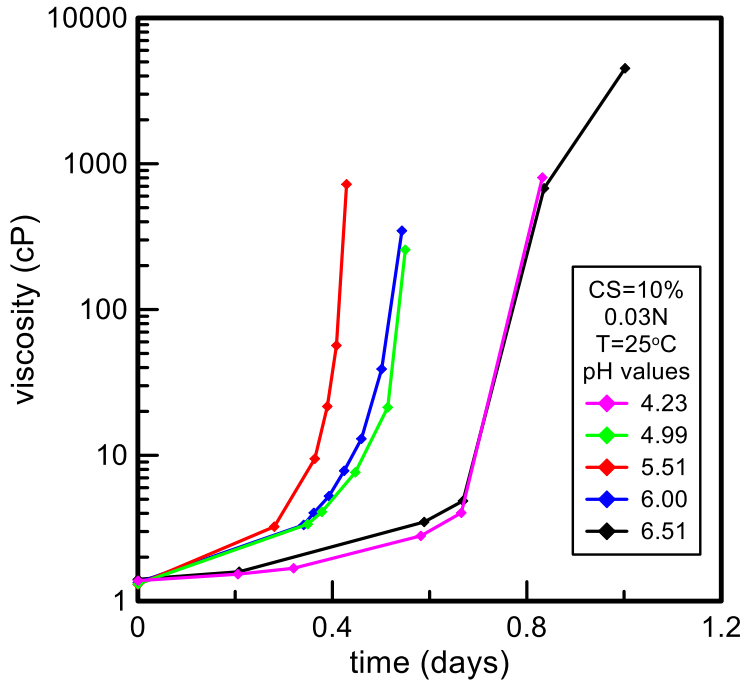

Figure A. 14 *Typical CS viscosity versus time curves for CS(%)=10 with 0.03N NaCl normality at temperature of T=25°C and different pH values.*

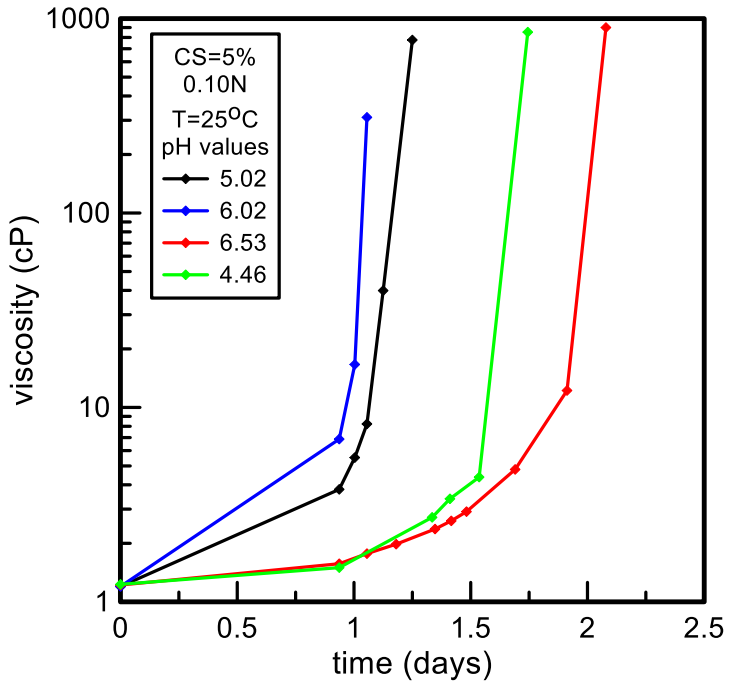

Figure A. 15 *Typical CS viscosity versus time curves for CS(%)=5 with 0.10N NaCl normality at temperature of T=25°C and different pH values.*

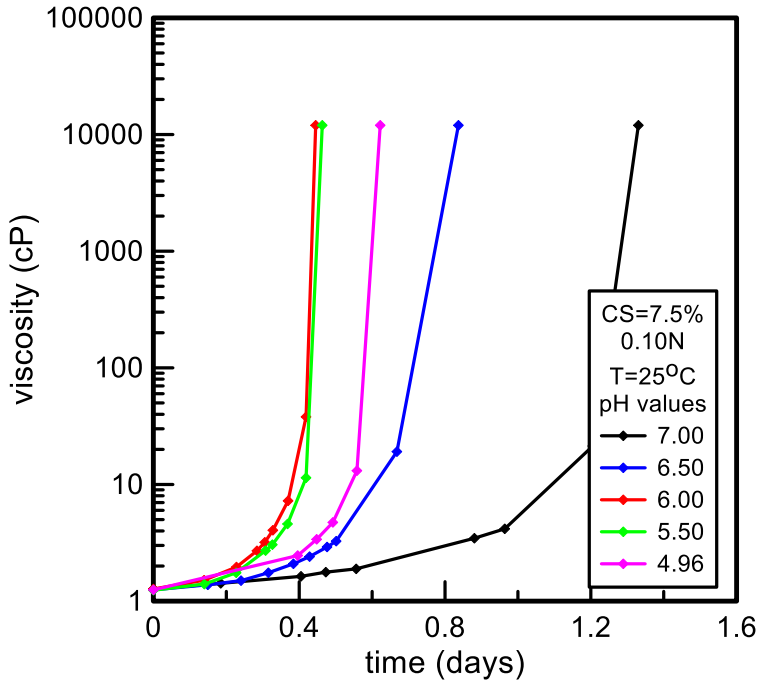

Figure A. 16 *Typical CS viscosity versus time curves for CS(%)=7.5 with 0.10N NaCl normality at temperature of T=25°C and different pH values.*

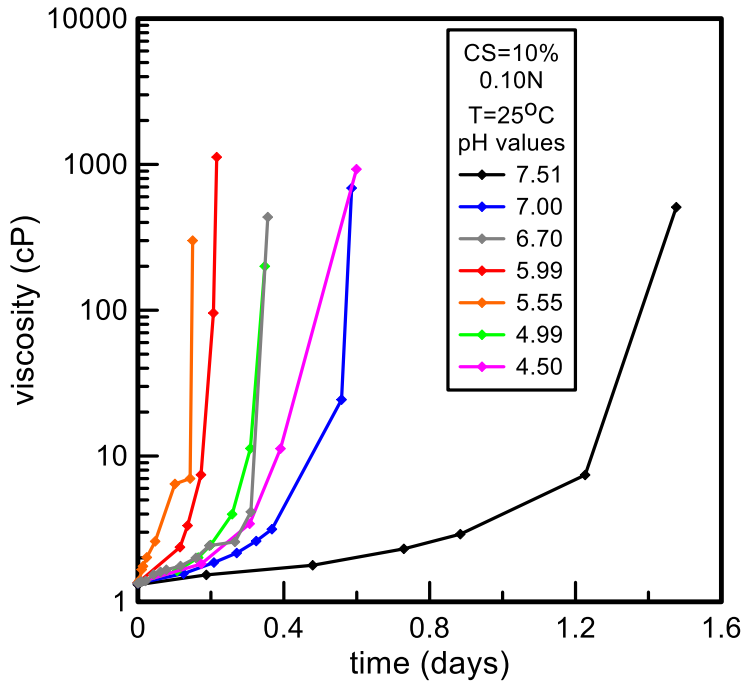

Figure A. 17 *Typical CS viscosity versus time curves for CS(%)=10 with 0.10N NaCl normality at temperature of T=25°C and different pH values.*

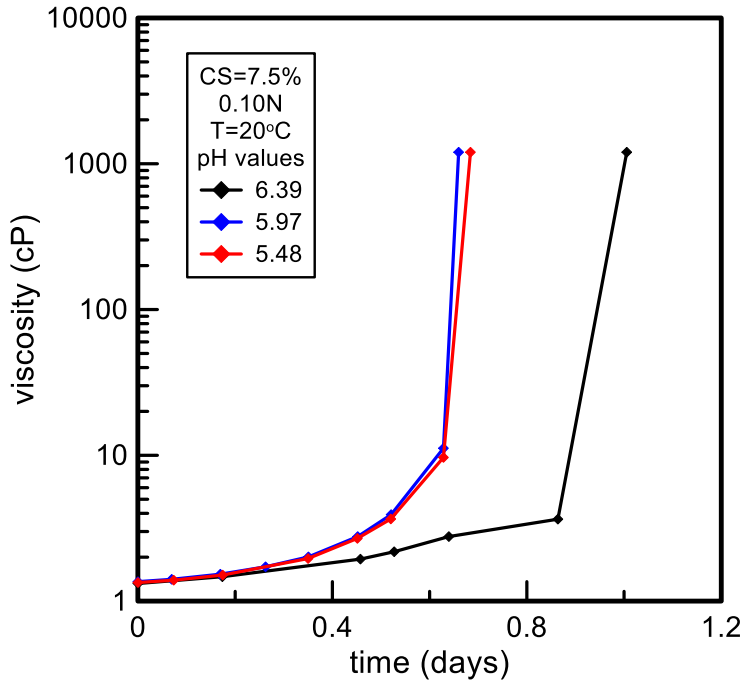

Figure A. 18 *Typical CS viscosity versus time curves for CS(%)=7.5 with 0.10N NaCl normality at temperature of T=20°C and different pH values.*

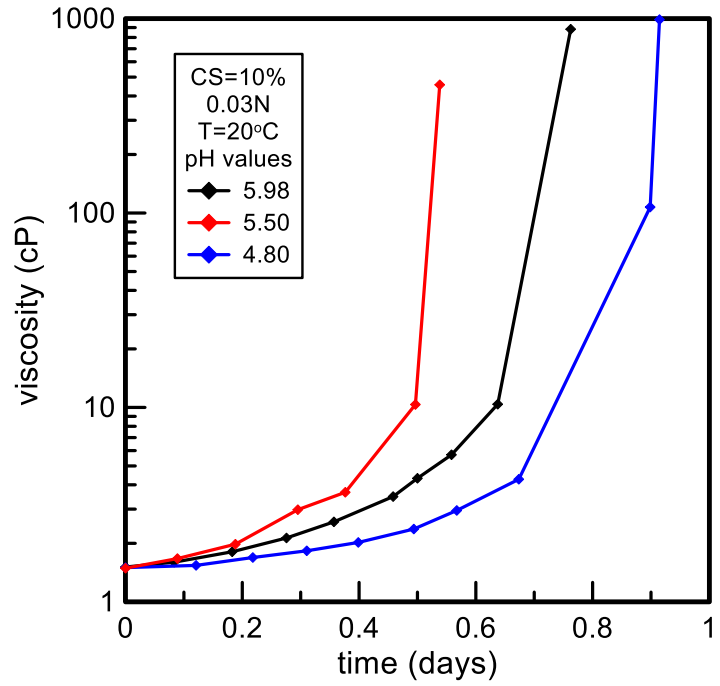

Figure A. 19 *Typical CS viscosity versus time curves for CS(%)=10 with 0.03N NaCl normality at temperature of T=20°C and different pH values.*

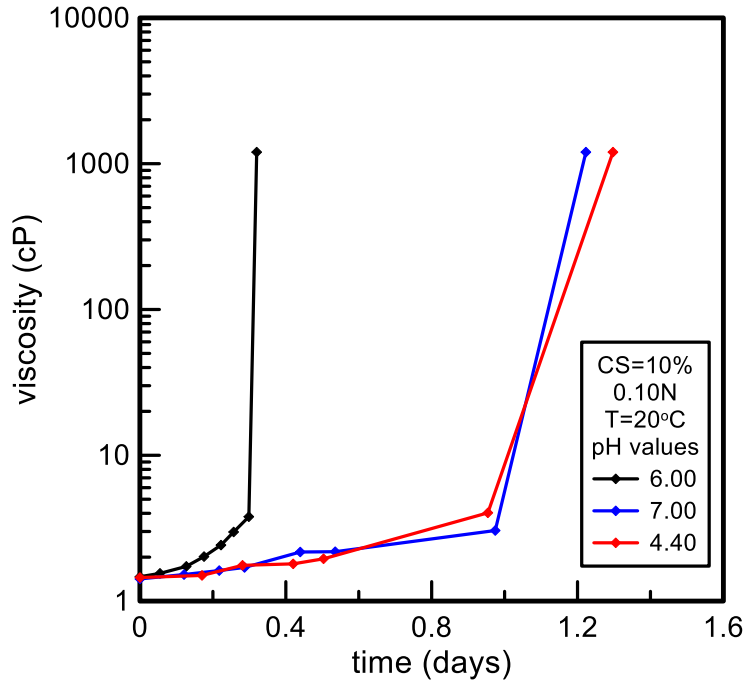

Figure A. 20 *Typical CS viscosity versus time curves for CS(%)=10 with 0.10N NaCl normality at temperature of T=20°C and different pH values.*

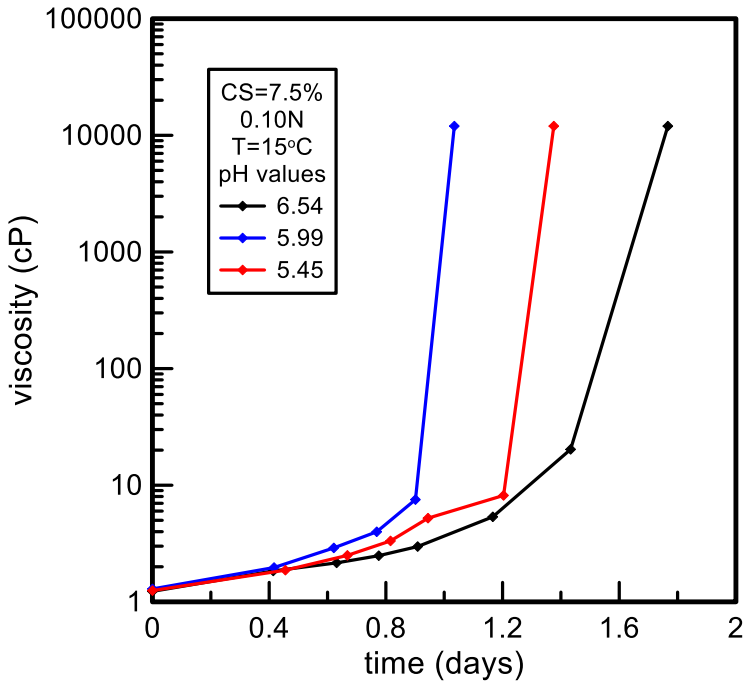

Figure A. 21 *Typical CS viscosity versus time curves for CS(%)=7.5 with 0.10N NaCl normality at temperature of T=15°C and different pH values.*

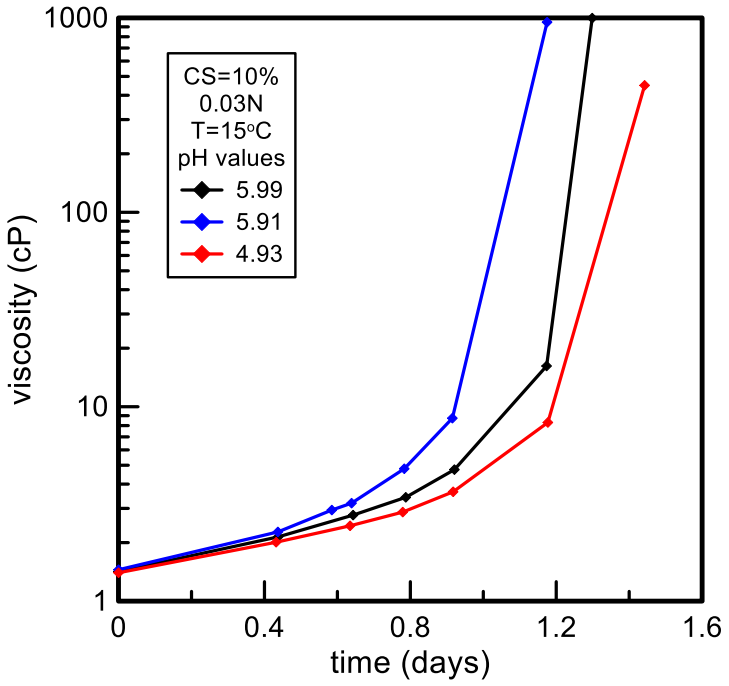

Figure A. 22 *Typical CS viscosity versus time curves for CS(%)=10 with 0.03N NaCl normality at temperature of T=15°C and different pH values.*

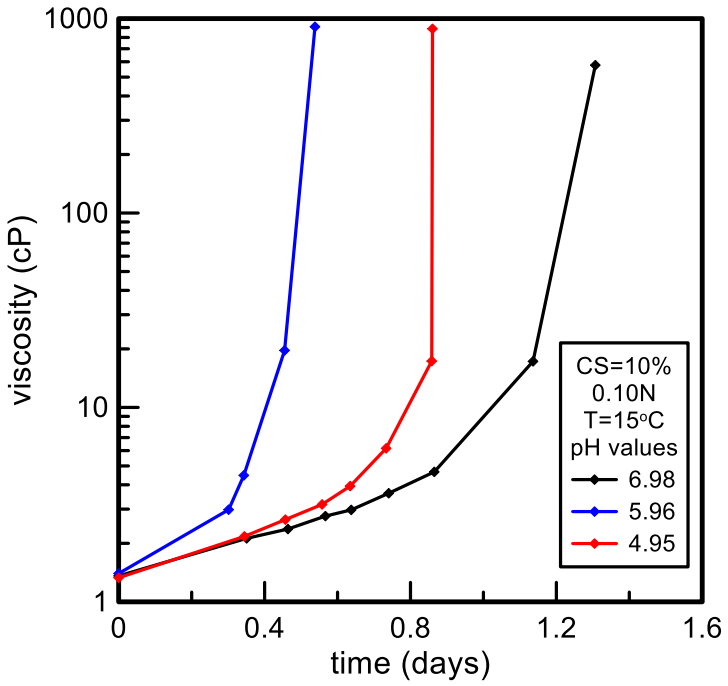

Figure A. 23 *Typical CS viscosity versus time curves for CS(%)=10 with 0.10N NaCl normality at temperature of T=15°C and different pH values.*

APPENDIX B

ELASTIC RESPONSE SPECTRA - ACCELERATION VELOCITY AND DISPLACEMENT TIME HISTORIES FOR THE 11 RECORDINGS